

ADA 040638

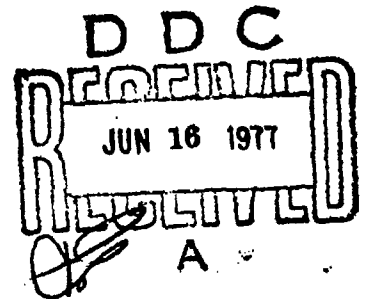
12
NW

Report No. FAA-EQ-77-3

AIRCRAFT EMISSIONS: POTENTIAL EFFECTS ON OZONE AND CLIMATE

A Review and Progress Report

R.C. Oliver
with
E. Bauer, H. Hidalgo, K.A. Gardner and W. Wasyluk



March 1977

FINAL REPORT

DISTRIBUTION STATEMENT A

Approved for public release;
Distribution Unlimited

Prepared for:

HIGH ALTITUDE POLLUTION PROGRAM

U.S. DEPARTMENT OF TRANSPORTATION
FEDERAL AVIATION ADMINISTRATION
Office of Environmental Quality
Washington, D.C. 20591

AD No. _____
DDC FILE COPY

This document is disseminated under the sponsorship of the Department of Transportation in the interest of information exchange. The United States Government assumes no liability for its contents or use thereof.

The work reported in this document was conducted under Contract No. DOT-FA76/WA-3757 for the Department of Transportation. The publication of this IDA Report does not indicate endorsement by the Department of Transportation, nor should the contents be construed as reflecting the official position of that agency.

Technical Report Documentation Page

1. Report Number 18 FAA-EQ-77-3 ✓	2. Government Accession No.	3. Recipient's Catalog No.
4. Title and Subtitle Aircraft Emissions: Potential Effects on Ozone and Climate - A Review and Progress Report.	5. Report Date March 1977	6. Performing Organization Code
7. Author(s) R.C. Oliver, E. Bauer, H. Hidalgo, K.A. Gardner, W. Wasyliwskyj	8. Performing Organization Report No. Paper P-1287	
9. Performing Organization Name and Address INSTITUTE FOR DEFENSE ANALYSES ✓ 400 Army-Navy Drive Arlington, Virginia 22202	10. Work Unit No. (TRIS)	11. Contract or Grant No. DOT-FA76WA-3757 new
12. Sponsoring Agency Name and Address U.S. Department of Transportation Federal Aviation Administration Office of Environmental Quality High Altitude Pollution Program	13. Type of Report and Period Covered 9 Final rept.	14. Sponsoring Agency Code
15. Supplementary Notes N/A 12401p.		
16. Abstract A critical review is made of information (as of December 1976) relative to effects of aircraft emissions (NO_x , SO_2 , H_2O) projected to 1990 on the earth's protective ozone shield and on mean surface temperature, as estimated from appropriate mathematical models. Potential biological effects are not reviewed. The review provides information showing the large uncertainties in computations of effects on ozone, due to uncertainties in NO_x emission indices (accepted values may be several-fold low), in chemistry, in troposphere-stratosphere interchange processes, and in future stratospheric composition (principally chlorine content); estimates of effects can be expected to change as new data are obtained. Current results indicate that aircraft NO_x effects on the ozone column change sign with aircraft altitude: subsonic aircraft, cruising at 6-km to 14-km altitude, enhance or have almost no effect on the ozone column; supersonic aircraft (mach-2 class), cruising at 16-km to 19-km, reduce total ozone, but, for given NO_x rates, by amounts less than previously reported. Computations based on a "high" (rapid growth) estimate for the 1990 total fleet of subsonic and supersonic aircraft, assuming current engines and accepted NO_x emission indices, including an estimated 142 Concorde and Tupolevs, showed an average ozone enhancement in the Northern Hemisphere of about 0.4 percent to 0.9 percent, varying with season. Potential surface temperature effects are very poorly established, but applications of existing model results suggest that such effects of the SST portion of this 1990 "high" fleet would be small (0 K to 0.02 K warming); the climatic effect of the subsonic portion of the 1990 "high" fleet was not estimated, because available models seemed to be not fully applicable. Problem areas needing further work are indicated.		
17. Key Words Ozone, Climate, Stratosphere, Troposphere, Aircraft emissions, Supersonic aircraft, Subsonic aircraft	18. Distribution Statement Document is available to the public through the National Technical Information Service, Springfield, Virginia 22151	
19. Security Classif. (of this report) UNCLASSIFIED	20. Security Classif. (of this page) UNCLASSIFIED	21. No. of Pages 404
		22. Price

Form DOT F 1700.7 (8-72)

Reproduction of completed page authorized

179350

LB

ABSTRACT

A critical review is made of information (as of December 1976) relative to effects of aircraft emissions (NO_x , SO_2 , H_2O) projected to 1990 on the earth's protective ozone shield and on mean surface temperature, as estimated from appropriate mathematical models. Potential biological effects are not reviewed.

The review provides information showing the large uncertainties in computations of effects on ozone, due to uncertainties in NO_x emission indices (accepted values may be several-fold low), in chemistry, in troposphere-stratosphere interchange processes, and in future stratospheric composition (principally chlorine content); estimates of effects can be expected to change as new data are obtained. Current results indicate that aircraft NO_x effects on the ozone column change sign with aircraft altitude: subsonic aircraft, cruising at 6-km to 14-km altitude, enhance or have almost no effect on the ozone column; supersonic aircraft (mach-2 class), cruising at 16-km to 19-km, reduce total ozone, but, for given NO_x rates, by amounts less than previously reported. Computations based on a "high" (rapid growth) estimate for the 1990 total fleet of subsonic and supersonic aircraft, assuming current engines and accepted NO_x emission indices, including an estimated 142 Concorde and Tupolevs, showed an average ozone enhancement in the Northern Hemisphere of about 0.4 percent to 0.9 percent, varying with season. Potential surface temperature effects are very poorly established, but applications of existing model results suggest that such effects of the SST portion of this 1990 "high" fleet would be small (0 K to 0.02 K warming); the climatic effect of the subsonic portion of the 1990 "high" fleet was not estimated, because available models seemed to be not fully applicable. Problem areas needing further work are indicated.

FOREWORD

This document was prepared for the High Altitude Pollution Program of the Federal Aviation Administration under Contract No. DOT-FA76WA-3757.

The authors are indebted to numerous individuals who have contributed data to or commented on various parts of this report. We are particularly indebted to Drs. J. S. Chang, W. H. Duewer, F. M. Luther, and D. J. Wuebbles of the Lawrence Livermore Laboratory for their many computations and analyses, to Dr. P. J. Crutzen of the National Center for Atmospheric Research (NCAR)* and the National Oceanic and Atmospheric Administration (NOAA), for including as part of his on-going investigations the problem areas reported in detail in Appendix A, and to Dr. G. F. Widhopf of the Aerospace Corporation for his modeling data reported herein. Valuable review comments were provided by the Lawrence Livermore Laboratory group, by Drs. R. E. Dickinson and V. Ramanathan of NCAR, and by Mr. R. Greenstone and Dr. N. Sundararaman of Operations Research, Inc. Appendix C was reviewed by Dr. J. D. Mahlman of Geophysical Fluid Dynamics Laboratory and Mr. K. Telegadas of National Oceanic and Atmospheric Administration; an early version was reviewed by Dr. D. M. Hunten of Kitt Peak National Observatory. However, the document as it stands is the responsibility of the authors. Comments and criticisms are invited.

* NCAR is sponsored by the National Science Foundation.

CONTENTS

SUMMARY	S-1
S.1 Scope	S-1
S.2 Purpose	S-1
S.3 Background	S-2
S.4 Current Findings	S-3
S.4.1 In Brief	S-3
S.4.2 In More Detail	S-4
S.5 Some Recommendations and Suggestions	S-17
1. Aircraft Emission: Potential Effects on Ozone and Climate	1-1
1.1 Introduction	1-1
1.2 Background	1-1
1.3 Objectives and Limitations	1-3
1.4 Organization and General Content of this Report	1-4
1.5 On Use of this Report	1-5
2. Air Traffic, Fuel Flows, and Emissions Projections	2-1
2.1 Introduction	2-1
2.2 CIAF Projections and Related Data	2-2
2.2.1 Projected Air Traffic and Fleets	2-2
2.2.2 Fuel Flow Projections	2-12
2.2.3 Emission Indices and Projections	2-14
2.3 FAA Projections	2-18
2.3.1 Procedures	2-18
2.3.2 Results	2-23
2.3.3 Fleet Size Estimates	2-32
2.4 A Word About Flight Altitudes	2-34
2.5 Concluding Comments	2-35
3. Effects of Aircraft Exhaust Products (Principally NO _x) on the Ozone Column	3-1
3.1 Introduction	3-1
3.2 Background	3-2
3.2.1 Stratospheric vs Tropospheric Ozone	3-2
3.2.2 Stratospheric Ozone	3-2
3.2.3 Effects of Altered Ozone Levels on Erythemally-Weighted Surface UV Flux	3-9
3.3 The Modeling Problem in General	3-16
3.3.1 Introduction	3-16
3.3.2 1-D Models	3-19
3.3.3 2-D Models	3-25
3.3.4 3-D Models	3-25
3.3.5 A Further Caveat	3-26

3.4	Results of Various Modeling Studies	3-27
3.4.1	CIAP, 1974, and NAS, 1975 Results	3-27
3.4.2	COMESA Modeling Results (1975)	3-36
3.4.3	Time-Dependent and Other Effects, 1-D Model	3-40
3.4.4	NASA-Ames 2-D Model Results (January 1976)	3-48
3.4.5	Crutzen 2-D Model Results	3-49
3.4.6	Reaction Rate Uncertainties and their Effects in 1-D Ozone Depletion Modeling	3-55
3.4.7	Fall 1976 Lawrence Livermore Laboratory Results	3-60
3.4.8	Average 2-D Model Results, "1990 High" Fleet Effects	3-73
3.5	Longitudinal Distribution Questions	3-82
3.6	Model Validation Attempts	
3.6.1	Introduction	3-85
3.6.2	Excess Carbon-14	3-85
3.6.3	HTO Transport	3-92
3.6.4	Zirconium-95	3-92
3.6.5	2-D and 3-D Model Studies and the 2-km Adjustment Question in the Hunten 1-D Model	3-93
3.6.6	Nuclear Weapons Tests--Injection of NO _x	3-95
3.6.7	Solar Proton Events, Polar Cap Absorption (PCA) Effects	3-96
3.7	A Summing Up	3-97
4.	Potential Effects on Mean Surface Temperature	4-1
4.1	Introduction	4-1
4.2	Background	4-2
4.2.1	Species and Effects of Concern	4-2
4.2.2	Some Observations on the Various Studies	4-3
4.2.3	Mean Changes and Their Limitations	4-4
4.3	Climate Change Modeling	4-5
4.3.1	Climate Modeling in General	4-5
4.3.2	CIAP Climate Modeling	4-6
4.3.3	COMESA Climatic Effect Studies	4-17
4.4	Computed Mean Temperature Effects--Fleet Effects	4-24
4.4.1	Introduction	4-24
4.4.2	Mean Temperature Impact of the 1990- High SST Fleet	4-24
4.4.3	Other Effects	4-29
4.5	Conclusions and Comments - Climatic Effects	4-30
APPENDIX A	Study of the Effects on Atmospheric Ozone of NO _x Emissions from Subsonic and Supersonic Aircraft Using the Crutzen 2-D Model	A-1
APPENDIX B	Some Details from the COMESA Report	B-1

APPENDIX C	On the use of Zr-95 Data from Chinese Atmospheric Thermonuclear Explosions to Study Atmospheric Motions in a One-Dimensional Parameterization	C-1
APPENDIX D	Computations of Injection Coefficients and Residence Times for 1-D Models	D-1
APPENDIX E	Emission Constraints on New SSTs: An Approach	E-1
APPENDIX F	Calculations of Time-Dependent Hypothetical SST Fleet Effects on Ozone Reduction and Mean Surface Temperature	F-1
APPENDIX G	Detectability of Environmental Changes Caused by Aircraft Effluents -- Some Comments	G-1
REFERENCES		R-1

FIGURES

S.1	Ozone Column Change Results by Various Models	S-11
S.2	Global Average Ozone Column Changes with Time Following Introduction of the Modified 1990 "High" Fleet NO _x Emissions, No Chlorine	S-14
S.3	Aerospace Model Results for Modified 1990 "High" Fleet	S-15
2.1	Air Traffic History and CIAP Projections	2-3
2.2	Flight Paths for Concorde and Tupolev-144 SSTs	2-22
2.3	Concorde Total NO _x Emissions, kg/Flight Above 13.2 km (After Reheat Cutoff), ISA Conditions	2-31
3.1	Ozone Distribution and Column Totals (22 March, 45° N)	3-3
3.2	Average (March 22) Ozone Concentration in Units of Molecules cm ⁻³ Expressed as Zonal-Average Contour Lines (7E12 means 7 x 10 ¹²)	3-4
3.3	Variation of Integrated Vertical Ozone Column with Season at Tropical, Temperate, and Polar Zones	3-4
3.4	Long-Term Variations in Total Ozone in the Northern Hemisphere	3-5
3.5	Average (March 22) Ozone Mole Fractions or Mixing Ratio by Volume (ppm)	3-5
3.6	Direct Solar UV Irradiance and Scattered UV Irradiance on a Horizontal Surface at Sea Level for Solar Zenith Angle θ of 0° and 0.341 atm-cm of Total Ozone	3-10
3.7	Analytical Models of Spectral Efficiencies for Biological Effects	3-11
3.8	Increase of "Carcinogenic" Solar UV Radiation with Decrease of Ozone Concentration, both in Percent	3-12
3.9	Percentage Increase in Sunburn Daily Dosage for a 10-Percent Decrease in Ozone Amount	3-14
3.10	Increase in Daily Sunburn Dosage for a 10-Percent Decrease in Ozone Amount (J/sq cm)	3-14
3.11	Yearly Sunburn Dosage (J/sq cm)	3-15
3.12	Latitudinal Distribution of Mean Tropopause Height, with CIAP Fleet Emission Projections and Data on the Latitudes of Nuclear Tests and CH ₄ Soundings	3-17

3.13	Six K_z Profiles	3-20
3.14	Schematic Diagram Indicating Water Vapor Fluxes Both into and in the Model Stratosphere	3-24
3.15	Correlations of McElroy et al., (1974) Estimates of Ozone Depletions	3-29
3.16	Ozone Columns as a Function of Season and Latitude, for Unperturbed (run 17) and Perturbed Atmospheres	3-34
3.17	Approach of Incremental NO_y to Final Value, 1.8 Mt NO_x/yr at 20 km and 45°N , L-D Model Results	3-36
3.18	Values of K_z from Hemispherically Averaged Annual Average Fluxes and Mixing Ratios (Average of Three Tracers) (m^2/sec)	3-38
3.19	Percentage Changes in O_3 Column Densities (Model A)	3-39
3.20	Normalized Ozone Depletions versus Time. Chang/1974 K_z	3-42
3.21	Normalized Ozone Depletions versus Time. Hunten/1974 K_z	3-43
3.22	1-D Time-Dependent Fleet and Model Ozone Effects Example. CIAP Chemistry	3-45
3.23	Assumed NO_x Emissions as a Function of Latitude at Levels 9, 10, 11, and 13. NCAR 2-D Runs	3-51
3.24	Percent Ozone Column Change Above Ground as a Function of Latitude and Season After Six Years of NO_x Emissions ($2.06 \times 10^9 \text{ kg}/\text{yr}$ at 35,000-ft Altitude	3-52
3.25	Normalized NCAR 2-D Results (Crutzen Model) for Ozone Column Changes with $1 \times 10^9 \text{ kg}/\text{yr}$ NO_x Injection Rate at Various Altitudes Distributed over 1.8-km Altitude Bands, and over Latitude According to Fig. 3.23	3-54
3.26	Effects of Background Chlorine Content on Ozone Sensitivity to NO_x Additions at Various Injection Altitudes	3-66
3.27	Effects of Background Chlorine Content on Ozone Sensitivity to NO_x Additions at Various Injection Altitudes	3-67
3.28	Data of Figs. 3.26 and 3.27 Replotted. (ClONO_2 Included)	3-68
3.29	Ozone Change Linearity Test. ClONO_2 Included	3-70
3.30	Water and NO_2 Effects on Ozone in the Presence of ~ 1 ppb Active Chlorine	3-72
3.31	Global Average Ozone Column Changes with Time Following Introduction of the Modified "1990-High" Fleet NO_x Emissions, No Chlorine	3-74
3.32	Ozone Columns (m-atm-cm) as a Function of Season and Latitude	3-77

3.33	Test of Widhopf 2-D Model Dynamics Using Zr-95 Data	3-78
3.34	Test of Widhopf 2-D Model Dynamics Using Zr-95 Data, Showing the need to Include Settling	3-79
3.35	Widhopf Model Results for Modified "1990-High" Fleet (see Table 2.33)	3-80
3.36	Excess Stratospheric C-14 from Atmospheric Thermonuclear Explosions	3-87
3.37	Decay Rate of Excess Carbon-14	3-88
3.38	Tests of Various K_z Profiles Using Data on Excess Carbon-14	3-89
3.39	Tests of Various K_z Profiles Using Data on Excess Carbon-14	3-90
3.40	Tests of Various K_z Profiles Using Data on Excess Carbon-14	3-91
3.41	Ozone Change Estimates by Various Models Illustrating Uncertainties Due to Chemistry and Dynamics	3-98
4.1	Residence Time Estimates	4-18
4.2	Surface Temperature Change as a Function of Fuel Burnt	4-20
A-1	Observed Total Ozone (m-atm-cm) as a Function of Season and Latitude in the Northern (London, 1963) and Southern (Sticksel, 1963) Hemispheres	A-11
A-2	Model Natural Total Ozone (m-atm-cm) Above Ground ($L=1$) as a Function of Latitude and Month of the Year after 15 Years of Integrations (Subsequent to Initialization)	A-12
A-3	Natural Water Vapor Volume Mixing Ratio During Winter (December 30) in the Northern Hemisphere and Summer in the Southern Hemisphere after 15 Years of Integration	A-13
A-4	Natural Methane Mixing Ratio During Winter (December 30) in the Northern Hemisphere and Summer in the Southern Hemisphere after 15 Years of Integration	A-14
A-5	Natural Ozone Concentration (molecules/cm ³) During Winter (December 30) in the Northern Hemisphere and Summer in the Southern Hemisphere after 15 Years of Integration	A-15
A-6	Natural Atomic Oxygen Concentration (atoms/cm ³) During Winter (December 30) in the Northern Hemisphere and Summer in the Southern Hemisphere after 15 Years of Integration	A-16
A-7	Natural NO + NO ₂ Volume Mixing Ratio During Winter (December 30) in the Northern Hemisphere and Summer in the Southern Hemisphere after 15 Years of Integration	A-17
A-8	Natural NO _x Volume Mixing Ratio During Winter (December 30) in the Northern Hemisphere and Summer in the Southern Hemisphere after 15 Years of Integration	A-18

A-9	Assumed NO _x Emissions (as NO ₂) as a Function of Latitude at Model Levels 9, 10, 11, and 13	A-19
A-10	Schematic Summary of Numerical Experiments Using the Crutzen Two-Dimensional Model of the Stratosphere and Troposphere	A-21
A-11	Percent Change of Ozone Column above Ground (L=1) at Middle Northern Latitudes (45° N) During Summer (August 30) after 6 Years of NO _x Emissions from Subsonic and Supersonic Aircraft	A-23
A-12	Percent Change of Ozone Column above Level 10 (12.66 km) at Middle Northern Latitudes (45° N) During Summer (August 30) after 6 Years of NO _x Emissions from Subsonic and Supersonic Aircraft	A-24
A-13	Percent Ozone Column Change as a Function of Latitude and Season after 6 Years of NO _x Emissions (2.06 x 10 ⁹ kg of NO ₂ /yr) at 10.8 km Altitude (L=9)	A-25
A-14	Percent Ozone Column Change as a Function of Latitude and Season after 6 Years of NO _x Emissions (0.455 x 10 ⁹ kg of NO ₂ /yr) at 12.7-km Altitude (L=10)	A-26
A-15	Percent Ozone Column Change as a Function of Latitude and Season after 6 Years of NO _x Emissions (0.455 x 10 ⁹ kg of NO ₂ /yr) at 14.5-km Altitude (L=11)	A-27
A-16	Percent Ozone Column Change as a Function of Latitude and Season after 6 Years of NO _x Emissions (0.226 x 10 ⁹ kg of NO ₂ /yr) at 18-km Altitude (L=13)	A-28
A-17	Natural Ozone Concentration at Middle Northern Latitudes (45° N) during Summer (August 30) after 15 Years of Integration	A-30
A-18	Percent Change in Ozone Concentration at Middle Northern Latitude (45° N) during Summer as a Function of Altitude after 6 Years of Aircraft NO _x Emissions	A-30
A-19	Natural NO _x Concentration at Middle Northern Latitudes (45° N) during Summer (August 30) after 15 Years of Integration	A-31
A-20	Percent Change in NO _x Concentration at Middle Northern Latitudes (45° N) during Summer as a Function of Altitude after 6 Years of Aircraft NO _x Emissions	A-32
A-21	NO _x Percent Increase as a Function of Latitude, Altitude, and Season after 6 Years of Fleet Operations for NO _x Emissions at Level 9 (approximately 10.3 km)	A-33
A-22	NO _x Percent Increase as a Function of Latitude, Altitude, and Season after 6 Years of Fleet Operations for NO _x Emissions at Level 13 (approximately 18 km)	A-34
A-23	Percent Ozone Column Change at Middle Northern Latitude (45° N) during Summer (August 30) and 6 Years of NO _x Emissions from Subsonic and Supersonic Aircraft	A-44

A-24	Percent NO_x Increase at Level 17 (25.2 km) at Middle Northern Latitudes (45° N) during Summer (August 30) and 6 Years of NO_x Emissions from Subsonic and Supersonic Aircraft	A-45
A-25	Percent Change of Natural Ozone Column above Ground ($L=1$) at Middle Northern Latitudes (45° N) during Summer (August 30) and 12 Years after Initialization (3 Years)	A-51
B-1	Summary of the State of Knowledge of Stratospheric Composition	B-5
B-2	Measured NO Profiles (Representative Values of Random Plus Systematic Errors are Indicated by Bars)	B-7
B-3	Oxford Pressure Modulator Radiometer Results, June 1975 (Representative Values of Random Plus Systematic Errors are Indicated by Bars)	B-8
B-4	Latitude Distribution of H_2O in the 15-km to 20-km Layer, Measured by Several Workers (identifications in text)	B-10
B-5	Recent Results of Balloon-borne Measurements of H_2O by the Oxford and NPL Groups	B-11
B-6	Values of K_z Hemispherically Averaged Annual Average Fluxes and Mixing Ratios (average of three tracers) (m^2/sec)	B-16
B-7	Percentage Changes in O_3 Column Densities (Model A)	B-24
B-8	Percentage Reduction in Total Global Ozone Amount	B-29
C-1	Height (decameters) of the 100-mb Surface on June 17, 1967 (0000 GMT)	C-5
C-2	Stratospheric Zirconium-95 Burdens (decay-corrected) Following the Chinese Nuclear Tests	C-7
C-3	Effective Vertical Transport of Radioactivity Estimated by Telegadas (1974, from Figs. 44 and 45)	C-8
C-4	Sketch of the Overall Character of the Solution for Injection at $z_i = 18$ km. We show nf, the total number of tracer particles per unit volume	C-12
C-5	The Function $U(x_i)$ Which Measures the Reduction in Tracer Burden with Time	C-14
C-6	Effective Injection Height for Aerosols as a Function of Time, $z(t)$	C-16
C-7	Decay of Stratospheric Tracer Burden as a Function of Time	C-17
C-8	Change of Stratospheric Tracer Burden with Time: Possible Effects of Sedimentation	C-18
C-9	Time for Stratospheric Tracer Burden to Decrease to 60 Percent of Its Peak Value, $t_{0.6}$, Computed With and Without Sedimentation, Shown as a Function of Eddy Diffusivity K_z	C-20

C-10	Time for Stratospheric Tracer Burden to Decrease to 60 Percent of the Peak Value, $t_{0.6}$, Computed With and Without Sedimentation, Shown as a Function of Eddy Diffusivity K_z	C-22
D-1	Three Eddy Diffusivity Profiles used During CIAP in 1974	D-4
D-2	Three Recent Eddy Diffusivity Profiles	D-5
D-3	Sedimentation Velocity for Spheres of Density 2 gm/cm^3	D-7
D-4	General Character of the Solution for Eddy Diffusivity Profile K_G	D-10
D-5	Case (ii): Scaling Factor $G(z_1)$ for $K = K_G$ and K_H for gases, $z_2 = 55 \text{ km}$	D-12
D-6	Case (ii): The Scaling Factor $G(z_1)$, which gives the Ratio of Flux Going Above the Point of Injection, z_1 , to the Flux Going Below the Point of Injection, for $K = K_H$, Gases and Aerosols, $z_2 = 55$ and 75 km	D-12
D-7	Residence Time for a Gas, $K = K_H$, for Cases (i)/(iii) and Case (ii) with $z_2 = 55$ and 75 km	D-13
D-8	Mean Atmospheric Residence Time for Gases and Aerosols, Case (iii), $K = K_G$	D-15
D-9	Mean Atmospheric Residence Time for Gases and Aerosols, Case (iii), $K = K_H$	D-15
E-1	Apparent Optimal Altitude as a Function of Mach Number (Velocity)	E-5
E-2	Fuel Flow as Permitted by Various Criteria and Models	E-7
F-1	Model-Generated Effects of Hypothetical SST Fleet Building up with Time	F-5
G-1	The Mean Global Total Ozone Distribution with the Ozone Amount given in Units of m-atm-cm (after Gebhart, Bojkov, and London, 1970)	G-5

TABLES

S.1	Projected Fuel Consumption Comparisons, 10^9 kg/yr	S-6
S.2	Projected Fuel Consumption Comparisons above 12-km by Subsonic Aircraft, 10^9 kg/yr	S-6
S.3	NO Concentration Measurements by Probe and Spectrometer Techniques	S-7
S.4	The Range of Estimates of Global Average Percentage Ozone Change Due to Uncertainties in Kinetics and Dynamics; NO_x Injection Rate at 17 km, 2.46×10^9 kg/yr as NO_2	S-8
S.5	Representative Changes in Computed Ozone Column Reductions Due to SST (Percent)	S-9
S.6	Distributions of NO_x From 1990 "High" Fleet (Modified); Total NO_x : 2.81×10^9 kg/yr	S-12
2.1	CIAP Upper-Bound Air Travel and Air Cargo Projections	2-4
2.2	CIAP Expected Air Travel and Air Cargo Projections	2-5
2.3	Aircraft Postulated in CIAP	2-7
2.4	CIAP Expected World Aircraft Fleets	2-8
2.5	Fleet Mix Developed in CIAP to Meet Upper-Bound 1990 Air Traffic Demand: Only Present SSTs Available	2-9
2.6	Fleet Mix Developed in CIAP to Meet Upper-Bound Air Traffic Demand; No SSTs Available	2-9
2.7	Flight Profiles for Emission Calculations; CIAP Model	2-10
2.8	Fuel Consumed at Specified Flight Altitudes in More Than 600 U.S. Boeing 707 Trans-continental Flights in January and February 1972	2-10
2.9	Annual Fuel Consumption Calculated in CIAP for the 1990 Expected Fleet (10^9 kg/yr)	2-11
2.10	Subsonic Fuel Consumption by Subsonics with Several Assumptions as to SSTs; CIAP Upper-Bound 1990 Traffic Model (10^9 kg/yr)	2-12
2.11	Fuel Consumption by Altitude Band; Present SSTs Only; CIAP Upper-Bound 1990 Traffic (10^9 kg/yr)	2-12
2.12	Distribution of Fuel Usage by Altitude and Latitude Bands; Present SSTs Only; CIAP Upper-Bound Traffic	2-13

2.13	Engine Emission Indices Assigned in CIAP to the Current Fleet	2-14
2.14	Current Technology Aircraft NO _x Emission Indices at Cruise as NO ₂ (Recommended Values)	2-14
2.15	Tentative Emission Indices. Kuznetsov NK-144 Engines	2-15
2.16	YJ93-GE-3 Engine Emission Measurement by Probe and Spectrometer Techniques	2-15
2.17	NASA Ad Hoc Committee 1973 Consensus Estimates of Cruise Emission Indices with Current and Projected Technology, JP Fuel	2-16
2.18	Projected NO _x Emission Indices as NO ₂	2-17
2.19	Aircraft Types and Engine Characteristics Assumed in FAA Predictions	2-19
2.20	Total Fuel Flow Rate vs Altitude Used in FAA Projections (kilograms per hour)	2-20
2.21	Emission Indices of Nitrogen Oxides (NO _x) Used in FAA Projections	2-21
2.22	Time Fraction-Cruise Altitudes for 747SP	2-23
2.23	Flight Hour Activity by Altitude Strata	2-23
2.24	Total Average Flight Hours/Day, Fuel Consumption and Emissions/Year, Above 6 km, 1975-1990, No Technology Improvements on Emissions. As Reported	2-24
2.25	Fuel Consumption Comparisons, CIAP and FAA (10 ⁹ kg/yr)	2-25
2.26	Fuel Consumption and NO _x Emissions, 1990 High Fleet. As Reported	2-26
2.27	1990 Worldwide Aircraft NO _x Emissions, High Forecast, kg/yr. Total and Three Aircraft Types. As Reported	2-27
2.28	1990 Worldwide Aircraft NO _x Emissions, High Forecast, kg/yr. Total and Three Aircraft Types. As Reported	2-28
2.29	Growth in Advanced Subsonics, 747SP Class and 7X7 Class, Flight Hours Per Day	2-29
2.30	Altitude Distribution of Flight Hours for 747SP and 7X7 Classes	2-29
2.31	Fuel Consumption Estimates for Advanced Subsonics in High Altitude Bands, 10 ⁹ kg/yr, 1990 High Fleet	2-29
2.32	Comparison for SST Emission Distribution Estimates (15-km to 18-km Band)	2-32
2.33	1990 Worldwide Aircraft NO _x Emissions, High Estimate, Adjusted 1.2; kg/yr	2-33
2.34	World Air Carrier Fleet Turbojet Composition (1990 Base Forecast)	2-34
3.1	Simplified Ozone Chemistry	3-7
3.2	The Instantaneous Ozone Balance (10 ²⁹) Molecules/Sec	3-8
3.3	Ratio of Diffuse to Direct UV Penetration	3-13

3.4	Erythemally Weighted Flux, $\mu\text{W}/\text{cm}^2$	3-13
3.5	Ozone Depletions (Hemispheric, Percent) with Injection of 10^8 kg/yr NO_x (as NO_2) at about 40°N , Hunten Model	3-30
3.6	Data and Correlations for Ozone Depletions (Global Average Percent) with Derived Coefficients, Chang Model (CIAP ROF, 1974)	3-32
3.7	Corridor Ozone Depletions, Percent, with Injection of 1×10^8 kg/yr NO_x (as NO_2) into Hemisphere, Chang Model (CIAP ROF, 1974)	3-32
3.8	Corridor Ozone Depletions, Percent, with Injection of 1×10^8 kg/yr NO_x (as NO_2) into Hemisphere; Hunten, Chang, and CIAP Models (CIAP ROF, 1974)	3-32
3.9	Ozone Depletions, Percent, with Injection of 1.8×10^9 kg/yr NO_x (as NO_2), MIT Model	3-35
3.10	Seasonal Hemispheric Average Ozone Depletions, Percent, with Injection of 1.8×10^9 kg/yr NO_x (as NO_2), MIT Model	3-35
3.11	Ozone Changes During Fleet Buildup and Phaseout	3-44
3.12	1-D Source Additivity Test	3-46
3.13	Residence Times for Added Odd Nitrogen	3-47
3.14	Ozone Depletions With and Without N Atom Reactions (Global; 17 km, 2.46×10^9 kg/yr NO_2)	3-48
3.15	Ozone Column Change (%) Near Ground ($L = 1$) After Six Years of Fleet Operating at Level L_1 (NO_x) _T = Total NO_x Annual Emissions, kg NO_2 /year. NCAR 2-D Runs, Crutzen Model.	3-53
3.16	Reactions, Reaction Designators and Rate Parameters for the Various Models Used in Uncertainty Analysis	3-56
3.17	Percentage Ozone Depletions (Global Average) with Variations in Thermal Rate Constraints, Chang/1974 K_z ; 2.46×10^9 kg/yr NO_x Injection	3-57
3.18	Ozone Depletions (Global Average) for Various K_z Profiles and Chemical Reaction Rate Sets; NO_x Injection: 2.46×10^9 kg/yr at 17 km	3-59
3.19	LLL 1976 Chemistry: O_x , NO_x , and HO_x	3-62
3.20	Ozone Modeling Results, Showing Effects of K_z Profile and ClX Content	3-65
3.21	Superposition Test in a Chlorine-Containing Atmosphere (1 ppb ClX). Equal NO_x Rates at Each Altitude. Ozone Change, Percent.	3-69
3.22	Chemical Reactions and Rate Coefficients	3-75
3.23	Ozone Columns and Changes, 45° on August 30, Crutzen 2-D Model Results	3-82
3.24	Ozone Replacement Times (Concentration/Production Rate) at 10 km, 45°N , Spring	3-85
3.25	Comparison of Injection Coefficients and Residence Times Derived from Zr-95 Data with those Calculated using Various K_z Profiles	3-93
3.26	Changes in Computed Ozone Depletion Results for SSTs	3-101

4.1	Sensitivity of Surface Temperature Increase ($^{\circ}\text{C}$) to Stratospheric Increase of Water Vapor (ppm)	4-7
4.2	Ratio of NO_2 Changes to NO_y ($\text{NO} + \text{NO}_2 + \text{HNO}_3$) Changes and Ozone Changes for Various Cases	4-11
4.3	Fuel Consumption Figures by Altitude Band, FAA "1990-High" Case, as Reported	4-25
4.4	Stratospheric Changes	4-26
4.5	Temperature Coefficients	4-27
4.6	Surface Temperature Changes Northern Hemisphere	4-28
A-1	Ozone Change Model Results After Six Years of Integration for Various Injection Altitudes; Latitudinally Distributed	A-4
A-2	Reaction Scheme and Coefficients	A-6
A-3	Change (%) of Ozone Column Above Ground ($L=1$) After 6 Years of Fleet Operations at Level L_1 ; $(\text{NO}_x)_T$ = Total NO_x Annual Emissions, kg NO_2/yr	A-36
A-4	Normalized Change (%) of Ozone Column Above Ground ($L=1$) After 6 Years of Fleet Operations at Level L_1 ; $(\text{NO}_x)_T$ = Total NO_x Annual Emissions, kg NO_2/yr	A-37
A-5	Change (%) of Ozone Column Above Level 10 After 6 Years of Fleet Operations at Level L_1 ; $(\text{NO}_x)_T$ = Total NO_x Annual Emissions, 10^9 kg NO_2/yr	A-38
A-6	Ozone Change on Zonal Band Between 25°N and 45°N , Percent (Sixth Year of Fleet Operations)	A-41
A-7	Northern Hemisphere Ozone Change, Percent (Sixth Year of Fleet Operations)	A-41
A-8	Southern Hemisphere Ozone Change, Percent (Sixth Year of Fleet Operations)	A-42
A-9	Global Ozone Change, Percent (Sixth Year of Fleet Operations)	A-42
A-10	Ratio of Ozone Change Averages	A-43
A-11	Change (Percent) of Ozone Column Above Ground ($L=1$) During Summer (August 30) as a Function of Time	A-47
A-12	NO_x Increase (Percent) on August 30 (Summer) as a Function of Time and Altitude	A-48
A-13	NO_x Increase (Percent) on August 30 (Summer) as a Function of Time and Altitude	A-49
A-14	NO_x Increase (Percent) at Level 17 (25.2 km) on August 30 (Summer) as a Function of Time	A-50
A-15	Natural Ozone Column (m-atm-cm) Above Ground ($L=1$) During Summer (August 30) as a Function of Time	A-52
A-16	Change (Percent) of Natural Ozone Column Above Ground ($L=1$) During Summer (August 30) as a Function of Time	A-53

B-1	Comparison of Effective Bimolecular Rate Constants $\text{OH} + \text{NO}_2 + \text{M} \rightarrow \text{HNO}_3 + \text{M}$	B-13
B-2	The Chemical Kinetic Mechanism Used in Model A	B-19
B-3	Rate Coefficients for Model B (with Activation Energy in cal/mole)	B-20
B-4	The Eddy Diffusion Coefficient (Chang Values)	B-21
B-5	The Eddy Diffusion Coefficients (Hunten Values)	B-21
B-6	Pollutant Input Rates Used in Model A (Molecules/cm ³ -sec)	B-22
B-7	Ozone Reductions Predicted by COMESA Model B	B-25
B-8	Aircraft Emissions in the 2-D Model	B-28
B-9	Ratio of Northern Hemisphere and 30° N-60° N Corridor Ozone Reductions to the Global Reductions	B-30
B-10	COMESA/CIAP Comparison	B-30
B-11	Ozone Reductions for Combined Fleets, COMESA Models	B-31
C-1	Stratospheric Inventory of Zirconium-95 Resulting from Chinese Tests	C-9
C-2	Effective K-values (in 10 ⁴ cm ² /sec = m ² /sec) from to .6 Values for the Various Chinese Tests, Computed With and Without Sedimentation. Tropopause Height Taken as 11 km	C-19
C-3	Effective K-values (in 10 ⁴ cm ² /sec = m ² /sec) from to .6 Values for the Various Chinese Tests, Computed With and Without Sedimentation. Tropopause Height Taken as 14 km	C-21
C-4	Comparison of Results from Different Models for 18-km Injection	C-26
D-1	Atmospheric Properties and Particulate Settling Velocities Used	D-17
D-2	McElroy K _z Profile	D-18
D-3a	Chan's K _z Profile (1974)	D-19
D-3b	Chang K _z Profile (1976)	D-19
D-4	Hunten/1974 K _z Profile	D-20
D-5	Crutzen/1974 K _z Profile	D-20
D-6	Wofsy 1975/K _z Profile	D-21
D-7	Crutzen-Isaksen 1975/K _z Profile	D-21
D-8	Computer Model	D-25
D-9	Variables	D-28
E-1	Fuel Flows at Altitude (10 ⁹ kg/yr) leading to 0.5 Percent Ozone Depletion, at Emission Index NO _x = 18 gm/kg as NO ₂	E-6
E-2	Fuel Flow Rates for Which Water Vapor Emissions Lead to 1.0 K Warming, Ignoring Other Effects, 10 ⁹ kg/yr, for Several Models	E-9

E-3 NO_x Emission Indices Leading to 0.5
Percent Ozone Depletion as a Function
of Yearly Fuel Flow
F-1 Input Data for Figure F-1
F-2 Steady-State Climatic Effects (1-D Models)

E-11
F-6
F-8

SUMMARY

S.1 SCOPE

In this paper, the potential effects that aircraft engine exhaust products, emitted at cruise altitude, may have on the earth's protective ozone shield and on the earth's mean surface temperature (here, loosely, "climate") are critically reviewed, using information available as of December 1976. The nominal time frame involved is from the present to 1990. The treatment is limited to direct effects, emphasizing potential changes in the ozone column (i.e., stratospheric plus tropospheric ozone); climatic effects are discussed, but given less emphasis. Derivative effects, such as changes in skin cancer incidence resulting from changes in the ozone column, or possible changes in biospheric productivity due to climatic changes, are not reviewed in this paper.

Data sources for this review have included the "Report of Findings" of the U.S. Department of Transportation Climatic Impact Assessment Program (CIAP, December 1974); the report of the National Academy of Sciences-National Research Council Climatic Impact Committee, titled "Environmental Impact of Stratospheric Flight," (NAS, 1975); and the United Kingdom Meteorological Office's "Report of the Committee on Meteorological Effects of Stratospheric Aircraft," (COMESA, 1975). Important newer material obtained under the High-Altitude Pollution Program (HAPP) of the Federal Aviation Administration, the successor program to CIAP, is also included. This latter material includes new fleet emissions forecasts, "Stratospheric Emissions Due to Current and Projected Aircraft Operations," (A. D. Little, August 1976), and new ozone modeling results from the Lawrence Livermore Laboratory (LLL), the National Center for Atmospheric Research (NCAR), and the Aerospace Corporation. Other results from the recent literature and from our own analyses are also included. Modeling results and applications to fleets, rather than the details of the models themselves, are emphasized.

S.2 PURPOSE

The purpose of this effort has been to gather and compare various modeling results, to note their bases and limitations, and to suggest areas which appear to be in need of further study or measurements. In a broader sense, the purpose of this effort and on-going studies under HAPP and elsewhere, is to be able to anticipate and, if required, to take appropriate action to prevent significant deleterious effects due to aircraft effluents.

S.3 BACKGROUND

The three major studies (CIAI, 1974; NAS, 1975; COMESA, 1975) cited above were carried out between 1971 (or 1972) and 1975. The focus of these efforts was on the effects on stratospheric ozone of nitrogen oxides (NO and NO_2 or NO_x) deposited in the stratosphere by high-altitude aircraft. At the outset of these studies, it had been proposed that NO_x would catalytically destroy stratospheric ozone, with possible deleterious biospheric effects. Water vapor emissions had been of concern earlier, but their effects on ozone had largely been dismissed by the time CIAP began. On completion, these several studies agreed with regard to the existence of the aircraft NO_x effect on ozone, but disagreed--by about a factor of six--as to its magnitude for aircraft (such as the Concorde SST) at 17 km, with NAS giving the largest and COMESA the smallest estimates. The NAS and CIAP studies both concluded that subsonic as well as supersonic aircraft would reduce the ozone column. Indeed, projections in CIAP of NO_x emissions by subsonics, and particularly by advanced subsonics (which may cruise to 14 km), implied, by the NAS and CIAP ozone depletion models, a significant and relatively near-term threat to the ozone column. The uncertainties in the SST case, and questions about the subsonic case, called for further study.

The climatic effects of SSTs were given less emphasis in these studies, but were recognized as potentially significant. The principal exhaust species studied for effects was SO_2 , which, when oxidized, forms particles of sulfuric acid which were argued to have a cooling effect on the earth's surface. The SO_2 comes from sulfur in the fuel which is present typically at 0.05 weight percent. Water vapor, which has an opposite temperature effect, was given less attention. Changes in NO_2 and in ozone were also noted to have possible climatic significance. Both NAS and CIAP studies, on the basis of calculated sulfur effects alone, recommended fuel desulfurization in the future. A review of climatic effects also seemed called for in this effort, although the climate problem appeared to be less urgent, in a time sense, than the ozone problem.

Subsequent to the CIAP (1974), NAS (1975), and COMESA (1975) efforts, the halocarbon problem attracted major study attention. The halocarbon studies (see NAS; 1976, 1976a) led to revisions in key reaction rates in the stratosphere, and introduced new chemistry, which had an impact on the aircraft NO_x -ozone problem. The sensitivity of calculated ozone reductions by NO_x to these rate changes and to uncertainties in these rates became evident, and have since been studied, with results described in the following material. In addition, a class of reactions associated with methane oxidation in the presence of NO_x which produce ozone and are important in the troposphere, were not included in CIAP and NAS modeling; inclusion of these reactions seemed called for in an evaluation of the effects of subsonic aircraft. As will be seen, inclusion of these various changes leads to substantial (if preliminary) changes in prior conclusions: current results

indicate that effects of NO_x injections on the ozone column change sign with altitude of injection, with enhancement below and depletions above about 14 km. The altitude distribution of emissions becomes of considerable importance, calling for careful evaluation in computing effects for both subsonic and supersonic aircraft.

Interactions between NO_x and chlorine chemistry, and other factors which change with time, add new uncertainties to projections of aircraft effects with time; future aircraft effects are dependent not only on fleet emissions, but also on worldwide decisions yet to be made about the release of halocarbons into the atmosphere and on the content of nitrous oxide, which may be affected by fertilizer usage, but is increasing with time. (The nitrous oxide question is not pursued herein.) Other more important uncertainties exist, however, with regard to chemical kinetics and atmospheric dynamics, and these are the matters of more immediate concern here.

As further background, it is clear that non-zero perturbations to the environment inevitably result from man's presence and from all of man's activities, and society must, in all cases, balance perceived benefits and penalties. "Acceptable" limits for ozone change or for climate change have yet to be established. As purely arbitrary working guidelines, however, the Federal Aviation Administration has set as goals to guide aircraft emissions the avoidance of calculated ozone depletions of greater than 0.5 percent and the avoidance of calculated changes in mean surface temperature of more than 0.1 K, both effects being computed for the Northern Hemisphere where traffic, and thus effects, are concentrated. Fleet projections are needed in computing future effects.

The current findings of this effort, first in brief and then in more detail, follow, with comparison to previous studies. Some suggestions for further work are then provided.

S.4 CURRENT FINDINGS

S.4.1 In Brief

Current results are as follows:

A. Uncertainties

In general, uncertainties are larger than indicated previously and include, in some cases, questions of sign as well as magnitude. These uncertainties must be reduced in order to improve confidence in forecast of future fleet effects relative to HAPP or possible other guidelines. Continuing revisions in estimates of effects are to be expected as work progresses.

B. Growth Rates, Fuel Consumption, and NO_x Emissions

Expected fleet growth rates, future fuel consumption by SSTs, and particularly fuel consumption by advanced subsonics at peak cruise altitudes (approximately 14 km), are lower than indicated in CIAP. A NO_x measurement technique uncertainty exists, however, which suggests current NO_x emission indices may be several-fold low; potential NO_x contamination rates thus need further examination. A mach-2.7 SST is not expected by 1990. Emission reduction schedules envisaged in CIAP may be difficult to achieve.

C. Aircraft Effects on the Ozone Column

Ozone chemistry is more complex and uncertainties regarding effects of NO_x injections are larger than previously recognized. Current chemistry, however, leads to smaller than previous estimates of reductions in the ozone column from NO_x additions at SST cruise altitudes (16-km to 19-km for present SSTs), and to enhancement or near-zero effects, rather than reductions, in the ozone column, from NO_x addition at altitudes typical of subsonics (6-km to 14-km). Reduction in ozone from NO_x additions by SSTs increases with increasing cruise altitude; higher-altitude, higher-mach-number SSTs would have greater effects than do current SSTs per unit of NO_x emitted. Computations using a 2-D model for a projected 1990 "high" (i.e., rapid growth) fleet of subsonics and supersonics (142 Concorde/Tupolevs), with current emission indices, showed a net average ozone enhancement in the Northern Hemisphere of 0.4 to 0.9 percent, varying with season.

D. Climatic Effects

Climate-modeling efforts have been inadequate; more emphasis on the overall effects of aircraft exhaust, rather than of individual species, seems to be needed. However, use of existing models suggest small effects from the SST portion of the FAA "high" fleet (0 to 0.02 K), with water vapor apparently having the dominant effect. It is argued that climatic effects of subsonics cannot be estimated using available models, at least partly because effects of contrails, which may be significant for subsonics, are not included in the models. Should an advanced SST with low NO_x engines be proposed, cruising at, say, 20 km, climatic effects would definitely need careful study.

S.4.2 In More Detail

A. Uncertainties

Significant uncertainties exist throughout the effects-computation process. Some of these are described further below. Fleet forecasts, the growth of SST traffic with time, the altitude (and latitudinal) distribution of emissions, and emission indices all involve substantial questions. Ozone chemistry, and reaction rates at stratospheric temperatures, are inadequately established for the problem at hand: wide variations in estimates of effects

of NO_x on the ozone column are possible within specified reaction rate uncertainties. Atmospheric dynamics, in particular stratospheric-tropospheric exchange processes, also involve wide variations in estimates, depending on whether a gaseous tracer (excess carbon-14), or particulate tracer (zirconium-95, strontium-90, etc.) is used. Future stratospheric chlorine contents affect future fleet effects, and depend on worldwide policy decisions not yet made. Possible feedback effects may affect water vapor in the stratosphere and may amplify or reduce both ozone and climatic effects; these have not been investigated. Numerous other uncertainties, some very fundamental in nature, also enter into the climate-change question.

Present overall uncertainties would seem to be unacceptably large in terms of the forecasting of future fleet effects. These uncertainties can, in general, be reduced by further measurement efforts in the laboratory and in the field, by further analysis of atmospheric motions, by further development and testing of atmospheric models, and by further refinement of fleet emission estimates.

B. Fleet and Emissions Forecast

Much of the emphasis in CIAP was on future fleets which included a large number of mach-2.7 aircraft by 1990; these scenarios are no longer considered realistic. Projections were also made in CIAP of possible future fleets which included only present SSTs and present and advanced (747SP type) subsonic aircraft. The CIAP and more recent FAA-sponsored projections [by Stanford Research Institute (SRI) and Arthur D. Little (ADL)] differ in several ways which impact on the magnitude of potential effects as a function of time.

Fuel consumption comparisons, which provide a rough measure of traffic growth, are shown in Table S.1. Note the substantial differences between the SRI/ADL and CIAP figures for fuel consumption by both subsonics and SSTs, the SRI/ADL figures being larger for subsonics and smaller for SSTs. The projected fuel consumptions in the 1990 "base" (or moderate growth) case would, according to the FAA, correspond to a fleet of about 88 Concorde/Tupolev SSTs,* 4025 widebody subsonics, and 1880 standard-body subsonics. Prorating, the number of such SSTs in the 1990 "high" (or rapid-growth) case is 142, or in the CIAP upperbound (present SST only) case, about 267. The figure quoted in CIAP for the CIAP upper bound case, allowing fewer hours per day per aircraft, was 378 Concorde/Tupolevs.

The altitude distribution of fuel consumption and pollutants emitted also differs between FAA and CIAP projections. An important point with regard to advanced subsonics follows from the data in Table S.2.

*The contractor's report (SRI, 1976) indicated a belief that even this level of SST usage in 1990 is highly optimistic.

TABLE S.1. PROJECTED FUEL CONSUMPTION COMPARISONS, 10^9 kg/yr

	CIAP ^a				SRI/ADL ^b			
	Expected		Upper Bound		Base		High	
	Subsonic	SST	Subsonic	SST ^c	Subsonic	SST	Subsonic	SST
1970	14.2	0	14.2	0	-	-	-	-
1975	-	-	-	-	45.5	0	45.5	0
1980	35.7	1.34 ^c	50.2	1.6	61.4	0.86	69.2	0.99
1985	-	-	-	-	81.0	2.54	107.2	3.39
1990	59.0	-	117.8	12.6	104.9	4.88	165.8	7.89

^aFrom 9 km up.

^bFrom 6 km up. Approximately 15 percent of the total subsonic fuel is used in the 6-km to 9-km band.

^cConcorde/Tupolev assumed for this case.

TABLE S.2. PROJECTED FUEL CONSUMPTION COMPARISONS ABOVE 12-km BY SUBSONIC AIRCRAFT, 10^9 kg/yr

Altitude Band, km	CIAP		FAA	
	1990 Expected	1990 Upper Bound	1990 "Base"	1990 "High"
12-13	Not resolved by 1-km increments		3.94	6.17
13-14			0.42	0.65
14-15			0	0
12-15	15.3	28.5	4.36	6.82

In CIAP studies, all subsonics flying beyond 3000 km were assumed to enter the 12-km to 15-km band, and all such emissions were then assumed to take place at the midpoint of the band, at 13.5 km. Neither assumption is correct, so that NO_x emissions of subsonics in the 12-km to 15-km band were overstated in CIAP terms of both magnitude and altitude. Similarly, advanced subsonics, such as the 747SP, were assumed to cruise at all times at 13.5 km (44,300 ft). These aircraft are capable of a maximum flight altitude of 13.7 km (45,000 ft) when near the end of cruise, but the emissions-weighted mean operating altitude is considerably lower, with a major portion of the emissions below 12 km. This point is important, in that NO_x effects on the ozone column vary significantly with altitude.

Fuel consumption figures, when multiplied by emission index data, provide the emissions data needed to compute aircraft effects. Currently accepted NO_x emission indices are based on techniques which involve probe sampling of the exhaust stream to obtain NO and NO_2 (much smaller) contents with known fuel-to-air ratios. An alternative *in-situ* measurement technique using ultraviolet spectrometry suggests the probe data may be in error. Data in Table S-3 are illustrative. Later data have not resolved the issue.

TABLE S.3. NO CONCENTRATION MEASUREMENTS BY
PROBE AND SPECTROMETER TECHNIQUES

<u>Simulated Mach No.</u>	<u>Altitude, ft</u>	<u>Power Setting</u>	<u>NO Concentration by Probe, ppm</u>	<u>NO Concentration by Ultraviolet Spectrometry, ppm</u>
2.0	55,000	Military	70	165
2.6	65,000	Military	100	323
2.6	65,000	Maximum afterburner	130	617

Source: Davidson and Domal, 1973

Calculations in this and prior reports are all based on the accepted procedures, which utilize probe-sampling techniques.

Emission-reduction schedules are outlined in CIAP, suggesting a six-fold reduction in the NO_x emission index for the fleet over the period 1985-1990, and larger reductions thereafter. This schedule may well be optimistic, considering the delays encountered in meeting more modest reductions in low-altitude emissions and the early status of the lean premix concepts involved. In fact, as older engines are replaced with more efficient modern engines, with higher operating temperatures, the average cruise emission index for the subsonic aircraft fleet may well increase over the figures used in CIAP.

An altitude-latitude distribution of NO_x emissions for a "1990-high" fleet, with today's NO_x emission indices for the aircraft specified, is given later in this summary.

C. Aircraft Effects on the Ozone Column

1. Uncertainties in Effects of SSTs due to Uncertainties in Chemical Kinetics and Dynamics Uncertainty studies have been done with one-dimensional (1-D) models, in which vertical motions in the atmosphere (dynamics) are parameterized by the so-called " K_z profile," a number of which are available and have been used. Two such profiles, one representing relatively rapid lower stratospheric-tropospheric exchange processes (Chang/1974) and one relatively slow (Hunten/1974), have received most use. Table S.4 shows the range of extreme ozone change values which can be calculated within quoted ranges of rate constants and with the two estimates for dynamics.

TABLE S.4. THE RANGE OF ESTIMATES OF GLOBAL AVERAGE PERCENTAGE OZONE CHANGE DUE TO UNCERTAINTIES IN KINETICS AND DYNAMICS; NO_x INJECTION RATE AT 17 km, 2.46×10^9 kg/yr AS NO_2

Kinetics	1-D Dynamics, K_z	
	Chang/1974	Hunten/1974
Maximized effects of NO_x	-8.06	-16.95
Minimized effects of NO_x	+2.22	+1.00

Source: Lawrence Livermore Laboratory, 1976.

The injection rate corresponds to an extremely large (approximately 4000), globally dispersed fleet of Concorde. Both large negative and small positive values of ozone change can be computed, although these extreme (maximized or minimized) computed effects have negligibly small (but difficult to quantify) associated probabilities. Uncertainties in parameterized dynamics also have a strong effect, as indicated in Table S.4; in some cases (not shown in Table S.4), the sign of the effect on the ozone column has been found to change with K_z choice. A further ambiguity arises in interpretation of 1-D results: some modelers consider such results to be mid-latitude effects and some consider them to be global average effects. A 2-km flight altitude adjustment recommended in NAS (1975), for mid-latitude traffic for the Hunten model, is not included in Table S.4 (see Table S.5 below). The model atmosphere used in the Table S.4 results included no chlorine chemistry.

Water effects from aircraft exhaust were also studied briefly in these uncertainty studies. It was found that when NO_x effects are maximized, water vapor, which is also present in the exhaust, increases ozone; where NO_x effects are minimized, the water emissions reduce ozone. These effects vary with K_z , and could be significant with large, low NO_x , possibly hydrogen-fueled, SST fleets.

2. Effects of Recent Revisions in Reaction Rates and Chemistry on SST Effects While uncertainties in ozone changes due to uncertainties in reaction kinetics must be recognized, the estimated effects using current values for reaction kinetics are of more interest. In this connection, it is found that, in general, as later more complex chemistry has been included, calculated effects of NO_x injections by SSTs seem to have decreased; this effect may, of course, not persist as new rate data are obtained or available rate data re-examined. Representative data are given in Table S.5.

TABLE S.5. REPRESENTATIVE CHANGES IN COMPUTED OZONE
COLUMN REDUCTIONS DUE TO SSTs (PERCENT) *

	Global average values ¹ , NO _x input = 2.46 x 10 ⁹ kg/yr				Hemisphere values ¹ , NO _x = 1.23 x 10 ⁹ kg/yr	
	Chang/1974 K _z		Chang/1976 K _z		Hunten/1974 K _z	
	17	20	17	20	17(15) ¹	20(18) ¹
Injection altitude, km						
CIAP Report of Findings, 1974	-5.1	-10.6	-	-	-16 ³	-23 ³
NAS, 1975	-	-	-	-	-8.97	-17.4
Revised OH + HO ₂ ; inclusion of CH ₄ oxidation ²	-1.75	-5.21	-	-	-6.68	-
LLL chemistry, 1976, no ClX	-0.065	-2.92	-1.15	-4.20	-4.06	-10.64
LLL chemistry, ^{4,5} 1976, 1 ppb ClX			-0.70	-3.26	-2.79	-8.76
LLL chemistry, ⁵ 1976, 2 ppb ClX	-	-	-0.40	-2.61	-2.33	-8.06

*Most of these results are from Lawrence Livermore Laboratory.

1. These calculations were made at Lawrence Livermore Laboratory with a global injection rate of 2.46 x 10⁹ kg/yr NO₂ at 17-km or 20-km model altitude. The results may, according to NAS, 1975, be interpreted as a hemispheric value for the Hunten model for half this injection rate for a mid-latitude fleet 2-km lower (as shown in parentheses) than the model injection altitude.
2. A simplified methane oxidation pathway is included.
3. The LLL computational model with CIAP chemistry gives higher depletions with the Hunten K_z profile than does the NAS formula. See Fig. A.38, p. 145, NAS, 1975.
4. Includes ClONO₂ in manner which may overestimate NO_x effects on ozone.
5. 1-ppb ClX may be a reasonable current value; 2 ppb might be 1990 value.

In Table S.5, the first two rows correspond to results based on chemistry used in the 1973-1974 period. During the halocarbon studies, a ten-fold reduction in the rate of the reaction OH + HO₂ → H₂O + O₂ was recommended. This reduction reduced computed effects at 17 km with the Chang/1974 K_z profile by about 60 percent. The third row entries show the combination of this revision plus the incorporation of a simplified methane oxidation pathway and certain other more detailed changes. A reexamination of the kinetics of certain critical reactions then led to use of a number of revised rates forming "LLL 1976 chemistry" with still lesser effects resulting. A shift to the Chang/1976 K_z profile (which was developed during studies on halocarbon effects), however, increased the effect over that computed with the Chang/1974 K_z profile.

Inclusion of 1-ppb active chlorine (a plausible current value) in the model then reduced the effects again; use of 2 ppb, as might be the case for 1990, caused further reductions. NO_x effects on the ozone column decrease as chlorine content increases; effects of water injections, however, may increase.

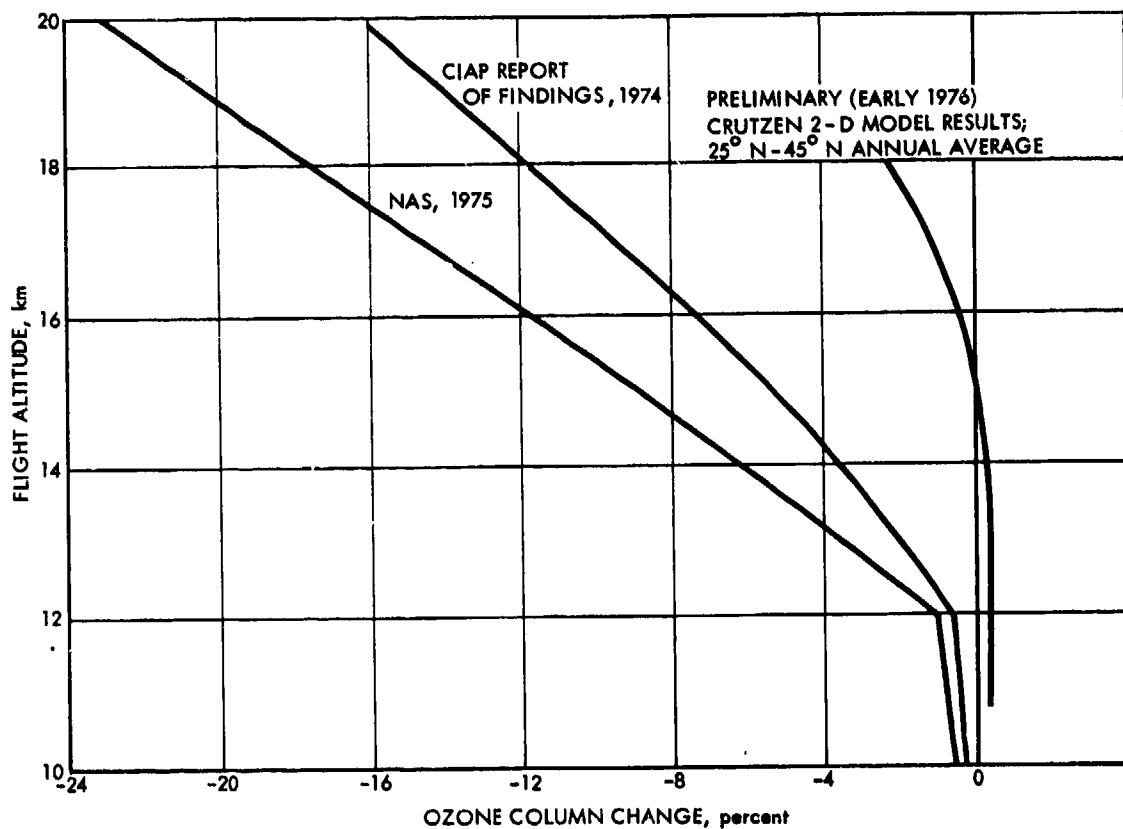
Uncertainties in dynamics to be used in 1-D models are not easily resolved, although they are clearly of major importance, as indicated by the above results. In general, the Hunten/1974 K_z profile has been supported (in the critical lower portion near the tropopause) by analysis of gaseous tracer (excess carbon-14) data, whereas the Chang profiles near the tropopause give better agreement with particulate tracer data. Uncertainties exist in both types of data. An analysis included here (Appendix C) of particulate tracer data (zirconium-95) injected by Chinese weapons tests supports previous estimates based on particulate tracers.

3. Effects of Aircraft NO_x at Different Altitudes (Subsonics vs Supersonics); Crutzen 2-D and Earlier Results Four perturbed atmosphere model runs were carried out at the National Center for Atmospheric Research (NCAR) in a joint effort between Dr. P. J. Crutzen, as part of his on-going studies there, and IDA, in early 1976. Details are reported in Appendix A. The model used was the Crutzen 2-D model. This model included the ozone-forming methane-oxidation reactions, and, being a 2-D model, permitted estimation of seasonal and latitudinal effects for latitudinally distributed sources.

The model used rather complete oxygen-hydrogen-nitrogen atmospheric chemistry, but did not include chlorine. The model used a three-fold lower rate for the $\text{OH} + \text{HO}_2$ reaction than was used in earlier CIAP and NAS efforts, but the rate used was still three-fold larger than recommended in the later halocarbon studies.

Four altitudes were studied (10.8, 12.7, 14.5, and 18.0 km) with NO_x sources distributed latitudinally according to CIAP traffic projections. The four altitudes used covered the range of present and advanced subsonics and the present mach-2 Concorde. A considerable mass of data was obtained (see Appendix A); however, the annually averaged results for the 25°N to 45°N latitude band are perhaps of greatest interest, and can be compared to the NAS and CIAP adjusted 1-D model results, as shown in Fig. S.1. Linearity of ozone effects with NO_x injection rate was assumed in converting the four available 2-D model runs to the hemispheric injection rate shown in Fig. S.1, the rate used earlier in Table S.5. Linearity of effects with NO_x injection rates has not, however, been studied in the 2-D models.

The Crutzen model results are considered to be preliminary by Dr. Crutzen in view of uncertainties in both the chemistry and dynamics and in recognition of the need for further model development. The great difference



3-11-77-1

FIGURE S.1. Ozone column change results by various models. The injection rate assumed at each altitude is 1.23×10^9 kg NO_x (as NO_2) per year into a hemisphere. The NAS and CIAP curves are based on 1-D model results, adjusted to correspond to changes to be expected in the "hemisphere" (NAS) or "corridor" (CIAP). The curve at the right represents annually averaged results for $25^\circ \text{N} - 45^\circ \text{N}$ from runs with the Crutzen 2-D model adjusted, assuming linearity, to the same total input rate, as for the other curves, but distributed by latitude according to CIAP traffic estimates. The Crutzen results are after 6 model years.

between these results and prior results should, however, be noted, as should the fact that the model shows enhancement rather than reduction (as in the other models) in the ozone column for NO_x injection below about 14 km. These results indicate that subsonics enhance but supersonics reduce ozone; furthermore, effects of SSTs are generally smaller than found in the earlier models. Where ozone enhancements occurred, the ozone increase came about due to increased ozone concentrations near flight altitude. Effects at low latitudes were smaller than at midlatitudes in the Northern Hemisphere. In some cases, enhancement was noted in the Northern Hemisphere and slight depletions in the Southern.

A full explanation of the differences between the Crutzen 2-D model and prior results cannot be offered. It should not be concluded that the reduced effects are due only to inclusions of the methane oxidation reactions and the use of a lower $\text{OH} + \text{HO}_2$ reaction rate.

4. 1990 Fleet Effects on Ozone An original goal of this effort was to estimate effects on ozone of future fleets as a function of time. The complexities in chemistry, possible changes in stratospheric chlorine content with time, an apparent need for further examination of fleet emission estimates, and limited modeling results have forced postponement of this goal. However, to gain an appreciation of possible effects, an IDA-modified "1990 high" emissions estimate was developed, based on SRI/ADL estimates, but with adjustments (upward in altitude) of SST emissions and of the total of subsonic emissions, both of which were done to achieve better correspondence with data reported elsewhere and believed to be reliable. No NO_x technology improvements were included. The various adjustments need further evaluation. The resulting total modified fleet emissions of NO_x were 2.81×10^9 kg/yr as NO_2 , with altitude and latitude distributions summarized as given in Table S.6. The actual emissions model used 1-km vertical (above 6 km) and 10-degree latitudinal resolution.

TABLE S.6. DISTRIBUTIONS OF NO_x FROM 1990 "HIGH" FLEET (MODIFIED); TOTAL NO_x : 2.81×10^9 kg/yr

Altitude Band, km	Percent of Total NO_x Emissions	Latitude Band	Percent of total NO_x Emissions
6- 9	17.91	60-90° N	2.10
9-12	75.78	30-60° N	73.80
12-14	3.46	0-30° N	18.04
14-16	0.84	0-30° S	4.74
16-18	1.67	30-60° S	1.32
18-19	0.34	60-90° S	0

This 1990 "high" fleet includes the equivalent of 142 Concorde and Tupolevs, based on FAA figures. (However, see note, p. S-5.) A larger number (201) would have been implied by the figures used in CIAP yearly for fuel flow per aircraft, wherein fewer hours per day were assumed per aircraft.

These emissions were studied in the 1-D model at Lawrence Livermore Laboratory (Fig. S.2) and in a 2-D model (Fig. S.3) at Aerospace. Neither run included chlorine effects nor the effects of added water. The Aerospace model used approximately the same "1976 chemistry" as did Lawrence Livermore Laboratory, but more complete (although still not well established) methane oxidation chemistry, slightly revised from that used by Crutzen. The dynamics used in the Aerospace 2-D model reasonably reproduce the excess carbon-14 data. Both modeling approaches showed slight enhancement in ozone columns, but magnitudes varied. For the 2-D model, ozone enhancements of 0.4 to 1.4 percent (after 5 years) were found in the Northern Hemisphere, varying with latitude and season; enhancements (not shown) were also found in the Southern Hemisphere. The 1-D model, with simplified methane oxidation chemistry (which probably underestimates ozone production) showed global average enhancements of less than 0.1 percent, with both Chang/1976 and Hunten/1974 K_z profiles. A netting out of ozone production and destruction effects is involved in both models, so that the ratio of results is sensitive to slight modeling differences.

5. Caveats on Fleet Results A number of caveats must be noted with regard to the foregoing results. The uncertainties in 1-D results already described apply; similar uncertainties, in general, apply to 2-D models. These runs did not include chlorine chemistry nor, like most modeling exercises, did they include any effects due to water injection from the exhaust. The 2-D models may not have reached steady-state, particularly in the Southern Hemisphere. Methane oxidation chemistry is not well established, and its uncertainties have not been explored. The assumed NO_x emission indices were based on probe-sampling techniques, which may be lower in general but not uniformly low for different aircraft; the SST (ozone-reducing) component of the fleet might increase relative to that of the subsonic portion. The chemical kinetics used will probably be revised as more data becomes available. Various thermal effects, and possible feedback effects, have not been explored.

A further point is that the enhancements noted include a combination of ozone enhancement at low to medium altitudes and ozone reduction at high altitude, the latter effect being of smaller absolute magnitude. The distribution of this average effect over the globe in the 1-D model or around the zones in a 2-D model is in question. The point is considered briefly in this document for the 2-D case; a tentative conclusion is drawn that zonal nonuniformity would not involve some regions with high enhancement and other regions with depletions. The point needs further study.

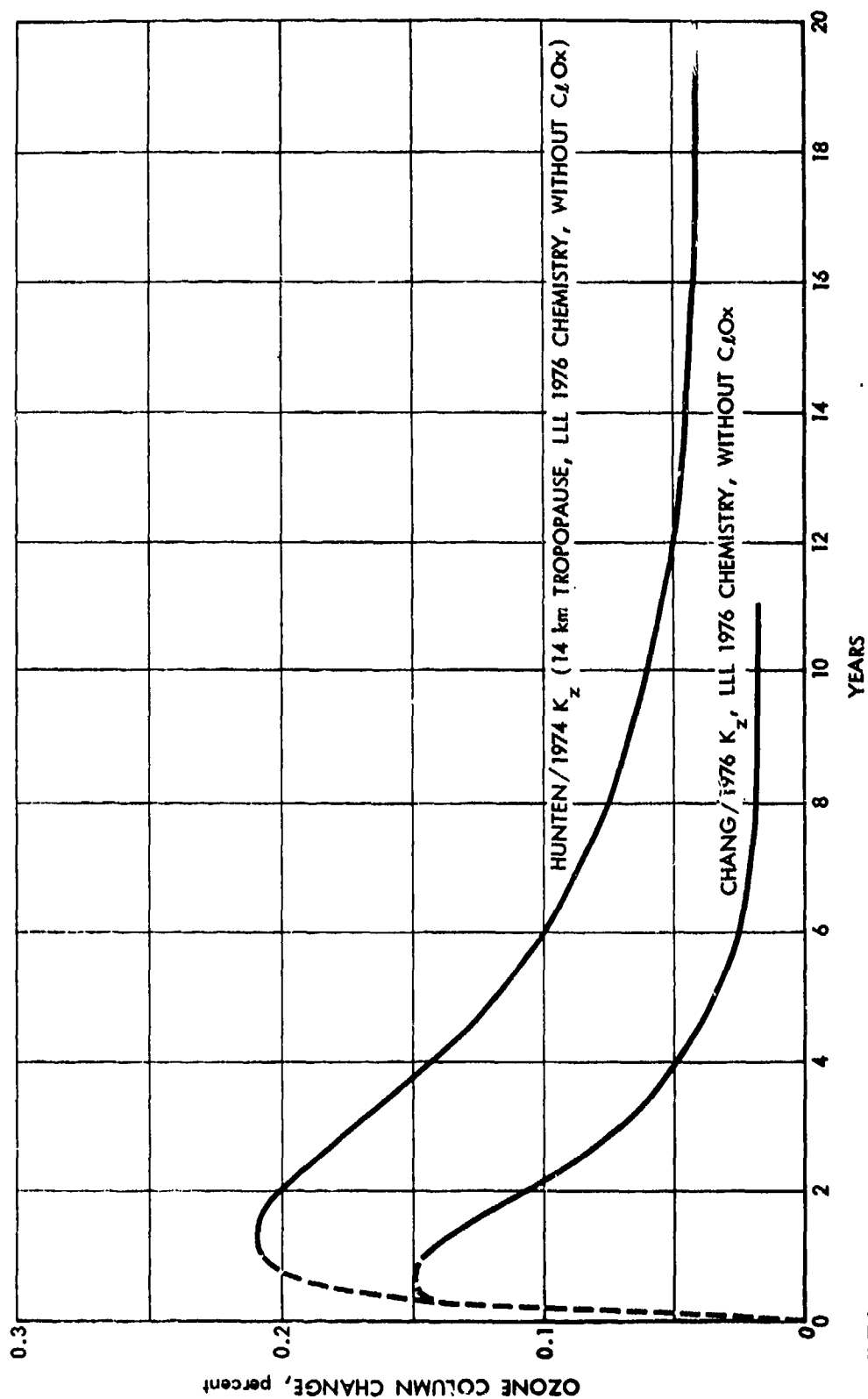
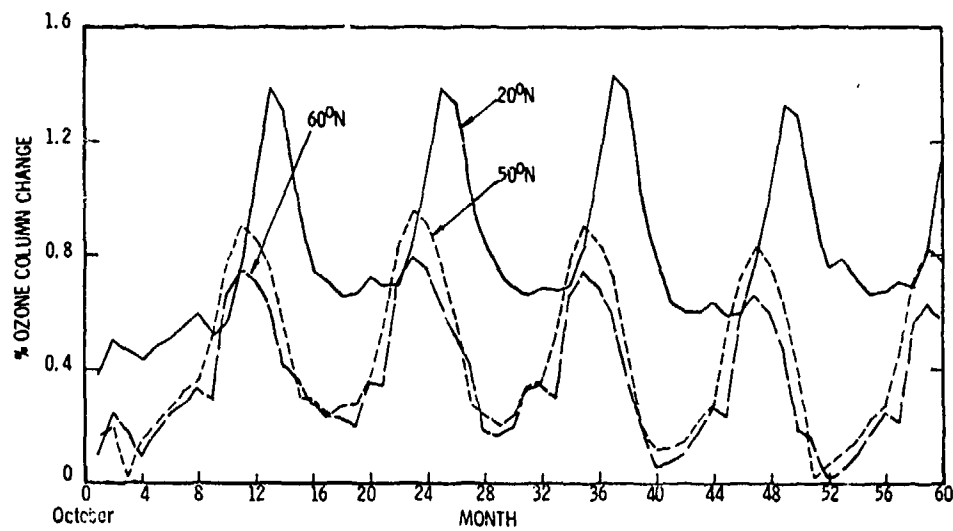


FIGURE S.2. Global Average Ozone Column Changes with Time
Following Introduction of the Modified 1990 "High"
Fleet NO_x Emissions, No Chlorine
Data Source: Lawrence Livermore Laboratory, 1976



(a)

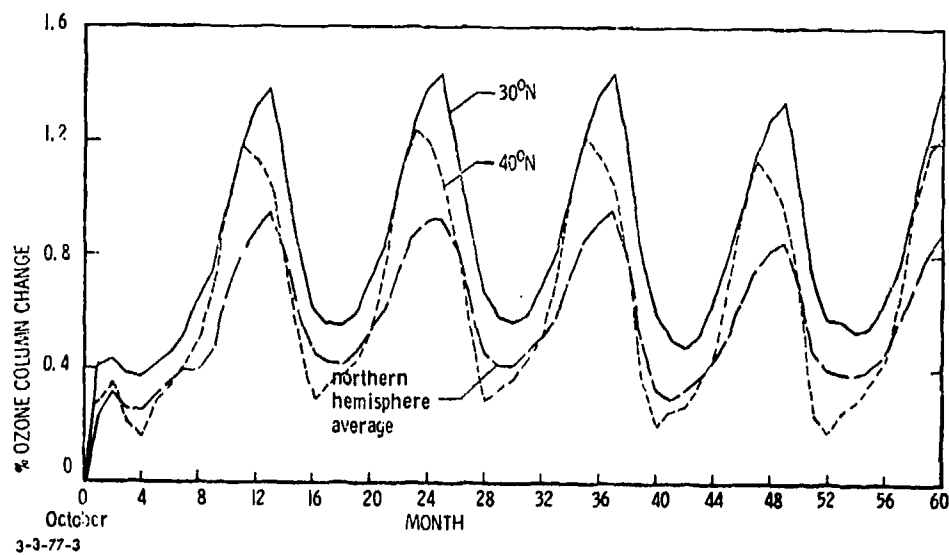


FIGURE S.3. Aerospace Model Results for Modified 1990 "High" Fleet
Source: Widhopf, 1976

D. Aircraft Effects on Climate

Potential climate changes due to aircraft exhaust species were studied in both CIAP and COMESA. The effort, however, (at least in CIAP) was considerably less intense than was the effort on the ozone problem. COMESA found the problem to be rather insignificant, finding that 1000 Concorde operating 5.5 hours per day would have a negligible impact on surface temperature [0.05 K or less (cooling)]. In the CIAP Report of Findings, the climate change question was converted to a criterion of a 10 percent change in stratospheric optical depth (emphasizing aerosol effects from the sulfur content in the fuel), which corresponds by CIAP methodology roughly to -0.07 K temperature change. The criterion of a 10-percent change in optical depth permitted a very large (2070) Concorde fleet. Both COMESA and CIAP found the aerosol effect to be larger than the water effect, roughly by a factor of 2. COMESA argued that net effects should be computed for the total of the various exhaust constituents. (The approximately 0.05 K cooling figure quoted above does not include this netting out.) COMESA, in general, indicated good agreement with CIAP, except that their estimate of ozone decrease was a factor of 2 or 3 smaller, and its climatic effect correspondingly lower than in CIAP.

The various climate modeling results are considered herein, but 1-D model results are emphasized; these results could be most easily applied to the aircraft problem. It is noted that available model results for different exhaust species involve different assumptions, and none include the potentially important effects of the altitude distribution of changes. The latter effect could not be included here; some rough approximations were made, however, to put the effects of various exhaust species on a common basis. As was done in CIAP, the burdens at steady-state were computed from 1-D K_z profiles (Chang/1974 and Hunten/1974); however, for aerosols, a correction was made for gravitational settling (sedimentation), which substantially reduced the burden of particulates relative to water vapor. This correction, along with certain other revisions in aerosol cooling and water vapor warming effects resulted in water vapor appearing to be the most important ingredient in the climatic-change sense. Further, if the long residence times implied by the Hunten/1974 K_z profile are used, a climate change criterion of 0.1 K (warming) could become of significance if a 20-km cruise altitude (mach 2.7) SST should be proposed.

Application of these adjusted models to the 1990 "high" SST fleet (142 Concorde/Tupolevs) led to a calculated hemispheric mean temperature change in the range of 0.0 to 0.016 K (warming). The models were not applied to the subsonic fleet portion, in view of the probable dominant effects of contrails, which are primarily a subsonic problem, but for which no tie to numbers of aircraft has been made. A COMESA model run suggested, however, possibly significant warming due to contrails.

The uncertainties in climate-change computations, such as described in the foregoing, can hardly be overstated. In our view, however, such estimates provide a necessary preliminary indication of the risks of climate change associated with SST operations. More sophisticated work, preferably in at least two dimensions, and recognizing altitude and latitudinal distribution effects, is to be encouraged.

S.5 SOME RECOMMENDATIONS AND SUGGESTIONS

This review has identified a number of problem areas which lead to significant uncertainties in the calculated results. Many of these problems have been recognized, and in some cases programs may well be under way directed towards their resolution. The following suggestions are made only on the basis of the problems indicated herein, and are not necessarily intended to imply that such work is not currently being done.

1. *Engine NO_x emission data uncertainties must be resolved, and forecasts of emissions estimates as a function of latitude, season, and altitude must be improved. Potential NO_x emission reduction schedules should be reexamined.*
2. *Detailed study is needed of the dynamics important in the region of principal aircraft traffic, 30° to 55° N, and at altitudes above and below the highly varying tropopause from, say, 6 km to 20 km.*

Such data, because of their seasonal and latitudinal variability, would be used most effectively in 2-D models, but a collapse of such data to 1-D would be useful in resolving uncertainties due to differing estimates of 1-D dynamics near the tropopause. "Rainout coefficients" also need better resolution for NO_x and its derivatives.

3. *Certain reactions and species critical to ozone production and destruction need additional measurement and study. Methane (and perhaps higher hydrocarbon) ozone-forming reactions, a number of reactions involving the HO_2 radical, the reactions forming and/or destroying HNO_3 , NO_3 , N_2O_5 , ClONO_2 (and perhaps other ClO_x - NO_x interacting species) are all in this category. Both laboratory and field measurements are needed; field measurements should include simultaneous measurements of the concentrations of a number of species as a function of altitude, particularly in mid-latitudes.*
4. *As stratospheric NO_x , chlorine, and water content all affect calculated ozone changes due to NO_x additions, results of new measurements or new projections (as policy decisions are made) should be incorporated into the models. The present large uncertainty in the N_2O budget raises questions about the understanding of all odd nitrogen budgets and needs resolution.*

5. More attention should be given to water vapor in general, its transport, its climatic effects (including possible feedback effects), its chemistry effects, and its use as a tracer in the stratosphere.

6. Ozone models need additional work, using 1-D, 2-D, and eventually 3-D models; present uncertainties seem to be unacceptably large:

a. 1-D models. Reduction in the uncertainties regarding the best representation of eddy diffusivity near the tropopause would be desirable; the studies outlined in (2) above may help. The implications of alternative chemistry and other variables to derived values of K_z in the mid and upper stratosphere, and resultant implications to aircraft NO_x effects would be of interest. Inclusion of water vapor injections along with NO_x (tied perhaps to excess odd nitrogen in the model by emission indices) would clarify water-effects questions. Uncertainties in results due to uncertainties in methane oxidation and related chemistry would be of interest. The effects of employing flux, rather than concentration boundary conditions, as for methane, should be investigated.

b. 2-D models. At present, models in two dimensions seem to be particularly useful in computing aircraft effects in view of nearly fixed aircraft cruise altitudes in an atmosphere in which tropopause heights and atmospheric dynamics vary with season and latitude. Such models are empirical, so that data from a variety of tracers need to be employed in model development. Chlorine chemistry should be included, as should be techniques to incorporate aircraft-added water vapor. Procedures to reduce computer requirements, perhaps by allowing the model to first distribute the pollutant without chemical reactions, should be considered. Linearity of effects with added NO_x for sources at different altitudes should be investigated, as should the effects of sources at different latitudes.

A study of past NO_x (and other contaminant) perturbations, matching computed results against ozone records, could be a valuable test of the models. Longer runs with simulated aircraft fleets should be made to insure that steady-state conditions are being reported, and transient effects should be considered for fleets changing with time.

Feedback effects may also be important and should be investigated (see item 7 below).

- c. 3-D models. These powerful models tend to be computer-limited. Such models, however, can be used without chemistry in studies of dynamics, and should be useful for improvement of 1-D and 2-D models. The use of such models in studies of the distribution with longitude of tropospherically enhanced and stratospherically depleted ozone, as deduced from 2-D models, would be of interest.
7. Improved climate modeling, designed to estimate the overall interactive climatic effects of aircraft exhaust, rather than of individual components, is needed to develop better understanding of the climate-change question. The various feedback effects (e.g., tropical tropopause temperature and water content) and latitudinal, and altitudinal distribution questions require at least a 2-D model. Since such modeling should incorporate chemistry, then the model would also be an ozone model. Aside from interactions with the ozone question, the climate question seems to be of significance primarily to the advanced SST problem. Some concern, however, exists with regard to contrail effects from present subsonics.
8. The problems associated with the monitoring of aircraft effects will require additional study, measurements, and modeling. The many sources of possible ozone change (aircraft NO_x , solar proton fluxes, N_2O from fertilizers and power plants, halocarbons, etc.) should, in principle, be separated in terms of time and place (latitude and altitude) where effects could be most easily discerned. Model exercises are necessary to guide efforts aimed at distinguishing among these presently small and complex effects.

1. AIRCRAFT EMISSION: POTENTIAL EFFECTS ON OZONE AND CLIMATE

1.1 INTRODUCTION

1.2 BACKGROUND

In 1970 and early 1971, during debates on the U.S. SST program, considerable controversy arose as to the effects stratospheric aircraft might have on stratospheric ozone, which shields the earth's surface from harmful ultraviolet light, and on climate, which, of course, affects all aspects of life on earth. The concerns related to the nature of the stratosphere, which tends to hold pollutants for long periods of time, and to the fragile nature of ozone, an unstable trace species, the concentration of which, it was argued, would be reduced by nitrogen oxides present in aircraft exhaust. As a result of these concerns (although the U.S. SST program was stopped, but recognizing the fact of SST development programs elsewhere in the world), the Climatic Impact Assessment Program (CIAP) was implemented by the U.S. Department of Transportation, and charged with pursuing the questions raised.*

The CIAP efforts, which involved expenditures of some \$25 million and inputs from hundreds of researchers of many disciplines, was organized in such a way as to provide predictions of the impacts in physical, biospheric, and economic terms under various forecast air traffic and emission control scenarios. The program was essentially completed in a technical sense in December 1974, with the summary report, the CIAP Report of Findings (Grobeck et al., 1974), being delivered to Congress in February 1975; detailed supporting documents, in particular, six large monographs, were delivered in later months in 1975.

*For readers desiring further historical background, certain papers and documents will be of particular interest. These include the SCEP (1970) report, the Crutzen (1971, 1972) and Johnston (1971) papers, the Commerce Technical Advisory Board (CTAB) (1972) report, the Australian Academy of Sciences (1972) report, the Report to the House Science and Astronautics Committee (1971), and the House (1971) and Senate (1971) Hearings in which various viewpoints were expressed. The testimonies of McDonald (1971) who first tied SST emissions to increased skin cancer incidence, and of Newell (1971) who discussed climatic and ozone effects of water vapor and of particulates and other matters of interest are noteworthy. Note that the original (pre-1971) concerns about ozone depletion due to SSTs were based on (erroneous) estimates of the effects of water vapor emissions, rather than NO_x emissions. Possible biological effects were reviewed by the National Academy of Sciences in the 1973 report (NAS-NAE, 1973).

In addition to the CIAP studies (although funded by CIAP), a concurrent and independent study was carried out by the Climatic Impact Committee of the National Academy of Sciences, their report, "Environmental Impact on Stratospheric Flight," (NAS, 1975), being distributed in April 1975. Independent studies were also carried out in Europe, by the British (COMESA, "Committee on Meteorological Effects of Stratospheric Aircraft"), and by the French (COVOS, "Comité sur les Conséquences des Vols Stratospheriques"). The COMESA report became available in May 1976. The complete COVOS report has not been received, although modeling results (Bertin et al., 1976) were received about the time this document was being finalized.

The CIAP studies were concerned not only with aircraft cruising in the stratosphere, but also with the flight of rocket-powered vehicles through the stratosphere. Partly as a result of this aspect of the CIAP investigations, the question of chlorine effects on the stratosphere arose (the space shuttle booster rockets emit HCl) and this led to studies of the fates of the halocarbons widely used in aerosol spray cans and refrigerants (see Molina and Rowland, 1974). These concerns led to a further study by the National Academy of Sciences, which has had an impact on the aircraft problem. Their results, (NAS 1976, 1976a) which became available in September 1976, were published in two related reports, "Halocarbons: Effects on Stratospheric Ozone," and "Halocarbons: Environmental Effects of Chlorofluoromethane Release." This investigation has led to revisions in the best estimates of certain reaction rates and to increased recognition of the complexities involved in the atmospheric ozone problem, as will be discussed later herein.

Both the CIAP Report of Findings* (1974) and NAS (1975) reports concluded that large-scale stratospheric flight, unless accompanied by drastic reductions in nitrogen oxide emissions, particularly by supersonic aircraft but not excluding subsonic aircraft, would lead to unacceptable reductions in stratospheric ozone. Water vapor emissions were concluded to have little effect on ozone. These reports also concluded that reductions in ozone would lead to increases at the earth's surface in the flux of ultraviolet light in the 295-320 nm erythematous (or sunburn) regime, and would thereby lead to increases in skin cancer rate, at about the rate of 2 percent increase in skin cancer for a 1 percent decrease in ozone column. The climatic effects were felt to be less predictable, but potentially significant, due to cooling effects of aerosols created from sulfur in the fuel; desulfurization was called for.

The magnitude of potential aircraft-induced effects depends on the rate and altitude (as well as on location and season) of introduction of pollutants to the stratosphere, all of which depend on the size, makeup, and route structure of future aircraft fleets (and, of course, on any emission reductions achieved). CIAP thus developed certain fleet forecasts, largely aimed at worst-case analysis;

* Or "ROF," for convenience.

these forecasts were largely developed, in their philosophical basis, prior to the steep fuel price rise following the oil embargo in late 1973. The projections included both subsonic and supersonic aircraft, but the emphasis in computational exercises and in the chemistry employed was on supersonic aircraft. Nevertheless, results were shown (CIAP, 1974; NAS, 1975) which implied possibly significant effects of subsonic aircraft alone, in the not too distant future. These projections and their suggested effects were clearly in need of further careful examination. The High Altitude Pollution Program (HAPP) was set up to pursue these matters, under the sponsorship of the Federal Aviation Administration. The work reported here has been carried out under HAPP.

In order to gain further perspective on the time frames involved in avoiding deleterious aircraft effects, recognizing current economic conditions, HAPP sponsored the development of revised fleet forecast to 1990, assuming present and projected subsonics and only current SSTs to be available. HAPP also suggested tentative guidelines as to possibly acceptable changes in the ozone column of 0.5 percent (decrease) and of 0.1 K, both in the Northern Hemisphere where fleets are concentrated. These tentative guidelines are noted frequently in the various discussions which follow.

1.3 OBJECTIVES AND LIMITATIONS

This study has several objectives. A principal objective is to review and compare results of three principal studies which have appeared on the aircraft effects question (CIAF ROF, 1974; NAS, 1975; COMESA, 1975). A second objective is to review and summarize progress made in these extremely difficult problem areas, as of December 1976, the nominal cutoff date for input to the report. A part of this second objective is to develop revised estimates of potential future aircraft effects (to 1990), using recent FAA projections as to aircraft fleets and emissions; effects of subsonic aircraft, and, in particular, the new higher flying subsonics, such as the 747SP, are of special interest. A third related objective is to consider time-dependent aspects of these effects, as fleets generally grow with time, and effects would be expected to lag fleet growth.

In a broader sense, the objective of this work, as with the CIAP and HAPP work in general, is to provide the understanding by means of which potentially significant deleterious effects of aircraft can be anticipated and thus avoided. Aircraft, however, have long life times, and new technologies tend to be proved and applied slowly. Possible adverse effects must thus be anticipated at least a decade before their occurrence, so that this, and similar work, must lean heavily on long-range, and clearly debatable, fleet forecasts.

The major focus of this review and study effort is on potential changes in the ozone column, with climatic effects being given lesser emphasis. As indicated earlier, the time frame emphasized is from the present to 1990. This study does not include possible biological or economic effects; for these subjects, the reader is referred to CIAP Report of Findings, 1974, Monographs 5 and 6 of the CIAP series (both 1975), and to NAS (1975) and NAS (1976, 1976a) reports.

Note that climatic effects, in the simple terms used here, refer only to computed mean hemispheric temperature changes based on certain mathematical models. In view, however, of current poor understanding of climate and climatic changes, such computed values should not be interpreted to be predictions, in the usual sense, of the effects of aircraft exhaust; these numbers should, instead, be viewed as semi-quantitative estimates of the climate risks involved, using temperature changes as a measure. Some quantification of these effects, in terms of best estimates using current models, is essential in view of the critical importance of climate.

Finally, before going in depth into these various matters, it must be appreciated that the atmosphere is an extremely complex system, and the science of trace species, their motions, and their effects on ozone and climate, is a developing one. While policy makers must always act on the basis of prudence and risk, the possibility always exists that new findings may drastically change previous conclusions. In general, of course, continued research leads to convergence of fact and theory. In this area, such continued research is clearly essential. In reporting on these matters, therefore, as described below, a basically chronological approach is used, the reasoning being that results have differed with time and, to date, at least in our opinion, few "final" answers have emerged.

1.4 ORGANIZATION AND GENERAL CONTENT OF THIS REPORT

The following material treats, first, CIAP and FAA projections as to aircraft fleets and their emissions, nominally to the year 1990. No attempt is made to include possible reductions in emission indices, although some comments are included. The study then turns to the major question of interest, i.e., the ozone column and changes in it which may result from these projected fleets (or parametric fleets), based on various 1-D and 2-D models. The treatment starts with model results available about at the end of CIAP (December 1974), and then discusses COMESA results and information based on post-CIAP modeling studies; 1-D and 2-D results on the FAA "1990-high" fleet are included. The uncertainties are discussed, as well as the research areas which appear to need emphasis.

The climate change question is addressed in the final section. For reasons to be discussed, it is concluded that little can be said about climatic effects of subsonic aircraft. Available 1-D model results are applied to the FAA projected SST fleet and results discussed.

Six appendices follow Section 4, which completes the main text. In the first of these (Appendix A), the detailed results of an ozone effects study are described for aircraft at different altitudes and distributed by latitude; this study used the Crutzen 2-D model, and was carried out at the National Center for Atmospheric Research (NCAR). The second appendix (Appendix B) discusses certain details of the studies by COMESA on the ozone question. In the third appendix (C), a study is reported in which the motion of zirconium-95, injected by Chinese weapons tests, is described in a 1-D parameterization. In the fourth appendix (D), available 1-D parameterizations of atmospheric motion are noted, and residence times (burden/flux for continuous injection) and injection coefficients computed. In Appendix E, possible emission index constraints on a new SST are discussed, assuming HAPP guidelines are followed; this treatment is considered primarily as indicating an approach rather than one of definitive treatment, in view of the great uncertainties involved. In Appendix F, the climatic and ozone effects of a hypothetical SST fleet building up with time are computed using a 1-D approach and a very simple model. The illustration provided is indicative of the type of time-dependent information (preferably, however, in more than one-dimension) which modelers might eventually be asked to provide. The final appendix, (F), discusses in a preliminary fashion some issues about detectability of changes in ozone and climate that arose during and to some degree subsequent to the CIAP program.

For convenience, the recommendations resulting from this work have been included in the summary.

1.5 ON USE OF THIS REPORT

As in any review, a possibility of misinterpretation of original sources exists. Furthermore, although the length of the following material might suggest otherwise, an effort has been made to incorporate as much material as possible herein by reference rather than by reproduction. For these reasons, the reader is urged to have available for ready reference at least the principal cited documents (CIAP ROF, 1974; NAS, 1975; and COMESA, 1975), and to go to other original published sources to the maximum extent feasible.

2. AIR TRAFFIC, FUEL FLOWS, AND EMISSIONS PROJECTIONS

2.1 INTRODUCTION

As indicated earlier, the environmental impacts of aircraft of concern here depend on the rates and locations--altitude, latitude, and longitude--of injection of certain exhaust species of interest. The rates of injection depend, in turn, on the air traffic demand (as well as aircraft types and load factors achieved), which sets fuel flow requirements, and on the emission characteristics of the fuels and combustors used. Altitude distribution depends on the types of aircraft, with supersonic aircraft operating higher than subsonic aircraft; geographical distribution depends on the markets served. All these factors change with time; furthermore, the environmental effects lag the aircraft operations, so that the effects at any given time depend on prior history, which means that the rate of traffic growth can also be important. (See Appendix F for an illustration.)

While these matters are, in fact, exceedingly complex, usable emission rate estimates can be developed by a combination of air traffic projections (passenger and freight), and their corresponding fuel flow requirements, and emission index data (emissions per unit of fuel burned), obtained from present engines and fuels. Emission indices of certain critical species (NO_x^* , SO_2) can be changed by technology; others (H_2O , CO_2) cannot, except by change of fuel. The time at which emission index changes may be necessary depends on computed effects as a function of time, recognizing air traffic growth projections. Projected fuel consumption rates, as a function of altitude (typically in kilograms of fuel burned per year) and emission index data are thus the fundamental working data needed. As noted above, altitude and geographical distribution of emissions depends on the types of aircraft assumed and markets served. The aggregation of emissions permitted depends on the model: for a 1-D model, global totals in each altitude band are used; for 2-D models, zonal totals** in each altitude band are used.

In quantifying these projections, one can make various optimistic or pessimistic assumptions about the rate of growth of air traffic; optimistic assumptions about growth rates obviously make any associated environmental problems more urgent in a time sense. One can also make various assumptions about SSTs, present or advanced. In these matters, the CIAP projections and the FAA projections which follow differ, based in large measure on the differing goals for

* NO_x on a molar basis is the sum of NO and NO_2 ; on a mass basis "as NO_2 " the molar sum is assumed to have the molecular weight of NO_2 .

** A zone, as used here, refers to the region between two latitudes as, e.g., between 30° and 40° N.

which the projections were made and on the differing times and economic conditions at which the projections were initiated. Thus, the CIAP projections were initiated in 1972, before the steep fuel price rise in late 1973, were long in time--in effect to 2025--and tended to be maximum-growth and mach-2.7-SST oriented. The FAA projections, initiated in 1975, were intended to recognize current economic conditions, and that a new SST would probably not be in commercial operation by 1990, the nominal end point of the FAA projections.

Actually, a number of CIAP projections were made, among which were "realistic upper-bound" and "expected traffic" projections. The upper-bound case was emphasized, and a number of fleets (subsonic and supersonic aircraft) computed to serve the associated traffic, including a fleet with an advanced SST, a fleet with only present SSTs available, and a fleet with no SSTs. The "expected traffic" case was treated only under the assumption that an advanced SST would be available, and concluded that 241 such aircraft would (or could) be in operation by 1990. These fleets are summarized in Appendix D of the CIAP Report of Findings and described in detail in Monograph 2 of the CIAP series. At present, however, and for purposes of this report, the advent of a mach 2.7 SST by 1990 is considered unrealistic. Emphasis in this report is thus on the cases where only current SSTs and subsonic aircraft are considered to be available. In general also, no assumptions are made as to when improved technology will result in fleets having reduced emission indices, i.e., the treatment is centered around projected fleets having the same emission index characteristics as do aircraft operating today.

2.2 CIAP PROJECTIONS AND RELATED DATA

2.2.1 Projected Air Traffic and Fleets

Air traffic projections for North America and the world, as prepared by English et al. (1975), are shown in Fig. 2.1; these data were also summarized in Appendix D, CIAP ROF (1974). Tabulated data are given in Tables 2.1 and 2.2.

Note (Table 2.1) that the upper-bound case involves an 8-fold growth in yearly world air passenger traffic between about 1970 and 1990 (Table 2.1a), and about a 24-fold growth in air freight (Table 2.1b). The expected case involves a 4-fold growth in passenger traffic and a 14-fold growth in freight in the same time frame. The growth in per-capita travel and cargo (Table 2.1c) is, of course, less than the total growth, because of population growth.

The upper-bound case was developed using the year 2025 as an "anchor point", assuming rapid growth in both population and per-capita affluence, with interpolation to intermediate years. Gompertz-type* growth curves were developed for

*Gompertz curves of the type $y = a \exp(-br^t)$, where $0 < r < 1$, have a characteristic slow initial rise, followed by a more rapid rise and subsequent maturation or leveling off.

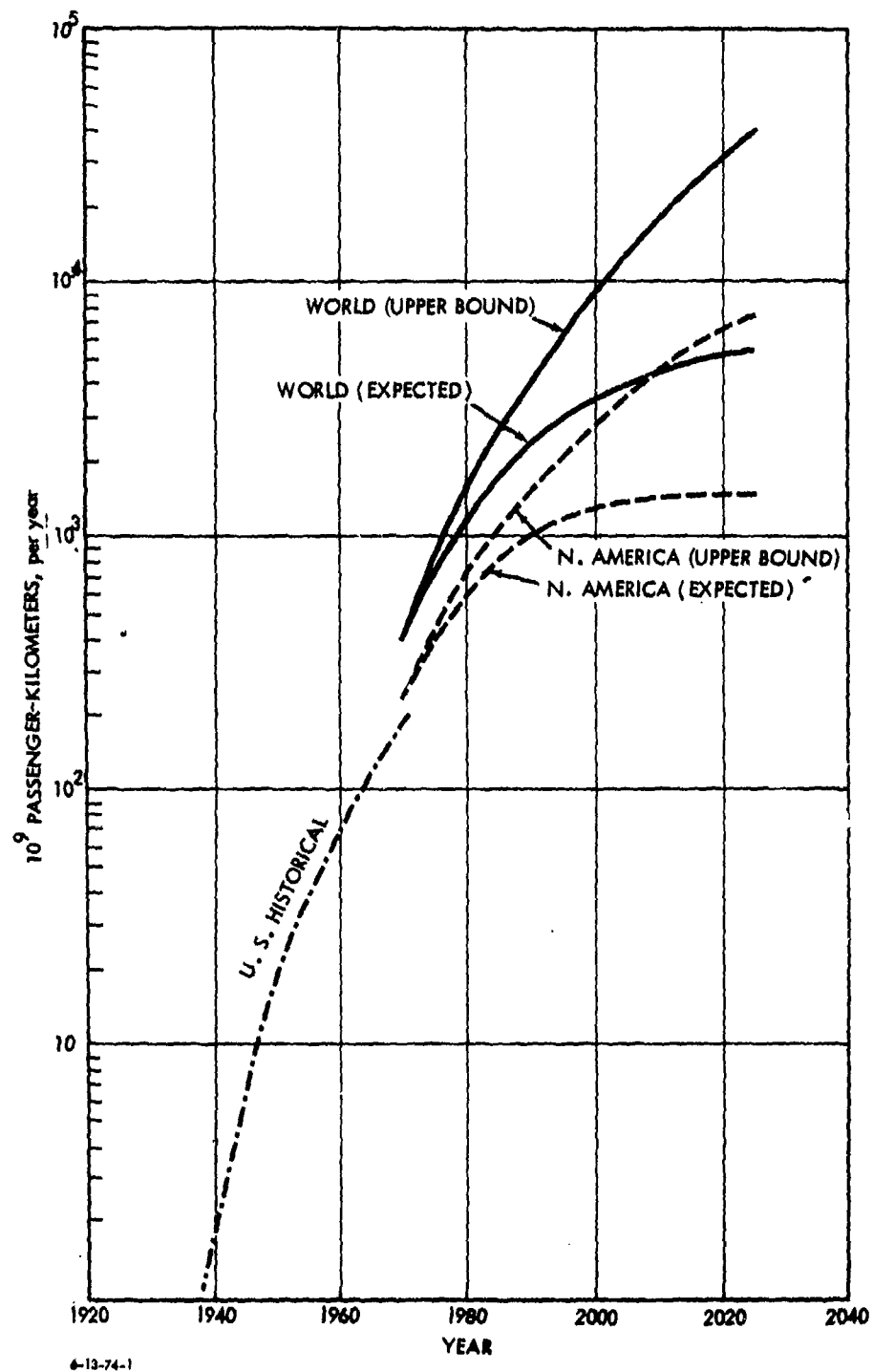


FIGURE 2.1. AIR TRAFFIC HISTORY AND CIAP PROJECTIONS
Source: CIAP ROF, p. D-71

TABLE 2.1. CIAP UPPER-BOUND AIR TRAVEL AND AIR CARGO PROJECTIONS
SOURCE: CIAP ROF, p. D-69

(a) Revenue air passenger demand, realistic upper-bound prediction (billions of pkm)

Region	1970	1980	1990	2000	2025
Africa	9	20	51	166	2,103
Latin America	16	47	163	565	4,238
North America	260	739	1,570	2,750	7,133
Asia	39	224	906	2,617	13,551
Europe	122	337	821	1,681	5,728
Oceania	11	31	107	308	1,731
U.S.S.R.	78	289	842	1,886	6,798
World	535	1,687	4,460	9,973	41,282

(b) Revenue air cargo demand, realistic upper-bound prediction (billions of tonne-km)

Region	1970	1980	1990	2000	2025
Africa	0.2	0.7	2.3	9.5	320.3
Latin America	0.5	2.3	13.7	66.1	996.9
North America	6.0	26.3	120.9	391.1	2,797.8
Asia	1.0	8.1	44.8	187.3	2,572.6
Europe	3.0	15.9	88.6	347.7	3,367.2
Oceania	0.3	1.2	5.7	20.0	186.0
U.S.S.R.	1.5	5.5	23.2	98.1	993.3
World	12.5	60.0	299.2	1,119.8	11,234.1

(c) Annual per capita travel and cargo, realistic upper-bound predictions.

Region	Passenger-kilometers					Cargo (tonne-km)				
	1970	1980	1990	2000	2025	1970	1980	1990	2000	2025
Africa	27	42	82	198	1,201	0.7	1.4	3.6	11.4	182.9
Latin America	57	124	324	846	3,106	1.7	6.1	27.3	99.0	730.6
North America	1,142	2,828	5,223	7,964	14,590	26.5	100.8	402.3	1,132.5	5,723.0
Asia	19	85	269	607	1,695	0.5	3.1	13.3	43.4	321.8
Europe	263	666	1,484	2,780	7,572	6.6	31.5	160.4	575.0	4,451.6
Oceania	565	1,193	3,068	6,555	17,580	13.9	46.2	163.3	426.2	1,889.9
U.S.S.R.	322	1,037	2,626	5,122	13,043	6.1	19.7	72.4	266.5	1,905.8
World	147	371	782	1,389	3,182	3.5	13.2	52.5	155.9	865.9

TABLE 2.2. CIAP EXPECTED AIR TRAVEL AND AIR CARGO PROJECTIONS
SOURCE: CIAP ROF, p. D-70

(a) Revenue air passenger demand (billions of pkm)

Region	1970	1980	1990	2000	2025
Africa	9	16	34	87	541
Latin America	16	34	86	202	490
North America	260	598	1,022	1,294	1,478
Asia	39	131	354	641	1,083
Europe	122	215	381	507	691
Oceania	11	20	55	117	291
U.S.S.R.	78	172	380	553	829
World	535	1,186	2,312	3,401	5,403

(b) Revenue air cargo demand (billions of tonne-km)

Region	1970	1980	1990	2000	2025
Africa	0.2	0.5	1.5	5.1	85.1
Latin America	0.5	1.7	7.4	24.2	119.8
North America	6.0	21.5	80.5	190.4	611.8
Asia	1.0	5.8	21.3	56.2	256.7
Europe	3.0	12.3	50.6	130.7	516.3
Oceania	0.3	1.0	3.6	9.5	39.2
U.S.S.R.	1.5	4.0	12.9	35.8	153.8
World	12.5	46.8	177.8	451.9	1782.7

(c) Annual per capita passenger travel and cargo, expected projections

Region	Passenger-kilometers					Cargo (tonne-km)				
	1970	1980	1990	2000	2025	1970	1980	1990	2000	2025
Africa	27	37	62	133	534	0.7	2.8	2.8	7.8	84.2
Latin America	57	96	195	402	714	1.7	4.8	16.7	48.2	174.6
North America	1,142	2,403	3,751	4,425	4,229	26.5	86.3	295.4	249.9	1,751.0
Asia	19	54	122	191	224	0.5	2.4	7.4	16.7	53.2
Europe	263	448	762	970	1,180	6.6	25.7	101.2	249.9	882.3
Oceania	565	895	2,087	3,872	6,673	13.9	42.7	137.5	312.8	900.1
U.S.S.R.	322	628	1,226	1,671	2,128	6.1	14.5	41.6	108.2	394.7
World	147	279	462	598	684	3.5	11.0	35.6	79.4	225.8

each of the major areas involved. The "expected" case (Table 2.2) was developed in similar fashion to that for the upper-bound case, except growth rates were taken to be lower (see pp. 8-25 and 8-26, CIAP Monograph 2).

The fleets of aircraft required to serve the projected traffic were developed by a computer model, using hypothesized aircraft, as given in Table 2.3, and economic selection rules as to the most profitable aircraft for each route. The model had no "memory" in that the fleets selected for a given year had no necessary relation to fleets selected for traffic, say 5 years earlier; as a consequence, severe fluctuations in fleet mix were found, as shown, for example, for the LR3J in Table 2.4, which gives projected numbers of aircraft for one CIAP case. This fact had little consequence in terms of fuel flows required, however, since different subsonic aircraft differed only by small amounts in terms of fuel consumption per passenger-kilometer. Of more importance was the assumption that the aircraft operated at 50 percent load factor for passengers and 60 percent for freight, requiring thereby, in effect, twice as large a fleet as theoretically (but not practically) possible. Also, the fleets predicted were designed to serve the peak summer season, without allowance for load factor increase in the summer. Seasonal splits were developed as follows, based on the peak summer values:

Summer	1.0
Fall	0.71
Winter	0.52
Spring	0.75
Average	0.75

In all calculations made using the CIAP estimates, the average yearly rates were used. The number of aircraft was not used directly. This procedure was preferred, partly due to the integrating effect of the atmosphere, and partly because load factors vary during the year, making fuel flow rate variations during the year less than indicated for these seasonal traffic values.

Two special case fleets of particular interest here were generated in CIAP as shown in Tables 2.5 and 2.6. In one, Table 2.5, it was assumed that no new SST would be built, and upper-bound traffic was served only by subsonic aircraft and by mach 2 (Concorde/Tupolev) SSTs. In the second, Table 2.6, it was assumed that no SSTs would be available, with upper-bound traffic served only by subsonic aircraft.

The CIAP model included no fuel penalty for carrying freight unless carried on all-freight aircraft. The effect of this assumption was that, when passengers were carried by SSTs, which carried no freight, "free" cargo space was lost, more air freighters were required, and little decrease in total fuel consumption by subsonic aircraft resulted, as will be shown in Section 2.2.2. (Note, for example, the model demand for 720 cargo aircraft in Table 2.5 versus 560 cargo aircraft in Table 2.6, also the number of passenger-carrying aircraft.) To some degree, this effect is an artifact of the model.

TABLE 2.3. AIRCRAFT POSTULATED IN CIAP
SOURCE: CIAP ROF, p. D-73

Aircraft type	Range (km)	Passenger capacity	All cargo capacity (kg)	Secondary cargo (kg)	Cruise speed (km/hr)	Gross weight (kg)	Fuel flow (kg/hr) ^a	Kg fuel per pkm ^b
S3J*	3,200	140	-	-	870	-	3,600	.060
ES3J*	3,500	170	-	-	900	99,000	3,900	.051
SST*	6,100	105	-	-	2,130	174,000	19,100	.171
ASST	6,300	170	-	-	2,130	226,000	20,500	.113
L4J*	9,000	380	75,000	18,000	900	362,000	10,000	.064
L3J*	5,500	295	50,000	10,000	880	200,000	6,600 (7,300)	.051
LR3J*	9,200	270	50,000	9,000	890	252,000	7,700 (8,200)	.064
T4J*	9,500	145	-	-	870	-	4,500	.071
L2J*	3,500	230	-	8,000	670	150,000	5,400 (6,200)	.054
LRL4J*	10,000	285	50,000	11,000	930	299,000	9,500(10,400)	.072
LRT4J*	12,000	200	27,000	5,000	870	163,000	4,500	.052
LASST	7,400	295	-	-	2,880	328,000	40,800	.096
LL4J	12,000	600	100,000	13,000	930	408,000	11,800	.042
HST	12,000	300	-	-	5,410/6,960 ^c	362,000	100,900/39,200 ^c	.038
ACX	12,000	1,000	150,000	23,000	870	544,000	16,100	.037

*Existing or near-term aircraft expected prior to 1980.

Nomenclature:

S3J	Small three-jet transport	L2J	Large two-jet transport
ES3J	Extended small three-jet transport	LRL4J	Long-range large four-jet transport
SST	Small supersonic transport	LRT4J	Long-range traditional four-jet transport
ASST	Advanced supersonic transport (mach 2)	LASST	Large advanced supersonic transport
L4J	Large four-jet transport	LL4J	Very large four-jet transport
L3J	Large three-jet transport	HST	Hypersonic transport
LR3J	Long-range three-jet transport	ACX	Advanced very large transport
T4J	Traditional four-jet transport		

^aFigures in parentheses apply to thrust uprated versions in year 2000; rest of table not applicable to year 2000 case.

^bAssumes 50-percent passenger load factor; ignores cargo. Computed at cruise speed.

^cClimb and cruise average, respectively.

TABLE 2.4. CIAP EXPECTED WORLD AIRCRAFT FLEETS
SOURCE: CIAP ROF, p. D-79

System*	1970**		1980		1990		2000		2025	
	Passenger	Cargo	Passenger	Cargo	Passenger	Cargo	Passenger	Cargo	Passenger	Cargo
LASST	-	-	42 (SST's)	-	241	-	615	-	1,064	-
HST	-	-	-	-	-	-	-	-	1	-
LS3J	-	-	23	-	161	-	374	-	-	-
L2J	-	-	21	-	87	-	763	-	2,442	-
L3J	18	18	31	4	183	78	674	460	1,209	30
LR3J	-	-	2,033	14	69	94	1,523	267	206	19
L4J	531	3	10	85	1,490	130	156	646	-	-
LL4J	-	-	-	-	14	26	3	108	131	21
LRL4J	-	-	-	2	75	11	1	7	51	5
ACX	-	-	-	-	246	177	342	528	905	5,655
S3J	266	-	71	-	-	-	-	-	-	-
T4J	82	24	166	11	-	-	-	-	-	-
TOTAL										
Supersonic	0	0	42	0	241	0	615	0	1,064	0
Hypersonic	0	0	0	0	0	0	0	0	1	0
TOTAL										
Subsonic	897	45	2,355	116	2,325	516	3,836	2,016	4,944	5,730

*See Table 2.3 for nomenclature.

**This is a model result, not the actual fleet.

TABLE 2.5. FLEET MIX DEVELOPED IN CIAP TO MEET UPPER-BOUND 1990
AIR TRAFFIC DEMAND; ONLY PRESENT SSTs AVAILABLE
SOURCE: CIAP ROF, p. D-77

<u>System*</u>	<u>Passenger</u>	<u>Cargo</u>
Concorde/Tupolev	378	-
ES3J	206	-
L2J	150	-
L3J	178	98
LR3J	53	145
L4J	3,490	237
LL4J	3	36
LRL4J	120	1
ACX	<u>543</u>	<u>203</u>
Total	5,121	720

TABLE 2.6. FLEET MIX DEVELOPED IN CIAP TO MEET UPPER-BOUND AIR
TRAFFIC DEMAND; NO SSTs AVAILABLE
SOURCE: CIAP ROF, p. D-77

<u>System</u>	<u>1990</u>		<u>2000</u>	
	<u>Passenger</u>	<u>Cargo</u>	<u>Passenger</u>	<u>Cargo</u>
ES3J	146	0	387	0
L2J	48	0	1,562	0
L3J	52	4	2,046	11
LR3J	133	33	4,890	4
L4J	3,412	265	1,111	2,219
LL4J	55	14	150	189
LRL4J	51	0	0	0
ACX	<u>679</u>	<u>244</u>	<u>1,860</u>	<u>938</u>
Total	4,576	560	12,006	3,361

The CIAP model also included no military traffic nor charter traffic to vacation spots. More importantly, it included only traffic traveling more than 700 km nonstop. The model-derived numbers for fuel flow, at least in total, and for current periods as, for example, 1970, were clearly low, by a factor of 1.5 to 2.0 (see ROF, p. D-65, and FAA figures, later herein).

Hypersonic aircraft, which would operate in the 27-km to 33-km range, are not expected until about the year 2015, according to CIAP, i.e., beyond the time frame of prime interest. Hence, they were not considered by CIAP, and are

*See Table 2.3 for nomenclature.

obviously excluded here. The altitude distribution of emissions was based on aircraft type and route length, as given in Table 2.7. These altitude distributions are somewhat arbitrary, particularly for subsonic aircraft. Thus, as seen in Table 2.8, Downie (1974) showed that, at least for U.S. transcontinental traffic in 1972, only a very small amount of traffic reached 12.5 km (41,000 ft).*

TABLE 2.7. FLIGHT PROFILES FOR EMISSION CALCULATIONS;
CIAP MODEL
SOURCE: CIAP ROF, p. D-81

<u>Aircraft Classification</u>	<u>Distance (km)</u>	<u>Altitude Band (km)</u>
Subsonic	0-3,000	9-12
	>3,000	12-15
Present supersonic	0-100	<9
	100-300	9-12
	300-700	12-15
	>700	15-18
Future supersonic	0-80	<9
	80-170	9-12
	170-260	12-15
	260-500	15-18
	>500	18-21

TABLE 2.8. FUEL CONSUMED AT SPECIFIED FLIGHT ALTITUDES
IN MORE THAN 600 U.S. BOEING 707 TRANS-
CONTINENTAL FLIGHTS IN JANUARY AND
FEBRUARY 1972
SOURCE: CIAP ROF, p. D-61

<u>Flight altitude 1,000 ft (km)</u>	<u>Fuel burned 1,000 lb (x 10⁴ kg)</u>		<u>Percent</u>
41 (12.5)	154	(7.0)	0.55
39 (11.9)	6,858	(311.1)	24.35
37 (11.3)	10,140	(459.9)	36.00
35 (10.7)	3,057	(138.7)	10.85
33 (10.1)	152	(6.9)	0.54
31 (9.4)	881	(40.0)	3.13
28 (8.5)	1,655	(75.1)	5.88
26 (7.9)	<u>5,268</u>	<u>(239.0)</u>	<u>18.70</u>
	28,165	(1,277.7)	100.0

The CIAP distance criterion resulted, even for the year 1970, in about 25 percent of the total subsonic fuel being in the 12-km to 15-km altitude range. This result was nearly invariant with time. In passing, it should be noted that in the computations reported in the CIAP ROF, long-range subsonic aircraft, such as the 747SP, were assumed to cruise at 13.5 km (44,280 ft), the midpoint of the

*See also Table 2.23, Section 2.3.1.

TABLE 2.9. ANNUAL FUEL CONSUMPTION CALCULATED IN CIAP FOR THE 1990
 EXPECTED FLEET (10^9 kg/yr)
 SOURCE: CIAP ROF, p. D-88

Year and altitude band (km)	Subsonic*	Supersonic
1970		
9-12	10.6	0
12-15	3.6	0
15-18	0	0
18-21	0	0
Total	14.2	0
1980		
9-12	26.7	0
12-15	9.0	0.16
15-18	0	1.18
18-21	0	0
Total	35.7	1.34
1990		
9-12	43.7	0
12-15	15.3	0
15-18	0	0.7
18-21	0	14.6
Total	59.0	15.3
2000		
9-12	75.0	0
12-15	29.8	0
15-18	0	1.8
18-21	0	37.4
Total	104.8	39.2

*The distribution by altitude is now considered unrealistic. See Section 2.3.

12-km to 15-km band, which, as will be seen later, is now believed to be too high as a mean value. More data on these points will be provided, but the figures shown in Table 2.7 were the basis for the CIAP computations.

2.2.2 Fuel Flow Projections

As noted earlier, the upper-bound case and the expected case both included an advanced mach 2.7 SST, introduced in the mid-1980s. Nevertheless, there are aspects of these projections that are of interest. Thus, in Table 2.9, the fuel flow is given for the expected subsonic fleet by the CIAP model. If we note, as shown in Table 2.10, that the presence of an advanced SST has little effect on fuel consumption by subsonics (in the CIAP model), the data in Table 2.9 can be compared to other fuel flow projections, without undue concern that the CIAP "expected fleet" includes a now-not-expected advanced SST.

TABLE 2.10. SUBSONIC FUEL CONSUMPTION BY SUBSONICS WITH SEVERAL ASSUMPTIONS AS TO SSTs; CIAP UPPER-BOUND 1990 TRAFFIC MODEL (10^9 KG/YR)
SOURCE: CIAP ROF, pp. D-85, D-87

<u>Scenario</u>	<u>Subsonic Fuel Flow</u>
Advanced SST	110.1
Present SST	117.8
No SST	118.0

Table 2.11 gives summarized data for the present SST-only case, assuming upper-bound traffic; in this case, the SST fleet consists of 378 Concorde/Tupolev aircraft. This case is of interest in that latitudinal distribution of emissions is provided for both large subsonic and supersonic (mach 2) fleets, which is considered to be of parametric value and has been used for 2-D modeling (Appendix A). The detailed fuel flow data are given in Table 2.12. As noted above, however, the altitude distribution for subsonic traffic is considered to be invalid, based as it is only on route length criteria.

TABLE 2.11. FUEL CONSUMPTION BY ALTITUDE BAND; PRESENT SSTs ONLY; CIAP UPPER-BOUND 1990 TRAFFIC (10^9 KG/YR)
SOURCE: CIAP ROF, p. D-87

<u>Altitude band</u>	<u>Subsonic</u>	<u>Supersonic</u>
9-12 km	85.7	0
12-15 km	32.1	1.3
15-18 km	0	11.3
18-21 km	0	0
Total	117.8	12.6

TABLE 2.12. DISTRIBUTION OF FUEL USAGE BY ALTITUDE AND LATITUDE BANDS;
PRESENT SSTs ONLY; CIAP UPPER-BOUND TRAFFIC
SOURCE: CIAP MONOGRAPH 2, pp. 9-62 to 9-64

Latitude Band	Subsonic				Supersonic			
	9-12 km		12-15 km		12-15 km		15-18 km	
	Fuel	%	Fuel	%	Fuel	%	Fuel	%
80-85° N	0.069	0.080	0.116	0.361				
75-80° N	0.104	0.121	0.194	0.603				
70-75° N	0.106	0.123	0.226	0.703				
65-70° N	0.157	0.182	0.227	0.706	0.0015	0.116	0.0105	0.093
60-65° N	1.610	1.871	1.927	5.992	0.0452	3.481	0.482	4.271
55-60° N	6.242	7.256	2.685	8.349	0.0389	2.996	1.100	9.747
50-55° N	11.279	13.110	6.378	19.832	0.237	18.253	3.477	30.810
45-50° N	9.773	11.350	5.585	17.366	0.144	11.090	1.596	14.142
40-45° N	12.346	14.351	3.121	9.705	0.285	21.949	0.808	7.160
35-40° N	12.291	14.287	2.447	7.608	0.163	12.554	0.331	2.933
30-35° N	9.581	11.137	2.015	6.266	0.0665	5.122	0.558	4.944
25-30° N	7.035	8.177	1.333	4.145	0.0091	0.701	0.610	5.405
20-25° N	4.517	5.250	1.459	4.537	0.958	7.378	0.720	6.380
15-20° N	4.052	4.710	1.150	3.576	0.0616	4.744	0.652	5.777
10-15° N	2.146	2.494	0.857	2.665	0.0632	4.867	0.304	2.694
5-10° N	0.920	1.069	0.665	2.068	0.0175	1.348	0.202	1.790
0-5° N	1.298	1.509	0.810	2.518	0.0092	0.709	0.293	2.596
0-5° S	0.490	0.570	0.301	0.936	0.100	0.770	0.0851	0.754
5-10° S	0.386	0.449	0.276	0.858	0.0345	2.657	0.0348	0.308
10-15° S	0.370	0.430	0.207	0.644	0.0155	1.194	0.0157	0.139
15-20° S	0.301	0.350	0.0988	0.307	0.00004	0.003	0.00004	0.0004
20-25° S	0.287	0.334	0.0523	0.163	0.00008	0.006	0.0044	0.0399
25-30° S	0.386	0.449	0.0258	0.080	0.00024	0.018	0.00075	0.0066
30-35° S	0.233	0.271	0.0039	0.012				
35-40° S	0.0361	0.042			0.00029	0.022	0.00029	0.0026
40-45° S	0.0085	0.010					0.00057	0.0051
45-50° S	0.0071	0.008			0.00029	0.022	0.00029	0.0026
Total	86.031	100.000	32.160	100.000	1.29844	100.000	11.2854	100.000

*The number of places carried here is for internal consistency only and is not intended to imply significance.

Examination of the data in Table 2.12 will show that almost all the aircraft fuel is consumed in the Northern Hemisphere, with a major fraction used in the 35° to 55° N band.

Longitudinal distribution of fuel flows is provided for selected cases in CIAP Monograph 2. These data are not used here, however, nor have they been used in any modeling work to date.

2.2.3 Emission Indices and Projections

A. Present Values

The emission indices used in the CIAP model in computing global emissions rates are given in Table 2.13. The NO_x values used for subsonic aircraft are based on data on older, low-compression-ratio engines (JT3D and JT8D). For more modern engines, higher values, as given in Table 2.14, are recommended. (Broderick, CIAP Monograph 2, p. 4-50). The CF-6, JT9D, and RB-211 engines are used on wide body subsonic aircraft; the Olympus 593 and NK-144 engines are used on the Concorde and Tupolev SSTs.

TABLE 2.13. ENGINE EMISSION INDICES ASSIGNED IN CIAP
TO THE CURRENT FLEET
SOURCE: CIAP ROF, p. D-81

<u>Emission species</u>	<u>Altitude (km)</u>	<u>Subsonic</u>	<u>Supersonic</u>
Oxides of nitrogen (as NO ₂)	9-12 12-15 15-21	10 g/kg fuel 7 -	10 g/kg fuel 18 18
Carbon monoxide (CO)		3	3
Total hydrocarbons (THC)		0.5	0.5
Soot		0.02	0.02
H ₂ O		1.25 x 10 ³	1.25 x 10 ³
CO ₂		3.22 x 10 ³	3.22 x 10 ³
SO ₂		1	1
Total trace elements		0.01	0.01
Lubricating oil		0.1	0.1

TABLE 2.14. CURRENT TECHNOLOGY AIRCRAFT NO_x EMISSION INDICES
AT CRUISE AS NO₂ (RECOMMENDED VALUES)
SOURCE: CIAP MONOGRAPH 2, p. 4-50

	<u>CF6, JT9D, RB211</u>	<u>Olympus 593, NK-144</u>	<u>JT3D, JT8D</u>
Oxides of nitrogen g(NO ₂)/kg fuel	16	18	6
Carbon monoxide g(CO)/kg fuel	4	3.5	4
Total hydrocarbons g(CH ₂)/kg fuel	0.1	0.2	0.1

Carbon monoxide and total hydrocarbons are (or have been) of little concern; in effect, such materials create ozone, although in negligible amounts.

The NO_x emission figures given in Table 2.14 are for "typical" cruise conditions. The values shown are satisfactory for first-cut analysis, but for more detailed study the variations along the flight path, in both fuel flow rates and NO_x emission indices (which decrease about with the square root of pressure and other factors) need to be examined.

Emission index estimates for the Kuznetsov NK-144 engine, in use on the Tupolev, were obtained during CIAP and are included as Table 2.15.

TABLE 2.15. TENTATIVE EMISSION INDICES.
KUZNETSOV NK-144 ENGINES
SOURCE: CIAP MONOGRAPH 2, p. 4-43

CO ₂	3,150 g/kg
H ₂ O	1,280
NO _x (as NO ₂)	18.4
CO	3.4
THC (total hydrocarbon)	0.17
SO ₂	1.0

A strong cautionary note must be added here relative to NO_x emission indices, in that values reported above (Tables 2.13 to 2.15) are based on probe sampling. A still unresolved discrepancy exists between probe sampling and a spectroscopic method tested at the Arnold Engineering Development Center (AEDC) (Davidson and Domal, 1973), which gives, particularly (almost five-fold) under afterburning conditions, much higher NO_x values than obtained by probe sampling. Data illustrating the effects are given in Table 2.16.*

TABLE 2.16. YJ93-GE-3 ENGINE EMISSION MEASUREMENT BY
PROBE AND SPECTROMETER TECHNIQUES
SOURCE: Davidson and Domal, 1973

Simulated flight condition, mach no.	Altitude, kft	Engine power setting	NO concentration (ppm)	
			Probe sampling	UV spectrometer
1.4	35	Military	56	75
2.0	55	Military	70	165
2.0	55	Min. afterburner	80	175
2.0	55	Max. afterburner	110	278
2.6	66	Military	100	323
		Max. afterburner	130	617

*The data of Few et al. 1977 (1974 and 1975 data), imply discrepancies similar to those shown for the max. afterburner case over a wide range of conditions. Other data, however, (Lyon et al. 1975; Gryvnak and Burch, 1976) imply negligible or small errors (~ 30 percent low) with probe sampling.

The questions associated with the validity of these two techniques are serious ones and in obvious need of resolution. A particular question relates to whether the NO, which may be present in the high-temperature stream, is indeed present after dilution with ambient air, or whether the NO is destroyed by the same processes (which may not be heterogeneous), resulting in lower values in the samples drawn through a probe.

For purposes here, values developed from probe sampling are used, as has been the case in CIAP and related programs. The clear possibility must be recognized, however, that these values may be several-fold low.

B. Potential Emission Index Reductions (other than SO₂)

Possible emission index values with improved combustor technology were estimated by a NASA *ad hoc* committee in 1973. The values are shown in Table 2.17; a CIAP interpretation is given in Table 2.18. In general, very low NO_x emission indices (3 or less) are based on the assumed implementation of lean premix combustion techniques, which have been demonstrated in the laboratory but have associated with them some rather significant questions (flashback, relight, safety, etc.). Ultra-low NO_x values (0.3) have also been demonstrated, using very lean flames or catalytic combustion techniques.

TABLE 2.17. NASA AD HOC COMMITTEE 1973 CONSENSUS ESTIMATES OF CRUISE EMISSION INDICES WITH CURRENT AND PROJECTED TECHNOLOGY, JP FUEL
SOURCE: CIAP MONOGRAPH 2, p. 5-84

<u>Mission propulsion system</u>	<u>NO_x g(NO₂)/kg fuel</u>	<u>CO g(CO)/kg fuel</u>	<u>THC g(CH₂)/kg fuel</u>	<u>Soot g(C)/kg fuel</u>
Current technology				
CF6, JT9D, RB211	16	4	0.1	0.1
Olympus 593, NK-144	18	3.5	0.2	0.1
JT3D, JT8D	6-8	4	0.1	0.1
CTOL turbofan (subsonic)				
1. Anticipated emission reduction technology	8	3	0.5	0.02
2. Advanced emission reduction technology	3	3	0.1	0.02
Nonaugmented SST/(dry) turbojet				
1. Anticipated emission reduction technology	14	3	0.5	0.02
2. Advanced emission reduction technology	3	3	0.1	0.02
ASST/duct-burning turbofan				
1. Anticipated emission reduction technology	12	30	10	0.02
2. Advanced emission reduction technology	3	15	3	0.02

TABLE 2.18. PROJECTED NO_x EMISSION INDICES AS NO₂
SOURCE: CIAP ROF, p. 103

<u>Engine Type (Aircraft System)</u>	<u>NO_x Emission Index: g(NO₂)/kg Fuel</u>
Current Technology (operational through 1985)	
- subsonic (JT9-D/B747)	16
- supersonic (Concorde)	18
Anticipated Reduction Technology (implemented 1980-1985 time frame)	
- subsonic	8
- supersonic	12 - 14
Advanced Reduction Technology (possible by 1985-1990)	
- subsonic	3
- supersonic	3
Projected Minimum	
- subsonic	0.3
- supersonic	0.3

The time schedule for NO_x emission index reductions suggested in Table 2.18 may well be optimistic. This observation (which is not based on detailed study) follows from the information presented by D.W. Bahr, at the 4th Conference on CIAP (February 4-7, 1975), and on testimony before the EPA* (January 27-28, 1976) by various engine companies. A two-fold reduction (at low altitudes still seems several years away from being implementable, although already pursued for 5 or more years. As noted above, concepts giving 6-fold or greater reductions will require new approaches and some years of testing. If, as may be possible, these new concepts can be applied only to new engines, reductions in fleet average values would take place very slowly, unless expensive engine replacement programs were to be implemented.

*Public Hearing on Control of Air Pollution from Aircraft and Aircraft Engines, Jan 27-28, 1976, EPA, Washington, D.C.

2.3 FAA PROJECTIONS

2.3.1 Procedures

The outlook for air travel, and particularly SST travel, changed substantially during the course of the CIAP program, due both to economic factors, such as the abrupt fuel price rise in 1973, and to environmental factors, such as were developed during the CIAP program itself. Also, the scope and nature of the problems had shifted from focus on advanced SSTs to focus on current SST and current and advanced subsonics. For these reasons, new projections were required, and were undertaken by the FAA in 1975, with contracts being issued to Stanford Research Institute (SRI) and to Arthur D. Little, Inc. (ADL). The SRI work provided projections of aircraft-operating (flight) hours in various altitude and latitude bands for 22 categories of aircraft, as given in Table 2.19 (reported by ADL). The ADL work used these data, along with fuel flow, as given in Table 2.20, and emission index data as given in Table 2.21 to generate rates of pollutant introduction. The base year was 1975, with high and low forecasts made for 1980, 1985, and 1990. Use of flight hours as a variable produces the desired pollutant flow data but does not indicate the number of aircraft involved.

The procedures used by SRI in developing forecasts are described in their contract report, only a draft of which has been available to us. The model used was an existing one adapted to the FAA forecasting problem. The model has been tested by "backcasting" historical data, with good results claimed. The model is an "aggregate model rather than a microanalytical one." The model does not attempt, as did CIAP, to select the most economic aircraft for each route, a procedure which may have caused the CIAP model results to exhibit large fluctuations in specific aircraft types with time. Routes of 400 miles or less were excluded, a procedure similar to that followed in CIAP, in which routes of 700 km or less were excluded.

The forecast use of SSTs was noted by SRI to be a particularly difficult problem in view of the uncertainties surrounding this type of travel; any projections are necessarily somewhat subjective. SRI noted that, according to fare and time elasticity estimates, the SST should capture most of the first-class traffic on applicable routes, which represents roughly a 6 percent passenger diversion, a smaller diversion than used in CIAP. However, because of FAA interest in SST effects, more generous assumptions were used which increased the size of the SST fleet; these assumed that, up to 1985, SST flights would divert roughly 30 percent of the flights in eligible markets, and in 1985-1990, 45 percent. SSTs were assumed to operate at 90 percent load factors versus 55 percent for subsonics. SRI states their belief that these forecasts of SST activity are extremely optimistic; the assumptions led to SST growth rates of 17 to 21 percent over the 1980-1990 period versus 4 to 7 percent for total traffic. SSTs

TABLE 2.19. AIRCRAFT TYPES AND ENGINE CHARACTERISTICS
 ASSUMED IN FAA PREDICTIONS
 SOURCE: Arthur D. Little, Inc., 1976, Tables 1 and 2

	<u>Aircraft Type</u>	<u>Airframe</u>	<u>Engine</u>	<u>Average Gross Weight, lb</u>	<u>Aircraft Included and Remarks</u>
(1)	L10	L1011	JT9D	340,000	L1011
(2)	707	707/320	JT3D	261,000	707, DC-8, 720, VC10, 880, 990
(3)	727	727	JT8D	154,000	727
(4)	737	737	JT8D	100,000	737, DC-9
(5)	747	747	JT9D	626,000	747 except 747SP
(6)	D10	DC10	CF6	360,000	DC10
(7)	A3	DC10	CF6	281,000	A300B; scale from DC-10
(8)	TR1	727	SPEY 511	117,000	Trident series; scale fuel flow from 727
(9)	F28	737	SPEY 511	83,000	F28, BAC111, Caravelle; scale fuel flow from 737
(10)	T34	737	JT8D	104,000	TU134, TU104; scale from 737
(11)	T54	707	JT3D	134,000	TU154, IL18; scale from 707
(12)	Y62	707	JT3D	302,000	IL62; scale from 707
(13)	Y86	DC10	CF6	360,000	IL86
(14)	Y40	Sabreliner	Typical T-1 engine	21,000	YAK40
(15)	7X7	DC10	CF6	300,000	7X7; scale from DC10
(16)	74S	747	JT9D	444,000	747SP; scale from 747
(17)	DCX	DC10	CF6	300,000	DCX200; same as 7X7
(18)	MISC	737	Typical P-2 engine	95,000	*; scale fuel flow from 737
(19)	LR	Learjet	Typical T-1 engine	12,000	Learjet
(20)	C5	Sabreliner	Typical T-1 engine	21,000	Falcon, HS125, Cita- tion
(21)	GULF	Sabreliner	Typical T-1 engine	21,000	Gulfstream, Saber- liner, Jetstar
(22)	SST	Concorde	Olympus	338,000	All SST

*All aircraft in scheduled service not otherwise included.

TABLE 2.20. TOTAL FUEL FLOW RATE VS ALTITUDE USED IN FAA PROJECTIONS (kilograms per hour)
SOURCE: Arthur D. Little, Inc., 1976, Table 3

Aircraft Type	ALTITUDE (Kilometers)											
	7	8.5	9.5	10.5	11.5	12.5	13.5	14.5	15.5	16.5	17.5	18.5
1	9,890	8,890	7,710	7,110	6,710	6,490						
2	6,920	6,170	5,900	5,530	4,760	3,990	3,180					
3	5,260	4,670	4,310	4,040	3,400	2,900	2,270					
4	3,030	2,620	2,450	2,340	2,300	2,270	2,270					
5	14,400	13,100	12,700	11,100	9,640	8,050	6,490					
6	9,800	8,620	8,120	7,440	6,580	5,530	4,540					
7	7,650	6,710	6,340	5,810	5,130	4,320	3,540					
8	4,000	3,550	3,270	3,070	2,280	2,210	1,720					
9	3,550	3,070	2,870	2,730	2,690	2,650	2,650					
10	3,150	2,730	2,550	2,430	2,390	2,360	2,360					
11	3,550	3,170	3,030	2,840	2,450	2,050	1,630					
12	8,000	7,140	6,820	6,400	5,510	4,620	3,670					
13	9,800	8,620	8,120	7,440	6,580	5,530	4,540					
14	980	950	900	820	780	750						
15	8,160	7,180	6,770	6,200	5,480	4,610	3,780					
16	14,200	13,300	12,400	11,200	9,660	7,980	6,120					
17	8,160	7,180	6,770	6,200	5,480	4,610	3,780					
18	2,880	2,490	2,330	2,220	2,180	2,150	2,150					
19	1,070	900	800	730	670	640	620					
20	980	950	900	820	780	750						
21	900	950	900	820	780	750	730					
22	49,000	45,000	41,900	38,800	35,900	33,000	29,900	27,200	24,300	21,600	18,300	15,800

TABLE 2.21. EMISSION INDICES* OF NITROGEN OXIDES (NO_x) USED IN FAA PROJECTIONS
SOURCE: Arthur D. Little, Inc., 1976, Table 4

Aircraft Type	ALTITUDE (Kilometers)													
	7	8.5	9.5	10.5	11.5	12.5	13.5	14.5	15.5	16.5	17.5	18.5		
1	23.4	20.8	18.2	16.3	14.9	13.4	12.1							
2	6.6	6.0	5.5	5.0	4.1	3.6	3.5							
3	13.9	12.8	11.6	10.1	9.2	8.5	7.8							
4	13.3	11.3	10.1	9.2	8.6	7.9	7.1							
5	23.4	20.8	18.2	16.3	14.9	13.4	12.1							
6	4.8	4.8	4.4	4.2	3.6	3.3	3.2							
7	4.8	4.8	4.4	4.2	3.6	3.3	3.2							
8	11.5	10.6	9.8	8.7	8.0	7.4	6.7							
9	11.5	10.6	9.8	8.7	8.0	7.4	6.7							
10	13.3	11.3	10.1	9.2	8.6	7.9	7.1							
11	6.6	6.0	5.5	5.0	4.1	3.6	3.5							
12	6.6	6.0	5.5	5.0	4.1	3.6	3.5							
13	4.8	4.8	4.4	4.2	3.6	3.3	3.2							
14	1.29	1.20	1.10	1.01	.74	.90	.90							
15	4.5	4.1	3.8	3.5	3.2	2.9	2.5							
16	23.4	20.8	18.2	16.3	14.9	12.4	12.1							
17	4.5	4.1	3.8	3.5	3.2	2.9	2.5							
18	2.7	2.7	2.3	2.2	1.9	1.7	1.6							
19	1.4	1.2	1.1	1.0	.97	.91	.86							
20	1.3	1.2	1.1	1.0	.94	.90	.90							
21	1.3	1.2	1.1	1.0	.94	.90	.90							
22	11.0	11.0	11.0	9.4	9.4	11.0	20.0	20.0	19.0	18.0	18.0	18.0		

*Some of these data are not in agreement with CIAP estimates. In particular, the emission indices for aircraft using the CF6 engine (types 6, 7, 13, 15, and 17) all appear to be low by a factor of 4 or 5. (See CIAP Monograph 2, p. 5-84.)

were considered ineligible for stage lengths less than 2,000 miles. For the 747SP class, it was assumed that these aircraft would be purchased for stage lengths exceeding 4,500 miles. As will be seen later, the total forecast use of aircraft of the 747SP class by 1990 is modest (approximately 800 flight hours per day).

Trajectories used by SRI, based on FAA recommendations for the SSTs, are given in Fig. 2.2. For the 747SP, the FAA-recommended altitudes are given in Table 2.22.

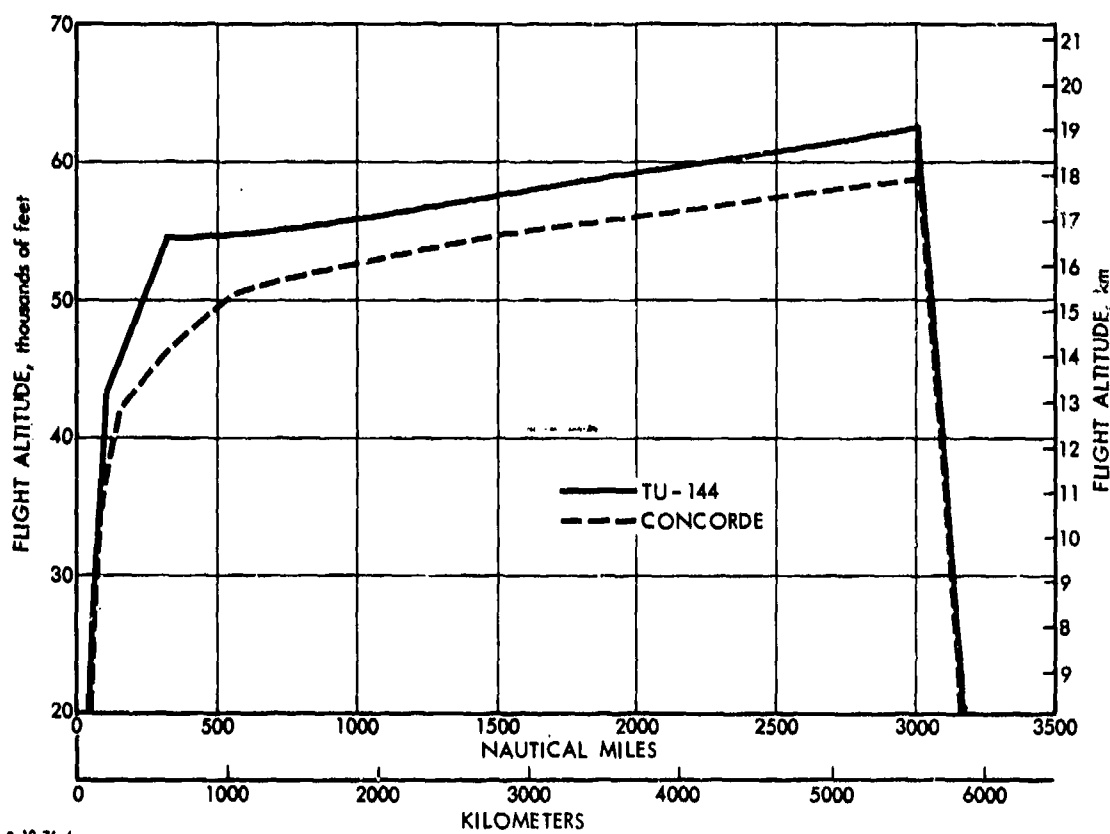


FIGURE 2.2. FLIGHT PATHS FOR CONCORDE AND TUPOLEV-144 SSTs
SOURCE: ICAO/OACI/NKAO, 1974

SRI assumed that, since most aircraft schedules are symmetric, as much time was spent going eastbound as westbound and adjusted flight hours at altitude accordingly. (Jet stream effects were apparently not included.) Ascent and descent times were treated separately, based on fixed time periods and rates for ascent and descent for each aircraft.

TABLE 2.22. TIME FRACTION-CRUISE ALTITUDES FOR 747SP
SOURCE: FAA, 1976

<u>Stage Lengths</u>	<u>Eastbound</u>	<u>Westbound</u>
0-2,000 miles	100% at 41,000 ft	100% at 43,000 ft
> 2,000 miles	50% at 37,000 ft	50% at 39,000 ft
	50% at 41,000 ft	50% at 43,000 ft

Data for other aircraft types were provided to SRI by FAA. By far the most heavily traveled band is the 10-km to 11-km band (32,800 to 36,100 ft). This is shown in the following data, included in the SRI report.

TABLE 2.23. FLIGHT HOUR ACTIVITY BY ALTITUDE STRATA*
SOURCE: Stanford Research Institute, 1976

<u>Altitude Stratum (km)</u>	<u>Daily Flight Hours</u>
6- 8	203
8- 9	485
9-10	898
10-11	1,314
11-12	433
12-13	99
13-14+	13

*These data are for June 1975 for the area over the Mid-western and Eastern United States. General aviation activity is excluded.

Note that this distribution is by flight hours, not by fuel consumption. Moreover, these data do not appear to agree with that shown in Table 2.8, where 60 percent of the fuel consumption (at 7.9 km and above) is in the 11-km to 12-km band, versus 13 percent (in flight hours) in this band in Table 2.23.

2.3.2 Results

Results obtained from the preceding studies follow. In the first set of these, the ADL results are given directly, i.e., as reported. In the second set, certain corrections to these results are made which appear to be called for on the basis of information reported or developed earlier in this report or elsewhere, as will be noted.

A. Fuels and Emissions Data as Reported

The as-reported data are summarized in Table 2.24.

TABLE 2.24. TOTAL AVERAGE FLIGHT HOURS/DAY, FUEL CONSUMPTION AND EMISSIONS/YEAR, ABOVE 6 km, 1975-1990,* NO TECHNOLOGY IMPROVEMENTS ON EMISSIONS. AS REPORTED.
SOURCE: Arthur D. Little, Inc., 1976

Item	1975	1980		1985		1990	
		Low	High	Low	High	Low	High
<u>Flight hr/day**</u>							
Total	24,625	30,266	34,010	36,295	47,484	44,402	68,849
SST	0	87.5	100.2	264.2	352.3	504.2	813.2
<u>Fuel, 10⁶ kg/yr</u>							
Total	45,540	62,250	70,150	83,520	110,590	109,780	173,660
SST	0	863	988	2,540	3,390	4,880	7,860
<u>Emissions, 10⁶ kg/yr</u>							
Total NO _x (as NO ₂)***	425	609	686	707	937	967	1,530
SST NO _x (as NO ₂)	0	13.1	15.0	39.2	52.3	75.1	121.2
Total H ₂ O	56,930	77,810	87,690	104,400	138,240	137,230	217,080
SST H ₂ O	0	1,080	1,235	3,175	4,240	6,100	9,825
Total SO _x (as SO ₂)	45.5	62.3	70.2	83.5	110.6	109.8	173.7
SST SO _x (as SO ₂)	0	0.863	0.988	2.54	3.39	4.88	7.86

*Note that, for internal consistency, more places are carried than are considered significant.

**Average of June and November forecasts; taken as yearly average.

***Subsonic NO_x emissions need to be reviewed. See footnote, Table 2.21.

These results are compared to the CIAP results in Table 2.25. Perhaps the most striking difference is in the fuel consumption estimates for subsonic aircraft, the FAA figures being about twice those of CIAP. Part of the difference is in the altitude bands employed; i.e., above 6 km with FAA and above 9 km by CIAP. However, in the FAA estimates, the fuel used above 9 km represents about 85 percent of the total subsonic fuel (based on 1990 figures), so this fact accounts for only a portion of the discrepancy. It was recognized during CIAP (and stated earlier, Section 2.2.1) that the CIAP model estimates for 1970 were low (see p. D-65, ROF), where 1970 fuel above 9 km was estimated at about twice the CIAP model figure. CIAP projections were, of course, primarily concerned with SST traffic; here it is of interest to note that the CIAP upper-bound case with only Concorde/Tupolev SSTs available utilizes considerably more SST fuel (12.6×10^9 kg/yr) than does the FAA "high" estimate case (7.89×10^9 kg/yr). The CIAP

"expected" case is not directly comparable, in that no estimate was made for this traffic with Concorde/Tupolev only available. However, if the CIAP 1990 "expected" fleet is taken as half the upper-bound fleet (based on fuel flows), it would appear that the CIAP "expected" fleet, with Concorde/Tupolev only, would have about the same SST usage as the FAA high estimate.

TABLE 2.25. FUEL CONSUMPTION COMPARISONS, CIAP AND FAA (10⁹ kg/yr)

	CIAP ^a		CIAP ^a		FAA ^b			
	Expected		Upper Bound		Low		High	
	Subsonic	SST	Subsonic	SST	Subsonic	SST	Subsonic	SST
1970	14.2	0	14.2	0	--	--	--	--
1975					45.5	0	45.5	0
1980	35.7	1.34 ^c	50.2	1.6 ^c	61.4	0.86	69.2	0.99
1985					81.0	2.54	107.3	3.39
1990	59.0 ^d	15.3 ^d	117.8 ^c 110.1 ^d	12.6 ^c 27.6 ^d	104.9	4.88	165.8	7.89

^aFrom 9 km up. Source: CIAP, ROF, pp. D-85 to D-88.

^bFrom 6 km up. Source: ADL. Approximately 15 percent of the total subsonic fuel is used in the 6-km to 9-km band.

^cConcorde/Tupolev assumed.

^dLarge advanced SST assumed.

CIAP SST fuel above 9 km (Concorde/Tupolev) is almost all (90 percent) in the 15-km to 18-km band; FAA SST fuel is only 59 percent (1990 high case) above 15 km in the total used above 9 km, or 50 percent of the total used above 6 km.

Growth rates can also be compared. The growth rate for subsonic travel 1970 to 1990 for the CIAP expected fleet is roughly 7 percent per year and for the CIAP upper-bound fleet roughly 11 percent per year, whereas the FAA fleet projections involve a growth rate (1975-1990) of 4 percent and 7 percent, respectively, for low and high projections. The CIAP "Concorde/Tupolev only" case involves SST growth rates (upper-bound) of 23 percent per year (1980-1990), whereas the FAA figures call for 19 percent and 23 percent, respectively, for low and high cases. As noted earlier, these growth rates were considered optimistic by SRI.

Fuel consumption and NO_x emissions by altitude band as reported are given for the 1990 high FAA fleet in Table 2.26. Longitudinal distributions of fuel consumption and NO_x emissions for the total fleet and for various aircraft of interest are given, again as reported, in Tables 2.27 and 2.28.

TABLE 2.26. FUEL CONSUMPTION AND NO_x EMISSIONS,
1990 HIGH FLEET. AS REPORTED.
SOURCE: Arthur D. Little, Inc., 1976

Altitude	Fuel, 10 ⁹ kg/yr		NO _x , 10 ⁶ kg/yr	
	Subsonic	SST	Subsonic*	SST
6- 8	10.67	0.652	110.98	7.17
8- 9	13.98	0.581	123.49	6.40
9-10	35.10	0.543	331.12	5.97
10-11	59.03	0.502	480.08	4.73
11-12	40.08	0.465	319.04	4.36
12-13	6.17	0.427	39.37	4.69
13-14	0.65	0.387	5.80	7.73
14-15		0.394		7.89
15-16		1.378		26.25
16-17		1.157		20.82
17-18		0.847		15.71
18-19		0.527		9.48
	165.68	7.860	1,409.88	121.20

*See footnote, Table 2.21.

Note (Tables 2.27 and 2.28) that the altitude distribution of SST NO_x emission differs somewhat from CIAP data. Thus, FAA peak NO_x emissions are in the 15-km to 16-km band, and extend into the 18-km to 19-km band. The higher altitude emissions (above 18 km) are presumably based on inclusion of higher flying (than Concorde) Tupolev aircraft in the fleet mix. In CIAP, NO_x emissions from current SSTs were assumed to be centered at 16.5 km, and not to extend above 18 km. Leach et al., at the 3rd Conference on CIAP (February 26 - March 1, 1974) also indicate peak SST (Concorde) fuel consumption and NO_x emissions to be in the 16-km to 17-km band, rather than in the 15-km to 16-km band as reported by ADL.

Note also (Table 2.23) that the total fuel used by subsonic aircraft in 1990 above 12 km is 6.82×10^9 kg/yr, of which 90 percent is in the 12-km to 13-km band. These figures can be compared to the figure of 15.3×10^9 kg/yr for the CIAP expected fleet (Table 2.9) in the 12-km to 15-km band.

Some further breakdown of the FAA figures is of interest: The FAA projections include 21 subsonic aircraft types, many of which are assumed to enter the 12-km to 13-km band (39,360 to 42,640 ft) a portion of the time. Only a few, however, are assumed to enter the 13-km to 14-km band. These are the 747SP, the 7X7, the "miscellaneous" category (of which the 737 is representative), and the Lear and Gulf business jets. Of these, two aircraft, the 747SP and the 7X7, may be considered to be advanced subsonics; "1990 high" data on these aircraft are given in Tables 2.27 and 2.28. Their projected growth is as shown in Table 2.29.

TABLE 2.27. 1990 WORLDWIDE AIRCRAFT NO_x EMISSIONS, HIGH FORECAST, kg/yr.
TOTAL AND THREE AIRCRAFT TYPES. AS REPORTED.
SOURCE: Arthur D. Little, Inc., 1976

FUEL	ALT (KM)	6-8	8-9	9-10	10-11	11-12	12-13	13-14	14-15	15-16	16-17	17-18	18-19
Total	N POLE	1.07E	2.81E	3.75E	3.94E	3.97E	3.97E	3.97E	3.97E	3.97E	3.97E	3.97E	3.97E
	50 TO 60	1.07E	2.81E	3.75E	3.94E	3.97E	3.97E	3.97E	3.97E	3.97E	3.97E	3.97E	3.97E
	40 TO 50	1.07E	2.81E	3.75E	3.94E	3.97E	3.97E	3.97E	3.97E	3.97E	3.97E	3.97E	3.97E
	30 TO 40	1.07E	2.81E	3.75E	3.94E	3.97E	3.97E	3.97E	3.97E	3.97E	3.97E	3.97E	3.97E
	20 TO 30	1.07E	2.81E	3.75E	3.94E	3.97E	3.97E	3.97E	3.97E	3.97E	3.97E	3.97E	3.97E
	10 TO 20	1.07E	2.81E	3.75E	3.94E	3.97E	3.97E	3.97E	3.97E	3.97E	3.97E	3.97E	3.97E
	0 TO 10	1.07E	2.81E	3.75E	3.94E	3.97E	3.97E	3.97E	3.97E	3.97E	3.97E	3.97E	3.97E
	-10 TO -20	1.07E	2.81E	3.75E	3.94E	3.97E	3.97E	3.97E	3.97E	3.97E	3.97E	3.97E	3.97E
	-20 TO -30	1.07E	2.81E	3.75E	3.94E	3.97E	3.97E	3.97E	3.97E	3.97E	3.97E	3.97E	3.97E
	-30 TO -40	1.07E	2.81E	3.75E	3.94E	3.97E	3.97E	3.97E	3.97E	3.97E	3.97E	3.97E	3.97E
	-40 TO -50	1.07E	2.81E	3.75E	3.94E	3.97E	3.97E	3.97E	3.97E	3.97E	3.97E	3.97E	3.97E
	-50 TO -60	1.07E	2.81E	3.75E	3.94E	3.97E	3.97E	3.97E	3.97E	3.97E	3.97E	3.97E	3.97E
	S POLE	1.07E	2.81E	3.75E	3.94E	3.97E	3.97E	3.97E	3.97E	3.97E	3.97E	3.97E	3.97E
TOTAL OF ALL FUEL = 1.7366E 11 (KILOGRAMS/YEAR)													
AIRCRAFT TYPE 10 (753)	ALT (KM)	6-8	8-9	9-10	10-11	11-12	12-13	13-14	14-15	15-16	16-17	17-18	18-19
	N POLE	3.66E	7.32E	9.76E	1.01E	1.01E	1.01E	1.01E	1.01E	1.01E	1.01E	1.01E	1.01E
	50 TO 60	3.66E	7.32E	9.76E	1.01E	1.01E	1.01E	1.01E	1.01E	1.01E	1.01E	1.01E	1.01E
	40 TO 50	3.66E	7.32E	9.76E	1.01E	1.01E	1.01E	1.01E	1.01E	1.01E	1.01E	1.01E	1.01E
	30 TO 40	3.66E	7.32E	9.76E	1.01E	1.01E	1.01E	1.01E	1.01E	1.01E	1.01E	1.01E	1.01E
	20 TO 30	3.66E	7.32E	9.76E	1.01E	1.01E	1.01E	1.01E	1.01E	1.01E	1.01E	1.01E	1.01E
	10 TO 20	3.66E	7.32E	9.76E	1.01E	1.01E	1.01E	1.01E	1.01E	1.01E	1.01E	1.01E	1.01E
	0 TO 10	3.66E	7.32E	9.76E	1.01E	1.01E	1.01E	1.01E	1.01E	1.01E	1.01E	1.01E	1.01E
	-10 TO -20	3.66E	7.32E	9.76E	1.01E	1.01E	1.01E	1.01E	1.01E	1.01E	1.01E	1.01E	1.01E
	-20 TO -30	3.66E	7.32E	9.76E	1.01E	1.01E	1.01E	1.01E	1.01E	1.01E	1.01E	1.01E	1.01E
	-30 TO -40	3.66E	7.32E	9.76E	1.01E	1.01E	1.01E	1.01E	1.01E	1.01E	1.01E	1.01E	1.01E
	-40 TO -50	3.66E	7.32E	9.76E	1.01E	1.01E	1.01E	1.01E	1.01E	1.01E	1.01E	1.01E	1.01E
	-50 TO -60	3.66E	7.32E	9.76E	1.01E	1.01E	1.01E	1.01E	1.01E	1.01E	1.01E	1.01E	1.01E
	S POLE	3.66E	7.32E	9.76E	1.01E	1.01E	1.01E	1.01E	1.01E	1.01E	1.01E	1.01E	1.01E
AIRCRAFT TYPE 15 (737)	ALT (KM)	6-8	8-9	9-10	10-11	11-12	12-13	13-14	14-15	15-16	16-17	17-18	18-19
	N POLE	5.75E	1.15E	1.53E	1.53E	1.53E	1.53E	1.53E	1.53E	1.53E	1.53E	1.53E	1.53E
	50 TO 60	5.75E	1.15E	1.53E	1.53E	1.53E	1.53E	1.53E	1.53E	1.53E	1.53E	1.53E	1.53E
	40 TO 50	5.75E	1.15E	1.53E	1.53E	1.53E	1.53E	1.53E	1.53E	1.53E	1.53E	1.53E	1.53E
	30 TO 40	5.75E	1.15E	1.53E	1.53E	1.53E	1.53E	1.53E	1.53E	1.53E	1.53E	1.53E	1.53E
	20 TO 30	5.75E	1.15E	1.53E	1.53E	1.53E	1.53E	1.53E	1.53E	1.53E	1.53E	1.53E	1.53E
	10 TO 20	5.75E	1.15E	1.53E	1.53E	1.53E	1.53E	1.53E	1.53E	1.53E	1.53E	1.53E	1.53E
	0 TO 10	5.75E	1.15E	1.53E	1.53E	1.53E	1.53E	1.53E	1.53E	1.53E	1.53E	1.53E	1.53E
	-10 TO -20	5.75E	1.15E	1.53E	1.53E	1.53E	1.53E	1.53E	1.53E	1.53E	1.53E	1.53E	1.53E
	-20 TO -30	5.75E	1.15E	1.53E	1.53E	1.53E	1.53E	1.53E	1.53E	1.53E	1.53E	1.53E	1.53E
	-30 TO -40	5.75E	1.15E	1.53E	1.53E	1.53E	1.53E	1.53E	1.53E	1.53E	1.53E	1.53E	1.53E
	-40 TO -50	5.75E	1.15E	1.53E	1.53E	1.53E	1.53E	1.53E	1.53E	1.53E	1.53E	1.53E	1.53E
	-50 TO -60	5.75E	1.15E	1.53E	1.53E	1.53E	1.53E	1.53E	1.53E	1.53E	1.53E	1.53E	1.53E
	S POLE	5.75E	1.15E	1.53E	1.53E	1.53E	1.53E	1.53E	1.53E	1.53E	1.53E	1.53E	1.53E

TABLE 2.28. 1990 WORLDWIDE AIRCRAFT NO. EMISSIONS, HIGH FORECAST, kg/yr. TOTAL AND THREE AIRCRAFT TYPES. AS REPORTED.
SOURCE: Arthur D. Little, Inc., 1976

SOURCE: Arthur D. Little, Inc., 1976

SOURCE: Arthur

[illegible]

Total of all NO₂ = 1.53123 E 9 kg/yr

[illegible]

AIRCRAFT TYPE	0-2	8-9	9-10	10-11	11-12	12-13	13-14	14-15	15-16	16-17	17-18	18-19
ALT (KV)												
LATITUDE												
N POLE	1-33E	1-11E	0-07E	7-33E	2-11E	7-33E	5-42E	0	00	00	00	0
30 TO 60	0-23E	0-04E	0-07E	7-33E	2-11E	7-33E	5-42E	0	00	00	00	0
60 TO 90	3-44E	2-32E	0-07E	1-06E	0-05E	2-35E	0-05E	0000	00	00	00	0
90 TO 120	0-00E	0-00E	0-00E	0-00E	1-06E	1-06E	1-06E	0000	00	00	00	0
120 TO 150	0-00E	0-00E	0-00E	0-00E	0-00E	0-00E	0-00E	0000	00	00	00	0
150 TO 180	0-00E	0-00E	0-00E	0-00E	0-00E	0-00E	0-00E	0000	00	00	00	0
-10 TO 10	0-00E	0-00E	0-00E	0-00E	0-00E	0-00E	0-00E	0000	00	00	00	0
-20 TO 10	0-00E	0-00E	0-00E	0-00E	0-00E	0-00E	0-00E	0000	00	00	00	0
-30 TO 10	0-00E	0-00E	0-00E	0-00E	0-00E	0-00E	0-00E	0000	00	00	00	0
-40 TO 10	0-00E	0-00E	0-00E	0-00E	0-00E	0-00E	0-00E	0000	00	00	00	0
-50 TO 10	0-00E	0-00E	0-00E	0-00E	0-00E	0-00E	0-00E	0000	00	00	00	0

[illegible]

TABLE 2.29. GROWTH IN ADVANCED SUBSONICS, 747SP CLASS AND 7X7 CLASS, FLIGHT HOURS PER DAY
SOURCE: Stanford Research Institute, 1976

<u>Year</u>	<u>747SP Class</u>		<u>7X7 Class</u>	
	<u>Low</u>	<u>High</u>	<u>Low</u>	<u>High</u>
1975	0	0	0	0
1980	145.32	163.42	0	0
1985	443.03	586.09	1,895.10	2,516.32
1990	527.83	833.83	6,623.76	10,444.67

The 7X7 class of aircraft is thus postulated to grow rapidly, replacing certain other aircraft in the process. However, the 7X7 is not postulated to spend an appreciable portion of its cruise at high altitudes, as does the 747SP. The estimates are given in Tables 2.30 and 2.31.

TABLE 2.30. ALTITUDE DISTRIBUTION OF FLIGHT HOURS FOR 747SP AND 7X7 CLASSES
SOURCE: Arthur D. Little, Inc., 1976

<u>Altitude</u>	<u>747SP*</u>	<u>7X7*</u>	
		<u>1985</u>	<u>1990</u>
10-11	0.011	0.323	0.328
11-12	0.479	0.310	0.270
12-13	0.239	0.0738	0.0811
13-14	0.237	0.0170	0.0120

*The distribution for the 747SP is almost invariant with time.

TABLE 2.31. FUEL CONSUMPTION ESTIMATES FOR ADVANCED SUBSONICS IN HIGH ALTITUDE BANDS, 10^9 KG/YR, 1990 HIGH FLEET
SOURCE: Arthur D. Little, Inc., 1976

	<u>Total Subsonic</u>	<u>747SP</u>	<u>7X7</u>
10-11	59.03	0.039	7.63
11-12	40.08	1.408	5.64
12-13	6.17	0.580	1.425
13-14	0.647	0.441	0.173

According to these data, the 7X7 and 747SP will (in 1990) burn 95 percent of the fuel used by subsonics in the 13-km to 14-km band. The 747SP itself will use 68 percent of the total; a small additional amount will be used by "miscellaneous" and business jet categories. These aircraft (the 747SP and 7X7) use only one-third of the total fuel in the 12-km to 13-km band, however, and lesser fractions below that.

The relative NO_x contribution by these various classes of aircraft depends, of course, on their emission indices. With the ADL emission index numbers (see Table 2.21), the 747SP class contributes a greater fraction of total NO_x emissions than indicated in Table 2.31.

B. Modified Emissions Estimates

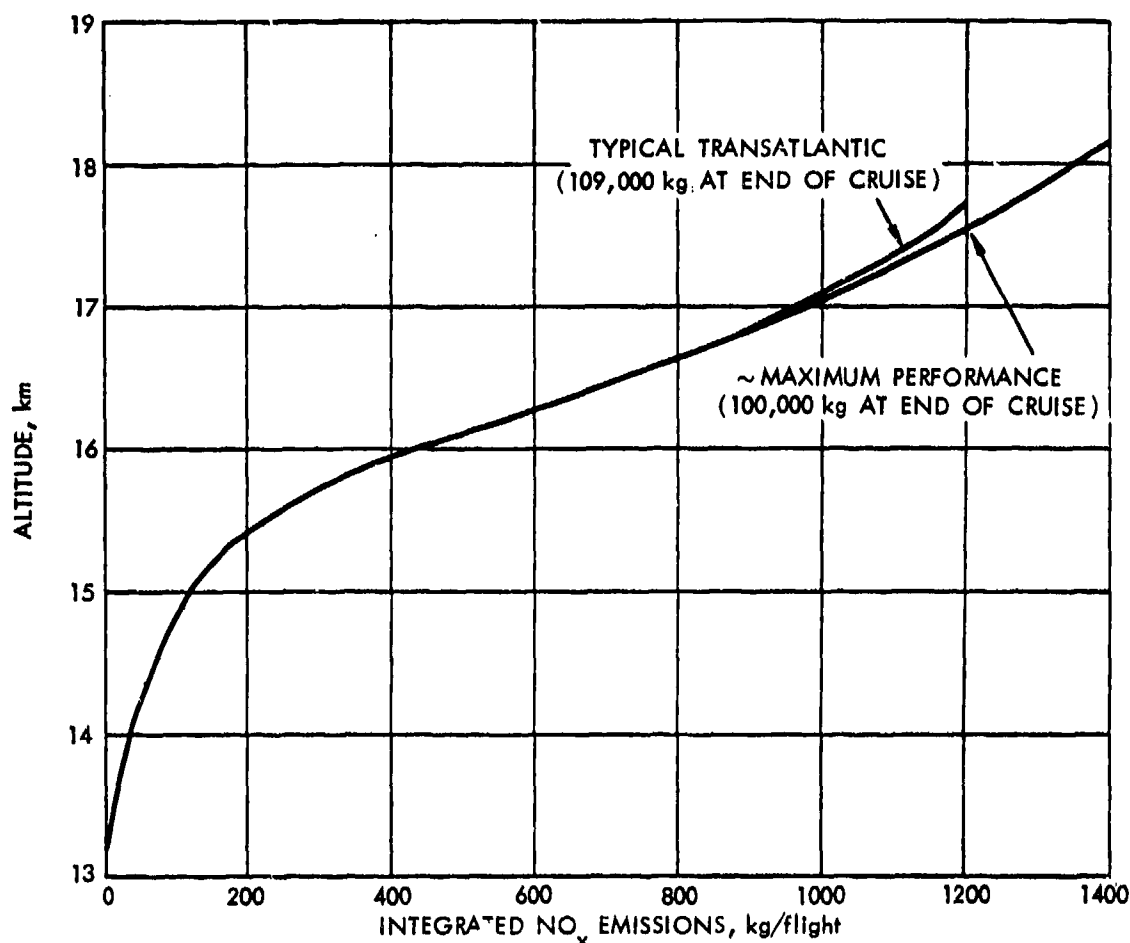
It has been noted* that the NO_x emission index used by ADL for CF6-engined aircraft appears to be low by a factor of about 4; it is our understanding, based on data in CIAP Monograph 2, that the CF6 and the JT9D engines have similar NO_x emission characteristics. It was also noted that the distribution in a vertical sense of NO_x emissions from Concorde was weighted towards lower altitudes than reported by Leach et al. (1974), of British Aircraft Corp. An independent (IDA) estimate was thus made of the Concorde distributions using Rolls-Royce published data by C. J. Scott (1974), with derived results as shown in Fig. 2.3. The data shown apply after reheat cutoff at 13.2-km altitude for ISA** conditions for two cases, one of which (109,000 kg end-of-cruise weight) corresponds to the North Atlantic run; the other is for a limiting altitude-range case, with lesser reserves. No data are available for shorter runs. The data given in Fig. 2.3 can be broken into whatever altitude increments are desired. The average Concorde emission index, computed by IDA from fuel flow data provided by Scott and the integrated NO_x emissions, corresponds to about 20 g NO_2 /kg fuel--about 10 percent higher than the value quoted in CIAP and elsewhere in this document.

Scott (1974) does not provide estimates of emissions during the descent phase, but these should be small; he also does not provide emissions during the time afterburners are operating below 13.2 km. Substantial quantities of fuel are burned during the initial acceleration phase, but because of the low altitude involved, effects on ozone are probably small. (See, however, Appendix A.) Also, Scott assumed a 0.6 power of NO_x emission index with pressure, which he cautioned might be high, but the measured values under simulated conditions seemed to agree reasonably well with the predicted figures. He included a +12 percent correction on measured NO_x values to correct the stratospheric humidity conditions. Scott also provides curves for various other ISA conditions; at higher (than ISA) temperatures the aircraft flies lower (and may need to off-load to obtain the necessary range). Seasonal effects may thus enter in computing altitude distributions of emissions. (See Section 2.4.)

Based on these and other relevant data, a revised set of figures (Table 2.28) was generated for NO_x emissions only, and for the 1990-high case only. The procedures used were as follows:

* See footnote on Table 2.21.

**International Standard Atmosphere Supplement, 1966.



3-2-77-3

FIGURE 2.3. CONCORDE TOTAL NO_x EMISSIONS, kg/FLIGHT
ABOVE 13.2 km (after reheat cutoff), ISA
CONDITIONS
SOURCE: Developed from data published by
C. J. Scott, 1974

1. The NO_x emissions for CF6-engined aircraft in each altitude-latitude box (ADL, 1976, pp. C-18 to C-24) were summed separately for (a) aircraft types 6, 7, and 13; and (b) for aircraft types 15 and 17, these groups having slightly different reported emission indices (p. 10). (See Table 2.19.) The incremental NO_x rate for each group was then calculated, assuming the same emission indices as given for the JT9D at the specified altitude. These two incremental rates were then summed and added to the reported total (Table 2.28).*

*The incremental rate for NO_x (kg/yr) for each aircraft in each box is simply the reported rate times the ratio

$$\left(\frac{E.I._{JT9D}}{E.I._1} - 1 \right)$$

where E.I._{JT9D} is the emission index (at the given altitude for the JT9D), and E.I.₁ is the quoted emission for the 1th aircraft.

2. The distribution of emissions with altitude for the SST was revised in rough accordance with the data in Fig. 2.4 by shifting the emissions in the 17-km to 18-km band into the 15-km to 16-km band and the other two up 1 km. No change was made to the 18-km to 19-km band or 14-km to 15-km band. The following data (Table 2.32) provided the justification for this redistribution.

TABLE 2.32. COMPARISON FOR SST EMISSION DISTRIBUTION ESTIMATES (15-km TO 18-km BAND)

Altitude, km	ADL, p. E-19		IDA		Leach et al., ³ 1974	
	NO _x	Percent ²	Fig. 2.2 ¹	Percent ²	45-60°N	Percent ²
15-16	2.625E7	41.8	23.0	25.1	22.5	25.2
16-17	2.082E7	33.1	40.0	43.7	45.6	51.1
17-18	1.571E7	25.0	28.5	31.1	21.1	23.7
Total	6.278E7					

¹Concorde only

²Normalized

³Report on 3rd CIAP Conference, p. 77, Fig. 22

No change was made to the altitude distribution of subsonic emissions, even though they appeared somewhat questionable, as noted earlier.

Leach et al. put about half the 15-km to 18-km NO_x emissions from Concorde in the 16-km to 17-km band, with about equal amounts above and below. About 44 percent are in this band, with somewhat more above than below, based on Scott's data (Fig. 2.2). ADL puts only 33 percent in this band. Also, the FAA fleet includes some TU-144s (number unspecified) which should increase emissions in the 17-km to 18-km band as well as put some in the 18-km to 19-km band. It thus seemed reasonable to adjust the quoted 15-km to 16-km and 16-km to 17-km band emissions as indicated above. The distribution becomes about as estimated for Concorde (Fig. 2.2), but with somewhat more in the 17-km to 18-km band than estimated by Leach.

The summarized results are shown in Table 2.33. Obviously, the revised figures should all be rechecked.

2.3.3 Fleet Size Estimates

The preceding results are based on average flight hours per day. The number of aircraft required is also of interest. These have been provided for the low or base case by B. Hannon of FAA, and are given in Table 2.34.

TABLE 2.33. 1990 WORLDWIDE AIRCRAFT NO_x EMISSIONS, HIGH ESTIMATE, ADJUSTED^{1,2}; kg/yr

Latitude	6-8	8-9	9-10	10-11	11-12	12-13	13-14	14-15	15-16	16-17	17-18	18-19	Total
N 60+	3.35E6	3.03E6	1.43E7	1.31E7	1.46E7	1.31E6	9.99E5	4.06E5	1.72E6	2.59E6	2.10E6	1.43E6	5.894E7
50-	2.15E7	2.59E7	9.44E7	1.06E8	9.09E7	8.26E6	3.72E6	2.12E6	6.57E6	1.03E7	8.06E6	3.71E6	3.814E8
40-	7.60E7	8.70E7	1.79E8	2.79E8	1.62E8	2.49E7	4.59E6	2.09E6	4.17E6	6.96E6	5.46E6	2.36E6	8.334E8
30-	7.74E7	9.20E7	1.67E8	3.09E8	1.72E8	2.97E7	3.11E6	1.74E6	1.30E6	2.73E6	2.07E6	8.63E5	8.589E8
20-	2.61E7	2.83E7	6.74E7	1.02E8	6.92E7	8.73E6	1.55E6	1.20E6	8.06E5	1.90E6	1.71E6	4.67E5	3.094E8
10-	1.11E7	1.18E7	2.65E7	4.28E7	3.99E7	3.67E6	4.74E5	1.54E5	3.24E5	5.38E5	4.22E5	1.71E5	1.379E8
0-	4.80E6	5.14E6	1.50E7	1.82E7	1.36E7	1.26E6	1.73E5	0	2.91E5	4.08E5	3.44E5	1.63E5	5.938E7
0-	3.31E6	3.77E6	1.22E7	1.38E7	1.09E7	8.65E5	1.38E5	0	3.01E5	4.22E5	3.56E5	1.65E5	4.623E7
10-	2.74E6	3.21E6	1.14E7	1.52E7	1.15E7	1.11E6	3.15E5	1.32E5	1.10E5	2.19E5	1.58E5	7.52E4	4.617E7
20-	3.67E6	4.01E6	9.47E6	1.37E7	8.66E6	9.31E5	5.10E4	0	9.85E4	1.38E5	1.16E5	6.63E4	4.091E7
30-	4.01E6	4.63E6	6.62E6	1.18E7	6.14E6	1.21E6	8.64E4	5.16E4	1.56E4	4.47E4	2.84E4	6.22E3	3.464E7
40-	2.36E5	3.05E5	3.19E5	8.28E5	4.46E5	9.29E4	1.5 E1	0	0	0	0	0	2.227E6
50-	4.77E4	3.79E4	2.99E4	2.52E4	1.04E4	1.45E3	0.97	0	0	0	0	0	1.526E5
S 60+	0	0	0	0	0	0	0	0	0	0	0	0	0
Total	2.343E8	2.691E8	6.036E8	9.255E8	5.999E8	8.197E7	1.521E7	7.894E6	1.571E7	2.625E7	2.082E7	9.477E6	2.810E9

Reference: ADL (1976), p. E-19

¹To make all "CF-6" aircraft have same emission indices as "JT-9D" aircraft.

²To distribute SST emissions in the 15-18 km band more closely to prior estimates.

TABLE 2.34. WORLD AIR CARRIER FLEET TURBOJET
COMPOSITION (1990 BASE FORECAST)*
SOURCE: FAA

	<u>Year</u>			
	<u>1975</u>	<u>1980</u>	<u>1985</u>	<u>1990</u>
<u>Supersonic</u>				
4 engine	--	20	47	88
<u>Wide Body</u>				
4 engine	240	414	741	1,103
3 engine	260	845	1,311	2,067
2 engine	5	35	765	855
<u>Standard Body</u>				
4 engine	1,464	834	415	--
3 engine	1,285	1,188	872	593
2 engine	2,375	1,075	569	132
(Other)	--	1,206	1,488	1,883
Total	5,629	5,617	6,208	6,721

*Source: B. Hannon, FAA, 20 August 1976.

A corresponding estimate for the "high case" is not available. On the basis of aircraft hours per day, however, the SST figure, which may be of greatest interest, would be $\frac{813}{504} \times 88$ or 142 aircraft in 1990.

The fuel consumption (kg) per SST per year in the FAA analysis is higher than in the earlier CIAP analysis. This is evident from the data in Table 2.25 $\left(\frac{4.88 \times 10^9}{88} \times .85 = 4.71 \times 10^7\right)$ vs that in Table 2.11 $\left(\frac{12.6 \times 10^9}{378} = 3.33 \times 10^7\right)$. The FAA estimate evidently assumes more hours per day per aircraft above 12 km than did CIAP. The CIAP estimate for the 1990-"High" fuel flow would be 201 SSTs.

2.4 A WORD ABOUT FLIGHT ALTITUDES

Altitudes used by aircraft, and quoted heretofore, are not true geometric altitudes above sea level, except in rare circumstances. Aircraft, in the absence of other constraints, operate at defined "pressure-altitudes," these being the indicated altitudes when a pressure altimeter is set at 1,013.25 mbar at sea level and calibrated with the standard atmosphere; a table of values is given in Table 5.3 of the U.S. Standard Atmosphere Supplements (1966). The "standard atmosphere" used is invariant with season and locale, as necessary for flight safety; geometric or absolute altitudes, of course, will vary, perhaps as much as 1/2 km or more above or below the nominal flight altitude. For example, an aircraft operating at 193 mbar, with a pressure altitude of 12.010 km, would

have a geopotential altitude (which is nearly the geometric altitude in this region of the atmosphere) of 11.214 km at 75° N in January and of 12.635 km at 30° N in July.

In some cases, as with the Concorde, additional complications enter; the turbine inlet temperature, e.g., cannot exceed recommended values. Where ambient temperatures are higher than standard values, this limits mach number, which in turn forces lower cruise altitudes (by as much as 2 km) (see Scott, 1974), off-optimum operating conditions, and use of reduced payloads. The altitude distribution as a function of season, including any variations in flight frequency and in weather (which must be treated statistically), becomes a matter of considerable complexity.

The pressure-altitude versus geometric-altitude question is of significance in modeling (for models set up in geometric coordinates), but the limited resolution of available models, the concentration of traffic in mid-latitudes, and the recognized presence of other uncertainties has precluded their inclusion to date.

2.5 CONCLUDING COMMENTS

The foregoing NO_x emission estimates are based on probe-sampling techniques. It should be reemphasized that these may be low by a factor of 2 to 5, judging by results from an *in situ* UV absorption method (see Section 2.2.3). This is an obviously critical uncertainty and must be resolved.

Note also that a number of significant differences are evident between the 1974/CIAP and current SRI/ADL/FAA projections as to aircraft operations. These can be summarized as follows:

1. The annual fuel consumed by subsonic aircraft, according to the ADL/FAA figures, is about twice as great as that estimated with the CIAP model. The low altitude (below 12 km) emissions of pollutants are correspondingly greater.
2. The fuel consumed by subsonic aircraft at altitudes above 12 km is considerably less in the FAA results than in the CIAP results, and weighted more closely to 12 km.
3. The CIAP projections emphasized a mach 2.7 advanced SST beyond about 1985. No such vehicle is now expected by 1990, the end point of the FAA projections.
4. According to FAA projections, the growth rate of SST travel, with only the Concorde/Tupolev available, is modest, calling for only 88 (as a low or base estimate) to 142 (as a high estimate) such aircraft by 1990. No directly comparable figures are available from CIAP, but the "high" estimate here would appear to be about the same as the "expected" estimate in CIAP.

5. NO_x emission estimates are in need of reexamination, not only because of the measurement uncertainties noted herein, but also because of questions that became evident while preparing this section, questions that led to the preparation of the "modified" fleet emissions included herein (Section 2.3.2-b and Table 2.33). The altitude distribution of emissions is rather critical; it is noted in later material herein (cf. Appendix A) that NO_x emissions appear to have opposite effects on the ozone column above and below about 14 km. Seasonal distributions, and altitude distribution changes with season, may also be significant.

3. EFFECTS OF AIRCRAFT EXHAUST PRODUCTS (PRINCIPALLY NO_x) ON THE OZONE COLUMN

3.1 INTRODUCTION

This chapter reviews available published studies and recent results (obtained under HAPP) on the effects aircraft exhaust products may have on the ozone column. The principal component of interest in such exhaust is NO_x ($\text{NO} + \text{NO}_2$), and most studies have dealt only with effects of NO_x . Some fragmentary information is, however, available on effects of water vapor. Emphasis here is on model results and interpretation of aircraft effects, rather than on the models themselves.

This review begins with some background material (Section 3.2) on ozone production and destruction, emphasizing stratospheric ozone. The effects that changes in the ozone column at various latitudes and seasons would have on the flux of "damaging ultraviolet" [or DUV, (NAS, 1976, 1976a)], which is associated with sunburn and skin cancer, are indicated briefly.

The modeling problem is then discussed in general terms (Section 3.3). Detailed modeling results follow in Section 3.4, in essentially chronological order, beginning with results published in the CIAP ROF (1974) and the NAS (1975) reports. The COMESA (1975) results are then reviewed briefly, with more details provided in Appendix B. More recent work, most of which has been carried out under HAPP, is then described. This more recent work includes time-dependent effects using a 1-D model, and effects of added or revised chemistry (methane oxidation reactions, chlorine effects, etc.). A discussion of effects of uncertainties in results due to reaction rate uncertainties is included. Finally, a recent 2-D model result for an FAA "1990 high" fleet is described; in this run, chlorine chemistry was not included but methane oxidation reactions and use of certain revised kinetics were included.

As will be described, inclusion of the methane oxidation reactions (possibly when coupled with minor changes in reaction rates), gives results for NO_x injections that indicate subsonic aircraft, in general, will increase rather than decrease [as in CIAP (1974); NAS (1975)] the ozone column. As zonal averages are involved in the results, however, the question arises regarding the distribution within the zone of the enhancements in ozone column. This question is discussed in Section 3.5.

The question of model validation, particularly for 1-D models, is discussed in Section 3.6. A summing up is then added as the final section (3.7).

3.2 BACKGROUND

3.2.1 Stratospheric vs Tropospheric Ozone

The great bulk of the protective ozone column is in the stratosphere, as is evident from Fig. 3.1. (The stratosphere was, in fact, once known as the "ozonosphere.") For this reason, when effects of supersonic aircraft, which would cruise well into the lower stratosphere, came under investigation (as in CIAP), emphasis was quite naturally on stratospheric ozone and the chemistry pertinent to it. For lower altitude flight, however, as is the case for subsonic aircraft, methane oxidation reactions, which form ozone in the troposphere, become significant, so that both stratospheric and tropospheric ozone chemistry must be treated in computing effects on the ozone column. The possible importance of these reactions was noted by Johnston and Quitevis (1974), and by Crutzen (1973), but were not included in CIAP ROF (1974), or NAS (1975), calculations; the COMESA (1975) effort considered them briefly. The importance of these reactions is evident from results to be reported later herein.

Tropospheric ozone is highly variable and its sources and sinks a matter of much current debate (see, e.g., Chameides and Stedman, 1976), and much work remains to be done. No attempt is made here to review the controversies and complexities in the general tropospheric ozone question. Rather, and what appears to be of more interest, the treatment is limited to the incremental ozone computed by modeling studies, based on methane oxidation and associated reactions. These reactions are probably, although not assuredly, the principal ones of interest at the altitudes at which typical subsonic aircraft cruise.

Stratospheric ozone is reviewed briefly in the following section.

3.2.2 Stratospheric Ozone

The stratospheric ozone question has intrigued researchers for many years, and while a great deal of progress has been made in recent years, it is clear that significant uncertainties remain. The problems are extremely complex and certain important aspects extremely sensitive, for example, to what appear to be minor uncertainties in reaction rates (as will be discussed in Section 3.4.6). These matters are treated in considerable detail elsewhere (Johnston, 1975; NAS, 1975; CIAP Monograph 1, 1975; Duewer et al., 1976a). A brief recapitulation, however, from the viewpoint of this work, seems appropriate.

The observed facts about ozone, based on NAS (1975), are indicated in sample form in Figs. 3.2, 3.3, 3.4, and 3.5, supplementing Fig. 3.1. Note in Figs. 3.2 and 3.3 that the ozone concentration (mol/cm^3) and the ozone column are at a maximum in the spring in the polar regions, and that (Fig. 3.4) there is considerable variability on various time scales, including those of the solar cycle. The maximum mixing ratio (molecules of O_3 /molecules of air), Fig. 3.5,

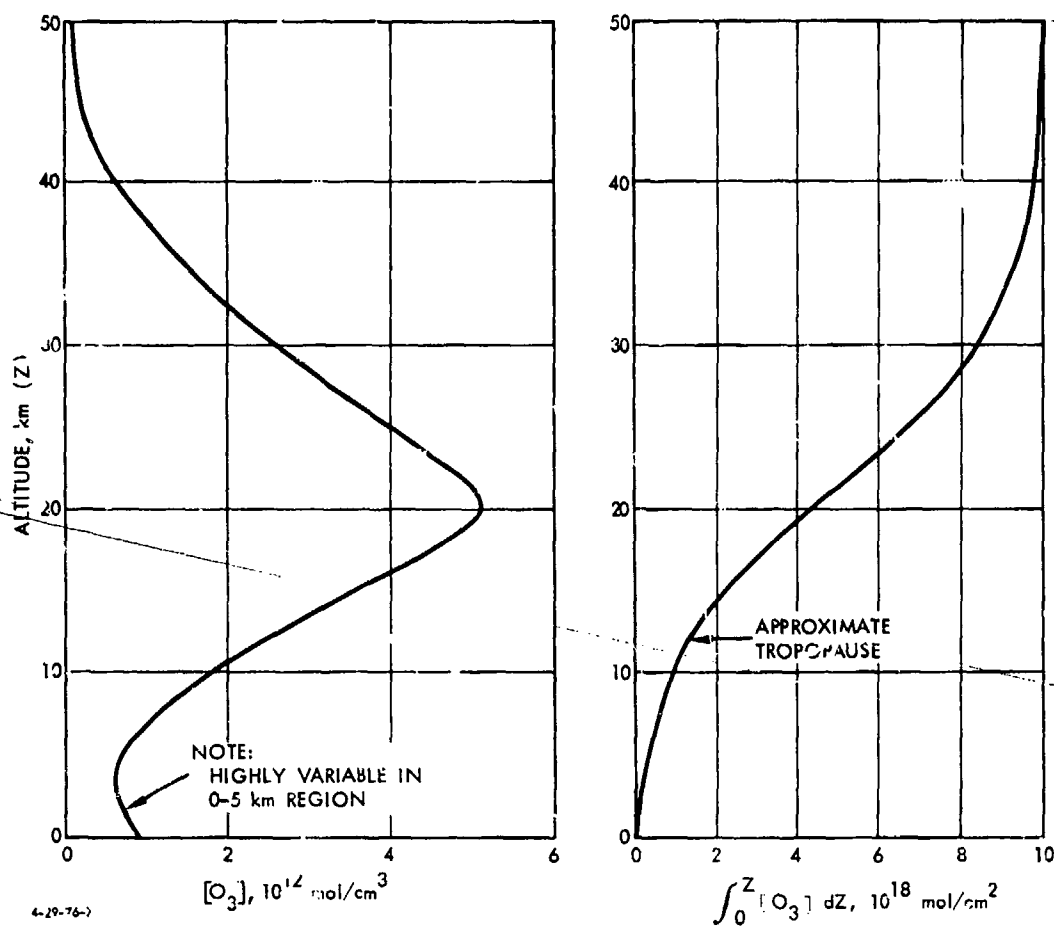
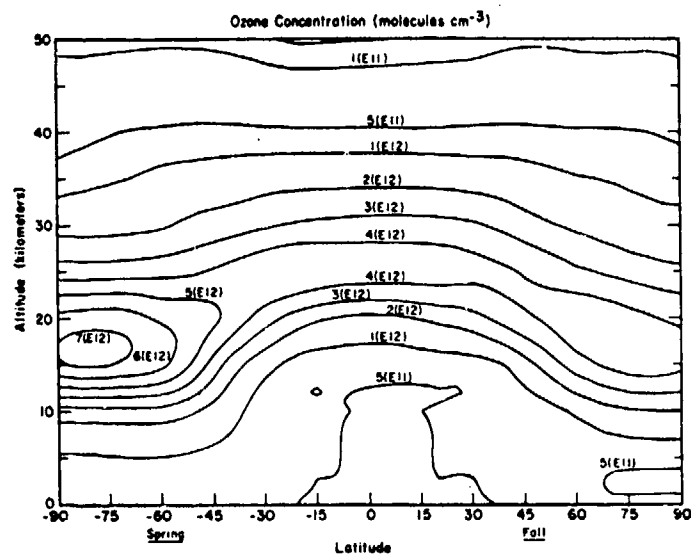


FIGURE 3.1. Ozone Distribution and Column Totals
(22 March, 45° N)
Source: after N.S., 1975 (Fig. A-9)

usually is found in the tropics, near about 30 km, although higher mixing ratios (up to 23 ppm) have been reported in small regions of the polar stratosphere (Heath, 1974) near 4 mbar, following a major stratospheric warming, suggesting unaccounted-for sources of ozone. The problem faced by atmospheric scientists is to explain the observed distributions of ozone in a time-dependent, three-dimensional (3-D) sense.

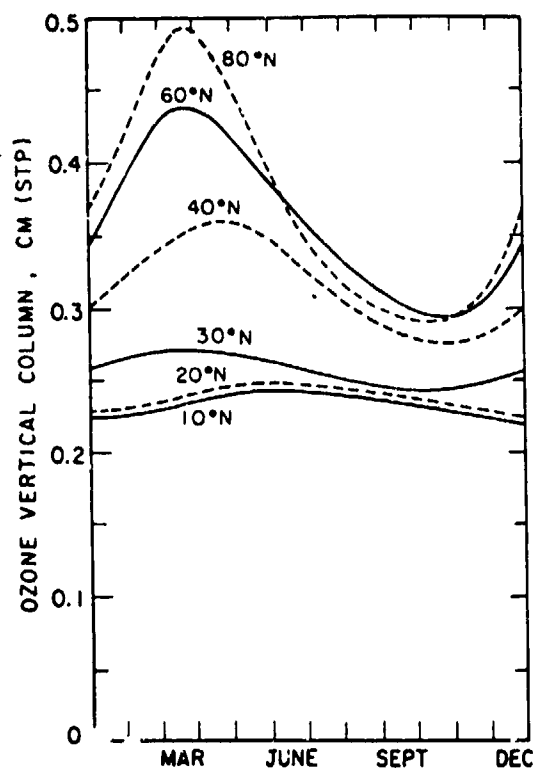
As Johnston (1975) points out, the ozone "problem" can be approached in two ways, depending on what one wishes to deduce. Thus, one can approach the problem in a very fundamental sense, using a combination of radiation data, photochemistry, and dynamics, to determine whether the ozone distribution can be matched. This approach, including dynamics, is clearly necessary if one wishes to determine the effects of a perturbing pollutant source, for the rate at which



3-2-77-10

FIGURE 3.2. Average (March 22) Ozone Concentration in Units of Molecules cm^{-3} Expressed as Zonal-Average Contour Lines (7E12 means 7×10^{12}). The variation of the ozone maximum with latitude can be read from the figure. The large concentration in the lower, spring, polar stratosphere is consistent with Fig. 3.3 below.

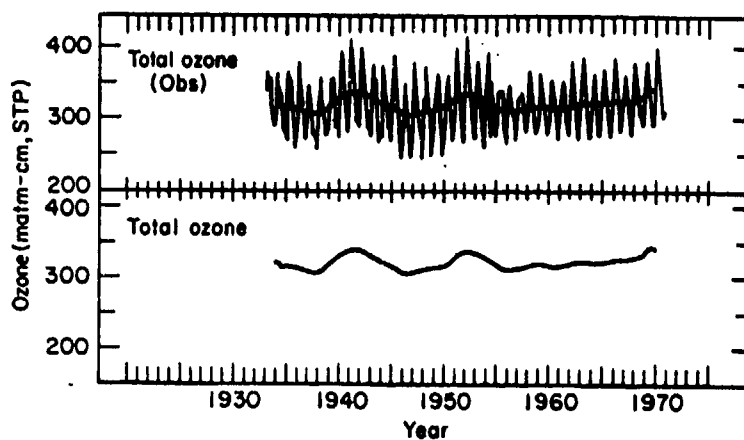
Source: NAS, 1975, p. 102



3-2-77-11

FIGURE 3.3. Variation of Integrated Vertical Ozone Column with Season at Tropical, Temperate, and Polar Zones.

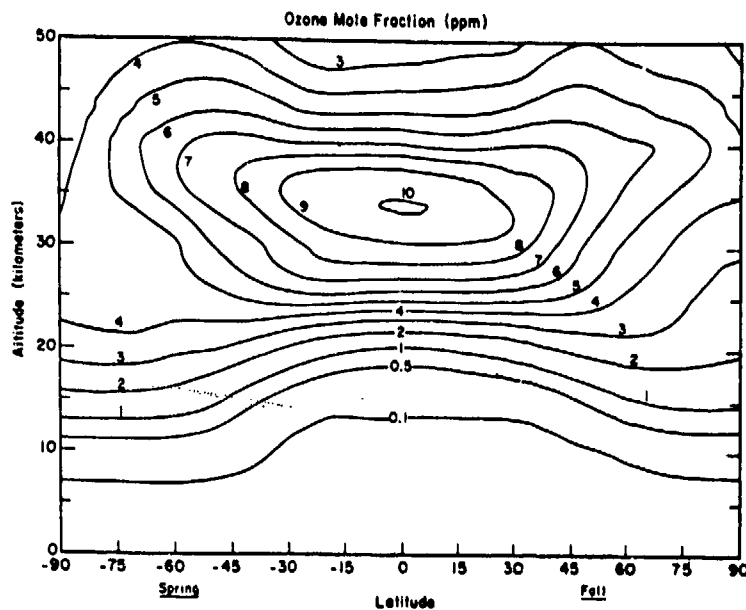
Source: NAS, 1975, p. 120



3-2-77-12

FIGURE 3.4. Long-Term Variations in Total Ozone in the Northern Hemisphere. The sharp seasonal variations are shown in the top panel. An 11-year running mean is inscribed in the top panel and repeated in the bottom panel. A possible 11-year cycle is indicated before 1960. An increasing trend is indicated for 1960-1970, but the 1970 high value is still less than high values before 1960. It is generally recognized that the data base before 1960 is too sparse to offer firm support to these suggested long-term trends.

Source: NAS, 1975, p. 121



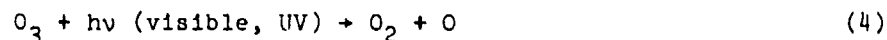
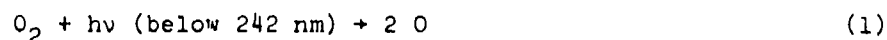
3-2-77-13

FIGURE 3.5. Average (March 22) Ozone Mole Fractions or Mixing Ratio by Volume (ppm)

Source: NAS, 1975, p. 123.

such materials are removed from (and distributed through) the stratosphere is critical to the problem. However, if one wishes simply to understand the factors controlling formation and destruction of ozone in the existing stratosphere, one can, according to Johnston, ignore dynamics (other than to show that transport to the troposphere, with destruction at the surface is small in comparison to the total ozone production rate) and utilize observed "snapshots" of ozone concentrations, along with knowledge of photochemistry and certain critical trace species, to see whether known instantaneous ozone production mechanisms match known ozone destruction mechanisms. The second approach would appear to be preferable from a chemical rate standpoint as various uncertainties can be explored in more expeditious fashion.

Using this latter approach, Johnston (1975) has argued that the classic pure air Chapman (1930) reactions,

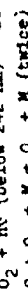


on a global basis, produce O_3 (reactions 1 and 2) at five times the rate that O_3 is destroyed by reaction 3. Reaction 4, the photodissociation of O_3 , is not of concern, since the most probable fate of the oxygen atom is to recombine with O_2 , according to (2) reforming O_3 . Johnston (1975) explores the uncertainties in this computation at length and demonstrates, beyond reasonable doubt, that other mechanisms (in effect catalyzing reaction 3), must be responsible for destruction of the majority of the ozone formed by reactions 1 and 2. He, and others, had, of course, come to this conclusion some years, perhaps a decade, earlier. It is of interest to note, historically, however, that as recently as 1963, using then-current reaction rates and Chapman chemistry, Prabhakara (1963) developed dynamics with which he was able to explain the ozone balance.

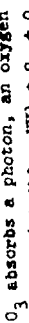
It is now clear the chemistry of stratospheric ozone is far more complex than indicated by the Chapman reactions. Reaction 3 is evidently catalyzed (homogeneously) by a number of cycles, which are of differing importance at different altitudes; these include cycles involving water chemistry (HO_x , including H, HO, and HOO), nitrogen oxide chemistry [NO_x , or $\text{NO} + \text{NO}_2$ and perhaps, NO_3 , the latter at low altitudes], halogen oxide chemistry (primarily ClO_x , but including BrO_x) and, of course, possibly heterogeneous catalysis. A simplified set of reactions important to the ozone balance is given in Table 3.1; more detailed listings are given later in this section. According to

TABLE 3.1. SIMPLIFIED OZONE CHEMISTRY

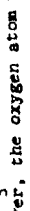
Ozone is formed by the Chapman (1930) reaction:



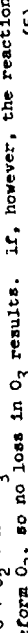
When O_3 absorbs a photon, an oxygen atom is released:



However, the oxygen atom usually recombines with oxygen

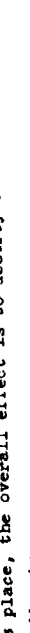


to reform O_3 , so no loss in O_3 results. If, however, the reaction



takes place, the overall effect is to destroy two ozone molecules,

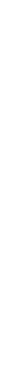
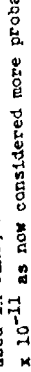
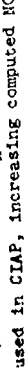
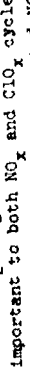
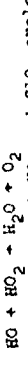
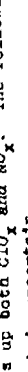
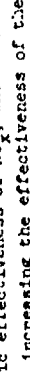
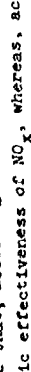
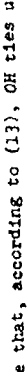
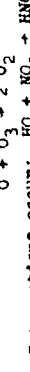
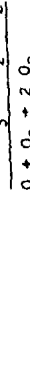
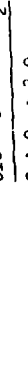
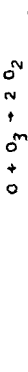
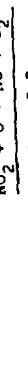
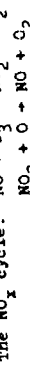
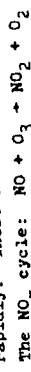
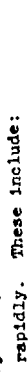
according to



Reaction (5) is too slow to account for the rate of loss of O_3 .

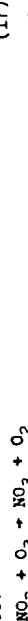
Catalytic cycles, however, exist by which Reaction (5) proceeds

more rapidly. These include:



The NO_x cycle, which may take place at low altitudes, is in

dispute:



In modeling exercises described later, it is assumed that one-

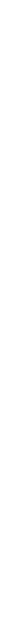
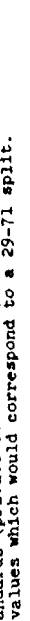
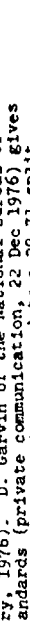
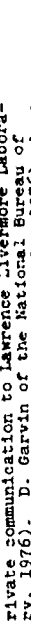
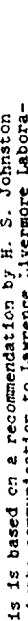
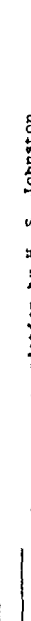
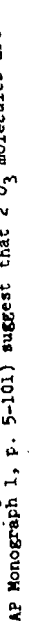
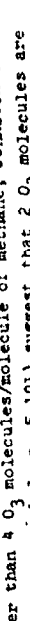
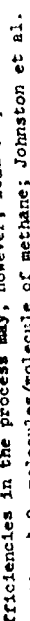
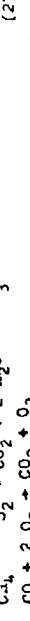
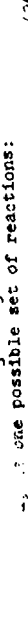
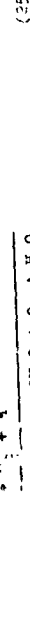
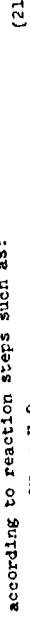
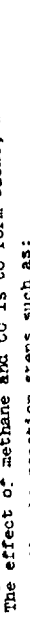
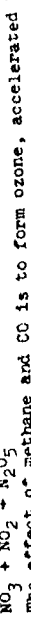
third of the NO_3 goes according to (18a), and 2/3 according to (18b)*

NO_3 reacts with NO_2 principally at night.



The effect of methane and CO is to form ozone, accelerated by

NO_x , according to reaction steps such as:



*This is based on a recommendation by H. S. Johnston (private communication to Lawrence Livermore Laboratory, 1976). D. Garvin of the National Bureau of Standards (private communication, 22 Dec 1976) gives J values which would correspond to a 29-71 split.

Johnston (1975), the NO_x cycle is the most important; he gives the instantaneous rates of formation and destruction of O_3 in Table 3.2.

TABLE 3.2. THE INSTANTANEOUS OZONE BALANCE, 10^{29} MOLECULES/SEC*
SOURCE: Johnston, 1975

	January 15	March 22
Gross rate of formation	500	486
Average transport to troposphere	6	6
Chemical loss by difference	494	480
Chemical loss by Chapman	86	89
Chemical loss by water reactions	56	54
Chemical loss by other mechanisms	352	337

Johnston (1975) further found that, if the combined concentration of NO and NO_2 is 3.6×10^9 molecules/cm³, ozone production and destruction would be in balance. This figure is within the (rather wide) range of measured values.

With inclusion of these various cycles, the problem becomes exceedingly difficult. It would appear, for example, that in order to establish the relative importance of the various cycles, data on trace species, such as H_2O , NO_x , ClO_x , etc., must be obtained in a detail to match that of the existing ozone data, and highly accurate reaction rate, photolysis, and radiation (scattered and direct) data must be available. Interactions between these different cycles (HNO_3 , ClONO , ClONO_2 , HCl , HOCl , etc.) would all need to be included.

Most stratospheric NO_x is thought to come from the oxidation of N_2O by energetic oxygen atoms [$\text{O}(^1\text{D})$] produced by photolysis of ozone. N_2O is produced in the soil by biological processes; it is also apparently produced during combustion, as in coal-fired power plants (Craig, 1976). Also, N_2O production by soil bacteria presumably increases with fertilizer use; hence, there has been increased concern with all sources of N_2O and fixed nitrogen as to potential effects on ozone (Liu et al., 1976; McElroy et al., 1976; Johnston, 1976; Crutzen, 1976a; Blackmer and Bremner, 1976). The calculations are highly uncertain because a large unknown sink for N_2O apparently exists in the troposphere and there is uncertainty as to the time delays involved (years vs. centuries).

Stratospheric ClO_x comes from photolytic dissociation in the upper stratosphere of chlorine-containing compounds such as CCl_4 , CH_3Cl , CF_2Cl_2 , and CFCl_3 . CH_3Cl is probably the only naturally occurring source of material; the others are man-made. The impact of chlorine-containing compounds, particularly CF_2Cl_2 and CFCl_3 , which are produced in large quantities for use as aerosol propellants and refrigerants, has been the subject of extensive study in the period since

*See Duewer, et al., (1976a) for revised estimates.

the CIAP Report of Findings was issued (see NAS, 1976, 1976a; also United Kingdom Department of the Environment, 1976). Much has been learned about stratospheric chemistry in the process. It is now evident that there are important interactions between the ClO_x , NO_x , and HO_x cycles, as will be shown in a later section. The present best estimate of chlorine content of the stratosphere in all forms is about 1 to 1.5 ppb, but this is expected to increase in the future, partly due to the large present reservoir in the troposphere, and partly due to continued manufacture of CF_2Cl_2 and CFCl_3 for at least some uses. This level of chlorine is thought to reduce ozone content somewhat less than 1 percent (NAS 1976, p. 5-13) based on 1-D modeling exercises, but is nevertheless of importance in estimating effects of NO_x added from aircraft.

3.2.3 Effects of Altered Ozone Levels on Erythemally-Weighted Surface UV Flux

A. General

Under typical mid-latitude conditions, almost no photon flux reaches the ground with wavelengths below about 295 nm, as shown in Fig. 3.6 (Cutchis, 1974) for a specific ozone column. For thinner ozone columns, the drop off in flux with decreasing wavelength is not as fast, but the behavior is similar. In any event, the absolute total flux in the region of Fig. 3.6 is of little interest; rather, what is desired is a weighted flux, recognizing that certain wavelengths have more biological effectiveness than others. The weighting curve usually used, that of the Commission Internationale de l'Eclairage [or CIE, see Cutchis (1974)] peaks at 297.5 nm. This curve is known as the erythema (reddening) efficiency curve, and was derived by determining the relative effectiveness of various wavelengths in producing detectable reddening (sunburn) on untanned white Caucasians. An analytical model of the CIE standard (STD) curve is given in Fig. 3.7, along with a curve showing the absorption spectrum of DNA. The assumption is usually made, based on skin cancer induction experiments on hairless mice, that the erythema weighting curve can also be used as a carcinogenic weighting curve. As damage due to ultraviolet light absorption might well be associated with integrated energy absorption by DNA, use of a DNA-absorption weighting curve might be preferable. However, as is evident in Fig. 3.7, the DNA absorption curve and the standard erythema curve, over the important 295-320 nm range, are roughly constant in ratio. As a result, the percentage changes in calculated dose with changes in ozone are nearly the same with use of either weighting curve. Erythemally weighted UV doses are sometimes known as "sunshine units." The term "damaging UV," or DUV, for weighted flux in the 290 nm to 320 nm region was used in halocarbon effect studies (NAS, 1976, 1976a), as noted earlier.

Changes in annual integrated erythemally weighted doses for various changes in ozone have been computed for various latitudes by Schulze (1974), with results given in Fig. 3.8. His curves are perhaps the easiest to use of various

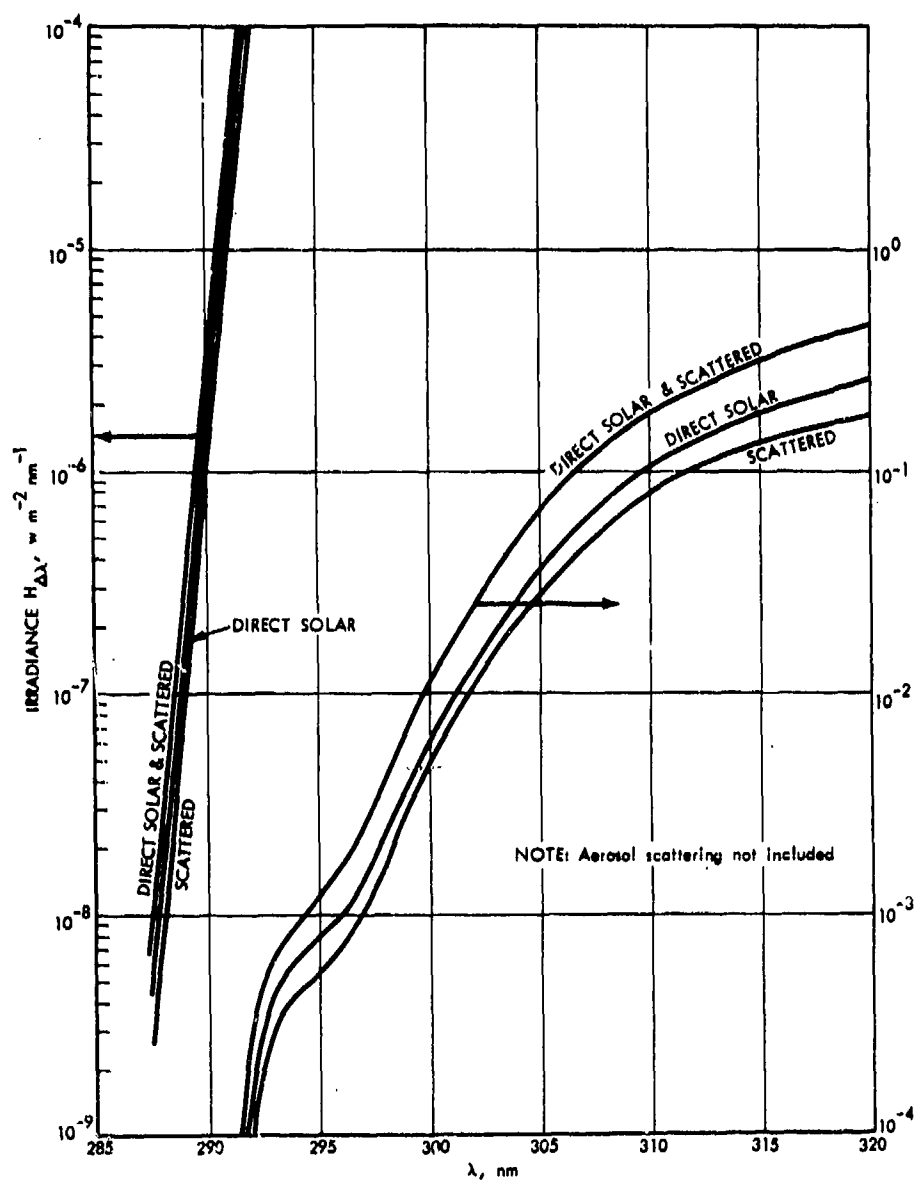
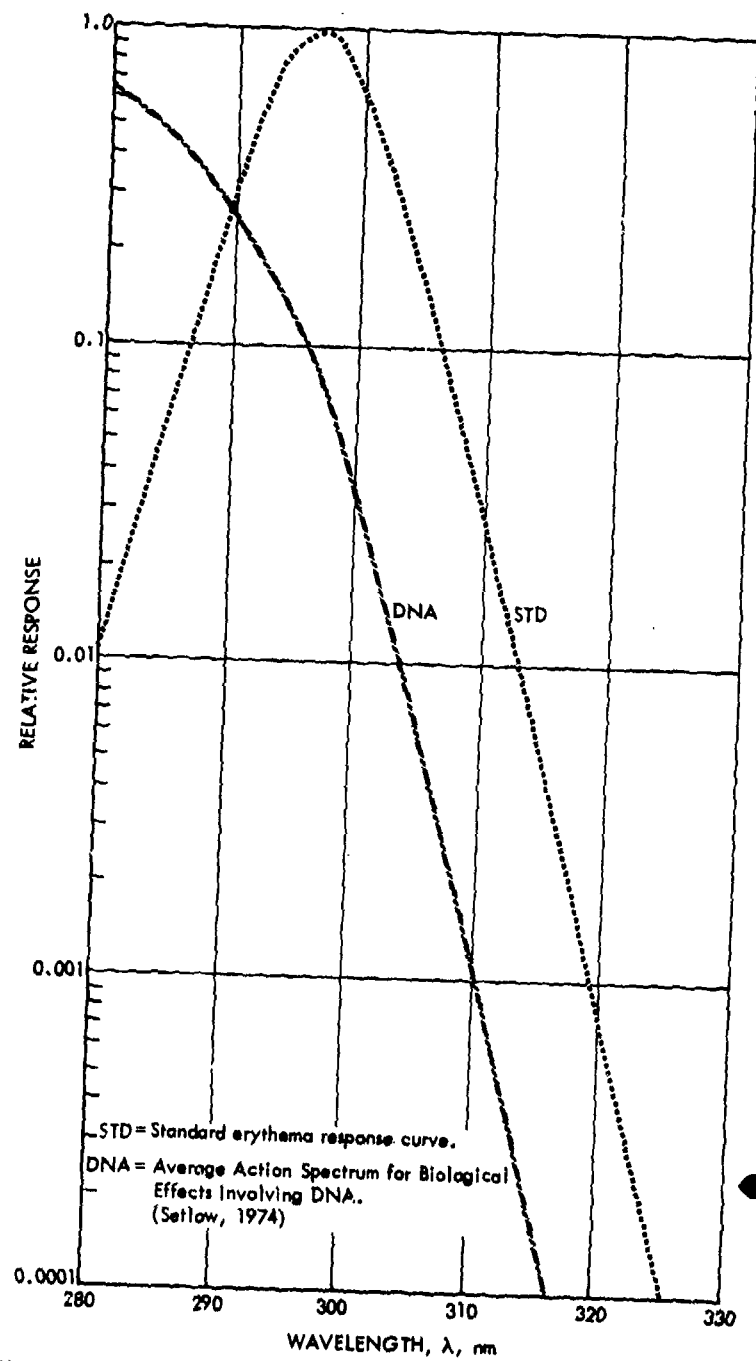


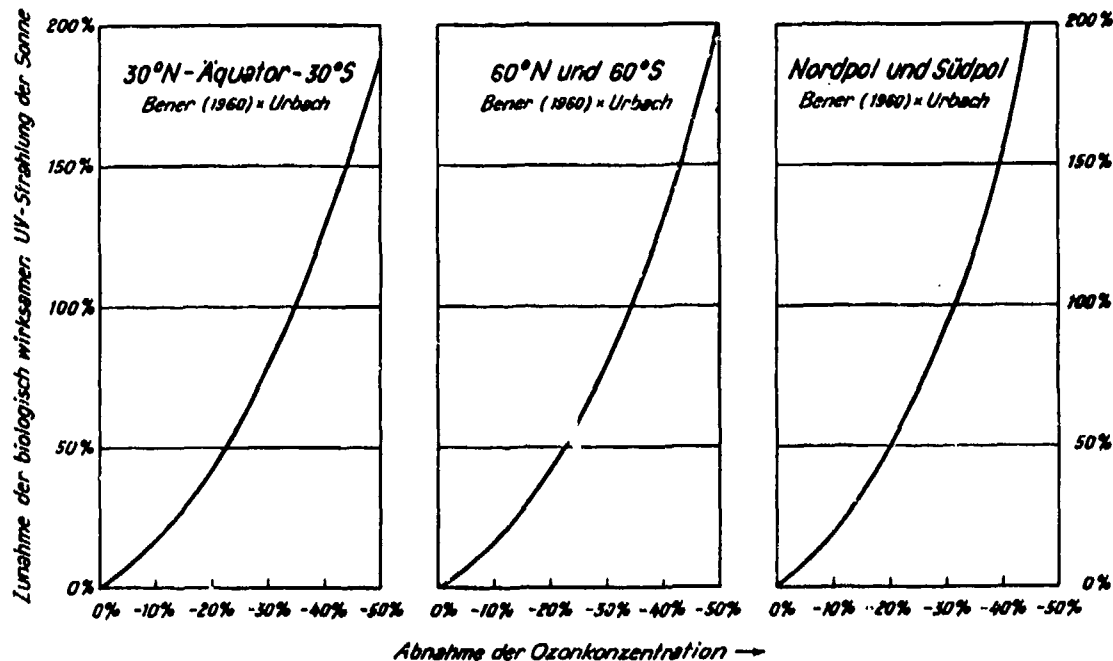
FIGURE 3.6. Direct Solar UV Irradiance and Scattered UV Irradiance on a Horizontal Surface at Sea Level for Solar Zenith Angle θ of 0° and 0.341 atm-cm of Total Ozone
Source: Cutchis, 1974



10-1-74-1

FIGURE 3.7. Analytical Models of Spectral Efficiencies for Biological Effects
Source: CIAP Monograph 5, Part 1, p. 2-56

curves, but suffer in detail by his failure to include radiation received below 300 nm. The error introduced thereby is insignificant for small changes in ozone, but become significant at large changes. Thus, according to computations by Cutchis (1974), the erythemal dose at 0.341 atm-cm and with a solar angle of 30 deg is 0.1385 units, of which 0.0085, or 6 percent, is below 300 nm; at 50 percent depletion, however, the total dose is 0.4290 units, of which 0.0978 or 23 percent is below 300 nm. The corresponding ratios of sunshine units are 2.55, ignoring the portion below 300 nm, and 3.10, including the portion below 300 nm.



3-2-77-14

FIGURE 3.8. Increase of "Carcinogenic" Solar UV Radiation with Decrease of Ozone Concentration, both in Percent. Calculations based on annual sums of irradiation from sunrise to sunset. Source: Schulze (1974)

Values developed by Schulze (1974) follow for a 10 percent decrease in ozone, for the increase in "carcinogenic UV."

At the equatorial zone	+18 percent
At middle latitude	+19 percent
At the north and south poles	+27 percent

B. COMESA Studies on UV Changes with Ozone Reduction

Studies by COMESA (1975) have clarified these issues further. They showed first that the ratio of scattered UV to direct UV is dependent only on zenith angle and wavelength, and not on ozone amount. This greatly simplifies the computational burden, and has been shown to be satisfactory by detailed study. Their results, which are independent of ozone amounts, are given in Table 3.3. It should be noted (Table 3.3) that the ratios developed are, in addition, almost independent of wavelength, except at high zenith angles, supporting an assumption made by Cutchis (1974).

One set of computations by COMESA that is of particular interest, shows the sensitivity of the change in erythemally weighted UV (to changes in ozone) to uncertainties in the absolute spectral location of the erythema efficiency curve. (See Table 3.4.)

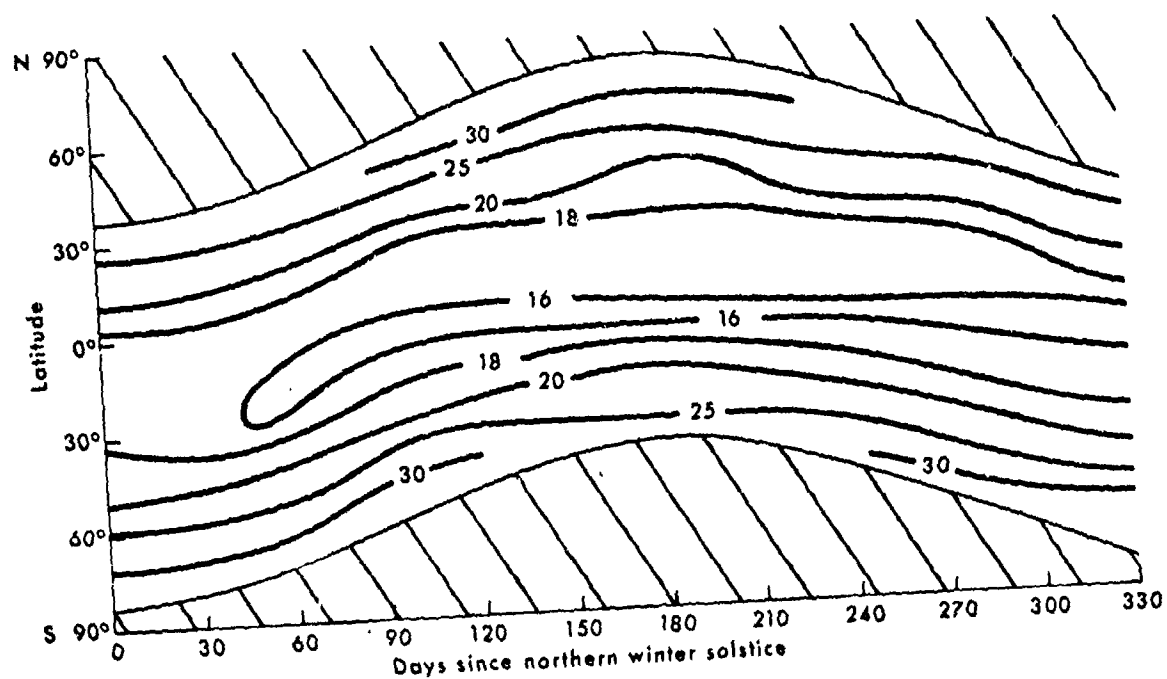
TABLE 3.3. RATIO OF DIFFUSE TO DIRECT UV PENETRATION
SOURCE: COMESA, 1975

Zenith Angle (deg), Wavelength Interval (nm)	0	30	60
290.0 - 291.5	0.76	0.93	4.76
294.5 - 296.0	0.82	1.01	4.30
299.0 - 300.5	0.85	1.07	3.90
305.0 - 306.5	0.90	1.13	3.56
309.5 - 311.0	0.93	1.13	3.16
314.0 - 315.5	0.93	1.12	2.89
318.5 - 320.0	0.90	1.08	2.64

TABLE 3.4. ERYTHEMALLY WEIGHTED FLUX, $\mu\text{W}/\text{cm}^2$
SOURCE: COMESA, 1975

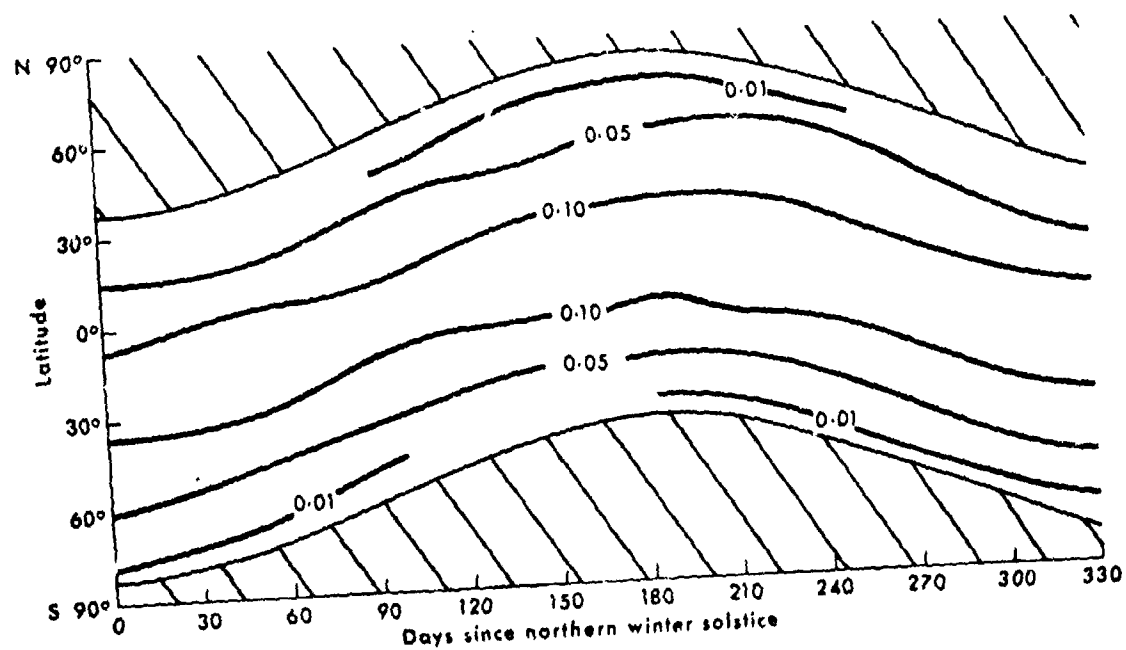
Erythema Curve Shift nm	Zenith Angle and O_3 Thickness		Ratio
	20 deg, 0.25 atm-cm	60 deg, 0.4 atm-cm	
+1.5	67.7	0.31	220
0	49.8	0.18	280
-1.5	35.7	0.09	400

The absolute erythemally weighted flux is clearly sensitive to the absolute location of the erythema weighting curve. Furthermore, as shown by the trend in the ratios (which have no other significance), the calculated change in erythemally weighted dose with given change in ozone will also depend



3-2-77-15

FIGURE 3.9. Percentage Increase in Sunburn Daily Dosage for a 10-Percent Decrease in Ozone Amount.
Source: COMESA, 1975

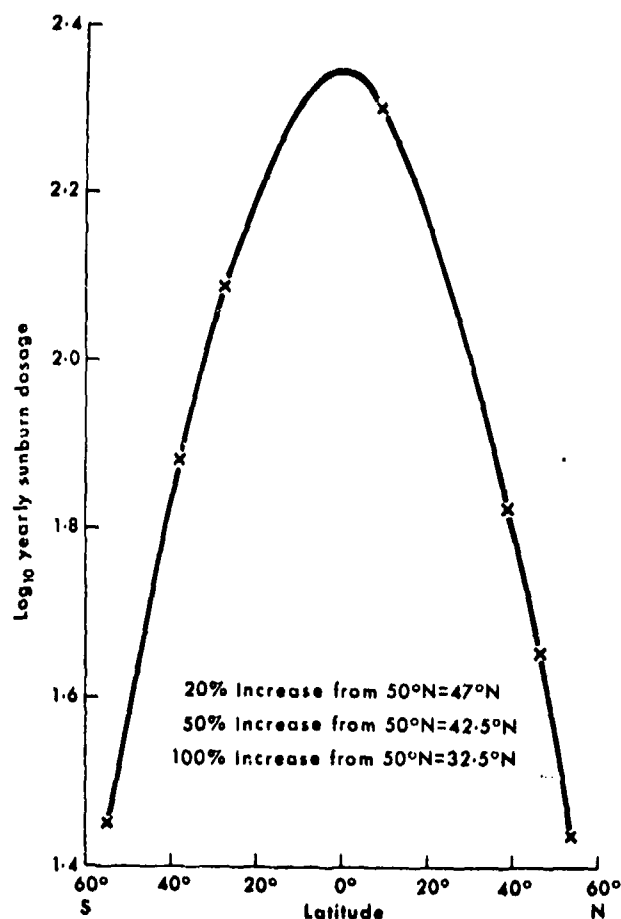


3-2-77-16

FIGURE 3.10. Increase in Daily Sunburn Dosage for a 10-Percent Decrease in Ozone Amount (J/sq cm)
Source: COMESA, 1975

on the absolute location of this curve. The shape of the curve itself was kept constant in these calculations but is itself not well established.

Latitudinal effects are shown in three COMESA curves. The first of these (Fig. 3.9) shows the percentage change in sunburn daily dosage (erythemally weighted UV dose) for 10 percent ozone change as a function of latitude and season. It is seen that the percentage changes are smallest in the tropics and largest in the arctic regions. The second (Fig. 3.10) shows the absolute (weighted) increase in Joules-cm⁻² for the same ozone change. The second curve (Fig. 3.10) looks quite different from the first, the change in flux being small in the arctic and large in the tropics. This is, of course, because of the very rapid change in yearly sunburn dosage with latitude, as shown in Fig. 3.11, on which the log scale should be noted.



3-2-77-17

FIGURE 3.11. Yearly Sunburn Dosage (J/sq cm)
 Source: COMESA, 1975

It will be seen later here that 2-D modeling results show ozone depletions due to SSTs to be small in a percentage sense in the tropics, but increase toward the poles. This fact, combined with trends as shown in Fig. 3.10 for a constant percentage depletion, suggests a compensation of factors, so that the absolute increase in flux may tend to be roughly constant over a given latitude band. If skin cancer incidence can be tied to absolute flux values, the observation might simplify the making of estimates of skin cancer changes due to NO_x injected by supersonic aircraft.

The COMESA analysis (p. 399) indicates that for a vertical sun a 10-percent decrease in ozone leads to a 16-percent increase in erythema dosage. For a 30-degree zenith angle, they find 20 percent versus 23 percent given by Cutchis (1974).

The variability in annual erythema dosage from year to year at various stations is also of interest. COMESA gives such data (p. 400) showing standard deviations of from 2.7 to 8.6 percent. Figure 3.11 is interpreted by COMESA to show that, for someone living at 50°N , a 20 percent increase in UV dosage is equivalent to moving to 47°N , 300 km south. These equivalences, of course, ignore changes in life style with latitude.

COMESA also notes the importance of aerosols and clouds, and the fact that stratospheric aerosols from aircraft reduce the penetration of UV, compensating somewhat for changes due to changes in ozone. They note that, if other factors remain constant, the change in erythema dosage is about 1.5 times the change in ozone at low latitudes, increasing up to about three times at 60°N in the summer.

C. Weather Effects

Penndorf (1976) brings up a point of considerable interest with regard to variability of ozone with weather. He quotes data which show the ozone column to be as much as 120 percent of the mean monthly value in the rear of a moving cyclone and as little as 70 percent of the mean value west of an anticyclone. Good weather is associated with such periods of low ozone, a point which could be important in computing exposures of the populace to damaging ultraviolet.

3.3 THE MODELING PROBLEM IN GENERAL

3.3.1 Introduction

It was noted in Section 3.2.1 that, if one is interested in the general problem of effects of high-altitude aircraft, subsonics as well as supersonics, the chemistry utilized must include reactions known to be important in both the troposphere and the stratosphere. It also follows that the dynamics of the atmosphere must be treated more carefully, particularly in the region of the tropopause. This is because, as shown in Fig. 3.12, aircraft traffic, in general, is concentrated in the region of the northern tropopause gap, a

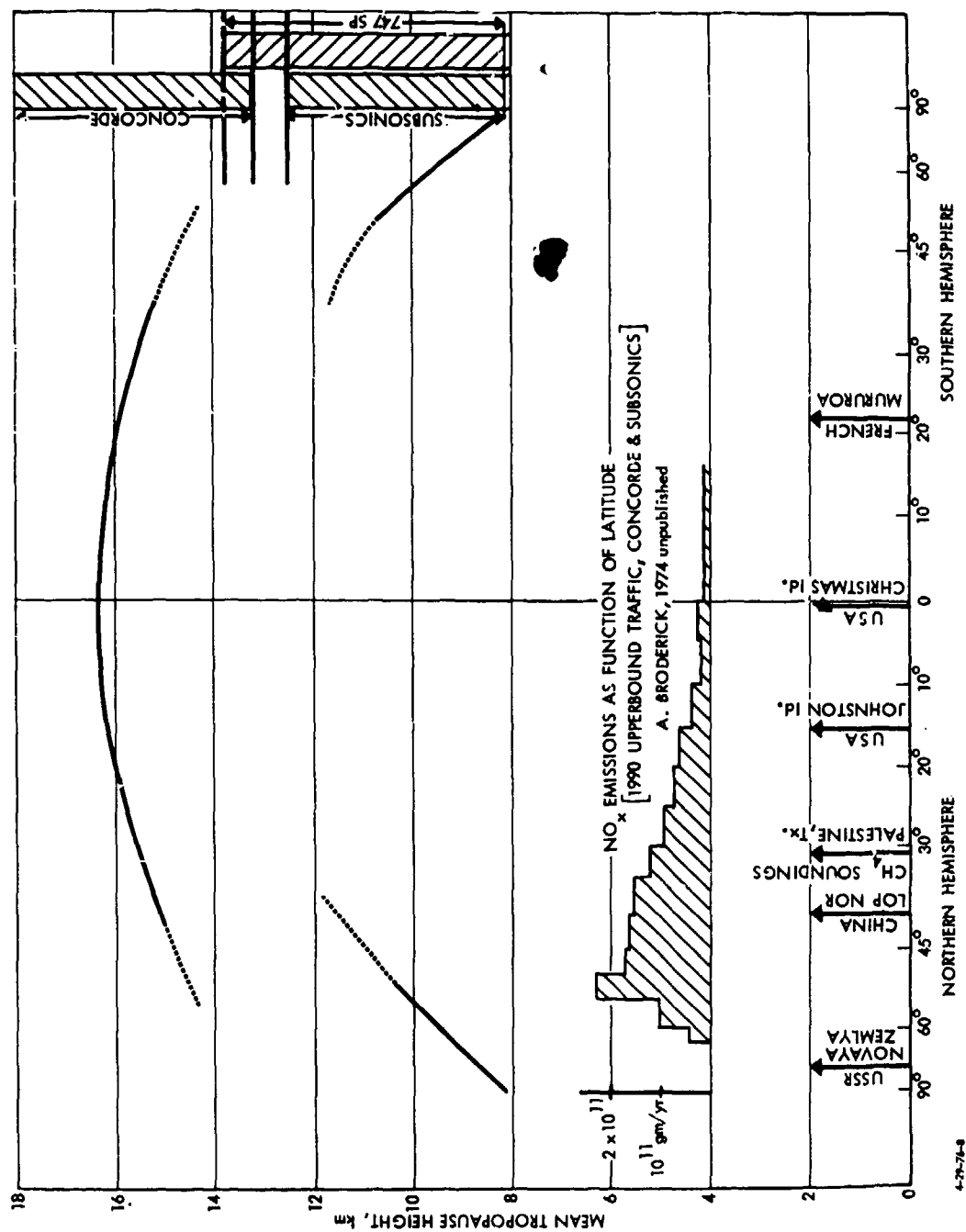


FIGURE 3.12. Latitudinal Distribution of Mean Tropopause Height, with CIAP Fleet Emission Projections and Data on the Latitudes of Nuclear Tests and CH₄ Soundings

region of the atmosphere which is highly variable in terms of tropopause height, sometimes having multiple, folded (or no) tropopauses; this region is also the region of jet streams and is generally complex in its behavior (see Danielsen et al., CIAP Monograph 1, Chapter 6; Downie, CIAP Monograph 2, Chapter 7). Subsonic aircraft operating in this region, at constant altitude, fly sometimes above and sometimes below the local tropopause, perhaps on subsequent days. Downie (CIAP ROF, p. D-62) gives some statistics on the probability that an aircraft at a given altitude will be in the stratosphere for different locales and seasons; the probability increases in the winter for flight farther north. Supersonic aircraft, on the other hand, particularly mach 2.7 aircraft at 20 km, cruise above these more complex regions, well into the stratosphere, reducing somewhat the uncertainties associated with transport of their exhaust products.

In order to determine the effects of added pollutants on ozone, one must first develop a model of the natural or unperturbed atmosphere which "credibly" reproduces certain observed characteristics of the real atmosphere, including natural sources of sinks of critical trace species. Perturbing sources (pollutants) are then introduced into the model, and the perturbed atmosphere compared to the natural atmosphere. Philosophically, of course, there is no proof that this process is valid, since many degrees of freedom exist in the modeling process; there is thus great interest in comparing observed effects of known perturbations (as, for example, from nuclear weapons tests) to model-predicted behavior. Unfortunately, this process also is faced with substantial difficulties, as shall be discussed later in this section.

The real atmosphere is far too complex to attempt to include its known behavior in any model, and various simplified models are used; these include 1-D (one dimension, height only), a 2-D (two dimensions, height and latitude), and 3-D (three dimensions, height, latitude, and longitude) representations. The computing time for these approaches varies with the complexities introduced, but generally increases rapidly with the number of dimensions used.

Models can be time-dependent or steady-state approximations and can approximate the chemistry involved with a widely varying number of reactions and elements. Order-of-magnitude computing times run from 1 minute for a 1-D (fixed solar zenith angle) run, to 2 hours for a 2-D run (at 20 minutes per model year), to perhaps 20 hours in a 3-D run, in all cases using a high-speed computer such as the CDC-7600 or IBM-360/95. These times are quoted for models with increasingly simplified chemistry with increases in dimensionality. 1-D models with fixed solar zenith angles also have the advantage of rapid convergence (with simulated times of 100 to 300 years) to a suitable number of decimal places, whereas in higher dimensionality models, the computed results do not necessarily ever repeat precisely from year to year, so that comparison of "natural" and "perturbed" atmospheres requires careful procedures (see

Appendix A). 1-D models have also been run with diurnally and seasonally varying solar zenith angles, which then involve long computational times and difficulties in convergence (and interpretation, as the computed ozone column is out of phase in a seasonal sense with measured values). 1-D models cannot include (or to date have not included) seasonally varying dynamics and tropopause heights, etc.

The mathematics, physics, and philosophy behind these different modeling approaches is discussed at length in Monograph 3 of the CIAP Series, and in briefer form in Appendix E of the CIAP Report of Findings. The philosophy behind 1-D modeling is discussed by Hunten (1975); limitations were noted by Mahlman at the 4th CIAP Conference, February 4-7, 1975. Discussions are also given in the COMESA report (1975). No attempt will be made to repeat these treatments. What follows is a brief discussion of these approaches, with emphasis on some of their characteristics and limitations. As 1-D models have been used most widely, these are discussed at greatest length.

3.3.2 1-D Models

The fundamental assumption in 1-D modeling is that for a given species, at a given altitude, in the absence of sources or sinks, the globally averaged mixing ratio gradient controls the globally averaged vertical flux, according to:

$$\phi = - K_z n \frac{\partial f}{\partial z}$$

where ϕ = flux, mol-cm⁻²-sec⁻¹

K_z = "eddy diffusivity" coefficient, cm²-sec⁻¹

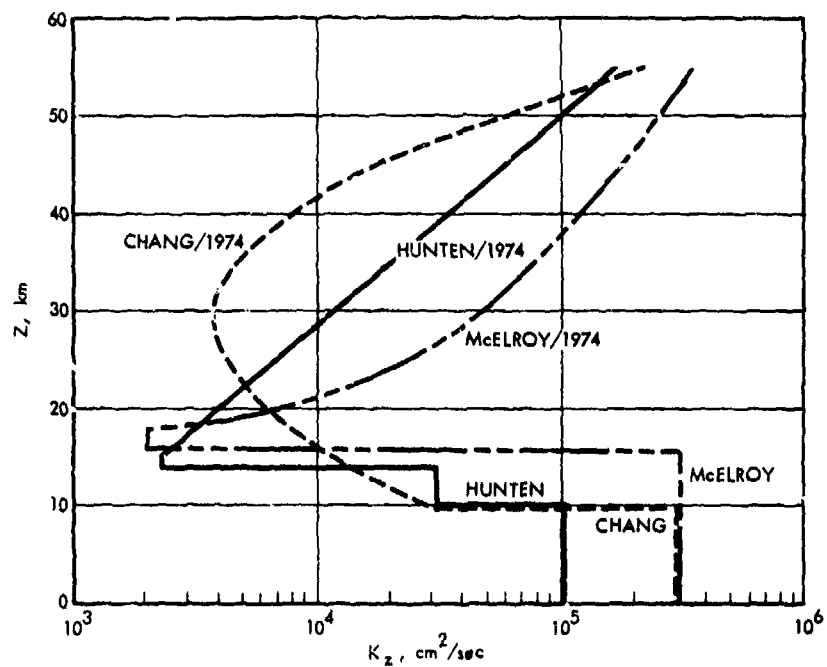
n = air density, mol-cm⁻³

f = mixing ratio of species being considered, (mol/mol)

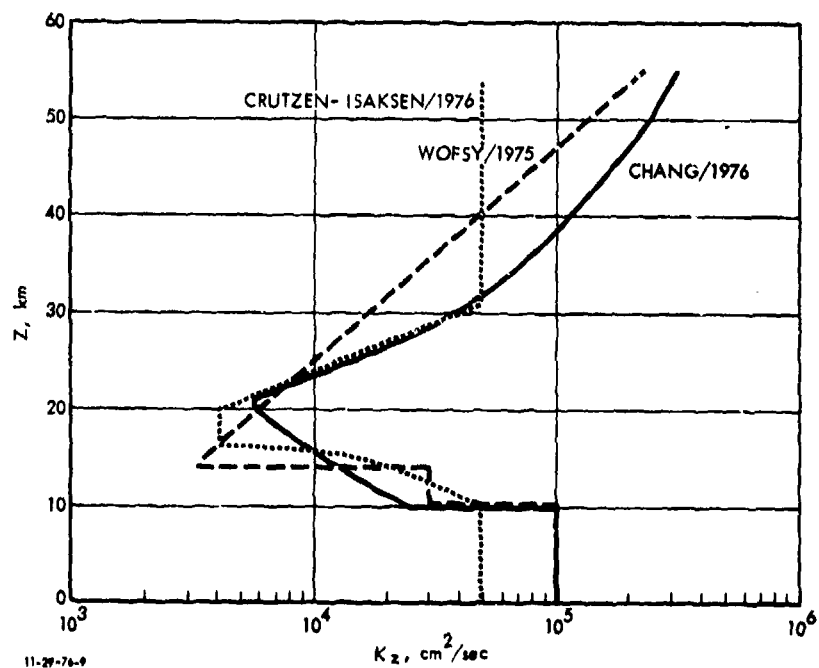
z = altitude, cm (but quoted in km)

K_z , in this formulation, is a function of altitude, the relationship with altitude forming a " K_z profile." The same value of K_z is assumed to apply to all trace species.

A large number of K_z profiles have been used, six of which are shown in Fig. 3.13. Typically, a large K_z value is used in the troposphere up to a model tropopause at 10 to 16 km, at which K_z drops abruptly by one or two orders of magnitude and after which, K_z increases with altitude. The Chang/1974 (upper figure) K_z is unique in that minimum K_z is at 30 km; the profile was revised following studies by Dickinson (NAS, 1976a) in the chlorofluoromethane work to give the "New Chang" or Chang/1976 (lower figure) K_z profile, in which minimum K_z is found at about 21 km. The Chang/1974 and Hunten/1974 K_z profiles played important roles in the CIAP Report of Findings. (See Section 3.4.)



(a)



(b)

FIGURE 3.13. Six K_z Profiles

Note that because modelers tend periodically to revise their preferred K_z profile, a date or reference should be given along with any model profile described by name.

It should be noted that some authors contend that their 1-D models represent mid-latitude conditions, rather than global or hemispheric average conditions. Mahlman at the 4th CIAP Conference, February 4-7, 1975, however, considers the interpretation of 1-D model results to be fundamentally ambiguous. Also, as different tracers have different sources and different sinks, K_z in principle and as computed from 3-D models (see Section 3.4.2 this report) may vary widely for different tracers, and can include negative values. Nevertheless, 2-D models have similar conceptual limitations (see Section B below), and 3-D models are, as noted earlier, computer-limited; much work has thus been done with 1-D models.

Several aspects of 1-D profiles control the computed effects of aircraft perturbations. The sink for NO_x is primarily in the lower troposphere (at or near the ground, with rainout) as the high-altitude photolysis sink is of only moderate significance (see Section 3.4.3F); at steady state there is essentially no upward flux. Thus, pollutants, introduced continuously, must in a model sense "diffuse" from the altitude of injection to the ground, at a rate equal to the injection rate. The resistance to diffusion and, hence, the mixing ratio gradient required to transport material at steady state, is proportional to the reciprocal of the product of K_z and air density at each altitude. The overall gradient between the point of injection and the ground (and thus the degree of contamination above the injection altitude at steady state) depends on the integrated resistance. The integrated resistance for a source above the tropopause depends on the tropopause height (and "thickness"), and on the minimum value of K_z below the altitude of injection. It is evident, therefore, that a source (see Fig. 3.13) at 15 km, above the Hunten tropopause but below the McElroy tropopause, would show vastly different effects with the two profiles. Similarly, a steady source at 20 km would show far less effect with either Chang profile (1974 or 1976) than with the Hunten profile.

K_z profiles have been deduced in various ways: The Chang/1974 K_z profile (see CIAP Monograph 3, p. 4-159) was developed from heat transport and particulate tracer data.* However, the preferred technique now appears to be to rely on measured changes in concentration of a reactive tracer with altitude, in particular, for upper altitudes, methane, and, to a lesser extent, N_2O . The techniques used and the uncertainties involved are discussed by R. Dickinson in the NAS report (1976a, Appendix B). The methane data are sparse, and available principally at one latitude (32°N). The technique used involves inversion of the measured concentration data to obtain an effective K_z between layers, assuming the concentrations of species which react with methane (OH , O^1D , and Cl) are known as well as the rates of reactions involved.

*An alternative technique, based on aerosol data, is given by Rosen and Hofmann (1975).

Some of the necessary species concentrations can be estimated from measurements (H_2O , O_3 , HCl , ClO), if such data exist and appropriate global averages can be deduced; other reactive species data (Cl , O^1D , OH) can be computed assuming photochemical equilibrium, using known rate constraints, and model-computed photon fluxes. As the rate of destruction of methane at any altitude depends on its concentration, and on concentrations of and rates of reaction with reactive species, there is a clear coupling between the concentrations of various species, and photon fluxes, chemistry, and the dynamics (K_z) generated. If the process were carried through iteratively to fit a specified methane profile, a consistent data set would result, although this has generally not been done. In any event, a question exists to what extent it is proper to decouple the process and use the K_z profile (generated with one set of chemistry, etc.) to explore effects of changes in chemical reaction rates or of changes in the radiative transport treatments, such as including multiple scattering, etc. This question would not apply if the K_z profile could be developed from "true" transport data.

It should be noted also that different tracers such as CH_4 and N_2O , do not lead to identical K_z profiles. This is shown by Dickinson (Appendix B, NAS report, 1976a). Furthermore, the available methane data lead to serious matching problems (that is, K_z values show erratic behavior) in the 20-km to 30-km region.

The critical low-altitude portion of the K_z profile, near the tropopause, cannot be obtained satisfactorily from methane profiles, as methane lifetime is too long at these altitudes. The tropopause height assignment is somewhat arbitrary, dependent on the problem being considered. Thus, Hunten (NAS, 1975) used 14 km (but, in effect, recommended 12 km for typical flight regions); Dickinson (NAS, 1976a) used 15 km, and McElroy et al., (1974) used 16 km. The assigned minimum in the K_z profile, and the thickness of the tropopause region, are also somewhat subjective but can be tested by studies of the rate at which a tracer is removed from the stratosphere. Carbon-14 data were so used in NAS, 1975 to argue for the Hunten/1974 profile, as discussed in Section 3.6. A study is included here (Appendix C) of the behavior of zirconium-95, which was injected at 40°N at an altitude of about 18 km, and thus is of particular interest to the Concorde SST problem. Results are given in Section 3.6; it is noted that eddy diffusivity value assignments and tropopause height assignments are necessarily coupled if tracer removal behavior is being considered.

For a K_z profile with a sharply defined tropopause, such as the Hunten profile, the relative position of the aircraft and tropopause is of crucial importance in determining computed effects. Where the aircraft is known to be above the tropopause only some fraction of the time, an averaging problem exists

which has been ignored to date. A seasonally varying K_z profile could, in principle, be developed, but it is not obvious how the necessary input data could be obtained, nor what the results might mean.

As noted earlier, in developing 1-D models of the natural atmosphere, tracer profiles of various trace species are given, such as ozone, nitrogen oxides, HNO_3 , etc., and compared to available measurements, which usually show wide variations and are not claimed to be global averages. One important tracer, however, namely water vapor, on which a great amount of (not very reliable) data exist, is normally excluded; water vapor is normally put into these models as a fixed or known species rather than as a computed quantity. A simple reason is that, with normally assigned tropopause temperatures, far too much water vapor would be present in the stratosphere if saturation at the tropopause is assumed. (The 45°N July standard atmosphere tropopause is at -57.5°C at 177.8 mb, for which saturation water vapor partial pressure would be 53 ppm.) The behavior of water vapor is not well understood, although measured data (which vary widely) can be reproduced empirically in reasonable fashion in 2-D models. A significant fraction of the stratospheric water vapor comes from methane oxidation. Because water vapor is an important component of aircraft exhaust, and affects the chemistry involved, it becomes important to understand its effects, particularly if NO_x emission indices are reduced. Water vapor is also an important tracer of atmospheric motion. (The question has been asked, if mid-latitude water vapor does not rise, why should NO_x from aircraft?) A model used by Hunt (1974) in studying stratospheric moisture (Fig. 3.14) is illustrative in this regard. Water vapor changes can be incorporated, but only crudely, in 1-D models, based on residence time considerations, mixing ratio enhancements, or by ratioing to augmentations in nitrogen oxides, etc.

The dryness of the stratosphere is usually explained by arguing that stratospheric air must, in large part, have entered the stratosphere where the cold tropical tropopause "traps out" water. Hunt (1974) appears to dispute this, but the calculated net fluxes are very sensitive to modeling assumptions, for example, whether the tropical tropopause is at 190 K as used by Hunt, or 193.15 K as given in the 1966 model atmosphere (15°N), over which range the saturation vapor pressure of ice varies by almost a factor of 2. Harries (1976) makes the same point in a careful review of water data. These matters need further investigation if the effects of aircraft water vapor are to be understood.

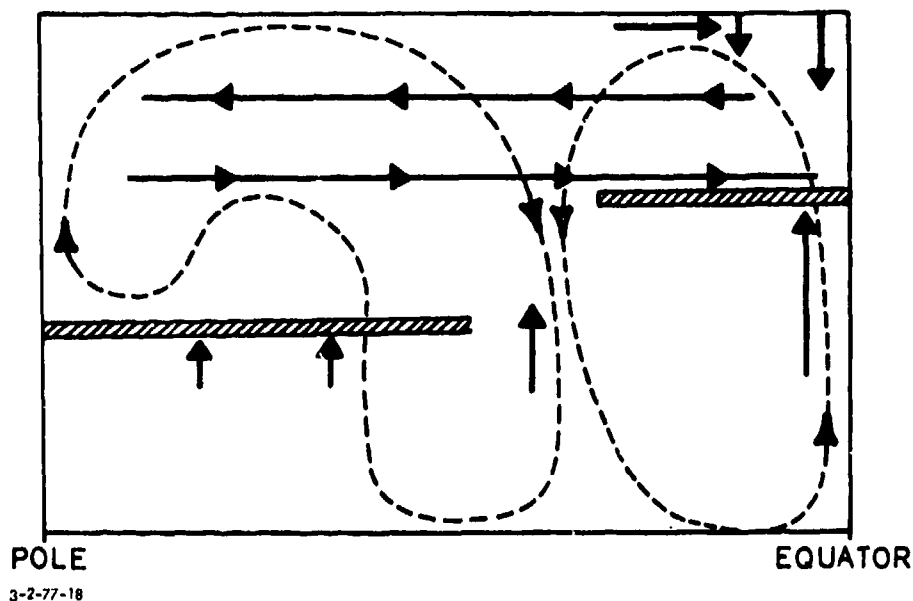


FIGURE 3.14. Schematic Diagram Indicating Water Vapor Fluxes both into and in the Model Stratosphere. The full lines represent the large-scale eddies, both vertical and horizontal, while the dashed lines represent the mean meridional circulations. The tropopause is shown by the hatched areas.
Source: Hunt, 1974

Another point should be noted with regard to the applicability of 1-D models to the aircraft problem as compared to the halocarbon problem. The halocarbons are released at the surface, dispersed worldwide in the troposphere, and destroyed by photolysis in the high stratosphere. Their degradation products are, of course, eventually removed in the troposphere and the details of the downward transport problem become of interest; however, the details of the upward transport process, whether or how often the materials are recycled to the troposphere, would seem to be of little interest. Aircraft sources, on the other hand, are released at altitude in a relatively concentrated region of the earth's atmosphere; the materials so released are not significantly destroyed in the stratosphere, but have a short lifetime in the troposphere. The effects on the ozone layer depend on the degree of contamination of the mid-stratosphere and this, in turn, depends on the rapidity with which the pollutants enter the troposphere, a process which varies with latitude, and on the rate of removal of the materials once they have entered the troposphere. Details of the stratospheric-tropospheric interchange processes, as well as the removal rates used (the "rainout" coefficients) become important. Two-dimensional model results for 20-km injections have shown a sensitivity to rainout coefficient

(Section 3.4.2) and relative effects will be expected to be greater at lower altitudes. For these reasons, as well as questions resulting from seasonal variations in tropopause height and dynamics as noted earlier, 1-D models, which may be appropriate for halocarbon studies, seem less appropriate than 2-D models for quantitative evaluation of aircraft effects.

3.3.3 2-D Models

Two-dimensional models, in which zonal, rather than global (or perhaps hemispheric) averages are used, are, like 1-D models, strictly empirical and obviously require a great deal more input data than do 1-D models. Such models can be purely diffusive (but in two dimensions), characterizing all motions in terms of eddy diffusion coefficients, or can include mean motions. The difficulties in obtaining good input data to describe the motions involved have led to criticism of such models (see NAS, 1975, p. 113, for example). However, a great deal of tracer data do exist, in 2-D and seasonal array, which can be applied in the development of such models without arbitrarily collapsing to 1-D behavior; much of the motion data are completely decoupled from the chemistry. There are still difficulties in that mean motions are highly correlated with eddy transports, so that mean and eddy motions tend to cancel (see CIAP Monograph 1, Chapter 6; also CIAP Monograph 3, Chapter 4). Nevertheless, as noted earlier, such models can empirically incorporate seasonally varying tropopause heights, seasonally varying dynamics, and water vapor, all of which are essential to the aircraft problem. As noted earlier, the computer time required for 2-D models is far greater (perhaps 100-fold) than for 1-D models, particularly because there is no known means to take increasingly large time steps, as is done in 1-D models, because all values in the computation change seasonally or continuously, and year-by-year computations must be continued until suitably close to equilibrium.

3.3.4 3-D Models

Three-dimensional (3-D) models, which give longitudinal as well as latitudinal effects, will ultimately be needed. These models have major theoretical advantages over 2-D models in terms of large-scale dynamics, but are seriously computer-limited in terms of including both adequate chemistry, radiative transport, and dynamics (see CIAP Monograph 3). Three-dimensional modeling efforts were undertaken under CIAP sponsorship at MIT (Cunnold and Alyea 1975, Alyea, et al., 1977; also CIAP ROF, 1974, pp. E-78 to E-88). The model was only partly developed at the end of CIAP, at which time it incorporated elements of 1-D (subgrid vertical transport), 2-D (NO_2 distribution), and 3-D (ozone distribution) models. Results on ozone depletion of SST sources were reported on a 2-D basis. Results are given in Section 3.4.2.

Three-dimensional models would appear to be of particular interest for study of the effects of subsonic aircraft because of questions relating to the uniformity of effects around a latitude zone in the troposphere (2-D models give only a zonal average). No studies of such source have been made in a 3-D model. Some preliminary consideration of this question is given in Section 3.5.

3.3.5 A Further Caveat

One further caveat should be noted before giving results of various models. That is that both fleet sizes and stratospheric composition will change with time, but not in predictable fashion. It has been noted that halogens, for example, will increase in the stratosphere over the next decade or more if for no other reason than due to the large present reservoir in the troposphere. Water vapor also changes with time, for reasons that are not understood. Effects on ozone of added water and NO_x will depend on the chlorine, and background NO_x water, contents. Also, changes in composition (NO_2 , H_2O , CH_4 , particulates, ozone) all affect stratospheric temperatures, changes in which affect stratospheric ozone. For the most part, however, with the doubtful exception of the CO_2 and halogen contents, any prognoses are too speculative to be of value, and have been ignored herein.

Results of various modeling exercises follow, arranged largely chronologically. Changes with time have come about due largely to changes in preferred rate coefficients, which have a considerable effect on the results, and to inclusion of more complex chemistry. For example, as indicated in Table 3.1 and as shown in Section 3.4.6, the rate of one particular reaction rate



has a strong effect on computed ozone depletion by SSTs. In the CIAP and NAS (1975) studies, a value of $2 \times 10^{-10} \text{ cm}^3/\text{sec}$ was used; in halocarbon studies, a value of $2 \times 10^{-11} \text{ cm}^3/\text{sec}$ was preferred, based on newer data and reevaluations. This change, if adopted, reduces the ozone-destroying effects of SSTs by some 60 percent (at 17 km). Also, important interactions exist between the NO_x and ClO_x cycles, which have only recently been recognized. And, as noted several times, CIAP and other studies in the CIAP time frame did not include methane oxidation (smog) ozone-producing reactions or the effects of chlorine. Nevertheless, for completeness, all these results are included in the following.

3.4 RESULTS OF VARIOUS MODELING STUDIES

3.4.1 CIAP, 1974, and NAS, 1975 Results

A. 1-D Models

The work of two investigators, Chang (see CIAP Monograph 3) and Hunten (see Hunten, 1975; also NAS, 1975), dominated conclusions drawn by CIAP in the ROF; only Hunten's work was accepted in the NAS report (1975). The CIAP results were based on an arithmetic average of the Hunten and Chang results. Discussion of the Hunten and the Chang models follows.

Hunten (1975) first derived a K_z profile, based on methane lifetimes and boundary flux estimates for the upper portion of his model atmosphere and other considerations for the tropopause portion; his K_z results were shown in Fig. 3.13. The lifetime estimates for CH_4 were based on OH and O^1D estimates from Wofsy and McElroy (1973), using then-current chemistry, adjusted to account for night-day effects. No attempt to "close" the K_z -chemistry iterative loop was made (see Chang, 4th CIAP Conference, February 4-7, 1975).

The rather slow vertical exchange implied by the Hunten 1974 K_z profile near the tropopause was argued to be consistent with the known rate at which excess carbon-14, produced by nuclear weapons tests, had been observed to leave the stratosphere (see NAS/CIC, pp. 146-149, also Johnston, et al, 1975). The validity of this has been questioned (Chang, 4th CIAP Conference, 1975); the point is further discussed in Section 3.6.

In developing the Hunten model, no new computer runs were made. Rather, the assumption was made, based on McElroy et al., (1974) that, in the absence of stratospheric sinks (NO photolysis was neglected), the augmented mixing ratio of NO_y ($\text{NO} + \text{NO}_2 + \text{HNO}_3$) above the point of injection would be constant, and dependent only on the K_z profile below the point of injection; an injection coefficient was derived to determine this augmented mixing ratio (see Appendix D, this report), and ozone depletions were estimated by using the ozone depletion results of McElroy et al., (1974), including a thermal feedback effect (which did not include effects of added NO_2 or H_2O). The temperature-feedback-corrected results showed smaller depletions than did the isothermal results. The model also included an approximation rather than a full modeling approach to estimate effects below about 28 km. The McElroy et al., (1974) depletions, as correlated by Hunten, are smaller than predicted using CIAP chemistry and the Hunten K_z profile (see NAS, 1975, p. 145).

Hunten (1975), (also NAS, 1975, pp. 110-119) gives the following formulae from which injection coefficients and ozone depletions can be

calculated, based on the Hunten K_z profile.

$$\alpha = C \left(e^{\left(\frac{z - z_t}{H_p} \right)} - D \right)$$

where

α is the injection coefficient (10^{-17} cm²-sec)

z is flight altitude (adjusted)

and the other symbols have numerical values as follows:

Height, km	z_t , km	H_p , km	C	D
0 - 10	10	6.2	0.087	0
10 - 14	10	6.2	0.29	0.70
14 up	14	18.1	16.7	0.979

Given α , the pollutant mixing ratio above the altitude of injection, χ , is obtained by

$$\chi = \alpha Q$$

where Q is in mol/cm²-sec. Hunten uses the area of a hemisphere (2.55×10^{18} cm²) in calculating Q .

Given χ , converted to ppbv, Hunten turned to McElroy et al., (1974) to obtain ozone depletions using his correlation of McElroy's results for the temperature-corrected case, obtaining, as shown in Fig. 3.15, the formula

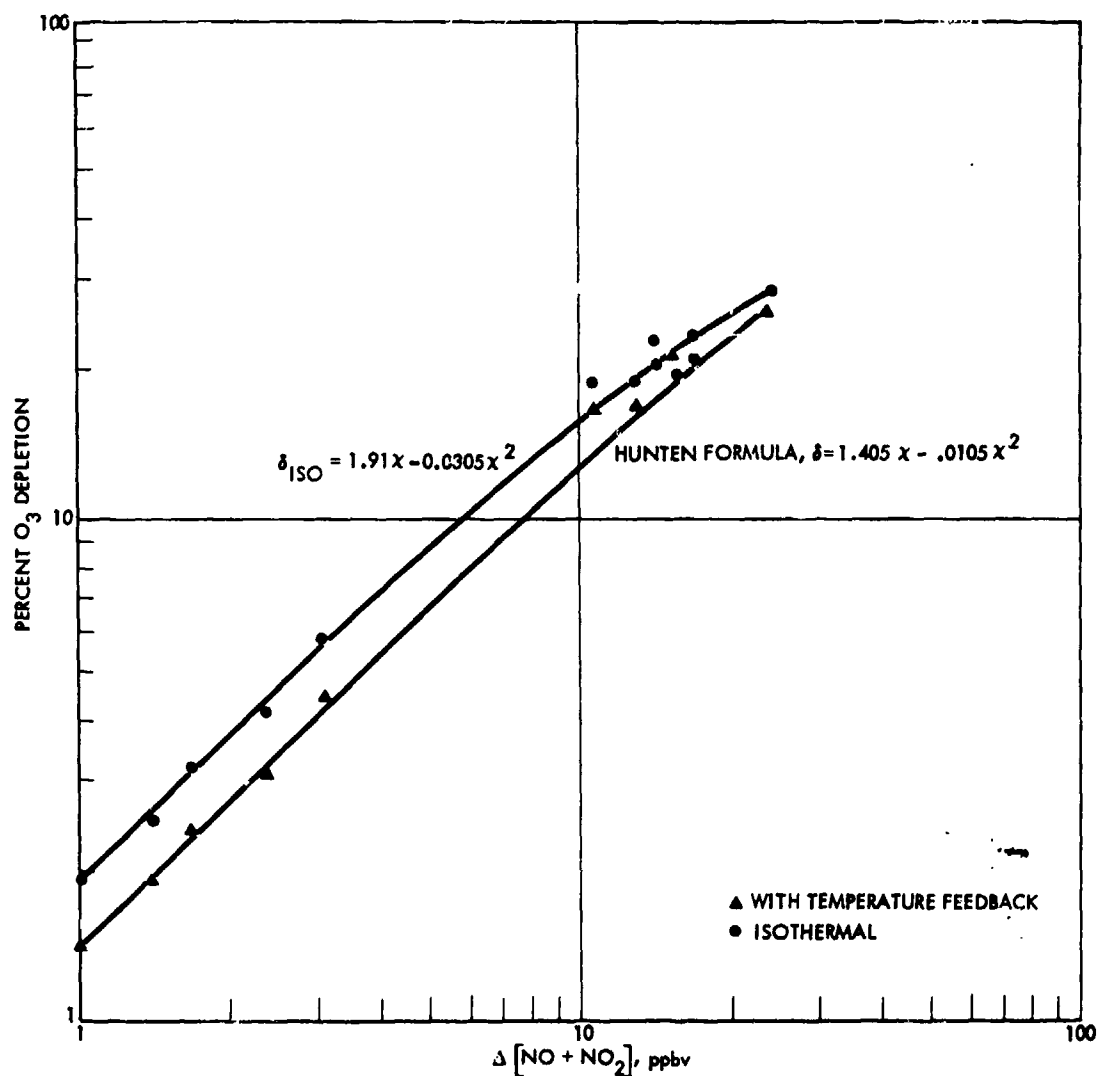
$$\delta_H = 1.405 \chi - 0.0105 \chi^2$$

where δ_H is the percentage ozone depletion by the Hunten formulae.

As noted earlier, because McElroy et al. ignored the compensating temperature effects of NO₂ (and any effects of H₂O), the temperature-corrected case may understate effects. McElroy's isothermal case is also shown on Fig. 3.15, and the results correlated, giving

$$\delta_{Iso} = 1.91 \chi - 0.0305 \chi^2$$

Hunten considered his K_z profile with a 14-km tropopause to be associated with 32° N, the latitude at which the CH₄ data were taken. For traffic at higher latitudes, he recommended use of his model with aircraft traffic shifted upwards in altitude, the argument being that contaminants mix along a surface parallel to the mean tropopause. In particular, for typical traffic, which he took to be at 40° N, he recommended 2-km flight altitude adjustments. At flight altitudes near the model tropopause, this



Reference: McElroy, et al (1974), Table 5

4-29-76-9

FIGURE 3.15. Correlations of McElroy et al. (1974) Estimates of Ozone Depletions

has a very large effect on calculated ozone depletions (6-fold at 12-km true flight altitude).

Values of ozone depletion computed via the Hunten procedure are given in Table 3.5, for an assumed 10^8 kg/yr NO_x injection. As a point of reference, 10^8 kg/yr NO_x corresponds to about 159 Concorde, or 256 advanced subsonics, based on the numbers used in the NAS (1975) report (p. 29).

TABLE 3.5 OZONE DEPLETIONS (HEMISPHERIC, PERCENT) WITH INJECTION OF 10^8 kg/yr NO_x (as NO_2) AT ABOUT 40°N , HUNTEN MODEL*

Altitude		$10^{-17} \text{ cm}^2 \text{ sec}$	$\chi - \text{ppbv}$	δ_{Hunten}	δ_{Iso}^{**}
True	Adjusted	α		$1.405 \chi - 0.0105 \chi^2$	$1.91 \chi - 0.0305 \chi^2$
9	11	0.1378	0.0224	0.032	0.043
12	14	0.3507	0.0570	0.080	0.109
13	15	1.318	0.2142	0.301	0.408
14	16	2.302	0.3741	0.524	0.710
17	19	5.664	0.9204	1.284	1.732
20	22	9.633	1.5654	2.174	2.915
23	25	14.316	2.326	3.211	4.278

*Treated in the CIAP Report of Findings as equal to the changes in the principal traffic "corridor."

**Not part of the Hunten model.

Note that the Hunten formulae, as used here, are for a fleet at about 40°N . The computed depletions are for the hemisphere; no mention is made of global average values. In CIAP 2-D studies (see Section B following), it was found that a value about twice the global average represented a "corridor value"; i.e., the depletion to be expected in the 30°N - 60°N region due to heavy traffic in that region. The hemispheric average was somewhat less than the corridor value. Thus, in the CIAP ROF, the Hunten "hemisphere" effect, as calculated, was treated as the "corridor" effect; this same procedure is used here.

Chang's extensive computational results on O_3 reduction which were performed in 1973 were correlated in the CIAP ROF (p. B-19), using a simple least-squares fit, according to the formulation,

$$\delta = a \chi^b$$

to give values for a and b at specified flight altitudes.* The results, however, were heavily influenced by cases for large ozone depletions. For cases involving low values of depletion, consistent with HAPP guidelines, it seems more reasonable to fit Chang's actual results, at injections of 0.124 and 1.24 ($\times 10^9$) kg NO_2/yr , giving values as in Table 3.6.

Ozone depletions, using these formulas, are given in Table 3.7, using 2×10^8 kg/yr as an input global value, to give corridor values corresponding to 1×10^8 kg/yr injection (for consistency with the Hunten formulas) and CIAP procedures.

As noted, the CIAP Report of Findings took a numerical average of the Hunten and Chang results. Following that approach, the values shown in Table 3.8 would be found.

Note that the largest differences between the two models lies in the 13- to 14-km region. This shows the powerful effect of the Hunten 2-km adjustment assumption on the effects of subsonic aircraft. In effect, this assumption puts all aircraft operating at 12 km or higher, above a sharp tropopause, on a continuous basis.

B. Higher Dimensionality Model Results

During CIAP, much was learned about the general behavior of a precipitation-scavengable pollutant introduced into the stratosphere through application of Mahlman's 3-D GCM (General Circulation Model) (see CIAP ROF, pp. E-90 to E-93). These data showed, for example, the buildup of pollutant with time as a function of latitude, for 20-km injection at 30° N, and were utilized in estimating hemispheric distribution of pollutants at steady state. In addition, Mahlman at the 4th CIAP Conference (1975) showed some of the limitations of 1-D modeling, if treated in terms of global average gradients, fluxes, and implied K_2 values for different tracers. Some information similar to this is given in Section 3.2.3. In addition, preliminary runs were made with fixed dynamics (constant October) 2-D model from Aerospace (George Widhopf); Rao-Vupputuri and Hesstvedt also presented results for steady-state conditions (see CIAP ROF, pp. E-62 to E-72). Of these models, the furthest advanced at the time of CIAP's completion appeared to be the MIT model (Alyea, Cunnold, Prinn, ROF, 1975, pp. E-78 to E-88).

Four runs, three perturbed atmosphere cases, and one natural atmosphere case, have been reported by the MIT group.** The three perturbed

*See also CIAP Monograph 3, pp. 4-170 to 4-172 for alternative correlation procedures and other discussion.

**The fourth run was analyzed by MIT after CIAP completion and reported in their contract final report. See Cunnold and Alyea (1975), and Cunnold et al. (1977).

TABLE 3.6 DATA AND CORRELATIONS FOR OZONE DEPLETIONS (GLOBAL AVERAGE PERCENT) WITH DERIVED COEFFICIENTS, CHANG MODEL (CIAP ROF, 1974)

Altitude, km	NO _x Rate, kg/yr (x)		Coefficients, $\delta = ax^b$	
	1.24×10^8	1.24×10^9	a	b
9	.005	.05	.0403	1.0
12	-	.35	.282	1.0
15	.14	1.37	1.107	.9906
17	.29	2.77	2.243	.9801
20	.72	6.29	5.137	.9413
23	1.33	10.33	8.525	.890

TABLE 3.7 CORRIDOR OZONE DEPLETIONS, PERCENT, WITH INJECTION OF 1×10^8 kg/yr NO_x (as NO₂) INTO HEMISPHERE, CHANG MODEL (CIAP ROF, 1974)

Altitude, km	Ozone Depletion, Percent
9	0.008
12	0.056
15	0.225*
17	0.463
20	1.129
23	2.035

*Interpolated

TABLE 3.8 CORRIDOR OZONE DEPLETIONS, PERCENT, WITH INJECTION OF 1×10^8 kg/yr NO_x (as NO₂) INTO HEMISPHERE, HUNTEN, CHANG, AND CIAP MODELS (CIAP ROF, 1974)

Flight Altitude, km	Huntен Model	Chang Model	CIAP (average)
9	0.032	0.008	0.020
12	0.080	0.056	0.068
13	0.301	0.090*	0.196
14	0.524	0.143*	0.334
17	1.284	0.463	0.874
20	2.174	1.129	1.652

*Interpolated graphically

cases all used an injection rate of 1.8×10^9 kg NO_2 /yr, injected in a 1-km thick, 10-degree-wide band, centered as shown:

Run 17	Natural atmosphere
Run 18	20-km injection, 45° N
Run 19	17-km injection, 45° N
Run 20	20-km injection, 10° N

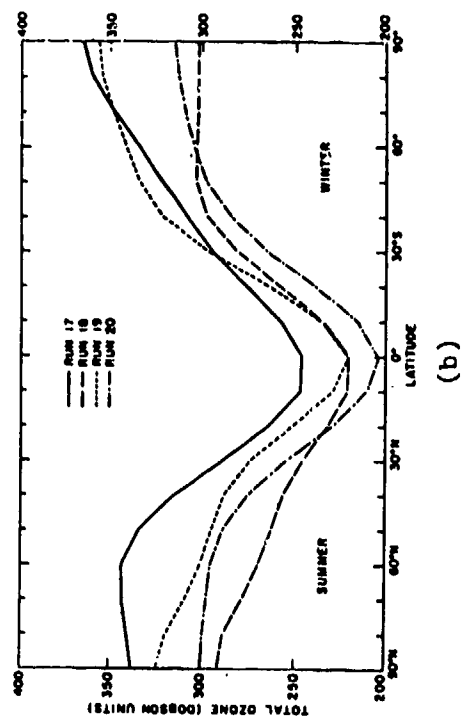
Three-year integrations of the perturbed atmosphere were used, after a much longer 2-D distribution run for the NO_2 . Results are given in Figs. 3.16a through 3.16d. The results show some anomalous behavior, in particular the ozone enhancement in the 17-km injection case in the Southern Hemisphere winter (Fig. 3.16b). Numerical results are given in Table 3.9 for annual global, hemispheric, and 45° N average, and for 45° N in the summer season. The hemispheric average seasonal depletion values are given in Table 3.10.

Note that the global average effect was not significantly changed with changes in latitude of injection, in these two cases at least. The Northern Hemisphere average value was, however, greater with more northern injection, as was the depletion in the important summer season at 45° N. The Southern Hemisphere effect was greater with tropical injection, as might be expected.

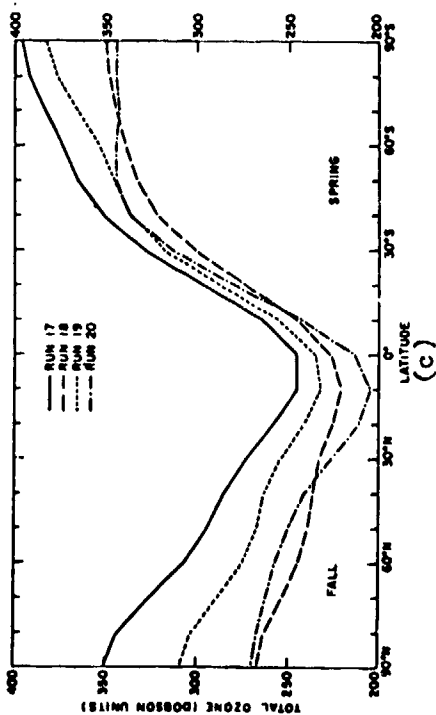
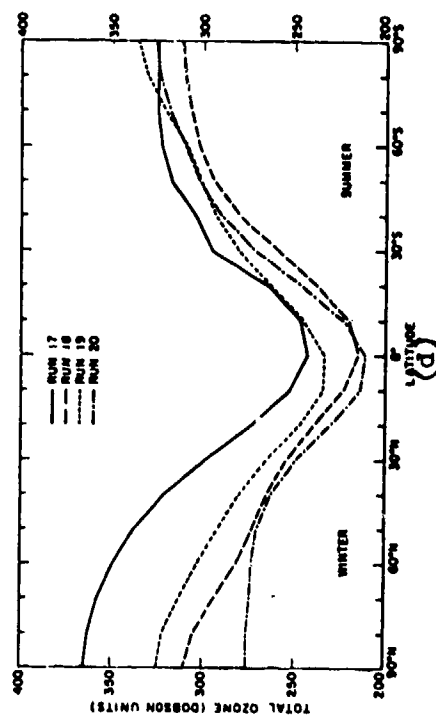
Also, the ratio of effects (Northern Hemisphere/Southern Hemisphere) was greater for farther-north and lower-altitude injections.

The MIT model used a 30-day rainout lifetime for NO_y in the troposphere. As a result, some fraction of the added NO_y was found to enter the troposphere in mid-latitudes, be transported equatorially, and returned to the stratosphere in the rising branch of the Hadley cell. The actual value to be used for the rainout coefficient is not well established, and is important in determining the effect of added NO_x in the stratosphere on the ozone layer. (See Prinn et al., 1975, 1974 for data on NO_x augmentations; ozone effects are not given.) The COMESA (1975) group used 7-day and 14-day rates in their 2-D modeling, and 30 days in their 3-D modeling (see Appendix B).

The rate of response of the MIT 3-D model atmosphere to an imposed NO_x source at 20 km at 45° N is shown in Fig. 3.17 for several locations. The Southern Hemisphere effect lags the Northern Hemisphere by 5 or more years, a point which would be important, for example, in monitoring effects of a growing fleet. In effect, since fleets may well change substantially in a 5-year period, the steady-state effects shown in Fig. 3.17 might never occur.



3-34



3-2-77-19

FIGURE 3.16. Ozone Columns as a Function of Season and Latitude, for Unperturbed (run 17) and Perturbed Atmospheres. Run 18, 450 N at 20 km; run 19, 450 N at 17 km; run 20, 100 N at 20 km. NO_x injection 1.8 Mt/yr in each case.
Source: Cunnold and Alyea, 1975.

TABLE 3.9 OZONE DEPLETIONS, PERCENT, WITH INJECTION OF 1.8×10^9 kg/yr NO_x (as NO_2) MIT MODEL
SOURCE: Cunnold and Alyea, 1975; 1977

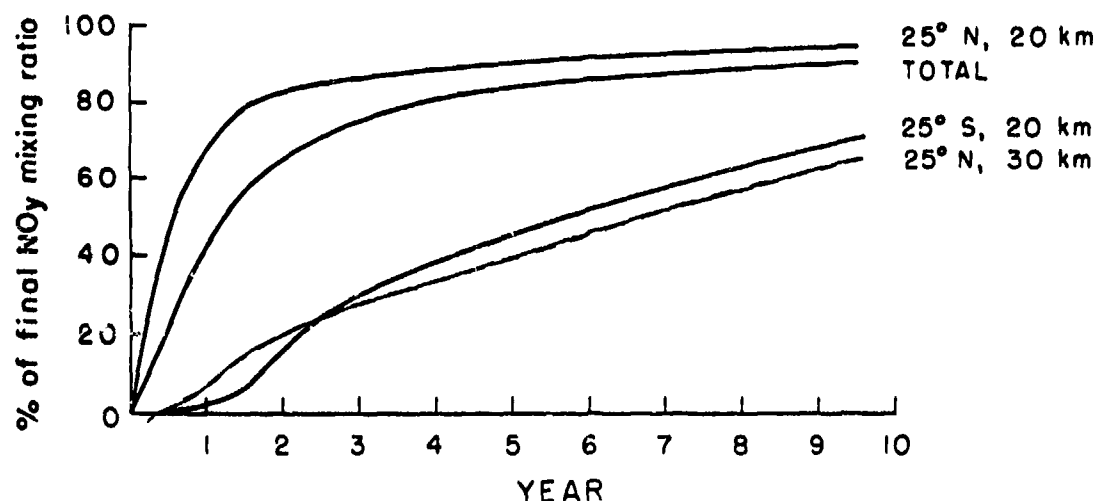
<u>Injection</u>	<u>Annual Global Average Depletion, %</u>	<u>Annual Hemispheric Average Depletions, %</u>		<u>At 45° N*</u>	
		<u>Northern Hemisphere</u>	<u>Southern Hemisphere</u>	<u>Summer Season</u>	<u>Annual Average</u>
45° N, 20 km	11.9	16.1	7.7	20	19
45° N, 17 km	5.8	8.2	3.4	11	10
10° N, 20 km	12.5	15.5	9.4	13	15

*Obtained graphically from Fig. 3.16

TABLE 3.10 SEASONAL HEMISPHERIC AVERAGE OZONE DEPLETIONS, PERCENT, WITH INJECTION OF 1.8×10^9 kg/yr NO_x (as NO_2) MIT MODEL
SOURCE: Cunnold and Alyea, 1975; 1977²

<u>Northern Hemisphere</u>				
<u>Injection at</u>	<u>Mar-May</u>	<u>Jun-Aug</u>	<u>Sep-Nov</u>	<u>Dec-Feb</u>
45° N, 20 km	17.4	15.9	15.5	15.7
45° N, 17 km	6.0	8.4	7.7	10.9
45° N, 20 km	13.7	13.6	16.8	18.3
<u>Southern Hemisphere</u>				
<u>Injection at</u>	<u>Mar-May</u>	<u>Jun-Aug</u>	<u>Sep-Nov</u>	<u>Dec-Feb</u>
45° N, 20 km	6.5	7.2	8.4	8.7
45° N, 17 km	5.9	2.3*	4.0	2.5
10° N, 20 km	13.3	11.0	7.2	6.2

*Anomalous behavior



3-2-77-20

FIGURE 3.17. Approach of Incremental NO_y to Final Value, $1.8 \text{ Mt NO}_x/\text{yr}$ (as NO_2) at 20 km and 45° N , 2-D Model Results.
Source: D. M. Cunnold, private communication, 1976.

The MIT results can be compared to the Hunten 1-D and Chang 1-D models. The Hunten model, for 45° N injection (with a 2-km adjustment) gives a Northern Hemisphere value of 31.2 percent depletion (which is slightly beyond the range of applicability of the correlation). The Chang model (p. E-59, ROF) gives a global average value of about 8 percent (interpolating); the hemispheric value (at double the rate) would be about 15 percent. These figures should be compared to the Cunnold-Alyea values of 12 percent and 16 percent. At 17 km, the Hunten model would give 20.4 percent; the Chang global average value is 3.7 percent, and a hemispheric value (at double the rate) is about 7.3 percent. These latter figures should be compared to the MIT values of 5.8 and 8.2 percent, respectively. The Hunten values are thus considerably higher, and the Chang values somewhat lower, than the Cunnold-Alyea results.

These results were all based on CIAP chemistry (in particular, $\text{OH} = \text{HO}_2 = 2 \times 10^{-10}$) and do not include "smog" reactions with methane or chlorine reactions.

3.4.2 COMESA Modeling Results (1975)

The COMESA program operated over the years 1972-1975. The report, which became available to us in May 1976, describes the extensive work carried out during that period. The two programs (CIAP and COMESA) operated during the same time frame and benefited from mutual interactions. Nevertheless, due to differences in approaches and some differences in chemistry,

results differed somewhat from those reported either in the CIAP ROF or in the NAS/CIC report. A review of the COMESA work is included as Appendix B to this report; a very brief review follows.

COMESA modeling efforts on the effects of aircraft effluents on ozone involved 3-D, 2-D, and 1-D models. The 1-D modeling exercises used diurnally and seasonally varying solar zenith angles, a departure from the procedures used in CIAP. The COMESA models also included the injection of H_2O , CH_4 , CO , and CO_2 in proportions expected from a Concorde fleet.

The COMESA 3-D general circulation model (without chemistry) was run for one year, studying the distribution of O_3 , H_2O , and NO_x as tracers. The results were collapsed to 1-D for comparison to published (Hunten/1974 and Chang/1974) K_z profiles). The different tracers showed widely differing behavior, including negative values of K_z as shown in Fig. 3.18. Gross averages, however, were developed which implied that the Hunten/1974 profile implies vertical motions to be too slow in the lower stratosphere and the Chang/1974 profile to be too slow in the upper stratosphere.*

With regard to the results from the 3-D tracer studies, COMESA concluded that: "Consideration of these results casts considerable doubts on the value of current 1-D models except for the purpose of first estimates and emphasizes the need for a more sophisticated treatment of the dynamics." In discussion, COMESA also questions the concept of 2-D models.

At the completion of the effort, the COMESA 2-D model was still at an early state of development, and considered unsuitable for perturbation predictions; it was used, however, to estimate latitudinal distribution of effects. Results on latitudinal distribution were similar to those reported in CIAP (p. B-20, ROF), although after only 3 years of equivalent running time, stationary state was not achieved.

Two 1-D models were used by COMESA, both using diurnally and seasonally varying sun angles, with fixed K_z profiles; Chang/1974 or Hunten/1974 model runs typically up to 10 years were used, but stationary state was not always evident. The first model (Model A) which included methane oxidation chemistry, 1-km resolution, and Chang K_z , a 10-km lower boundary and 50-km upper boundary, showed initial ozone enhancement by subsonics (at 11 km to 13 km) but (after 3 years) a slight depletion, varying with season, as shown in Fig. 3.19. SSTs showed depletions at all times. The second model (Model B) extended from the ground to 48 km, with 2-km resolution, but utilized simplified chemistry (no smog reactions). Runs with 1-D models included SSTs

*The Chang/1976 profile (Fig. 3.13) utilizes a larger value of K_z in the upper stratosphere.

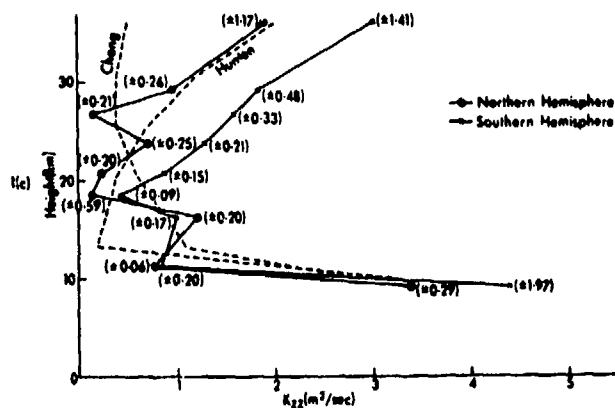
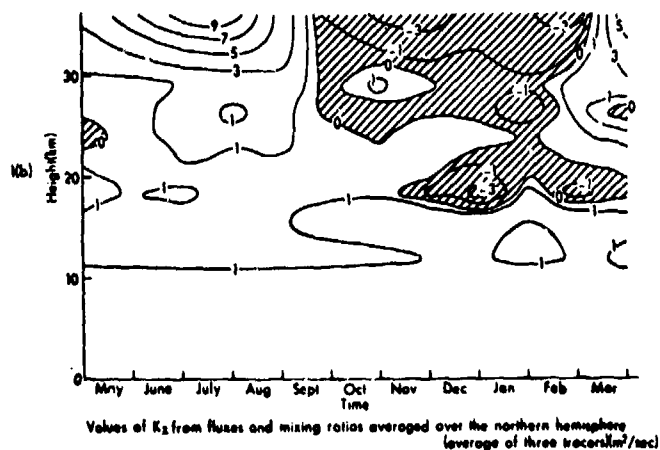
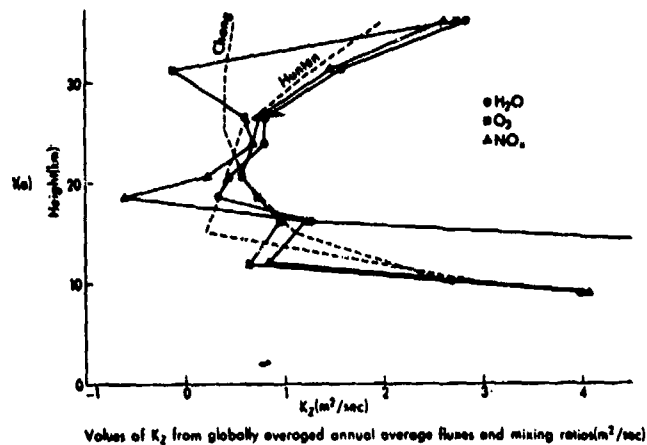
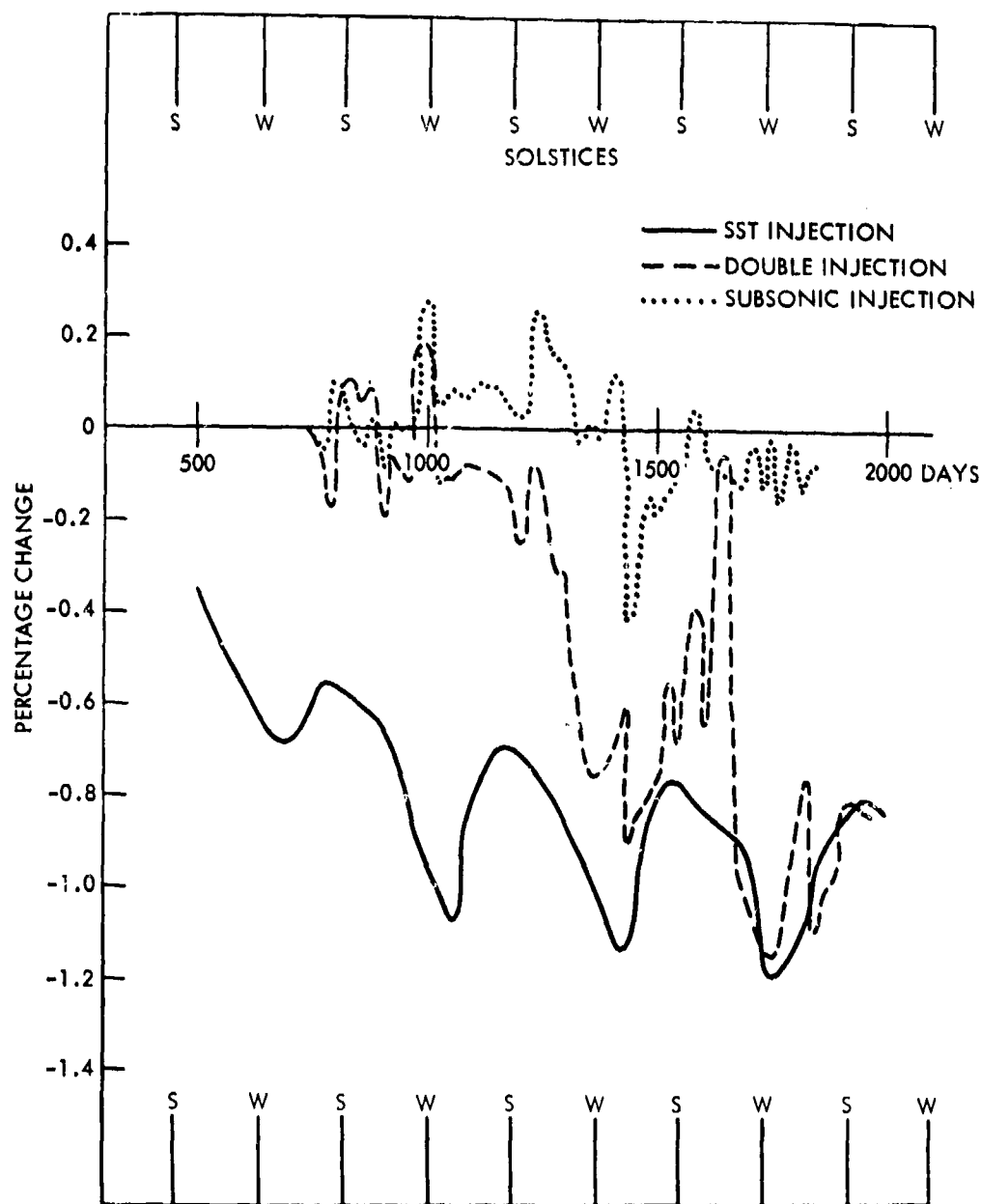


FIGURE 3.18. Values of K_z from Hemispherically Averaged Annual Average Fluxes and Mixing Ratios (average of three tracers) (m^2/sec)
Source: COMESA, 1975



1-21-77- 34

FIGURE 3.19. Percentage Changes in O_3 Columns (Model A). The injection rates at both altitudes were taken as 1.24×10^{34} molecules NO_2 /yr (9.5×10^8 kg NO_2 /yr), corresponding to approximately 1200 Concorde and about twice as many subsonics. The model lower boundary was 10 km, probably too close (as noted by COMESA) to the subsonic injection level.
Source: COMESA, 1975

and subsonics, alone and in combination. The most surprising result was an insensitivity to K_z for SSTs (Concorde/Tupolev), with Chang/1974 and Hunten/1974 K_z profiles giving about the same effect on ozone; with subsonics, however, the difference in results was substantial.

The COMESA report concluded that about 600 Concorde (each producing 8×10^5 kg NO_x/yr) would be required to cause 1 percent ozone depletion in the $30^\circ \text{N} - 60^\circ \text{N}$ region; a global average value would be about 1/2 percent, and the Southern Hemisphere value would be about 1/4 percent. The effects, as interpreted by COMESA, are about 1/6 those given by the NAS/CIC and about 1/3 those given in CIAP. They further comment that the results "indicate that the reduction of ozone caused by present subsonic fleets (which is widely regarded as negligible) will be less than doubled by addition of a hundred or more Concorde-like SSTs," (COMESA, 1975, p. 388). The reference to the present subsonic fleet is apparently based on the 0.1 percent figure quoted in the CIAP ROF, rather than to COMESA's own (Model A) results.

The COMESA report does not utilize the 2-km adjustment to aircraft altitude used by NAS and by CIAP in applying the NAS model. COMESA also notes that their ozone depletion results are about half those found by Chang for the same K_z . They comment that the diurnal treatment may reduce the effects. Part of the reduced effect, however, (based on later studies by Lawrence Livermore Laboratory, Section 3.2.6) can be attributed to a lower value for the rate constant (6.7×10^{-11} rather than 2×10^{-10}) for the $\text{OH} + \text{HO}_2$ reaction. A larger NO_x column also entered (See Appendix B, p. 6).

The COMESA report also describes their measurements work, and discusses uncertainties in the understanding of certain important trace species. In their view, the measured NO_x in the stratosphere is larger than implied by the models, suggesting sources other than N_2O . If the point is verified, the stratosphere would be less sensitive to added NO_2 than predicted by the models. A brief review of their arguments is included in Appendix F.

3.4.3 Time-Dependent and Other Effects, 1-D Model [CIAP chemistry (no chlorine or "smog" reactions), Lawrence Livermore Laboratory/IDA studies, December 1975]

A. Time-Dependent Effects

In preceding sections, approximate "steady-state" changes on ozone were reported, assuming a continued injection at constant rate for many years--in some cases, 30 to 300 years, to be reasonably certain of reaching steady-state results. In any real situation, the rate of approach to the steady-state value is also important, since fleets change continuously with time; it is obviously of interest to be able to estimate time-dependent effects for various fleets from steady-state and respective data. While substantial questions may exist about whether the rate of approach to

equilibrium in a 1-D model has any physical reality in terms of the rate of approach in the atmosphere, it would seem that if the 1-D parameterization has any validity the rate of response might also. Latitudinal variations, of course, are expected, as was shown in Fig. 3.17. In any event, by using 1-D response time data along with 1-D steady-state data, simplified procedures have been developed here which give time-dependent, 1-D effects for fleets changing with time, and which, for the SST case at least, can be made to match the results obtained in a full computer simulation, as will be shown in the following. The data are from runs made at Lawrence Livermore Laboratory, 12-13 December 1975, using the same chemistry as used by Chang in CIAP, except that a "half sun" (signifying an average of night and day) was used, whereas in CIAP a "full-sun" was used.

Normalized ozone depletions versus time, using a step change in source, are shown for several cases in Figs. 3.20 (Chang/1974, K_z) and 3.21 (Hunten/1974 K_z). The labeled data show the altitudes of injection and source strengths in $\text{kg NO}_x/\text{yr}$ ($1\text{E}9 = 1 \times 10^9 \text{ kg NO}_x$, as NO_2 , per year). In each case, the inset graph gives time to e-fold and half the time for two e-folds. Note, however, that particularly for low-altitude injections, the initial response to the perturbing NO_x is to increase the ozone column, rather than to decrease it, so that an e-folding time, which implies an exponential approach to equilibrium ($1 - e^{-kt}$) is invalid; an e-folding approach, however, is not unreasonable as an approximation technique for injections at higher altitudes. The initial opposite effect at low altitude was obtained even in the absence of "smog" reactions, and was due to NO_2 interference* with the HO_x cycle at low altitude prior to diffusion of the pollutant NO_2 to ozone destruction altitudes. Modeling of this behavior for time-dependent fleets might be accomplished by assuming superposition of sources, but no data are available to support such an approach.

The overall response time (e-folding) increases with decreasing altitude, and, thus, residence time, directly opposite to the effect which would be expected on a box model of the stratosphere. Presumably, at some altitude, the response time would increase with altitude as residence time effects become dominant, an effect hinted at by the shape of one of the inset curves in Fig. 3.21. Response time may also be somewhat injection-rate-dependent (see inset on Fig. 3.21).

To test a simple approach to the time-dependent problem, square-wave response time and equilibrium data were applied to an hypothesized Concorde buildup and phaseout case, and compared to a detailed computer run.

*W. Duewer, private communication, January 1977

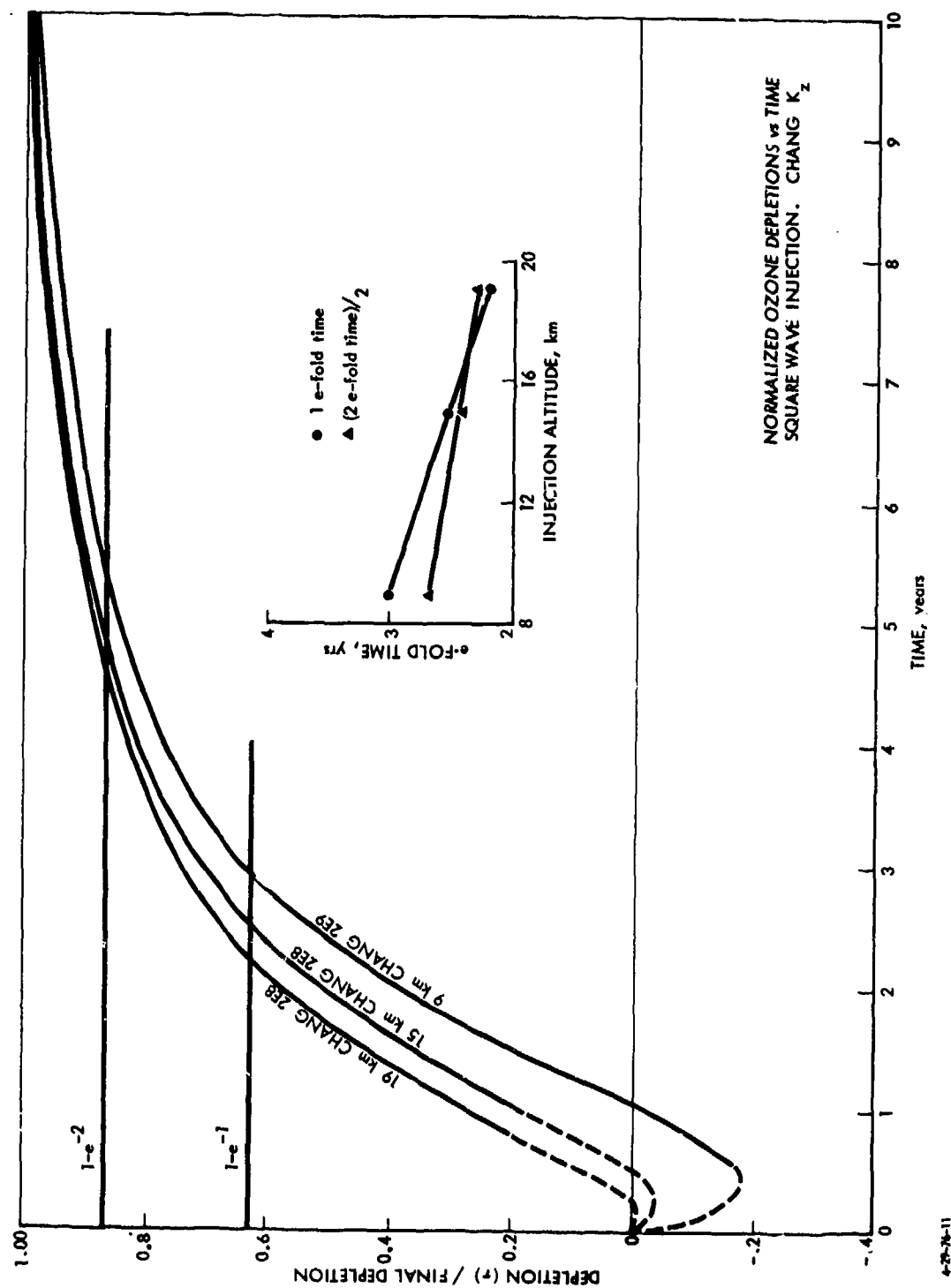


FIGURE 3.20. Normalized Ozone Depletions versus Time. Chang/1974 K_z

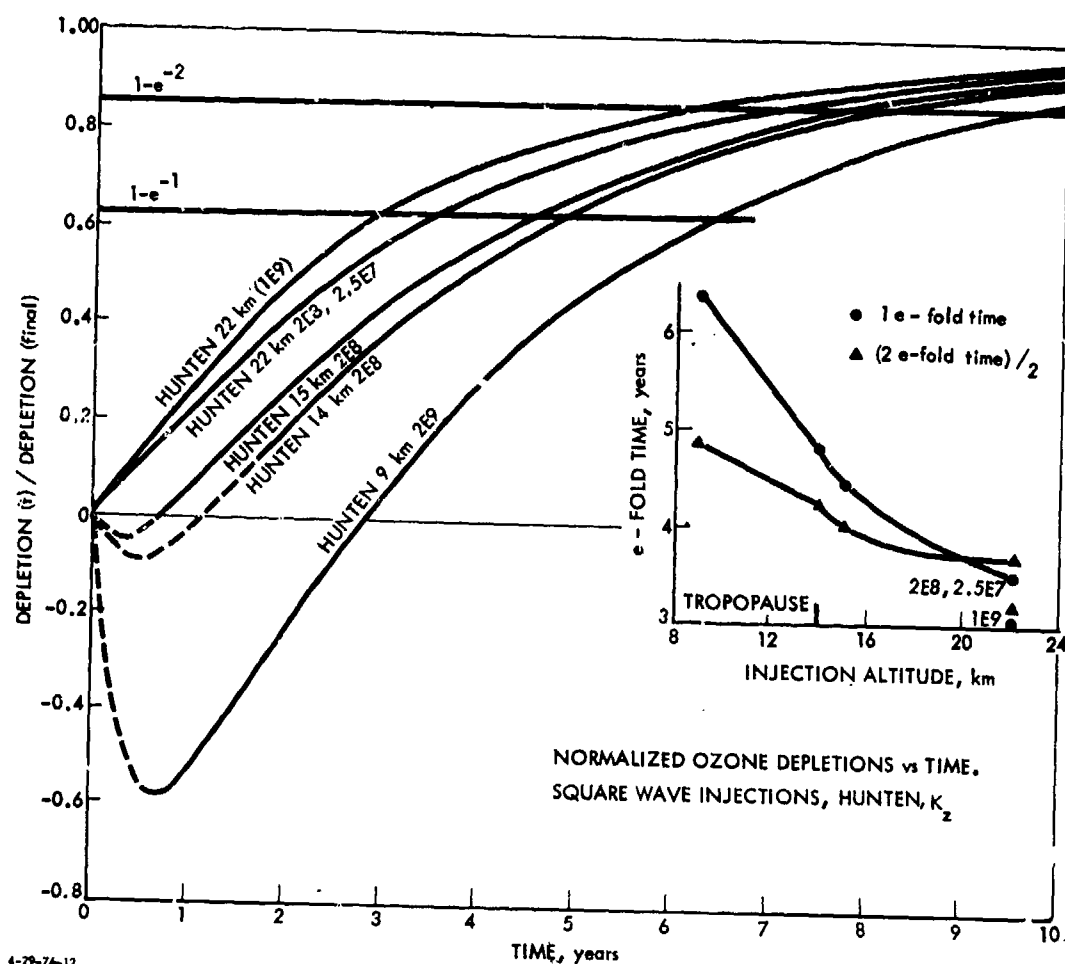


FIGURE 3.21. Normalized Ozone Depletions versus Time. Hunten/1974 K_z

The approach used assumed ozone depletions, in each band, to change with time according to

$$\delta_{n+1} = \delta_n e^{-1/R_t} + \delta_{n+1}^0 (1 - e^{-1/R_t}),$$

where δ_{n+1} = ozone depletion at the end of the year $n+1$,

δ_n = ozone depletion at end of year n (beginning of year $n+1$),

δ_{n+1}^0 = steady-state ozone depletion for NO_x injection rate at beginning of year $n+1$,

R_t = response time, years; here taken as half the e-folding and two e-folding times.

The functional relationships for steady-state O_3 decrease used in the simplified procedure (above) follow:

$$\begin{aligned} 14 \text{ km} \quad \delta^{\circ} &= 0.7258 R \\ 17 \text{ km} \quad \delta^{\circ} &= 2.34 R^{0.98}, \end{aligned}$$

where δ° is global average O_3 depletion in percent and R is in units of 10^9 kg/yr NO_x injection.

The depletion function used at 17 km is slightly higher than that used previously (which was based on Chang's 1973 results, pp. 13-17, CIAP ROF), in accordance with results obtained in December 1975. NO_x injections were taken to be at 14 km and 17 km, rather than at 13.5 km and 16.5 km, as in CIAP, as even injection altitudes are required in the Chang model.

The SST was assumed to build up and be phased out over a 29-year period. The NO_x emissions, per aircraft year, were taken as 1.082×10^5 kg at 14 km and 9.414×10^5 kg at 17 km. A response time of 2.56 years was used at 14 km and 2.38 years at 17 km, averaging one and two e-fold times. Final results are shown in Fig. 3.22. Good agreement was found, although a slightly larger response time could be argued. (Three years was tried, and found to be much too large.) Tabulated results for even years are presented in Table 3.11.

TABLE 3.11. OZONE CHANGES DURING FLEET BUILDUP AND PHASEOUT

Year	Actual* (LLL)	Simplified (IDA)
2	0.0075	0.0091
4	0.0226	0.0242
6	0.0401	0.0416
8	0.0587	0.0601
10	0.0777	0.0789
12	0.0895	0.0892
14	0.094	0.0936
16	0.096	0.0955
18	0.097	0.0964
20	0.0975	0.0967
22	0.0903	0.0882
24	0.0756	0.0737
26	0.0581	0.0564
28	0.0394	0.0380
30	0.0205	0.0187
32	0.0086	0.0081
34	0.0041	0.0035
36	0.0020	0.0015
38	0.0011	0.0007
40	-	0.0003

*Provided by J. Chang, Lawrence Livermore Laboratory, 13 December 1975

The procedure appears to be satisfactory. It should be noted that the response time question was not addressed in CIAP, or taken into account in fleet-effect considerations.

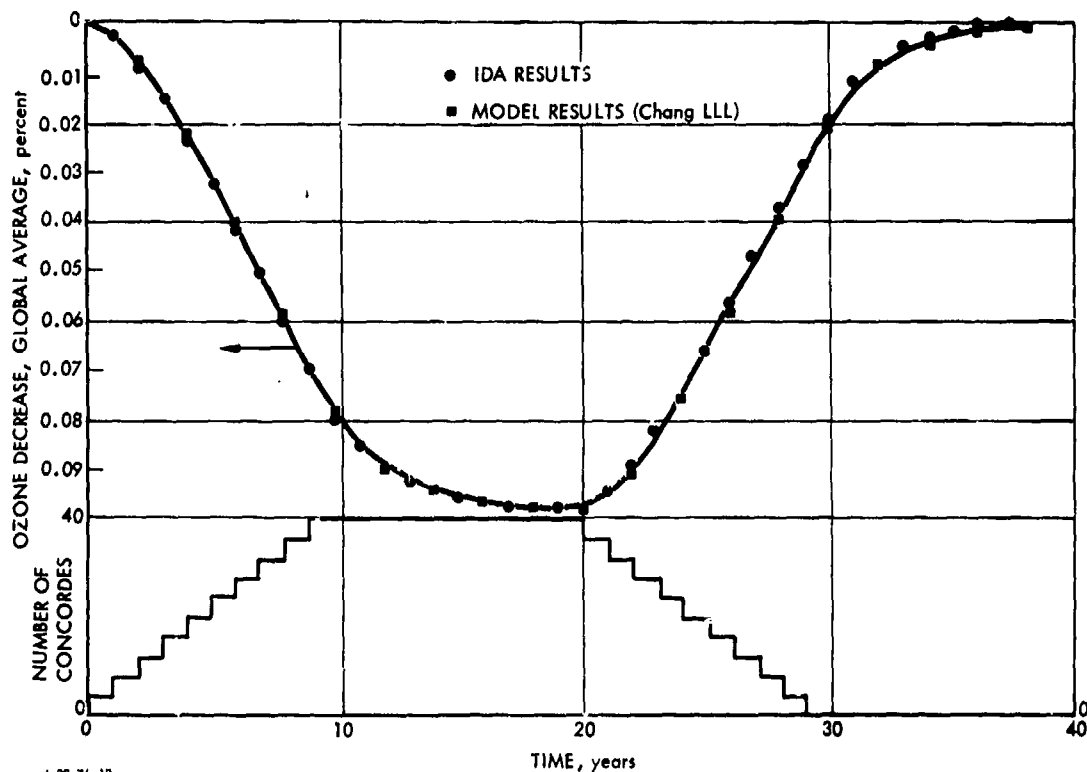


FIGURE 3.22. 1-D Time-Dependent Fleet and Model Ozone Effects Example. CIAP chemistry.

B. Reversibility With Elimination of NO_x Source

From a mathematical point of view, the sudden removal of a source of NO_x at a given altitude from a column in equilibrium is equivalent to the sudden addition of an NO_x source to a column in equilibrium. In a sense, one is an instantaneous negative source and the other an instantaneous positive source. To demonstrate the point, however, several cases were run by Lawrence Livermore Laboratory, 12-13 December 1975.

The first test involved a source at 9 km held constant for 30 years, using the Chang/1974 K_z profile. The final condition (which involved a slightly greater time than 30 years) was then taken as the initial condition, the source was set to zero, and the model again run for 30 years.

Reproducibility was found in this case to be good to five places (8.35069 x 10¹⁸ mol/cm² initial versus 8.35072 mol/cm² final). The behavior as a function of time was found also to be essentially symmetrical either with a suddenly imposed NO_x input or to a suddenly imposed NO_x shut-off, up to about 10 years after the change. The symmetry included the initial response; in this case, NO₂ removal initially decreased ozone.

Beyond about 10 years, small random errors appeared to distort the behavior very slightly. This initially opposite behavior might be of interest if confirmed and if emission controls on a fleet were being considered.

C. Additivity of Sources at Different Altitudes

One run was made to test the additivity of several sources at different altitudes. The summed run used the same sources as in three single-source runs, all using Hunten's K_z profile. Results, at steady state are presented in Table 3.12, using run numbers as assigned at the time of the runs:

TABLE 3.12. 1-D SOURCE ADDITIVITY TEST

Run	Altitude, km	NO _x Source, 10 ⁹ kg/yr	-ΔO ₃ /O ₃ Percent
1.2	9	2.0	0.0829
1.4	15	0.2	0.577
1.6	22	0.2	3.92
Sum			4.58
2.3	Summed sources		4.48

The summed results from the three initial runs were found to be slightly above the result with summed sources, as expected (since ozone depletions cannot exceed 100 percent).

The time-phased response in the summed case (run 2.3) was dominated by the large source at 22 km (run 1.6).

The choice of input conditions used here was probably not a good one in view of the dominance of a single component.

Note that in the correlations of Chang's results (p. B-19, CIAP ROF) and in the plot (p. E-59, CIAP ROF), which are of the form $y = ax^b$, where b varies above and below unity, the additivity of sources is imperfect, even for sources at constant altitude injection.

D. Effects of Water Added Simultaneously With NO_x

Five runs were made to test the effects of water vapor augmentation on ozone depletion. These data will be of principal interest if low NO_x combustors are developed. Steady-state conditions were considered, which seemed to be reached somewhat slowly. In each case, equilibration with added water was carried out before NO_x was added, and the end point distribution used as the starting point. The added water vapor was arbitrary, and based simply on a constant multiplier at every point in the column.

Results showed the effect of added water vapor to be K_z -dependent as to sign, and smaller in magnitude than reported by Crutzen (1974). With Chang's/1974 K_z profile, added water caused a slight decrease in ozone (a 25 percent increase in water causing a 0.016 percent decrease in ozone), whereas with the Hunten/ K_z profile, a 25 percent increase in water led to a 0.15 percent increase in ozone. Effects with small input NO_x rates, in addition, were additive.

As noted, the water effect found here, even with Hunten's K_z , for which the effect is positive, is still considerably less than that reported by Crutzen (1974), who found a 1.5 percent increase in ozone with a doubling of water vapor (compared to the equivalent of 0.5 percent for a doubling found here). McElroy et al., (1974) found a 0.1 percent increase in ozone for a 24 percent increase in water vapor (NAS, 1975, p. 161), compared to the 0.15 percent found with the Hunten/1974 K_z at 25 percent increase found here. Crutzen (1976) has since reported a minor decrease in ozone with increased water vapor.

Water effects might be of greater significance in a more realistic chlorine-containing model stratosphere (see Section 3.2.7). Thermal effects of water vapor on stratospheric ozone would also need to be considered with low NO_x emission-index combustion.

E. Residence Times

As a matter of additional interest, the added burdens of NO_y ($\text{NO} + \text{NO}_2 + \text{HNO}_3$) were computed for comparison to inert tracer computations by Chang in the CIAP ROF (p. 19) and by Bauer et al. (Appendix D).

TABLE 3.13. RESIDENCE TIMES FOR ADDED ODD NITROGEN

Altitude, km	K_z	Run	Δ Burden NO_y , mol/cm ²	Input Rate (mol/cm ² -sec)	Residence Time, Years
9	Chang	1.1	2.150E14	1.616E8	0.042
9	Hunten	1.2	4.146E14	1.616E8	0.081
22	Hunten	1.6	2.2439E15	1.616E7	4.39
22	Hunten	1.7	11.3347E15	8.08E7	4.35

For comparison, residence times at 9 km in the CIAP ROF (p. 19) are 0.08 (Chang) and 0.25 (Hunten) years. For these same conditions, Bauer finds 0.072 and 0.21 years (Appendix D). At 22 km, the ROF (p. 19) would give approximately 5.3 years.

The burden buildup of NO_y with time was also examined for run 1.6. In the case of run 1.6 (22 km, Hunten K_z), it appeared that the NO_y burden buildup followed the ozone depletion change fairly closely, with both responding (e-folding) in about 3.7 or 3.8 years, somewhat faster than the

apparent residence time). However, in runs 1.1 or 1.2 (9 km, Chang and Hunten K_z), the NO_y column buildup was much faster than the ozone depletion. In run 1.1, 78 percent of the equilibrium incremental $\text{NO} + \text{NO}_2$ burden was reached in 1 year (HNO_3 data were not available, but should not affect the result much); in run 1.2, 82 percent of the $\text{NO} + \text{NO}_2$ incremental burden was reached in 1 year.

Response time and residence time are evidently not well related. Also, residence times (burden/flux) apparently vary with the tracer. In the case of NO_y , this may be explainable by interaction with N_2O , the concentration of which was found to be affected by an artificial NO_x source, and by reactions with atomic nitrogen.

F. Pollutant Mixing Ratio Constancy

A fundamental tenet of the injection coefficient approach, as used by Hunten, is that the augmented mixing ratio of pollutants above the point of injection is constant.

The point was investigated, using the run data generated at Lawrence Livermore Laboratory (LLL) for several cases, and compared to values read from the graphical data presented by McElroy et al. (1974). The LLL results showed a definite decrease with altitude, decreasing by a factor of 2 or more between 28 km and 40 km, whereas McElroy's results were more nearly constant. In a subsequent analysis, Duewer et al. (1976), showed this effect to be due to destruction of NO and NO_x by N atom reactions. However, ozone depletion results were found to be not significantly affected by the inclusion or deletion of these reactions as shown in Table 3.14.

TABLE 3.14. OZONE DEPLETIONS* WITH AND WITHOUT N ATOM REACTIONS
(Global; 17 km, 2.46×10^9 kg/yr NO_2)

K_z	With	Without
Chang/1974	1.75	1.77
Hunten/1974	6.68	7.25
Crutzen-Isaksen/1975	1.31	1.36

*Source: Duewer et al., 1976.

3.4.4 NASA-Ames 2-D Model Results (January 1976)

Borucki et al. (1976) have published preliminary results of a 2-D model study of ozone depletions due to supersonic aircraft. The model extended from the ground to 60 km in 2.5-km intervals, and from 80° S to 80° N. Results were considered to be preliminary in that further work was felt to be needed on the transport parameters. The model did not include the methane oxidation reactions, but did use a lower value (6×10^{-11} cm³/sec)

for the $\text{OH} + \text{HO}_2$ reaction than was used in CIAP ($2 \times 10^{-10} \text{ cm}^3/\text{sec}$). The authors compared their results to those of Cunnold and Aleya (see Section 3.4.1.B). The agreement was found to be good for similar runs in the Northern Hemisphere but not as good in the Southern Hemisphere.

These authors reported ozone depletions as a function of latitude for NO_x injection at the rate of 1.8×10^6 metric tons/year at 20-km altitude for three different latitudes of injection ($30\text{--}40^\circ \text{ N}$, $40\text{--}50^\circ \text{ N}$, and $50\text{--}60^\circ \text{ N}$). Results were largely insensitive to the latitude of injection. At 45° N , the calculated depletion was 20 percent for $30\text{--}40^\circ \text{ N}$ injection and for $50\text{--}60^\circ \text{ N}$ injection, but 19 percent for $40\text{--}50^\circ \text{ N}$ injection.

3.4.5 Crutzen 2-D Model Results (early 1976); methane reactions included; chlorine reactions excluded

As noted in Section 3.1, the methane oxidation reactions produce ozone in the presence of NO_x ; Johnston (1974), in fact, pointed out that the rate of ozone-generating reactions crosses the rate of ozone-destroying reactions at about 13 or 14 km altitude in a 1-D model. These reactions were not included in any of the CIAP or NA modeling work described heretofore; one of the 1-D models used by COMESA did include these reactions, but use of a lower boundary of 10 km made any results due to aircraft at 11-13 km rather dubious, as COMESA points out (see Section 3.4.2, this report). The Crutzen 2-D model, from which first results with SST sources were reported in the 4th CIAP Conference (February 1975) did, however, include these reactions, so that it became of particular interest to carry out runs with this model to compute the effects of aircraft at various altitudes. Such runs were made, with the cooperation of P.J. Crutzen and NCAR in the winter and early spring of 1976.

The Crutzen model is described in his 4th CIAP Conference paper (Crutzen, 1975); at the time of the runs to be described, however, the model had been modified in the rate of meridional transport to fit data accumulated following the Fuego eruption.

Detailed results of these runs are given in Appendix A, and summarized briefly in this section. The most interesting aspect of the results was that the model runs simulating subsonic and advanced subsonic aircraft generally showed increases in the total ozone column in northern flight latitudes, as will be seen; however, it must be emphasized that the results are tentative, in that the chemistry is uncertain and work is needed on the model for use near the tropopause, the region which was of prime interest here; also steady state may not have been achieved in the six-year model period utilized. In addition, it was found that the model does not handle water injections properly, so results include only the effects of NO_x injections (as, of course, do most other modeling results).

The model uses 6×10^{-11} cm³/sec for the critical $\text{OH} + \text{HO}_2 \rightarrow \text{H}_2\text{O} + \text{O}_2$ reaction, somewhat lower than 2×10^{-11} value recommended in NAS, 1976a (see Section 3.4.7). (Larger values of this reaction rate increase the ozone depletion.) The model did not include the NO_3 cycle described by Johnston (see Table 3.1), but judging from other results (see Section 3.4.8) it is doubted that inclusion of the cycle would have substantially altered results. The point should, of course, be checked.

The model was used for latitudinally distributed NO_x injections, based on Table 2.12 (Section 2, this report), at four levels (level 9, approximately 11 km; level 10, approximately 12.5 km; level 11, approximately 14.3 km; and level 13, approximately 18 km). The model is in pressure units, so quoted geometric levels represent standard atmosphere pressure altitudes (see Section 2.14).

Inputs were parametric, in that the 1.8 vertical km resolution of the model could not be matched to the actual flight trajectories of the various aircraft. The injection rates selected, however, were related to the data given in Table 2.12 only in a general sense. For example, the level 9 run was based on a 50 percent increase over the total subsonic fleet fuel values given in Table 2.12 (to allow for low-altitude traffic) and an emission index of 16 gm NO_2 /kg fuel, corresponding to fan jet engines, was used, rather than 10 gm/kg as in CIAP, which corresponded more to current low-pressure-ratio engines. Small perturbations resulted with the injection rates used; to gain accuracy, both the perturbed and natural stratosphere were run beyond initial starting conditions, and the changes noted at corresponding times. The runs were carried for six years, which appeared to give stable results; however, long slow changes could not be ruled out, particularly in the Southern Hemisphere (see Fig. 3.17).

The input conditions, which were not varied seasonally, are shown in Fig. 3.23. A sample 2-D seasonally varying result is plotted for 11-km injections in Fig. 3.24; detailed tabular data are given in Table 3.15. The variations with injection altitude for 35° N, 45° N and 55° N are shown in Fig. 3.25 for a normalized input of NO_x of 1×10^9 kg/yr, assuming linearity for the input rates shown in Table 3.16; linearity, however has not been demonstrated. The variations in latitudinal distribution between different levels were also ignored in preparing Fig. 3.24, but this effect should have been small.

The enhancements found in ozone column are small. In terms of mixing ratios, it can be deduced from the data in Appendix A, Figs. A-11 and A-12, that the increase in ozone for 11-km injection is about 12 percent, or about 0.12 (5×10^{11}) or 6×10^{10} mol/cm³. At 11 km, the atmospheric density is about 7.6×10^{18} mol/cm³ (U.S. Standard Atmosphere, 1962) so that the mixing ratio augmentation is 8 ppbv.

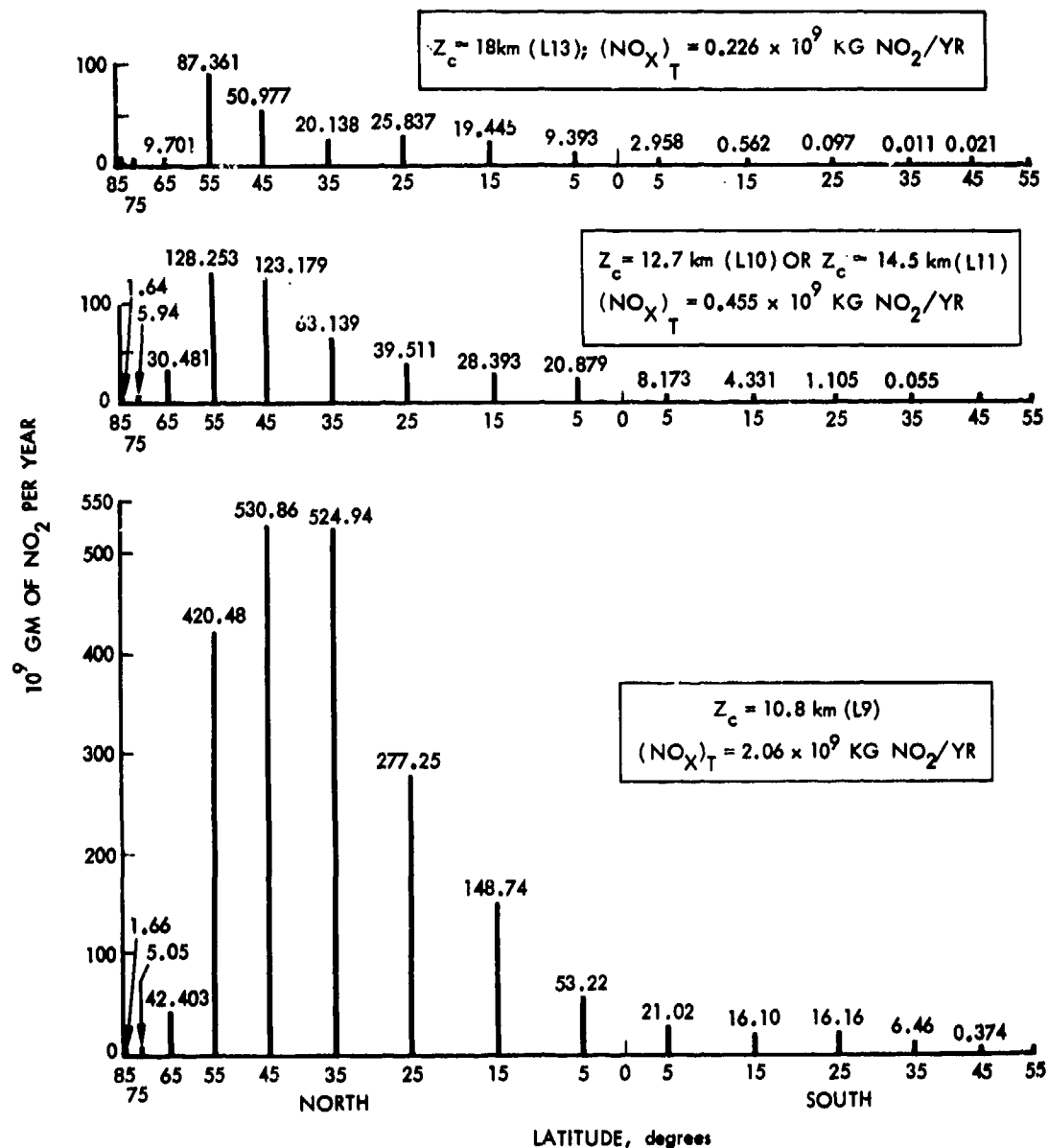


FIGURE 3.23. Assumed NO_x Emissions as a Function of Latitude at Levels 9, 10, 11, and 13. NCAR 2-D runs.

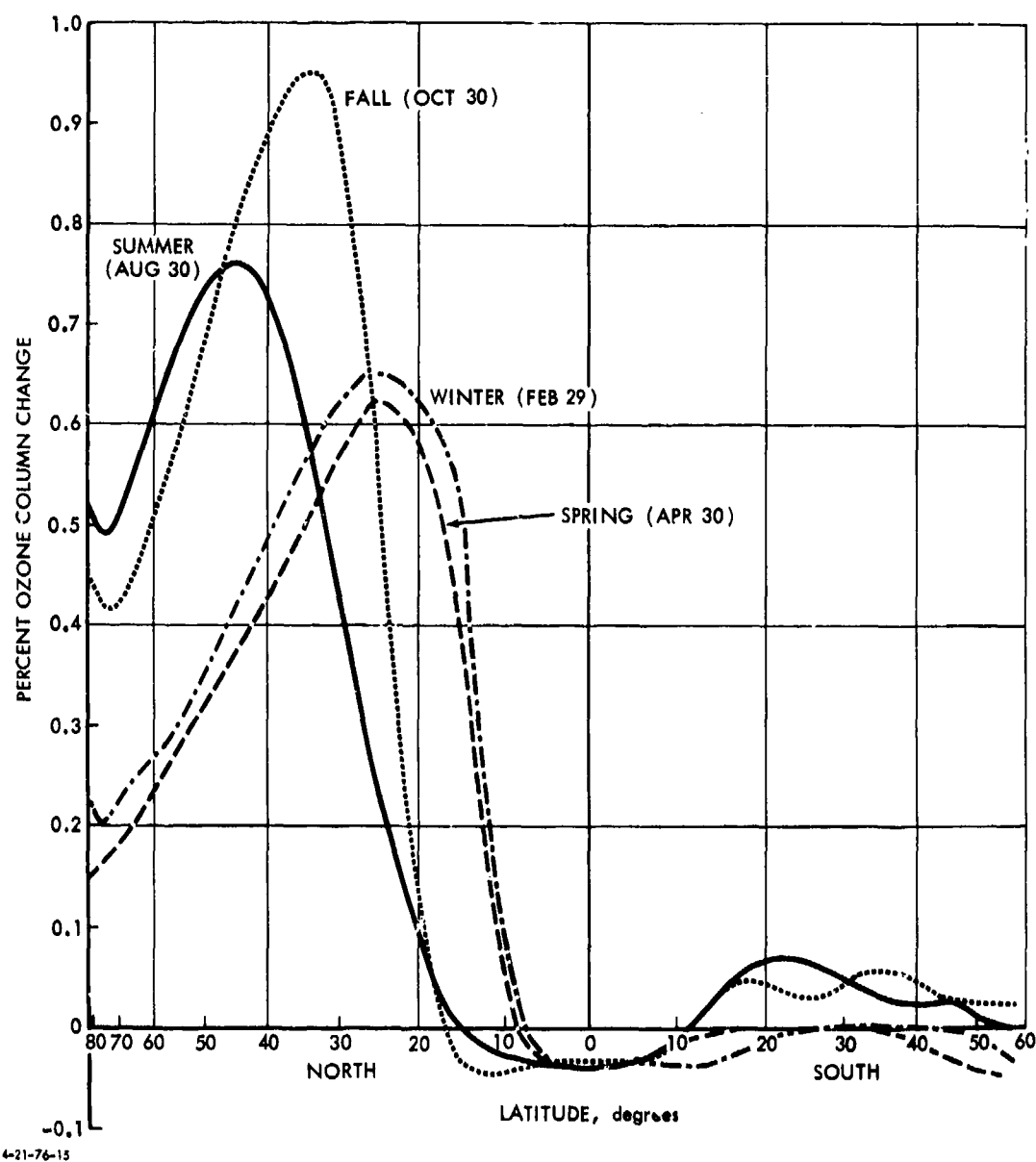
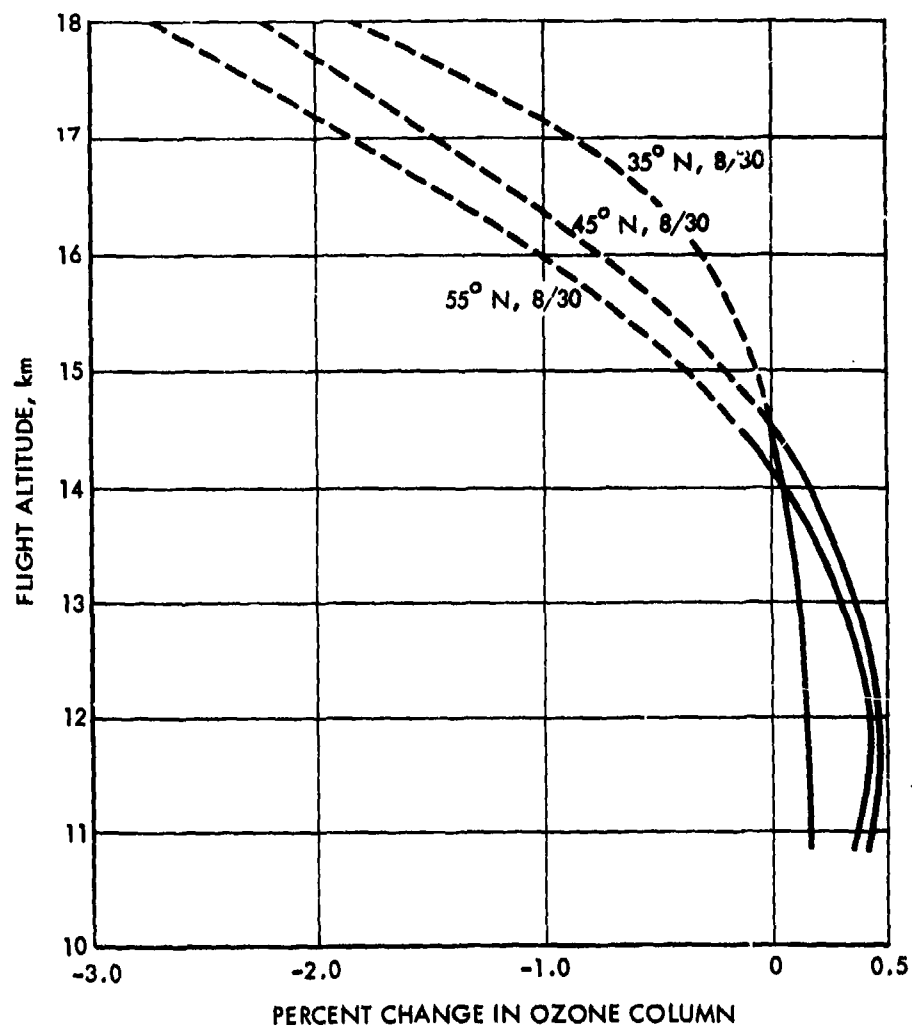


FIGURE 3.24. Percent Ozone Column Change Above Ground as a Function of Latitude and Season after Six Years of NO_x Emissions (2.06×10^9 kg of NO_2/yr) at 35,500-ft Altitude. NCAR 2-D runs; Crutzen model

TABLE 3.15. OZONE COLUMN CHANGE (%) NEAR GROUND (L = 1) AFTER SIX YEARS OF FLEET OPERATIONS AT LEVEL L_i .
 $(NO_x)_T$ = TOTAL NO_x ANNUAL EMISSIONS, kg NO_2 /YEAR. NCAR 2-D RUNS, CRUTZEN MODEL.

L_i	April 30 (Spring)				August 30 (Summer)				October 30 (Fall)			
	9	10	11	13	9	10	11	13	9	10	11	13
$(NO_x)_T$	2.064×10^9	0.455×10^9	0.455×10^9	0.226×10^9	2.064×10^9	0.455×10^9	0.455×10^9	0.226×10^9	2.064×10^9	0.455×10^9	0.445×10^9	0.226×10^9
Lat 85	0.48	-0.025	-0.246	-0.764	0.524	0.062	-0.246	-0.955	0.443	0.059	-0.236	-0.856
75	0.169	-0.024	-0.217	-0.698	0.489	0.058	-0.230	-0.863	0.419	0.030	-0.239	-0.867
65	0.201	0.000	-0.176	-0.628	0.562	0.089	-0.178	-0.769	0.450	0.064	-0.193	-0.835
55	0.287	0.052	-0.104	-0.522	0.681	0.148	-0.059	-0.593	0.589	0.131	-0.098	-0.687
45	0.372	0.080	-0.053	-0.426	0.761	0.183	0.000	-0.487	0.813	0.203	0.000	-0.576
35	0.493	0.116	0.000	-0.348	0.625	0.099	0.000	-0.428	0.941	0.290	0.109	-0.435
25	0.620	0.155	0.062	-0.279	0.237	0.068	-0.034	-0.305	0.567	0.151	0.038	-0.340
15	0.361	0.066	0.000	-0.230	0.000	-0.034	-0.102	-0.273	-0.037	-0.037	-0.112	-0.300
5	-0.035	-0.035	-0.104	-0.243	-0.034	-0.034	-0.103	-0.206	-0.036	-0.036	-0.107	-0.214
-5	-0.036	-0.036	-0.073	-0.181	-0.035	-0.035	-0.071	-0.177	-0.035	0.000	-0.070	-0.140
-15	-0.038	-0.038	-0.075	-0.150	0.035	0.000	-0.035	-0.104	0.033	0.000	-0.033	-0.100
-25	0.000	-0.036	-0.072	-0.108	0.069	0.000	-0.035	-0.069	0.031	0.000	-0.031	-0.093
-35	0.000	-0.034	-0.068	-0.102	0.032	-0.032	-0.032	-0.129	0.056	0.000	-0.028	-0.084
-45	0.000	0.000	-0.065	-0.129	0.029	0.000	-0.029	-0.117	0.026	-0.026	-0.051	-0.129
-55	-0.032	-0.032	-0.064	-0.127	0.000	-0.026	-0.053	-0.132	0.025	0.000	-0.051	-0.127
-65	-0.035	-0.035	-0.069	-0.138	0.000	0.000	-0.052	-0.130	0.000	-0.027	-0.080	-0.161
-75	-0.038	-0.038	-0.075	-0.150	0.000	-0.027	-0.053	-0.133	0.029	0.000	-0.059	-0.147
-85	-0.038	-0.038	-0.077	-0.115	0.000	-0.026	-0.053	-0.132	0.000	-0.030	-0.091	-0.182

*Corresponding flight altitudes: level 9 (~35,500 ft); 10 (~41,500 ft); 11 (~47,500 ft); 13 (~59,150 ft)



3-9-77-18

FIGURE 3.25. Normalized NCAR 2-D Results (Crutzen Model) for Ozone Column Changes with 1×10^9 kg/yr NO_x Injection Rate at Various Altitudes Distributed over 1.8-km Altitude Bands, and over Latitude According to Fig. 3.23. Linearity of effects with injection rate was assumed in making the adjustment.

3.4.6 Reaction Rate Uncertainties and Their Effects in 1-D Ozone Depletion Modeling (ClO_x Reactions excluded), August 1976

During CIAP, a considerable effort went into the study of reaction rates, and recommended rates, with estimated uncertainties, were established (see CIAP Monograph 1, Chapter 5). As a practical matter, the recommended values, and the same general sets of reactions (ignoring methane oxidation reactions) and rates were generally used by the various modelers. The principal differences between different modelers' results thus came about due to differences in the 1-D "dynamics" employed; i.e., the K_z profile. As a result, modelers tended to agree as to the sign, but not necessarily the magnitude of the effects, of NO_x on ozone. Also, some tendency resulted to underestimate the uncertainties involved, a factor of 2 being quoted in the NAS report (p. 29) for the Hunten model results at 19.5 km, a factor of 3 at 16.5 km, and a factor of 10 "either way" for subsonic aircraft.

The question of uncertainties in ozone effects due to uncertainties in the chemical thermal reaction rates has been pursued subsequent to the CIAP effort by a group at Lawrence Livermore Laboratory (Duewer et al., 1976a). Uncertainties in photodissociation rates, or those due to thermal feedback effects, scattering, etc., were not included. The results show that true uncertainties are generally larger than estimated, as well as the possibility (or as shown earlier for the case of subsonic aircraft, the probability) that the sign of the effect may be incorrect.

The procedure used by Duewer et al., (1976a) was to study ozone column perturbations in a 1-D model, for given NO_x input conditions, as reaction rates were systematically varied, within the uncertainty ranges quoted by the NBS, to maximize or minimize the effects on ozone. The reactions used, and their range, are given in Table 3.16. Three basic cases were considered. In Model A, rates used in CIAP were used, with the important exception that reaction 19 ($\text{OH} + \text{HO}_2 \rightarrow \text{H}_2\text{O} + \text{O}_2$) was set equal to $2 \times 10^{-11} \text{ cm}^3/\text{sec}$, [a value preferred by modelers of the halocarbon problem (NAS, 1976a)] rather than 2×10^{-10} , as in CIAP. With 2×10^{-10} , the model was termed Model A'. In Model B, the rates were set to the end of the uncertainty range which maximized the destruction of ozone. In Model C, the reactions were set to minimize destruction of ozone. In further refinements, the fate of NO₃ was varied, either to form NO + O₂, which destroys ozone, or to NO₂ + O, which has no effect on ozone; these possibilities were given subscripts 1 or 2, respectively. Finally, in recognition of the low probability of either Model B or C being correct, a model study was made (models C'₁ and C'₂) in which only four critical rates were set (plus Reaction 19) to the NO_x-minimizing end, and these reactions thus examined further. Photolysis rates and temperature-dependence factors were left unchanged. The K_z profile used was that of Chang/1974, with exceptions to be noted.

TABLE 3.16. REACTIONS, REACTION DESIGNATORS AND RATE PARAMETERS FOR THE VARIOUS MODELS USED IN UNCERTAINTY ANALYSIS
SOURCE: Duewer et al., 1976a

Reaction		Photolysis Rates at the Indicated Altitudes for Model A ₂			
Formula	Number	55 km	30 km	15 km	
O ₂ + hv → 2O	J1	7.76 × 10 ⁻¹⁰	1.90 × 10 ⁻¹¹	8.42 × 10 ⁻¹⁶	
O ₃ + hv → O + O ₂	J2	2.80 × 10 ⁻⁴	2.41 × 10 ⁻⁴	2.07 × 10 ⁻⁴	
O ₃ + hv → O(¹ D) + O ₂	J3	4.79 × 10 ⁻³	5.85 × 10 ⁻⁵	7.90 × 10 ⁻⁶	
NO ₂ + hv → NO + O	J4	5.03 × 10 ⁻³	4.85 × 10 ⁻³	4.74 × 10 ⁻³	
N ₂ O + hv → N ₂ + O(¹ D)	J5	4.14 × 10 ⁻⁷	2.89 × 10 ⁻⁹	1.44 × 10 ⁻¹⁵	
NO + hv → N + O	J6	1.35 × 10 ⁻⁶	8.90 × 10 ⁻¹⁰	7.30 × 10 ⁻³⁷	
HNO ₃ + hv → OH + NO ₂	J7	6.38 × 10 ⁻⁵	4.78 × 10 ⁻⁶	3.21 × 10 ⁻⁷	
H ₂ O ₂ + hv → 2OH	J8	8.25 × 10 ⁻⁵	6.39 × 10 ⁻⁶	2.22 × 10 ⁻⁶	
HO ₂ + hv → OH + O	J9	1.98 × 10 ⁻⁴	3.40 × 10 ⁻⁶	1.70 × 10 ⁻¹⁰	
NO ₃ + hv → NO + O ₂	J10 ₁	Either J10 ₁ or J10 ₂ is assumed to be the only fate of NO ₃ as is indicated by model subscript.			
NO ₃ + hv → NO ₂ + O	J10 ₂				
Arrhenius A Factor ⁺ for Indicated Model					
		A	B	C	Temperature Dependence
O + O ₂ + M → O ₃ + M	K1	1.07 × 10 ⁻³⁴	0.91 × 10 ⁻³⁴	1.26 × 10 ⁻³⁴	+ 510.
O + O ₃ → 2O ₂	K2	1.9 × 10 ⁻¹¹	1.5 × 10 ⁻¹¹	2.4 × 10 ⁻¹¹	-2300.
O ₃ + NO → NO ₂ + O ₂	K3	9 × 10 ⁻¹³	11.6 × 10 ⁻¹³	7. × 10 ⁻¹³	-1200.
O + NO ₂ → NO + O ₂	K4	9.1 × 10 ⁻¹²	10.4 × 10 ⁻¹²	7.9 × 10 ⁻¹²	--
H ₂ O + O(¹ D) → H ₂ + O ₂	K5	1.1 × 10 ⁻¹⁰	0.7 × 10 ⁻¹⁰	1.74 × 10 ⁻¹⁰	--
H ₂ O + O(¹ D) → 2HO	K6	1.1 × 10 ⁻¹⁰	0.7 × 10 ⁻¹⁰	1.74 × 10 ⁻¹⁰	--
H + O ₂ → HO + O	K7	1.1 × 10 ⁻¹⁴	0.7 × 10 ⁻¹⁴	1.74 × 10 ⁻¹⁴	-3150.
H + NO → H ₂ + O	K8	2.7 × 10 ⁻¹¹	2.1 × 10 ⁻¹¹	3.4 × 10 ⁻¹¹	--
H + NO ₂ → 2HO	K9	6 × 10 ⁻¹²	6 × 10 ⁻¹²	0.	--
O(¹ D) + H ₂ O → 2OH	K10	3.5 × 10 ⁻¹⁰	2.8 × 10 ⁻¹⁰	4.4 × 10 ⁻¹⁰	--
O(¹ D) + CH ₄ → OH + CH ₃	K11	4. × 10 ⁻¹⁰	3.2 × 10 ⁻¹⁰	5 × 10 ⁻¹⁰	--
O ₃ + OH → HO ₂ + O ₂	K12	1.6 × 10 ⁻¹²	0.8 × 10 ⁻¹²	3.2 × 10 ⁻¹²	-1000.
O + OH → O ₂ + H	K13	4.2 × 10 ⁻¹¹	2.7 × 10 ⁻¹¹	6.7 × 10 ⁻¹¹	--
O ₃ + HO ₂ → OH + 2O ₂	K14	1.0 × 10 ⁻¹³	0.5 × 10 ⁻¹³	2.0 × 10 ⁻¹³	-1250.
O + HO ₂ → OH + O ₂	K15	8 × 10 ⁻¹¹	2 × 10 ⁻¹¹	32. × 10 ⁻¹¹	- 500.
H + O ₂ + M → HO ₂ + M	K16	2.08 × 10 ⁻³²	2.44 × 10 ⁻³²	1.77 × 10 ⁻³²	+ 290.
H + O ₃ → OH + O ₂	K17	1.23 × 10 ⁻¹⁰	1.0 × 10 ⁻¹⁰	1.55 × 10 ⁻¹⁰	- 562.
HO ₂ + HO ₂ → H ₂ O ₂ + O ₂	K18	3 × 10 ⁻¹¹	6 × 10 ⁻¹¹	1.5 × 10 ⁻¹¹	- 500.
HO ₂ + OH → H ₂ O + O ₂	K19 ^{aa}	2 × 10 ⁻¹¹	2 × 10 ⁻¹⁰	1.5 × 10 ⁻¹¹	--
OH + NO ₂ → HNO ₃	K20 ^{aa}	4 × 10 ⁻¹²	2 × 10 ⁻¹²	8 × 10 ⁻¹²	-- ^{aa}
OH + HNO ₃ → H ₂ O + NO ₃	K21	8.9 × 10 ⁻¹⁴	4.5 × 10 ⁻¹⁴	1.8 × 10 ⁻¹³	--
H ₂ O ₂ + OH → H ₂ O + HO ₂	K22	1.7 × 10 ⁻¹¹	2.7 × 10 ⁻¹¹	1.1 × 10 ⁻¹¹	- 910.
N ₂ + O(¹ D) → M + N ₂ O + M	K23	2.8 × 10 ⁻³⁶	5.6 × 10 ⁻³⁶	1.4 × 10 ⁻³⁶	--
N + O ₂ → N ₂ O + O	K24	9 × 10 ⁻¹²	9 × 10 ⁻¹²	1 × 10 ⁻¹²	--
NO + O + M → NO ₂ + M	K25	3.96 × 10 ⁻³³	2 × 10 ⁻³³	8 × 10 ⁻³³	+ 940.
NO + HO ₂ → NO ₂ + OH	K26	2 × 10 ⁻¹³	6.3 × 10 ⁻¹⁴	6.3 × 10 ⁻¹³	--
OH + OH → H ₂ O + O	K27	1 × 10 ⁻¹¹	1.6 × 10 ⁻¹¹	0.63 × 10 ⁻¹¹	- 550.
N + O ₃ → NO + O ₂	K28	5.7 × 10 ⁻¹³	1.8 × 10 ⁻¹²	1.8 × 10 ⁻¹³	--
HO ₂ + v ₃ → NO ₃ + O ₂	K29	1.23 × 10 ⁻¹³	1.55 × 10 ⁻¹³	1. × 10 ⁻¹³	-2470.
OH + CH ₄ → H ₂ O + CH ₃	K30	2.36 × 10 ⁻¹²	2.15 × 10 ⁻¹²	2.6 × 10 ⁻¹²	-1710.
OH + OH + M → H ₂ O ₂ + M	K31	2.5 × 10 ⁻³³	4. × 10 ⁻³³	1.6 × 10 ⁻³³	+2500.
H ₂ O ₂ + O → OH + HO ₂	K32	2.75 × 10 ⁻¹²	2.34 × 10 ⁻¹²	3.23 × 10 ⁻¹²	-2125.
O(¹ D) + H → O + H	K33	5.85 × 10 ⁻¹¹	4.14 × 10 ⁻¹¹	8.26 × 10 ⁻¹¹	--
CH ₃ + 2HO ₂ → CO		Assumed to be the only fate of CH ₃			

⁺Constant A in K = A exp(C/T) in units of cm³/sec (cm⁶/sec for 3 body processes)

⁺Constant C in K = A exp(C/T)

^{aa}Model A' differs from A only in that K19 is set to 2 × 10⁻¹⁰, the value used in most of the CIAP experiments.

^{aa}K20 is pressure dependent. In our model K20 = K[M]/(1.12 × 10¹⁸ + [M]) where K is value tabled above. This is a fit to the altitude dependent expression given by Hampson and Garvin (1975).

Input NO_2 rate was $2000 \text{ mol/cm}^3\text{-sec}$ over a 1-km band; this corresponds to $2.46 \times 10^9 \text{ kg/yr}$ of NO_x (as NO_2 on a global basis. Results might also be interpreted as "corridor" results for a Northern Hemisphere fleet emitting $1.23 \times 10^9 \text{ kg/yr}$, as was done in the CIAP ROF (1974). In round numbers, for the 17-km injection case, using COMESA NO_x rates per Concorde per year ($8 \times 10^5 \text{ kg/yr}$), the $1.23 \times 10^9 \text{ kg/yr}$ figure corresponds to 1500 Concorde; with NAS (1975) numbers ($6.28 \times 10^5 \text{ kg/yr}$), nearly 2000 Concorde are implied. The equivalent number of Boeing 2707s (at 20 km) is arguable; if based on the 1974 figures (p. 101, CIAP ROF) of $9.2 \times 10^5 \text{ kg NO}_2/\text{yr}$ per B-2707, the figure corresponds to 1340 Boeing 2707s. If based on the 1970 estimate (same reference), the figure corresponds to 354 Boeing 2707s. These figures ignore a slight altitude correction; i.e., 17 km and 20 km are not the proper weighted cruise altitudes for these aircraft.

Water effects were studied briefly by arbitrarily increasing the water content of the stratosphere at all points by 10 percent in several cases. The various results are summarized in Table 3.17.

TABLE 3.17. PERCENTAGE OZONE DEPLETIONS (GLOBAL AVERAGE)
WITH VARIATION IN THERMAL RATE CONSTANTS,
CHANG/1974 k_2 ; $2.46 \times 10^9 \text{ kg/yr NO}_x$ INJECTION
SOURCE: Duewer et al., 1976a

Injection Altitude, km	"CIAP" $k_{19} = 2 \times 10^{-10}$		$k_{19} = 2 \times 10^{-11}$		Maximized	Minimized		Minimized 4 Rates	
	A ₁	A ₂	A ₁	A ₂	B	C ₁	C ₂	C ₁	C ₂
17	-4.34	-3.52	-1.75	-1.16	-8.06	+1.74	+2.22	+0.61	+1.01
20	-9.79	-8.47	-5.21	-4.03	-15.92	+1.61	+2.64	-0.20	+0.70
35	-17.24	-15.34	-14.06	-12.46	-25.11	-6.42	-4.77	-9.20	-7.80
1.1 x H_2O^*	+0.03	-0.01	-0.14	-0.21	+0.15	-0.52	-0.54	-0.35	-0.38
1.1 x H_2O , 17	-4.25	-3.48	-1.88	-1.34	-7.89	+1.23	+1.67	+0.26	+0.63
1.26 x H_2O , 20**	-9.56	-8.37	-5.55	-4.50	-15.48	+0.28	+1.21	-1.11	-0.29

*No NO_x injection.

**Estimated by IDA. The water effect in all cases is taken as the difference between the first and fifth rows.

The "CIAP" A₁ and A₂ results are not identical to those reported in the ROF [p. B-17 (note that there is a 10-fold NO_x rate error on page B-17 ROF); also p. E-59], which at 17 km would be about 5.1 percent, or at 20 km, about 10.7 percent. The CIAP ROF numbers corresponded to A₁ in terms of the NO_3 photolysis reactions. The differences between CIAP and current results may be due to inclusion of the $\text{CH}_3^{(\text{O}_2)}_2 \text{HO}_2 + \text{CO}$ ozone-forming reactions; also, a "half sun" (current) rather than a full sun (CIAP) or change in removal mechanism (rainout) may have affected results.

The data shown in Table 3.17 are of obvious significance to the SST problem. The first point is that use of a smaller value of K_{19} (2×10^{-11} cm³/sec) reduces effects previously computed substantially. If, following a recent recommendation attributed to H.S. Johnston (see Table 3.1), it is assumed that the NO₃ photolysis goes one-third via route 1 and two-thirds via route 2, then a weighted A_1-A_2 value can be estimated as -1.36 percent at 17 km versus -4.34 percent in A'_1 or -5.1 percent in CIAP, a reduction of some 70 percent. A second point is that the uncertainty as to the effect is much greater, with results at 17 km, for example, ranging from -8.06 percent to +2.22 percent. Note that the CIAP result (-5.1 percent) is closer to the Model B result (-8.06 percent) than to the Model C result (+2.22 percent). This is because of the powerful effect of the reaction 19 on the CIAP result. Similar points could be noted with regard to the higher altitude injections. The 35-km injection is, of course, purely academic, involving as it would necessarily, some form of hypersonic (ca. mach 8) vehicle.

No rigorous way (even within the 1-D context!) apparently exists to model the water effect in a 1-D model. However, using an injection coefficient approach,* with the Chang/1974 profile a water mixing ratio enhancement of 10 percent is found for 17-km injection. Similarly, at 20 km, the enhancement is 26 percent. The values quoted in the two bottom rows of Table 3.17, which include, in an approximate way, the simultaneous effects of water and NO_x addition, may thus be considered the most plausible for this K_z profile under the various conditions. Note that, where NO_x effects are minimized, water effects are maximized, so that it appears to be important to include the water effects. The figures in the bottom row have been estimated assuming linearity and ignoring differences in the profile below 20 km for the injection coefficient and Lawrence Livermore Laboratory approaches.

Runs were also made by Duewer et al., (1976a) using the Hunten/1974 (without 2-km adjustment), Crutzen/1974, and Wofsy/1975 profiles, for various sets of chemical reaction rates. Results are shown in Table 3.18.

*The injection coefficient (Appendix D) at 17 km is 1.223×10^{-17} cm²-sec; the water emission index is taken as 1250 gm/kg; the NO_x emission index is taken as 18 gm/kg. Background water vapor was^x about 4.32 ppmv on this model. Calculated enhancement is 0.434 ppmv.

TABLE 3.18. OZONE DEPLETIONS (GLOBAL AVERAGE) FOR VARIOUS K_z PROFILES AND CHEMICAL REACTION RATE SETS; NO_x INJECTION: 2.46×10^9 kg/yr AT 17 km
SOURCE: Duewer et al., 1976a

K_z	A_1	A_2	B	C_1	C_2
Chang/1974	-1.75	-1.16	- 8.06	+1.74	+2.22
Crutzen-Isaksen/1975	-1.32	-0.95	- 5.10	+0.68	+1.02
Wofsy/1975	-4.88	-3.41	-14.74	+0.47	+2.08
Hunten/1974	-6.68	-4.60	-16.95	-1.69	+1.00

Note the powerful effects of the rate uncertainties; even the Hunten K_z profile gives ozone enhancement in Model C_2 .

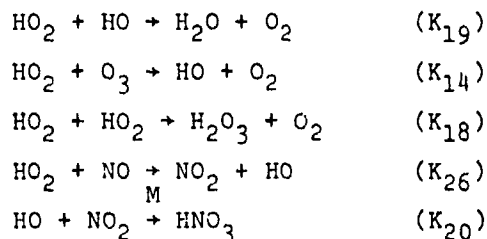
In intercomparing the results in Table 3.18, an interpretation problem arises. As noted earlier, the "corridor" value at a given NO_x input rate was taken in the CIAP ROF as being equal to the global average value at twice the input rate. For the Hunten profile, the further problem enters of the 2-km adjustment recommended for mid-latitude flight; according to this recommendation, the value shown for the Hunten profile should apply to the hemisphere for flight at 15 km, for half the total input rate, i.e., 1.23×10^9 kg/yr. For comparison to these results, the formulae given earlier (Section 3.4.1; also NAS, 1975, pp. 116-119) can be used (for 1.23×10^9 kg/yr, at a model injection altitude of 17 km) to give 8.97 percent depletion.

Duewer et al., (1976a) make several additional important points. The first, and probably most important of these, is that in spite of the wide diversity of reaction sets employed, the available trace measurements data are sufficiently spread so that none of the models can be excluded on the basis of measured NO , NO_2 , N_2O , HNO_3 , or O_3 data. Observed OH data, however, (Anderson, 1976) are most easily consistent with the lower value for K_{19} , which would eliminate Model B as constituted. Computed CH_4 data, using these different chemistries, which would be of interest, are not given. Also, computed profiles of various species are given only for the Chang/1974 K_z profiles.

A second point, of perhaps less practical interest, is that, with the different models, the relative importance of ozone destruction rate by the NO_x and HO_x cycles and the Chapman reactions is greatly altered. The HO_x cycles become more important and the NO_x cycles less important as reaction sets move from B to C. (ClO_x reaction cycles were not included in these calculations.)

Five reactions are considered to be of greatest importance by Duewer et al., (1976a). These reactions, set to their appropriate uncertainty

limits, comprise Model C'. As shown in Table 3.17, ignoring H₂O, effects on ozone are small or positive with this set, independent of K_z profile. The reactions are:



HO₂ reactions, in general, are very important to the ozone problem. Because of reaction 26, NO₂ formation, followed by photolysis, is a source of ozone. These reactions have been reviewed by Duewer (private communication, September 1976).^{*} In general, more data are needed on all, and all are difficult on which to get data. Temperature dependence data for several of the reactions are unavailable. Available data are in conflict, particularly in view of measurements which yield reaction rates, not in absolute terms, but in terms of certain products and ratios of rates (see DeMore and Tschuikow-Roux, 1974). However, of these five reactions, Duewer (private communication, September 1976) on reviewing the data considers only K₁₄ and K₂₆ to approach values used in Model B, whereas the other three all seem to approach (or in the case of K₂₀ to be more extreme than) those used in Model C. He estimates subjectively that the probability of Model C' representing the stratospheric response to NO_x is of the order of 1 percent.

The foregoing results have, of course, all come from 1-D models with all their limitations. Furthermore, as noted earlier, the decoupling of chemistry-generated stratosphere dynamics in several of the profiles^{**} while studying effects of varying chemistry can be questioned. Also, unless C or C' chemistry is correct, a probably more important question relates to which of the various K_z profiles is to be preferred. Uncertainties in effects will be reduced only as more kinetic data become available and as more tracer data are used, preferably in models of higher dimensionality.

3.4.7 Fall 1976 Lawrence Livermore Laboratory Results (1-D, showing chlorine effects, water effects, and 1990 fleet effects)

A. Introduction

The intensive studies carried out during 1975-1976 on the effects of halocarbons on stratospheric ozone had an impact in a number of important ways in the evaluation of NO_x aircraft effects on stratospheric ozone.

^{*} See Duewer, et al., 1976c for detailed discussion of reactions K12, K14, K18, K19, K20, and K26.

^{**}The Chang/1974 profile was not based on methane profiles or the chemistry of methane destruction.

These changes came about due to revisions in "best values" of certain rate constants and due to recognition of interaction between chlorine catalytic cycles and NO_x catalytic cycles, and to revisions in K_z profiles, in particular the Chang/1974 profile. To illustrate these effects and to show computed effects of future fleets, a series of 1-D runs were made at Lawrence Livermore Laboratory (September-October, 1976). These results are summarized here. The revisions in input data follow.

B. Chemistry

A complete listing of "1976 chemistry" as used by Lawrence Livermore Laboratory is given in Table 3.19. This listing, in general, follows the "A" chemistry listed before, with revisions in $\text{O}(^1\text{D})$ reactions (K_5 , K_6 , K_{10} , K_{11} , K_{33}) and in reactions K_{18} ($\text{HO}_2 + \text{HO}_2$) and K_{20} ($\text{OH} + \text{NO}_2 + \text{M}$); of these, the last change is the most important, the expressions as used being satisfactory in the stratosphere, although somewhat too slow in the troposphere (D. Wuebbles, private communication, October 1976). Note that, as in "A" chemistry, the critical reaction $\text{OH} + \text{HO}_2 \rightarrow \text{H}_2\text{O} + \text{O}_2$ has been assigned a rate of $2 \times 10^{-11} \text{ cm}^3/\text{sec}$. NO_3 photolysis was assumed to proceed 66 percent in the "do-nothing" cycle ($\text{NO}_2 + \text{O}$) and 34 percent in the ozone-destroying path ($\text{NO} + \text{O}_2$).

Chlorine chemistry as used by Lawrence Livermore Laboratory is included in Table 3.19. Note that important interactions occur between the ClO_x and the NO_x cycles in reactions K_{45} and K_{48} . Also, K_{19} , which strongly affects the calculated OH content, interacts with K_{20} and K_{54} , with low values of K_{19} reducing the effects of added NO_x and increasing the effects of added chlorine.

Perturbation runs made with the above chemistry follow below. However, for comparison, runs were also made with "partial Widhopf chemistry," which differs from the above by excluding chlorine chemistry and in choice of rates for the $\text{O}(^1\text{D})$ reactions K_5 , K_6 , K_{10} , and K_{33} . The Lawrence Livermore Laboratory model assumes instantaneous conversion of CH_3 to $2 \text{ HO}_2 + \text{CO}$ as a simplified substitute for the more complex methane oxidation reactions used by Widhopf (see Section 3.4.8) and Crutzen (Section 3.4.5) and may well understate ozone production in this process (W. Duewer, private communication, September 1976).

In addition, because of still-remaining uncertainties about chlorine nitrate, runs are reported below with and without inclusion of chlorine nitrate. The rationale is that the computed quantity, and thus significance,

TABLE 3.19. LLL 1976 CHEMISTRY: O_x, NO_x, and HO_x
Source: Lawrence Livermore Laboratory, Fall 1976

ClO _x Chemistry		
Designation*	Reaction	Arrhenius A Factor**
J1	O ₂ + hv → O + O	QJ(1)
J2	O ₃ + hv → O + O ₂	QJ(2)
J3	O ₃ + hv → O(¹ D) + O ₂	QJ(3)
K1	O + O ₂ + M → O ₃ + M	1.07 x 10 ⁻³⁴ exp(810/T)
K2	O + O ₃ → 2O ₂	1.9 x 10 ⁻¹¹ exp(-2300/T)
J4	NO ₂ + hv → NO + O	QJ(4)
K3	O ₃ + NO → NO ₂ + O ₂	9.0 x 10 ⁻¹³ exp(-1200/T)
K4	O + NO ₂ → NO + O ₂	9.1 x 10 ⁻¹²
J5	N ₂ O + hv → N ₂ + O(¹ D)	QJ(5)
K5	N ₂ O + O(¹ D) → N ₂ + O ₂	7 x 10 ⁻¹¹
K6	N ₂ O + O(¹ D) → 2NO	7 x 10 ⁻¹¹
J6	NO + hv → N + O	QJ(6)
K7	N + O ₂ → NO + O	1.1 x 10 ⁻¹⁴ exp(-3150/T)
K8	N + NO → N ₂ + O	2.7 x 10 ⁻¹¹
K10	O(¹ D) + H ₂ O → 2OH	2.1 x 10 ⁻¹⁰
K11	O(¹ D) + CH ₄ → OH + CH ₃	1.3 x 10 ⁻¹⁰
J7	HNO ₃ + hv → OH + NO ₂	QJ(7)
K12	O ₃ + OH → HO ₂ + O ₂	1.6 x 10 ⁻¹² exp(-1000/T)
K13	O + OH → O ₂ + H	4.2 x 10 ⁻¹¹
K14	O ₃ + HO ₂ → OH + 2O ₂	1.0 x 10 ⁻¹³ exp(-1250/T)
K15	O + HO ₂ → OH + O ₂	3 x 10 ⁻¹¹
K16	H + O ₂ + M → HO ₂ + M	2.08 x 10 ⁻³² exp(290/T)
K17	O ₃ + H → OH + O ₂	1.23 x 10 ⁻¹⁰ exp(-562/T)
K18	HO ₂ + HO ₂ → H ₂ O ₂ + O ₂	1.7 x 10 ⁻¹¹ exp(-500/T)
K19	HO ₂ + OH → H ₂ O + O ₂	2.0 x 10 ⁻¹¹
K20	OH + NO ₂ + M → HNO ₃ + M	$\frac{2.76 \times 10^{-13} \exp(880/T)}{1.166 \times 10^{-18} \exp(222/T) + M}$
K21	OH + HNO ₃ → H ₂ O + NO ₃	8.9 x 10 ⁻¹⁴
J8	H ₂ O ₂ + hv → 2OH	QJ(8)
K22	H ₂ N ₂ + OH → H ₂ O + NO ₂	1.7 x 10 ⁻¹¹ exp(-910/T)
K23	H ₂ + O(¹ D) + M → N ₂ O + M	2.8 x 10 ⁻³⁶
K24	N + NO ₂ → N ₂ O + O	1.4 x 10 ⁻¹²
K25	NO + O + M → NO ₂ + M	3.96 x 10 ⁻³³ exp(940/T)
K26	NO + HO ₂ → NO ₂ + OH	2.0 x 10 ⁻¹³
K26a	H ₂ + O(¹ D) → OH + H	2.9 x 10 ⁻¹⁰
K27	OH + OH → H ₂ O + O	1.0 x 10 ⁻¹¹ exp(-550/T)
K28	N + O ₃ → NO + O ₂	6.7 x 10 ⁻¹³
K29	NO ₂ + O ₃ → NO ₃ + O ₂	1.2 x 10 ⁻¹³ exp(-2450/T)
J9	HO ₂ + hv → OH + O	QJ(9)
K30	OH + CH ₄ → H ₂ O + CH ₃	2.36 x 10 ⁻¹² exp(-1710/T)
K31	OH + OH + M → H ₂ O ₂ + M	2.5 x 10 ⁻³³ exp(2500/T)
K32	H ₂ O ₂ + O → OH + HO ₂	2.76 x 10 ⁻¹² exp(-2125/T)
K32a	O + CH ₄ → OH + CH ₃	3.6 x 10 ⁻¹¹ exp(-4550/T)
K32b	CO + OH → H + CO ₂	1.4 x 10 ⁻¹³
K33	O(¹ D) + M → O + M	2.2 x 10 ⁻¹¹ exp(92/T)
J10 ₂	NO ₃ + hv → NO ₂ + O	0.66
J10 ₁	→ NO + O ₂	0.34
-	CH ₃ $\xrightarrow{O_2}$ 2 NO ₂ + CO	Instantaneous fate assumed for CH ₃

* Follows table 3.16.

**In cm³/sec for two-body or cm⁶/sec for three-body reactions.

TABLE 3.19. (CONTINUED)

Designation*	Reaction	Arrhenius A Factor**
K34	$\text{Cl} + \text{O}_3 \rightarrow \text{ClO} + \text{O}_2$	$2.97 \times 10^{-11} \exp(-243/T)$
K35	$\text{Cl} + \text{OCIO} \rightarrow 2\text{ClO}$	5.9×10^{-11}
K36	$\text{Cl} + \text{O}_2 + \text{M} \rightarrow \text{ClO}_2 + \text{M}$	$1.7 \times 10^{-33} (300)$
K37	$\text{Cl} + \text{CH}_4 \rightarrow \text{HCl} + \text{CH}_3$	$5.4 \times 10^{-12} \exp(-1133/T)$
K38	$\text{Cl} + \text{ClO}_2 \rightarrow \text{Cl}_2 + \text{O}_2$	5×10^{-11}
K39	$\text{Cl} + \text{ClO}_2 \rightarrow 2\text{ClO}$	1.4×10^{-12}
K40	$\text{Cl} + \text{NO} + \text{M} \rightarrow \text{ClNO} + \text{M}$	$1.7 \times 10^{-32} \exp(553/T)$
K41	$\text{Cl} + \text{ClNO} \rightarrow \text{Cl}_2 + \text{NO}$	3.0×10^{-11}
K42	$\text{Cl} + \text{NO}_2 + \text{M} \rightarrow \text{ClNO}_2 + \text{M}$	$6.9 \times 10^{-34} \exp(2115/T)$
K43	$\text{Cl} + \text{ClNO}_2 \rightarrow \text{Cl}_2 + \text{NO}_2$	3.0×10^{-12}
K44	$\text{ClO} + \text{O} \rightarrow \text{Cl} + \text{O}_2$	$3.38 \times 10^{-11} \exp(+75/T)$
K45	$\text{NO} + \text{ClO} \rightarrow \text{NO}_2 + \text{Cl}$	$1.13 \times 10^{-11} \exp(+200/T)$
K46	$\text{ClO} + \text{O}_3 \rightarrow \text{ClO}_2 + \text{O}_2$	$1.0 \times 10^{-12} \exp(-2763/T)$
K47	$\text{ClO} + \text{O}_3 \rightarrow \text{OCIO} + \text{O}_2$	$1.0 \times 10^{-12} \exp(-2763/T)$
K48	$\text{ClO} + \text{NO}_2 \xrightarrow{\text{H}} \text{ClNO}_3$	0.05 = HNO_3 formation
K49	$\text{ClO} + \text{ClO} \rightarrow \text{Cl} + \text{OCIO}$	$2.0 \times 10^{-12} \exp(-2300/T)$
K50	$\text{ClO} + \text{ClO} \rightarrow \text{Cl}_2 + \text{O}_2$	$2.0 \times 10^{-13} \exp(-1260/T)$
K51	$\text{ClO} + \text{ClO} \rightarrow \text{Cl} + \text{ClO}_2$	$2 \times 10^{-13} \exp(-1260/T)$
K52	$\text{HCl} + \text{O}(^1\text{D}) \rightarrow \text{Cl} + \text{OH}$	2×10^{-10}
K53	$\text{ClNO}_3 + \text{HCl} + \text{O}_2 \rightarrow \text{HNO}_3$	0.0
K54	$\text{OH} + \text{HCl} \rightarrow \text{H}_2\text{O} + \text{Cl}$	$2.0 \times 10^{-12} \exp(-310/T)$
K55	$\text{O} + \text{HCl} \rightarrow \text{OH} + \text{Cl}$	$1.75 \times 10^{-12} \exp(-2273/T)$
K56	$\text{ClO}_2 + \text{M} \rightarrow \text{Cl} + \text{O}_2 + \text{M}$	$1.5 \times 10^{-8} \exp(-4000/T)$
K57	$\text{O} + \text{OCIO} \rightarrow \text{ClO} + \text{O}_2$	5.0×10^{-13}
K58	$\text{NO} + \text{OCIO} \rightarrow \text{NO}_2 + \text{ClO}$	3.4×10^{-13}
K59	$\text{M} + \text{OCIO} \rightarrow \text{NO} + \text{ClO}$	5.0×10^{-13}
K60	$\text{H} + \text{OCIO} \rightarrow \text{OH} + \text{ClO}$	5.7×10^{-11}
K61	$\text{Cl} + \text{OH} \rightarrow \text{HCl} + \text{O}$	$2.0 \times 10^{-12} \exp(-1878/T)$
K62	$\text{Cl} + \text{HO}_2 \rightarrow \text{HCl} + \text{O}_2$	3.0×10^{-11}
K63	$\text{Cl} + \text{HNO}_3 \rightarrow \text{HCl} + \text{NO}_3$	$4.0 \times 10^{-12} \exp(-1500/T)$
K64	$\text{ClO}_2 + \text{HO}_2 \rightarrow \text{HCl} + 2\text{O}_2$	3.0×10^{-12}
	$\text{Cl}_2 + h\nu \rightarrow 2\text{Cl}$	QCJ(1)
	$\text{HCl} + h\nu \rightarrow \text{H} + \text{Cl}$	QCJ(2)
	$\text{ClO}_2 + h\nu \rightarrow \text{ClO} + \text{O}(^1\text{D})$	QCJ(3)
	$\text{ClO} + h\nu \rightarrow \text{Cl} + \text{O}$	QCJ(4)
	$\text{ClO} + h\nu \rightarrow \text{Cl} + \text{O}(^1\text{D})$	QCJ(5)
	$\text{ClNO} + h\nu \rightarrow \text{Cl} + \text{NO}$	QCJ(6)
	$\text{ClNO}_2 + h\nu \rightarrow \text{Cl} + \text{NO}_2$	QCJ(7)
	$\text{OCIO} + h\nu \rightarrow \text{ClO} + \text{O}(^1\text{D})$	QCJ(8)
	$\text{OCIO} + h\nu \rightarrow \text{ClO} + \text{O}$	QCJ(9)
	$\text{CF}_2\text{Cl}_2 + h\nu \rightarrow 2\text{Cl}$	QCJ(10)
	$\text{CFCl}_3 + h\nu \rightarrow 2.5 \text{ Cl}$	QCJ(11)
	$\text{CCl}_4 + h\nu \rightarrow 2\text{Cl}$	QCJ(12)
K65	$\text{CFCl}_3 + \text{O}(^1\text{D}) \rightarrow 2\text{Cl}$	5.8×10^{-10}
K66	$\text{CF}_2\text{Cl}_2 + \text{O}(^1\text{D}) \rightarrow 2\text{Cl}$	5.3×10^{-10}
K67	$\text{Cl} + \text{H}_2 \rightarrow \text{HCl} + \text{H}$	$5.7 \times 10^{-11} \exp(-2400/T)$
K68	$\text{Cl} + \text{H}_2\text{O}_2 \rightarrow \text{HCl} + \text{HO}_2$	$1.0 \times 10^{-11} \exp(-810/T)$
K69	$\text{O} + \text{ClNO}_3 \rightarrow \text{ClO} + \text{NO}_3$	2.1×10^{-13}
K70	$\text{OH} + \text{CH}_3\text{Cl} \rightarrow \text{H}_2\text{O} + \text{HO}_2 + \text{HCl}$	$1.58 \times 10^{-12} \exp(-1049/T)$

of ClONO_2 depends on diurnal averaging procedures as well as on the multiple scattering effects. Results cited with ClONO_2 are thought to provide a best estimate if multiple scattering is not included. The "truth" may lie between effects computed with and without ClONO_2 , although ClONO_2 is necessarily included in any best estimate, and diurnal effects are clearly significant.

C. K_z Change

As noted in Section 3.2.1 in discussing Fig. 3.13, analysis of methane profile data by Dickinson (NAS, 1976a, Appendix B), CFM led to a revision of the upper portion of the "old Chang" or Chang/1974 K_z profile, increasing eddy diffusivity values appreciably in the region above 20 km. In the "new Chang" or Chang/1976 profile, the minimum K_z occurs at 20 km, whereas the minimum was at 29 km in the "old Chang" profile. (At 29 km, the new value is $2.56 \times 10^4 \text{ cm}^2/\text{sec}$ rather than $3.65 \times 10^3 \text{ cm}^2/\text{sec}$; at 50 km, the new value is 2.35×10^5 rather than 5.41×10^4 .) In addition, the "new Chang" profile uses a lower value for tropospheric K_z , 1×10^5 rather than $3 \times 10^5 \text{ cm}^2/\text{sec}$. The remainder of the profile (10-20 km) was not changed. Further profile data are given in Appendix D of this report (Table D-3).

D. Results

Results obtained for a variety of cases are given in Table 3.20. The following points can be made:

1. Altitude Effects at Constant Injection Rates A series of runs were made at a constant input rate of 2000 molecules NO_2/cm^3 over a 1-km altitude layer. As before, this corresponds to $2.46 \times 10^9 \text{ kg/yr}$ as NO_2 into the global atmosphere, but if assumptions made in CIAP (1974) are utilized, can be interpreted as the effects in the flight corridor of a fleet of half the size (about 2000 Concorde or 3000 advanced subsonics, using NAS, 1975 figures) operating in the Northern Hemisphere. Effects at different altitudes of injection as a function of the background chlorine level in the stratosphere are shown in Fig. 3.26 for the Chang/1976 K_z profile and in Fig. 3.27 for the Hunten K_z profile. Results are shown with and without ClONO_2 . Water effects are not included. The chlorine contents correspond roughly to current values at about 1 ppb, to a nominal 1990 value at about 2 ppb (assuming minimal further growth or perhaps a cutback in fluorocarbon production), and to a 4 ppb level, which is probably implausible, representing continued production at current levels or some growth, at some undefined time in the future. The same data are plotted in different fashion in Fig. 3.28.

The results with the Chang/1976 K_z profile show slight enhancement or very small decreases in the ozone column for subsonic aircraft operating

TABLE 3.20. OZONE MODELING RESULTS, SHOWING EFFECTS OF K_z PROFILE
AND CIX CONTENT
SOURCE: Lawrence Livermore Laboratory (LLL), Fall 1976
Chemistry

Injection Altitude, km	NO _x , cm ⁻³ sec ⁻¹	ClX, ^{1,2} ppb	Ozone Columns (10 ¹⁸ cm ⁻²) or % Change (+ or -) With (+) and Without (-) ClONO ₂				
			Chang/1976		Huntten/1974 ³		Chang/1974
			+ ClONO ₂	- ClONO ₂	+ ClONO ₂	- ClONO ₂	- ClONO ₂
--	--	0	8.541		8.2135		7.8266
9	2000	0	+0.066		- .10		--
13	2000	0	-0.098		.08		--
17	2000	0	-1.147		-4.059		-0.065
20	2000	0	-4.198		-10.636		-2.916
--	--	~1	8.3689 ^(1.02)	8.2141 ^(1.02)	8.0197 ^(1.19)	7.8955 ^(1.19)	7.5112 ^(1.32)
9	200	~1	--	+0.0085	--	--	--
9	2000	~1	+0.011	+0.090	0.117	-0.043	
13	200	~1	--	+0.0097	--	--	
13	2000	~1	-0.703	+0.099	0.163	+0.057	
17	200	~1	-0.063	-0.029	-0.160	--	
17	600	~1	-0.194	-0.096	-0.794	--	
17	2000	~1	-0.703	-0.399	-2.788	-2.157	+0.108
20	200	~1	--	-0.202	--	--	--
20	2000	~1	-3.259	-2.605	-8.762	-7.841	-1.289
--	--	~2	8.2511 ^(1.93)	7.9569 ^(2.0)	7.9433 ^(1.98)	7.7126 ^(2.0)	
9	2000	~2	+0.091	+0.108	0.126	+0.143	
13	2000	~2	+0.088	+0.216	0.198	+0.283	
17	200	~2	-0.028	+0.030	-0.103	--	
17	600	~2	-0.092	+0.079	-0.388	--	
17	2000	~2	-0.398	+0.140	-2.333	-1.167	
20	2000	~2	-2.607	-1.420	-8.057	-6.314	
--	--	~4	8.0125 ^(3.7)	7.4354 ^(4.0)			
9	2000	~4	+0.110	+0.144			
13	2000	~4	+0.242	+0.483			
17	200	~4	+0.045	+0.152			
17	600	~4	+0.117	+0.436			
17	2000	~4	+0.231	+1.241			
20	2000	~4	-1.269	+1.029			

¹ClX is the sum of active chlorine species (principally Cl, ClO, HOCl, ClONO₂).

²Values superscripted on total O₃ column indicate actual ClX used, where reported.

³2-km flight altitude adjustment not included.

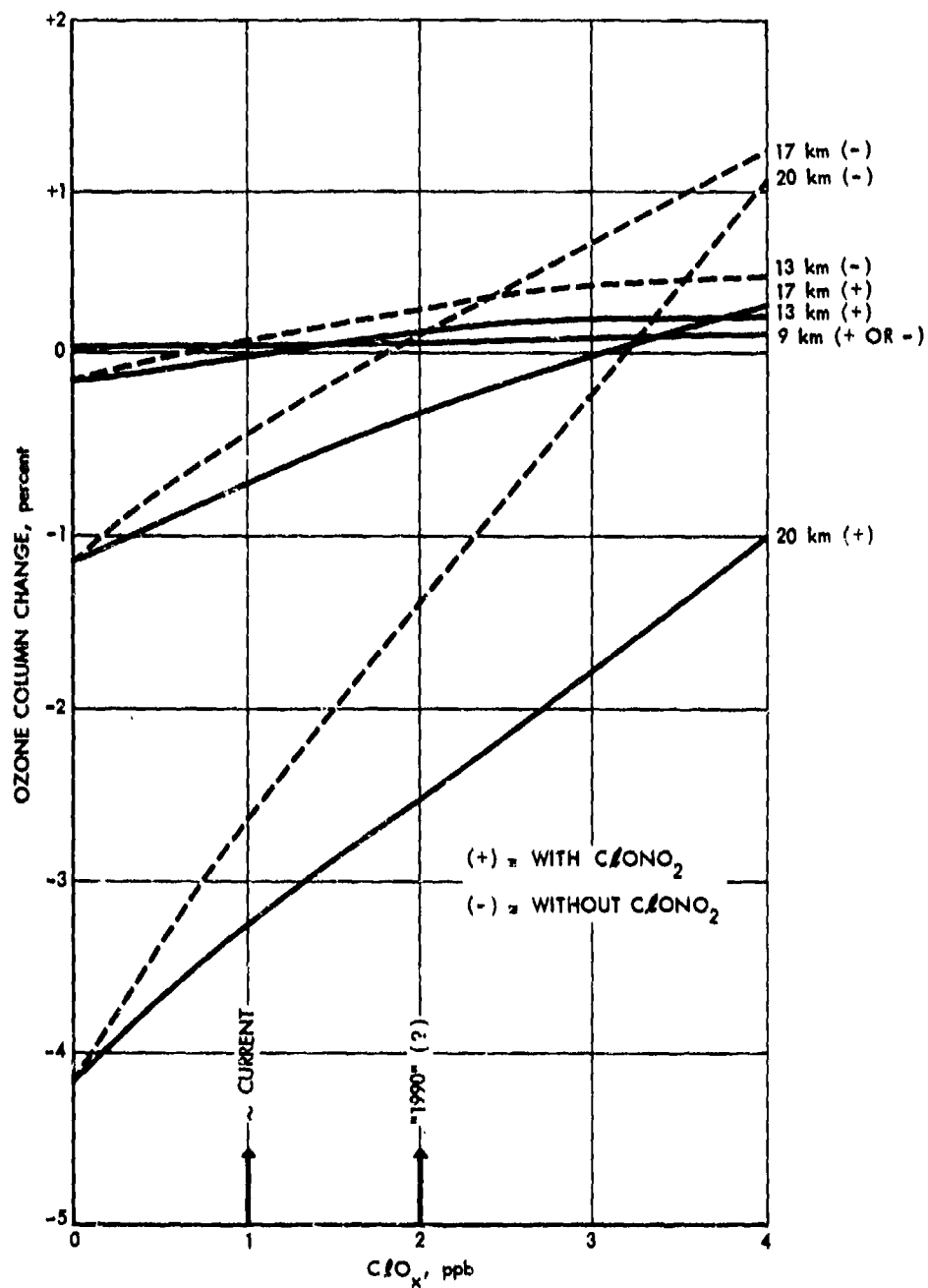
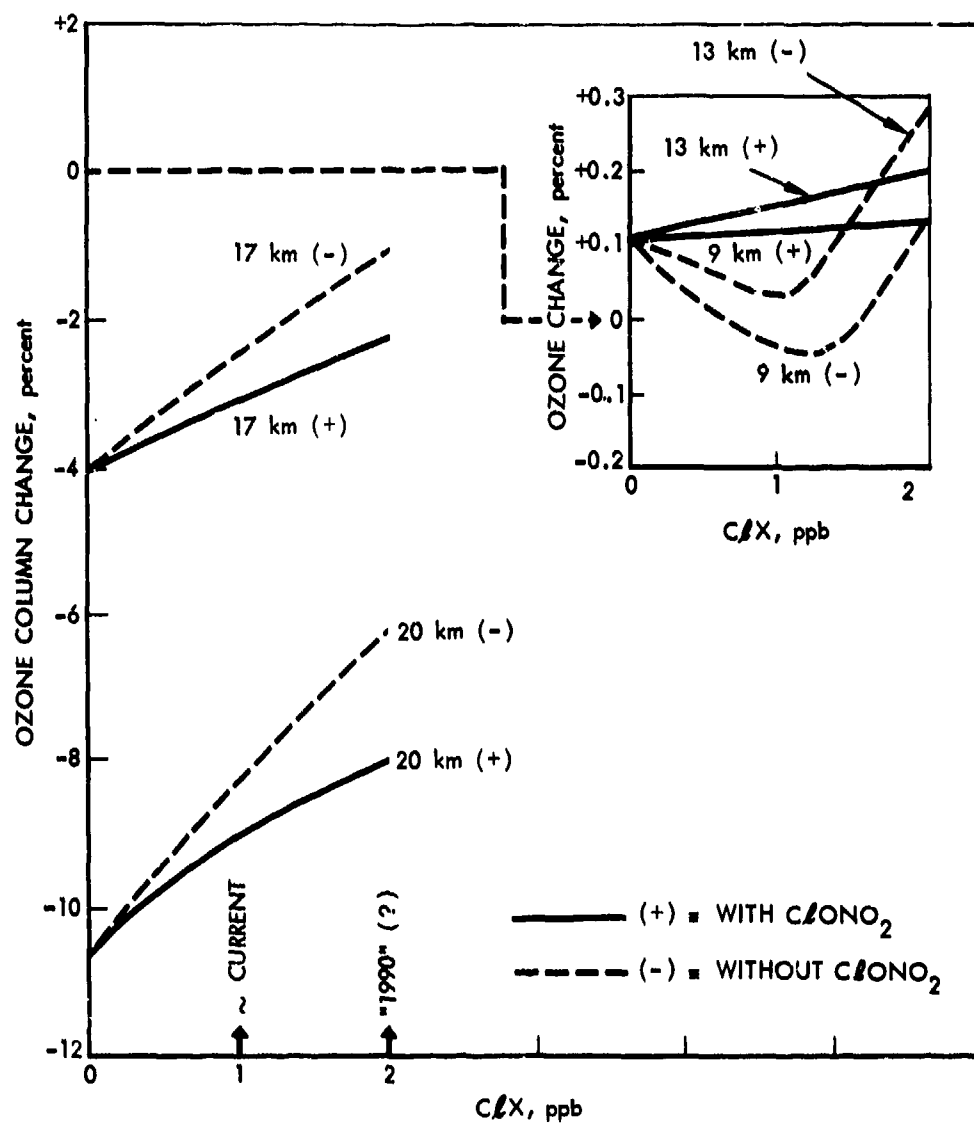
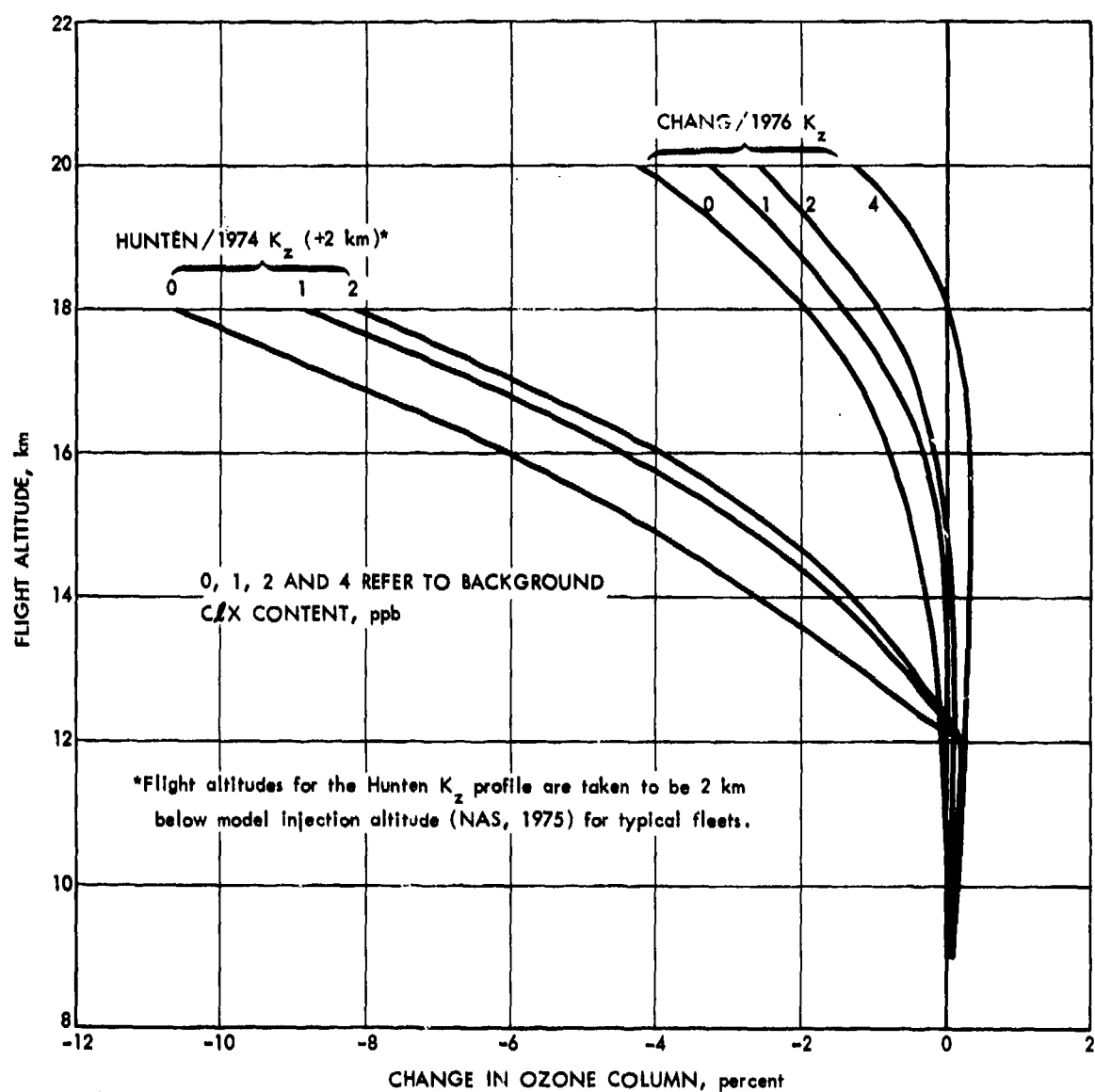


FIGURE 3.26. Effects of Background Chlorine Content on Ozone Sensitivity to NO_x Additions at Various Injection Altitudes. Chang/1976 K_z Profile. NO_x injection rate $2000 \text{ mol/cm}^3\text{-sec}^{-1}$ over 1 km at each altitude
Data Source: Lawrence Livermore Laboratory, 1976



11-18-76-7

FIGURE 3.27. Effects of Background Chlorine Content on Ozone Sensitivity to NO_x Additions at Various Injection Altitudes. Hunt/1974 R_z profile, without 2 km adjustment in flight altitude. NO_x injection rate 2000 mol/cm³-sec over 1 km at each altitude. Data Source: Lawrence Livermore Laboratory, 1976



11-18-76-5

FIGURE 3.28. Data of Figs. 3.26 and 3.27 Replotted.
($ClONO_2$ included)

to 13 km. The Hunten profile shows the same effects, but the 2-km adjustment and the known strong change in effect at 14 km (12 km adjusted) suggests that aircraft operating above 12 km might lead to ozone depletion, but more runs would be necessary to establish the point.

2. Linearity The question of linearity of effects was studied in a series of runs also with and without ClONO_2 at 17-km injection. Results with ClONO_2 are shown in Fig. 3.29. Some curvature appears in the plot, but it is not clear how much of this is due to small round-off errors or convergence criteria differences. Based on these data, however, the assumption of linearity would seem to be acceptable only as a rough approximation, even for conditions yielding only a few percent ozone reduction.

A superposition run was made for the following conditions:

K_z profile: "new Chang"

Background 1 ppb

No ClONO_2

Injection rates: 200 molecules/cm³ sec

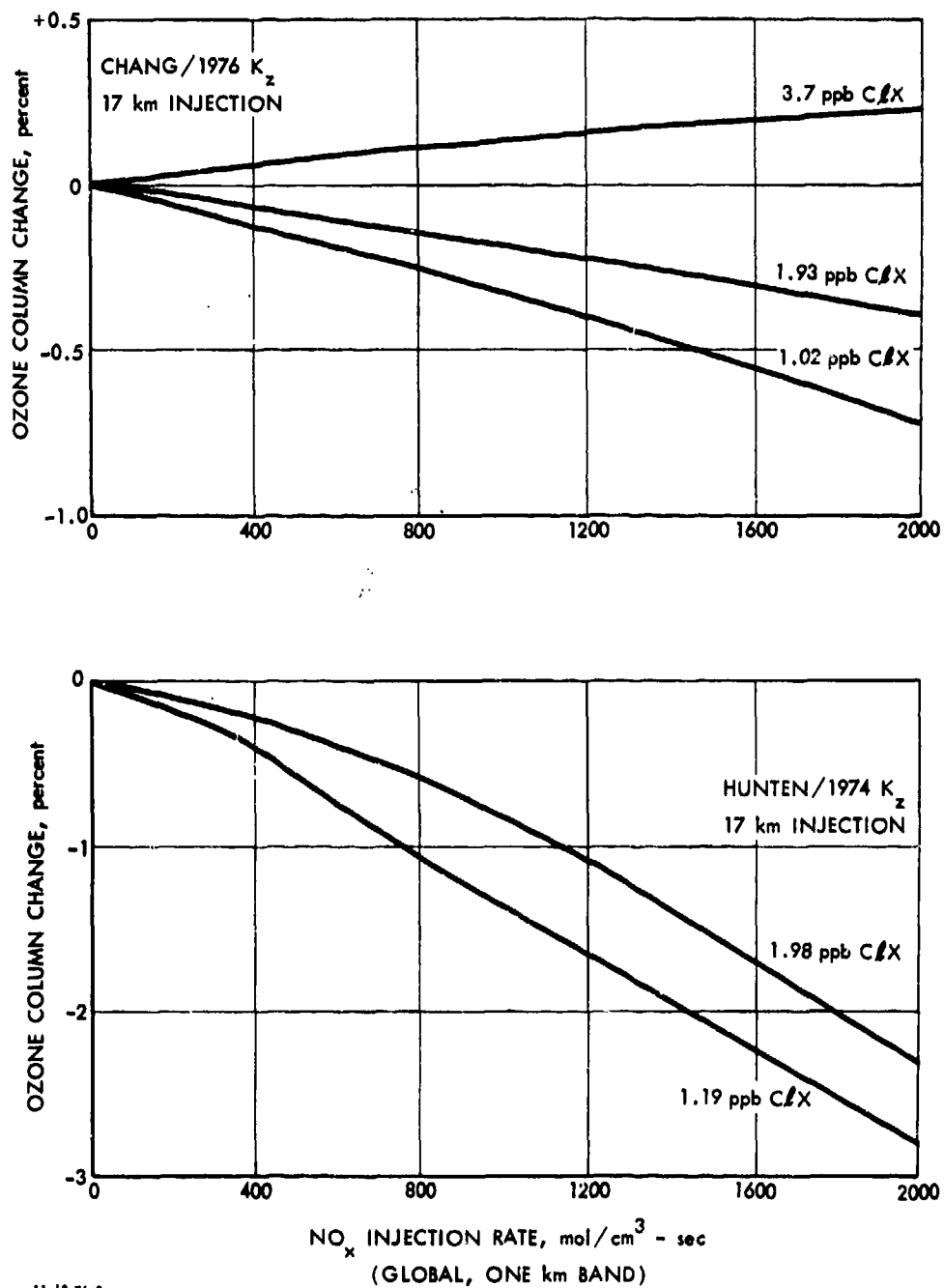
Results at each altitude and for the summed injections are as shown in Table 3.21.

TABLE 3.21. SUPERPOSITION TEST IN A CHLORINE-CONTAINING ATMOSPHERE (1 ppb ClX). EQUAL NO_x RATES AT EACH ALTITUDE. OZONE CHANGE, PERCENT.
SOURCE: Lawrence Livermore Laboratory, 1976

Altitude, km	Ozone Change,* Percent
9	+0.0085
13	+0.0097
17	-0.0292
20	-0.2021
Sum	-0.2131 (simple addition)
9,13,17,20	-0.2204 (computed)

*The final digit is probably not significant.

The dominance of the value at 20 km precludes firm conclusions, but linear superposition appears to be a reasonably good assumption, as was the case without chlorine chemistry (Section 3.4.3).



11-18-76-8

FIGURE 3.29. Ozone Change Linearity Tests. $ClONO_2$ Included. The curves are based on points at 200, 600, and 2000 $mol/cm^3 \cdot sec$ over 1 km at 17 km.
Data Source: Lawrence Livermore Laboratory, 1976

3. Water Effects The importance of water in a stratosphere polluted by ClX and NO_x was suggested by Liu et al., (1976). The paper implied a considerable sensitivity of ozone depletion results to stratospheric water vapor content. The point was further studied at Lawrence Livermore Laboratory, using conditions as follows:

Injection rate: $2000 \text{ mol/cm}^3\text{-sec}$, 1-km global

K_z profiles: Chang/1976, Hunten/1974

ClX contents: 1.12 ppb at 40 km (Chang/1976)
1.28 ppb at 40 km (Hunten)

Water multipliers: 0, 1, 1.1 (or 1.2), 2, 5

Baseline water content above 14 km: 4.32 ppmv

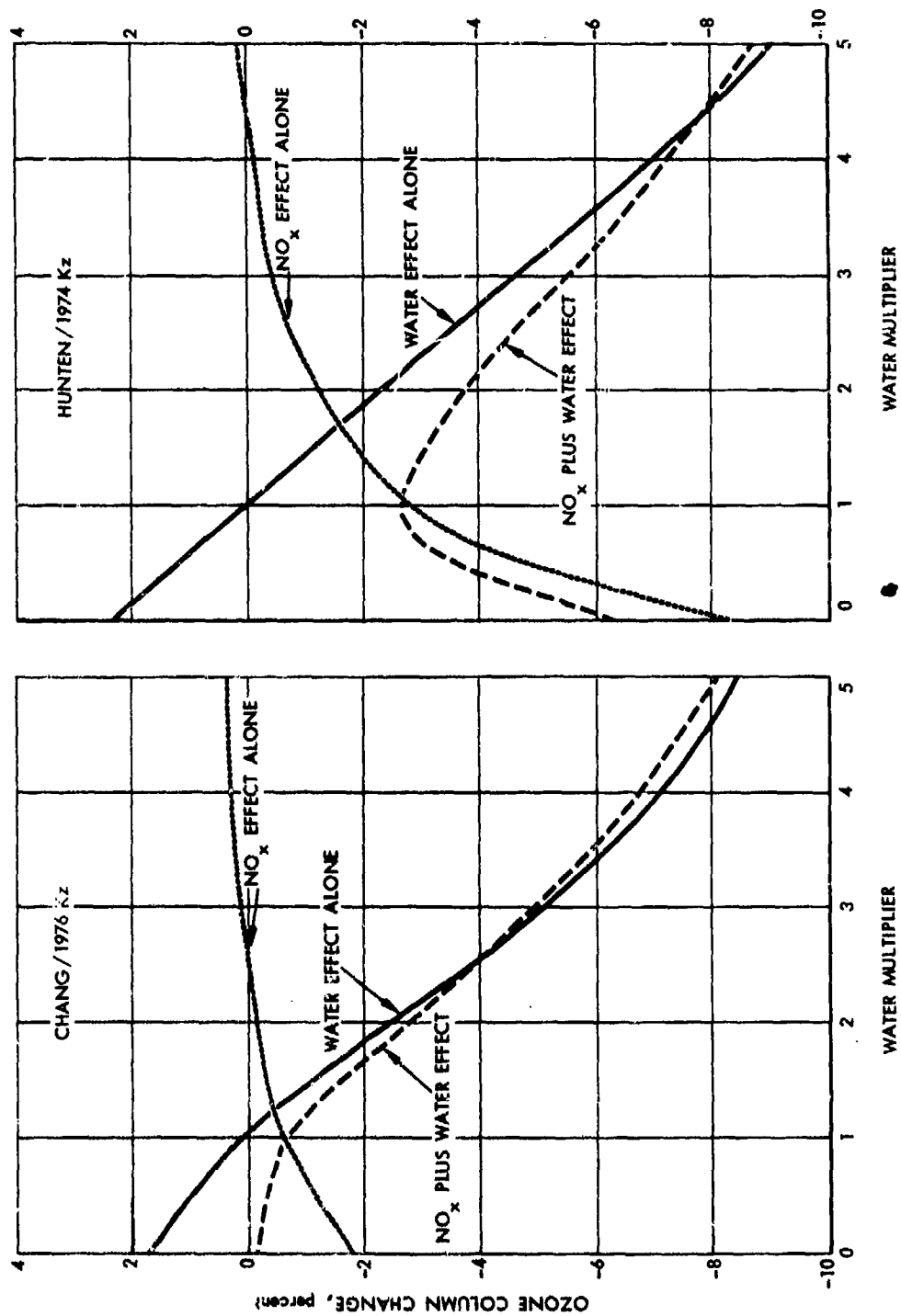
The chemistry used was "1976" chemistry (Table 3.19)

Results are shown for the "new Chang" profile in Fig. 3.30a and for the Hunten profile (without altitude adjustment) in Fig. 3.30b. Results follow the same general trends as reported by Liu et al., (1976). However, some interpretation is called for.

First of all, the scale of the water multiplier must be noted: A five-fold change in water vapor would be possible only with very great positive feedback effects, as very large fleets of SSTs,* at 20 km, even with residence times corresponding to the Hunten K_z profile, would be required to as much as double the stratospheric water content due to aircraft water emissions alone; most estimates are for much smaller changes. The large values used by Liu et al. (1976) were based on an assumed positive feedback in which a depletion of ozone due to NO_x was assumed to lead to an increase in the tropical tropopause cold trap temperature and a corresponding increase in water content. The most probable effect on the tropical tropopause temperature is, however, unknown, as effects of NO_2 , water vapor, and sulfates would need to be determined in a satisfactory model. If the aircraft exhaust water vapor effect is the dominant climatic effect, the tropopause temperature should decrease rather than increase, providing a negative feedback effect (Manabe-Wetherald, 1967; COMESA, 1976, p. 494). A strong effect, however, is implied, and the question needs further study.

The solid lines on Fig. 3.30 show the change in ozone with increased or decreased water in the stratosphere; an increase in water above

*Using fuel flow per advanced SST as in the NAS study ($9.1 \times 10^7 \text{ kg/yr}$), a 1.25 gm/gm water emission index, a residence time of 5.2 yr (CIAP ROF, p. 19), a hemisphere factor of 1.4, and stratospheric water content of $2 \times 10^{12} \text{ kg}$, a fleet size of 2400 advanced SSTs is required to double stratospheric water content.



11-18-76-4

FIGURE 3.30. Water and NO_x Effects on Ozone in the Presence of ~ 1 ppb Active Chlorine. A water multiplier of 1.0 represents the standard model. NO_x injection rate 2000 mol/cm³ sec over 1 km at 17 km altitude. Source: Lawrence Livermore Laboratory, 1976

the normal value (a multiplier of 1.0) decreases ozone. The dashed lines show the change in ozone due to a specified change in water vapor when coupled with a NO_x injection of $2000 \text{ mol/cm}^3\text{-sec}$ over 1 km at 17 km. The dotted lines show the change in ozone resulting from the added NO_x , relative to what might be termed a natural stratosphere containing more or less water than the normal model atmosphere. Note that crossovers occur (at a multiplier of about 2.5 with Chang/1976 and a multiplier of about 4 with Hunten/1974) where the NO_x addition does not change the ozone column. If the stratosphere is drier than the model atmosphere implies, NO_x effects are increased, relative to those in the model atmosphere. A further interpretation can also be made using the dashed curve directly if an estimate of the change in stratospheric water for a given NO_x input rate can be made: ignoring feedbacks, the Chang/1976 K_z dashed curve should be read at about 1.1 multiplier to get the combined effect and about 1.3 for the Hunten K_z curve, assuming a water to NO_x emission index ratio of 1250/18. Without feedback, the water effect appears to be rather small.

4. Results (1990-high fleet, modified; no chlorine) The modified 1990 fleet collapsed to 1-D was run by Lawrence Livermore Laboratory without chlorine species, to be consistent with the Widhopf model runs. Results were printed out each year until several years showed the same values. Results are shown in Fig. 3.31. Note that both K_z profiles show slight ozone enhancements, in spite of the presence of an equivalent of about 140 Concordes and Tupolevs operating up to the 18-km to 19-km region. The "partial Widhopf" chemistry described earlier shows slightly smaller net effects. A 14-km tropopause was used with the Hunten model; i.e., a 2-km altitude adjustment was not made. This correction, if made, might well have put the total fleet effect with the Hunten K_z profile on the negative side. Note that a substantial number of years of operation are required to bring effects near to equilibrium, particularly with the Hunten K_z profile.

3.4.8 Average 2-D Model Results, "1990 High" Fleet Effects

A. Model Description and Tracer Studies

Widhopf et al., (1976) have recently summarized progress and results in their 2-D time-dependent photochemical model of the atmosphere. This model has been under development for several years, first under CIAP and for about the past year under HAPP. The model is briefly described by Widhopf as follows:

The atmospheric model solves the time-dependent species conservation equations for the transient and spatial variation of the following trace species: $\text{O}(^3\text{P})$, $\text{O}(^1\text{D})$, O_3 , NO , NO_2 , N_2O , HNO_3 , N , OH , HO_2 , H_2O_2 , H , CH_4 , and CO in the entire meridional plane continuously throughout the year. A 10-deg latitudinal and a 1-km resolution from the surface up to 35 km

is used in the computations. A 2.5-km resolution is used from 35 to 50 km. Transport by mean meridional circulation and large scale turbulent eddies is also included by parameterization. A second order accurate numerical finite difference scheme is used to solve the system of conservation equations which is outlined by Widhopf at the 4th CIAP Conference, February 4-7, 1975. The reaction system and reaction rates used in the model are listed (in Table 3.22). This system includes smog chemistry together with the other important atmospheric reaction cycles. Rain-out/washout of NO_x , HNO_3 , and H_2O_2 is included in the model, whereas the distribution of water vapor is prescribed.

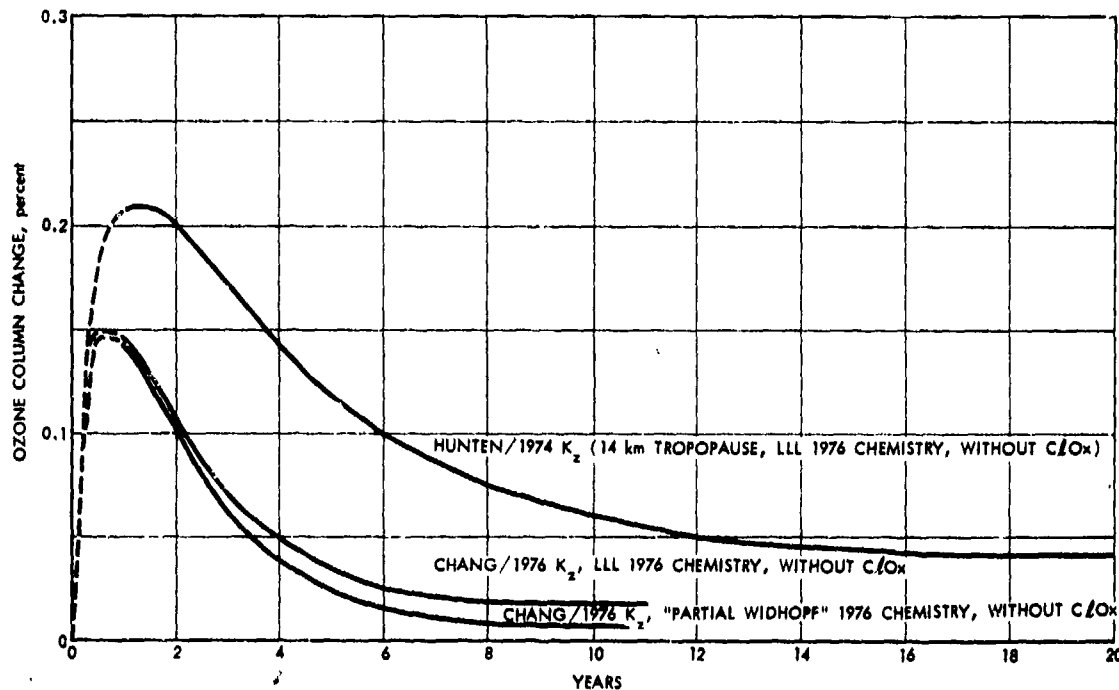


FIGURE 3.31. Global Average Ozone Column Changes with Time Following Introduction of the Modified "1990-High" Fleet NO_x Emissions, No Chlorine. Data Source: Lawrence Livermore Laboratory, 1976

The smog chemistry referred to by Widhopf in the quotation above is the methane oxidation chemistry, as used by Crutzen (see Appendix A) (reactions R47 through R53), but with certain rate constant changes recommended by D. Garvin (private communication, August 1976), in particular reactions 44, 46, and 51, for which the Crutzen model values are given in Appendix A. The rest of the set, in particular changes made in the important reactions 12 and 16, was developed from CIAP (NBS) recommendations and as a result of recommendations by Lawrence Livermore Laboratory.

The Widhopf model was developed initially using diffusion coefficients as presented by Luther (1973) and the mean meridional winds as

TABLE 3.22. CHEMICAL REACTIONS AND RATE COEFFICIENTS
Source: Widhopf, 1976

1.	$\text{O}^3\text{P} + \text{O}_3 \rightarrow \text{SO}_2$	$1.9(10)^{-11} \exp(-2300/T)$	J_{26}
2.	$\text{O}_2 + h\nu \rightarrow 2\text{O}^3\text{P}$	J_2	$1.02(10)^{-14} T \exp(3130/T)$
3.	$\text{O}_3 + h\nu \rightarrow \text{O}^3\text{P} + \text{O}_2$	J_3	$2.7(10)^{-11}$
4.	$\text{NO}_2 + h\nu \rightarrow \text{O}^3\text{P} + \text{NO}$	J_4	0.0
5.	$\text{O}^3\text{P} + \text{C}_2 \cdot \text{M} \rightarrow \text{O}_3 + \text{M}$	$1.07(10)^{-34} \exp(510/T)$	$2.8(10)^{-36}$
6.	$\text{O}^3\text{P} + \text{NO}_2 \rightarrow \text{O}_2 + \text{NO}$	$9.1(10)^{-12}$	$1.4(10)^{-12}$
7.	$\text{O}_3 + \text{NO} \rightarrow \text{O}_2 + \text{NO}_2$	$9(10)^{-13} \exp(-1200/T)$	$2.32(10)^{-10}$
8.	$\text{O}_3 + \text{NO}_2 \rightarrow \text{O}_2 + \text{NO}_3$	$1.23(10)^{-13} \exp(-2470/T)$	$1.38(10)^{-10}$
9.	$\text{NO}_3 + h\nu \rightarrow 2/3[\text{NO}_2 + \text{O}^3\text{P}] + 1/3[\text{NO} + \text{O}_2]$	$1.6(10)^{-12} \exp(-1000/T)$	$4.2(10)^{-11}$
10.	$\text{O}_3 + \text{OH} \rightarrow \text{O}_2 + \text{HO}_2$	$2.3(10)^{-13}$	$2.08(10)^{-32} \exp(290/T)$
11.	$\text{NO} + \text{HO}_2 \rightarrow \text{OH} + \text{NO}_2$	0.0	$1.23(10)^{-10} \exp(-562/T)$
12.	$\text{O}^3\text{P} + \text{H}_2\text{O} \rightarrow \text{OH} + \text{OH}$	$2.76(10)^{-13} \exp(280/T)$	$3.96(10)^{-33} \exp(940/T)$
13.	$\text{OH} + \text{NO}_2 + \text{M} \rightarrow \text{HNO}_3 + \text{M}$	$1.166(10)^{-10} \exp(220/T) + [M]$	$1(10)^{-11} \exp(-550/T)$
14.	$\text{HNO}_3 + h\nu \rightarrow \text{OH} + \text{NO}_2$	J_{13}	$5.7(10)^{-13}$
15.	$\text{HO}_2 + \text{O}_3 \rightarrow \text{OH} + \text{O}_2 + \text{O}_2$	$1(10)^{-13} \exp(-1250/T)$	J_{40}
16.	$\text{HO}_2 + \text{O}^3\text{P} \rightarrow \text{OH} + \text{O}_2$	$3(10)^{-11}$	$2.36(10)^{-12} \exp(-1710/T)$
17.	$\text{OH} + \text{HO}_2 \rightarrow \text{H}_2\text{O} + \text{O}_2$	$2(10)^{-11}$	$2.5(10)^{-33} \exp(2500/T)$
18.	$\text{OH} + \text{HNO}_3 \rightarrow \text{H}_2\text{O} + \text{NO}_3$	$8.9(10)^{-14}$	$2.75(10)^{-12} \exp(-2125/T)$
19.	$\text{HO}_3 + h\nu \rightarrow 2/3[\text{NO}_2 + \text{O}^3\text{P}] + 1/3[\text{NO} + \text{O}_2]$	J_{18}	$\log_{10} K = -12.95 + 3.94(10)^{-4} T$
20.	$\text{H}_2\text{O}_2 + h\nu \rightarrow \text{OH} + \text{OH}$	$1.7(10)^{-11} \exp(-910/T)$	J_{45}
21.	$\text{H}_2\text{O}_2 + \text{OH} \rightarrow \text{H}_2\text{O} + \text{HO}_2$	$1.7(10)^{-11} \exp(-500/T)$	$5(10)^{-12}$
22.	$\text{HO}_2 + \text{HO}_2 \rightarrow \text{H}_2\text{O}_2 + \text{O}_2$	J_{21}	$2.6(10)^{-31}$
23.	$\text{O}_3 + h\nu \rightarrow \text{O}_2 + \text{O}^3\text{P}$	$2.2(10)^{-11} \exp(92/T)$	$1.5(10)^{-12} \exp(-560/T)$
24.	$\text{O}^3\text{P} + \text{M} \rightarrow \text{M} + \text{O}^3\text{P}$	J_{23}	$3.0(10)^{-11} \exp(-500/T)$
25.	$\text{N}_2\text{O} + h\nu \rightarrow \text{N}_2 + \text{O}^3\text{P}$	$5.7(10)^{-11}$	J_{50}
26.	$\text{N}_2\text{O} + \text{O}^3\text{P} \rightarrow \text{N}_2 + \text{O}_2$	$5.7(10)^{-11}$	$1.6(10)^{-13} \exp(-3300/T)$
27.	$\text{N}_2 + \text{O}_2 \rightarrow \text{N}_2 + \text{O}_2$		J_{52}
28.	$\text{N}_2 + \text{NO} \rightarrow \text{N}_2 + \text{O}^3\text{P}$		$1.4(10)^{-11}$
29.	$\text{N}_2 + \text{NO}_2 \rightarrow \text{N}_2 + \text{NO}$		
30.	$\text{N}_2 + \text{O}^3\text{P} + \text{M} \rightarrow \text{N}_2\text{O} + \text{M}$		
31.	$\text{NO}_2 + \text{N} \rightarrow \text{N}_2\text{O} + \text{O}^3\text{P}$		
32.	$\text{O}^3\text{P} + \text{H}_2\text{O} \rightarrow \text{OH} + \text{OH}$		
33.	$\text{O}^3\text{P} + \text{CH}_4 \rightarrow \text{OH} + \text{CH}_3$		
34.	$\text{OH} + \text{O}^3\text{P} \rightarrow \text{O}_2 + \text{H}$		
35.	$\text{H} + \text{O}_2 + \text{M} \rightarrow \text{HO}_2 + \text{M}$		
36.	$\text{H} + \text{O}_3 \rightarrow \text{OH} + \text{O}_2$		
37.	$\text{NO} + \text{O}^3\text{P} + \text{M} \rightarrow \text{N}_2\text{O}_2 + \text{M}$		
38.	$\text{OH} + \text{OH} \rightarrow \text{H}_2\text{O} + \text{O}^3\text{P}$		
39.	$\text{N} + \text{O}_3 \rightarrow \text{NO} + \text{O}_2$		
40.	$\text{HO}_2 + h\nu \rightarrow \text{OH} + \text{O}$		
41.	$\text{OH} + \text{CH}_4 \rightarrow \text{H}_2\text{O} + \text{CH}_3$		
42.	$2\text{OH} + \text{M} \rightarrow \text{H}_2\text{O}_2 + \text{M}$		
43.	$\text{H}_2\text{O}_2 + \text{O} \rightarrow \text{OH} + \text{HO}_2$		
44.	$\text{CO} + \text{OH} \rightarrow \text{H} + \text{CO}_2$		
45.	$\text{CH}_2\text{O} + h\nu \rightarrow \text{H}_2 + \text{CO}$		
46.	$\text{CHO} + \text{O}_2 \rightarrow \text{HO}_2 + \text{CO}$		
47.	$\text{CH}_3 + \text{O}_2 + \text{M} \rightarrow \text{CH}_3\text{O}_2 + \text{M}$		
48.	$\text{CH}_3\text{O}_2 + \text{NO} \rightarrow \text{CH}_3\text{O} + \text{NO}_2$		
49.	$\text{CH}_3\text{O}_2 + \text{HO}_2 \rightarrow \text{CH}_3\text{O}_2\text{H} + \text{O}_2$		
50.	$\text{CH}_3\text{O}_2\text{H} + h\nu \rightarrow \text{CH}_3\text{O} + \text{OH}$		
51.	$\text{CH}_3\text{O} + \text{O}_2 \rightarrow \text{CH}_2\text{O} + \text{HO}_2$		
52.	$\text{CH}_2\text{O} + h\nu \rightarrow \text{H} + \text{CHO}$		
53.	$\text{CH}_2\text{O} + \text{OH} \rightarrow \text{H}_2\text{O} + \text{CHO}$		

developed from various sources, including transport of particulate radioactive debris. Widhopf, however, found these data to provide an inadequate simulation of excess carbon-14, a gaseous tracer, produced by nuclear weapons tests, as well as incorrectly predicting ozone at high latitudes. Widhopf thus modified the transport coefficients using the data on excess carbon-14 as a guide, and developed modified coefficients which adequately simulated the movement of excess carbon-14 for a 3-year period (with some exceptions as, e.g., the 9-km to 13-km region at high latitudes), and also provided better ozone-matching at polar latitudes. Other photochemically active tracer species (NO , NO_2 , HNO_3 , OH , and CO) were also examined, with a reasonable match found for model-derived values to the various, rather uncertain, measurements. The model-derived O_3 values are compared to measurements in Fig. 3.32. The general agreement is seen to be quite good.

Widhopf has carried out two additional tests of the dynamics of his model. The first involved the data on tungsten-185 which isotope was deposited by an explosion at 11°N in the summer of 1958. This tracer has been used in a number of studies of stratospheric motion. Widhopf found his revised coefficients to give a somewhat better fit to this data than did his earlier values. Particulate settling was not included in these calculations. The second test involved the behavior of zirconium-95, an isotope deposited at about 18 km and 40°N by Chinese weapons tests in 1967 and subsequently. These tests were of particular interest being at mid-latitude (rather than equatorial, as were the tungsten-185 injections, or polar, as were the bulk of the excess carbon-14 injections), and at an injection altitude near that at which mach 2 SSTs travel. The zirconium-95 data are treated in a 1-D sense in Appendix C of this report. These data showed strong differences with season, with slow removal noted following summer injections and rapid removal noted following winter injections. The particular case studied (to date) by Widhopf was for a summer injection (17 June 1967), using data collected in October 1967 and thereafter. In this case, Widhopf found it necessary to make a rather large* allowance for settling of the particulates in order to match the tracer behavior, as shown in Figs. 3.33 and 3.34, but the general behavior of the model was good.

*Note that Widhopf used (in Figs. 3.33 and 3.34) a density of 6.44 gm/cc and a radius of 0.15μ . Telegadas and List (1969) quoted a density of 2 gm/cc and radii ranging from 0.02μ to 0.15μ . As settling velocity is proportional to the square of the radius times the density, the settling velocity used by Widhopf (at, say, 20 km) corresponds to a particle of density 2 gm/cc and a radius of 0.27μ .

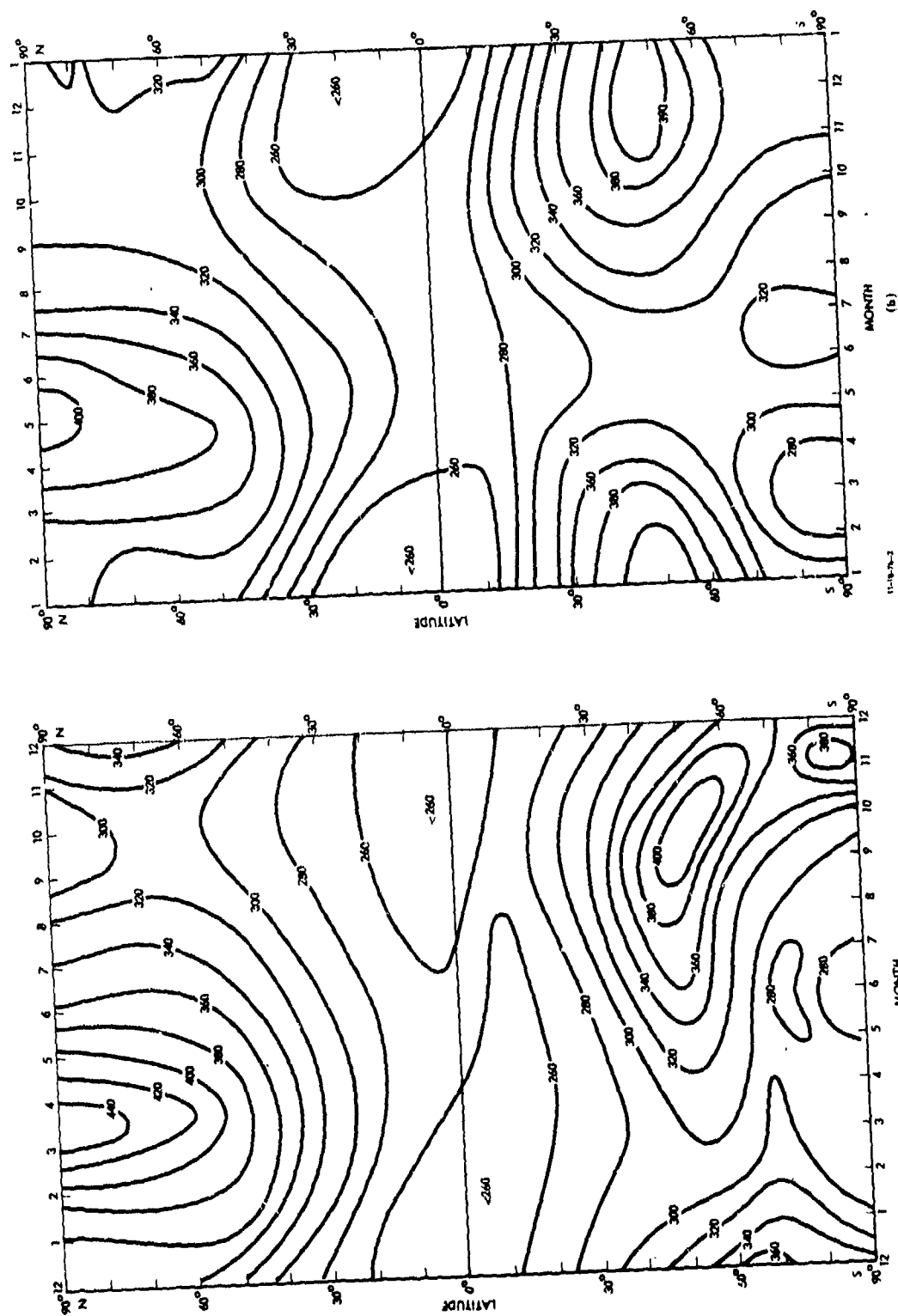


FIGURE 3.32. Ozone Columns (m-atm-cm) as a Function of Season and Latitude. The plot on the left represents measured data (Dütsch, 1971); the plot on the right represents results from the Widhopf 2-D model. Source: Widhopf, 1976

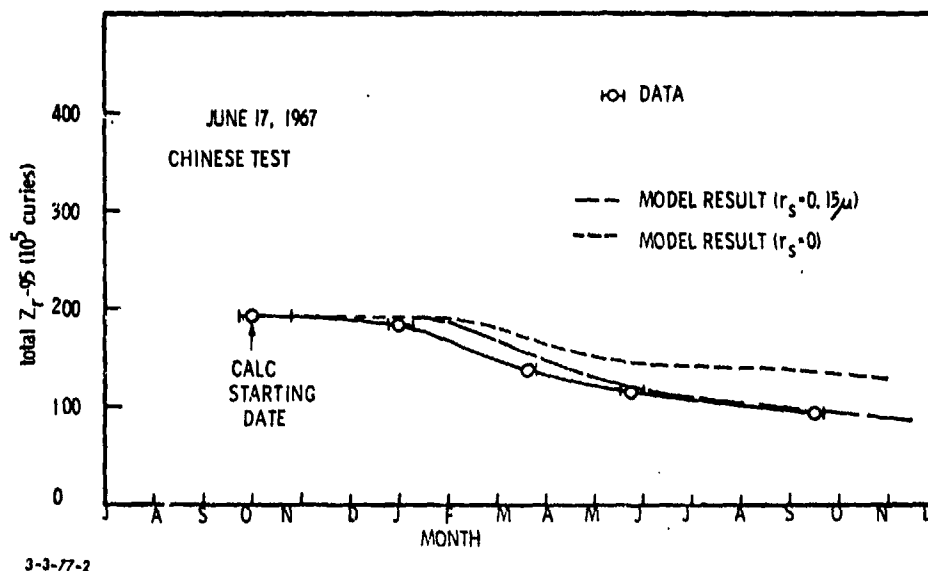


FIGURE 3.33. Test of Widhopf 2-D Model Dynamics Using Zr-95 Data. Total burden vs. time, with and without settling. Particle density of 6.44 gm/cm³ assumed. Source: Widhopf, 1976

B. Fleet Effects Results

The model was run using NO_x injections (at constant rates) based on the modified fleet forecast (1990-high) given in Table 2.33. The model was run, using an October start, for five model years, extending both the natural and perturbed atmospheres for comparison. Results are shown in Fig. 3.35 for the Northern Hemisphere, covering latitudes 20° N to 60° N. An enhancement in the ozone column was found over the entire hemisphere at all seasons. Enhancements were found to decrease with increasing latitudes. An apparent slight downward trend with time suggests the desirability of extending the runs for additional years (see Fig. 3.17 describing the MIT results).

The maximum enhancements were found to occur in the fall and minimum enhancements to occur in late winter or early spring, varying somewhat with latitude. The average ozone column enhancement at 30° N to 40° N in the summer period (months 56 to 59) is about 0.8 percent.

Quantitative results for the Southern Hemisphere are not yet available (15 November 1976); however, appreciable enhancements were found (Widhopf, private communication, November 1976). This result is a principal disagreement with the Crutzen model results, which showed little or negative effects in the Southern Hemisphere for subsonic aircraft.

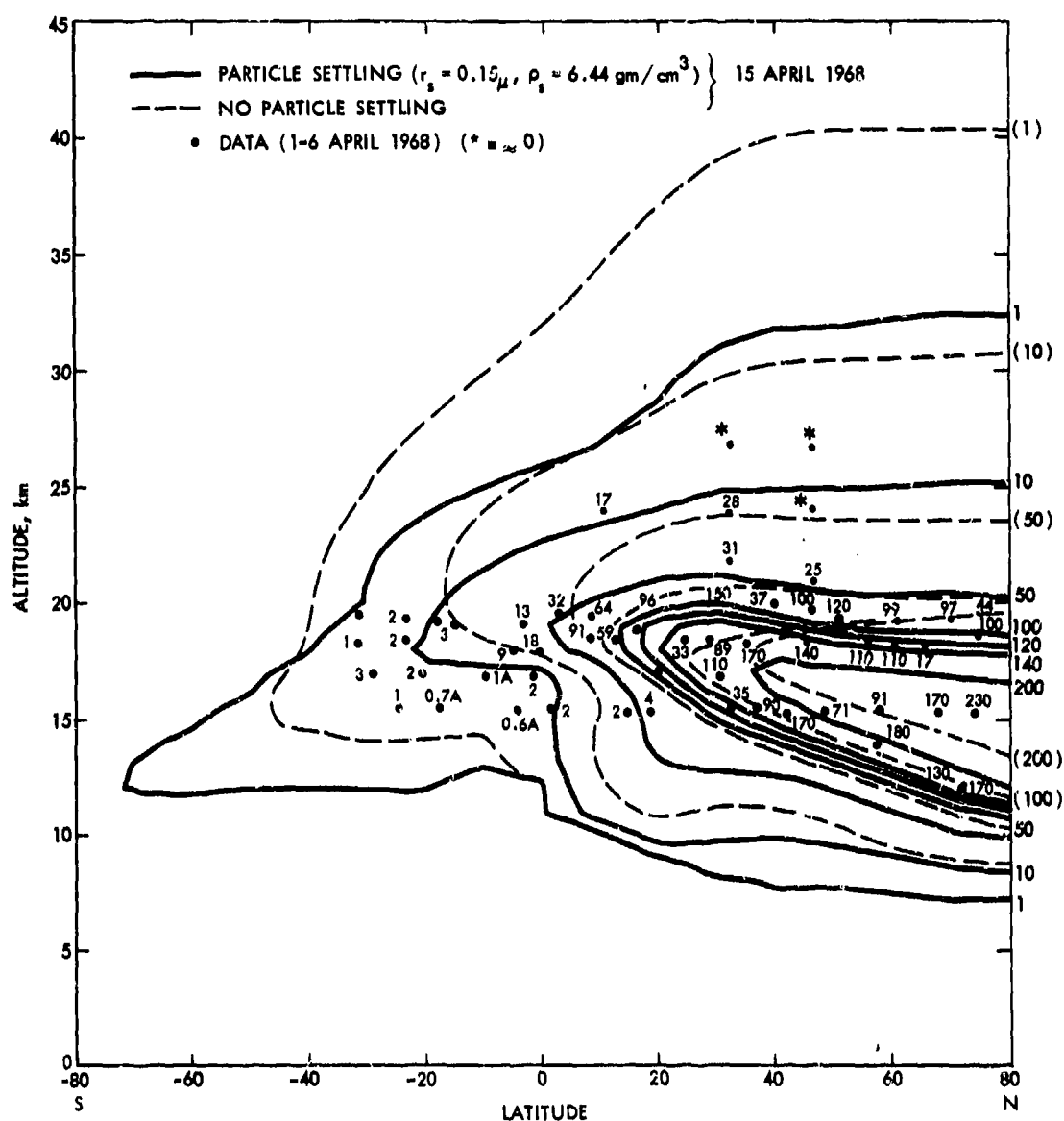
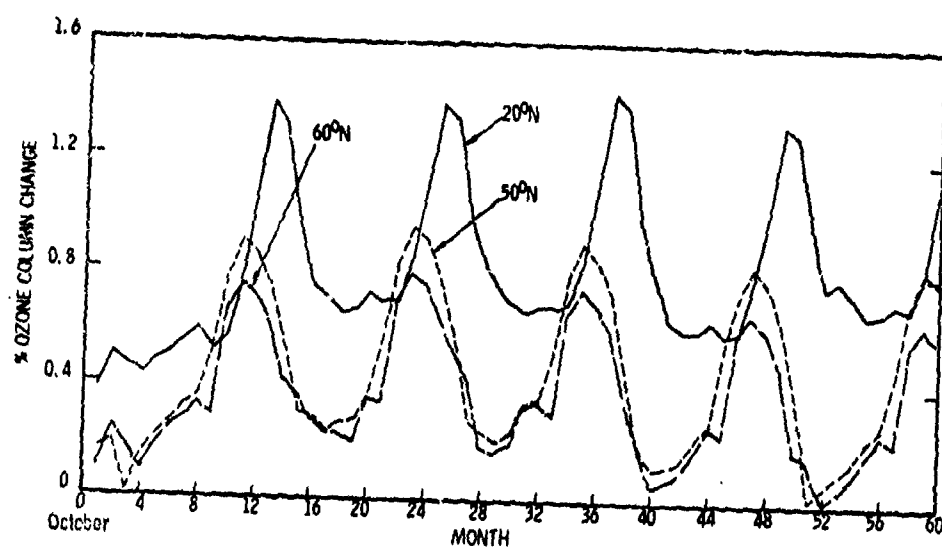
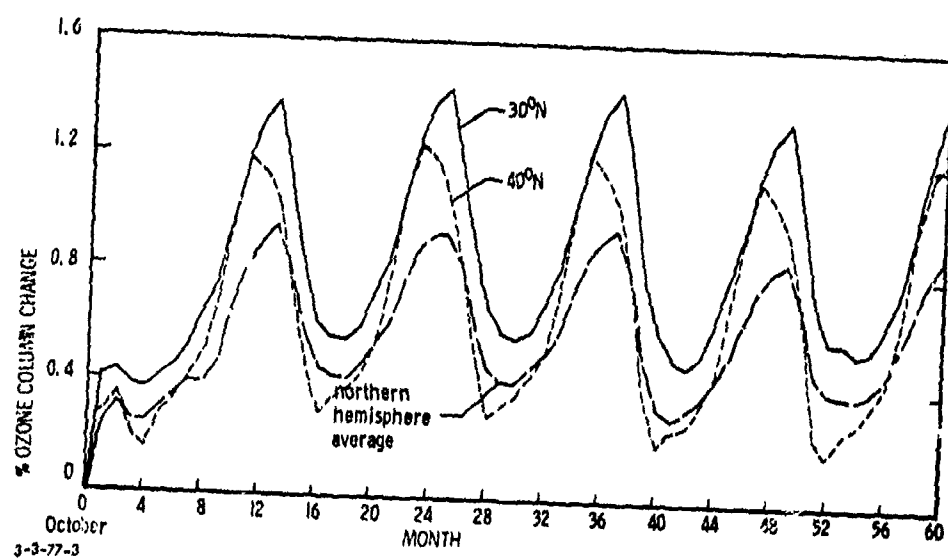


FIGURE 3.34. Test of Widhopf 2-D Model Dynamics Using Zr-95 Data, Showing the Need to Include Settling.
Source: Widhopf, 1976



(a)



(b)

FIGURE 3.35. Widhopf Model Results for Modified "1990-High" Fleet (see Table 2.33).
Source: Widhopf, 1976

C. Comments

While some disagreement and considerable uncertainty surrounds both the Crutzen and Widhopf model results, it seems evident that inclusion of methane oxidation chemistry has a powerful effect on the computed effects of aircraft fleets. Note that the Widhopf result included the effects of some 142 Concorde-Tupolev aircraft, as well as a large increase in subsonic traffic (both "present" and "advanced" types) in all cases using emission indices typical of today's engines. The total effect of this fleet, as computed, is an enhancement of the ozone column.

The substantially greater net ozone production in the Widhopf 2-D results when compared to the Lawrence Livermore Laboratory 1-D results, is probably due to a number of factors. However, the greater ozone production by the Widhopf methane oxidation path relative to the simpler path used in the 1-D results may well have a strong effect, as the net change is a result of a variety of production and destruction mechanisms.

Quite obviously, the above result, as well as the components which make up these results, need further study and verification. The uncertainty range should be determined, using plausible estimates for critical reaction rates. Chlorine chemistry, N_2O_5 (in Widhopf's model), and water effects all should be included. Further studies on the dynamics using all available tracer data would also be desirable. For example (see Section 3.6), a "hidden source" of carbon-14, if present as suggested by Chang at the 4th CIAP Conference, February 4-7, 1975, would lead to erroneous model dynamics if carbon-14 data were used exclusively, but anomalies, and the need for corrections, should become evident with the use of additional tracers.

3.5 LONGITUDINAL DISTRIBUTION QUESTIONS

Results have been described herein from two separate 2-D models which show ozone column enhancements due to subsonic aircraft as a function of latitude. Inasmuch as these results are based on zonal averages in the troposphere (in which zonal uniformity would hardly be expected) as well as on the combination of a tropospheric enhancement with a stratospheric depletion, a further examination of the distribution of these effects is necessary. The possibility might exist, for example, that the tropospheric air mass crossing the Pacific might be cleared of incremental NO_x and ozone, leaving the West Coast of the United States exposed only to the effects resulting from a stratospheric depletion. These questions are in detail extremely complex. However, on examining the model data in connection with some elementary considerations, some useful observations seem possible.

Data from the Crutzen model runs are shown in Table 3.23. The data are for 45° N on August 30 after six model years, a time selected for its expected relevance to biospheric UV exposure, as noted earlier. The different injection rates at different altitudes should be noted. In all cases, a depletion is found above 19.8 km, and in all cases an enhancement is found over the 0-km to 16.3-km altitude range. If the tropospheric component is taken as that portion to 12.7 km, and complete zonal uniformity is assumed above 12.7 km, it follows that a reduction below the tropospheric zonal mean of even 100 percent would not lead to a column deficit for 10.8-km and 12.7-km injections, but any reduction below the tropospheric zonal mean would result in a deficit for injections at 14.5 km and above.

TABLE 3.23. OZONE COLUMNS AND CHANGES, 45° ON AUGUST 30, CRUTZEN 2-D MODEL RESULTS

Altitude Increment, km	Ozone Column, Natural Atmosphere, Dobson Units	Ozone Column Change in Dobson Units in Increment, With NO_x injections at () km of 10^9 [] kg/yr			
		(10.8)	(12.7)	(14.5)	(18.0)
		[2.06]	[0.455]	[0.455]	[0.226]
19.8-55	233.3	-0.4	-0.3	-0.7	-1.6
16.3-19.8	43.7	+0.2	+0.1	0	-0.1
12.7-16.3	18.8	+0.5	+0.3	+0.4	+0.1
0.2-12.7	32.8	+2.2	+0.5	+0.3	0
0.2-16.3	51.6	+2.7	+0.8	+0.7	+0.1
16.3-55	277.0	-0.2	-0.2	-0.7	-1.7
0.2-55	328.6	+2.5	+0.6	0	-1.6
0.2-55 percent ozone change	-	+0.76	+0.18	0	-0.49

The above results would seem to indicate that, at least for present subsonics and for the 40-50° N zone, even if the computed zonal mean value is composed of a larger-than-mean increase over regions of heavy air traffic (the U.S., the North Atlantic, and Europe), and a smaller-than-mean increase over the Pacific, there would still be no region within the zone where an enhanced UV-B dose rate would be expected. The same conclusion would appear to follow for advanced subsonics (recognizing that the model run at 12.7 km nominal was, in fact, spread over the 11.8-13.6-km altitude band) but the "safety margin" is reduced. For higher-altitude flight, as at 14.5 km and above, depletions would likely be expected in some or all parts of the zone. Some increase in zonal uniformity might, however, be expected as residence times (particularly above the tropopause) increase with altitude (see, e.g., Reiter, 1975; Bach, 1976).

While zonal nonuniformity may not lead to regions of enhanced UV-B with present and advanced subsonics, it is still of some interest to estimate the degree of nonuniformity that might result. To do so, a nominal upper troposphere residence time of 30 days is adopted as suggested by Newell (1971), noting that Machta et al., (1970) quoted a higher figure (90 days). As used here, the term residence time refers to the time after which 1/e of the mass of a pulse of precipitation-scavengable material would remain in the atmosphere. Residence time would, in fact, vary with season, altitude, and latitude. In order to gain some estimate of zonal uniformity, the time to circle the globe is needed. Newell (1971) shows zonal east-west wind speeds in the 30° N to 60° N latitude band at altitudes of 9 km to 15 km to be of the order of 10 m/sec to 35 m/sec, with winter speeds (20 m/sec to 35 m/sec) being roughly twice those of summer (10 to 15 m/sec). At, say, 15 m/sec, the time required to circle the globe is 22 days. Values of 22 days or so are less than or near the quoted e-folding time at 10 km so that a circling of the globe would result in only partial removal of pollutant materials. In fact, the comparison of minimum normalized value of pollutant level, which might be, say, 0.52 (based on $1-e^{-22/30}$), relative to the peak level, should instead be compared to the mean zonal value which, with the same numbers would be 0.71 [based on $(30/22) \times (1-e^{-22/30})$] rather than the peak value, so that for this set of numbers the minimum value is only 27 percent below the mean value.

Furthermore, the use of the globe-circling time is probably overly conservative, in that some of the polluted air masses, as from the U.S. and the North Atlantic, are further polluted in moving over Europe and the Soviet Union. Thus, the travel time in which no pollutant is added would often or usually be considerably less than the 22 days used above for illustration. As a result, zonal effects would be more uniform than indicated.

The above result is based on literature values of upper tropospheric residence times, which are reasonable for a region in which clouds are few and precipitation is rare (except in the tropics). It is of interest, however, to couple in independent cloud spreading data to see whether such data are compatible with the quoted times. To do so, we turn to Bauer (1974) who provides plots of horizontal and vertical spread of clouds with travel time.

For large clouds, which are equivalent conceptually to clouds which have traveled for a long period, Bauer gives an horizontal eddy diffusivity which characterizes the further spreading of the order of $5 \times 10^9 \text{ cm}^2/\text{sec}$. For vertical spreading, the data are less convincing, but a K_z of the order of $10^5 \text{ cm}^2/\text{sec}$, as is often used in 1-D modeling, would seem appropriate.

Given these eddy diffusivity figures, an estimate can be made of the additional horizontal and vertical spreading which would occur after, say, 20 days additional travel time. The calculation is based on the simple relationship $r^2 = aKt$, where r is a characteristic cloud width, K is eddy diffusivity, a is a constant with a value of 4 for horizontal spreading or 2 for vertical spreading, and t is time. It follows that if the cloud has an initial dimension r_0 , the corresponding effective initial time t_0 is ar_0^2/K , and the cloud dimension at time t_t later is simply $[r_0^2 + aKt_t]^{1/2}$, where t_t is the travel time being considered. It follows that a cloud initially 1000-km wide by 5-km thick would grow to 2200 km in width and 7.9 km in thickness after 22 days of travel. The horizontal spreading, of course, removes no pollutant, but the vertical spreading, by moving material into the rainout region, does. The vertical spreading in this concept is in terms of mixing ratio, which because of increasing density with decreasing altitude, means the center of mass of the material moves downward. If the 58 percent spread in depth should thereby result in a 58 percent loss of material in 22 days, an e-folding "residence time" of 40 days would result. These figures have but little quantitative significance, but some rough consistency is implied between this approach and the figures (30 to 90 days) quoted from the literature.

In all the above discussion, it has been implicitly assumed that incremental ozone concentrations are related directly to the incremental NO_x added by aircraft; processes which remove NO_x are assumed to also remove excess ozone. As noted in Section 3.1, however, there are controversies in this field, engendered largely by Chameides and Walker (1973) who argue that methane oxidation provides large local sources of ozone, particularly at ground level. These authors argued for a photochemical lifetime of 10 days at 10 km, photochemical lifetime being the local concentration divided by the local production rate. These estimates have since been revised; Chameides and Stedman (1976) now quote 10 days at low altitudes, 100 days at 5 km, and 700 days at 10 km. Even so, their results are not in full agreement with earlier results, suggesting ozone to be largely inert in the upper troposphere, as shown by the figures in Table 3.24.

TABLE 3.24. OZONE REPLACEMENT TIMES (CONCENTRATION/
PRODUCTION RATE) AT 10 KM, 45° N, SPRING

Ozone concentration, mol cm ⁻³	1.6 x 10 ¹² (CIAP Monograph 1, Fig. 5-23)
Ozone production rate, without methane reactions, mol-cm ⁻³ sec ⁻¹	1.0 x 10 ⁻² (NAS, 1975 Fig. A-22)
Ozone production rate from CH ₄ - NO _x reactions	8 x 10 ³ (CIAP Monograph 1, Fig. 5-26)
Replacement time, without methane reactions, yr	5 x 10 ⁵
Replacement time, with methane reactions, yr	6

Obviously, uncertainties still exist in the tropospheric ozone question, and in the relative importance of photochemistry and transport at various altitudes in the troposphere. See Fabian (1974), Chameides and Walker (1976), Chatfield and Harrison (1976), and Dimitriadis et al., (1976), Danielson and Mohnen (1976), for further discussion. From the standpoint of the problem at hand, however, it should be noted that even a replacement time of 10 days, the shortest figure cited, is far longer than necessary to eliminate any concerns about significant diurnal effects (i.e., for example, whether the enhanced ozone column might not appear until, say, noon or later, permitting increased ultra-violet during the morning).

3.6 MODEL VALIDATION ATTEMPTS

3.6.1 Introduction

Demonstration that a given model reasonably reproduces certain observed characteristics of the natural atmosphere, e.g., the distribution of ozone or other trace species, is never proof that the model will correctly predict the effect of some hypothesized perturbation. It is thus always of interest to compare the observed behavior of the atmosphere following some known perturbation, such as NO_x introduced by a nuclear weapons test, to the model predictions. Several validation efforts merit comment.

3.6.2 Excess Carbon-14

It has been noted that methane profile data are not very useful in determining the critical tropopause region portion of the K_z profile. Yet, this portion, in effect, controls the rate at which (in a 1-D model) a pollutant introduced above the tropopause will leave the stratosphere. A considerable variation exists between the various models in this region. To find which of these profiles most nearly duplicate the behavior of a gaseous tracer,

Johnston et al. (1975) turned to published data on excess carbon-14 (as $C^{14}O_2$) formed in the stratosphere by nuclear weapons tests, largely in the 1958 to 1962 period (see NAS, 1975 pp. 146-149). This tracer is removed from the stratosphere more slowly than are particulate tracers; as a gas, however, it was argued to be a better simulant for NO_x than are particulates, for which settling may influence removal rates. Johnston et al. thus took the available excess carbon-14 data (concentrations at various altitudes and longitudes) collapsed it along lines parallel to the mean tropopause, and found it to fit into more extensive profile data taken at 32° N. He then took initial conditions at various times, and studied predictions of later concentration profiles using various K_z profiles. He concluded that the Hunten K_z profile best represented the removal of the tracers, most other profiles showing far too rapid a removal rate.

A number of questions have been, or can be, raised about this data, its treatment, and its interpretation. As a start, the principal contributors to the atmospheric burden of carbon-14 at the time of interest were large Soviet devices exploded at 75° N latitude, in particular one 57-Mt device. No reliable data seem to be available for the height of cloud formed from such devices; much of the cloud, however, should have gone higher than the maximum sampling altitude in northern latitudes of 20 km. (Seitz et al., 1968, give 20 km to 30 km as the cloud height spread for a 30-Mt USSR test.) Chang (1975) has argued that an unsampled reservoir of excess carbon-14 was "feeding" the region at 30° N, although Johnston argues that he sees no evidence for it. The suitability of carbon-14, which is not removed by precipitation in the troposphere, as a tracer to simulate a scavengeable tracer has also been questioned; COMESA, e.g., argues that each tracer has in effect its own K_z profile. Mahlman (1975) also discusses the issue, showing that lack of a sink in the troposphere does have some effect on apparent K_z 's, but more modeling work was needed to clarify the effect as a function of time. The Johnston argument is that mixing ratios in the troposphere were too small during the study period to significantly affect the back transport. The total amount of carbon-14, and the confounding of data by earlier tests, is also at question. This is shown by Fig. 3.36, which shows the amount of carbon-14 which should have been formed, according to accepted estimating procedures, and the amount measured. Note, in particular, that the sum of the 1961 and 1962 inputs seem to be inconsistent with the measured amount in 1963. Note also that earlier tests also contributed to the burden for many years, as material is cycled into the troposphere and returned to the stratosphere. The effective residence time for carbon-14 increases with time, as shown by Telegadas (1971, Fig. 3.37). The period selected for study affects the results achieved. The data and analysis also show somewhat anomalous behavior. Thus (see Fig. 3.38), in January 1964, the data show the Hunten model to slightly underpredict the

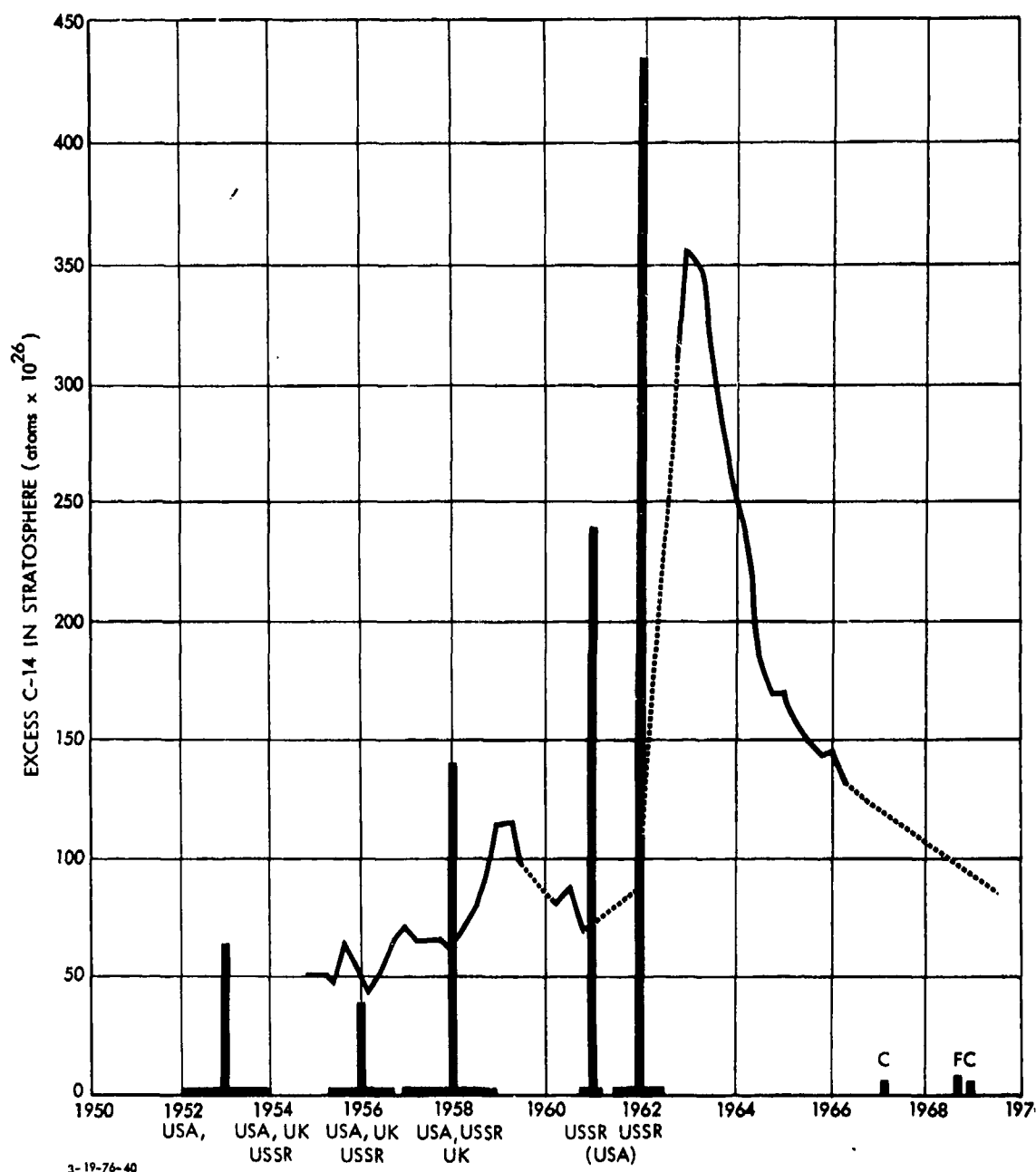


FIGURE 3.36. Excess Stratospheric C-14 from Atmospheric Thermonuclear Explosions. The total injected C-14 is shown (2×10^{26} atoms/Mt for airbursts, half that for surface bursts) as well as the origin of the injection (U.S., UK, F-tropical, USSR-arctic, C-midlatitude).
Source: Telegadas et al., 1971

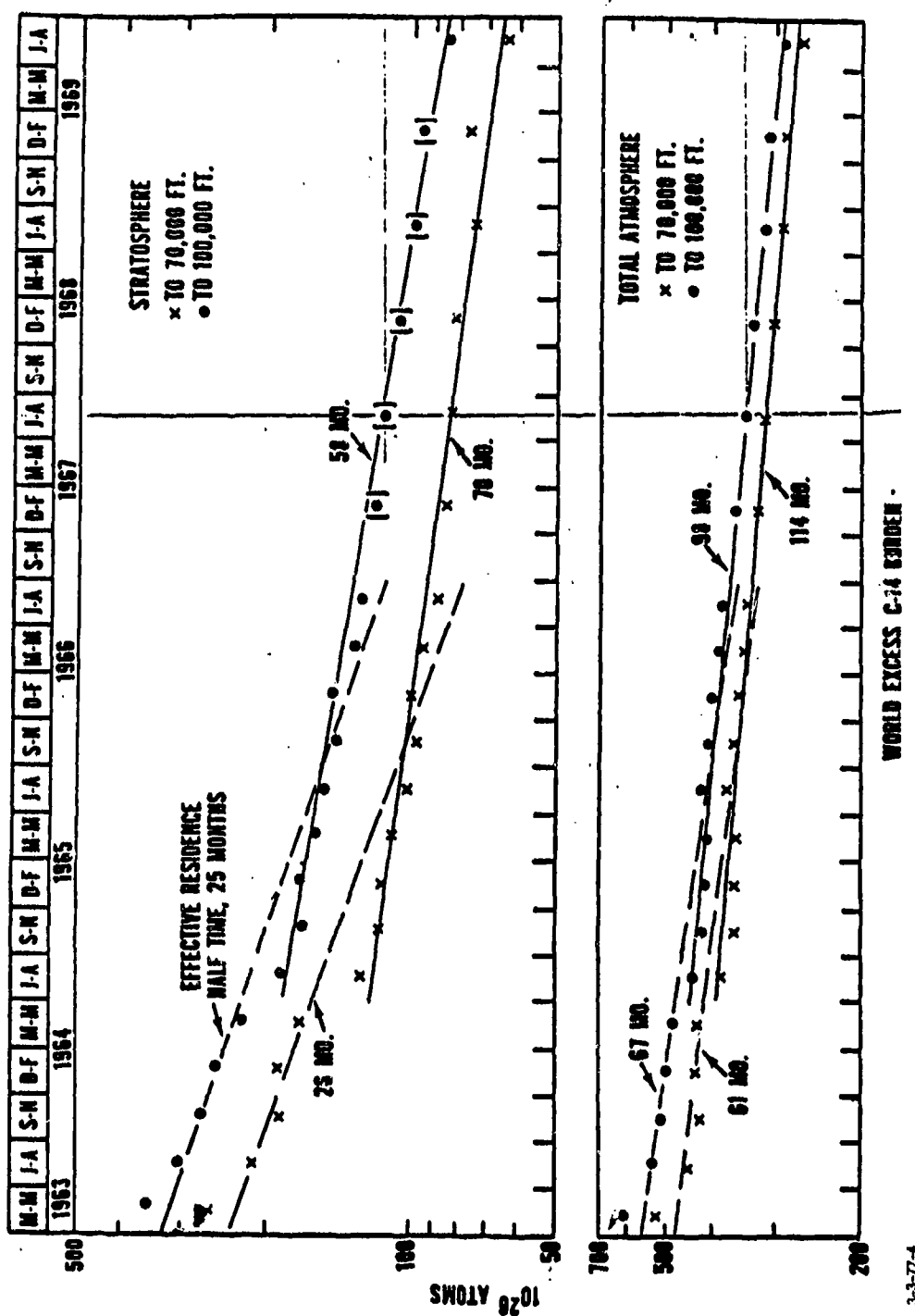
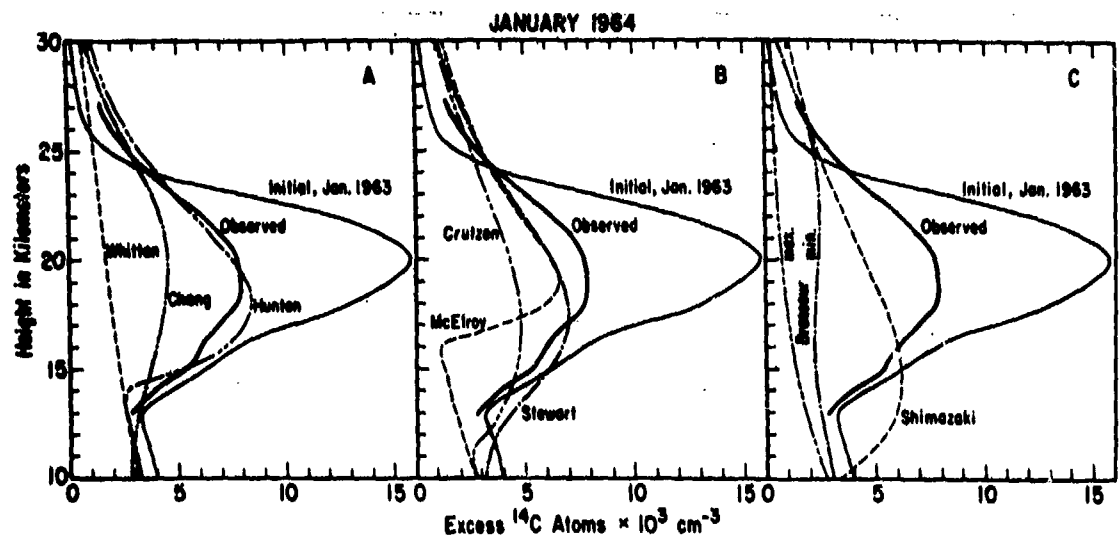


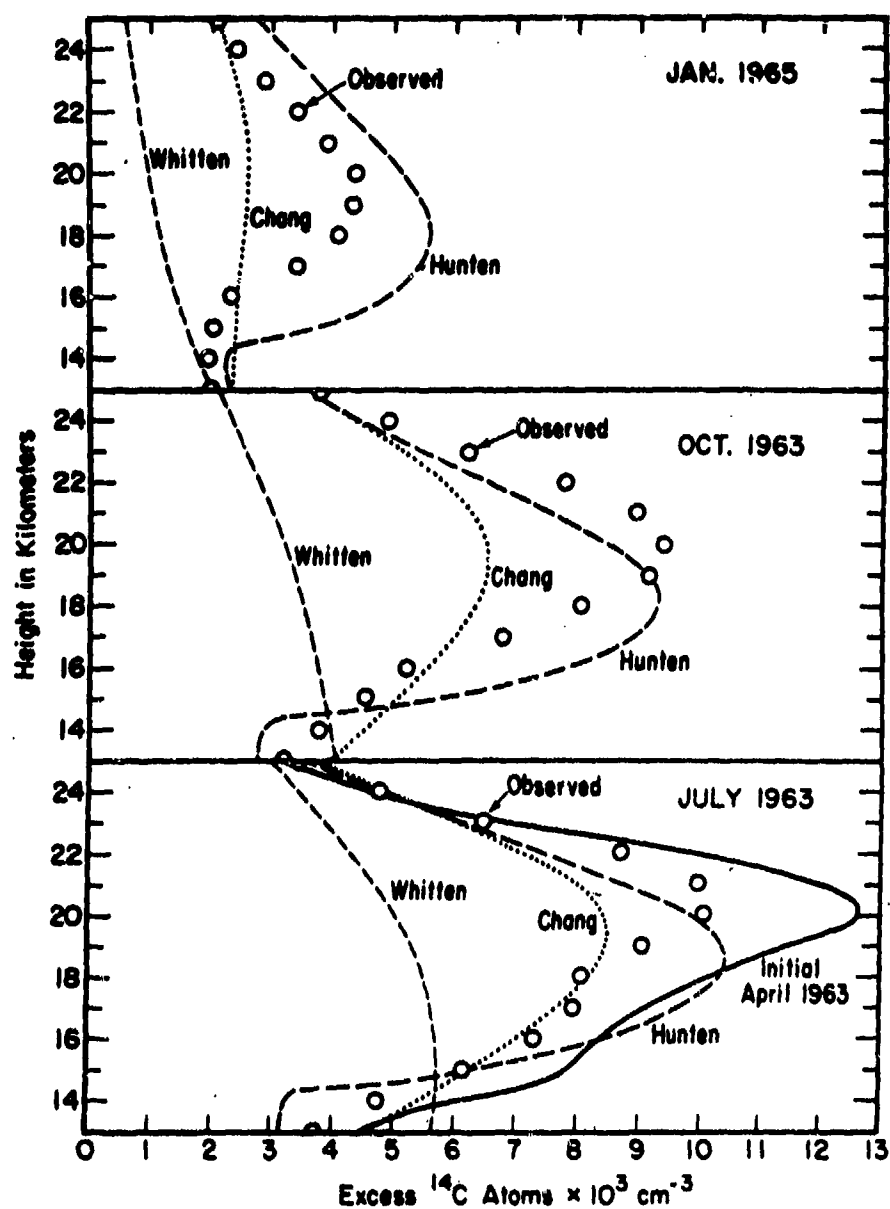
FIGURE 3.37. Decay Rate of Excess Carbon-14
 Source: Telegadas, 1971



3-3-77-3

NBL 7410-7436

FIGURE 3.38. Tests of Various K_z Profiles Using Data on Excess Carbon-14. Period January 1963-January 1964. Source: Johnston, Kattenhorn, and Whitten, 1975

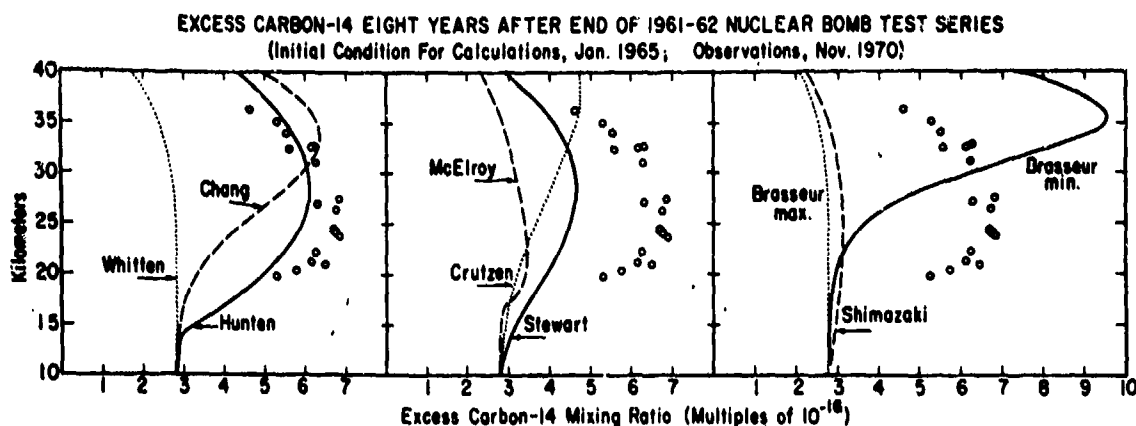


3-3-77-6

XBL 7410-7438

FIGURE 3.39. Tests of Various K_z Profiles Using Data on Excess Carbon-14.
Period April 1963-January 1965
Source: Johnston, Kattenhorn, and Whitten, 1975

rate but, nevertheless, to be the best of all shown; the January 1965 data (Fig. 3.39) show serious unprediction by the Hunten model. The later data (eight years after the tests, Fig. 3.40) actually show the Hunten model to overpredict the rate of removal, a fact probably related to the general return to the stratosphere of material removed earlier.



3-3-77-7

FIGURE 3.40. Tests of Various K_2 Profiles Using Data on Excess Carbon-14.
Period: eight years after tests.
Source: Johnston, Kattenhorn, and Whitten, 1975

The treatment of the data and the interpretation of the results also merit some comment. Thus, in order to obtain a representation for an effective global gradient, applicable to a global average profile, Johnston corrected each time period for "leakage" to the Southern Hemisphere. The problem being solved thus seems more applicable to a uniformly polluted global stratosphere, with the same concentration profile at all latitudes, than to an aircraft source in a rather narrow latitude band. In reality, as shown by Mahlman (1972) and others, localized aircraft sources, at steady-state, create strong local gradients which presumably increase the rate of transport. Chang [private communication (1976)] has argued that his is a mid-latitude model, so there appear to be conceptual differences involved. Also, as lesser points, as noted earlier, the Hunten profile was later adjusted by 2 km for use in the aircraft problem, whereas none of the other profiles have been. And Johnston et al., (1975) adjusted the data at 40° by 1 km rather than 2 km as recommended by Hunten; however, most SST traffic at least would be farther north than 40° in any event, so this adjustment, if acceptable in concept, would seem to be appropriate.

In our view, none of the questions about carbon-14 as a tracer preclude its use to provide what may be a conservative estimate of the rate of transport between the stratosphere and the troposphere. However, in view of the fact that the data are 2-D in character, and that transport does take place between hemispheres and back and forth between the troposphere and the stratosphere, the data can best be utilized in a 2-D model.

3.6.3 H₂O Transport

Mason and Östlund (1976) have discussed removal of water vapor from the stratosphere, using tritium oxides as a tracer. These data do not appear to have been given the extensive analysis which has been given to the excess carbon-14 data, but are of interest as a precipitation-scavengeable gaseous tracer, more analogous to NO_x than excess carbon-14. The data indicate an e-folding time of water vapor in the lower stratosphere (10-18 km) of 2 ± 0.2 years. In Mason and Östlund's analysis, an eddy diffusivity of $3.45 \times 10^4 \text{ cm}^2/\text{sec}$ at 40° N was used with a 10-km tropopause, implying much more rapid transport than does the much lower Hunten tropopause value ($2.3 \times 10^3 \text{ cm}^2/\text{sec}$ at 14 km) which Johnston et al. (1975) argue to be supported by the carbon-14 data.

Note also that Newell (1971) quotes mean residence times for carbon-14 and tritium as 3.3 and 3.5 years, respectively, citing L. Machta (private communication, 1970) and Gulliksen (1970). He notes that these times are longer than those for particulates, which he quotes as 1-1/2 to 2 years in the region below 25 km.

These various data appear to be worthy of further examination.

3.6.4 Zirconium-95

A brief study of downward transport in the region of prime aircraft traffic was carried out in this work (see Appendix C), using data from the Chinese weapons tests, which took place at 40° N and 90° E. These data seemed to more closely simulate the aircraft problem than earlier tests, which took place mostly in the tropics or at 75° N. Debris from the tests was initially emplaced at about 18 km; the tracer was zirconium-95. The Chinese tests were carried out at several seasons. Summer injections and winter injections were found to behave quite differently, with material injected in the summer being retained until the following winter, whereas winter injections began to come out immediately. The analysis used a time-dependent diffusion model. The technique used was to determine an effective K_z between the altitude of injection and the tropopause, based on known global removal rates from the stratosphere, followed by calculation of an injection coefficient and residence time for continuous injection. An approximate correction was included for settling. The analysis showed that the mean effective K_z is strongly dependent on assumed tropopause height, which in this region is highly variable. However, because the mean K_z and the distance between the injection altitude and the tropopause are coupled together, it was found that the injection coefficient and the resulting residence time for continuous injection were not strongly affected by variations in assumed tropopause height.

Results, which are applicable only to 18-km injections in midlatitudes, are shown in Table 3-25, with comparison to values calculated for other profiles:

TABLE 3.25. COMPARISON OF INJECTION COEFFICIENTS AND RESIDENCE TIMES DERIVED FROM Zr-95 DATA WITH THOSE CALCULATED USING VARIOUS K_z PROFILES

<u>Source</u>	<u>Injection coefficient</u> <u>10^{-17} cm²-sec</u>	<u>t_R</u> <u>yr</u>
This analysis		
$K_z = 1 \times 10^4$ (11-km tropopause)	1.77	1.52
$K_z = 5 \times 10^3$ (14-km tropopause)	2.37	1.78
$K_z = 1.75 \times 10^4$ (11-km tropopause)	1.04	0.95
$K_z = 7 \times 10^3$ (14-km tropopause)	1.73	1.33
Chang/1974 (18 km)	1.71	1.42
Chang/1976 (18 km)	1.76	1.58
Hunten/1974 (18 km)	4.60	3.55
Hunten/1974 + (18 km, latitude adjusted)	5.19	4.61
Wofsy/1975 (18 km)	3.21	2.57

This analysis suggested that the Hunten K_z profile, with or without the 2-km latitude adjustment, gives excessive residence times and injection coefficients. The results are in agreement with those computed using the Chang/1974 or Chang/1976 profiles and do not seem to be inconsistent with the Mason and Ostlund data (1976) on tritium oxides, described earlier.

A preliminary attempt was made to use the same model using the C-14 data. However, uncertainties, particularly in initial injection heights and burden, in the proper way to handle highly varying seasonal behavior, and in the proper period to be used made the effort questionable. A further examination of the data may, however, be useful in putting some upper and lower bounds on the estimates.

3.6.5 2-D and 3-D Model Studies and the 2-km Adjustment Question in the Hunten 1-D Model

While the testing of a model with another model is objectionable in principle, it is of interest to compare results from models of higher dimensionality to those from the 1-D models. In particular, the 2-km adjustment recommended by Hunten for midlatitude flight merits attention, because it has a powerful effect (6-fold by formula) on computed ozone changes for flight at 12 km, i.e., for present and advanced subsonics.

Based on results from his 3-D model, Mahlman (private communication, 1975) has estimated the residence time (burden/flux at steady state) for a precipitation scavengeable tracer continuously injected at 20 km and 30° N as 16 months (1.3 yr). The Hunten K_z profile gives 4.6 years for the same injection altitude; the Chang/1974 profile gives about 2.0 years at the same altitude.

Using their 2-D pure diffusive transport model, Machta (private communication, 1976) found that for continuous injection of a precipitation-scavengeable tracer at 11 km to 13 km in the 40° N to 50° N band, the residence time (burden/flux at steady state) corresponded to 0.25 yr. The Hunten profile, with a 2-km upward adjustment on the injection, taking an average according to $\frac{(R_{13} + 2R_{14} + R_{15})}{4}$ gives 0.71 years. Without the 2-km adjustment, $\frac{(R_{11} + 2R_{12} + R_{13})}{4}$ gives 0.37 yr. The difference is due to raising the injection across the model tropopause with the 2-km adjustment. The Chang profile, on the same basis, gives 0.27 yr.

Ozone depletion modeling efforts by the MIT group have already been described for 20-km injections at 10° N and 45° N (Section 3.4.1). On a global average basis, the effects were slightly greater at 10° N than at 45° N (12.5 percent versus 11.9 percent). The Northern Hemisphere value was slightly larger, however, with 45° N injection (16.1 percent versus 15.5 percent). The depletion value (which might be taken as the "corridor" value) at 45° N, however, was considerably larger for 45° N than for 10° N injection (20 percent versus 13 percent) (See Table 3.9).

The NASA-Ames results (see Section 3.2.5) gave ozone depletions which were insensitive to the latitude of injection, over the 30° N to 60° N region.

The MIT results can be argued to support the philosophical basis for the adjustment in flight altitude with latitude in the Hunten 1-D model if the computed depletion is taken to be applicable to the region of heavy traffic. The data would not support the adjustment if computed depletions by the Hunten model are taken to apply to hemispheric average depletions.

Dickinson (NAS, 1976a p. B-10), working the methane-inversion-to- K_z problem, used a mathematical coordinate transformation such that the region from the local tropopause to 20 km is linearly stretched into the assigned mean tropopause (15 km, his case) to 20-km region. If his procedure were applied to the aircraft problem and to the Hunten K_z profile, there would be no adjustment for flight at 20 km, an adjustment to 14 km for all flight at (above) the tropopause (whether the tropopause is 17 km or 8 km), and linear transformation in between, i.e., flight at the half-way altitude between the tropopause and 20 km would be assigned to 17 km, halfway between the 14-km Hunten tropopause and 20 km. Flight at 17 km in mid-latitudes, taking the mean tropopause at 12 km, would be assigned to $14 + \frac{5}{8}(6)$ or 17.75 km, rather than 18 km as it would with the Hunten approach. Flight below the tropopause could be similarly transformed between the surface and tropopause levels, but would stay below the tropopause. This approach would appear to be preferable if adjustments of this type are to be attempted.

3.6.6 Nuclear Weapons Tests--Injection of NO_x

In principle, nuclear weapons tests should provide excellent tests of the NO_x-O₃ theories, in that very large quantities of NO_x (perhaps 1.5 million tons during the period 1958-62) were injected into the stratosphere by such tests. The first authors to raise this point were Foley and Ruderman (1972); the issue has subsequently been examined by Johnston, Whitten and Birks (1973), by Bauer and Gilmore (1975), by the NAS (pp. 158-159), by COMESA (1975), and by COVOS* (Bertin et al., 1976). Model results, using the Chang/1974 K_z profile were presented in the NAS (1975) report; an average depletion of 4 percent was computed by Chang for the year 1963; decreasing to about 1 percent by 1967. The peak depletion, however, as discussed below, was computed at about 5 percent (Duewer, private communication, 1976). The question of whether or not the effects were or should have been noticeable or detectable has been argued at length. The NAS (1975) report (p. 159) suggests the tests were responsible for a "missing rise" in ozone, which should have occurred due to effects associated with sunspot cycles at about that time. (See Fig. 3.4 this report.) Ellsaesser (private communication, 1976) finds alternative explanations related to sudden stratospheric warmings. Johnston (1976a abstract) suggests that there is an initial ozone production by nuclear weapons explosions and the time required for the initial ozone production to be removed is substantial. He concludes that an initial enhancement of ozone, as observed following a 2-Mt test at 15° S, is compatible with the theory. The short-term effects with larger weapons, which rise to altitudes where photochemical equilibrium is reached more rapidly, would appear to need additional examination.

As noted earlier, NAS (1975) accepted the Chang results in discussing the effects of bomb-injected NO_x on ozone, but rejected the Chang model in determining aircraft effects. To explore this matter further, the problem was rerun at Lawrence Livermore Laboratory using the Hunten/1975 K_z profile, as well as with the Chang/1974 and Chang/1976 K_z profiles, and with revised chemistry and NO production rates per megaton. It was found (Duewer, private communication, 1976) that the peak depletions with the Chang/1976 profile and the Hunten profile were similar; furthermore, presumably because of the lower K_z values near 30 km with Chang/1974 than in the Hunten model, the rates of recovery were not greatly different. The Chang/1976 profile showed greater ozone destruction effects for injections near 30 km, and rapid recovery, but with the LLL 1976 chemistry and NO/megaton estimates, the peak effects were similar to those computed earlier. More analysis of these results may be desirable, as is the carrying out of the same computations with a 2-D model. A 2-D seasonally varying model would allow for the great variability in dynamics and effects between tropical and far north injections at different seasons, and would provide better predictions as to where and when effects should have been maximized.

*Received too late for discussion and intercomparison herein.

The COMESA report also discusses the bomb tests at some length. They find that the bomb tests, according to their calculations, should have produced about a 1 percent decrease, much smaller than that given in the NAS report. They then argue that since this could not be detected, the effects of over 1000 Concorde would be similarly undetectable. (The detectability question is in need of careful definition.) A considerable difference exists between the detectability of a pulsed event, a long-term slow change as fleets or halocarbons build-up with time, and a more-or-less abrupt change should a step-function fleet be imposed and operated continuously. See Appendix G for further discussion.

3.6.7 Solar Proton Events, Polar Cap Absorption (PCA) Effects

The solar proton event of August 1972 was an unusually large one which produced, according to Crutzen, (1975) some 6×10^{15} mol/cm² of NO, mostly above 60° geomagnetic latitude. Assuming, as does Crutzen et al. (1975), that this flux was produced over one-sixth the earth's surface, the total number of NO molecules was of the order of 5×10^{33} molecules, or equivalent on a global basis to the NO introduced by detonation of some 50 to 300 Mt of nuclear bombs, depending on the value used for NO molecules/Mt. [The smaller yield would result from the value used by Bauer and Gilmore (1975) of 1×10^{32} molecules NO/Mt. The larger value corresponds to 0.17×10^{32} molecules of NO/Mt, the lower value suggested by Johnston et al., 1973]. Most of this NO was produced at high altitudes, with the maximum (in mol/cm³) being in the 40 km to 50 km region. Crutzen (1975) proposed that this event be used as a validation test for photochemical models, and in a subsequent paper, Heath, Krueger, and Crutzen (1975) compared ozone measurements with model prediction. The record showed a dramatic change above 4 mbar (38 km) at 75° N to 80° N following the event, the ozone column dropping about 2 mbar out of 13 mbar, in reasonable agreement with model predictions. This was taken to be confirmation of the chemical scheme, in regions where photochemical equilibrium prevails. The change at lower levels, where the ozone column was greatest, would obviously be less easy to detect, as the absolute change of 2 mbar was nearly 20 percent of the total above 4 mbar; the percentage changes on the ozone column above the surface, however, would be much less. Further analysis will be necessary to see whether the NO effects can be traced to lower altitudes and latitudes as a function of time.* (It might be possible, using a 2-D model and careful observation, to exclude certain sets of chemistry and dynamics as leading to predicted effects outside the uncertainty bounds on those observed.)

An earlier event, with energy deposited at higher altitudes (54 km to 67 km), where the HO_x cycle, rather than the NO_x cycle as above, is thought to control ozone, demonstrated the effects of increased HO_x on ozone [Crutzen, private communication (1976)].

*Photolytic destruction of NO may be important in this case. Such destruction is definitely important in the case discussed in the mesosphere (following paragraph).

Zinn and Sutherland (1975) point out that four large solar flares occurred in May-July 1959, each producing 5×10^{15} mol/cm² NO above 65° for a total some 2.5 times that of the August 1972 event. These authors state that these four together should have produced about a 1 percent decrease in O₃ inventory. Obviously, any detailed modeling efforts studying bomb effects in 1958 to 1962 should include the solar proton events.

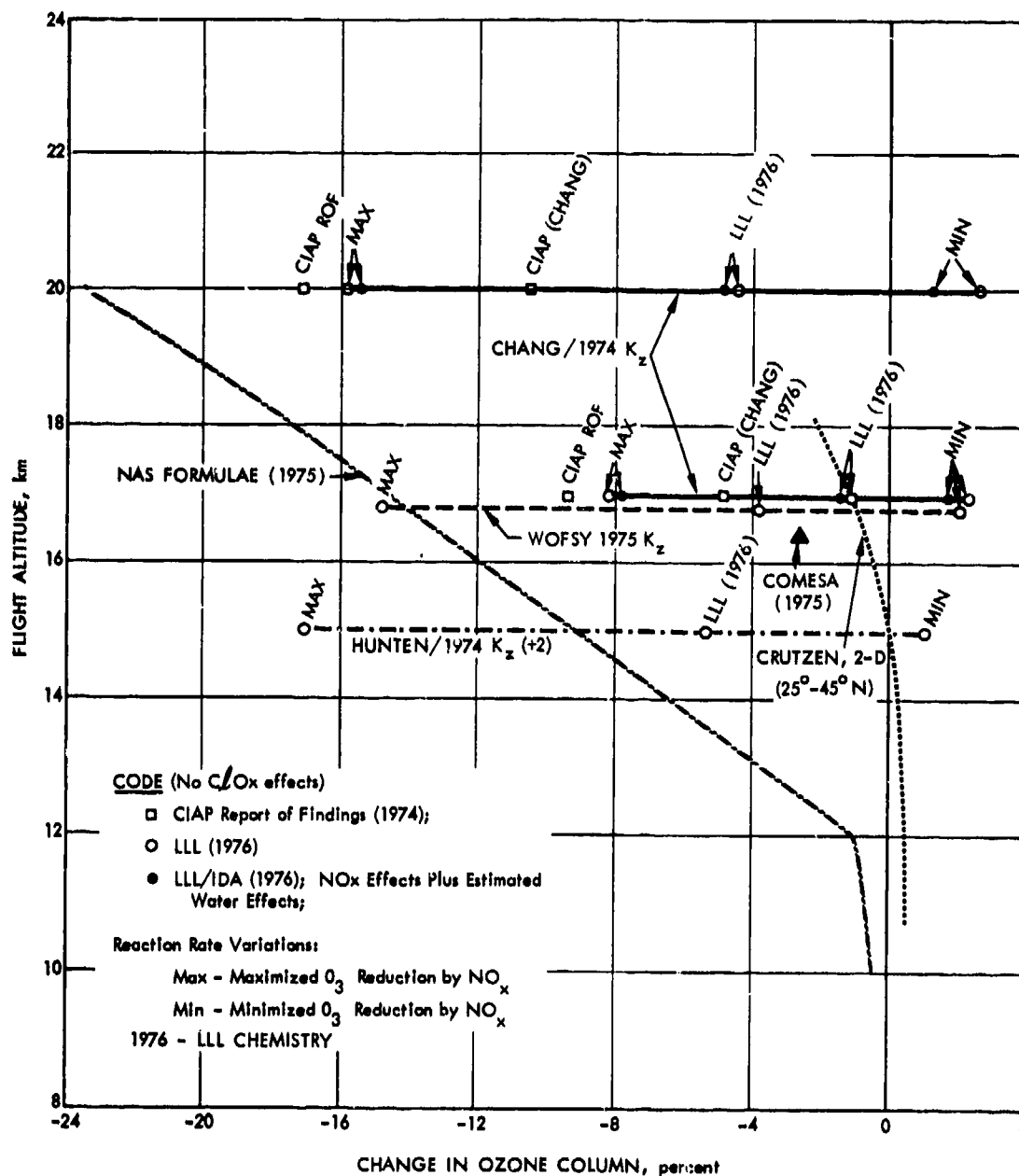
Two points should be noted about the PCA work. First, detection of the effect was made vastly simpler by coupling model predictions about where and when the effect should be sought with observations; detection would have been much more difficult from total ozone column measurements. This point is in line with the discussion in Appendix G. A second point is that the solar proton events deposit NO_x in a different altitude and latitude region than do aircraft sources. Aircraft effects involve questions of transport to these altitudes and the chemistry in a considerably lower region of the atmosphere.

3.7 A SUMMING UP

It is evident from the preceding sections that large uncertainty bars must be put on any estimate of ozone change due to aircraft operation. An array of estimates results from considering various chemistries, various kinetics (thermal rate coefficients), and various dynamics, as illustrated in Fig. 3.41, which figure does not include chlorine chemistry or uncertainties therein. Other aspects of such modeling exercises involve large further uncertainties--feedback effects, thermal effects, photolysis rates, radiation phenomena, and the finer points of the chemistry, including activation energies, quantum yields, absorption cross section reaction paths, etc. And, to return to basics, the NO_x emission indices still involve the unresolved discrepancy between *in-situ* UV absorption methods and direct sampling techniques (see Table 2.16, Chapter 2).

Although necessary, statements of uncertainty are inherently unsatisfactory. Of more value, perhaps, is a discussion of apparent trends in results, as work has progressed, operating on the assumption that continuing work and more detailed examination of the various phenomena lead to more nearly correct results. On this basis, the data in the previous section can be argued to show the following:

1. For subsonic aircraft, inclusion of the methane oxidation reactions has completely altered the CIAP (1974) and NAS (1975) picture of the effects of this class of aircraft on the ozone column. However, uncertainties in these reactions have not been explored. The methane oxidation reaction (like much of the stratospheric chemistry) is not adequately understood, and tropospheric dynamics and tropospheric stratospheric interchange processes are exceedingly complex and difficult to model. Nevertheless, present computational results do



11-18-76-20

FIGURE 3.41. Ozone Change Estimates by Various Models Illustrating Uncertainties Due to Chemistry and Dynamics. The NO_x injection rate at each altitude is constant at $2000 \text{ mol/cm}^3\text{-sec}$ over 1 km, or $1.23 \times 10^9 \text{ kg (as NO}_2\text{)/year}$ if assumed in one hemisphere. Chlorine chemistry is not included. Procedures as used in CIAP, 1974, have been used to compare 1-D and 2-D models by taking midlatitude "corridor" effects to be the same as global effects at half the rate. The Hunden/1974(+2) result is for model injection at 17 km, which is argued to apply to flight (in midlatitude) at 15 km. Linearity has been assumed where necessary.

suggest that subsonic aircraft, particularly those typical of the bulk of today's fleets, increase rather than decrease the ozone column, at least in the hemisphere in which they are operating. For the so-called advanced subsonics, such as the 747SP (which, in fact, is in operation now), the picture is less sure, for these aircraft will spend a greater fraction of their cruise time in the stratosphere than do the shorter-range aircraft; the advanced subsonics may increase the ozone column very slightly, but there may be areas wherein the latitudinal zone where slight depletions may occur. A discrepancy exists between the Crutzen and Widhopf 2-D model results for subsonic aircraft, in that one model shows ozone enhancement in the Southern Hemisphere and the other shows very slight depletions.

Other important points should be noted about subsonic aircraft, their NO_x emissions, and their injection altitudes relative to the tropopause. It was noted in Section 2 that a number of assumptions made in the CIAP subsonic fleet computations seem to be in error, in particular, the flight altitude versus range assumption, which, when coupled with the 3-km resolution employed, put a substantial fraction (approximately 25 percent) of the subsonic emissions at 13.5-km altitude (44,280 ft), an erroneous result. This fraction, being based largely on distances between cities, was nearly invariant with time. This approach, coupled with the NAS recommendation that 2 km should be added to actual flight altitude for mid-latitude operation in using the NAS model, put a substantial portion of subsonic aircraft as well as "advanced" subsonics (like the 747SP) continuously above the model tropopause at 14 km. Such subsonic aircraft are, in fact, above the tropopause only a portion of the time, the fraction depending on the route. Growth rates in CIAP were also assumed to be substantial, (4.15-fold from 1970 to 1990). Using CIAP figures for the expected fleet in 1990 (Table 2.9) and the NAS model (see p. 29, NAS), one would estimate an ozone depletion of

$$\frac{15.3 \times 10^9}{2.6 \times 10^9} \times 0.16, \text{ or } 0.94\%$$

by 1990, due to high-altitude subsonics; the corresponding CIAP estimates (see p. xvi, ROW) would be

$$\frac{15.3 \times 10^9}{2.0 \times 10^9} \times 0.079 \text{ or } 0.60\% \text{ depletion,}$$

both results exceeding the tentative FAA 0.5 percent guideline. If, however, the SRI/ADL forecast, with its subsonic altitude distributions, are taken with the "high" 1990 projections (Table 2.26), the Crutzen model results (Table 3.15), using an average of the level 10 and 11 results, would give an estimate for the high-altitude portion of the subsonic fleet without controls at 45° N and August 30, as follows:

$$\frac{45 \times 10^6}{0.455 \times 10^9} \left(\frac{0.183 + 0}{2} \right) \text{ or } 0.009\% \text{ enhancement.}$$

For lower-altitude subsonics, computed enhancements are greater. These results must, of course, be considered tentative for reasons already discussed and summarized below.

2. For supersonic aircraft operating at 17 km to 20 km, the results of all studies to date, except those with highly improbable combinations of thermal reaction rates, indicate depletions of the ozone column. The magnitude of the resulting effects for any given number of aircraft is, however, in considerable doubt, as evidenced by the horizontal bars in Fig. 3.41. Again, however, if the trends are examined, there appears to be some reason to believe the effects of such aircraft NO_x emissions (for a specified fleet) are smaller than indicated in NAS or CIAP. These effects are summarized in Table 3.26.

The computed smaller effects, with more recent calculations, as illustrated in Table 3.26, result primarily from revisions in certain key reaction rates, primarily the OH + HO₂ reaction, plus certain other effects resulting from a simplified methane-oxidation (ozone-forming) path and from inclusion of chlorine chemistry. It must be cautioned, however, that the revised reaction rates used in the LLL 1976 chemistry are based only on careful examination of limited data, in which data on individual reactions rather than on ratios of reaction rates were emphasized. Other groups analyzing the same limited data could well settle on different estimates of the most probable rate of values. In any event, no amount of analysis can substitute for new and careful measurements. Further changes in these estimates may be expected, particularly as new data are obtained.

Results equivalent to those given in Table 3.26 are not available for 2-D models. Note, however, that the Crutzen 2-D model, with distributed emissions from a fleet at 17 km (see Fig. 3.25) would, assuming linearity, give with 1.8 Mt/yr NO_x injection, about 1.8 x 1.5 or 2.7 percent ozone depletion at 45° N on August 30. The Cunnold-Alyea results for summer season (Fig. 3.16), however, give about 10 percent depletion for a 17-km injection. The differences undoubtedly lie in

different chemistries (the Crutzen model being more complete, and including methane oxidation and N_2O_5 , for example) and probably in different dynamics, but are obviously not fully resolved.

TABLE 3.26. CHANGES IN COMPUTED OZONE DEPLETION RESULTS FOR SSTs

	Global average values ²				Hemisphere values ²	
	NO_x input = 2.46×10^9 kg/yr				NO_x = 1.23×10^9 kg/yr	
	Chang/1974 K_z	Chang/1976 K_z	Chang/1974 K_z	Chang/1976 K_z	Hunten/1975 K_z	Hunten/1975 K_z
Injection altitude, km	17	20	17	20	17(15) ²	20(18) ²
CIAP ROF, 1974	-5.1	-10.6	-	-	-16 ⁴	-23 ⁴
NAS, 1975	-	-	-	-	-8.97	-17.4
Revised OH + HO_2 , inclusion of CH_4 oxidation ³	-1.75	-5.21	-	-	-6.68	-
LLL chemistry, 1976, no ClX	-0.065	-2.92	-1.15	-4.20	-4.06	-10.64
LLL chemistry, 1976, 1 ppb ClX ^{5, 6}	-	-	-0.70	-3.26	-2.79	-8.76
LLL chemistry, 1976, 2 ppb ClX ⁵	-	-	-0.40	-2.61	-2.33	-8.06

¹ Most of these results are from calculations made at Lawrence Livermore Laboratory.

² The calculations at LLL were made with a global injection rate of 2.46×10^9 kg/yr NO_2 at 17 to 20 km model altitude. The results may be interpreted by the Hunten Model according to NAS, 1975 as a hemispheric value at half this injection rate for a mid-latitude fleet 2 km lower than the model injection altitude, i.e., at the altitude shown in parentheses.

³ Approximate. A simplified methane oxidation pathway is included. For illustration here, the pathway $\text{NO}_3 + \text{NO} + \text{O}_2$ is used. See Table 3.17 for further data. (Dewer, et al., 1976b)

⁴ The Chang computational model, with CIAP chemistry, gives higher depletions with the Hunten K_z profile than does the NAS formula. See Fig. A.38, p. 145, NAS.

⁵ Includes ClONO_2 in a manner which may overestimate NO_x effects. See Section 3.4.7.

⁶ 1 ppb ClX may be a reasonably correct present value; 2 ppb might be a 1990 value.

Questions about dynamics, particularly near the tropopause, are still serious and unresolved, as indicated by the large differences between the results using the Chang (1974 or 1976) and Hunten/1974 K_z profiles. The Chang profiles reasonably match particulate data and the Hunten/1974 profile reasonably matches gaseous carbon-14 data. Both sets of tracers involve imperfect data, so that the questions cannot be resolved unambiguously. The Hunten/1974 K_z profile may, nevertheless, be somewhat extreme; the Wofsy/1975 profile (Fig. 3) which is of the same form, was developed after the Hunten/1974 profile was developed and shows somewhat lesser effects. (See Table 3.18.)

The latitudinal adjustment of aircraft altitudes in a 1-D model to compensate for changes in tropopause height as recommended in NAS (1975), merits a brief further comment. Where the adjustment artificially puts aircraft continuously above the tropopause, whereas it is known that the aircraft spend a significant portion of the yearly flight time below the tropopause, the adjustment is clearly incorrect. At SST flight altitudes (17-20 km), the correction is in the proper direction if the so-computed depletions are taken to apply to the latitudes of heavy flight, but, based on limited 2-D results, the correction does not seem to be appropriate if results are to be treated as hemispheric averages. Alternative transformations of the altitude coordinates with latitude (tropopause height) as used by Dickinson (NAS, 1976a; see Section 3.6.5) might be preferable. In any event, such arguable corrections obviously become unnecessary if 2-D models are employed.

The above comments need to be viewed in terms of a progress report on complex problems. Much additional study, analysis, and data-taking will be necessary before understanding of these processes can be considered adequate.

A partial list of problems needing attention on 2-D models is included at the end of Appendix A.

4. POTENTIAL EFFECTS ON MEAN SURFACE TEMPERATURE

4.1 INTRODUCTION

In this section, the possible effects that high-altitude aircraft exhaust may have on mean surface temperature are discussed and applied to a postulated SST fleet. The extreme limitations in current understanding of what causes changes in climate, and thus in our ability to predict such changes, are recognized. Nevertheless, if a reasonable probability exists that some activity may affect climate, it is only prudent to make a best estimate with available knowledge of the magnitude and sign of the effect, along with estimates of the uncertainties involved. This is done here, using various climate model results developed elsewhere, primarily in CIAP. The COMESA efforts are also reviewed, as are NAS (1975) views on the subject.

A number of climate-modeling approaches are noted in the following material, but the application studies will be based largely on 1-D models. This is not because of any preference for such models; it is rather because more "usable" results are available from such models at the present time. Discussion will be limited to mean temperature effects at "steady-state," by which is meant effects resulting after a decade or more of continued operations at some constant rate. Time-dependent effects, which add uncertainty to the already severe uncertainties implied with steady-state effects, are discussed in Appendix F, wherein the type of time-dependent information that modelers may eventually be asked to provide is illustrated.

Before proceeding further, it is important to note that climate modeling of aircraft effects has not been given nearly the emphasis that has been given to the ozone-depletion problem. A single effect -- that of the sulfate aerosols -- was emphasized in CIAP studies; other effects, those from ozone depletion and NO_2 and water addition, were treated briefly. Furthermore, few post-CIAP results are available. Those that are, and which are mostly qualitative and related to the recognition of the importance of the altitude distribution of aircraft-related perturbations (R.E. Dickinson, 1976; V. Ramanathan, 1977, private communication), tend to cast doubt on earlier treatments. Thus, quantitative

*Indeed, in our opinion, in order to account for known latitudinal and altitude distribution of sources, and to include possible feedback effects (as on the tropical tropopause temperature) higher-dimension models, including some chemistry, are mandatory. Ultimately, ozone-depletion models and climate models may, in fact, converge.

estimates given in the following treatment must necessarily be viewed with considerable reserve. However, the results to be discussed have involved significant research effort, and are believed to be the best general set of results available for application at this time.

As noted earlier, application studies here rely heavily on results generated or included in CIAP. However, an important departure is made from CIAP techniques (as described in the Report of Findings, Appendix B), in that a correction for sedimentation is made in the case of sulfate aerosols, thereby giving exhaust gases greater residence times than particulates; this point was made in NAS (1975) and by others (e.g., Newell, 1971) earlier. Also, in view of the currently unmodeled effects of contrails, and other uncertainties in the case of subsonics (see however, Section 4.3.3 in the following), the available techniques are considered applicable only to aircraft operating primarily in the stratosphere, that is, SSTs. The case studied thus involves only SSTs.

4.2 BACKGROUND

4.2.1 Species and Effects of Concern

It was noted in Section 2 that the primary products of combustion of aircraft fuels are CO_2 and H_2O , with much smaller quantities being produced of NO_x , CO , SO_2 , unburned hydrocarbons, soot, and various metal oxides. Of these various ingredients, the NAS and CIAP reports both concluded that the ingredients of primary concern in a climatic sense are SO_2 , NO_x , and H_2O , and these will be emphasized here. CO_2 , while an obvious candidate, is present in massive quantities in the atmosphere (~500 ppm by mass) so that atmospheric CO_2 content is relatively unaffected, even by large fleets of aircraft; furthermore, because of the long atmospheric residence time of CO_2 , the effects of aircraft CO_2 are probably not significantly related to the altitude of emission. To clarify these points, some numbers on the CO_2 question are provided later in this section. Water vapor, because it is present in small concentrations in the stratosphere (~3 ppm by mass) could be significantly altered in content by large fleets, and because of its importance in the earth's radiation balance, is of concern in a climatological sense. SO_2 , after being discharged from the engines, is converted to sulfuric acid particles (nominally 75 percent H_2SO_4), and such particles would also affect the radiation balance. NO_x has a twofold effect. First, because its addition to the stratosphere reduces ozone, which is important in ultraviolet, visible, and infrared regions, and, second, because NO_2 (as part of the NO_x) is a brown gas which itself absorbs and reemits energy over a wide spectral range.

In addition to such direct effects, various possible feedback effects can be suggested which could be important. Thus, any changes in stratospheric temperatures due to ozone depletion, NO_2 or water addition, etc., could affect the tropopause "cold-trap" temperature which is thought to have a strong effect

on stratospheric water content. Any change in cloudiness is important climatologically (Manabe and Wehner, 1967; Schneider, 1972) and could come about due to changes in the stratosphere* or directly by contrails. Some discussion of effects of change in cloudiness will be included in the following material, but changes in cloudiness are generally not predictable.

Numerous other effects, presumably secondary in significance, can also be suggested. Thus, changes in stratospheric temperatures due to particulates or water, etc., affect ozone content by affecting reaction rates. SO_2 itself, prior to conversion to H_2SO_4 particulates, is an absorber of UV-B. Heat added by combustion and turbulence induced by aircraft motion could affect atmospheric dynamics, although probably in a minor way.

4.2.2 Some Observations on the Various Studies

Before going into further detail on climatic effects, certain philosophic differences should be noted among the NAS (1975), CIAP (1974),** and COMESA (1975) reports. The NAS (1975) document, after some discussion, but before drawing conclusions, states (p. 55) that

In summary, it is possible that emissions of NO_x , SO_x , and water vapor by high-altitude aircraft flying in the stratosphere may produce long-term climatic changes; such changes may or may not be negligible in terms of effects on life at the earth's surface. Although climatic effects, if they occurred, would be of enormous importance, the link between stratospheric modification and change of climate is very poorly known. (emphasis added)

Nevertheless, the NAS document, provides some rough estimates of possible climatic changes from aircraft exhaust, as shall be noted in further discussion. However, it is clear that the NAS gives less credence to the predictability of climate change than is implied in the CIAP Report of Findings, wherein model-derived estimates of effects from specific constituents (SO_2 and H_2O), while admittedly of large uncertainty, are computed, costed out, and plotted against fleet size.

Both CIAP and NAS reports treat questions of climate change due to sulfate particles independently from climate changes due to water vapor, even though these are believed to be of opposite sign in terms of temperature changes, and

*Greenstone (1976) has, in fact, noted that a correlation exists between reduced ozone and increased cloudiness in the 1966-1975 period. Pena and Hosler (1970) suggested that shock waves from SSTs could create condensation nuclei in supercooled clouds.

**Here the "CIAP report" refers primarily to the first 130 pages of the Report of Findings.

both come from the same aircraft exhaust; however, the CIAP report (Report of Findings, p. xxiii, p. 74) does argue that climatic effects of ozone depletion are compensated by NO_2 addition; the COMESA report (p. xxi) argues that compensating effects should be netted out. No evaluation is given of the effects of aircraft exhaust, in its totality, in either CIAP or the NAS reports; the COMESA report, while claiming to take compensating effects into account (p. xviii) is difficult to interpret quantitatively in terms of fleet effects (see Section 4.3.3). The NAS report emphasizes particulate effects, but does note possible water effects at various points in the text (e.g., p. 54); however, in the Issue and Findings (p. 7), the water vapor question is specifically discounted, as follows:

Although large fleets of SSTs could bring about a small increase in the (stratospheric) water vapor content, this would have only a small influence on the radiative balance, because the radiative effect of water is small compared with that of carbon dioxide, whose concentration is a hundred times larger.

This statement is not otherwise elaborated by the NAS. Nevertheless, some comparative effects numbers are provided by the NAS. In fact, the NAS, the CIAP, and COMESA reports all suggest, without, in the case of NAS, being explicit, that the climatic effect (cooling) of aerosols, from fuels containing a nominal 0.05 percent sulfur, is greater than the climatic effect (warming) of water vapor from burning the same fuels. (On NAS, p. 54, it is stated that global average warming due to H_2O may be of the order of 0.1°C due to "high-altitude aircraft" of unspecified quantity; on p. 56, it is stated that "high-altitude flight operations ...would produce long-term global changes of no more than a few tenths of a degree Celsius;"). The CIAP Report of Findings comparison states (p. 74) that the SO_2 effect is about 1.75 times the H_2O effect. The COMESA report (p. 516) shows a water vapor effect to be about half the SO_2 effect, but the numbers on which this plot is based are difficult to reconstruct (see Section 4.3, this report.) Both the NAS and CIAP reports conclude that sulfur should be removed from aircraft fuels in the future. COMESA makes no recommendation on this matter.

The procedures used by CIAP and COMESA are described below. The NAS document includes no independently derived techniques, although an exploration is made therein (Section K) of the uncertainties in the CIAP procedures.

4.2.3 Mean Changes and Their Limitations

An important limitation applies to all the model approaches to be discussed. This is that, at best, an estimate of a global or hemispheric mean change (or in the 2-D case, a zonally averaged change) is obtained. It is recognized that climatic changes, which occur naturally, are usually greater in high latitudes

than in tropic latitudes, but for aircraft sources concentrated in the mid-latitudes, these observations might be misleading. Furthermore, it is not known how any resultant mean changes might be distributed in an east-west sense nor in a seasonal sense. That is, an average decrease in temperature might involve a cooling in one part of the world or one part of the year, and a warming elsewhere or at a different time. Similarly, a zonal average model might show reduced average precipitation in certain latitude bands, but this might involve an averaging of, say, rainfall in the Pacific Northwest rain forest and the Sahara Desert, a case where the distribution of the change would be all-important. It is, of course, also possible that a net effect of some perturbation on, say, mean hemispheric temperature could be zero, but that a redistribution of some type in a time or geographical sense would be involved which could be significant. Such questions are far beyond the modeling work discussed in the following.

4.3 CLIMATE CHANGE MODELING

4.3.1 Climate Modeling in General

The various climatic modeling approaches are discussed in Chapters 6 and 7 of Monograph 4; Appendix F, of the CIAP Report of Findings; and Chapter 5 of the COMESA report. A large body of literature also exists -- papers by Gates (1975), Smagorinsky (1974), and Schneider and Dickinson (1974) are particularly noteworthy.

The best models, from a theoretical point of view, are time-dependent, 3-D models; these incorporate as much fundamental physics as possible. A number of such models exist. At this time, however, it is probably fair to state that even the most advanced such models -- although having made great progress -- are still in an early state of development, and faced with severe computational, data, and even theoretical problems. The computational problems are such that only a small number ["one to several dozen," (Gates, 1975), assuming coordinated usage] of "experiments" can be performed each year. Data questions are numerous as, for example, in whether the sun has been constant during known climatic changes and possible effects thereof [see Dickinson (1975), Lockwood (1975)], how the oceans circulate, etc. Cloud behavior is critical, but poorly known. Theoretical questions have, in fact, been raised about whether climate is even deterministic, i.e., whether it can shift to various alternative states without shifts in external forcing functions. A decade or more may yet be required before such models can be expected to treat the aircraft-induced climate change question quantitatively.

As noted above, a full discussion of CIAP-climate-modeling approaches is available in CIAP Monograph 4, and of COMESA modeling efforts in Chapter 5 of the COMESA report. Only a very brief review of these efforts is attempted here.

4.3.2 CIAP Climate Modeling

A. Discussion

The CIAP climate change computations (cf. Appendices B, E, and F, CIAP Report of Findings) were based primarily on 1-D modeling, modified somewhat, however, for possible ice-albedo feedback effects, and for hemispheric effects (as compared to global average effects) from 2-D and 3-D (ozone depletion) and 3-D (general circulation models, inert tracer) models. These results are discussed herein. CIAP also sponsored, and preliminary results were obtained from, a 2-D zonally averaged climate model (ZAM), but no quantitative conclusions were drawn from the results in terms of potential aircraft effects (see CIAP Report of Findings, pp. 46 and F-127 to F-130).

In discussing climate change modeling "in CIAP," it is necessary to distinguish the material used in the Report of Findings in the main text, prepared about September/October 1974, from additional, mostly later, modeling results, -- which became available in time for inclusion in Appendices E and F. Subsequent material also has come from Ramanathan et al. (1976), Harshvardhan and Cess (1976), and Pollack et al. (1976, 1976a). Thus, the water vapor effect in the main text of the CIAP Report of Findings was based (p. B-28) on Manabe and Wetherald (1967); the ozone-NO₂ changes were assumed to cancel out, based on preliminary calculations (CIAP Report of Findings, p. 74); and aerosol effects were apparently based on early single wavelength calculations of Herman. However, additional later data were presented in the appendices (see, e.g., pp. B-23 and F-116). The available data will be discussed below. However, these data leave much to be desired in terms of consistency and other factors. Thus, effects of water vapor increases, ozone reductions, and NO₂ increases were all treated in a model in which the distribution of tropospheric relative humidity was held constant for any given surface temperature (but varied with surface temperature changes), whereas, in CIAP, the aerosol effects were computed without coupling in changes in tropospheric water vapor; a late paper (Pollack et al., 1976a) includes such effects for aerosols but gives no results for water vapor or other gaseous constituents. The constant relative-humidity-distribution model gives about twice the effects that an earlier constant-absolute-humidity-distribution model did (Manabe and Wetherald, 1967; Ramanathan, 1976). In Ramanathan's modeling studies (1974), the changes in H₂O, NO₂, and O₃ were assumed to be constant with altitude in terms of percentage mixing ratio changes; however, Ramanathan et al. (1976) note the importance of the distribution of changes in a vertical sense (as well as in a latitudinal sense) but the tie to aircraft effects has not yet been made. Aerosol computations in CIAP were based on an assumed uniform loading from 15 km to 25 km over the hemisphere, which is probably unrealistic. Furthermore, the CIAP work on aerosols included what, in effect, is a 2-D ice-albedo feedback correction which makes computed

effects about 1.5 times those computed in certain 1-D models, as were used in computing gaseous effects. The change in results if this factor is included is noted below.

Different modeling approaches were thus used in CIAP in determining the climatic effects of added stratospheric aerosols and of changes in the gaseous constituents (water and NO_x additions and ozone decreases). Latitude and altitude-distribution questions were not addressed. Effects were not considered simultaneously or interactively. Some data on additivity (i.e., the absence of interactions), were developed by COMESA (Section 4.4.5).

B. Gaseous Constituent Changes (H_2O , O_3 , NO_2)

1. Models Used The data that follow are based on the 1-D radiative equilibrium, constant relative humidity distribution modeling results of Ramanathan (see material following p. F-90 and p. F-125, ROF). Two sets of his modeling results are available, based on constant cloud-top altitude (CCTA) and constant cloud-top temperature (CCTT) models. At one point recently, based on the work of Cess (1975), the constant cloud-top temperature model was believed to be preferred; more recently, however, it appears there is no theoretical preference for one or the other (Ramanathan, private communication, 1976).

As shown by Manabe and Wetherald (1967), the constant relative humidity assumption seems to fit existing data on tropospheric humidity better than the assumption of constant absolute humidity; unfortunately, this agreement does not necessarily establish the validity of the model under perturbed conditions. Also, because these are equilibrium models, there is no information provided on the rate of approach to a new equilibrium state.

2. Water Vapor The water vapor change/surface temperature effects obtained by Ramanathan (1974) and CIAP Report of Findings (p. F-125) for a CCTA model, assuming an initial 3-ppm (mass) mixing ratio of H_2O in the stratosphere are shown in Table 4.1.

TABLE 4.1. SENSITIVITY OF SURFACE TEMPERATURE INCREASE ($^{\circ}\text{C}$)
TO STRATOSPHERIC INCREASE OF WATER VAPOR (ppm)
SOURCE: Ramanathan, 1974

Stratospheric Mass Mixing Ratio of H_2O	Temperature Increase ($^{\circ}\text{C}$) Constant Cloud-Top Altitude
3.0×10^{-6}	0
3.3×10^{-6}	0.06
3.6×10^{-6}	0.12
4.5×10^{-6}	0.27
6.0×10^{-6}	0.50

For small changes in the range of interest, the range appears to be, for the CCTA model,*

$$\Delta T = 0.6 \frac{\Delta H_2O}{H_2O}$$

where ΔT is in $^{\circ}\text{C}$ or K (Kelvins).

Note that, while the model is developed in terms of a ratio, the temperature change is not extremely sensitive to the background water vapor value used. Thus, for 1.5-ppm change from 3.0 to 4.5 ppm, the temperature change is 0.27 K; for the next 1.5 ppm, the change is 0.23 K. The constant (0.6) should be changed with the background water assumed, although later herein we treat 2.67 ppm \approx 3 ppm, and make no correction.

For the CCTT model, the results are 60 percent larger, giving

$$\Delta T = 1.0 \frac{\Delta H_2O}{H_2O}$$

The CCTA model implies a χ value of 100 K, i.e., an 0.01 change in solar constant leads to a temperature change of 1 K, whereas the CCTT model implies a χ value of 160 K. One of us (H. Hidalgo), and J. Coakley (private communication, 1976), argue as noted earlier, that these values should be multiplied by 1.5 to include the ice-albedo, decade time-frame, feedback effects included in the treatment of aerosols.** However, the implications of this have not been pursued in terms of the implied energy balances within the models (Ramanathan, 1976, private communication).

Several techniques have been used to estimate the fractional change in stratospheric water vapor for a given aircraft source strength. The approach used in the CIAP Report of Findings (and herein) treats water vapor as a gaseous pollutant with removal at the ground or in the troposphere. Weickmann (p. 7-22, CIAP Monograph 3) and the COMESA report (see below) ratio an aircraft source strength to the natural flux into (and out of) the stratosphere; this method

*CIAP Report of Findings (p. B-28) used a proportionality constant of 0.5 K rather than 0.6 K, basing the number on results from an assumed doubling of water vapor. Also, V. Ramanathan (private communication, 1977) points out that a preferred form for this relationship

would be $\Delta T = 1.2 \left(\sqrt{\frac{H}{H_0}} - 1 \right)$, where H is the perturbed water content and H_0 is 3 ppm (mass). The differences are negligible in the range of interest.

**Also Coakley (1976) based on different emissivity data (Cess, 1974) finds the temperature change due to added water to be considerably smaller than does Ramanathan, obtaining values about 65 percent of those found by Ramanathan.

ignores changes in residence time with changes in aircraft altitude, and may well give low estimates of stratospheric water perturbations by SST and high values for subsonics. A third method is that of the 1-D injection coefficient as used by Hunten (pp. 116-118, NAS Report; also Appendices C and D, this report), which computes the augmentation in mixing ratio above the point of injection; as the injection coefficient increases more rapidly with altitude than the residence time (the mixing ratio decreases below the point of injection), this method tends to maximize aircraft altitude effects. As the fluxes of water vapor in the stratosphere are not well understood (see Chapter 7, CIAP Monograph 3; also Section 3.3.2, CIAP Monograph 1), the "correct" method is obviously unknown and debatable. In all cases, some correction is necessary to adjust for the concentration of air traffic within a hemisphere.

According to Weickmann et al. (CIAP Monograph 3, p. 7-19), the global stratospheric water content is 1.78×10^{12} kg, based on 2.67 ppm (mass) and a stratospheric mass of 6.67×10^{17} kg. Hidalgo (p. F-126, CIAP Report of Findings) quotes 1.6×10^{12} kg. Sundararaman (CIAP Report of Findings, p. B-28) used 2.2×10^{12} kg. Weickmann questions (p. 7-18), however, whether the 2.67 ppm figure is consistent with other data (the cold-trap temperature, calling for 3.4 ppm, and the recognized CH_4 oxidation flux), so the figure may be low. Nevertheless, as the Monograph 3 panel estimate, the figure of 1.78×10^{12} kg is adopted here for the unperturbed global stratospheric burden of water vapor.

These calculations for water effects do not include changes in earth albedo due to changes in water vapor, a positive feedback effect which would increase the water vapor warming results about 10 percent (Ramanathan, 1976), nor a change in tropopause cold-trap temperature, a feedback effect which could be important for all perturbations, but which is not quantified by Ramanathan. These points need further study, but probably will require use of a 2-D or 3-D model.

3. Ozone Reductions* Ramanathan's results for NO_2 and O_3 changes in CCTT models are given in the CIAP Report of Findings, p. F-90. The temperature change is roughly linear in fractional ozone change, again assuming that ozone is fractionally depleted uniformly between 12 km and 40 km. For ozone depletions up to 10 percent, in the absence of NO_2 changes, we interpret his results as follows:*

*Here we must note that a demurrer has been entered by Ramanathan (private communication, 1977) to the effect that the separation of NO_2 and ozone effects as done here may be invalid. We do not disagree in principle, but argue that the technique used fits (reasonably) the data points generated by his model, and in view of some evidence of linearity, should not be overly misleading as an interpolation procedure where both effects are present.

$$\Delta T_{\text{CCTA}} = 0.76 \frac{\Delta O_3}{O_3},$$

$$\Delta T_{\text{CCTT}} = 1.25 \frac{\Delta O_3}{O_3}.$$

Again, it would appear that a factor of 1.5 should be applied to these values if ice-albedo decade time-frame feedback effects are to be included (Hidalgo, private communication, 1976) in the same fashion as recommended for aerosol effects.*

The proportionality "constants" (0.76 and 1.25) change slightly at greater depletions (being 0.854 and 1.38, respectively, at 50 percent depletion). The calculations are based on an ozone column of 0.344 atm-cm of O_3 , with a peak ozone density at an altitude of 22 km.

Note that in developing these data, Ramanathan assumed changes in ozone only between 12-km and 40-km altitude. In 1-D ozone depletion modeling however, the computed change reported is in terms of the percentage change in the total ozone column. The great bulk of atmospheric ozone is, of course, in the 12-km to 40-km range, so that relatively little error should be introduced by treating the two depletions as equivalent; this approximation is made here.

Ramanathan et al. (1976) also report briefly on effects (deduced from their 1-D model) of vertical and latitudinal distribution of ozone changes, and their resultant effects on surface temperature. The conclusions are that, if ozone is reduced nonuniformly, being greater at lower altitudes, the surface-temperature effects increase; also, the effects will be amplified several-fold in polar regions.

4. NO₂ Changes Ramanathan, 1974 (p. F-90, CIAP Report of Findings), using the same 1-D model, reported surface temperature changes as a function of NO₂ changes in the presence of ozone changes. Changes were again assumed to be uniformly fractional with altitude. The initial NO₂ distribution used was one provided him by J. Chang of Lawrence Livermore Laboratory. By algebraic manipulation** of his results, we obtain:

*The recent results of Reck (1976) should also be noted. She finds that the effects of ozone depletion on surface temperatures are dominated by the presence or absence of low-lying particulate layers, cooling in the absence of particles but heating in their presence. These results have not been confirmed by other studies, to our knowledge.

**Note again Ramanathan's demurrer about the separation of NO₂ and O₃ effects (previous page).

$$\Delta T_{\text{CCTA}} = 0.0278 \frac{\Delta \text{NO}_2}{\text{NO}_2},$$

$$\Delta T_{\text{CCTT}} = 0.0445 \frac{\Delta \text{NO}_2}{\text{NO}_2}.$$

As was the case with ozone, $\Delta \text{NO}_2/\text{NO}_2$ refers to the fractional change in NO_2 column between 12 km and 40 km. The unperturbed NO_2 column above 13* km used by Ramanathan, based on Chang's 1974 K_z profile, is 4.06×10^{15} mol/cm²; his NO_2 perturbation results assume uniform changes (percentage-wise) in NO_2 column between 12 km and 40 km. In order to obtain $\Delta \text{NO}_2/\text{NO}_2$, it is necessary to know what fraction of the added NO_x becomes NO_2 . Data on this point were obtained from four of the runs at Livermore made 12-13 December 1975. Results are given in Table 4.2.

TABLE 4.2. RATIO OF NO_2 CHANGES TO NO_y ($\text{NO} + \text{NO}_2 + \text{HNO}_3$) CHANGES AND OZONE CHANGES FOR VARIOUS CASES

<u>K_z</u>	<u>Chang/1974</u>	<u>Hunten/1974</u>	<u>Chang/1974</u>	<u>Hunten/1974</u>
NO_2 injection, kg/yr	2.E8	2.E8	2.E8	1.E9
Altitude, km	15	15	19	22
$-\Delta \text{O}_3/\text{O}_3$	0.002355	0.005767	0.00952	0.15208
ΔNO_2	0.07165E15	0.14270E15	0.21196E15	0.38206E16
ΔNO_y	0.29615E15	0.55627E15	0.7130E15	1.13347E16
$\Delta \text{NO}_2/\Delta \text{NO}_y$	0.242	0.257	0.297	0.337
$(\Sigma \text{NO}_2 > 12)^a_{\text{unp}}$	4.1627E15	5.1109E15	4.1627E15	5.1109E15
$\Delta \text{NO}_2/(\Sigma \text{NO}_2 > 12)_{\text{unp}}$	0.0172	0.0279	0.0509	0.7475
δ^b	7.309	4.84	5.35	4.92

^aUnperturbed

$$\delta^b = [(\Delta \text{NO}_2/(\Sigma \text{NO}_2 > 12)_{\text{unperturbed}})]/[-\Delta \text{O}_3/\text{O}_3]$$

Note in Table 4.2 that $\Delta \text{NO}_2/\Delta \text{NO}_y$ varies from 24 percent to 34 percent over a wide range of conditions. Note also that the NO_2 column above 12 km varies with the K_z profile. The ratio (δ) of total NO_2 column change to original NO_2 column above 12 km to the fractional change in ozone varies in

*A slight discrepancy appears to be implied between Ramanathan's use of this figure, which refers to a column above 13 km, and the use by him of a perturbed atmosphere above 12 km.

these cases from 4.8 to 7.3. A figure of 6 was quoted by Ramanathan.* The total change in NO_2 column is used here largely because no other data are available; however, Ramanathan (private communication, 1976) has argued that the altitude distribution of NO_2 changes is not critical to surface temperature change calculations, and most of the NO_2 change is in the stratosphere. However, stratospheric temperatures are affected by the altitude distribution of this added NO_2 .

The complexities are many and there is little point in attempting too many refinements with available data. We thus use (see Section E below) an NO_2 cooling figure, as discussed, and assign 27 percent as the NO_2 fraction of the added NO_x burden, which is computed from the NO_x input rate and residence time, as computed from K_z profiles. On a global total, Ramanathan's NO_2 value of $4.06 \times 10^{15} \text{ mol/cm}^2$ is equivalent to $1.58 \times 10^9 \text{ kg}$. It follows that:

$$\Delta T_{\text{CCTA}} = 0.0278 \times 0.27 \times \Delta \text{NO}_x / 1.58 \times 10^9 = 0.0075 \frac{\Delta \text{NO}_x}{1.58 \times 10^9} .$$

$$\Delta T_{\text{CCTT}} = 0.0445 \times 0.27 \times \Delta \text{NO}_x / 1.58 \times 10^9 = 0.012 \frac{\Delta \text{NO}_x}{1.58 \times 10^9} .$$

As was noted for water vapor and ozone effects, it has been argued that a factor of 1.5 should be applied to these numbers for consistency with the x value quoted for particulates.

The NO_2 warming effect is a relatively small one, as later comparison will show.

C. Particulates

Particulates from jet fuel exhaust come primarily from sulfur in the fuel, but may also come from metals in the fuels, erosion of the engines, and from soot and hydrocarbons due to incomplete combustion. Sulfur contents appear to be ~ 0.05 percent on the average, but vary from ~ 0.02 to 0.15 percent (CIAP Monograph 2, p. 2-5); the COMESA report gives 0.05 to 0.12 percent for British fuels. The value permitted by specification is 0.3 weight percent for commercial fuels. At 0.05 percent sulfur, converted to 75 percent sulfuric acid, the particulate emission index becomes 2.04 g/kg of fuel. The nonsulfur components are small in a relative sense at 0.05 percent sulfur, but would need further examination if the fuels are desulfurized.

The climatic impact of the sulfur-containing oxidation products of jet fuels involves a number of poorly determined factors (see CIAP Monograph 3, Chapters 6 and 8). The kinetics of the oxidation, nucleation, and condensation

*Note also that Cunnold (p. E-80, CIAP Report of Findings) gives a 12 percent global decrease in O_3 for a 38 percent increase in NO_y , which, if the NO_2 portion of the total NO_y remains roughly constant, gives a δ value of 3.2. (Table 4-2)

processes are not well known; the optical properties and the size distribution and shape of the resultant particulates are critical, but by no means unequivocally established, the Mie theory may not be valid for the shapes involved, etc., [although Pollack et al. (1976a), argue that it is a good approximation]. The residence times to be used for SO₂-based particulate products is almost certainly less than for gaseous products, but how much less is unclear, in view of questions regarding the altitude and rate at which the gases are converted to particles (which may differ from the altitude of injection) and the appropriate mean particle size. Larger particles (e.g., 0.3- μ m-radius diameter) settle more rapidly but also have more effect on light scattering than do smaller particles. At high altitudes (above 30 km to 35 km); the temperatures may be high enough to evaporate sulfuric acid particles (Hamill et al., 1976); also, the particles would be expected to grow as they settle.*

As noted earlier, the computations in CIAP assumed, for working purposes, that the aerosol particles were uniformly distributed in a shell 10-km thick (at an altitude of 15 km to 25 km) over the earth; this shell has a volume of $5.1 \times 10^{18} \text{ m}^3$. The Friend particle size distribution (see CIAP ROF p. E-135) was used, with a mean particle radius of 0.3 μ m. The scattering properties of this layer were estimated, originally by Herman p. F-116, CIAP Report of Findings using a single wavelength of light (0.5 μ m), but later extended to include an integration over the visible wavelength regime. However, none of the CIAP calculations included the longwave effects, which may reduce the cooling effects by about 20 percent (Harshvardhan and Cess, 1976) to about 40 percent (Pollack et al., 1976a). The increased optical depth was estimated from these calculations, using best estimates of the optical properties. The increased optical depth was found (see p. F-116, CIAP ROF) to be linear in the increased particulate loading; the increase in optical depth was used as one possible measure of acceptability of change in the CIAP Report of Findings. For climatic change estimates, however, the optical depth increase has been converted to a change in equivalent solar constant, and then, based on various model estimates, converted to a change in global mean temperature; the procedures thus differ from, and are not directly comparable to, models such as that used by Ramanathan et al. (1976), in which humidity and cloudiness parameters are prescribed. Herman's single wavelength values were apparently used in the main text of the CIAP Report of Findings; it would appear, however, that the wavelength-integrated numbers should be preferable. On this basis, using Pollack-Toon results (p. F-116, CIAP ROF),

*The source of the natural sulfate layer (the Junge layer) is a matter of debate. Crutzen (1976b) suggests that the source is not SO₂ from the troposphere but CSO, which is oxidized above the Junge layer.

$$\frac{\delta\sigma}{\sigma} = - 0.0061 \Delta S_d ,$$

where $\delta\sigma/\sigma$ is the fractional change in solar constant and ΔS_d is the increase in particulate loading, in $\mu\text{g}/\text{m}^3$. (Note that $1 \mu\text{g}/\text{m}^3$ in $5.1 \times 10^{18} \text{ m}^3$ corresponds to 5.1 Mt.) The proportionality constant (0.0061) was found by two other investigators to be 0.0046 and 0.011, respectively, (see p. F-116, CIAP ROF). In recent modeling work, however, Pollack et al. (1976a) on re-evaluating the correcting (~ 40 percent) for longwave effects and incorporating constant relative humidity (and other) specifications, found considerably lower effects. Their results are not presented directly in the CIAP format, but they provide data* for a constant relative humidity model from which the proportionality constant can be calculated to be 0.00232, ~ 40 percent of the value derived from their earlier work. Pollack et al. (1976a), do not describe their work in terms of constant cloud-top altitude or constant cloud-top temperature; their model assumed 50 percent cloud cover, with the clouds at 3 km to 6 km.

In the CIAP work, to convert to global average temperature change, a χ value of 150 K (after about 10 years) was recommended, giving,

$$\begin{aligned} \Delta T &= - 150 (0.0061) \Delta S_d = - 0.915 \Delta S_d \\ &= - 0.179 \Delta M_s \end{aligned}$$

where ΔM_s is the mass of added sulfate particles in the global stratosphere, in megatons. A slightly different relationship, $\Delta T = - 0.8 \Delta S_d$ is reported by Coakley and Grams (1976) in recently published work which followed their CIAP efforts.

Pollack et al. (1976a) develop a χ value of 112 K which they find to be in good agreement with Manabe-Wetherald (1967) who used a value of 120 K; their temperature change relationship becomes for the case described:

$$\begin{aligned} \Delta T &= - 112 (0.00232) \Delta S_d = - 0.260 \Delta S_d \\ &= - 0.051 \Delta M_s . \end{aligned}$$

The significance of these results, using the $0.915 \Delta S_d$ relationship, is that, on a global average basis, the cooling resulting from a loading of 1 Mt of particles at 15 km to 25 km, consisting of 75 percent H_2SO_4 with a specified

*Using their (1) Fig. 7, Model A (constant relative humidity), (2) Eq. 3b, and (3) $\chi = 112$ (p. 255):

$$\frac{\delta\sigma}{\sigma} = \frac{\Delta T}{112} \approx \frac{-8.4 \Delta T}{112} \approx \frac{-0.2604 \Delta S_d}{112} = -0.00232 \Delta S_d .$$

size distribution, if maintained for 10 years, would be 0.279°C . Using the Pollack et al. (1976a) results, the global average cooling resulting from a loading of 1 Mt would be 0.051°C . This result is in reasonable agreement with values found empirically by Oliver (1976), in which dust loadings were based on a hemisphere, and were thus two-fold larger per Mt.

Several possible adjustments may be considered in estimating particulate effects, or when considering various authors' results. One, the fraction of SO_2 converted to sulfate particles, has been estimated in a 1-D model by Chang (see p. F-98, CIAP ROF) as 0.965 for injections at 20 km and 0.883 at 17 km, with slightly lower values at lower altitudes. This correction will be closer to unity for longer residence time models (CIAP report and Hunten), but no values are available; in view of other uncertainties (as, for example, in residence times of gases versus particles), the correction will be ignored in later work here. A second correction, which may be necessary when comparing different investigators, involves the particle density, as scattering involves the volume rather than mass of the particles. A value of 2 g/cm^3 , as used by Pollack et al. (1974, 1976a), is believed to be approximately correct. (A value of 2 g/cm^3 at stratospheric temperatures seems reasonable, somewhat above the hand-book value of 1.67 g/cm^3 for 75 percent sulfuric acid at room temperature.) A third correction relates the mass of aerosols (at 75 percent H_2SO_4) to the mass of SO_2 converted. We have used the figure $2.04 \left[= \frac{98 (\text{mol wt } \text{H}_2\text{SO}_4)}{64 (\text{mol wt } \text{SO}_2)} \cdot \frac{1}{(0.75)} \right]$; Pollack et al. (1976a) quote 1.6. In general, these corrections are not of great concern, considering the uncertainties in the computation of $\frac{\delta\sigma}{\sigma}$ or in the value of χ .

D. Hemispheric Factors

Calculations based on techniques given in Sections B and C are for global average changes. Most traffic, however, is in the Northern Hemisphere, and most of the pollutant burden will be in the Northern Hemisphere. To correct for this, a "hemispheric factor" recognizing the work of Mahlman (see p. E-95, CIAP ROF) and Alyea et al. (1974) is needed to obtain Northern Hemisphere loadings compared to a uniformly distributed global burden for the same input rate. Available data suggest that a figure of 1.3 to 1.4 is applicable for flight in the 17 km to 20 km region at 40° to 60°N , implying that 65 percent to 70 percent of the equilibrium burden is in the Northern Hemisphere and 30 percent to 35 percent in the Southern Hemisphere (see pp. E-89, E-95, E-99, CIAP ROF). However, this factor would likely vary from perhaps nearly 2.0 (100 percent in the Northern Hemisphere) for low-altitude, high-latitude flight, to perhaps 1.1 or 1.2 for high-altitude, low-altitude flight (see Alyea et al., 1974). It could also vary with the gas or species being considered and for particulates relative to gases. These points have not been studied adequately.

E. Residence Times

Residence time, as defined in the CIAP report for use in applying 1-D modeling results, signifies the stratospheric burden at steady state divided by the input flux, using a 1-D model, assuming a ground sink. This burden is necessary to estimate mean temperature changes. The computations in the CIAP Report of Findings are based on this concept, except, there, the residence times quoted are total atmospheric residence times, including the tropospheric component. For gases with no high-altitude sink, a model of this type leads to a constant augmented mixing ratio above the point of injection (see NAS report, Appendix A, pp. 114-119). For particulates, however, settling retards upward diffusion, and enhances downward transport, reducing the total burden relative to gaseous injectants (see Hunten, 1975a). The concepts and residence times for various K_z profiles are discussed in detail in Appendix D.

Residence time is, of course, an oversimplified concept. Its utility lies in its simplicity, and for computing 1-D mean temperature changes, in the absence of better techniques (e.g., coupled models) cannot readily be improved upon. Even so, due to questions about how to handle the tropospheric component, some problems exist. The tropospheric component is of relatively little significance, however, for flight at 17 km to 20 km i.e., for typical SST altitudes.

Residence time calculations in CIAP were made on the basis of an average value between two K_z profiles, that of Hunten/1974 and that of Chang/1974 (see p. 19, CIAP ROF). In carrying out the averaging, however, the Hunten recommendation that flight altitudes at $\sim 40^\circ$ N be adjusted upward by 2 km was not used. To make temperature change estimates, we have thus recomputed residence times (see Appendix D) for continuously injected gaseous and particulate pollutants, based on the Chang/1974, Hunten/1974, and CIAP approaches; we have also made certain assumptions about the tropospheric component as follows:

1. For gaseous pollutants (H_2O and NO_2), the tropospheric component has been subtracted. For H_2O , stratospheric water is obviously not enhanced directly by tropospheric water; for NO_2 , reactions with water in the troposphere would completely alter its absorption characteristics.
2. For particulates, the residence time was taken as the total atmospheric residence time for particles of $0.3 \mu m$ radius, including the tropospheric component. The assumption was that inclusion of a somewhat fallacious tropospheric burden (the particles would, in fact, be rained out 5 km or more above the assumed ground sink) would compensate for the fact that SO_2 (prior to conversion to particulates) may diffuse to altitudes higher than would particulates, and may thereby build up a larger burden than calculated, assuming instantaneous conversion at exhaust altitude, as was implied in residence-time calculations. We have also ignored kinetic factors, thus increasing the burden slightly.

Using these assumptions, residence times for gases and aerosols were estimated for Chang/1974, Hunten/1974, (with a 2-km adjustment for flight altitude), and CIAP methods. The results are shown in Fig. 4.1. The computations for particulate residence times were carried out by Bauer (Appendix D). Residence times for other K_z profiles and other particle diameters are also given in Appendix D.

F. Response Time

The CIAP Report of Findings treats climate changes as occurring instantaneously. The actual time required is not well known. It seems reasonable, however, to assume that the time involved consists of two components, that due to transport and chemical delays in building up pollutant effects, typically several years, and that due to the inertia of the earth-ocean system plus possible feedback effects.

It was shown in Chapter 3 of this report that the time delays in effecting ozone changes tend to increase with decreasing altitude in the range studied; however, at SST altitudes, the response times do not differ to a large degree from residence times; in any event, the dominating delay is probably that of the thermal inertia of the ocean. A number of estimates for thermal inertia delays are available. For example, Budyko (1974) used 2.5 years in one set of calculations based on a seasonal march of temperatures. In empirical studies, Oliver (1976) found mean surface temperature response times to stratospheric dust changes to be 6 ± 3 years. Schneider and Mass (1975) used a 6.9-year figure based on a 75-meter mixed layer assumption. Pollack et al. (1976), refer to a 4-year relaxation time. Two-dimensional feedback effects undoubtedly exist on various time scales, ranging from less than a decade to thousands of years; the χ values quoted in the CIAP report (50 K at 1 year, 150 K at 10 years), however, fit an empirical relationship involving a time constant (2.53 years) similar to that recommended by Budyko (1974). Thus, $\chi \approx 152.9$ ($1 - e^{-t/2.53}$) gives a value of 50 K at 1 year and 150 K at 10 years.

4.3.3 COMESA Climatic Effect Studies

A. Introduction

COMESA climate-change studies were based on 2-D and 3-D models; 1-D models were not employed. As with the CIAP effort, effects of changes in aerosols, water, NO_2 , and ozone were studied. In addition, two other studies of particular interest were made: one of these related to the possible interactions involved with simultaneous perturbations simulating several of the ingredients in aircraft exhaust; a second related to the climatic consequences of contrails, particularly those from subsonic aircraft.

Much of the COMESA climate discussion is based on a fleet of 1,000 Concorde. This fleet, in its stratospheric operations, is taken to have the following characteristics, with page references to the COMESA report:

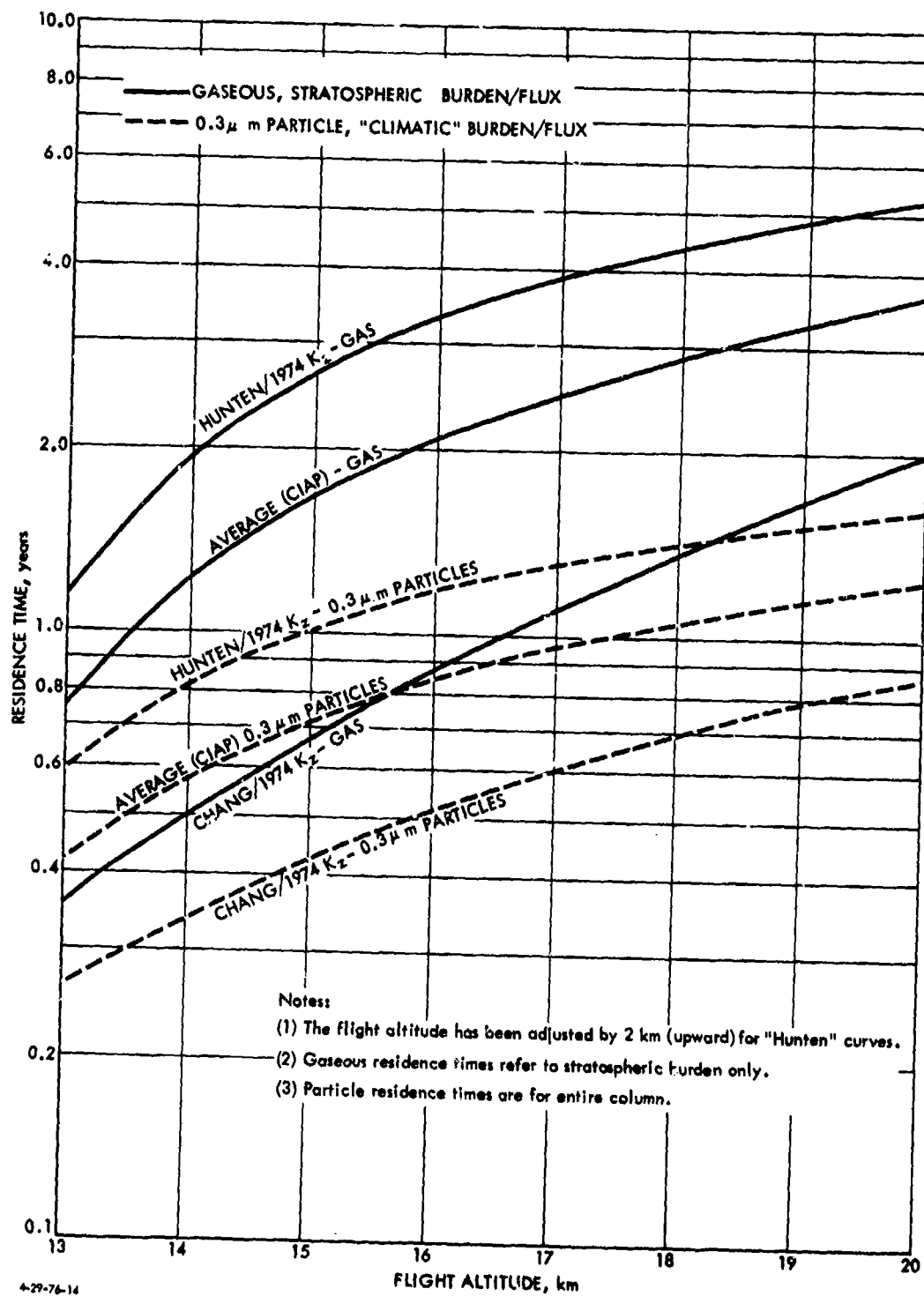


FIGURE 4.1. Residence Time Estimates

Fuel burned/yr:	4.3×10^{10} kg (p. 23, from SO_2)
Average flight hr/day:	5.5
NO_x emissions:	1.13×10^{34} molecules/yr (p. 24) 8.0×10^8 kg/yr (p. 17)
SO_2 emissions:	U.S. fuel (0.05 percent sulfur) 4.3×10^7 kg/yr (p. 22) U.K. fuel (0.12 percent sulfur) 1.03×10^8 (p. 15)
Emission indices:	CO 3140 (p. 15) H_2O 1270 (p. 15) SO_2 1.0 or 2.4 (p. 15) NO_x 18.5 - 20 (p. 15) CO 3.5 (p. 15) Unburned hydrocarbons 0.2 (p. 15) Soot 0.1 (p. 15)

Nominal flight altitude: 17 km (p. 24). Distribution, however, is noted to be important (p. 16).

The COMESA results are summarized in Fig. 4.2 (their Fig. 5.6.1). This figure will be referred to frequently in the following discussion.

B. Sulfates

The COMESA computation of aerosol burden from Concorde is through analogy to computations in SCEP (1970) for the U.S. SST (pp. 451-453). They quote 500 U.S. SSTs (p. 451) using a 2-year residence time as adding a burden of 2×10^8 kg; they argue that more than 1,000 Concorde would be required to produce a similar amount, but then state (p. 453) that 500 Concorde may produce an amount equal to the background (10^8 kg, p. 452). Apparently, 2×10^8 kg was used as the sulfate burden from 1,000 Concorde. CIAP procedures, with the COMESA fuel flow, using a residence time of 1.70 years and 86.7 percent conversion (6.5 km, p. B-24, ROF) would give 1.3×10^8 kg; without the conversion factor, the burden would be 1.5×10^8 kg. An allowance for higher sulfur content may be implied.

Climatic effects of aerosols were studied with both pure absorbing layers and a scattering layer. The pure absorbing layer computations were apparently not used in making estimates of aircraft effects. Effects computed in the 2-D model were much smaller than in the 3-D model. The surface cooling due to the scattering layer (p. 461) was based on prorating of an assumed aerosol layer with total backscattering of 0.6 percent, which corresponded in their model to 0.6 K cooling. The mass of this layer is given as 4×10^9 kg. Prorating to 2×10^8 kg, the cooling from 1,000 Concorde was estimated as 0.03 K. However, (see Fig. 4.2), the plotted cooling effect at 4.3×10^{10} kg fuel per year is 0.05 K. [The source of the discrepancy is unclear. It is not in sulfur content, since the SO_2 scale on top of Fig. 4.2 implies an SO_2 emission index of unity (0.05 percent sulfur).]

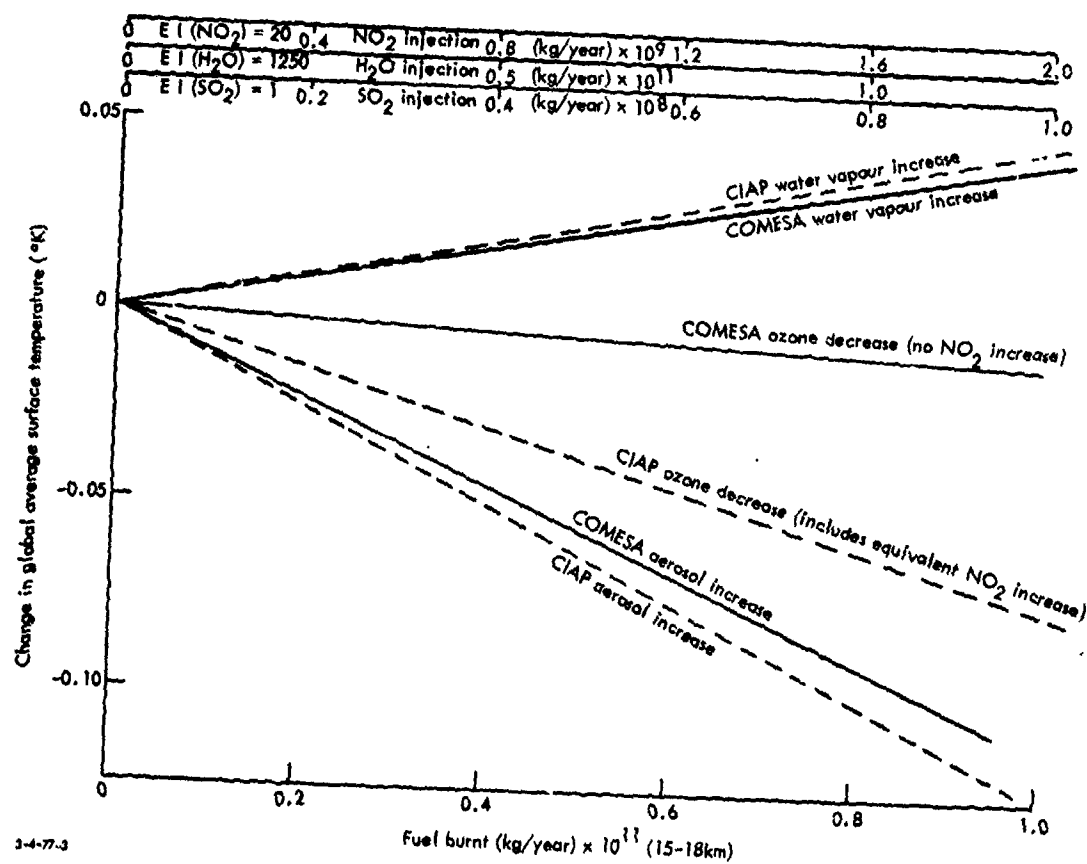


FIGURE 4.2. Surface Temperature Change as a Function of Fuel Burnt
Source: COMESA, 1975

The basis for the dotted line showing the "CIAP aerosol increase" is also unclear, if procedures in Appendix B of the CIAP ROF are applied. Thus, on a global average basis, the 1.3×10^8 kg increased loading, if spread in a 10-km-thick layer, is $0.0255 \mu\text{g}/\text{m}^3$. The temperature change (pp. B-23, E-9, B-6) is -1.311×0.025 or -0.033 K. The plotted value is about -0.06 K. The CIAP and COMESA figures both seem to be 0.03 K (although this agreement is clearly fortuitous, considering the differences in procedures, χ values, etc.), but the plotted values both seem to be different from the values computed here.

COMESA distinguishes between changes in equivalent solar constant due to reduced solar flux from absorbing aerosols and true changes in solar constant. The effects are said to be quite different, the aerosol layer having much less (about 1/6) effect (p. 451). We have not pursued this question further.

C. Water Vapor Perturbations

1. Stratospheric Water Vapor Changes COMESA carried out studies on water vapor changes with both their 2-D and 3-D models. The 3-D model (p. 492) showed essentially no effect of increased water vapor, but the run was not carried to equilibrium and was discounted. The 2-D runs used a baseline stratospheric humidity of 0.1×10^{-6} g/g, with perturbed cases at 2.5 and 5×10^{-6} . The figures from the 2.5- to 5.0-ppm runs are of particular interest; the results show a 0.495 K change in global average temperature and a change of 0.457 K in Northern Hemisphere average (p. 493). The overall change in going from 0.1 ppm to 5.0 ppm is 1.47 K, which COMESA states is in agreement with Manabe-Wetherald (M-W) model result of 1.5 K. (This is apparently not a published M-W result, as the M-W started with 3 ppm.) However, the 1-D Ramanathan results for doubling of stratospheric water vapor (CIAP ROF, p. F-125) from 3 ppm to 6 ppm is 0.5 K in agreement with the COMESA 2-D result.

As to perturbing effects of aircraft on stratospheric water vapor content, the COMESA group adopted the procedure of ratioing natural and aircraft fluxes (p. 7-22, Monograph 3). The claim is made that $1,000$ Concorde might increase stratospheric water vapor by 1 to 4 percent (p. 494 and p. 20); however, the figures quoted are a natural flux of 1.5×10^{12} kg/yr versus the $1,000$ Concorde flux of $4.3 \times 10^{10} \times 1.27$ or 5.5×10^{10} kg/yr, giving an increase in flux of 3.7 percent (global). This corresponds to 0.037×0.5 or 0.019 K increase in temperature, which matches the plotted value on Fig. 4.2.

The CIAP value, with a 1.7 -year residence time, would be $0.5 \times [4.3 \times 10^{10} \times 1.25 \times 1.7 \text{ kg burden} / 2.2 \times 10^{12} \text{ natural (p. B-28)}]$ or 0.021 K. Use of a 1.6×10^{12} kg natural water burden figure (Section 4.3.2.B, or p. F-124, CIAP ROF) increases this to 0.029 K. This near-agreement appears to be happenstance, as the CIAP figures are based on an average water residence time [("Hunten," without the 2 -km recommended adjustment, plus "Chang")/2], and the flux ratio technique ignores the altitude of the source entirely.

2. Changes in Cloudiness and Contrails The COMESA report includes 2-D modeling results on changes in low clouds and high clouds, effects of which, on surface temperature, are, according to their models, opposite in sign. Surface temperatures are very sensitive to changes in low cloudiness (600 mbar to 800 mbar), with increased low cloudiness substantially lowering surface temperature [47.3 K for 100 percent low cloudiness versus no clouds in their specific experiment (p. 474)]. Because such changes are difficult to predict (such changes would be a feedback effect of aircraft, not a direct effect), the studies in changes in cirrus cloud, which can be related to contrail formation, are of more interest. The COMESA study (p. 475) showed that a climatological global average cirrus cover (22.0 percent) increased global average surface temperatures by 0.86 K (versus no such clouds). The clouds were placed between 260 and 410 mbar (33,000 ft to 23,000 ft; 10 km to 7 km), reflected 20 percent of incoming radiation, and were half black to infrared. [They note, however, a 3-D study elsewhere (Hunt, 1975, as reported in the COMESA report) which showed little effect of cirrus.] As to ties to aircraft, they note, in agreement with CIAF, that SSTs will produce very little change in cirrus. However, the COMESA report quotes Singer (1968), who argued that, in 1968, aircraft contrails had increased (high) cloud cover by 1 percent, which corresponds to a warming of 0.04 K. This figure is larger than most SST fleet effects and would presumably be increasing. This question was of concern following introduction of jets in about 1960. See Machta, 1971.

Feedback studies in the 2-D model were also made to see if changes in low cloudiness resulted from changes in ozone or aerosols. The results were essentially inconclusive, although the changes which were found implied a regenerative cooling effect with ozone changes (increased clouds and decreased temperature with decreased ozone), and a compensating effect (decreased cloud and warming, with increased aerosol, p. 477).

D. Ozone Decreases and NO₂ Increases

Ozone decreases of 25 and 50 percent were studied in 2-D and 3-D models. The 3-D model showed a decrease in surface temperature at the land/ice point of 0.26 K with 25 percent ozone decrease and 1.05 K with 50-percent decrease. However, the authors tended to discount these results. The 2-D model showed a 0.199 K global decrease at 25-percent reduction in ozone (but only a 0.081 K Northern Hemisphere change) and 0.068 K global average change for 12.5 percent ozone reduction (but only 0.015 K for Northern Hemisphere). Results were thus not linear in ozone change.

The latitudinal distribution of changes merits further comment. Results from the COMESA 2-D model, assuming 25-percent reduction in ozone everywhere, follow:

85.5° N	-0.007 K
49.5° N	0.020 K
4.5° N	-0.197 K
49.5° S	-0.374 K
85.5° S	-0.475 K

It is not explained why the Northern Hemisphere changes are so different from those in the Southern Hemisphere.

These results are, according to COMESA, much smaller than predicted by Manabe and Wetherald, due apparently to the fact that M-W changed both ozone distribution and ozone amount; the M-W figure for 25-percent decreases in ozone is -0.8 K. The CIAP figure (Ramanathan, p. F-90, constant cloud-top altitude, as in M-W, would give a figure of about -0.22 K).

The NO₂ effect was studied more briefly (COMESA report p. 495). No global average figures were given. It was argued that the NO₂ effect would be greatest at high latitude, but probably insignificant. Callis et al. (1975) were quoted as indicating that solar heating decrease due to ozone reduction is largely compensated by NO₂ additions.

NO₂ effects were not considered by COMESA in computing aircraft effects (COMESA report p. 491). It was argued that a high estimate of ozone reductions from 1,000 Concorde would be about 2.5 percent (p. 491), which is 1/10 one of the decreases studied, leading to ~ 0.02 K cooling. The plot, however, ["COMESA ozone decrease (no NO₂ increase)"], (Fig. 4.2) shows less than 0.01 K at 4.3×10^{10} kg/yr fuel. The plot (Fig. 4.2) apparently reflects a lower ozone change estimate than does the text on p. xvii of the COMESA report. One thousand Concorde lead to 0.8 percent global average ozone decrease for a temperature change of less than 0.01 K.

A line is given in Fig. 4.2 labeled "CIAP ozone decrease (includes equivalent NO₂ increases)." The source of this curve is uncertain; the summary section of the CIAP Report of Findings assumed NO₂ and ozone effects balanced (p. 39, CIAP ROF). However, if a NO_x injection rate of 8×10^8 kg/yr is used, and the results on p. B-31, CIAP Report of Findings (1990^c case), prorated, the ozone reduction is about 4×1.505 or 6 percent in the Northern Hemisphere corridor, or 3 percent globally. Hidalgo, p. F-92 CIAP ROF, suggests that the net change due to NO_x injections is equal, in °K, to the fractional change in ozone. The global change should then be -0.03 K. The plotted value (Fig. 4.2) is about -0.035 K, suggesting that this procedure may have been used.

E. Carbon Dioxide

CO₂ is discussed by COMESA on pp. 17-18 of their report. They estimate that 5 years of operations of 1,000 Concorde at 5.5 hr/day in the stratosphere, would increase CO₂ contents about 0.05 ppmv in the atmosphere, with no relative

buildup of CO₂ in the stratosphere. They also estimate the corresponding change due to fossil fuel consumption at the ground to be 10 ppmv. The 0.5 ppmv figure apparently assumes half of the CO₂ leaves the atmosphere in this period. Note that this calculation implies 5 percent of the total fossil fuel consumed in this period is used by SSTs, certainly an upper-bound assumption. The CO₂ question is discussed further in Section 4.5.

F. Interactive Effects, 2-D Model

COMESA conducted a study in their 2-D model of the additivity of the effects of various changes due to the different components of engine exhaust. The combined perturbations included a 25-percent decrease in ozone, an absorbing layer (0.008 optical thickness), and an increase in water vapor of 2.5 ppm. On a global average basis, the additivity was found to be excellent (0.65 K interactive versus 0.63 K additive). Latitudinal differences, if any, are not reported (p. 497). This important result adds credence to the additivity concept, but the aggregation involved in global averaging must be considered, as well as the fact that the perturbations were imposed rather than computed, so that any altitudinal or latitudinal distribution effects would not have been discovered.

4.4 COMPUTED MEAN TEMPERATURE EFFECTS--FLEET EFFECTS

4.4.1 Introduction

The foregoing sections have given modeling results which are necessary inputs to estimates of changes that might result from specified aircraft operations. The severe uncertainties, and lack of consistency between models, have been illustrated. The time-dependent aspects of such changes are discussed in Appendix E. Here we ignore time-dependent aspects and compute the "steady-state" (after approximately 10 years) effects of the FAA as reported (Table 2.27) "high estimate" 1990 SST fleet.

4.4.2 Mean Temperature Impact of the 1990-High SST Fleet (As Reported)

The 1990-high SST fleet as reported has the following fuel-consumption characteristics in the altitude bands for which the climate models may be applicable. (See Table 4.3.)

TABLE 4.3. FUEL CONSUMPTION FIGURES BY ALTITUDE
BAND, FAA "1990-HIGH" CASE; AS REPORTED
SOURCE: Arthur D. Little, Inc.

Altitude band, km	Fuel burned, 10^8 kg/yr	SO ₂ , 10^5 kg/yr	H ₂ O, 10^8 kg/yr	NO _x , 10^6 kg/yr
13-14	3.8656	3.8656	4.8320	7.7338
14-15	3.9447	3.9447	4.9309	7.8936
15-16	13.7792	13.7792	17.2240	26.2497
16-17	11.5669	11.5669	14.4586	20.8244
17-18	8.7420	8.7420	10.9275	15.7061
18-19	5.2662	5.2662	6.5828	9.4767
	47.1646	47.1646	58.9558	87.8843

The above tabulation includes a small (~ 3 percent) Southern Hemisphere component, which will have a negligible impact on the hemispheric distribution of effects.

In using the models, a substantial matrix of choices is evident; these include:

1. K_z profile choice (and any tropopause height corrections).
2. Perturbation computation approach: residence time, injection coefficient, or ratio to natural flux across the tropopause.
3. Particle size selected to correct for settling.
4. Model:
 - Constant cloud-top altitude or constant cloud-top temperature
 - Constant relative or absolute humidity
 - Inclusion or exclusion of ice-albedo feedback effects
5. Modeler, primarily with regard to particulates, and optical characteristics selected.

There is little point to pursuing the array in great depth. Some bounds on the possible effects and on their range of uncertainty are of more interest. To obtain some estimates, the fleet emissions were simplified by lumping all emissions into a single 1-km band, which was taken as 17 km to 18 km; the results are for this reason 20 percent to 40 percent high in comparison with the FAA distribution.* An attempt is then made to derive self-consistent sets of numbers based on the two K_z profiles which have been given the most

*Furthermore, by so doing, the altitude adjustments made to obtain the "modified" fleet, as described for NO_x effects (Table 2.33 of this report) become unnecessary.

TABLE 4.4. STRATOSPHERIC CHANGES^a

Item	K ₂ profile	
	Chang/1974)	Hunten/1974 (+ 2) ^b
t _{RG} = stratospheric residence time, gas (yr)	1.2	4.2
t _{RP} = residence time, 0.3 μm particles (yr)	0.65	1.37
Burden computations, residence time basis (global)		
H ₂ O: 5.90E9 x t _{RG} (kg)	7.08E9	2.48E10
Particles: 4.72E6 x t _{RP} x 2.04 (kg)	6.25E6	1.32E7
NO _x : 8.79E7 x t _{RG} (kg) ^c	1.06E8	3.69E8
Unperturbed global burdens		
H ₂ O (kg)		1.78E12
NO ₂ (kg) ^d		1.58E9
Changes (global average)		
ΔH ₂ O/H ₂ O	3.98E(-3)	1.39E(-2)
ΔNO _x /NO ₂	6.70E(-2)	2.34E(-1)
ΔS (μg/m ³) ^e	1.23E(-3)	2.59E(-3)
ΔO ₃ /O ₃	-0.002 ^f	-0.0063 ^g

^a1E9, e.g., refers to 1 x 10⁹.

^bIn this computation, the flight altitude has been adjusted upwards 2 km in accordance with the NAS (1975) recommendation.

^cNO₂ taken as 0.27 x ΔNO_x.

^dThis figure should, in fact, be model-dependent, with a greater burden for the Hunten model. The NO₂ cooling effect with the Hunten profile is thus overestimated in Table 4.6, but little error is introduced in the net effects computed.

^eVolume taken as 5.1 x 10¹⁸ m³.

^fFrom p. E-59, CIAP Report of Findings.

^gUsing NAS/1975 method, pp. 117-119.

consideration, that of Hunten/1974 (+ 2) and Chang/1974. The stratospheric changes resulting are given in Table 4.4; the temperature change coefficients are given in Table 4.5; and the range of temperatures resulting is given in Table 4.6. The net change is found to be in the range 0.000K to 0.016 K (warming).

It should be remembered that material presented elsewhere in this report suggests that the Hunten/1974 K_z profile may give an excessively large (a factor of 2 or more) burden at steady-state. The combination of Hunten/1974 K_z profile with the ice-albedo-coupled feedback factor of 1.5 with the CCTT model may thus well be several-fold high in the estimates of overall effects. Also, the ozone depletion estimates presented in Table 4.4 are now believed to be high in view of revised chemical reaction rates.

The principal difference between the net heating result here and the net cooling effect found in CIAP is the use here of a residence time correction for particulates relative to gases. In addition, current results, in particular, Pollack et al. (1976a), in which correction for longwave effects is included, indicate particulates have smaller climatic effects than were used in CIAP.

TABLE 4.5. TEMPERATURE COEFFICIENTS

	<u>CCTA, $\chi = 100$</u>	<u>CCTT, $\chi = 150$</u>
$\Delta H_2O/H_2O$	0.6	1.44
$\Delta NO_x/NO_2$	0.0075	0.018
$\Delta O_3/O_3$	0.76	1.88
ΔS	<u>$\chi = 100$</u>	<u>$\chi = 150$</u>
Pollack-Toon ^a	-0.61	-0.915
Coakley-Schneider ^a	-0.46	-0.69
Luther ^a	-1.10	-1.65
CIAP ^a	-0.90	-1.35
Pollack et al. (1976a)	0.23 ^b	0.35 ^b
Hemisphere factor	1.4	1.4

^aFrom p. F-116, CIAP Report of Findings.

^bAdjusted from Pollack et al. (1976a), who developed a χ of 112.

TABLE 4.6 SURFACE TEMPERATURE* CHANGES^a
NORTHERN HEMISPHERE

Causative agent	K _z profile and model	
	Chang/1974, CCTA, $\chi = 100$	Hunten/1974 (+ 2), CCTT, $\chi = 150$
Gases		
$\Delta H_2O/H_2O$	3.35E(-3)	2.80E(-2)
$\Delta NO_x/NO_2$	7.03E(-4)	5.90E(-3)
$\Delta O_3/O_3$	-2.13E(-3)	-1.18E(-2)
Sum (gases)	1.92E(-3)	2.21E(-2)
Particulates	$\chi = 100$	$\chi = 150$
Pollack-Toon ^b	-1.05E(-3)	-3.32E(-3)
Coakley-Schneider ^b	-7.92E(-4)	-2.50E(-3)
Luther ^b	-1.89E(-3)	-5.98E(-3)
CIAP ^b	-1.55E(-3)	-4.90E(-3)
Pollack et al. (1976a)	-4.00E(-4)	-6.00E(-4)
Range	-4.00E(-4) to -1.89E(-3)	-6.00E(-4) to -5.98E(-3)
Sum (gases + particulates)	0.03E(-3) to 1.47E(-3)	2.15E(-2) to 1.61E(-2)
Net ^c	0.000 to 0.016	

^aAfter about a decade of steady operations

^bFrom CIAP Report of Findings, p. F-116

^cAssuming additivity

*As in Table 4.5, 3.35E(-3) e.g., refers to 3.35×10^{-3}

These results, which need further study to ensure both credibility and self-consistency, indicate that the largest effect is always that of water vapor, the NO_2 effect is small, as is the effect of particulates if the latest results (Pollack et al., 1976a) are to be accepted. The ozone temperature effect is smaller than the water effect, and in the opposite direction. The net overall effect is very small, and slightly on the positive side. This positive effect would be increased if NO_x emission indices are reduced and if the fuel is desulfurized.

The 1990-high FFA SST fleet corresponds to perhaps 142 aircraft. Even if the extreme net 0.016 K temperature change is taken from Table 4.6, some 900 to 1,000 Concorde-type SSTs would be required to create the HAPP guideline change of 0.1 K.

4.4.3 Other Effects

A. Carbon Dioxide

COMESA comments on CO_2 were noted in Section 4.3.3 E. Here some further discussion and quantification is offered.

The lifetime of CO_2 in the atmosphere appears to be long in comparison to stratospheric-tropospheric interchange processes (see e.g., Machta, 1973) so that to first order, at least, it would seem to be of little importance whether CO_2 from aircraft is added to the stratosphere or the troposphere. Hence, to make a crude upper-bound estimate of the climate effects of CO_2 from aircraft, we need only to select a time interval of interest, compute the total CO_2 added by aircraft, thus ignoring any sinks, and compare the results to values considered either in modeling studies as, e.g., Manabe and Wetherald (1967).

To illustrate, consider the "expected" fleet, as defined by CIAP, for the period 1970-2000 (see p. D-88, CIAP ROF). The integrated total kerosene consumed in this period is about 2×10^{12} kg, which would produce about 6×10^{12} kg of CO_2 . Assuming, as a limiting case, that none of this CO_2 leaves the atmosphere, the increased CO_2 could correspond to $6 \times 10^{12} / 5 \times 10^{18}$ or 1.2 ppm on a mass basis; on a volumetric basis, the figure drops to about 0.8 ppm. According to Machta (1973), interpreting Manabe-Wetherald, an increase of 65 ppm corresponds to a warming of about 0.5°C . The integrated net effect of aircraft, based on the figures given on p. D-88, CIAP Report of Findings, which excludes certain classes (traffic below 700 km) of aircraft, but without allowing for any loss mechanisms, would be $(0.8/65 \times 3.5)$ or about 0.006 K. The figure is small and essentially unavoidable, as all forms of traffic generate at least some extra CO_2 ; it is thus given no further consideration here.

B. Stratospheric Clouds and Contrails

The possible effects of contrails were noted in Section 4.4.3. The contrail problem is primarily a phenomenon associated with subsonics; however, as pointed out by Weickmann et al., (CIAP Monograph 3, pp. 7-31 to 7-33), a possibility exists that SSTs, particularly at Concorde altitudes in the tropics and the polar night, would generate persistent contrails. No quantification of these effects in terms of aircraft fleets is possible with available data.

4.5 CONCLUSIONS AND COMMENTS - CLIMATIC EFFECTS

The many uncertainties in the estimating procedures for climatic changes due to aircraft effluents should be clear from the description of the techniques employed and examination of Table 4.6. Many of these uncertainties are due to input data--size, shape, optical properties, aircraft-generated aerosols, background NO_2 and water vapor, etc.--on which, if effort is continued, gradual improvement in understanding can be expected. Other uncertainties, however, are related to the limited amount of modeling work performed to date, and to the fact that different models have been used, e.g., in computing aerosol effects and for computing gaseous constituent effects. Also, the distributions of expected changes in a vertical sense have not been incorporated in the modeling computations, nor have interactive effects (if any) of simultaneously injected pollutants been included: To obtain more useful temperature change estimates--estimates which would be based on internally consistent calculations, if not true climatic predictions--requires, in our opinion, as a minimum, the coupling of 1-D climate change models (radiative-equilibrium, constant relative humidity distribution, and cloud-top temperature or altitude) with 1-D kinetics codes. A 2-D model study would be preferred, permitting latitudinal distribution, and possibly certain feedback effects, to be incorporated. These combined codes should incorporate techniques for including water vapor, NO_2 , SO_2 , particulates (with settling), NO_x , and ozone changes.

In view of the above comments, it is clear that considerably more study would be required before firm conclusions could be drawn on the various climate change issues. Available models do, however, lead to the preliminary conclusion that the various individual climatic effects, and particularly the net effects, of forecast SST fleets through 1990 would be extremely small. It might also be noted that, according to available models, fuel desulfurization, which might be desirable, for example, from a stratospheric optical depth standpoint, or NO_x emission index reduction, would increase net climatic warming.

Improved climate modeling would seem to be a particular requirement should a large advanced SST be proposed. The reasons may not be obvious, in view of the small effects computed herein for a modest fleet, and the small effects reported by COMESA for a "1000-Concorde" fleet. However, if higher altitude aircraft are proposed, and if the longer residence times associated with such altitudes and with the atmospheric dynamics implied by the Hunten/1974 K_z profile are used, the effects from plausible fleets approach the 0.1-K criterion suggested in the HAPP sidelines. These issues are further discussed in Appendix F, where possible emission constraints on new SSTs are discussed.

APPENDIX A

STUDY OF THE EFFECTS ON ATMOSPHERIC OZONE OF NO_x EMISSIONS FROM
SUBSONIC AND SUPERSONIC AIRCRAFT USING THE CRUTZEN 2-D MODEL

H. Hidalgo

APPENDIX A

STUDY OF THE EFFECTS ON ATMOSPHERIC OZONE OF NO_x EMISSIONS FROM SUBSONIC AND SUPERSONIC AIRCRAFT USING THE CRUTZEN 2-D MODEL

A.1 INTRODUCTION AND SUMMARY

Johnston and Quitevis (1974) have pointed out that there is a "cross-over" altitude for the direction (or sign) of atmospheric ozone effects from nitrogen oxides in the natural atmosphere. Their results indicated that below 13 km there is a net rate of (local) ozone formation from the methane oxidation reactions; whereas, above 13 km there is a net rate of (local) ozone destruction from the NO_x catalytic cycle. These competing local effects suggest that the altitude of aircraft NO_x emissions can also be important in determining the sign of the NO_x emission effects on the atmospheric ozone column above the ground. To determine the effect on the total ozone column for NO_x injections at any given flight altitude, the local ozone effects must be integrated vertically, which requires the coupling of transport and photochemical processes in an atmospheric model. Results of these effects are reported here, based on the use of (a) a two-dimensional (2-D) photochemical model developed by Crutzen (1975), and (b) hypothetical aircraft fleets, distributed latitudinally and operating in altitude bands typical of present subsonics, future subsonics, and present SSTs. Each fleet type is further assumed to operate individually so as to isolate the effect of flight altitude on the atmospheric ozone column.

The methane oxidation reactions are of relatively little importance in the stratosphere, and were not included in the recent CIAP (Grobecker et al., 1974) and NAS (1975) studies of the impact of stratospheric aviation on atmospheric ozone. However, because of the cross-over altitude at 13 km, the methane oxidation reactions can change the sign of the ozone column effects in such results for the lower flight altitude of the subsonics.

The results of this study, summarized below, are considered preliminary because they do not include certain effects (e.g., water vapor emissions, chlorine chemistry), which may be important; furthermore, the methane oxidation reactions are not well characterized. Details follow the summary of results. These include, in the specified order, the modeling of the natural atmosphere, assumed aircraft NO_x emissions, numerical experiments performed, ozone and NO_x perturbations from the aircraft emissions, latitudinal averages of the ozone perturbations, approach to equilibrium conditions in the

natural and perturbed atmospheres, correlation of model results, and outstanding problem areas for further numerical investigations.

The results of this study are summarized in Table A-1. The first column shows the assumed average cruise altitudes for the present subsonics (10.8 km), future subsonics (12.7 or 14.5 km), and present SSTs (18 km). The second column gives the assumed total NO_x emission rate for each aircraft type, which are distributed as a function of latitude (see Fig. A-9). This latitudinal distribution assumes the heaviest traffic at middle northern latitudes. Aircraft numbers equivalent to the total NO_x emission rates cannot be established with confidence, inasmuch as aircraft operate over various altitudes during any given flight. However, to provide some appreciation of these NO_x rates, the NAS (1975) emission indexes, based on current engines, can be used. On this basis, the total NO_x emission rates listed in the second column of the table would correspond to 5282 subsonics, 1167 advanced subsonics, and 360 SSTs.

TABLE A-1. OZONE CHANGE MODEL RESULTS AFTER SIX YEARS OF INTEGRATION FOR VARIOUS INJECTION ALTITUDES; LATITUDINALLY DISTRIBUTED

Average Cruise Altitude, km*	NO_x Rate, 10^9 kg/yr (as NO_2)	O_3 Column Change, Percent and Column (Natural), D.U.** 45° N, August 30			O_3 Column Change, Percent, Annual Average		
		0-12.7 km (32.8 D.U.)	12.7-55 km (295.8 D.U.)	0-55 km (328.6 D.U.)	Hemispherical		
					North	South	Global
10.8	2.06	6.71	0.10	0.76	0.39	-0.002	0.19
12.7	0.455	1.52	0.03	0.18	0.08	-0.019	0.03
14.5	0.455	0.91	-0.10	0	-0.05	-0.057	-0.05
18.0	0.266	0.0	-0.54	-0.49	-0.42	-0.127	-0.27

* NO_x was distributed over 1.8 km centered at these altitudes.

** Dobson Units, m-atm-cm.

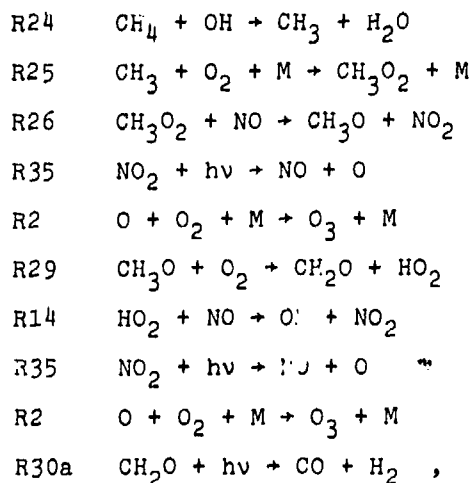
The third to fifth columns in the table give the percentage change at 45° N in the "tropospheric" (0 to 12.7 km), "stratospheric" (12.7 to 55 km), and total (0 to 55 km) ozone columns. Note that only about 10 percent (32.8 D.U.) of the total ozone (328.6 D.U.) is in this 0 to 12.7 km region of the atmosphere, so that small absolute changes correspond to large percentage changes; the data in the fifth column show that ozone column enhancements result from NO_x injections at 10.8 and 12.7 km, no change results for injections at 14.5 km, and depletion occurs with 18.0 km injections. The distribution of these changes between the "tropospheric" and "stratospheric" portions of the ozone column can be noted from the third and fourth columns.

The last three columns give the hemispheric and global annual averages of the percent change of the total ozone column.

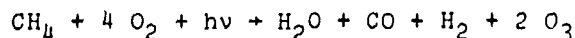
These preliminary results indicate that a slight enhancement of the ozone column results from NO_x injections by present subsonics, while a depletion occurs with supersonic aircraft. Advanced subsonics, such as the recently introduced 747SP, operate at a maximum altitude of 13.7 km, at which altitude there appears to be little (positive) or no effect on the ozone column.

A.2 MODELING OF THE NATURAL ATMOSPHERE

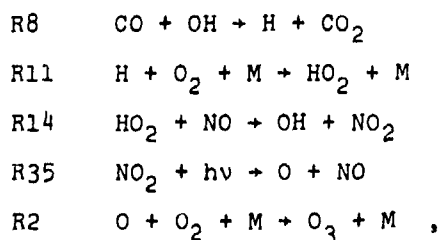
The modeling of the CH_4 - HO_x - O_x - NO_x system for the natural and perturbed atmospheres is based on the reactions given in Table A-2 (Crutzen, 1975; see also Hidalgo and Crutzen, 1976). It is important to note that Table A-2 includes the conventional O_x (R1 to R5), HO_x and NO_x , but not the ClO_x systems.* The production of ozone from the methane oxidation reactions in the presence of NO_x becomes evident by considering the following reactions (Crutzen, 1974):



which yields the balance B_1



These reactions are followed by:



*Following earlier practice, NO_x emissions from aircraft are quoted on a mass basis as equivalent NO_2 . NO_x in the atmosphere is defined here on a volumetric basis as the sum of the $\text{NO} + \text{NO}_2 + \text{NO}_3 + 2 \text{N}_2\text{O}_5$.

TABLE A-2. REACTION SCHEME AND COEFFICIENTS*

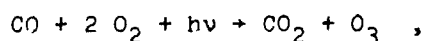
Oxygen Reactions	
R1	$O_2 + h\nu \rightarrow O + O$
R2	$O + O_2 + M \rightarrow O_3 + M$
R3a	$O_3 + h\nu \rightarrow O_2 + O(^1D)$
R3b	$O_3 + h\nu \rightarrow O_2 + O$
R4	$O_3 + O \rightarrow O_2 + O_2$
R5	$O(^1D) + M \rightarrow O + M$
Reactions Defining Relative Concentrations of Odd Hydrogen Related Species	
R6	$O + OH \rightarrow H + O_2$
R7	$O_3 + OH \rightarrow HO_2 + O_2$
R8	$CO + OH \rightarrow H + CO_2$
R9	$H_2 + OH \rightarrow H + H_2O$
R10	$O_3 + H \rightarrow OH + O_2$
R11	$O_2 + H + M \rightarrow HO_2 + M$
R12	$O + HO_2 \rightarrow OH + O_2$
R13	$C_3 + HO_2 \rightarrow OH + 2 O_2$
R14	$HO_2 + NO \rightarrow OH + NO_2$
R15	$OH + NO_2 (+M) \rightarrow FNO_3 (+M)$
R16	$HNO_3 + h\nu \rightarrow OH + NO_2$
R17	$HO_2 + HO_2 \rightarrow H_2O_2 + O_2$
R18	$H_2O_2 + h\nu \rightarrow OH + OH$
Production and Loss Reactions for Odd Hydrogen	
R19a	$H_2O + O(^1D) \rightarrow OH + OH$
R19b	$CH_4 + O(^1D) \rightarrow CH_3 + OH$
R19c	$H_2 + O(^1D) \rightarrow H + OH$
R20	$H + HO_2 \rightarrow H_2 + O_2$
R21	$OH + HO_2 \rightarrow H_2O + O_2$
R22	$OH + H_2O_2 \rightarrow H_2O + HO_2$
R23	$OH + HNO_3 \rightarrow H_2O + NO_3$
	$\lambda < 242 \text{ nm}$
	$k_2 = 1.1 \times 10^{-34} \exp(500/T)$
	$\lambda < 310 \text{ nm}$
	$\lambda < 1140 \text{ nm}$
	$k_4 = 1.9 \times 10^{-11} \exp(-2300/T)$
	$k_5 = 6.0 \times 10^{-11}$
	$k_6 = 4.2 \times 10^{-11}$
	$k_7 = 1.6 \times 10^{-12} \exp(-1000/T)$
	$k_8 = 2.1 \times 10^{-13} \exp(-75/T)$
	$k_9 = 2.3 \times 10^{-11} \exp(-2450/T)$
	$k_{10} = 2.6 \times 10^{-11}$
	$k_{11} = 2.1 \times 10^{-32} \exp(290/T)$
	$k_{12} = 2.0 \times 10^{-11}$
	$k_{13} = 1.0 \times 10^{-13} \exp(-1250/T)$
	$k_{14} = 2.2 \times 10^{-13}$
	$k_{15} = [4.2 \times 10^{-22} \exp(-170/T)(M)] \sigma^{-1}$
	$\lambda < 546 \text{ nm}$
	$\sigma = 4 \times 10^{-11} (M) + 1.6 \times 10^{-2} T$
	$k_{17} = 3.0 \times 10^{-11} \exp(-500/T)$
	$\lambda < 565 \text{ nm}$
	$k_{19a} = 3.0 \times 10^{-10}$
	$k_{19b} = 4.0 \times 10^{-10}$
	$k_{19c} = 3.0 \times 10^{-10}$
	$k_{20} = 10^{-11}$
	$k_{21} = 5.0 \times 10^{-11}$
	$k_{22} = 1.7 \times 10^{-11} \exp(-900/T)$
	$k_{23} = 9 \times 10^{-14}$

TABLE A-2. (Continued)

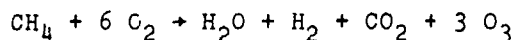
Methane Oxidation Reactions	
R24	$\text{OH} + \text{CH}_4 \rightarrow \text{H}_2\text{O} + \text{CH}_3$
R25	$\text{CH}_3 + \text{O}_2 + \text{M} \rightarrow \text{CH}_3\text{O}_2 + \text{M}$
R26	$\text{CH}_3\text{O}_2 + \text{NO} \rightarrow \text{CH}_3\text{O} + \text{NO}_2$
R27	$\text{CH}_3\text{O}_2 + \text{HO}_2 \rightarrow \text{CH}_3\text{O}_2\text{H} + \text{O}_2$
R28	$\text{CH}_3\text{O}_2\text{H} + \text{hv} \rightarrow \text{CH}_3\text{O} + \text{OH}$
R29	$\text{CH}_3\text{O} + \text{O}_2 \rightarrow \text{CH}_2\text{O} + \text{HO}_2$
R30a	$\text{CH}_2\text{O} + \text{hv} \rightarrow \text{H}_2 + \text{CO}$
R30b	$\text{CH}_2\text{O} + \text{hv} \rightarrow \text{H} + \text{CHO}$
R31	$\text{CH}_2\text{O} + \text{OH} \rightarrow \text{H}_2\text{O} + \text{CHO}$
R32	$\text{CHO} + \text{O}_2 \rightarrow \text{HO}_2 + \text{CO}$
Odd Nitrogen Reactions	
R33	$\text{NO} + \text{O}_3 \rightarrow \text{NO}_2 + \text{O}_2$
R34	$\text{NO}_2 + \text{O} \rightarrow \text{NO} + \text{O}_2$
R35	$\text{NO}_2 + \text{hv} \rightarrow \text{NO} + \text{O}$
R36	$\text{N} + \text{O}_3 \rightarrow \text{NO} + \text{O}_2$
R37	$\text{N} + \text{O}_2 \rightarrow \text{NO} + \text{O}$
R38	$\text{N} + \text{OH} \rightarrow \text{NO} + \text{H}$
R39	$\text{N} + \text{HC}_2 \rightarrow \text{NO} + \text{OH}$
R40	$\text{NO} + \text{hv} \rightarrow \text{N} + \text{O}$
R41	$\text{N} + \text{NO} \rightarrow \text{N}_2 + \text{O}$
R42	$\text{N}_2\text{O} + \text{hv} \rightarrow \text{N}_2 + \text{O}$
R43a	$\text{N}_2\text{O} + \text{O}(^1\text{D}) \rightarrow \text{NO} + \text{NO}$
R43b	$\text{N}_2\text{O} + \text{O}(^1\text{D}) \rightarrow \text{N}_2 + \text{O}_2$
R44	$\text{NO}_2 + \text{O}_3 \rightarrow \text{NO}_3 + \text{O}_2$
R45	$\text{NO}_3 + \text{hv} \rightarrow \text{NO}_2 + \text{O}$
R46	$\text{NO}_3 + \text{NO} \rightarrow 2 \text{NO}_2$
R47	$\text{NO}_3 + \text{NO}_2 + \text{M} \rightarrow \text{N}_2\text{O}_5 + \text{M}$
R48	$\text{N}_2\text{O}_5 + \text{M} \rightarrow \text{NO}_2 + \text{NO}_3 + \text{M}$
R49	$\text{N}_2\text{O}_5 + \text{hv} \rightarrow \text{NO}_2 + \text{NO}_3$
	$k_{24} = 2.5 \times 10^{-12} \exp(-1660/T)$
	$k_{25} = 2.6 \times 10^{-31}$
	$k_{26} = 1.5 \times 10^{-12} \exp(-500/T), \text{ assumed}$
	$k_{27} = 3.0 \times 10^{-11} \exp(-500/T), \text{ assumed}$
	$J_{\text{CH}_3\text{O}_2\text{H}} = J_{\text{H}_2\text{O}_2}, \text{ assumed}$
	$k_{29} = 4.2 \times 10^{-13} \exp(-3000/T)$
	$\lambda \lesssim 350 \text{ nm}, J_{30a} = 1.1 \times 10^{-4}$
	$\lambda \lesssim 350 \text{ nm}, J_{30b} = 3.3 \times 10^{-5}$
	$k_{31} = 1.4 \times 10^{-11}$
	$k_{32} = 1.7 \times 10^{-13}$
	$k_{33} = 9.0 \times 10^{-13} \exp(-1200/T)$
	$k_{34} = 9.2 \times 10^{-12}$
	$\lambda < 400 \text{ nm}$
	$k_{36} = 3.0 \times 10^{-11} \exp(-1200/T)$
	$k_{37} = 1.1 \times 10^{-14} \exp(-3150/T)$
	$k_{38} = 5.3 \times 10^{-11}$
	$k_{39} = 2.0 \times 10^{-10}$
	$\lambda < 191 \text{ nm}$
	$k_{41} = 2.7 \times 10^{-11}$
	$\lambda < 337 \text{ nm}$
	$k_{43a} = 1.1 \times 10^{-10}$
	$k_{43b} = 1.1 \times 10^{-10}$
	$k_{44} = 1.23 \times 10^{-13} \exp(-2470/T)$
	Johnston & Graham (1974)
	$k_{46} = 8.7 \times 10^{-12}$
	$k_{47} = [1.2 \times 10^{-21} (\text{M})] / [2 \times 10^5 + 1.7 \times 10^{-10} (\text{M})]$
	$k_{48} = [4000 (\text{M}) \exp(-9650/T)] / [2 \times 10^8 + 1.7 \times 10^{-10} (\text{M})]$
	Johnston & Graham (1974)

*Units: two-body reactions, $\text{cm}^3 \text{ molecules}^{-1} \text{ s}^{-1}$; three-body reactions, $\text{cm}^6 \text{ molecules}^{-2} \text{ s}^{-1}$.

which yields the balance B_2

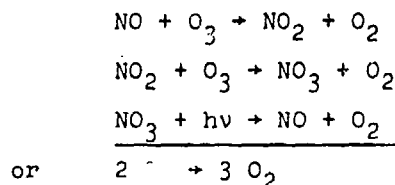


taking B_1 and B_2 together



In the stratosphere, the same reactions take place, but other reactions become more important. In the stratosphere, ozone content is far greater than in the troposphere, as is atomic oxygen generated from ozone by photolysis. As a result, in the stratosphere, addition of NO_x leads to net ozone destruction through the NO_x catalytic cycle, which is given by reactions R33 and R34.

Note in Table A-2 that the reaction rate for the critical reaction (R21) of $OH + HO_2 \rightarrow H_2O + O_2$ is taken as 6×10^{-11} , i.e., a geometrical mean value in the uncertainty range of $2 \times 10^{-11} < k_{21} < 2 \times 10^{-10}$, as considered by Duewer et al. (1976). Note also that Table A-2 incorporates N_2O_5 (R47, R48), which species can represent a significant fraction of the NO_x species. The reaction set as used did not include NO_3 photolysis to $NO + O_2$, a pathway which destroys ozone according to:



because this pathway for NO_3 photolysis was thought to be unimportant relative to R45, which has no effect on ozone. Current thinking based on late work by H. S. Johnston (D. Garvin, private communication, December 1976) is that about one-third of the NO_3 photolysis proceeds by this ozone-destroying path. Effects on the results presented here should be small, but need to be quantified*.

The modeling of the atmospheric dynamics is subject to two basic constraints: (1) the use of a time-dependent, three-dimensional (3-D) model of the atmosphere with the CH_4 - HO_x - O_x - NO_x system is not currently feasible with current operational computers. These constraints lead to the use of the simpler time-dependent, two-dimensional (2-D) models that use longitudinal or zonal averages of the conservation equations. The atmospheric dynamics is modeled by two components: (a) average circulations in the latitude-altitude meridional domain, and (b) eddy transports superimposed on the

*Note that Widhopf's results (Section 3.2.8) allowed one-third of the NO_3 photolyzed to proceed to $NO + O_2$, yet obtained significant ozone enhancements. More recent use of the Crutzen 1-D model also verifies these results (private communication, February 1977).

meridional circulations. In contrast with the use of 3-D models, the use of 2-D models requires an empirical representation of the eddy transports on all the scales of wave motions, i.e., the horizontal macroscale, mesoscale, and microscale, as well as the vertical mesoscale and microscale; or equivalently in the large scale as well as the subgrid scales of the numerical models; (2) the lack of statistics for the meridional circulation and eddy transports in the critical region of interest of the upper troposphere and lower stratosphere (Öort and Rasmusson, 1971). Because of these constraints, the 2-D model adopts the mean wind data derived by Louis (1974) as a function of season from considerations of observed temperature fields. The coefficients for the eddy poleward and vertical transports are obtained by "trial and error" to give the best agreement between the observed and calculated natural ozone column as a function of latitude and month in both hemispheres as well as that of the water vapor mixing ratio in the stratosphere.

The vertical resolution of the tropospheric-stratospheric 2-D model is defined by 31 pressure levels between 980 (level 1) and 0.415 mbar (level 31), which yield a vertical resolution between two consecutive levels of about 1.8 km. The vertical resolution in the lowest levels below 1.8 km is finer. The height interval chosen is about 0.45 km. The latitudinal resolution is 10 degrees. The time step in the numerical integrations is 2 hr, which allows a full one-year integration on the CDC 7600 computer in about 18.2 min. Other features of interest of this 2-D model are as follows: (a) mean daytime (sunlit hours) dissociation probabilities are calculated at the start of each 15-day period in a year that is assumed to have 360 days; (b) at night, the photochemistry is "frozen," except for the conversion of NO and NO₂ to NO₃ and N₂O₅; (c) the variation of the solar zenith angle during the year is closely simulated; and (d) the scattering of solar radiation is taken into account approximately at wavelengths $\lambda \geq 300$ nm (Crutzen and Isaksen, 1976).

Numerical integrations for the natural atmosphere were made for as long as 15 years. The numerical results provide data for the CH₄-HO_x-O_x-NO_x species in the meridional plane for every other month of the year (every 60 days), but with microfilm plots for every month. Numerical data is thus available for every 10 degrees latitude between 85° S and 85° N, and every pressure level between the ground (approximately level 1) and about 55-km altitude (level 31). The scope of the data includes total ozone column above any given pressure level, ozone concentration (molecules/cm³) and mixing ratio; atomic oxygen concentration; water volume mixing ratio; water humidity; cloudiness probability; water relative humidity; and the volume mixing ratio for the H₂, H, OH, HO₂, H₂O₂, NO, NO₂, HNO₃, NO₃, N₂O₅, NO_x, N₂O, CH₄, and CO species.

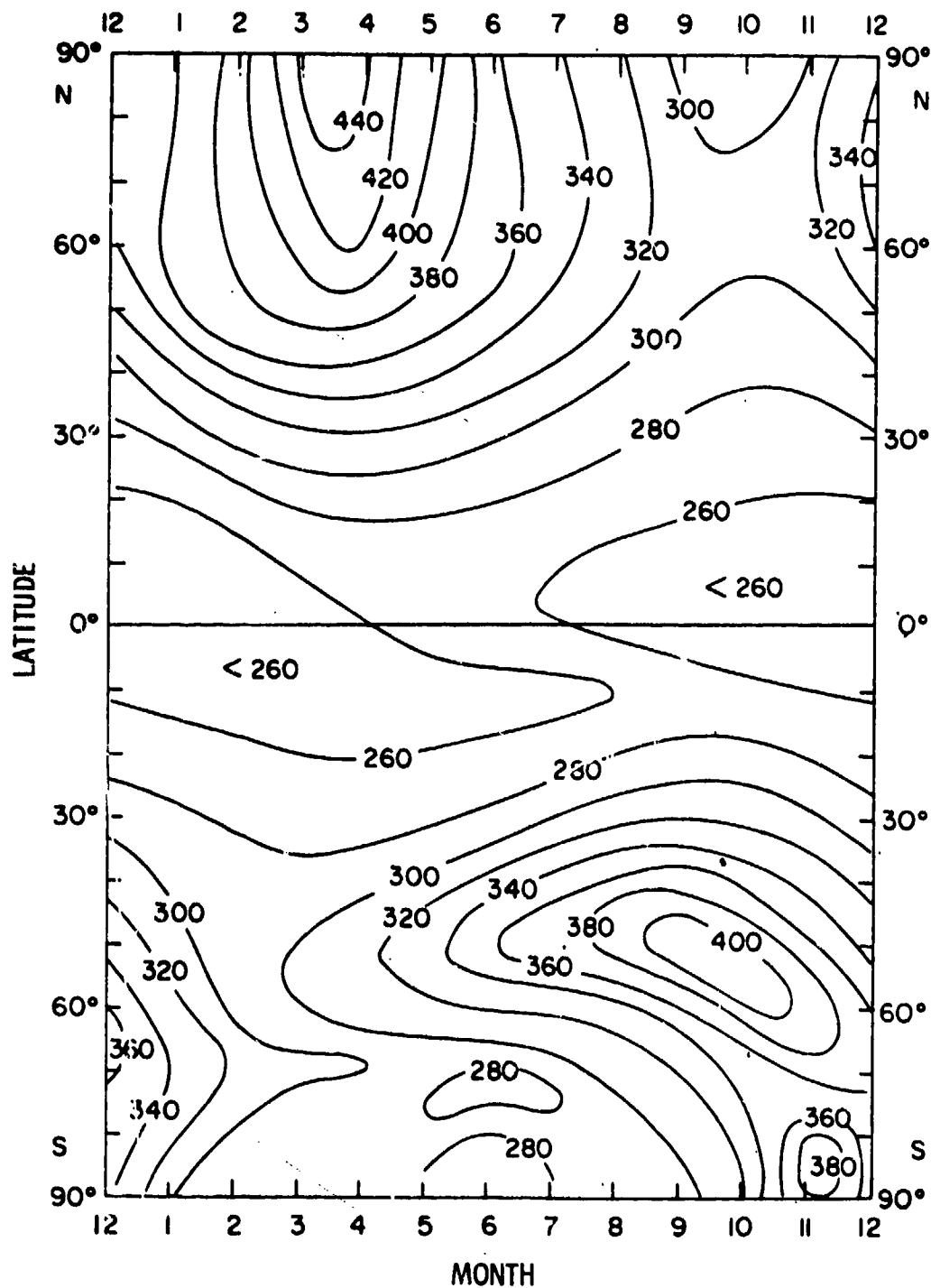
Figures A-1 and A-2 show the matching of the total ozone column as a function of latitude and month of the year. These figures show that the model satisfactorily duplicates the magnitude of the ozone column as well as its temporal and latitudinal gradients in both hemispheres. By further adjustments of the eddy transport coefficients, it would be possible to increase the accuracy in the matching of these characteristics of the ozone column in regions such as at high latitudes in the Southern Hemisphere. Figure A-3 shows the water vapor mixing ratio in the stratosphere during winter (December 30) in the Northern Hemisphere and summer in the Southern Hemisphere. This figure shows water mixing ratios in the stratosphere that are consistent with but perhaps somewhat higher than mean observations (Harries, 1973, 1976; Mastenbrook, 1974). Note that the mixing ratios in Fig. A-3 are lower (drier) than the original values reported by Crutzen (1975). The improved values in Fig. A-3 are the result of adjustments made to the horizontal eddy transports (K_{yy}) at low latitudes based on recent aerosol data from the Fuego volcanic eruption. The horizontal eddy transports are coupled to the vertical transports because of the "compression" of the atmosphere or isobaric surfaces with increasing latitude relative to the earth's surface.

Figures A-4 to A-8 illustrate meridional profiles during winter (December 30) in the Northern Hemisphere and summer in the Southern Hemisphere for the remaining species of interest in the $H_2O-CH_4-O_x-NO_x$ system. These species are, respectively, methane, ozone, atomic oxygen, nitrogen oxide plus nitrogen dioxide, and NO_x .

A.3 AIRCRAFT NO_x EMISSIONS

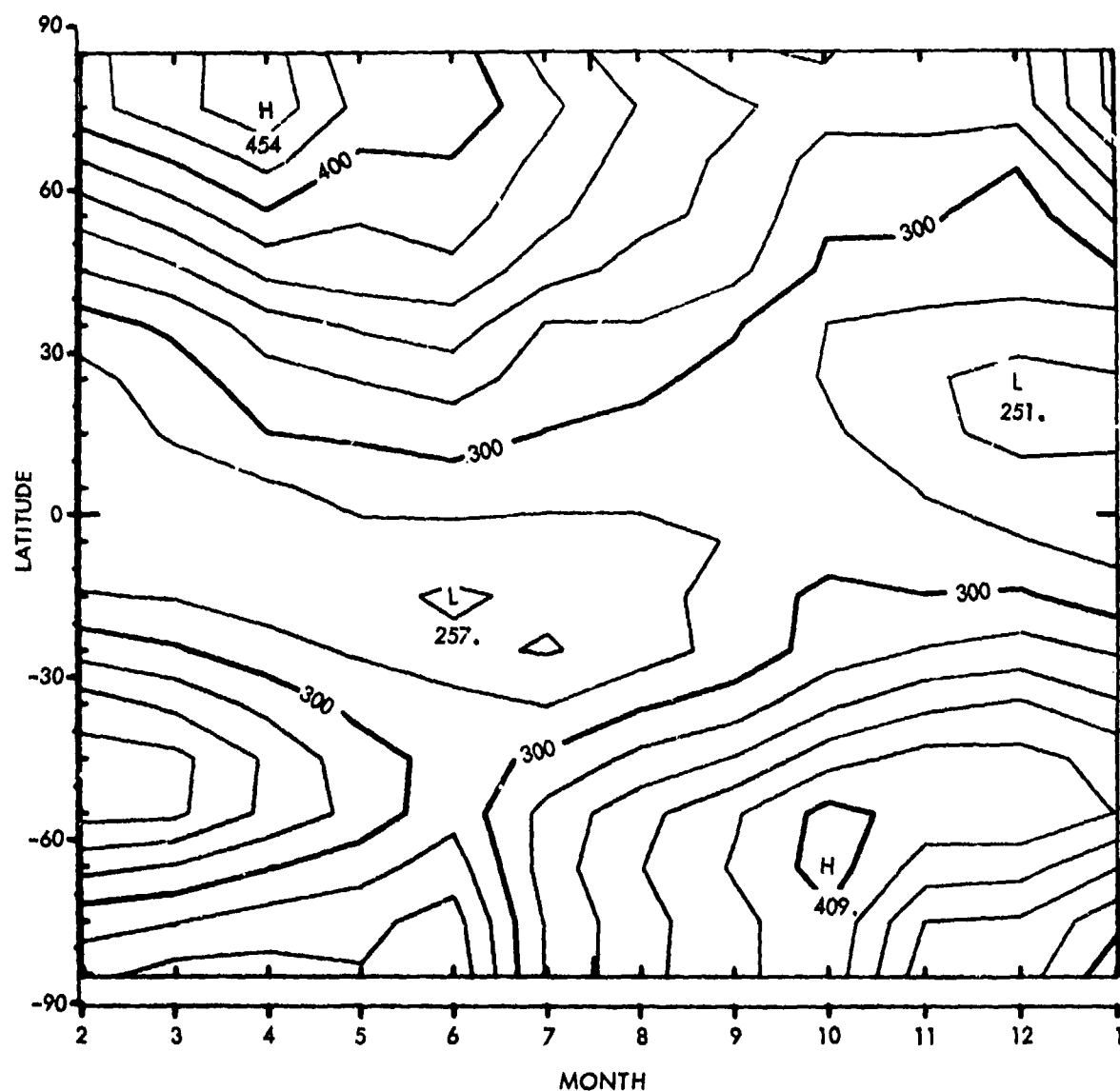
A set of NO_x emissions as a function of latitude and altitude was assumed to represent typical but hypothetical fleets that operate individually in an altitude range from 10.8 to 18 km. Figure A-9 shows the assumed NO_x emissions for three types of aircraft: current subsonics with an average cruise altitude of 10.8 km (35,500 ft), advanced subsonics with cruise altitudes at either 12.7 km (41,500 ft) or 14.5 km (47,500 ft)*, and supersonic transports or SSTs (Concorde and Tupolev) with cruise altitudes of 18 km (59,150 ft). This latter altitude is more representative of the Tupolev because the 18-km altitude represents about the peak altitude rather than the average cruise altitude of the present NO_x emissions for each type of aircraft. The emission levels for the present subsonic type are based on CIAP upper-bound projections to 1990 (English and Guo-An Pan, 1975), arbitrarily increased by 50 percent to account for short range (< 700 km) traffic ignored in

*These altitudes were dictated by the available model levels. A peak cruise altitude of 13.7 km (45,000 ft) is associated with an actual subsonic aircraft (the 747SP) now entering operation.



4-21-76-6

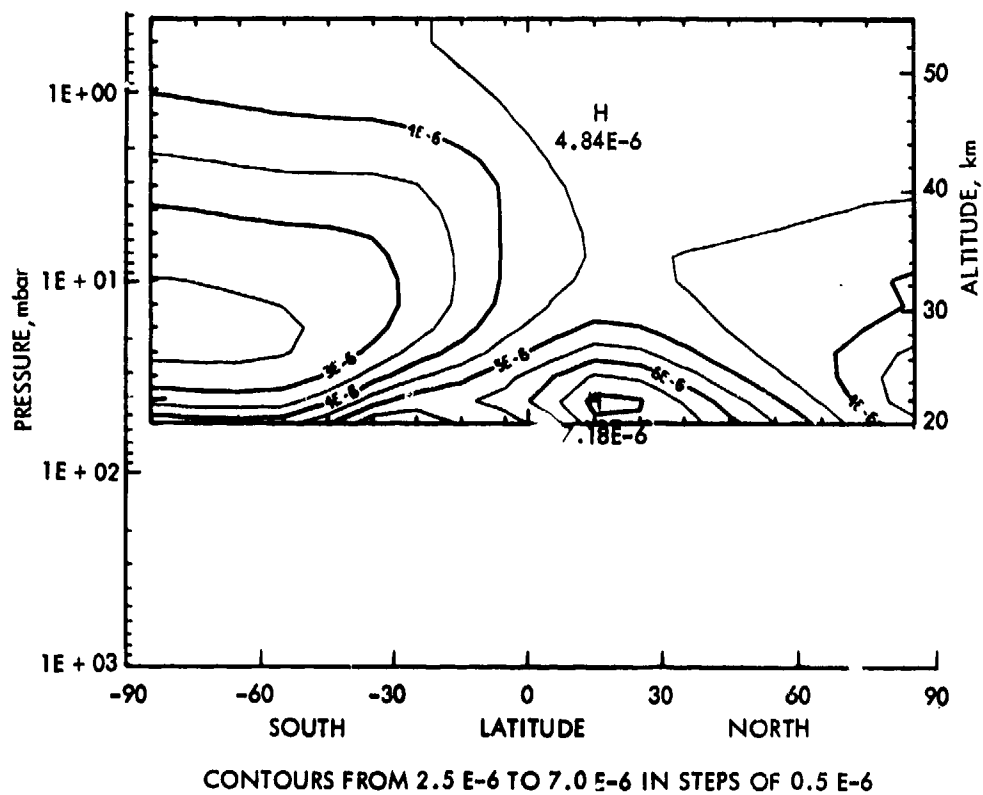
FIGURE A-1. Observed Total Ozone (m-atm-cm) as a Function of Season and Latitude in the Northern (London, 1963) and Southern (Sticksel, 1963) Hemispheres.
Source: H.U. Dütsch, 1971



4-21-76-7

CONTOURS FROM 200 TO 600 IN STEPS OF 20.0

FIGURE A-2. Model Natural Total Ozone (m-atm-cm) above Ground (L=1) as a Function of Latitude and Month of the Year after 15 Years of Integration. Note the asymmetric ozone distribution in the two hemispheres. Notations L and H denote "low" and "high" values, respectively.



6-11-76-12

FIGURE A-3. Natural Water Vapor Volume Mixing Ratio During Winter (December 30) in the Northern Hemisphere and Summer in the Southern Hemisphere after 15 Years of Integration. The mixing ratio values in the troposphere have been deleted to enhance the scale shown above 20-km altitude. The positive latitude values denote the Northern Hemisphere. For example, the notation 4E-6 denotes 4×10^{-6} .

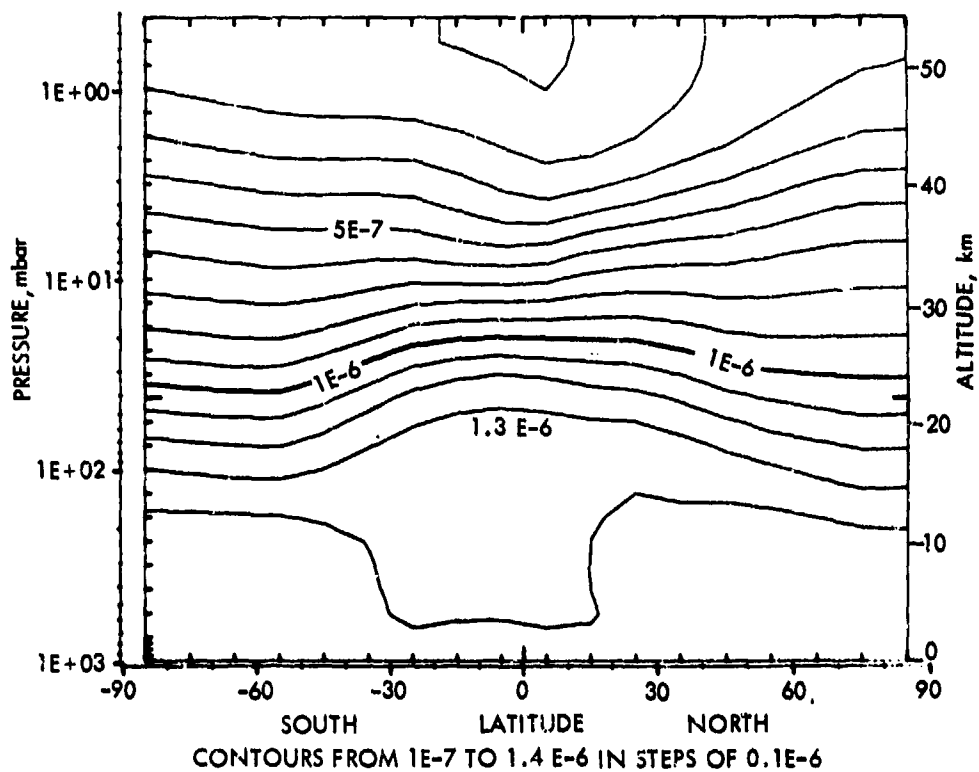


FIGURE A-4. Natural Methane Mixing Ratio During Winter (December 30) in the Northern Hemisphere and Summer in the Southern Hemisphere after 15 Years of Integration

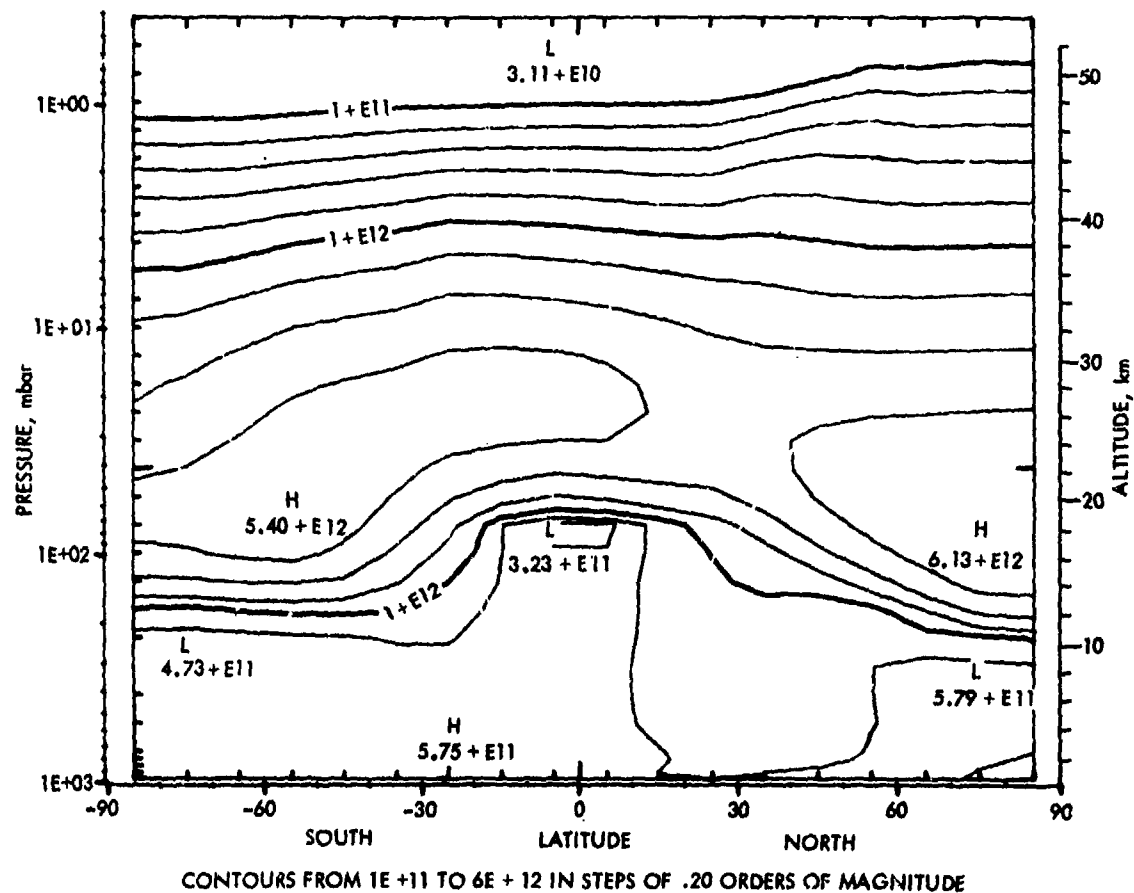
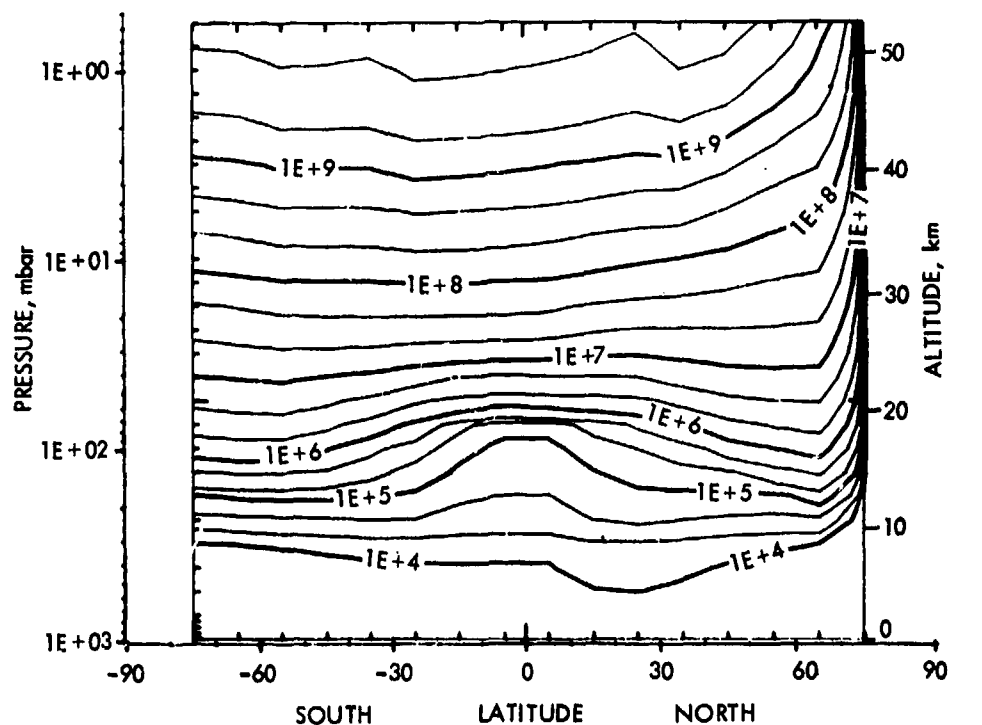


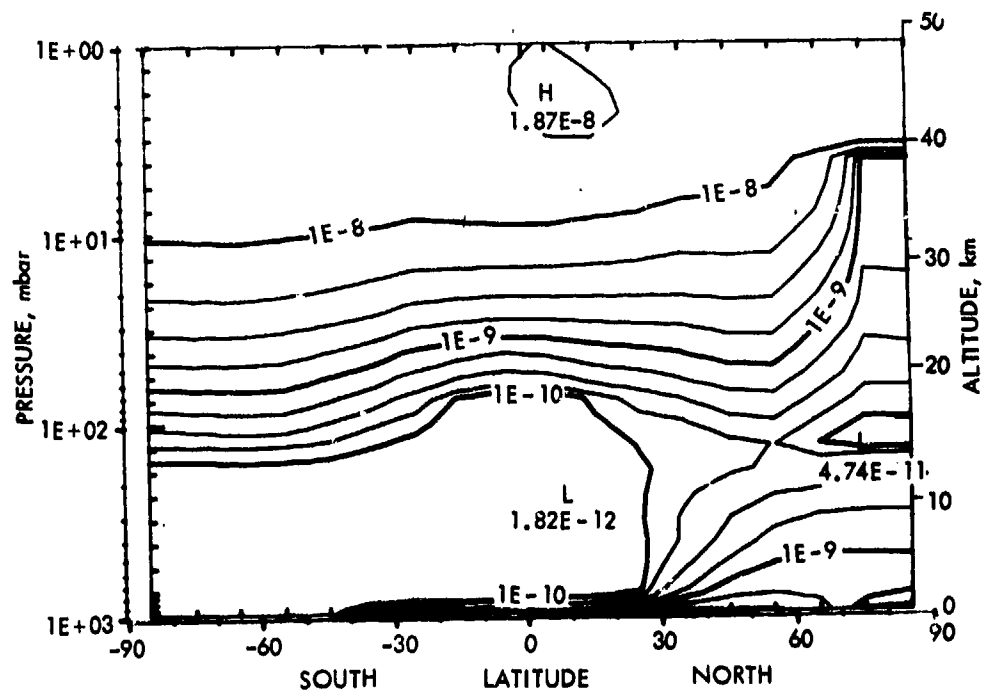
FIGURE A-5. Natural Ozone Concentration (molecules/cm^3) During Winter (December 30) in the Northern Hemisphere and Summer in the Southern Hemisphere after 15 Years of Integration



CONTOURS FROM $1\text{E} + 4$ TO $6.67\text{E} + 9$ IN STEPS OF .33 ORDERS OF MAGNITUDE

10-12-76-5

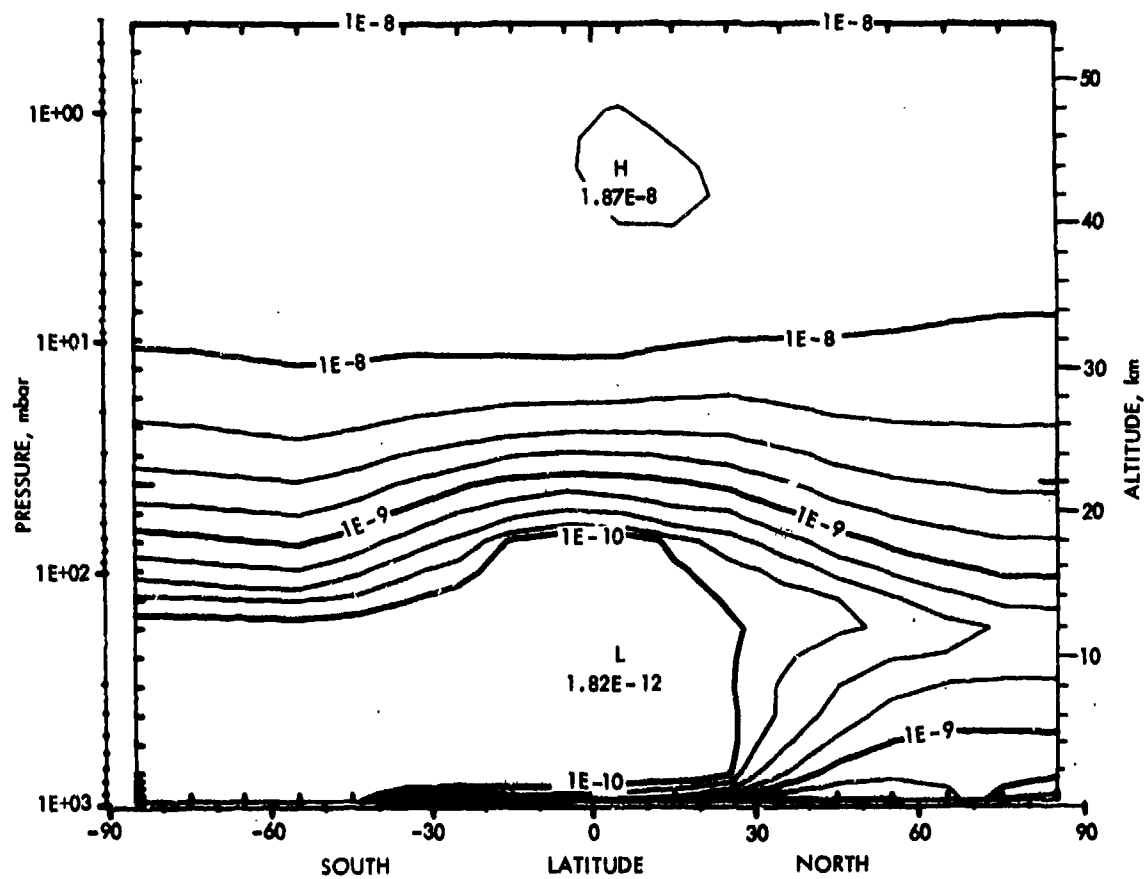
FIGURE A-6. Natural Atomic Oxygen Concentration (atoms/cm^3) During Winter (December 30) in the Northern Hemisphere and Summer in the Southern Hemisphere after 15 Years of Integration



CONTOURS FROM $1\text{E} - 10$ TO $1\text{E} - 8$ IN STEPS OF .25 ORDERS OF MAGNITUDE

10-12-76-6

FIGURE A-7. Natural $\text{NO} + \text{NO}_2$ Volume Mixing Ratio During Winter (December 30) in the Northern Hemisphere and Summer in the Southern Hemisphere after 15 Years of Integration



CONTOURS FROM $1\text{E}-10$ TO $1\text{E}-8$ IN STEPS OF .25 ORDERS OF MAGNITUDE

4-21-76-9

FIGURE A-8. Natural NO_x Volume Mixing Ratio During Winter (December 30) in the Northern Hemisphere and Summer in the Southern Hemisphere after 15 years of integration. Note that the NO_x mixing ratio increases with increasing altitude in the lower and middle stratosphere.

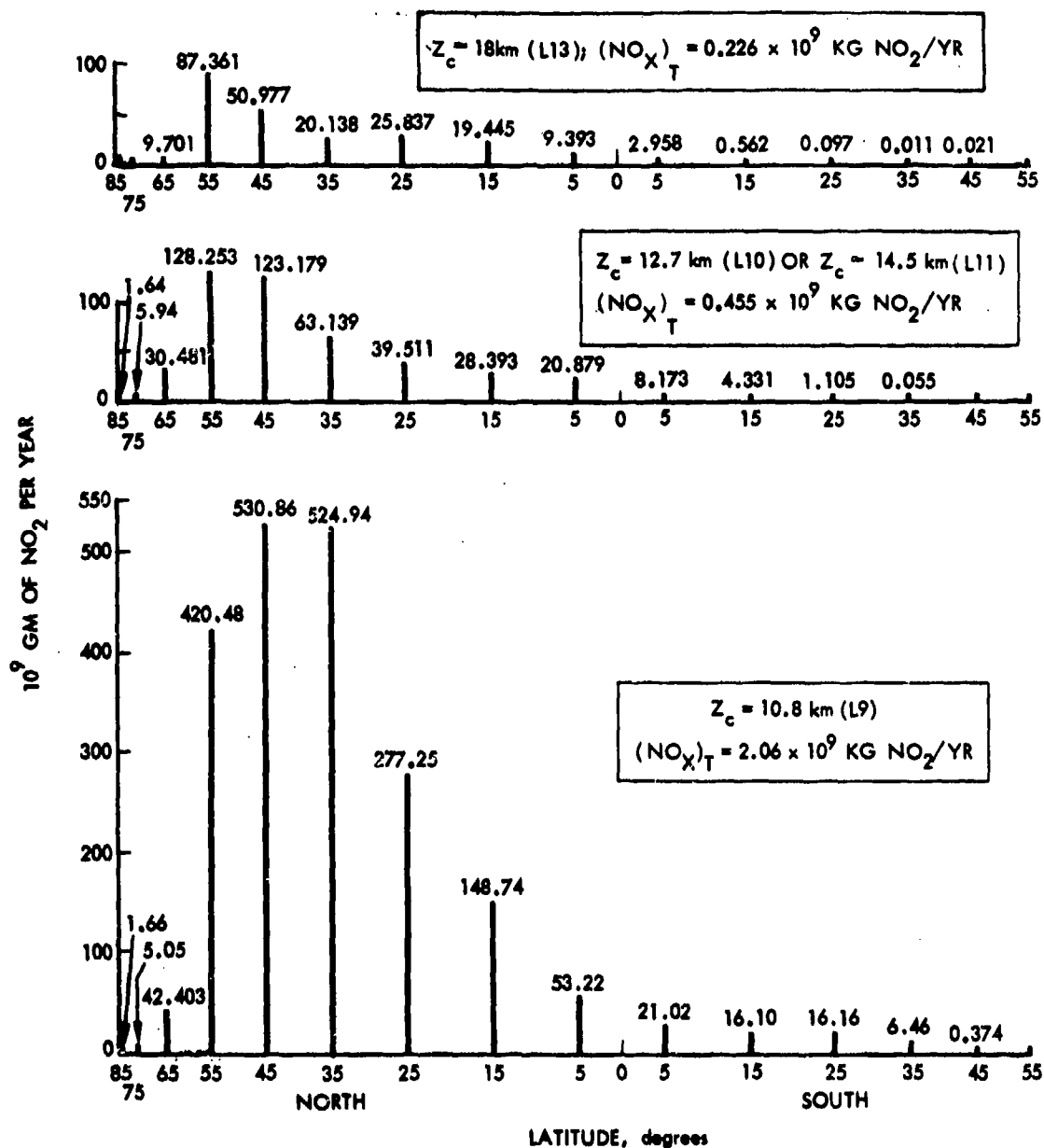


FIGURE A-9. Assumed NO_x Emissions (as NO_2) as a Function of Latitude at Model Levels 9, 10, 11, and 13.

CIAP. The emission levels at each altitude or model level were chosen to provide ozone changes high enough that they could be scaled down, instead of extrapolated, to lower NO_x emissions of practical interest. Because of the 1.8-km vertical resolution of the model, the aircraft NO_x emissions at a particular level are distributed uniformly about 0.9 km (approximately 3000 ft) above and below that level. This altitude distribution, of course, does not perfectly simulate real traffic, but provides an unambiguous model result.

An estimate of the number of aircraft for each of the fleets in Fig. A-9 may be derived by using, for example, the annual NO_x (as NO_2) rates per 100 aircraft for each aircraft type given in Table 4 of the National Academy of Sciences (1975) report. These NO_x rates are 39×10^6 kg of NO_x/yr for either present or advanced subsonics and 62.8×10^6 kg of NO_x/yr for present SSTs. On this basis, the number of aircraft for the fleets in Fig. A-9 would be 5282 subsonics, 1167 advanced subsonics, and 360 SSTs.

A.4 NUMERICAL EXPERIMENTS PERFORMED

Figure A-10 provides a summary of the numerical experiments performed using the 2-D model and the NO_x emissions for the three fleet types in Fig. A-9. The method used to calculate the small perturbations in the ozone column simulates two earth planets: a natural one, without aircraft flights; and a perturbed one with a particular type of aircraft, one at a time. This method is necessary to eliminate time effects, by comparing every perturbation with the corresponding natural state at the same time in the evolutions of the photochemical and dynamical processes in the natural and perturbed atmospheres.

The current 2-D model allows time integrations of up to 3 years to be performed for each numerical run, a constraint that stems from the extensive demand on computer time for such integrations. Thus, the numerical runs shown schematically in Fig. A-10 are made up of 3-year segments. The characteristics shown in Fig. A-10 are as follows:

- (1) Point A represents the initialization of the natural atmosphere, i.e., the atmospheric state derived after 3 years of integrations from the initial conditions at time $t = 0$.
- (2) Point B represents the state of the natural atmosphere 6 years subsequent to that of state A. Note that there are two paths for the natural atmosphere subsequent to point B: one path utilizes two segments (3 years each), and another one three segments (3, 2, and 1 years, respectively). This latter path was used to detect the effect, if any, of restarting procedures on the results.
- (3) The four paths starting at point B and designated by the end points as L9, L10, L11, and L13 represent the perturbation runs for NO_x

emissions at the respective model levels; i.e., L9 for emissions at 10.8 km, L10 at 12.7 km, L11 at 14.5 km, and L13 at 18 km. These altitudes correspond to summer (August 30) conditions. Since the pressure level (in millibars) remains fixed, there is a small variation in the corresponding level altitude with season.

- (4) The dashed B-L10 path represents an initial run that included the aircraft H₂O emissions.
- (5) The path A-L9 represents the following preliminary runs: (a) the first two 3-year segments are for NO_x emissions alone, and (b) the three subsequent segments of 1, 2, and 3 years include the H₂O emissions.

The results that included the H₂O emissions indicated no increase in stratospheric water vapor at the end of the third year. Since these results could not be understood, it was decided to exclude the effect of H₂O emissions on the ozone column during these numerical investigations.

A.5 OZONE AND NO_x PERTURBATIONS FROM AIRCRAFT EMISSIONS

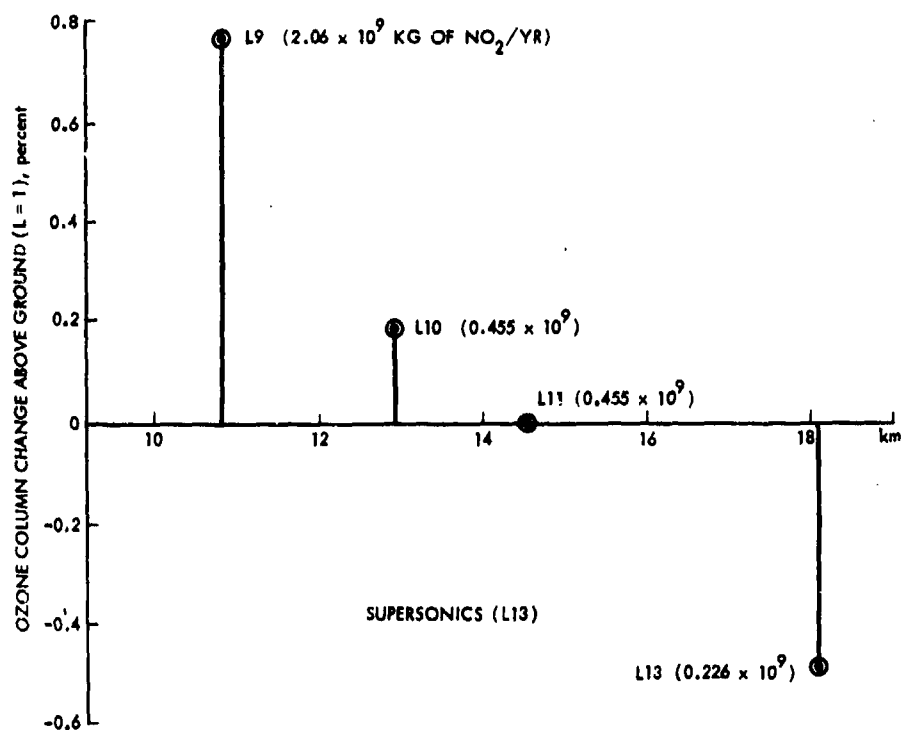
Before describing specific results from the foregoing numerical experiments, it is important to emphasize the following two factors:

- (a) The practical interest in the magnitude of the net change in the natural ozone column from aircraft NO_x emissions is more of the order of 1 percent than 10 percent (or more). The latter is a result of the usual hypothesis of an operation in the distant future (say, early in the 21st century) of a very large worldwide fleet of supersonic transports equipped with current engine technology (i.e., with an NO_x emission index of 18 g of NO₂/kg of fuel).
- (b) The summer season is of primary interest because it is characterized by the longest days at the middle northern latitudes of heavy traffic (Fig. A-9); i.e., by conditions that amplify the impact of the aircraft NO_x emissions on the biosphere.

Figure A-11 shows the change in the ozone column above the ground (or level 1), during summer (August 30) at 45° N latitude after the sixth year of integration for the present subsonics (L9), advanced subsonics (L10 or L11), and SST (L13). This figure indicates that the subsonics give an ozone increase of about 0.76 percent, an effect that decreases with increasing flight altitude of the advanced subsonics. The net increase of the ozone column for the present subsonics indicate that the effect of ozone production from the methane-smog reactions in the upper troposphere dominates over that of ozone destruction from the NO_x and HO_x catalytic cycles in the middle stratosphere. However, the ozone production mechanism from the methane-smog

reactions becomes weaker with increasing flight altitude; whereas the ozone destruction mechanism from the NO_x and HO_x catalytic cycles at the same time becomes more important (see Johnston, 1975). These two opposing effects become about equal at the 14.5-km altitude for level 11 of the advanced subsonics. The net decrease in the ozone column for the SSTs indicates that the effect of ozone destruction from the NO_x and HO_x catalytic cycles in the middle stratosphere dominates over that of ozone production from the methane-smog reactions in the upper troposphere.

SUBSONICS (LEVELS 9, 10, 11)



4-21-76-13

FIGURE A-11. Percent Change of Ozone Column above Ground ($L=1$) at Middle Northern Latitudes (45° N) During Summer (August 30) after 6 Years of NO_x Emissions from Subsonic and Supersonic Aircraft.

Figure A-12 shows the change in the ozone column above level 10 (12.7 km) during summer (August 30) at 45° N latitude after the sixth year of integration for the three types of aircraft fleet. The results in Figs. A-11 and A-12 indicate that, for the present subsonics, most of the increase of the ozone column above the ground (level 1) takes place below level 10. However, as the flight altitude increases, the perturbation of the ozone column

below level 10 by the methane-smog reactions become increasingly smaller. Thus, for the SSTs, the ozone perturbation is caused almost exclusively by the NO_x catalytic cycle in the stratosphere.

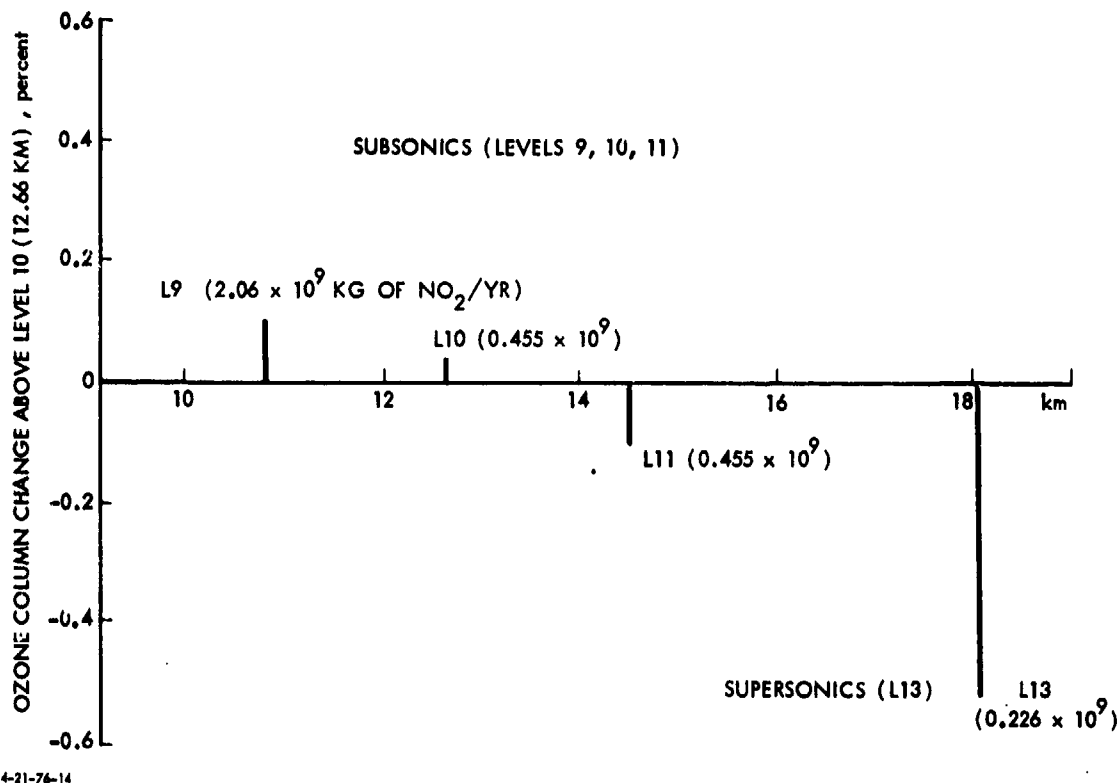


FIGURE A-12. Percent Change of Ozone Column above Level 10 (12.66 km) at Middle Northern Latitudes (45° N) during Summer (August 30) after 6 years of NO_x Emissions from Subsonic and Supersonic Aircraft.

A generalization of the foregoing results is given by Figs. A-13 to A-16, which show the perturbation of the ozone column above level 1 as a function of latitude and season after the sixth year of integrations for the present subsonics (L9), advanced subsonics (L10 or L11), and SSTs (L13). Figure A-13 shows that the present subsonics give the largest ozone increase (0.94 percent) during fall (October 30) at a latitude of about 35° N. Figure A-14 indicates the same relative seasonal effects, but at lower levels of the percent ozone increase. Figure A-16 shows that for the SSTs, the decreases in ozone as a function of latitude tend to become more independent of season.

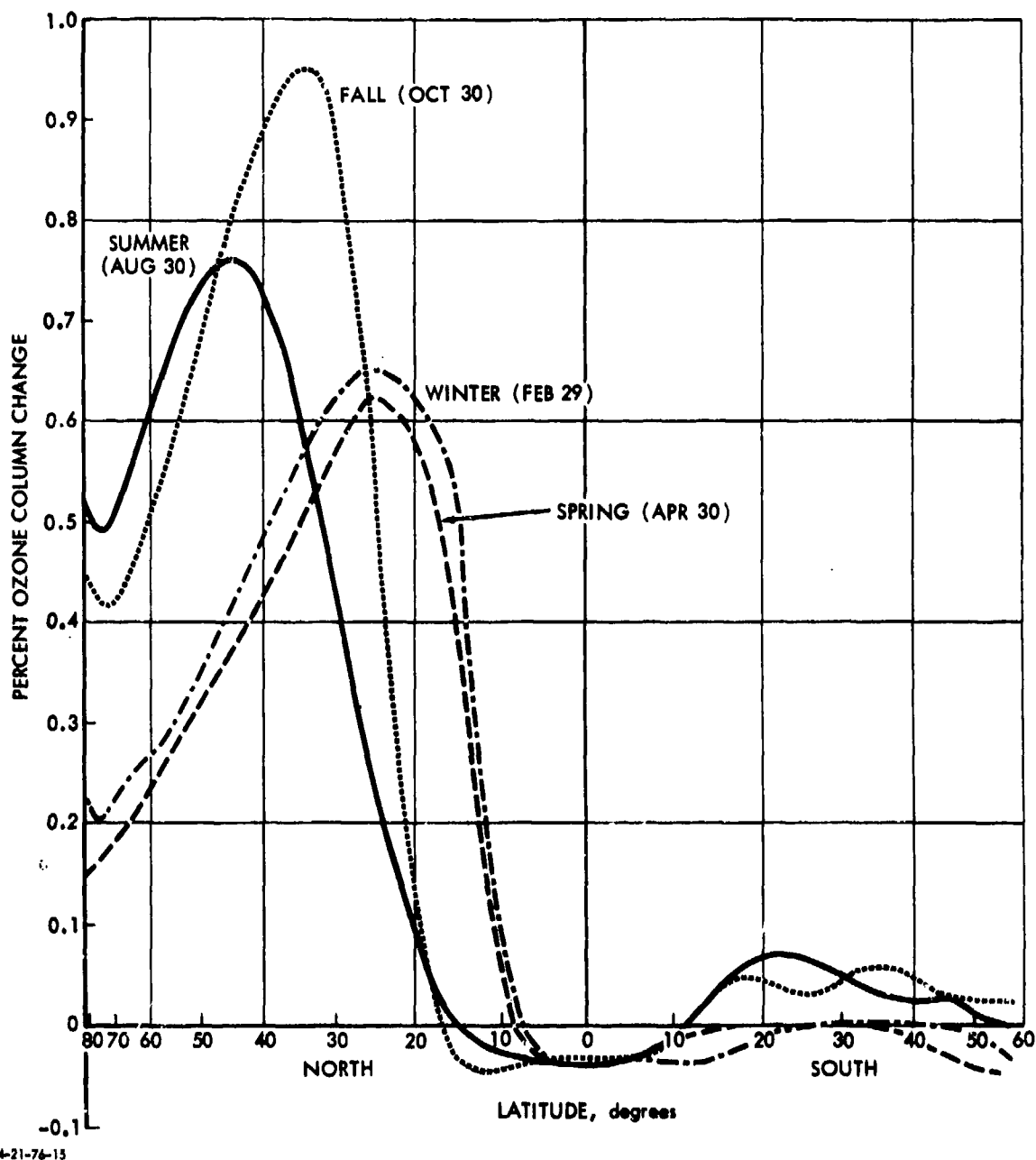
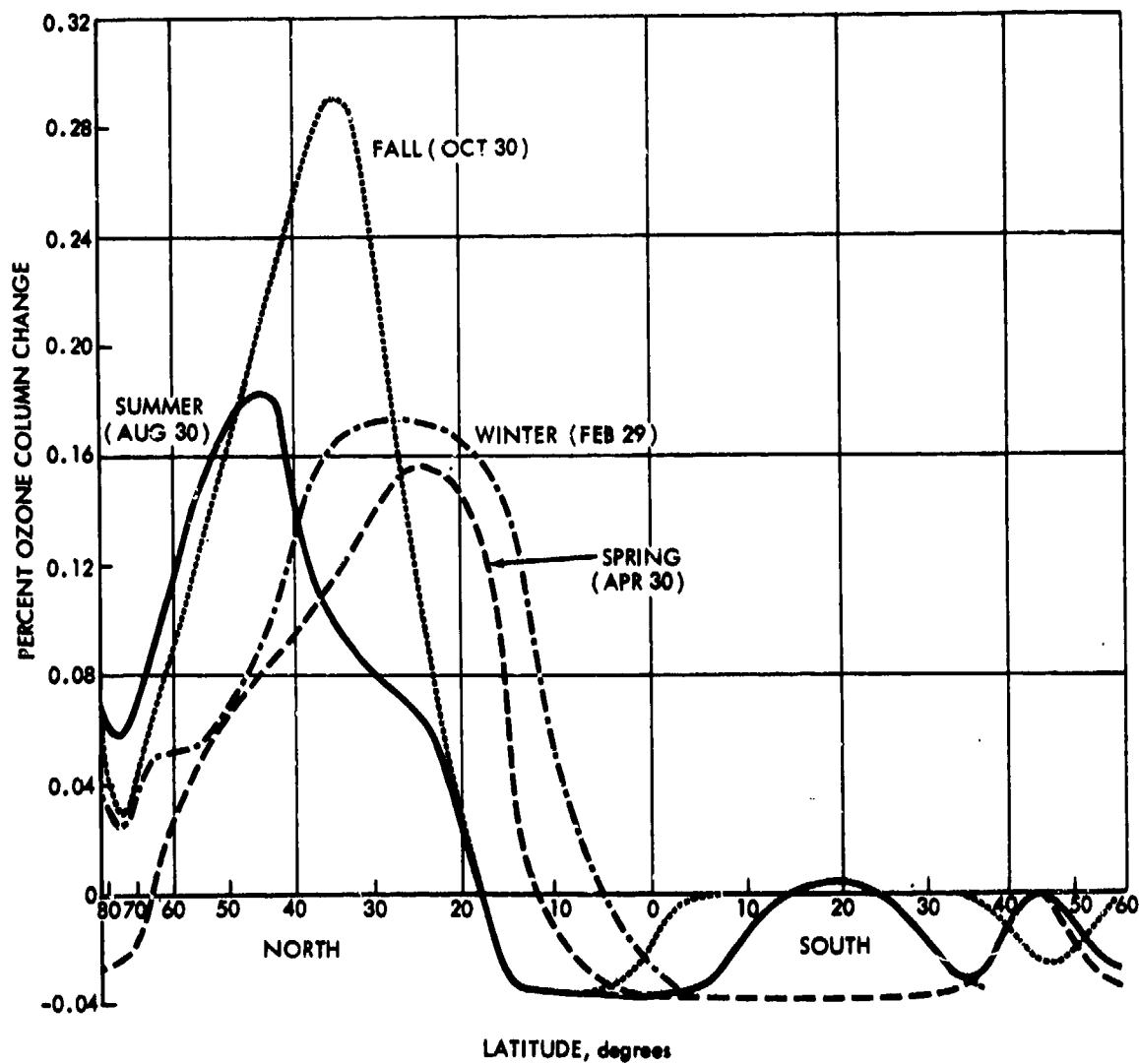
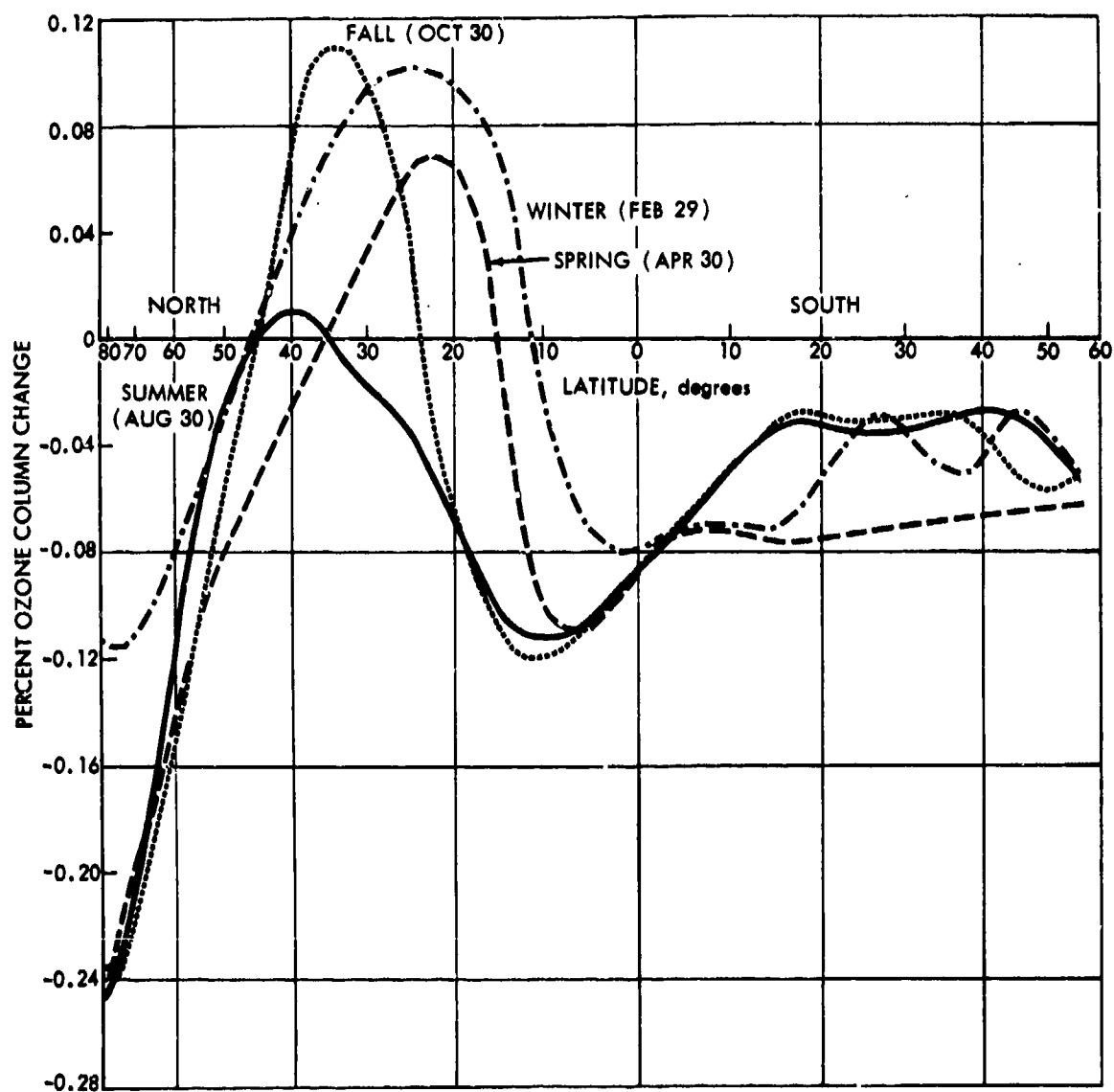


FIGURE A-13. Percent Ozone Column Change as a Function of Latitude and Season after 6 years of NO_x Emissions (2.06×10^9 kg of NO_2/yr) at 10.8-km Altitude ($L=9$)



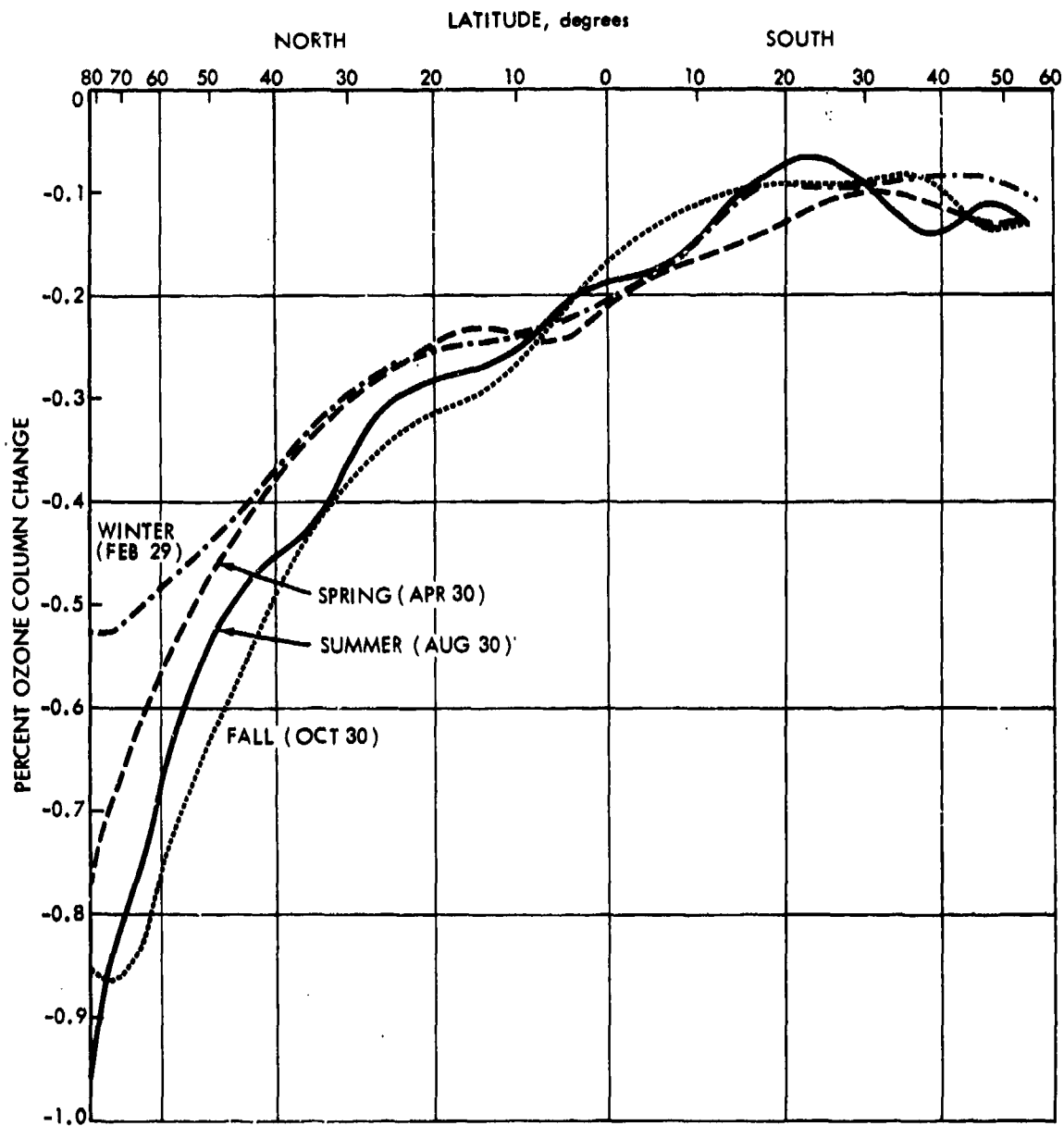
9-28-76-13

FIGURE A-14. Percent Ozone Column Change as a Function of Latitude and Season after 6 years of NO_x Emissions (0.455×10^9 kg of NO_2/yr) at 12.7-km Altitude ($L=10$)



5-28-76-13

FIGURE A-15. Percent Ozone Column Change as a Function of Latitude and Season after 6 Years of NO_x Emissions (0.455×10^9 kg of NO_2/yr) at 14.5-km Altitude ($L=11$)



5-28-76-14

FIGURE A-16. Percent Ozone Column Change as a Function of Latitude and Season after 6 years of NO_x Emissions (0.226×10^9 kg of NO_2/yr) at 18-km Altitude ($L=13$)

The vertical distribution of the natural ozone concentrations at 45° N during summer (August 30) is shown in Fig. A-17, whereas that of the ozone perturbations is shown in Fig. A-18. Figure A-17 shows the natural ozone concentration after 12 years of integrations subsequent to the initialization (Point A, Fig. A-10) of the natural atmosphere. This figure is thus a vertical cross section at 45° of the meridional ozone concentration as shown in Fig. A-5 for summer in the Southern Hemisphere. Figure A-17 shows a peak in the ozone concentration near 22-km altitude, and a low-altitude minimum of about 5.2×10^{11} molecules/cm³ at about 11-km altitude. The concentration at 11 km is higher by a factor of 4 than the corresponding value from the Chang 1-D model given in the CIAP Report of Findings by Grobecker et al. (1974). Figure A-18 shows the percent change in the natural ozone concentration (i.e., Fig. A-17) during summer (August 30) at 45° N latitude as a function of altitude after the sixth year of integration for the NO_x emissions from present subsonics (L9), advanced subsonics (L11), and SST (L13) types of aircraft. Note that for the NO_x emissions at level 9, the methane-smog reactions produce an 11.9 percent increase in the ozone concentration at the flight altitude (10.8 km); whereas the NO_x catalytic cycle produces a decrease in the ozone concentration above 19-km altitude. This figure shows that the stratospheric NO_x catalytic cycle dominates the effect of the methane-smog reactions for the NO_x emissions at level 13.

The corresponding vertical distributions of the natural and perturbed NO_x at 45° N during summer (August 30) are shown in Figs. A-19 and A-20. Figure A-19 shows the natural NO_x concentration after 12 years of integrations subsequent to the initialization of the natural atmosphere. This figure is also a vertical cross section at 45° N of the meridional NO_x distribution such as that shown in Fig. A-8 for June in the Southern Hemisphere. Figure A-19 shows a peak in the NO_x concentration near 27-km altitude, and a low-altitude minimum of about 4.4×10^8 molecules/cm³ at about 12-km altitude. Figure A-20 shows the percent change in the natural NO_x concentration (Fig. A-19) during summer (August 30) at 45° N latitude as a function of altitude after the sixth year of integrations for the NO_x emissions at levels 9, 11, and 13. Note that for the NO_x emissions at level 9, there is a 330 percent increase in NO_x at the flight altitude (10.8 km); i.e., at an altitude near the low altitude minimum of the natural NO_x concentration (Fig. A-19). Also, the NO_x increase above 20 km becomes larger as the flight altitude increases from level 9 for the present subsonics to level 13 for the SSTs.

A generalization of the vertical distributions for the NO_x increases to other latitudes and seasons is provided in Figs. A-21 and A-22. Figure A-21 indicates that the large vertical gradients in the NO_x increase at 45° N

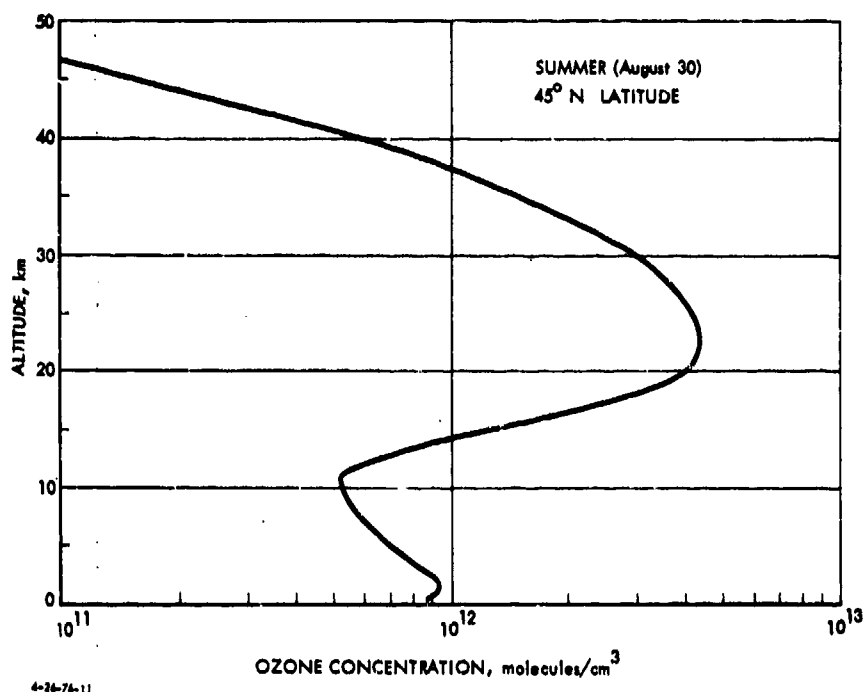


FIGURE A-17. Natural Ozone Concentration at Middle Northern Latitudes (45° N) during Summer (August 30) after 15 years of integration

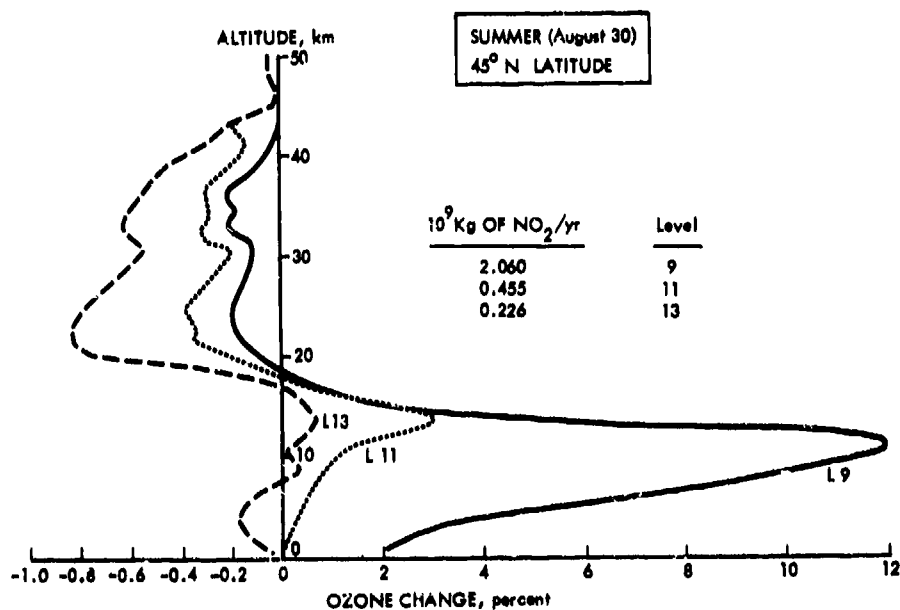


FIGURE A-18. Percent Change in Ozone Concentration at Middle Northern Latitude (45° N) during Summer as a Function of Altitude after 6 Years of Aircraft NO_x Emissions. Note that the negative scale is amplified by a factor of 5.

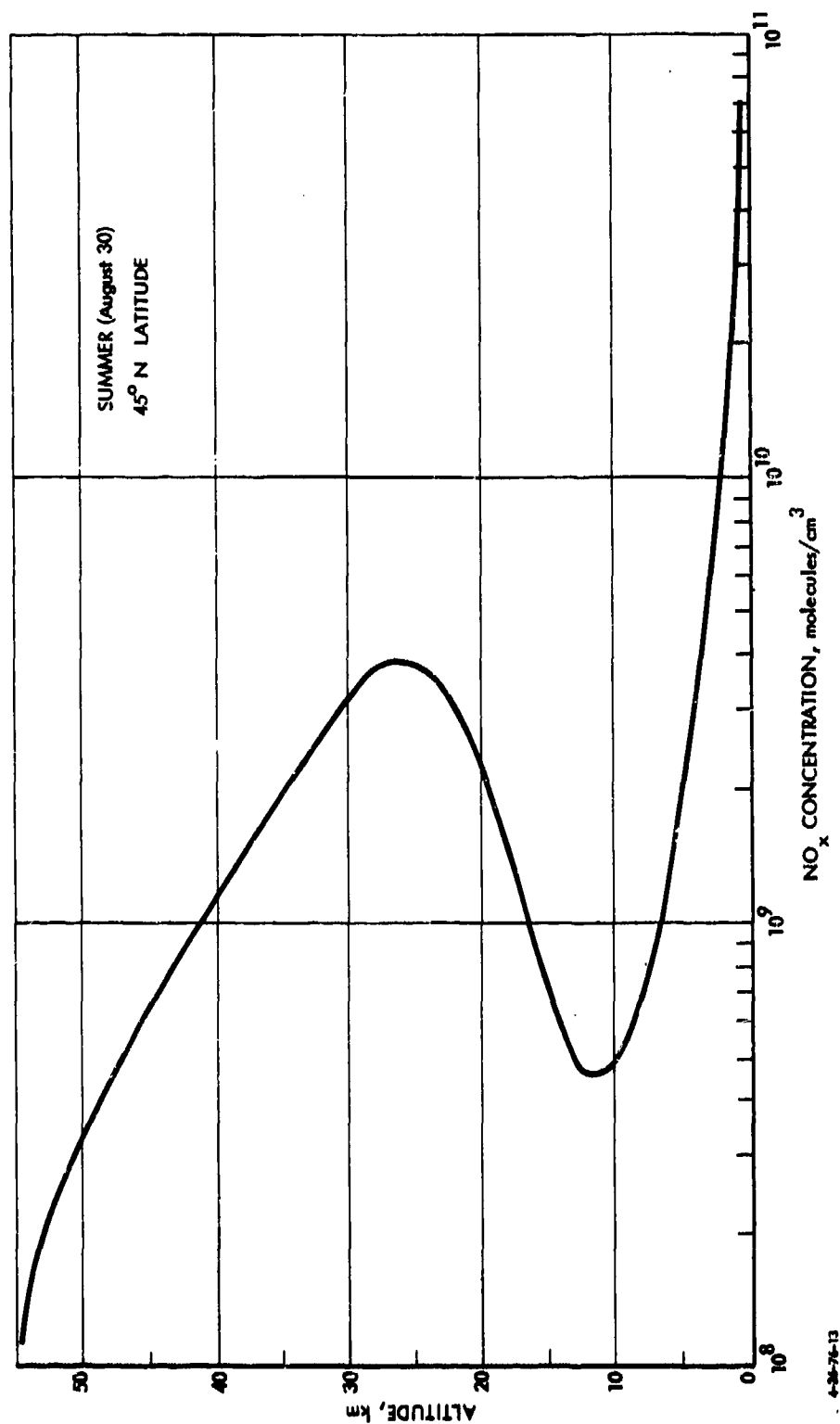


FIGURE A-19. Natural NO_x Concentration at Middle Northern Latitudes (45° N) during Summer (August 30) after 15 Years of Integration

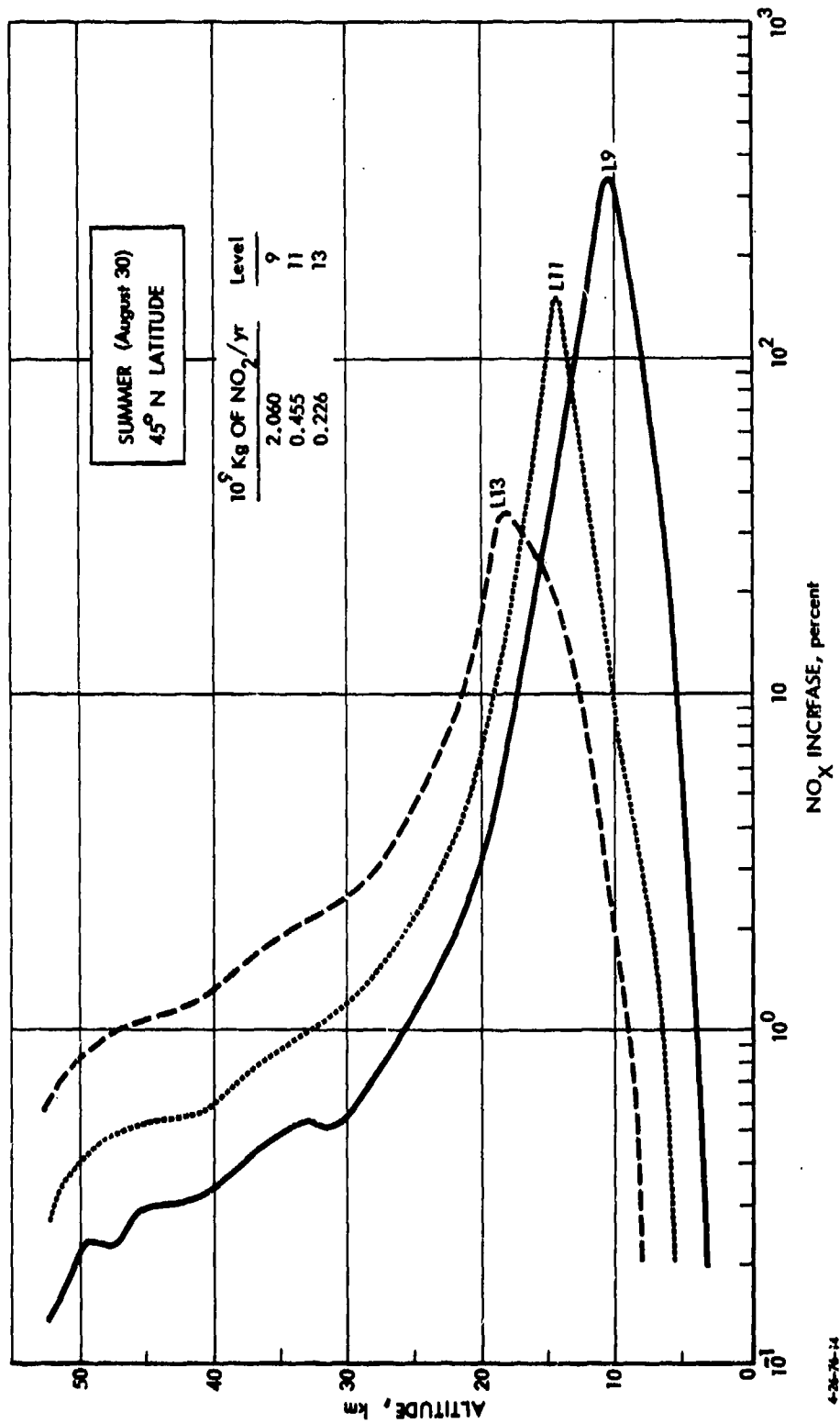
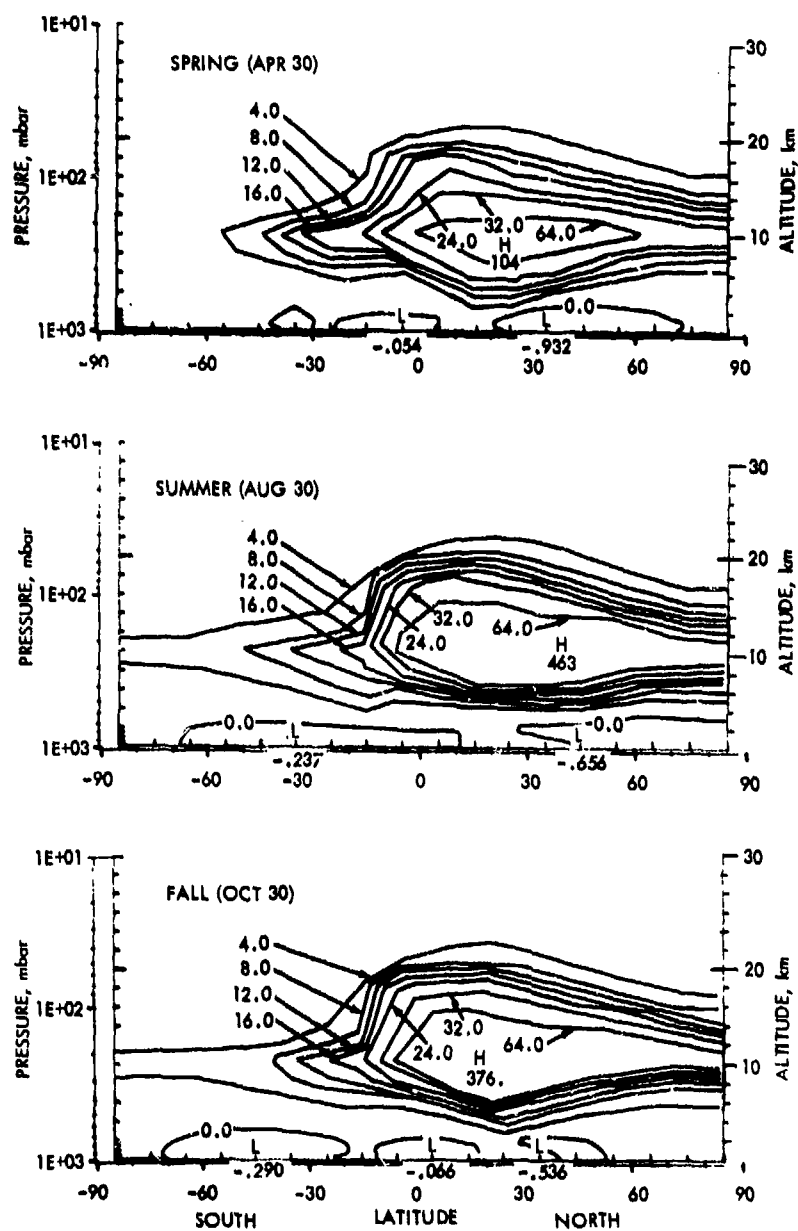
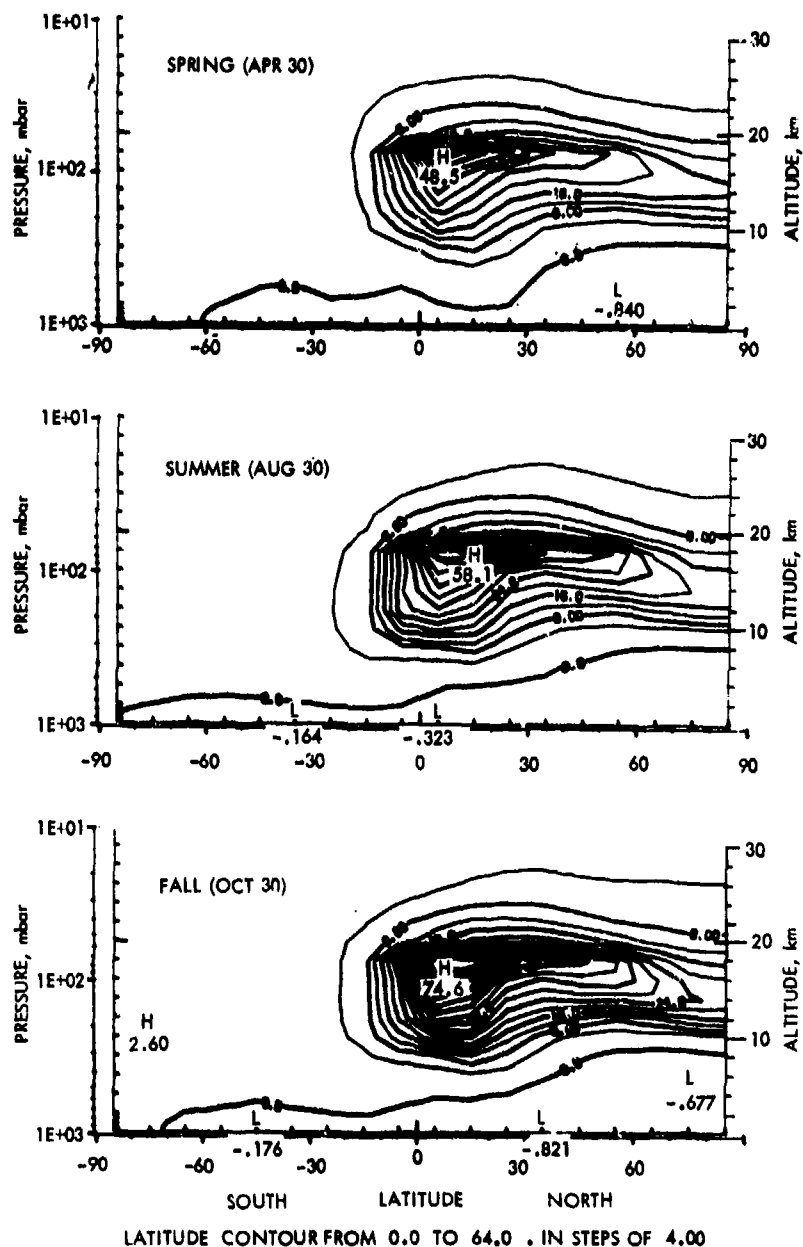


FIGURE A-20. Percent Change in NO_x Concentration at Middle Northern Latitudes (45° N) during Summer as a Function of Altitude after 6 Years of Aircraft NO_x Emissions.



4-21-76-18

FIGURE A-21. NO_x Percent Increase as a Function of Latitude, Altitude, and Season after 6 Years of Fleet Operations for NO_x Emissions at Level 9 (approximately 10.8 km).



4-21-76-19

FIGURE A-22. NO_x Percent Increase as a Function of Latitude, Altitude, and Season after 6 Years of Fleet Operations for NO_x Emissions at Level 13 (approximately 18 km).

during summer for the NO_x emissions at level 9 are also present at other latitudes and seasons. This figure further shows that the peak values of the percent NO_x increase are smallest during spring (104 percent) as compared with those in summer (463 percent) and fall (376 percent). Also, an important characteristic in this figure is the significant latitudinal gradients at low latitudes in the Southern Hemisphere, gradients that prevent a significant NO_x increase at higher latitudes in that hemisphere. Figure A-22 shows similar results for the NO_x emissions at level 13. This figure indicates that the peak values of the NO_x increase are more nearly independent of season as compared with those from the NO_x emissions at level 9. Also, it should be noted that these peak NO_x increases take place at low latitudes in the Northern Hemisphere at about the flight altitude (18 km).

Table A-3 provides numerical data for the change in the ozone column above the ground (level 1) after 6 years of fleet operations as a function of latitude, season, and level of the NO_x emissions. The data are for the lowest level of the model (L1) at 980 mbar. Table A-4 adjusts the results in the previous table to a constant value of NO_x emissions equal to that at level 9. This normalization is, of course, based on the as yet unproven assumption of a linear relationship between small ozone perturbations and the total NO_x emissions. The results in Table A-4 indicate that the ozone reductions at level 13 would dominate the ozone increase from the NO_x emissions at level 9 when the ratio of the total NO_x emissions at level 13 to that at level 9 acquires the unlikely value of unity. Finally, a generalization of the results in Fig. A-12 is given by Table A-5, which gives the change in the ozone column above level 10 as a function of latitude and season for the NO_x emissions at levels 9, 10, 11, and 13.

A.6 LATITUDINAL AVERAGES OF OZONE PERTURBATIONS

There are two reasons for the interest in averages of the ozone perturbations on latitudinal bands that may include an entire hemisphere and even the whole globe: (1) to assess the impact of NO_x emissions on ozone over particular political entities, such as a state, country, etc., and (2) to correlate model results for the ozone perturbations as derived from 3-D, 2-D, and 1-D photochemical models of the atmosphere.

The numerical results provide data for the zonal average of the ozone column at 10-degree increments in latitude for the last day of every other month (every 60 days) and for both the natural and perturbed atmospheres. Numerical integrations with respect to latitude have been performed for each perturbed case (Fig. A-10) over a latitudinal range corresponding to the following cases: (a) a zonal band between 25° N and 45° N, which is intended

TABLE A-3. CHANGE (%) OF OZONE COLUMN ABOVE GROUND (L=1) AFTER 6 YEARS OF FLEET OPERATIONS AT LEVEL L_i ; $(NO_x)_T$ = TOTAL NO_x ANNUAL EMISSIONS, $kg\ NO_2/yr$

L_i^*	April 30 (Spring)				August 30 (Summer)				October 30 (Fall)			
	9	10	11	13	9	10	11	13	9	10	11	13
$(NO_x)_T$	2.064×10^9	0.455×10^9	0.455×10^9	0.226×10^9	2.064×10^9	0.455×10^9	0.455×10^9	0.226×10^9	2.064×10^9	0.455×10^9	0.445×10^9	0.226×10^9
Lat 85	0.148	-0.025	-0.246	-0.764	0.524	0.062	-0.246	-0.955	0.443	0.059	-0.236	-0.856
75	0.169	-0.024	-0.217	-0.698	0.489	0.058	-0.230	-0.863	0.419	0.030	-0.239	-0.867
65	0.201	0.000	-0.176	-0.628	0.562	0.089	-0.178	-0.769	0.450	0.064	-0.193	-0.835
55	0.287	0.052	-0.104	-0.522	0.681	0.148	-0.059	-0.593	0.589	0.131	-0.098	-0.687
45	0.372	0.080	-0.053	-0.426	0.761	0.183	0.000	-0.487	0.813	0.203	0.000	-0.576
35	0.493	0.116	0.000	-0.348	0.625	0.099	0.000	-0.428	0.943	0.290	0.109	-0.435
25	0.620	0.155	0.062	-0.279	0.237	0.068	-0.034	-0.305	0.567	0.151	0.038	-0.340
15	0.361	0.066	0.000	-0.230	0.000	-0.034	-0.102	-0.273	-0.037	-0.037	-0.112	-0.300
5	-0.035	-0.035	-0.104	-0.243	-0.034	-0.034	-0.103	-0.206	-0.036	0.000	-0.107	-0.214
-5	-0.036	-0.036	-0.073	-0.181	-0.035	-0.035	-0.071	-0.177	-0.035	0.000	-0.070	-0.140
-15	-0.038	-0.038	-0.075	-0.150	0.035	0.000	-0.035	-0.104	0.033	0.000	-0.033	-0.100
-25	0.000	-0.036	-0.072	-0.108	0.069	0.000	-0.035	-0.069	0.031	0.000	-0.031	-0.093
-35	0.000	-0.034	-0.068	-0.102	0.032	-0.032	-0.032	-0.129	0.056	0.000	-0.028	-0.084
-45	0.000	0.000	-0.065	-0.129	0.029	0.000	-0.029	-0.117	0.026	-0.026	-0.051	-0.129
-55	-0.032	-0.032	-0.064	-0.127	0.000	-0.026	-0.053	-0.132	0.025	0.000	-0.051	-0.127
-65	-0.035	-0.035	-0.069	-0.138	0.000	0.000	-0.052	-0.130	0.000	-0.027	-0.080	-0.161
-75	-0.038	-0.038	-0.075	-0.150	0.000	-0.027	-0.053	-0.133	0.029	0.000	-0.059	-0.147
-85	-0.038	-0.038	-0.077	-0.115	0.000	-0.026	-0.053	-0.132	0.000	-0.030	-0.091	-0.182

*Corresponding flight altitudes: level 9 (~35,500 ft); 10 (~41,500 ft); 11 (~47,500 ft); 13 (~59,150 ft)

TABLE A-4. NORMALIZED CHANGE (%) OF OZONE COLUMN ABOVE GROUND (L=1) AFTER 6 YEARS OF FLEET OPERATIONS AT LEVEL L_i ; $(NO_x)_T$ = TOTAL NO_x ANNUAL EMISSIONS, kg NO_2 /yr

L_i	April 30 (Spring)			August 30 (Summer)			October 30 (Fall)		
	9	10	11	9	10	11	9	10	11
$(NO_x)_T$	2.064×10^9	2.064×10^9	2.064×10^9	2.064×10^9	2.064×10^9	2.064×10^9	2.064×10^9	2.064×10^9	2.064×10^9
Lat 85	0.148	-0.113	-1.116	0.524	0.281	-1.116	0.443	0.268	-1.070
75	0.169	-0.109	-0.984	0.489	0.263	-1.043	0.419	0.136	-1.084
65	0.201	0.000	-0.798	0.562	0.404	-0.807	0.450	0.290	-0.875
55	0.287	0.236	-0.472	0.681	0.671	-0.268	0.589	0.594	-0.444
45	0.372	0.363	-0.240	0.761	0.830	0.000	0.813	0.921	0.000
35	0.493	0.526	0.000	0.625	0.449	0.000	0.943	1.315	0.494
25	0.620	0.703	0.281	0.237	0.309	-0.154	0.567	0.685	0.172
15	0.361	0.299	0.000	0.000	-0.154	-0.463	-0.037	-0.168	-0.508
5	-0.035	-0.159	-0.472	-0.034	-0.154	-0.467	-0.036	-0.163	-0.485
-5	-0.036	-0.163	-0.331	-0.035	-0.159	-0.322	-0.035	0.000	-0.317
-15	-0.038	-0.172	-0.340	0.035	0.000	-0.159	0.033	0.000	-0.150
-25	0.000	-0.163	-0.327	0.069	0.000	-0.159	0.031	0.000	-0.141
-35	0.000	-0.154	-0.308	0.032	-0.145	-0.145	0.056	0.000	-0.127
-45	0.000	0.000	-0.295	0.029	0.000	-0.131	0.026	-0.118	-0.231
-55	-0.032	-0.145	-0.290	0.000	-0.118	-0.240	0.025	0.000	-0.231
-65	-0.035	-0.159	-0.313	0.000	0.000	-0.236	0.000	-0.122	-0.363
-75	-0.038	-0.172	-0.340	0.000	-0.122	-0.240	0.029	0.000	-0.268
-85	-0.038	-0.172	-0.349	0.000	-0.118	-0.240	0.000	-0.136	-0.413

*Corresponding flight altitudes: level 9 (~35,500 ft); 10 (~41,500 ft); 11 (~47,500 ft); 13 (~59,150 ft)

TABLE A-5. CHANGE (%) OF OZONE COLUMN ABOVE LEVEL 10 AFTER 6 YEARS OF FLEET OPERATIONS AT
LEVEL L_i : $(NO_x)_T$ = TOTAL NO_x ANNUAL EMISSIONS, $109 \text{ kg } NO_2/\text{yr}$

L_i	April 30 (Spring)				August 30 (Summer)				October 30 (Fall)			
	9	10	11	13	9	10	11	13	9	10	11	13
$(NO_x)_T$	2.064	0.455	0.455	0.226	2.064	0.455	0.455	0.226	2.064	0.455	0.455	0.226
Lat 85	-0.139	-0.111	-0.360	-0.859	-0.107	-0.107	-0.393	-1.107	-0.067	-0.100	-0.366	-0.965
75	-0.134	-0.107	-0.349	-0.805	-0.066	-0.098	-0.361	-0.984	-0.033	-0.067	-0.334	-0.935
65	-0.112	-0.112	-0.307	-0.726	0.000	-0.033	-0.266	-0.832	0.000	-0.036	-0.285	-0.891
55	-0.058	-0.058	-0.234	-0.613	0.066	0.000	-0.165	-0.694	0.036	0.000	-0.218	-0.800
45	-0.030	-0.060	-0.180	-0.540	0.101	0.034	-0.101	-0.541	0.076	0.000	-0.153	-0.687
35	0.033	0.000	-0.132	-0.431	0.181	0.072	-0.036	-0.434	0.123	0.041	-0.082	-0.576
25	0.035	0.000	-0.106	-0.353	0.111	0.037	-0.037	-0.370	0.084	0.042	-0.084	-0.420
15	0.000	-0.037	-0.110	-0.293	0.000	-0.037	-0.112	-0.298	-0.041	-0.041	-0.124	-0.330
5	-0.038	-0.038	-0.114	-0.228	-0.037	-0.037	-0.112	-0.225	-0.039	-0.039	-0.117	-0.235
-5	-0.040	-0.040	-0.080	-0.199	-0.039	-0.039	-0.077	-0.194	-0.038	-0.038	-0.077	-0.191
-15	-0.041	-0.041	-0.083	-0.165	-0.040	-0.040	-0.080	-0.120	-0.037	-0.037	-0.074	-0.148
-25	0.000	0.000	-0.040	-0.121	-0.041	-0.041	-0.081	-0.122	-0.035	-0.035	-0.070	-0.105
-35	0.000	0.000	-0.038	-0.113	-0.037	-0.037	-0.074	-0.148	-0.031	-0.031	-0.062	-0.125
-45	-0.036	-0.036	-0.071	-0.142	-0.033	0.000	-0.066	-0.131	-0.028	-0.028	-0.085	-0.141
-55	-0.035	-0.035	-0.104	-0.174	-0.029	-0.029	-0.058	-0.146	-0.028	-0.028	-0.083	-0.166
-65	-0.038	0.000	-0.076	-0.152	-0.029	-0.029	-0.087	-0.144	-0.058	-0.029	-0.088	-0.175
-75	-0.042	-0.042	-0.083	-0.125	-0.030	-0.030	-0.089	-0.148	-0.032	-0.032	-0.096	-0.161
-85	-0.043	-0.043	-0.086	-0.129	-0.029	-0.029	-0.059	-0.147	-0.067	-0.067	-0.100	-0.200

*Corresponding flight altitudes: level 9 (35,500 ft); 10 (41,500 ft); 11 (47,500 ft); 13 (59,150 ft)

to include the United States between Miami, Florida, and Portland, Oregon,* (b) the Northern Hemisphere, (c) The Southern Hemisphere, and (d) the whole globe.

The several types of latitudinal averages are obtained from integrations with respect to latitude of the ozone columns for the perturbed and natural atmospheres. If $\bar{\Omega}(\theta)$ denotes the zonal average of the ozone column at a given latitude, (θ) , and A_z the area of the zonal region of interest, the latitudinal average ($\bar{\Omega}$) of the ozone column is then given by

$$\bar{\Omega}_n = \frac{\int_{A_1}^{A_2} \bar{\Omega}_n(\theta) dA_z}{A_z} \quad (1)$$

for the natural atmosphere, and by

$$\bar{\Omega}_p(L) = \frac{\int_{A_1}^{A_2} \bar{\Omega}_p(\theta, L) dA_z}{A_z} \quad (2)$$

for the perturbed one, where the subscripts n and p denote, respectively, natural and perturbed conditions; the latter being a function of the altitude or level (L) of the NO_x emissions. For the small latitudinal increments of 10 degrees in the numerical data, the area of the zonal ring at a given latitude is given by

$$dA_z = 2\pi a^2 \cos\theta d\theta, \quad (3)$$

where "a" is the earth's radius. Denoting the percent change in the latitudinal average of the ozone column by $(\delta\bar{\Omega}/\bar{\Omega}_n)_L$ for NO_x emissions at a given level L, i.e.,

$$\left(\frac{\delta\bar{\Omega}}{\bar{\Omega}_n}\right)_L \equiv \left(\frac{\bar{\Omega}_p(L) - \bar{\Omega}_n}{\bar{\Omega}_n}\right) 10^2,$$

then

$$\left(\frac{\delta\bar{\Omega}}{\bar{\Omega}_n}\right)_L = \left(\frac{\bar{\Omega}_p(L)}{\bar{\Omega}_n} - 1\right) 10^2, \quad (4)$$

* The 25° N latitude also crosses, approximately, the following countries: Northern Mexico, Algeria, Libya, Egypt, Saudi Arabia, Northern India, Burma, and Southern China. The 45° N latitude also crosses Minneapolis, Minnesota; Montreal, Canada; Southern France; Northern Italy; Romania; Manchuria; and Northern Japan.

where from Eqs. (1) to (3):

$$\frac{\tilde{n}_p(L)}{\tilde{n}_n} = \frac{\int_{\theta_1}^{\theta_2} \tilde{n}_p(\theta, L) \cos \theta d\theta}{\int_{\theta_1}^{\theta_2} \tilde{n}_n(\theta) \cos \theta d\theta} \quad (5)$$

The numerator and denominator in the right-hand side of Eq. (5) have been evaluated numerically in the latitudinal bands of interest as fixed by the limits of integration θ_1 and θ_2 , the level of NO_x emissions, and for each bimonth (every 60 days) as dictated by the availability of the numerical data. The integrands in these integrations involve the product of the zonal ozone column and $\cos \theta$. Since $\cos \theta \rightarrow 0$ as $\theta \rightarrow \pi/2$ at the polar regions, the ozone perturbations at high latitudes are less important for the latitudinal averages than the perturbations at middle and low latitudes.

The annual averages of the six bimonthly percent values were determined by both the arithmetical mean and the weighted average, using the natural ozone column for each bimonth, i.e., from

$$\frac{\delta \tilde{n}}{\tilde{n}_{n, L, a}} = \frac{\sum_{b=1}^6 \left(\frac{\delta \tilde{n}}{\tilde{n}_{n, L, b}} \right) \tilde{n}_{n, b}}{\sum_{b=1}^6 \tilde{n}_{n, b}} \quad (6)$$

where the subscripts a and b denote, respectively, annual and each bimonth value. Because of the small percent change in the ozone column for each bimonth, it was found that there was no significant difference between the arithmetical mean and the weighted average given by Eq. (6).

Tables A-6 to A-9 give, respectively, the zonal band (25° N to 45° N), northern hemispheric, southern hemispheric, and global averages for every other month for subsonic (levels 9, 10, 11) and supersonic (L13) aircraft. These tables include also the annual averages of the bimonthly values. Table A-6 shows that the present subsonics (L9) would produce a change of 0.63 percent in the ozone annual average between 25° N and 45° N for the NO_x emissions assumed at that level in Fig. A-9; whereas the SSTs (L13) would yield a 0.40 percent ozone decrease for the NO_x emissions assumed at level 13. Table A-7 shows that over the Northern Hemisphere, the present subsonics would give a 0.39 percent ozone increase; whereas the SST would produce a 0.42 percent ozone decrease. Table A-8 shows that for the Southern Hemisphere, all types of aircraft would give an ozone decrease. This is a consequence of the small NO_x increases in this hemisphere as a result of

the large latitudinal gradients for the NO_x emissions at level 9 in Fig. A-21, for example. Table A-9 shows that, on the global basis of the 1-D models, the subsonics at level 9 would produce a 0.19 percent ozone increase; whereas the SSTs at level 13 would give a 0.27 ozone decrease.

TABLE A-6. OZONE CHANGE ON ZONAL BAND BETWEEN 25° N AND 45° N, PERCENT
(SIXTH YEAR OF FLEET OPERATIONS)

Level	9	10	11	13
Altitude, km	10.8	12.7	14.5	18.0
$(\text{NO}_x)_T, 10^9 \text{ kg/yr}$	2.064	0.455	0.455	0.226
February 29	0.551	0.153	0.062	-0.332
April 30	0.496	0.117	0.002	-0.348
June 30	0.670	0.164	0.016	-0.402
August 30	0.577	0.106	-0.006	-0.415
October 30	0.856	0.252	0.079	-0.440
December 30	0.621	0.152	0.039	-0.473
Annual Average (Arithmetic)	0.629	0.157	0.032	-0.402
Annual Average (Weighted)	0.626	0.155	0.030	-0.397

TABLE A-7. NORTHERN HEMISPHERE OZONE CHANGE, PERCENT
(SIXTH YEAR OF FLEET OPERATIONS)

Level	9	10	11	13
Altitude, km	10.8	12.7	14.5	18.0
$(\text{NO}_x)_T, 10^9 \text{ kg/yr}$	2.064	0.455	0.455	0.226
February 29	0.383	0.095	0.002	-0.351
April 30	0.328	0.060	-0.056	-0.383
June 30	0.407	0.071	-0.071	-0.428
August 30	0.370	0.060	-0.074	-0.433
October 30	0.429	0.099	-0.057	-0.468
December 30	0.429	0.097	-0.043	-0.481
Annual Average (Arithmetic)	0.391	0.080	-0.050	-0.424
Annual Average (Weighted)	0.391	0.080	-0.050	-0.420

TABLE A-8. SOUTHERN HEMISPHERE OZONE CHANGE, PERCENT
(SIXTH YEAR OF FLEET OPERATIONS)

Level	9	10	11	13
Altitude, km	10.8	12.7	14.5	18.0
(NO _x) _T , 10 ⁹ kg/yr	2.064	0.455	0.455	0.226
February	-0.018	-0.019	-0.056	-0.113
April 30	-0.022	-0.032	-0.072	-0.136
June 30	0.001	-0.017	-0.061	-0.134
August 30	0.018	-0.017	-0.044	-0.124
October 30	0.025	-0.004	-0.046	-0.116
December 30	-0.019	-0.025	-0.067	-0.140
Annual Average (Arithmetic)	-0.003	-0.019	-0.058	-0.127
Annual Average (Weighted)	-0.002	-0.019	-0.057	-0.127

TABLE A-9. GLOBAL OZONE CHANGE, PERCENT
(SIXTH YEAR OF FLEET OPERATIONS)

Level	9	10	11	13
Altitude, km	10.8	12.7	14.5	18.0
(NO _x) _T , 10 ⁹ kg/yr	2.064	0.455	0.455	0.266
February 29	0.185	0.039	-0.027	-0.233
April 30	0.168	0.018	-0.063	-0.270
June 30	0.202	0.030	-0.066	-0.290
August 30	0.191	0.021	-0.059	-0.276
October 30	0.210	0.043	-0.051	-0.277
December 30	0.193	0.033	-0.056	-0.301
Annual Average (Arithmetic)	0.192	0.031	-0.054	-0.275
Annual Average (Weighted)	0.191	0.031	-0.054	-0.274

Table A-10 provides ratios for the zonal-band-to-global and northern-hemispheric-to-global averages for both the bimonthly and annual averages for levels 9, 10, 11, and 13. For the SSTs, the ratio of the zonal-band (Table A-6) to the northern hemispheric averages (Table A-7) is, approximately, 0.95; hence, the near same annual average value (approximately 1.5) for the two averages for level 13 in Table A-10. It should further be noted that the northern-hemispheric-to-global ratios in Table A-10 for level 10 are significantly higher than 2 because of the opposite signs of the ozone effects in the two hemispheres, as shown in Tables A-7 and A-8.

TABLE A-10. RATIO OF OZONE CHANGE AVERAGES

Level	Zonal band (25-45°N) Global				Northern Hemisphere Global			
	9	10	11	13	9	10	11	13
Altitude, km	10.8	12.7	14.5	18.0	10.8	12.7	14.5	18.0
(NO _x) _T , 10 ⁹ kg/yr	2.064	0.455	0.455	0.226	2.064	0.455	0.455	0.226
February 29	2.98	3.92	-2.30	1.42	2.07	2.44	-0.07	1.51
April 30	2.95	6.50	-0.03	1.29	1.95	3.33	0.89	1.42
June 30	3.32	5.47	-0.24	1.39	2.01	2.37	1.08	1.48
August 30	3.02	5.05	0.10	1.50	1.94	2.86	1.25	1.57
October 30	4.08	5.86	-1.55	1.59	2.04	2.30	1.12	1.69
December 30	3.22	4.61	-0.70	1.57	2.22	2.94	0.77	1.60
Annual Average	3.26	5.24	-0.79	1.46	2.04	2.71	0.84	1.55

A.7 APPROACH TO EQUILIBRIUM CONDITIONS

The foregoing ozone and NO_x perturbations are for the sixth year of integrations, using constant NO_x emissions, as indicated in Fig. A-9. The reaching of the equilibrium values for these perturbations is of interest because they represent ultimate values of such perturbations.

Figure A-23 shows the changes in the ozone column above level 1 and at 45° N during summer (August 30) for the NO_x emissions of the present subsonics and SSTs during each of the 6 years of integrations. This figure shows that the ozone increase for the present subsonics is nearly the same during each year of integration, a characteristic that suggests a rather fast reaching of equilibrium conditions when the tropospheric effects from the methane-smog reactions dominate over those of the stratospheric NO_x catalytic cycle. However, the results in this figure for the SSTs indicate significant oscillations in the ozone decrease at 45° N latitude during summer, oscillations that appear to decay only during the fifth and sixth years of integrations. Figure A-24 shows the corresponding NO_x perturbations at about 25 km at 45° N during summer (August 30) for the NO_x emissions of the present subsonics and SSTs during each of the 6 years of integration. This figure shows the same time-distribution of NO_x at 25 km for both types of aircraft, but with significant larger values for the SST perturbations. The smaller values of these NO_x perturbations for the subsonics indicate that they produce a small ozone decrease from the NO_x cycle; hence, the small oscillations in the corresponding ozone increases in the previous figure. However, the larger values of the NO_x perturbations for the SSTs indicate that they control the oscillations of the ozone decrease in the previous figures. Nevertheless, the rather small change of the NO_x increase between the fifth and sixth years for both aircraft types suggests that equilibrium conditions may have already been reached by the end of the fifth year. If this is indeed the case,

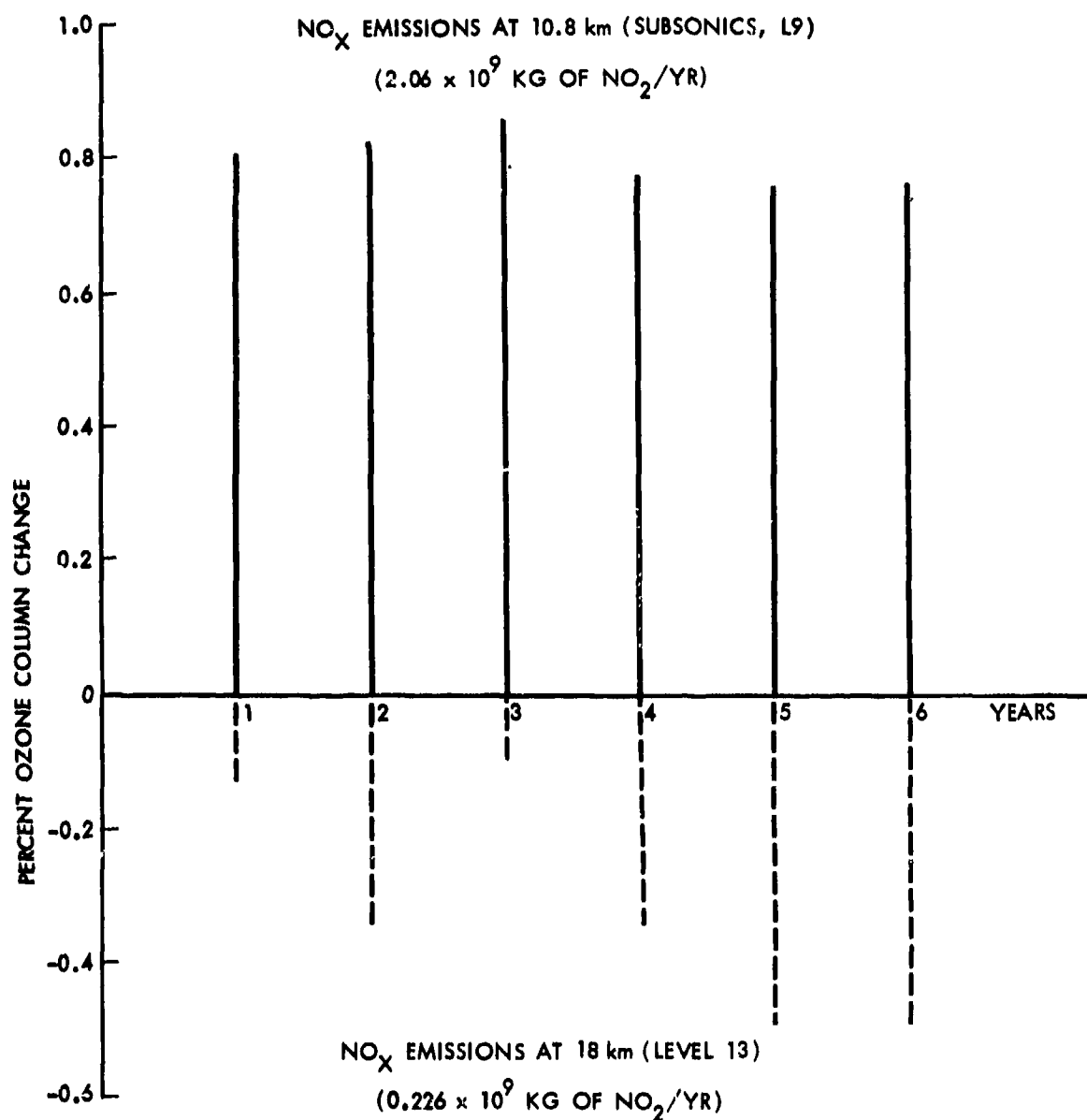
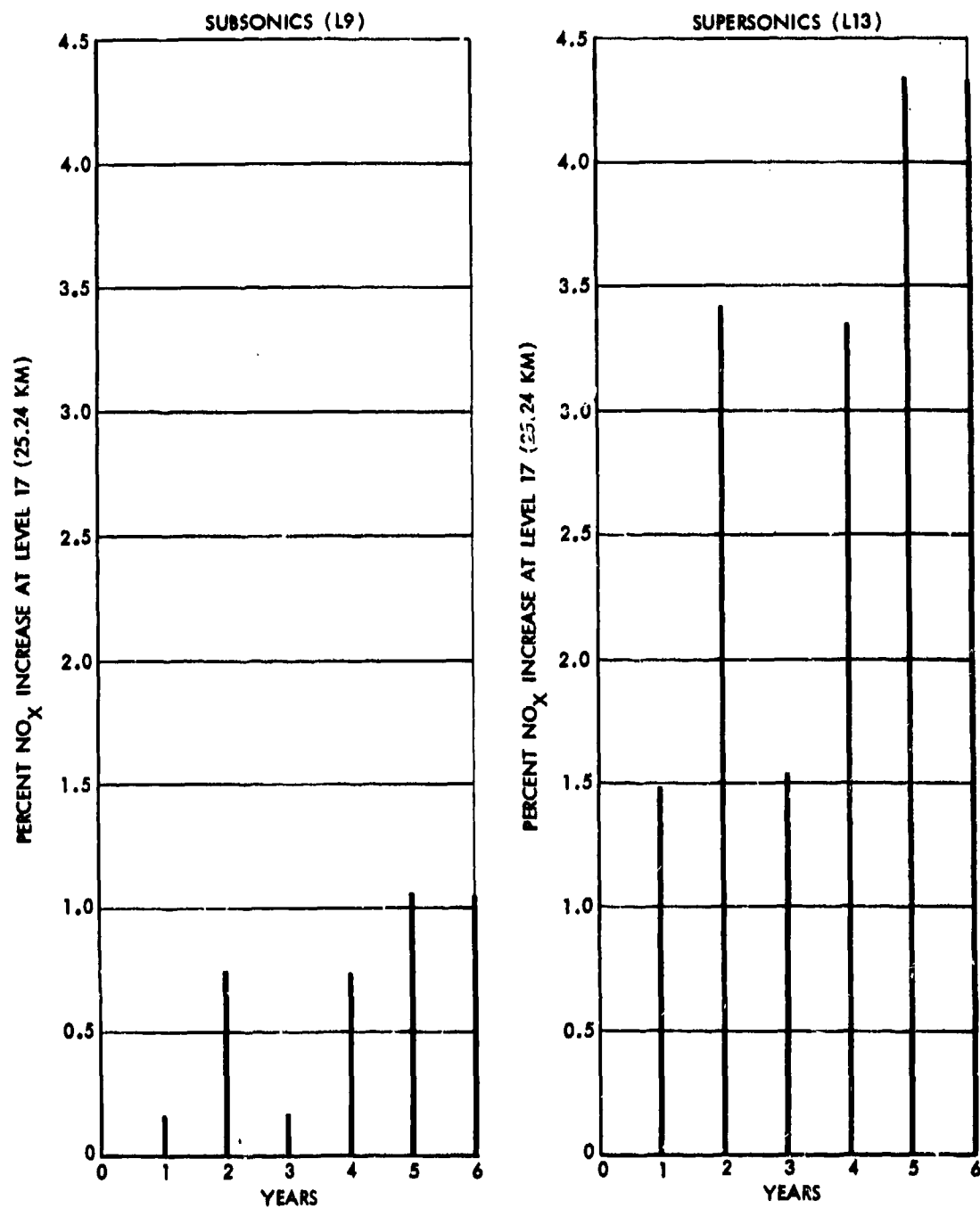


FIGURE A-23. Percent Ozone Column Change at Middle Northern Latitudes (45° N) during Summer (August 30) and 6 Years of NO_x Emissions from Subsonic and Supersonic Aircraft.



4-21-76-17

FIGURE A-24. Percent NO_x Increase at Level 17 (25.2 km) at Middle Northern Latitudes (45° N) during Summer (August 30) and 6 Years of NO_x Emissions from Subsonic and Supersonic Aircraft.

numerical integrations beyond the sixth year would essentially duplicate the perturbations at the 45° N latitude during summer.

A generalization of the foregoing results to other latitudes during summer is provided by the numerical data in Table A-11, which shows the perturbations in the ozone column above level 1 of the model as a function of latitude and year of integration for the NO_x emissions at levels 9 and 13. For the most part, the numerical data in this table show similar results at latitudes other than 45° N. The vertical propagation of the NO_x perturbations to the 25-km region (level 17) as a function of latitude during the first and sixth years of integration is indicated by the numerical data in Tables A-12 and A-13, respectively, for the NO_x emissions at levels 9 and 13. The results shown in Table A-12 indicate a small difference in the NO_x increase between the first and sixth years at the lower levels (8, 9, 10) but rather significant differences at the higher levels (15, 17). These results suggest, then, that the NO_x increases reach equilibrium conditions much faster for the smog reactions at the lower levels than those for the NO_x catalytic cycle at the higher levels. However, the results shown in Table A-13 suggest that the approach to equilibrium conditions takes a longer time as the altitude of NO_x emissions increases from level 9 of the present subsonics to level 13 of the SSTs. Table A-14 shows the NO_x increase at level 17 (i.e., at the highest level of the previous two tables) after each of the 6 years of integrations as a function of latitude for the NO_x emissions at levels 9 and 13; this table is thus a generalization of the results in Fig. A-24 at 45° N to other latitudes during the summer (August 30). This table indicates that the results for the fifth and sixth years are about the same at every latitude, results that suggest that the approach to equilibrium conditions may have already been reached, even for the stratospheric NO_x catalytic cycle.

The approach to equilibrium conditions in the numerical simulation of the natural atmosphere is also of interest in considerations of the monitoring of small ozone column changes in the perturbed atmosphere. Figure A-25 illustrates the changes in the natural ozone column above level 1 at 45° N during summer after each of the 12 years of integration (Fig. A-10). This figure shows that the amplitude of the natural ozone column changes are of the order of ± 1 percent. This result is extended to other latitudes by the numerical data in Tables A-15 and A-16, which show, respectively, the magnitude of the ozone column and their annual oscillations. The results in Table A-15 reveal that the values of the natural ozone column after the ninth year of integration duplicates those after the sixth year at every latitude. However, this condition does not repeat itself in the subsequent years. Table A-15 indicates the presence of annual oscillations at every latitude. It is important to note that the presence of these annual and latitudinal oscillations does not prevent the calculation of the smaller

TABLE A-11. CHANGE (PERCENT) OF OZONE COLUMN ABOVE GROUND (L=1) DURING SUMMER (AUGUST 30) AS A FUNCTION OF TIME

(NO _x) _T Year	NO _x Emissions at Level 9 (~ 35,500 ft)						NO _x Emissions at Level 13 (~ 59,150 ft)					
	2.064 x 10 ⁹ kg NO ₂ /yr						0.226 x 10 ⁹ kg NO ₂ /yr					
	1	2	3	4	5	6	1	2	3	4	5	6
Lat 85	0.700	0.586	0.714	0.601	0.523	0.524	-0.223	-0.709	-0.217	-0.696	-0.953	-0.955
75	0.651	0.576	0.666	0.560	0.488	0.489	-0.207	-0.633	-0.203	-0.649	-0.862	-0.863
65	0.729	0.651	0.714	0.635	0.561	0.562	-0.152	-0.533	-0.179	-0.544	-0.738	-0.769
55	0.786	0.741	0.804	0.724	0.680	0.681	-0.151	-0.444	-0.119	-0.422	-0.621	-0.593
45	0.805	0.822	0.855	0.772	0.760	0.761	-0.124	-0.335	-0.092	-0.340	-0.486	-0.487
35	0.633	0.691	0.726	0.632	0.557	0.625	-0.100	-0.296	-0.099	-0.266	-0.427	-0.428
25	0.205	0.271	0.305	0.204	0.237	0.237	-0.068	-0.237	-0.068	-0.239	-0.304	-0.305
15	0.069	0.034	0.068	0.034	0.000	0.000	-0.069	-0.205	-0.063	-0.206	-0.273	-0.273
5	0.000	0.000	0.000	0.000	-0.069	-0.034	-0.069	-0.137	-0.034	-0.138	-0.240	-0.206
-5	0.000	-0.035	0.000	-0.035	-0.035	-0.035	-0.035	-0.106	-0.035	-0.106	-0.142	-0.177
-15	0.068	0.035	0.069	0.034	0.069	0.035	0.000	-0.069	0.035	-0.068	-0.069	-0.104
-25	0.067	0.069	0.069	0.067	0.069	0.069	0.000	-0.035	0.000	-0.034	-0.069	-0.069
-35	0.063	0.065	0.065	0.063	0.064	0.032	0.000	-0.032	0.032	-0.031	-0.097	-0.129
-45	0.058	0.058	0.059	0.057	0.000	0.029	0.000	-0.029	0.000	-0.057	-0.146	-0.117
-55	0.052	0.053	0.053	0.026	0.000	0.000	0.000	-0.053	0.000	-0.052	-0.132	-0.132
-65	0.026	0.026	0.026	0.026	0.000	0.000	0.000	-0.078	0.000	-0.052	-0.130	-0.130
-75	0.053	0.027	0.027	0.026	0.000	0.000	0.000	-0.053	0.000	-0.053	-0.133	-0.133
-85	0.053	0.027	0.053	0.026	0.000	0.000	0.000	-0.053	0.027	-0.053	-0.133	-0.132

TABLE A-12. NO_x INCREASE (PERCENT) ON AUGUST 30 (SUMMER) AS A FUNCTION OF TIME AND ALTITUDE

Years	NO _x Emissions at Level 9 (35,500 ft)										
	First					Sixth					
Level*	8	9	10	15	17	8	9	10	15	17	
Lat 85	46.37	103.25	37.21	0.285	0.057	26.11	102.39	37.02	1.241	0.808	
75	27.35	117.90	41.30	0.269	0.071	27.10	117.15	41.24	1.235	0.794	
65	33.73	156.33	68.36	0.361	0.090	33.56	155.88	68.17	1.420	0.843	
55	62.18	257.18	114.86	0.507	0.125	61.79	256.76	115.65	1.716	0.928	
45	114.19	333.94	125.91	0.916	0.173	112.42	333.18	128.59	2.210	1.053	
35	184.47	466.90	138.00	1.521	0.284	180.89	463.55	138.72	3.072	1.219	
25	220.41	462.50	173.49	1.852	0.286	216.51	440.77	164.32	3.632	1.271	
15	161.82	292.20	144.70	1.803	0.222	160.35	280.43	137.39	3.719	1.127	
5	55.56	137.52	102.80	1.275	0.125	57.78	135.29	98.11	3.135	0.872	
-5	33.33	98.20	107.69	0.757	0.050	31.91	75.61	64.47	2.154	0.621	
-15	15.24	17.96	11.78	0.177	0.024	15.15	18.12	11.00	1.041	0.391	
-25	11.76	14.22	6.22	0.080	0.024	11.91	15.60	6.78	0.683	0.297	
-35	8.33	11.36	4.79	0.000	0.000	8.82	12.24	5.39	0.496	0.250	
-45	6.04	6.04	4.57	0.039	0.000	6.25	9.29	5.16	0.358	0.220	
-55	3.95	6.65	3.89	0.000	0.000	4.73	7.34	4.44	0.325	0.187	
-65	3.52	5.54	2.28	0.000	0.000	4.32	6.48	2.83	0.284	0.191	
-75	3.01	5.85	1.98	0.000	0.000	3.82	6.38	2.60	0.324	0.198	
-85	2.92	5.34	1.90	0.000	0.000	2.96	5.50	2.59	0.320	0.179	

*Corresponding altitudes in km: level 8 (8.9 km); 9 (10.8 km); 10 (12.7 km); 15 (21.6 km); 17 (25.2 km)

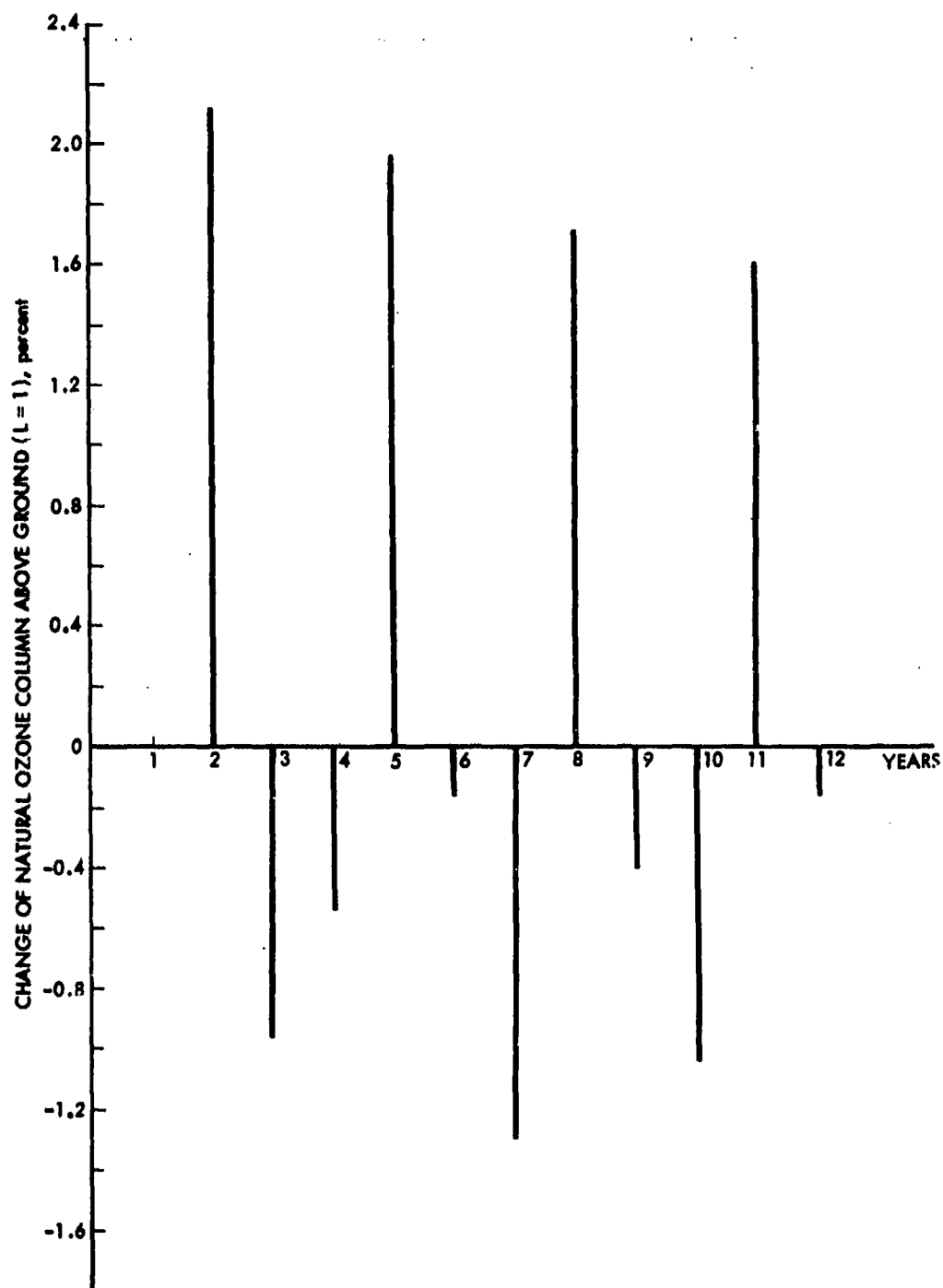
TABLE A-13. NO_x INCREASE (PERCENT) ON AUGUST 30 (SUMMER) AS A FUNCTION OF TIME AND ALTITUDE

NO _x Emissions at Level 13 (~59,150 ft)																
Years	Level*	First					Sixth									
		8	9	10	15	17	8	9	10	15	17					
Lat 85	0.219	2.428	9.830	2.025	0.777	0.000	3.988	15.072	5.323	3.330						
75	0.317	2.045	9.784	1.946	0.764	-0.104	3.202	14.689	5.218	3.268						
65	0.200	1.798	8.180	2.530	0.884	-0.098	2.805	12.167	5.984	3.504						
55	0.318	1.629	5.840	3.732	1.125	0.104	2.350	8.754	7.497	3.862						
45	0.797	2.041	6.331	5.632	1.476	0.786	2.905	9.253	9.732	4.372						
35	1.618	3.286	7.511	7.478	1.926	1.911	4.907	10.979	12.092	4.965						
25	3.061	6.115	10.233	7.971	1.907	1.883	9.013	14.545	12.922	4.961						
15	7.273	14.679	19.616	7.211	1.433	8.621	18.478	25.225	12.362	4.233						
5	4.444	15.768	24.299	5.313	0.824	6.667	19.508	32.075	10.190	3.113						
-5	4.444	20.120	34.615	3.243	0.425	6.383	17.073	26.316	7.029	2.187						
-15	2.857	3.873	4.140	0.887	0.120	4.040	5.625	5.667	3.122	1.296						
-25	2.206	2.219	2.008	0.400	0.073	3.175	4.000	3.939	2.135	1.039						
-35	1.389	1.580	1.473	0.105	0.020	2.941	2.857	3.194	1.434	0.833						
-45	1.342	1.443	1.333	0.077	0.000	2.083	2.655	3.099	1.152	0.714						
-55	0.658	1.036	1.237	0.064	0.017	1.351	2.752	2.896	1.008	0.647						
-65	0.000	1.143	0.870	0.031	0.000	1.439	2.315	2.594	0.979	0.641						
-75	0.000	0.763	0.731	0.032	0.000	1.527	2.128	2.489	1.003	0.667						
-85	0.730	1.049	0.699	0.031	0.000	1.481	2.000	2.478	0.991	0.662						

*Corresponding altitudes in km: level 8 (8.9 km); 9 (10.8 km); 10 (12.7 km); 15 (21.6 km); 17 (25.2 km)

TABLE A-14. NO_x INCREASE (PERCENT) AT LEVEL 17 (25.2 km) ON AUGUST 30 (SUMMER) AS A FUNCTION OF TIME

(NO _x) _T Year	NO _x Emissions at Level 9 (~35,500 ft)						NO _x Emissions at Level 13 (~53,150 ft)					
	2.064 x 10 ⁹ kg NO ₂ /yr						0.226 x 10 ⁹ kg NO ₂ /yr					
	1	2	3	4	5	6	1	2	3	4	5	6
85	0.057	0.550	0.077	0.520	0.813	0.808	0.777	2.437	0.845	2.349	3.330	3.330
75	0.071	0.516	0.054	0.506	0.799	0.794	0.764	2.394	0.810	2.294	3.269	3.268
65	0.090	0.579	0.073	0.550	0.849	0.843	0.884	2.598	0.931	2.494	3.507	3.504
55	0.125	0.630	0.108	0.618	0.935	0.928	1.125	2.926	1.157	2.816	3.869	3.862
45	0.173	0.754	0.174	0.742	1.061	1.053	1.476	3.411	1.527	3.319	4.386	4.372
35	0.284	0.902	0.241	0.892	1.207	1.219	1.926	3.945	1.906	3.925	4.965	4.955
25	0.286	0.929	0.261	0.973	1.260	1.271	1.907	3.912	1.824	4.013	4.942	4.951
15	0.222	0.803	0.170	0.858	1.117	1.127	1.433	3.239	1.286	3.456	4.213	4.213
5	0.125	0.574	0.072	0.638	0.858	0.872	0.824	2.195	0.675	2.499	3.078	3.113
-5	0.050	0.372	0.024	0.434	0.627	0.621	0.425	1.414	0.313	1.661	2.182	2.187
-15	0.024	0.218	0.024	0.221	0.367	0.391	0.120	0.727	0.095	0.785	1.248	1.296
-25	0.024	0.147	0.000	0.148	0.297	0.297	0.073	0.539	0.048	0.543	1.039	1.039
-35	0.000	0.103	0.000	0.104	0.228	0.250	0.020	0.370	0.020	0.395	0.810	0.833
-45	0.000	0.072	0.000	0.073	0.201	0.220	0.000	0.308	0.000	0.293	0.712	0.714
-55	0.000	0.084	0.000	0.068	0.187	0.187	0.017	0.270	0.000	0.273	0.662	0.647
-65	0.000	0.069	0.000	0.070	0.190	0.191	0.000	0.274	0.000	0.278	0.656	0.641
-75	0.000	0.071	0.000	0.072	0.198	0.198	0.000	0.285	0.018	0.290	0.665	0.667
-85	0.000	0.071	0.000	0.072	0.179	0.179	0.000	0.283	0.000	0.288	0.660	0.662



4-21-76-14

FIGURE A-25. Percent Change of Natural Ozone Column above Ground (L=1) at Middle Northern Latitudes (45° N) during Summer (August 30) and 12 Years after Initialization (3 Years).

TABLE A-15. NATURAL OZONE COLUMN (m-atm-cm) ABOVE GROUND (L=1) DURING SUMMER
(AUGUST 30) AS A FUNCTION OF TIME

Years*	1	2	3	4	5	6	7	8	9	10	11	12
Lat 85	306.7	320.1	314.4	311.6	323.0	322.2	314.4	324.5	322.2	315.9	325.3	324.6
75	330.1	343.1	337.5	334.9	345.9	345.2	337.7	347.4	345.2	339.2	348.2	347.5
65	322.9	334.2	329.5	327.0	336.6	336.0	329.3	337.9	336.0	330.6	338.6	338.0
55	325.5	334.6	330.7	328.7	336.5	335.9	330.7	337.5	335.9	331.7	338.1	337.5
45	311.9	326.3	323.2	321.5	327.8	327.3	323.1	328.6	327.3	323.9	329.1	328.6
35	296.8	302.1	299.7	298.9	303.4	303.0	300.1	304.0	303.0	300.7	304.4	304.0
25	290.0	293.9	291.8	291.8	294.9	294.6	292.9	295.4	294.6	293.4	295.7	295.4
15	288.3	291.4	289.5	290.0	292.3	292.1	290.9	292.8	292.1	291.4	293.1	292.9
5	287.3	289.7	288.0	288.9	290.6	290.6	289.8	291.1	290.6	290.2	291.4	291.3
-5	279.4	280.8	279.2	281.0	281.7	281.8	281.9	282.2	281.8	282.4	282.4	282.5
-15	292.7	287.1	285.5	294.5	288.2	288.4	295.6	288.8	288.4	296.2	289.0	289.3
-25	293.3	286.4	284.6	295.4	287.6	287.9	296.6	288.2	287.9	297.2	288.5	288.8
-35	312.6	307.6	305.2	315.3	309.1	309.4	316.8	309.9	309.4	317.6	310.3	310.7
-45	341.9	339.2	336.1	345.4	341.1	341.5	347.3	342.1	341.5	348.3	342.7	343.0
-55	375.4	374.8	371.0	379.5	377.1	377.5	381.8	378.3	377.5	383.0	379.0	379.4
-65	378.5	379.2	375.2	382.8	381.7	382.1	385.3	383.0	382.1	386.5	383.6	384.0
-75	370.1	371.3	367.4	374.4	373.7	374.2	376.8	375.0	374.2	378.1	375.7	376.1
-85	371.7	372.8	368.8	376.0	375.2	375.6	378.4	376.5	375.6	379.7	377.2	377.6

*Note that 9th year matches exactly the 6th year values at every latitude.

TABLE A-16. CHANGE (PERCENT) OF NATURAL OZONE COLUMN ABOVE GROUND (L=1) DURING SUMMER
(AUGUST 30) AS A FUNCTION OF TIME

Year	1	2	3	4	5	6	7	8	9	10	11	12
85	-	4.369	-1.781	-0.891	3.659	-0.248	-2.421	3.212	-0.709	-1.955	2.976	-0.215
75	-	3.938	-1.632	-0.770	3.285	-0.202	-2.173	2.872	-0.633	-1.738	2.653	-0.201
65	-	3.500	-1.406	-0.759	2.936	-0.178	-1.994	2.612	-0.562	-1.607	2.420	-0.177
55	-	2.796	-1.166	-0.605	2.373	-0.178	-1.548	2.056	-0.474	-1.250	1.929	-0.177
45	-	2.320	-0.950	-0.526	1.960	-0.153	-1.283	1.702	-0.396	-1.039	1.605	-0.152
35	-	1.786	-0.794	-0.267	1.506	-0.132	-0.957	1.300	-0.329	-0.759	1.230	-0.131
25	-	1.345	-0.715	0.000	1.062	-0.102	-0.577	0.854	-0.271	-0.407	0.784	-0.101
15	-	1.075	-0.652	0.173	0.793	-0.068	-0.411	0.653	-0.239	-0.240	0.583	-0.068
5	-	0.835	-0.587	0.313	0.588	0.000	-0.275	0.449	-0.172	-0.138	0.414	-0.034
-5	-	0.501	-0.570	0.645	0.249	0.035	0.035	0.106	-0.142	0.213	0.000	0.035
-15	-	-1.913	-0.557	3.152	-2.139	0.069	2.497	-2.300	-0.139	2.705	-2.431	0.104
-25	-	-2.353	-0.628	3.795	-2.640	0.104	3.022	-2.832	-0.104	3.230	-2.927	0.104
-35	-	-1.599	-0.780	3.309	-1.966	0.097	2.392	-1.178	-0.161	2.650	-2.298	0.129
-45	-	-0.790	-0.914	2.767	-1.245	0.117	1.698	-1.497	-0.175	1.991	-1.608	0.088
-55	-	-0.160	-1.014	2.291	-0.632	0.106	1.139	-0.917	-0.211	1.457	-1.044	0.106
-65	-	0.185	-1.055	2.026	-0.287	0.105	0.837	-0.597	-0.235	1.152	-0.750	0.104
-75	-	0.324	-1.050	1.905	-0.187	0.134	0.695	-0.478	-0.213	1.042	-0.635	0.106
-85	-	0.296	-1.073	1.952	-0.213	0.107	0.745	-0.502	-0.239	1.092	-0.658	0.106

perturbations in the ozone column from the NO_x emissions because of the methodology described in Fig. A-10. However, this methodology could not be extended to the actual perturbed atmosphere because the "reference" natural atmosphere would be unavailable, i.e., it would be difficult to detect changes of the ozone column in the perturbed atmosphere that are smaller than the amplitude of the oscillations of the natural atmosphere (Fig. A-25).

A.8 COMPARISON OF PREVIOUS 1-D AND PRESENT 2-D MODEL RESULTS

The use of the annual global average of the ozone column perturbations after 6 years of integration for the NO_x emissions from SSTs (Table A-9) allows "comparison" with earlier results from 1-D models, which, however, did not use the same chemistry. As an example, the Chang 1-D ozone decrease for equilibrium conditions is given in the CIAP Report of Findings (p. E-57) as

$$\left(\frac{\delta\tilde{n}}{\tilde{n}}\right)_{1-D} = [2 + 0.8(z-17)][\dot{E}_{\text{NO}_x} \times 10^{-9}]^{0.88 + (0.07/3)(20-z)} \quad (7)$$

where $(\delta\tilde{n}/\tilde{n})_{1-D}$ is the global average of the ozone decrease, z is the flight altitude in the range $17 < z < 20$ km, and \dot{E}_{NO_x} is the annual rate of NO_x emissions (as NO_2) in kg/yr in the range $0.1 < \dot{E}_{\text{NO}_x} \times 10^{-9} < 3$. Using the data in Table A-9 for level 13, i.e., $z = 18$ km and $\dot{E}_{\text{NO}_x} = 0.226 \times 10^9$, Eq. (7) yields

$$\left(\frac{\delta\tilde{n}}{\tilde{n}}\right)_{\text{Chang CIAP}} \approx 0.71\%$$

which is a factor of 2.6 higher than the corresponding 2-D average value (0.27) in Table A-9. It is not surprising that the Chang value is higher because of the following factors: (1) the Chang use of 2×10^{-10} for the rate of the $\text{OH} + \text{HO}_2 + \text{H}_2\text{O} + \text{O}_2$ reaction (R21), an effect that has been studied by Duewer et al. (1976); (2) the difference in the dynamics (K_z vs K_{zz} , etc.); (3) the assumed latitudinal distributions of the NO_x emissions in the 2-D model (Fig. A-9) vs a uniform one for the 1-D model; (4) the present uncertainty concerning the reaching of equilibrium conditions for the 2-D model results; and (5) the omission of the smog reactions in the Chang 1-D model.

The present 2-D model results may also be compared with previous ones obtained with the same model (Crutzen, 1975). Such comparison indicates

that the earlier 2-D model results for NO_x emissions at 18-km altitude are higher than the present ones by a significant factor. The reason for this discrepancy appears to be an input error in the previous calculations concerning the number of NO_x molecules per unit volume per second corresponding to the assumed number of SSTs. The previous and current 2-D model results also show a difference in the latitudinal distribution of the ozone perturbations. This difference might be produced by the change in these calculations of the K_{yy} eddy transport coefficients at low latitudes, with the current values being based on the aerosol distribution of the Fuego volcanic eruption. A detailed analysis of the difference between the previous and current results is not possible because of the unavailability of the numerical data for the previous calculations.

A.9 AREAS FOR FURTHER INVESTIGATIONS

Areas for further numerical investigations may be classified as short- and long-range problems, the latter depending on the need to modify the 2-D model. They are identified below.

a. Short-Range Problems

1. Verification of the equilibrium conditions for the NO_x catalytic cycle by extending the present numerical integrations for the perturbed atmosphere from 6 to 9 years (e.g., Figs. A-23, A-24).
2. Use of a 6-year segment of integration (Fig. A-10) to test the effect, if any, of restarting integrations on the reaching of equilibrium conditions (Figs. A-23, A-24).
3. Development of procedures for reducing computing time by using tracer spreading without chemistry in subsequent integrations that include the chemistry. For example, initial use of the total NO_x emissions as inert species to determine the time to reach dynamic equilibrium (without chemical effects) of the NO_x emissions.
4. Evaluation of both the linear scaling of the changes in the ozone column as a function of the total NO_x emission for a given aircraft type, and the linear superposition of effects for the simultaneous operation of present subsonics, advanced subsonics, and SST types of aircraft.
5. Use of the time-dependent Crutzen 1-D model (which incorporates the methane oxidation reactions) to investigate the sensitivity of the ozone column increase to the uncertainty in the reaction rates for the methane system as well as the effect of the possible photolysis of NO_3 to produce $\text{NO} + \text{O}_2$.

b. Long-Range Problems

1. Incorporation of chlorine reactions to evaluate the coupled effect of the ClO_x and NO_x chemistry in the stratosphere for the ozone perturbations from SST aircraft. Review and modification of other rates according to best available data.
2. Incorporation of aircraft H_2O emissions by reformulation (possibly) and reprogramming of the water vapor processes in the stratosphere.
3. Increase of the vertical resolution of the model in the region of the flight altitudes of interest so as to allow more accurate simulations of the NO_x emissions along typical flight trajectories. It should be noted that this has already been done between the first and fifth levels of the model near the earth's surface for applications other than the High Altitude Pollution Program (HAPP).
4. Evaluation of the stratospheric dynamics for tracers other than ozone and water vapor. Attempt also better matching of the ozone column at high southern latitudes (Figs. A-1 vs A-2).
5. Calculation of NO_x injection runs at various latitudes, altitudes, and total NO_x injection rates.
6. Performance of numerical experiments to simulate effects of past nuclear explosions in the atmosphere as well as such natural phenomena as solar proton events.

APPENDIX B

SOME DETAILS FROM THE
COMESA REPORT

(With Reviewer's Comments)

R.C. Oliver

APPENDIX B

SOME DETAILS FROM THE COMESA REPORT (With Reviewer's Comments)

B.1 INTRODUCTION AND SUMMARY

The report of the Committee on Meteorological Effects of Stratospheric Aircraft (COMESA) documents extensive efforts over several years in analysis, modeling, and measurements, both in the field and in the laboratory. Some discussion of their ozone modeling work was included in Section 3 and of their climate modeling work in Section 4 of this report. Certain additional points which seem to be of particular interest are noted here; no attempt is made to be comprehensive. Readers are referred to the documents themselves for full exposition.

The topics discussed here include the state of knowledge of the stratosphere, as viewed by COMESA, certain laboratory measurements of reaction rates, and a further discussion of ozone modeling. Some comparisons (by this reviewer) to CIAP results and other numbers are included.

COMESA modeling efforts on the effects of aircraft effluents on ozone involved 3-D, 2-D, and 1-D models.

The COMESA 3-D general-circulation model (without chemistry) was run for one year, studying the distribution of O_3 , H_2O , and NO_x as tracers. The results were collapsed to 1-D for comparison to published (Hunten and Chang) K_z profiles. The different tracers showed widely differing behavior, including negative values of K_z . Gross averages, however, were developed which implied that the Hunten profile implies vertical motions to be too slow in the lower stratosphere and the Chang profile to be too slow in the upper stratosphere.

The COMESA 2-D model, being at an early state of development, was considered unsuitable for perturbation predictions; it was used, however, to estimate latitudinal distribution of effects. Results were similar to those reported in CIAP, although after only 3 years of equivalent running time, stationary state was not achieved.

Two 1-D models were used by COMESA, both using diurnally and seasonally varying sun angle, with fixed K_z profiles, Chang or Hunten. Model runs typically up to 10 years were used, but stationary state was not always

evident. The model (Model A) with methane chemistry, 1-km resolution and Chang K_z , but a 10-km lower boundary (and 50-km upper) showed initial ozone enhancement by subsonics (at 11 km to 13 km) but (after 3 years) a slight depletion, varying with season. The second model (Model B) extended from the ground to 48 km, with 2-km resolution, but utilized simplified chemistry (no smog reactions). Runs with 1-D models included SSTs and subsonics, alone and in combination. The most surprising result was an insensitivity to K_z for SSTs (Concorde/Tupolev), with Chang and Hunten K_z profiles giving about the same effect on ozone; with subsonics, however, the difference in results was substantial.

The COMESA group concluded that about 600 Concorde (each producing 8×10^5 kg NO_x/yr) would be required to cause 1 percent ozone depletion in the 30° to 60° N region. The results "indicate that the reduction of ozone caused by present subsonic fleets (which is widely regarded as negligible) will be less than doubled by addition of a hundred or more Concorde-like SSTs," (COMESA, p. 388). The reference to the present subsonic fleet is apparently based on the 0.1 percent figure quoted in the CIAP Report of Findings, rather than to their own (Model A) results.

Valuable discussion is included in the COMESA report of inadequacies of models, of questions as to the NO_x budget, of the problems of monitoring (with known variations in N_2O), and on important chemical reaction rate uncertainties.

B.2 THE NATURAL STRATOSPHERE, AS VIEWED BY COMESA

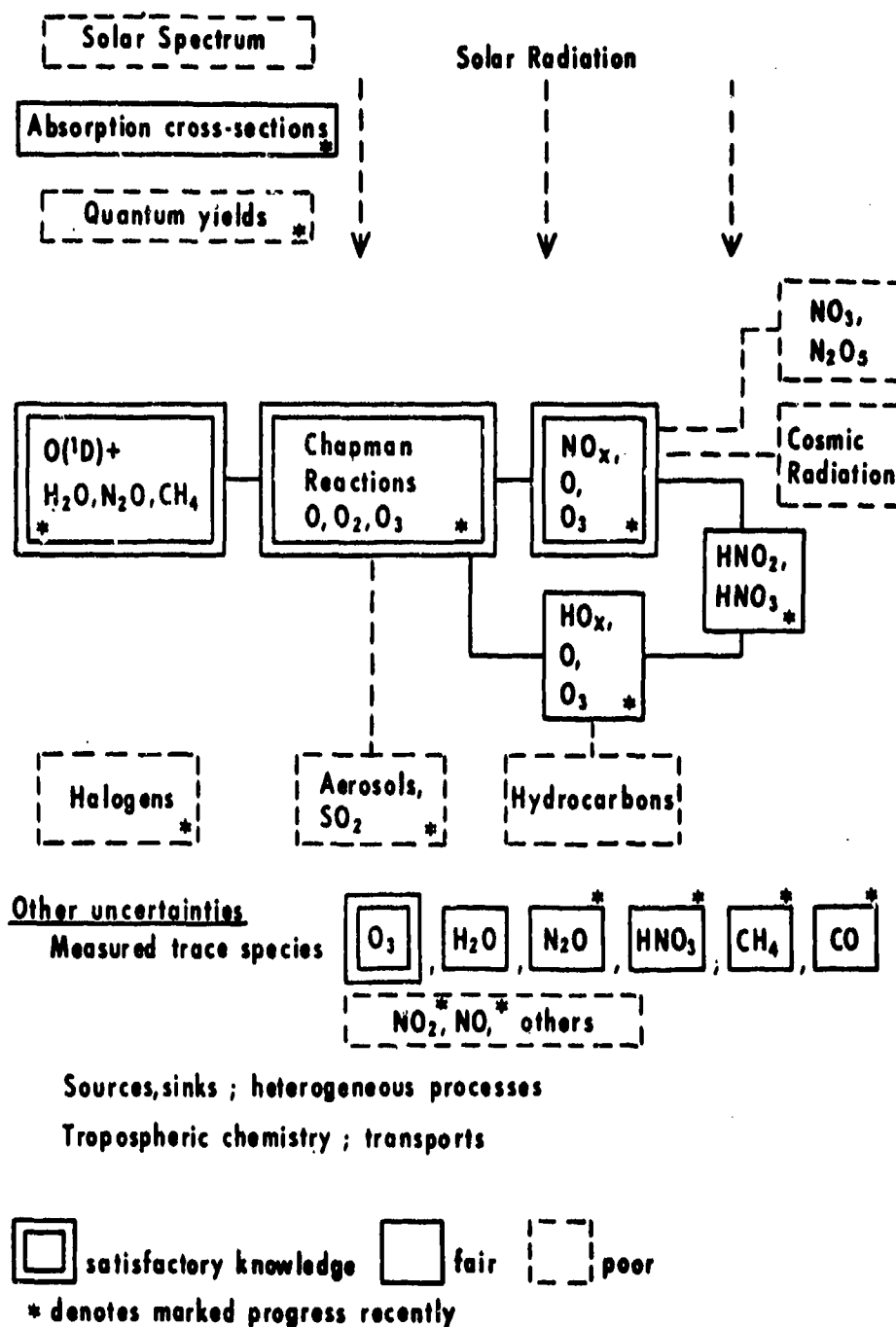
B.2.1 State of Knowledge

The COMESA view of the state of knowledge of stratospheric composition is given in Fig. B-1. Note that in their view many important areas of the problem, beginning with solar radiation and the solar spectrum, are not accurately known. Certain items are shown on which COMESA feels that important progress has been made recently. Two of these items, "sources and sinks" and "transports," listed under the heading "other uncertainties," are given considerable discussion elsewhere in the report; heterogeneous processes and tropospheric chemistry are not given much treatment.

B.2.2 Measurements and Composition Data

The COMESA (with COVOS*) effort involved stratospheric measurements of a number of species from both aircraft and balloons. The H_2O , NO , NO_2 , and HNO_3 measurements are of particular interest.

*Comite d'Etudes sur les Conséquences des Vols Stratosphériques



1-21-77-29

FIGURE B-1. Summary of The State of Knowledge of Stratospheric Composition
SOURCE: COMESA, 1975

A. NO

Oxford daytime NO measurements (by balloon-borne instrument, 5.3- μ m band of NO, 14 June 1975, S.E. France) are shown in Fig. B-2. A factor of 2 uncertainty is ascribed to the curve as shown, which is expected to be reduced by further analysis (COMESA report, p. 57). Note that the Oxford results are higher than others in the 15- to 40-km region.

B. NO₂

The variation of NO₂ found by COMESA in a diurnal sense and with altitude is shown in Fig. B-3. The profiles are considered uncertain to the order of ± 50 percent (COMESA report, p. 64). To first order the sum NO + NO₂ should be constant over the diurnal cycle, as NO is essentially quantitatively converted to NO₂ by reaction with O₃ [at 30 km (COMESA report, p. 65), the mixing ratio decreases from day to night from 10^{-8} to 10^{-10}]. The COMESA (Oxford) measurements (COMESA report, p. 65) meet this test within the uncertainties. The total column density (apparently above 15 km) has been estimated (COMESA report, p. 63) as 1.4×10^{16} cm⁻²; they compare this to 1.0×10^{16} cm⁻² reported by Noxon in 1975. For comparison, the Chang model (based on the "old Chang" profile, 12-13 December 1975 runs at Lawrence Livermore Laboratory) above 15 km gives 7.24×10^{15} cm⁻², although the total column density is 9.99×10^{15} cm⁻² above 0 km.*

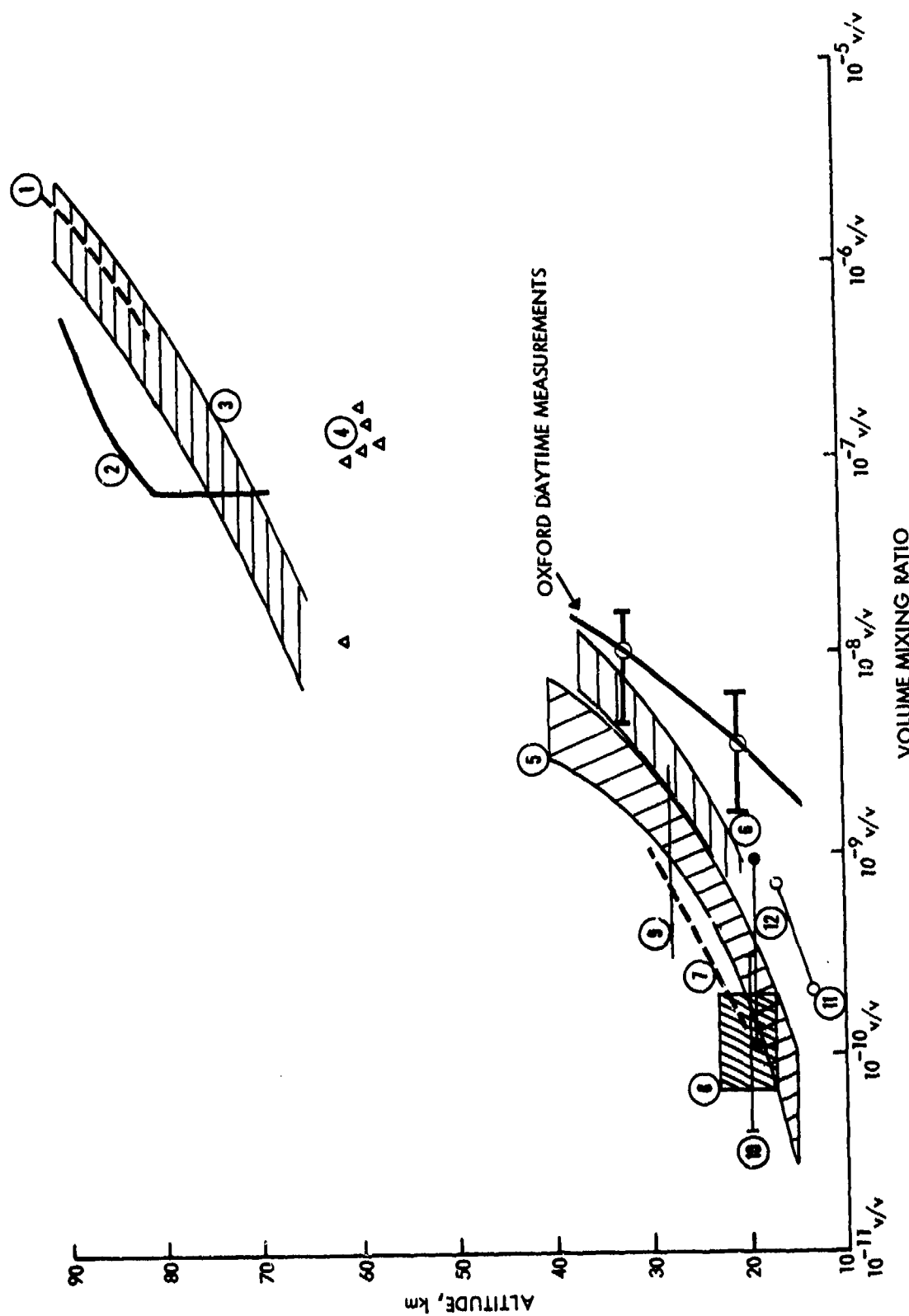
HNO₃ is not included in this summation as it is apparently nearly constant during the day (formation = destruction). N₂O₅ and NO₃, while formed at night and decomposed during the day, are implicitly small contributors. The possibility exists, however, (see Ridley et al., 1976), that N₂O₅ could be a significant part of the total odd nitrogen budget.

The COMESA report considers these higher odd nitrogen values to be significant, indicating sources of NO_x other than from N₂O, and thus lesser sensitivity to added NO_x (COMESA report, p. xviii).

C. HNO₃

HNO₃ exists in a broad layer (10-km half-height) with maximum mixing ratio 3 to 8 ppbv occurring near 20 km to 25 km. The layer is lower and the column greater at high latitudes (COMESA report, p. 68). There are possible seasonal and hemispheric differences. COMESA measurements found an increase

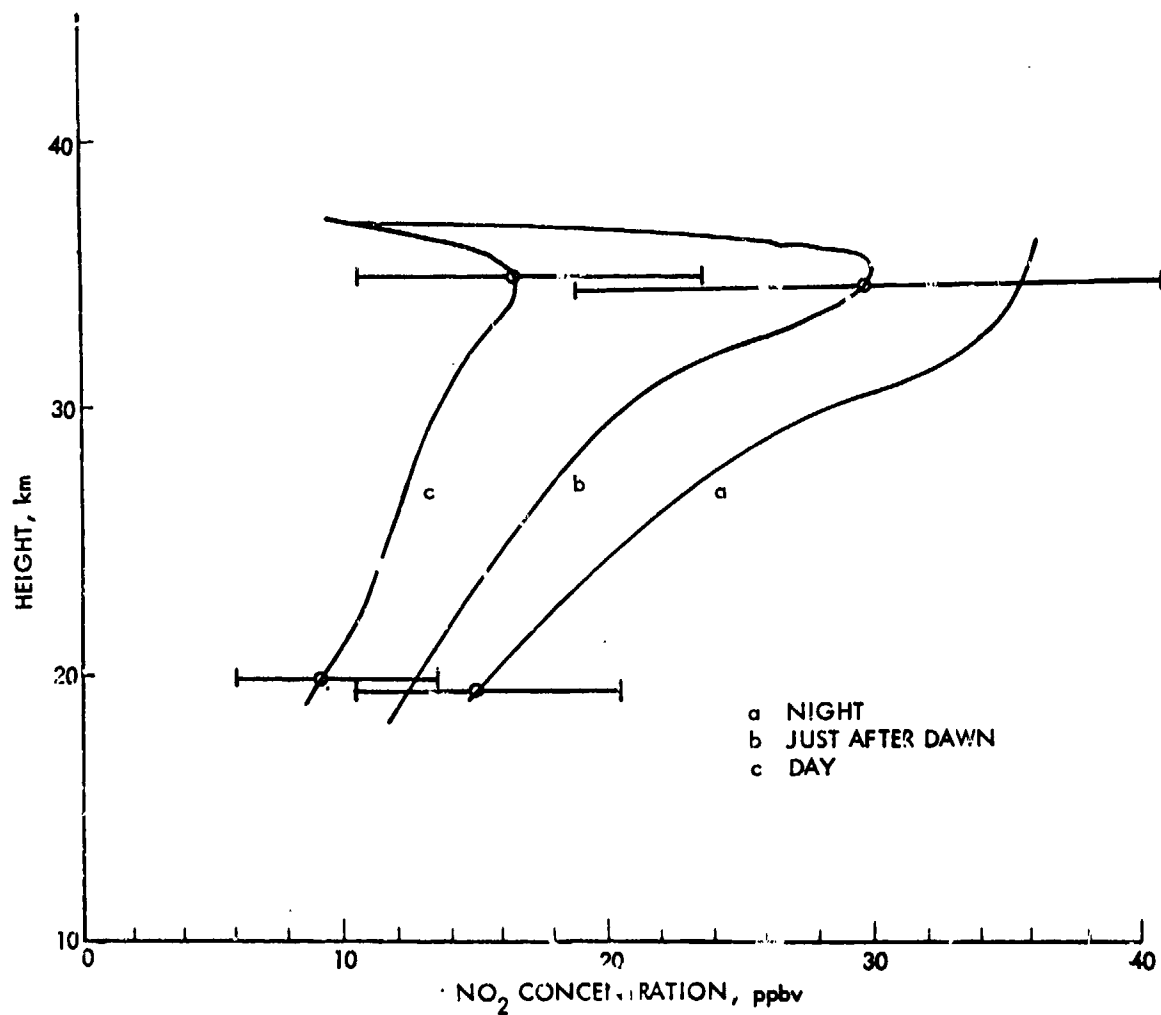
*The Lawrence Livermore Laboratory First Annual Report (p. 26, 30 June 1976) notes that the Lawrence Livermore model has roughly half the NO_x column of other models and traces this fact to the quantum yield formulation used for O(¹D) from ozone as a function of wavelength. The doubled NO_x column decreases ozone sensitivity to NO_x injections from 1.75 percent to 1.35 percent for a 17-km injection.



1-29-77:30

FIGURE B-2. Measured NO Profiles (Representative Values of Random Plus Systematic Errors are Indicated by Bars).

Source: COMESA, 1975



1-29-77-31

FIGURE B-3. Oxford Pressure Modulator Radiometer Results, June 1975
(Representative Values of Random Plus Systematic Errors
are Indicated by Bars).
Source: COMESA, 1975

in HNO_3 column poleward, but did not find significant hemispheric differences. These findings contributed to the totality of data on this important species, but there seems to be no exceptional COMESA position on the matter.

D. N_2O

In common with other researchers, COMESA finds N_2O to be fairly uniformly distributed in the troposphere, falling off with increasing height in the stratosphere, and with no apparent variation with latitude over about 70°N to 40°S (COMESA report, p. 75). COMESA notes, however, inconsistencies in both absolute values (factor of 3 variability) and trends, some of which may be instrumental in nature. It is suggested that this important gas has been given inadequate research attention.

It might be noted here that Junge (1974) has correlated tropospheric variability in concentration with lifetimes. High variability would have considerable significance, if confirmed.

E. CH_4

CH_4 data (versus altitude) have been used to estimate K_z profiles; good N_2O data could also be so used. COMESA summarizes the literature (COMESA report, pp. 77, 126) but reports no original measurements. The variation in data from different researchers suggest considerable uncertainty remains. CH_4 is rather constant in the troposphere at 1.4 ppmv, but decreases in the middle or upper stratosphere.

F. CO

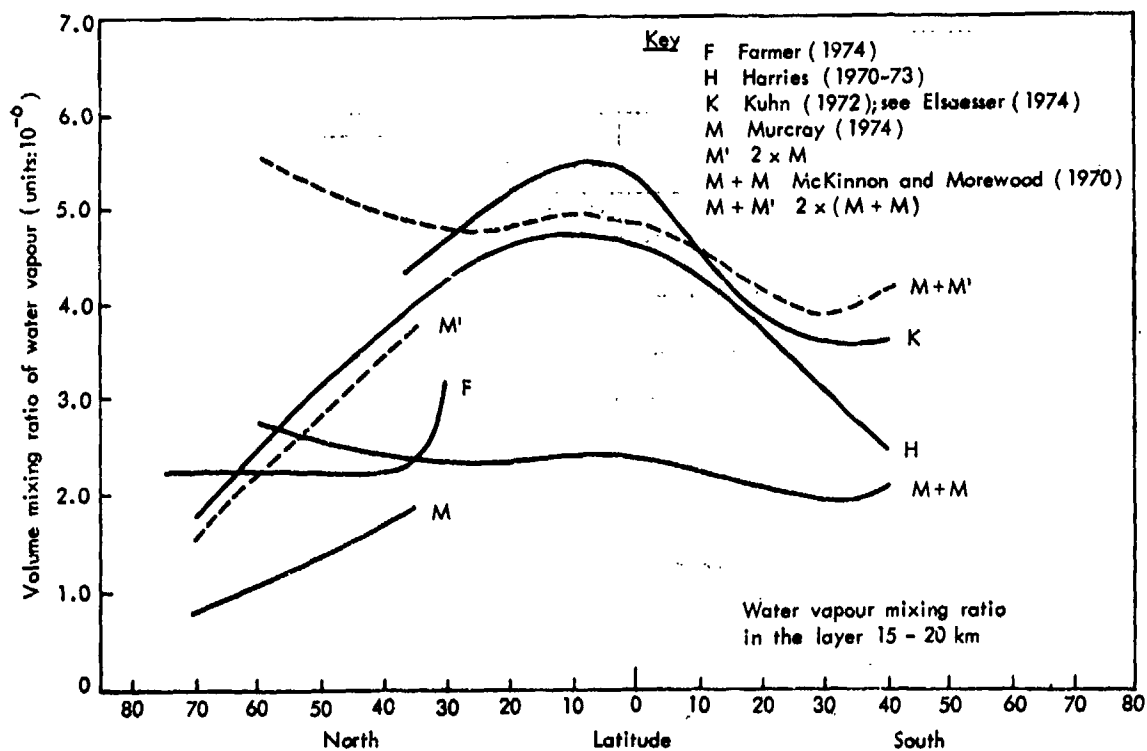
CO , unlike CH_4 , drops off rapidly with altitude (presumably due to destruction by OH) directly above the tropopause. CH_4 oxidation is apparently the principal source of CO at higher altitudes. COMESA reported no measurements of CO .

G. H_2O

H_2O is an important tracer to the dynamics of the stratosphere; however, it is not well understood, despite extensive measurements. A detailed discussion is provided by COMESA of the stratospheric water question. The possible importance of the Antarctic regions as sinks for H_2O are noted, as are layering and changes reported with time.

It is of interest that the Kuhn data (Fig. B-4) show a maximum mixing ratio of 4.5 ppmv at 17 km to 19 km at 10°N . The general shape of the different curves seems to fit this.

COMESA measurements, even though only data obtained above the local tropopause (COMESA report, p. 84) were used, showed a significant increase



11-8-76-1

FIGURE B-4. Latitude Distribution of H_2O in the 15-km to 20-km Layer, Measured by Several Workers (identifications in text).
Source: COMESA, 1975

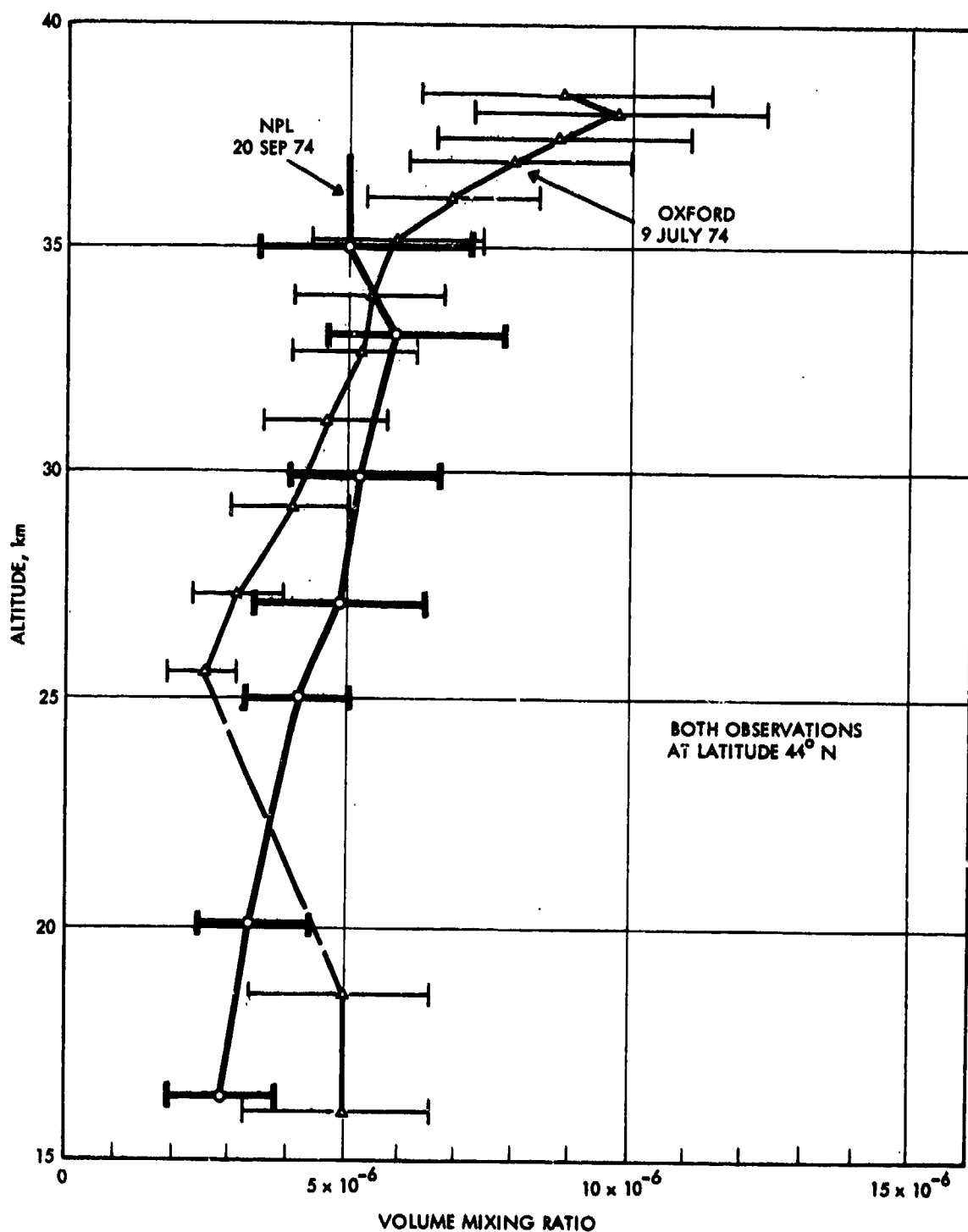
in total water amount towards the equator. Their results are shown on Fig. B-4 as curve H.

COMESA also found a significant increase in H_2O mixing ratio with altitude as shown in Fig. B-5. The result is considered to be explained by CH_4 oxidation.

Water, in the COMESA view, remains an important research topic.

B.2.3 Summary (The Natural Stratosphere)

The COMESA document reemphasizes the points made above (COMESA report, pp. 91-95) and adds certain additional points. COMESA views resolution of differences in N_2O measurements as a matter of priority. (Their modeling exercises showed the effects on ozone of variability in N_2O , with the time delays involved, suggesting a possible erroneous attribution of an ozone



1-21-77-32

FIGURE B-5. Recent Results of Balloon-borne Measurements of H_2O by the Oxford and NPL Groups
Source: COMESA, 1975

decline to stratospheric aircraft.) Important uncertainties in water vapor persist, particularly above 30 km. The ClO_x question is also noted.

The point is also made that simultaneous measurements are needed of NO , NO_2 , HNO_3 , and O_3 as a function of latitude, altitude, and time of day. Ground-state $\text{O}(^3\text{P})$ oxygen atoms, together with OH and O_3 , also need simultaneous measurement.

B.3 LABORATORY CHEMISTRY

B.3.1 Discussion and Measurements

The COMESA report (pp. 143-204) discusses at some length the problems and uncertainties of stratospheric chemistry. The possible importance of excited-state chemistry, and of alternative pathways in estimating the effects of various species are noted; however, the points were not tied in to the chemical models, so that no quantitative appreciation of their significance can be deduced from the discussion. Nevertheless, one gains the impression (which has been well established by Lawrence Livermore Laboratory in later studies) of the large uncertainties in these modeling exercises. (See Section 3, this report.)

Much of the discussion centers around the nitrogen oxyacids, HNO_3 and HNO_2 , and their various reactions. Four two-body reactions are discussed specifically, with results as follows:

	<u>Rate Data Found</u>
$\text{O} + \text{HNO}_3 \longrightarrow \text{products}$	$k < 3 \times 10^{-17}$ (300 K)
$\text{H} + \text{HNO}_3 \longrightarrow \text{products}$	$k \approx 1 \times 10^{-15}$ (300 K)
$\text{OH} + \text{HNO}_3 \longrightarrow \text{H}_2\text{O} + \text{NO}_3$	$k = (0.8 \pm 0.2) \times 10^{-13}$ (298 K, little temperature effect)
$\text{OH} + \text{HNO}_2 \longrightarrow \text{H}_2\text{O} + \text{NO}_2$	$k = (2.2 \pm 0.2) \times 10^{-12}$

The third reaction is the most important; however, while not discussed by COMESA, its importance depends also, to some degree, on the subsequent fate of NO_3 (i.e., to $\text{NO} + \text{O}_2$, or to $\text{NO}_2 + \text{O}$), which pathway is not fully established.*

COMESA also discusses 3 three-body reactions.

	<u>Rate constants</u> <u>$\text{M} = \text{N}_2, 300 \text{ K}$</u>
$\text{OH} + \text{NO}_2 + \text{M} \rightarrow \text{HNO}_3 + \text{M}$	$(15 \pm 5) \times 10^{-31} \text{ cm}^6 \text{ mol}^{-2} \text{ sec}^{-1}$
$\text{OH} + \text{NO} + \text{M} \rightarrow \text{HNO}_2 + \text{M}$	$(26 \pm 10) \times 10^{-31}$
$\text{OH} + \text{SO}_2 + \text{M} \rightarrow \text{HSO}_3 + \text{M}$	$(7.2 \pm 5) \times 10^{-31}$

*Current thinking (see Section 3.0) is that about one-third of the NO_3 goes to $\text{NO} + \text{O}_2$ and two-thirds to $\text{NO}_2 + \text{O}$.

The first one of this set has been shown to be of considerable importance to ozone modeling by Lawrence Livermore Laboratory; hence, a comparison to the CIAP/NBS number is called for.

The rate constant used in CIAP for the equivalent bimolecular reaction is given as

$$\kappa = \frac{\kappa[M]}{(1.12 \times 10^{18} + [M])}, \text{ where } \kappa[M] = 4 \times 10^{-12}.$$

(See Lawrence Livermore Laboratory preprint, UCRL -77917, p. 20, March 1976)

The effective bimolecular rate constant is also given by the COMESA report (p. 179) for this reaction, along with values of [M] at various altitudes. Selected values follow, along with computed values using the CIAP/NBS relationship (Table B-1).

TABLE B-1. COMPARISON OF EFFECTIVE BIMOLECULAR RATE CONSTANTS $\text{OH} + \text{NO}_2 + \text{M} \rightarrow \text{HNO}_3 + \text{M}$

Altitude, km	$10^{-17}[\text{M}],$ (mol-cm ⁻³)	κ_{COMESA}	κ_{NBS}
15	39.8	1.3×10^{-11}	3.12×10^{-12}
20	18.6	8.0×10^{-12}	2.49×10^{-12}
25	8.5	4.2×10^{-12}	1.73×10^{-12}
30	3.8	1.8×10^{-12}	1.01×10^{-12}
35	1.8	8.5×10^{-13}	5.54×10^{-13}
40	0.83	3.2×10^{-13}	2.76×10^{-13}
45	0.40	1.4×10^{-13}	1.38×10^{-13}
50	0.23	5.8×10^{-14}	8.05×10^{-14}

The COMESA results for this reaction support a higher rate than used by CIAP at altitudes to 45 km. The higher rate reduces the effects of added NO_x from aircraft. COMESA modeling efforts, however, adopted the NBS values, with an expression equivalent to that given by Lawrence Livermore Laboratory (COMESA report, p. 299).

The $\text{OH} + \text{SO}_2$ rate found leads, in agreement with information in CIAP, to the opinion that $\text{OH} + \text{SO}_2$ is important in the oxidation of SO_2 in the stratosphere. No discussion of the importance of HNO_2 is given.

Various bimolecular reactions with OH are discussed. The $\text{OH} + \text{HNO}_3$ reaction has already been noted. The important $\text{OH} + \text{HO}_2$ reaction is not mentioned. The reaction $\text{OH} + \text{CO} \rightarrow \text{CO}_2 + \text{H}$ is discussed.

The wavelength dependence for the quantum yield for $O(^1D)$ production in O_3 photolysis is discussed (COMESA report, pp. 161-162, 193). The major point of interest is that COMESA believes a step function (at $\lambda = 308$ nm) from 1.0 to 0 at 233 K may be the most satisfactory for this relationship. This is in contrast to the view expressed by Lawrence Livermore Laboratory in their draft annual report (p. 26).

Quantum yields of HNO_3 photolysis, and questions thereto, are discussed. More work seems to be needed on this important problem.

A number of other reactions and species are discussed, including HNO_2 and NO photolysis, the HO_2 radical, $O(^1D)$ reactions, HO_2 reactions (but not the critical one with OH and HO_2), excited NO_2 , etc., but no particular point is made of the results.

B.3.2 Summary (Laboratory Chemistry)

The COMESA report concludes (pp. 175-176) that, while considerable progress has been made in the last several years, there is still a need for better rate coefficients in the $OH-HO_2-NO_x$ system. The gas kinetic behavior of the higher oxides of nitrogen, as well as methane oxidation processes, are not well understood. Excited species chemistry, particularly in the high stratosphere, needs to be considered, but for this, high quality data on solar UV, its penetration, and on the wavelength dependence of the quantum yield for ozone photodissociation below 310 nm are needed. Chlorine species are also expected to play a central role.

The COMESA group also points out that none of their results contradicts the basic hypothesis that NO_x from stratospheric aircraft will lead to some reduction in stratospheric ozone.

B.4 COMESA OZONE MODELING

B.4.1 Introduction

The COMESA used a number of models in their studies. A major difference with CIAP modeling efforts was the exclusive use by COMESA of 1-D models in which the sun angle is varied diurnally and seasonally. The computer time requirements in such models is vastly larger than in fixed solar angle models, so that the COMESA results were not always assuredly at stationary state conditions. Also, intercomparison of perturbed and unperturbed atmosphere is more difficult with time-dependent, diurnally varying models since all variables change continuously, so that considerable "noise" is evident in the plots of ozone changes versus time.

The following discussion follows that of the COMESA report. The 3-D modeling work, in which only the study of tracers was attempted, is described first. The 2-D work is then discussed, and an intercomparison of the COMESA and CIAP/NAS work follows.

B.4.2 3-D Modeling

The COMESA 3-D general circulation model is described in philosophical terms and in detail on p. 209 and following pages of the COMESA report. The model grid density is nearly uniform, with 4626 points representing the globe with an average grid length of about 320 km. Vertical resolution is typically 3 km, with 13 levels spaced over 0 to 44 km. The model shows many interesting features of the natural atmosphere, including a strong gradient of ozone mixing ratio across the model tropopause and also a downward slope of the mixing ratio isopleths towards the poles in the lower stratosphere.

A. 3-D Injected Tracer Results

The 3-D model was run with simulated NO_x injections from 9 km to 18 km, according to the "Standard CIAP Problem" (1973), but excluding subsonics and the advanced supersonic transport (AST)*, and thus emissions above 18 km (p. 226) (see below, however). The effective NO_x e-folding time in the troposphere due to rainout was taken as 30 days, depleting NO_x where rain was predicted. Seasonal variation in the Standard CIAP Problem was included, making comparison of the data with steady injection models difficult. Also, the model was run for only 360 days, so that stationary state was not achieved. Nevertheless, the results could be interpreted in terms of average flux-gradient relationships for comparison to 1-D models, as shown in Fig. B-6.

The buildup of burden was found to be as follows, in 10^{-8} g-cm $^{-2}$ globally averaged.

<u>Day</u>	Total NO_x <u>Injected</u>	NO_x <u>Rained Out</u>	NO_x <u>Burden</u>
120	3.2	0.9	2.3
240	9.1	3.6	5.5
360	13.4	7.8	5.6

The total NO_x injected after one year (COMESA, p. 253) was $13.4 \times 10^{-8} \times 5.1 \times 10^{18} \times 10^{-3} = 3.417 \times 10^8$ kg, whereas the CIAP Standard Problem, excluding subsonics and the AST, called for 6.86×10^8 kg/yr. The source of the apparent discrepancy is not evident, but is of no apparent consequence. The altitude distribution of the emissions is about as shown

*A vehicle postulated early in the CIAP.

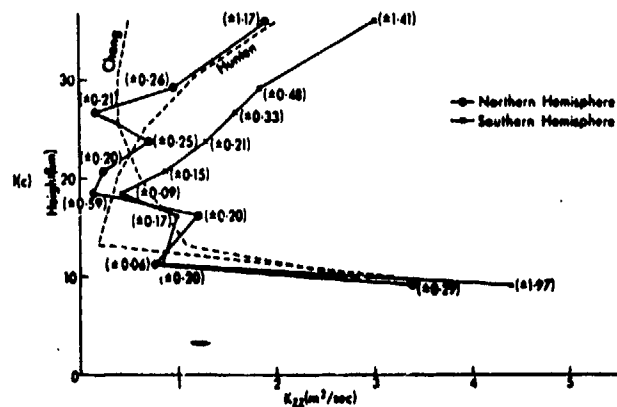
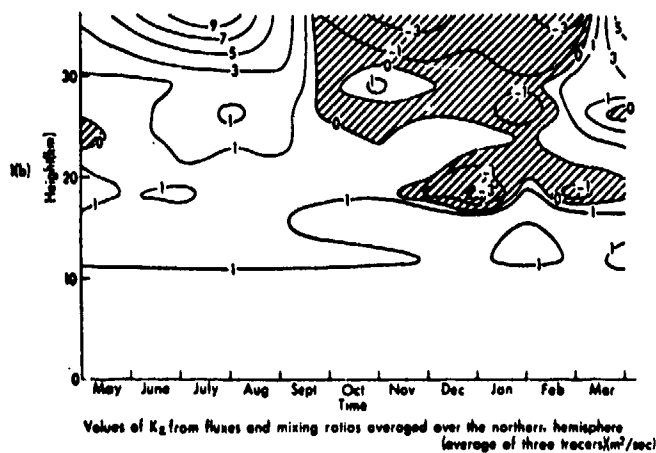
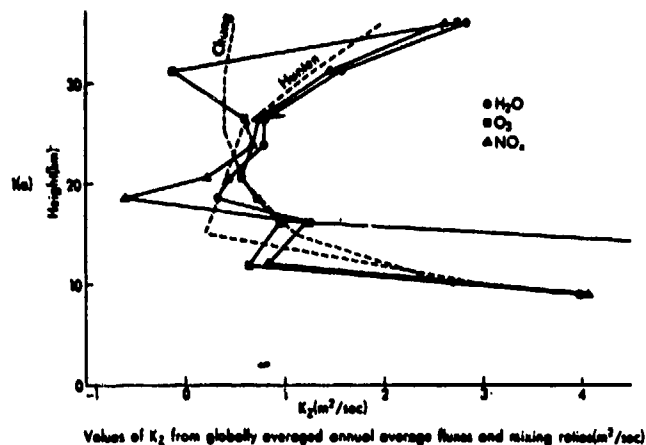


FIGURE B-6. Values of K_2 Hemispherically Averaged Annual Average Fluxes and Mixing Ratios (average of three tracers) (m^2/sec)
Source: COMESA, 1975

in the Standard Problem (63.1 percent 15-18, 31.5 percent 12-15, and 5.4 percent 9-12). Because the model was not at stationary state, and because of the seasonal variation in input, residence times (burden/flux), etc., cannot be determined from this run.

The 3-D results were subjected to averaging processes in order to compare them to 1-D models. Several points of interest were noted. First, three tracers, all treated as inert in the stratosphere (O_3 , H_2O , NO_x) gave different K_z results with, in some cases, negative (Fig. 1a) values being evident, even on a globally averaged annual flux basis. Second, strong seasonal variability (Fig. 1b) was evident, involving both positive and negative values, averaging all three tracers over the Northern Hemisphere. Third, a comparison (Fig. 1c) to Chang and Hunten K_z profiles was made which could be interpreted in a broad sense to support the Chang profile in certain regions and the Hunten profile in others (See Fig. 1). In detail, the comparisons were not very satisfactory. In the critical (to subsonic aircraft) low-altitude region (about 10 km to 13 km), the Chang K_z values were too large, as were Hunten's* at 10 km to 11 km. The extreme minimum at 14 km in the Hunten model was not found in the 3-D studies but low values were found in the 3-D model near about 18 km. The K_z values in the Chang profile above 30 km were too low. [The "new Chang" (1976) profile has, of course, corrected this.] The Northern Hemisphere and Southern Hemisphere values were different.

B. COMESA Interpretation of 3-D Results

The COMESA results (Fig. F-6) have been interpreted by COMESA as follows (pp. 228-229):

"As regards these profiles of \tilde{K}_z **, on the whole, they agree best with the Hunten values above about 26 km. There is fairly good agreement with both Chang and Hunten between 20 and 26 km, there is better agreement with Chang than Hunten between about 14 and 20 km and rather considerable spread at lower levels. The physical implication of these values is that, compared with the 3-D model, the vertical fluxes for all constituents implied by current 1-D models will be too slow in the upper stratosphere when Chang's values are used and too slow in the lower stratosphere when Hunten's values are used....

"Consideration of these results casts considerable doubts on the value of current 1-D models, except for the purpose of first estimates, and emphasizes the need for a more sophisticated treatment of the dynamics."

*As plotted. The 3-km resolution used, however, is too coarse to make much out of this.

**Averaged values.

B.4.3 One-Dimensional Models

A. Discussion

The COMESA report discusses the limitation of various models and of the averaging processes involved at considerable length (pp. 257-ff). Their evident feeling is that 1-D and 2-D models involve internal inconsistencies which cannot be resolved. The call is made for more observations and for comparison of models only to observations (COMESA, p. 258), and not to other models. It is also pointed out (COMESA, p. 274) that "1-D models cannot hope to generate profiles which may be compared with measured distributions."

The discussion points out (COMESA, p. 259) the factor of 2 uncertainty in the solar flux below 270 nm.

An important point is made that it is not clear how to handle some sources and sinks in 1-D models, in which transport for all species at a given altitude is assumed to be dependent on the mixing ratio gradient and the same "eddy diffusion" coefficient, independent of species. Thus, COMESA (pp. 19, 260), notes that the water vapor mixing ratio decreases with altitude; yet water is formed from CH_4 oxidation in the stratosphere and the flux is evidently downward. Mean motions downward must be important, but are not included in the 1-D concept. (Ellsaesser, pp. 7-13, CIAP Monograph 3, makes the same point; in essence, the question is, if water is not carried upward at midlatitudes, why should NO_x from aircraft be carried upward?). As was suggested in the 3-D work, a different K_z should perhaps be applied to each constituent. Excess carbon-14 (COMESA, p. 263), having a completely different sink from NO_x , cannot, in the COMESA view, be given any special significance in explaining the movements of NO_x . Also according to COMESA, the use of CH_4 data near the downward branch of the Hadley cell will give overestimates of residence times because of the sharp gradients near the tropopause.

It is argued (COMESA, p. 260) that, since not all sources and sinks can be known, the model results will be an overestimate of effects, because a balance between too small opposing terms is involved. Furthermore, there is evidence that 1-D models underestimate the rate of vertical transport in the stratosphere as a whole (COMESA, p. 267).

It is argued extensively that the mean motions are supposedly represented by the K_z profile, but the gradients, and thus the transports are, in fact, determined by the photochemistry (COMESA, p. 263). The boundary conditions selected play an important role (COMESA, p. 264).

There are numerous rate constants which are not well established. COMESA agrees (p. 260) that the most critically needed rate is $\text{OH} + \text{NO}_2 + \text{M} \rightarrow \text{HNO}_3 + \text{M}$.

TABLE B-2. THE CHEMICAL KINETIC MECHANISM USED IN MODEL A
SOURCE: COMESA, 1975

O_2	+	hv	+	O + O	OH + NO ₂	+	M	+	HNO ₃ + M
O_3	+	hv	+	O + O ₂	OH	+	O ₃	+	HO ₂ + O ₂
O_3	+	hv	+	O + O ₂ (¹ Δ _g)	HO ₂	+	O ₃	+	OH + O ₂ + O ₂
O_3	+	hv	+	O(¹ D) + O ₂ (¹ Δ _g)	H	+	O ₃	+	OH(v=1-9) + O ₂
NO	+	hv	+	N + O	O	+	OH	+	O ₂ + H
NO ₂	+	hv	+	NO + O	O	+	HO ₂	+	OH + O ₂
N ₂ O	+	hv	+	N ₂ + O(¹ D)	OH	+	OH	+	O + H ₂ O
NO ₃	+	hv	+	NO + O ₂	OH	+	H ₂	+	H + H ₂ O
N ₂ O ₅	+	hv	+	O + NO ₂ + NO ₂	H	+	HO ₂	+	OH + OH
H ₂ O	+	hv	+	H + OH	H	+	HO ₂	+	H ₂ + O ₂
HNO ₂	+	hv	+	OH + NO	H	+	OH	+	O + H ₂
HNO ₃	+	hv	+	OH + NO ₂	O(¹ D)	+	H ₂ O	+	OH + OH
HCHO	+	hv	+	H ₂ + CO	O(¹ D)	+	H ₂	+	H + OH
HCHO	+	hv	+	H + HCO	H + OH	+	M	+	H ₂ O + M
CO ₂	+	hv	+	O + CO	OH + OH	+	M	+	H ₂ O ₂ + M
H ₂ O ₂	+	hv	+	OH + OH	H + O ₂	+	M	+	HO ₂ + M
HO ₂	+	hv	+	O + OH	OH	+	H ₂ O ₂	+	H ₂ O + HO ₂
CH ₃ O ₂	+	hv	+	O + CH ₃ O	O	+	H ₂ O ₂	+	OH + HO ₂
CH ₃ NO	+	hv	+	CH ₃ + NO	HO ₂	+	HO ₂	+	O ₂ + H ₂ O ₂
CH ₃ ONO	+	hv	+	CH ₃ O + NO	OH	+	HNO ₂	+	H ₂ O + NO ₂
O(¹ D)	+	M	+	O + M	OH	+	HNO ₃	+	H ₂ O + NO ₃
O ₂ (¹ Δ)	+	M	+	O ₂ + M	OH	+	CO	+	CO ₂ + H
O ₂ (¹ Σ _g ⁺)	+	M	+	O ₂ + M	H	+	NO ₂	+	NO + OH
OH(v=1-9)	+	M	+	OH + M	N	+	OH	+	NO + H
O + O ₂	+	M	+	O ₃ + M	NO	+	HO ₂	+	OH + NO ₂
O	+	O ₃	+	O ₂ + O ₂	N	+	O ₃	+	NO + O ₂
O(¹ D)	+	O ₃	+	O ₂ + O ₂	N	+	NO	+	N ₂ + O
O(¹ D)	+	O ₃	+	O + O	N	+	O ₂	+	NO + O
O(¹ D)	+	O ₃	+	O ₂ + O ₂ (¹ Σ _g ⁺)	N	+	NO ₂	+	N ₂ O + O
O(¹ D)	+	O ₂	+	O + O ₂ (¹ Σ _g ⁺)	N	+	NO ₂	+	NO + NO
O ₂ (¹ Δ)	+	O ₂ (¹)	+	O ₂ + O ₂ (¹ Σ _g ⁺)	O(¹ D)	+	CH ₄	+	OH + CH ₃
O ₂ (¹ Σ _g ⁺)	+	O ₃	+	O + O ₂ + O ₂	OH	+	CH ₄	+	H ₂ O + CH ₃
O ₂ (¹ Δ)	+	O ₃	+	O + O ₂ + O ₂	OH	+	HCHO	+	H ₂ O + HCO
NO	+	O ₃	+	NO ₂ + O ₂	HCO	+	O ₂	+	HO ₂ + CO
O	+	NO ₂	+	NO + O ₂	CH ₃ + O ₂	+	M	+	CH ₃ O ₂ + M
NO ₂	+	O ₃	+	NO ₃ + O ₂	CH ₃ + NO	+	M	+	CH ₃ NO + M
NO ₂ + NO ₃	+	M	+	N ₂ O ₅ + M	CH ₃ O ₂	+	NO	+	CH ₃ O + NO ₂
O	+	N ₂ O ₅	+	NO ₂ + NO ₂ + O ₂	CH ₃ O ₂	+	CH ₃ O ₂	+	CH ₃ O - CH ₃ O + O ₂
NO	+	NO ₃	+	NO ₂ + NO ₂	OH	+	HO ₂	+	H ₂ O + O ₂
O + NO	+	M	+	NO ₂ + M	CH ₃ O	+	NO	+	CH ₃ ONO
O + NO ₂	+	M	+	NO ₃ + M	CH ₃ O	+	NO ₂	+	CH ₃ ONO ₂
O(¹ D)	+	N ₂ O	+	NO + NO	CH ₃	+	NO ₂	+	CH ₃ NO ₂
O(¹ D)	+	N ₂ O	+	N ₂ + O ₂	CH ₃ O	+	O ₂	+	HCHO + HO ₂
OH + NO	+	M	+	HNO ₂ + M					

TABLE B-3. RATE COEFFICIENTS FOR MODEL B
(with activation energy in cal/mole)
SOURCE: COMESA, 1975

$O_2 + hv$	$\rightarrow O + O$	} Fully time-dependent 45° N sun, J values computed every 30 min Ackerman's solar spectrum
$O_3 + hv$	$\rightarrow O_2 + O(^1D)$	
$O_3 + hv$	$\rightarrow O_2 + O$	
$NO_2 + hv$	$\rightarrow NO + O$	
$HNO_3 + hv$	$\rightarrow OH + NO_2$	
$O(^1D) + M$	$\rightarrow O + M$	$7.0 \times 10^{-11} \text{ cm}^3 \text{ molec}^{-1} \text{ s}^{-1}$
$O + O_2 + M$	$\rightarrow O_3 + M$	$1.05 \times 10^{-34} \exp(1014/RT) \text{ cm}^6 \text{ molec}^{-2} \text{ s}^{-1}$
$O + O_3$	$\rightarrow O_2 + O_2$	$2.00 \times 10^{-11} \exp(-4522/RT) \text{ cm}^3 \text{ molec}^{-1} \text{ s}^{-1}$
$NO + O_3$	$\rightarrow NO_2 + O_2$	$9.50 \times 10^{-13} \exp(-2460/RT) \text{ cm}^3 \text{ molec}^{-1} \text{ s}^{-1}$
$O(^1D) + N_2O$	$\rightarrow NO + NO$	$1.1 \times 10^{-10} \text{ cm}^3 \text{ molec}^{-1} \text{ s}^{-1}$ (other channel allowed for)
$OH + NO_2 + M$	$\rightarrow HNO_3 + M$	$4.0 \times 10^{-12} \frac{[M]}{[M] + 1.1 \times 10^{18}} \text{ cm}^3 \text{ molec}^{-1} \text{ s}^{-1}$
$OH + O_3$	$\rightarrow HO_2 + O_2$	$1.6 \times 10^{-k2} \exp(-1990/RT) \text{ cm}^3 \text{ molec}^{-1} \text{ s}^{-1}$
$OH + HO_2$	$\rightarrow H_2O + O_2$	
$O(^1D) + H_2O$	$\rightarrow OH + OH$	$3.5 \times 10^{-10} \text{ cm}^3 \text{ molec}^{-1} \text{ s}^{-1}$
$O + HO_2$	$\rightarrow OH + O_2$	$2.0 \times 10^{-11} \text{ cm}^3 \text{ molec}^{-1} \text{ s}^{-1}$
$NO + hv$	$\rightarrow N + O$	Assume J_{NO}/J_{O_2} has constant ratio and use Cieslik & Nicolet (1973)
$N + NO$	$\rightarrow N_2 + O$	$2.7 \times 10^{-11} \text{ cm}^3 \text{ molec}^{-1} \text{ s}^{-1}$
$O + NO_2$	$\rightarrow NO + O_2$	$9.1 \times 10^{-12} \text{ cm}^3 \text{ molec}^{-1} \text{ s}^{-1}$

TABLE B-4. THE EDDY DIFFUSION COEFFICIENTS (CHANG VALUES)
SOURCE: COMESA, 1975

$10^{-4}K,$ $\text{cm}^2 \text{ sec}^{-1}$	$z,$ km	$10^{-4}K,$ $\text{cm}^2 \text{ sec}^{-1}$	$z,$ km
2.87	48.5	0.367	28.5
2.33	47.5	0.372	27.5
1.91	46.5	0.382	26.5
1.58	45.5	0.397	25.5
1.33	44.5	0.417	24.5
1.13	43.5	0.443	23.5
0.965	42.5	0.476	22.5
0.837	41.5	0.517	21.5
0.734	40.5	0.568	20.5
0.652	39.5	0.631	19.5
0.585	38.5	0.708	18.5
0.530	37.5	0.805	17.5
0.487	36.5	0.925	16.5
0.452	35.5	1.07	15.5
0.424	34.5	1.26	14.5
0.402	33.5	1.50	13.5
0.386	32.5	1.80	12.5
0.375	31.5	2.19	11.5
0.368	30.5	2.69	10.5
0.365	29.5	30.0	0.5-9.5

TABLE B-5. THE EDDY DIFFUSION COEFFICIENTS (HUNTEN VALUES)
SOURCE: COMESA, 1975

$10^{-4}K,$ $\text{cm}^2 \text{ sec}^{-1}$	$z,$ km
7.2	47
5.9	45
4.7	43
3.8	41
3.0	39
2.4	37
2.0	35
1.6	33
1.3	31
1.1	29
0.9	27
0.72	25
0.56	23
0.45	21
0.37	19
0.30	17
0.23	15
3.0	13
3.0	11
10.0	1-9

B. 1-D Results

COMESA 1-D results were based on models using a diurnally and seasonally (45° N) varying sun, with a fixed K_z profile. It is noted that results from such models cannot show correct seasonal values for a hemisphere (COMESA, p. 207). Two models (A and B) were used, one with 1-km resolution and detailed chemistry (including CH_4 reactions) extending from 10 km to 50 km, and one with abbreviated chemistry (no CH_4 reactions) and 2-km resolution extending from 0 km to 48 km. Further details of the chemistry and dynamics used are given in Tables B-2 to B-5. The first model required 112 sec/day and the second 13 sec/day on an IBM 360-195.

Model A. Model A included N_2O_5 as well as the CH_4 reactions (neither of which were included in CIAP). N_2O_5 has a response time of the order of 24 hours (COMESA, p. 273) in the middle and low stratosphere; furthermore, NO_2 photolysis is not a square wave but rather increases through the day, so that models which do not include the diurnal variation do not evaluate the term $k[\text{NO}_2][\text{O}]$ correctly; a fixed sun is a poor approximation (COMESA, p. 274).

The model was run for 6 years, both for natural and perturbed cases. The perturbed case included H_2O , CO , CH_4 , and CO_2 injections in quantities proportional to Concorde emission indices, with NO_2 injected at the rate of 1.24×10^{34} molecules/yr (COMESA, p. 277.* In molecules- cm^{-3} -sec $^{-1}$ the figures are as given in Table B-6 (COMESA, p. 297).

TABLE B-6. POLLUTANT INPUT RATES USED IN MODEL A
(molecules/ cm^3 -sec)

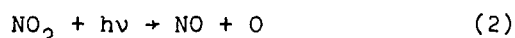
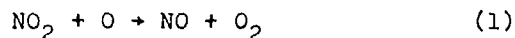
NO_2	768
H_2O	172,800
CO	267
CO_2	91,200
CH_4	77

The injection rate was apparently held constant. The eddy diffusivity profile used was that due to Chang (Table B-4).

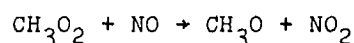
The reduction in ozone was found to vary (COMESA, p. 277) from about 0.8 percent in summer to 1.2 percent in winter. Another experiment was run in which the same injection rate was put in at 11 km to 13 km. The model base, however, is at 10 km, so the results were in some question. However, it was found that an increase in O_3 took place initially, followed after

*Relative to the figure of 1.13×10^{34} for 1000 Concordes (COMESA, p. 24), this is 1097 Concordes; converted to 9.475×10^8 kg NO_x /yr, relative to p. 17 at 8×10^8 kg/yr, this is 1184 Concordes.

about 3 years by a decrease in O_3 , of the order of 0.1 percent, above 10 km. The model showed maximum ozone production at low solar penetration (winter); at summer conditions, the production rate of O atoms was high enough for the injected NO_2 to cause O_3 reduction. The behavior was explained in terms of a tradeoff between NO_2 photolysis which produces O_3 , and NO_2 reaction with O atoms, which destroys O_3 . Thus, if O atom concentration is low, the first of the following two reactions is less important than the second. If O atom concentration is high, the second reaction is less important.



This model included the methane oxidation steps so that



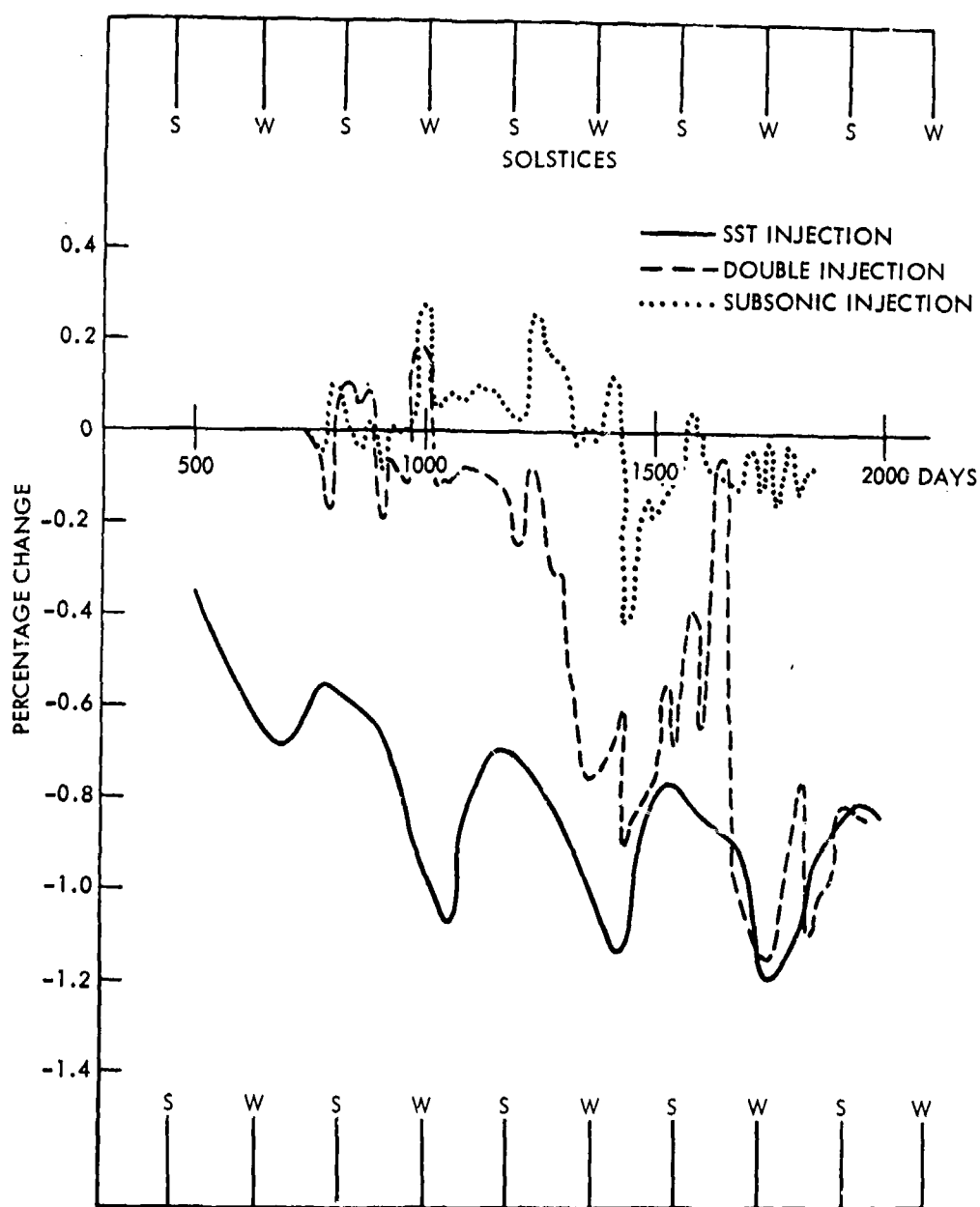
also produced ozone, via reaction (2).*

The model also was run with simultaneous injection at both altitude levels. The results were somewhat inconclusive, since the run was for only 3-1/2 years, but there was some evidence of interference (in the model) between the two sources, each tending to slow transport through the other layer, upwards or downwards. The noisy nature of the results is shown in Fig. B-7, which plots the individual and combined cases.

Model B. The second model used simplified chemistry (Table B-3) (12 species, 18 reactions, and excluding many HO_x reaction and methane oxidation reactions) and extended from 0 to 48 km with 2-km resolution. The model took 1-1/4 hr/yr on the IBM 360-195 and was fully time-dependent. The abbreviated chemistry utilized increased the model sensitivity to NO_x injections. Nine experiments, each involving about a 10-year integration period were performed. The experiments were run with the natural atmosphere, 100 SSTs, and 100 SSTs + 2000 subsonics, with Chang and Hunten K_z profiles. One experiment involved variation with time of N_2O ; in two others, the temperature was changed according to radiative equilibrium considerations. A fixed temperature profile was used in the other experiments.

The NO_x injection rates used were 1.08×10^8 kg/ NO_2 /yr at 16 to 18 km for 100 Concorde equivalents, and 9.16×10^8 kg NO_2 /yr for 2000 subsonics, at 12 km (COMESA, p. 297). The results are discussed in detail in the COMESA report. They are summarized for the aircraft perturbations (COMESA, p. 285) in Table B-7.

*The NO_3 photolysis mechanism (to $NO + O_2$) which destroys O_3 was included; the alternate pathway (to $NO_2 + O$) was not. (See Table B-2.)



I-21-77-34

FIGURE B-7. Percentage Changes in O_3 Column Densities (Model A)

TABLE B-7. OZONE REDUCTIONS PREDICTED BY COMESA MODEL B

<u>Experiment</u>	<u>K_{zz} Author</u>	<u>Percent Reduction in O₃, Late Winter</u>	<u>Percent Reduction in O₃, Late Summer</u>	<u>Annual Mean, Percent</u>
100 SSTs	Chang	0.15	0.09	0.12
2000 subsonics + 100 SSTs	Chang	0.28	0.18	0.23
100 SSTs	Hunten	0.17	0.11	0.14
2000 subsonics + 100 SSTs	Hunten	0.45	0.33	0.39

The conclusion is drawn (by COMESA) that the choice of K_z profile has little effect on predicted O₃ changes due to 100 SSTs (0.12 versus 0.14 percent); however, a considerable effect is noted on O₃ changes due to subsonics. The conclusion with regard to SSTs is surprising in view of other model results,* and may relate to the exact manner in which the numerical modeling was done (with 2-km resolution) to chemistry differences (e.g., 6.7×10^{-11} for the OH + HO₂ reaction, rather than 2×10^{-10} as in CIAP), differences between fixed and varying sun angle, lack of stationary state, etc. The Hunten K_z, for example, was set at a minimum value of 2.3×10^3 at 15 km versus 3×10^4 at 13 km; with finer resolution, a value of 2.3×10^3 is called for at 14 km also.

*The NAS results (NAS report, p. 29) can be prorated to an injection of 1.08×10^8 kg NO₂/yr to give, on a global average basis, for the Hunten K_z profile

$$\frac{0.72}{2} \times \frac{108}{62.8} = 0.619\%.$$

This figure, however, includes a 2-km adjustment for aircraft altitude relative to the tropopause at midlatitudes versus that at which the model was derived. If this correction is removed (see NAS, p. 118), the change in injection coefficient changes the result to 0.345 percent. In contrast (for 16.5-km injection), the Chang results (CIAP ROF, p. B-19) would be,

$$\delta = 1.4972 (0.108)^{0.9091} = 0.198\%.$$

Furthermore, if the Chang chemistry had been used with the Hunten K_z profile (Lawrence Livermore Laboratory/IDA runs of 12-13 December 1975) figures about 50 percent higher (than 0.619 percent) would have been found.

The considerable differences in odd nitrogen budget and ozone distribution in the natural atmosphere between the Hunten and Chang K_z profiles were noted (COMESA report, p. 285). It is suggested that the larger NO_x burden in the natural atmosphere with the Hunten profile decreases the sensitivity to NO_x injections. It should be noted, however, that the Lawrence Livermore Laboratory model results include this effect, also showing considerably more NO_x in the natural atmosphere; yet substantial differences in results are evident between Chang and Hunten K_z profiles.

The importance of the $\text{OH} + \text{NO}_2 + \text{M} \rightarrow \text{HNO}_3 + \text{M}$ rate constant was noted by the COMESA report (p. 287), although no sensitivity results were reported. The rate constant formulation used was apparently that prescribed in the CIAP (NBS) recommendations.

The initial formation of O_3 due to NO_2 injection, even without CH_4 reactions, is noted in their report by COMESA (p. 288).

The model runs in which temperature was calculated rather than prescribed were inconclusive, although suggesting that a minor reduction in the ozone decrease would result.

Runs with varying N_2O in the troposphere were made which showed the time delays involved (12 years to stationary state, COMESA, p. 290) and the effects on O_3 . The point is made, noting the measured increase in N_2O in 1966-69 (Schütz et al., 1970), that ozone reductions of the order of 1 percent to 2 percent would be expected into the mid-1970s and would have important implications for monitoring possible anthropogenic effects.

Several points follow in the COMESA discussion (p. 291). It is argued that subsonic aircraft at 11 km to 13 km cannot be neglected in comparison with supersonic at 16 km to 18 km. It is stated that Model A results show that about 600 Concorde would produce about 1 percent O_3 depletion on a global scale. However, the actual Model A results (COMESA report, p. 277) of 1.24×10^{34} NO_x molecules/yr, or 9.5×10^8 kg/yr as NO_2 , corresponds more closely to about 1200 Concorde, based on information elsewhere in the report. A hemispheric value and a global value were apparently intermixed in this comparison; in the COMESA Summary (p. xvii) and later herein, the information is reported correctly.

It is also pointed out (COMESA report, p. 291) that the constant K_z 1-D model implies higher transport in the summer than in the winter, because of the photochemically created gradients involved, whereas the actual atmosphere has higher transport rates in the winter. It is also argued (COMESA report, p. 292) that the use of average solar zenith angle does not lead to a realistic simulation of the dynamics over an annual cycle. All models are extremely dependent on bottom boundary conditions.

B.4.4 2-D Modeling

A. Discussion

A comprehensive 2-D model at Oxford was not yet complete at the time the COMESA report was prepared (COMESA report p. 332). Work was thus reported with a simplified model in which "known" values of mean winds \bar{v} and \bar{w} , along with empirically determined eddy diffusivity coefficients, were used. Climatological \bar{v} data exist only to about 30 km, and major gaps exist, particularly in the Southern Hemisphere. For higher altitudes, estimates have been made (as, e.g., by J.F. Louis, 1974). The \bar{w} data can be calculated, given \bar{v} data and assuming \bar{w} at the upper boundary is zero. Eddy diffusivity coefficients (K_{yy} , K_{yz} , K_{zz}) have been derived by the various workers, assuming the same values apply to all constituents, but there is a great deal of uncertainty involved, and no guarantee that a set of "tuned values" will be correct (particularly for the perturbed atmosphere). Correct averaging around latitude circles is also difficult to achieve (COMESA report, p. 334). Boundary conditions, or tropospheric sinks, are difficult to specify properly. In short, numerous disposable parameters exist to tune the model to a given observation, but credibility is not necessarily enhanced.

The Oxford 2-D model (COMESA report, p. 338) extends from 0 to 80 km, with a vertical resolution of about 3.5 km (0.75 pressure ratio); the model utilizes a latitudinal resolution of 9.47 deg, and a time resolution of 6 hours. Luther (1973) K_z values have been used. Heating and cooling are calculated explicitly. The model did not assume hemispheric symmetry. Removal of NO_x in the troposphere was simulated by using a time constant for destruction of one week (considerably faster than the 30 days used in the 3-D work). The maximum NO_x mixing ratio (based on a 1-D argument) is increased about 20 percent by doubling the washout time constant to 14 days (COMESA report, p. 342).*

B. Results

At the time of report preparation, the model included a simple treatment of ozone photochemistry, which was not considered suitable for perturbation experiments, although proving runs were carried out, including both tracer and perturbation results.

Tracer experiments (COMESA report, pp. 343 ff) with the model included both W-185 and C-14. The simulation was imperfect in both cases, although perhaps not unreasonably so.

*It is of interest that Prinn et al. (1975) used 30 days (as a "lifetime") below 8 km.

The model was run, for the natural atmosphere, for 3 years -- too short a time to achieve a stationary state. Some evidence of a possible tropospheric source of NO_x was noted (COMESA report, p. 319). Model water vapor distribution was quite realistic in the stratosphere, although volume mixing ratios were rather high, up to 21 km to 23 km levels. (No further data on this point are given.)

The model experiments also included simulated emissions from a fleet of about 100 Concorde and 2000 subsonics. The latitudinal and seasonal distributions were taken from the CIAP Standard Problem, (0.6 winter to spring, 1.08 spring to summer, 1.52 summer to autumn, and 0.8 autumn to winter). Water vapor was taken as 69.3 gm H_2O /gm NO_2 .

The injection rates were taken as shown in Table B-8.

TABLE B-8. AIRCRAFT EMISSIONS IN THE 2-D MODEL

(a) Weighting of Aircraft Flight Frequency

Latitude	85° N	75° N	65° N	55° N	45° N	35° N	25° N	15° N	5° N	5° N	15° S	25° S	35° S
Height													
10-12 km	0.25	0.25	4	23	33	24	8	1.125	1.125	1.125	1.125	1.5	1.5
12-14 km	0.25	0.25	4	23	33	24	8	1.125	1.125	1.125	1.125	1.5	1.5
16-18 km	0.5	0.5	5	29	30	20	8	1	1	1	1	1.5	1.5

(b) Details of Aircraft Types and Total Injections

Height	Aircraft Type	Total NO_2 Injection
10-12 km	500 narrow-bodied, 4-engined	
	1000 wide-bodied, 3-engined	7.0×10^8 kg/yr
	200 wide-bodied, 4-engined	
12-14 km	300 wide-bodied, 4-engined	2.16×10^8 kg/yr
16-18 km	100* Concorde type	1.08×10^8 kg/yr

* (If the conversion rate recommended in Section 2.2 of 0.8×10^8 kg/yr⁻¹/100 Concorde is used, the value of 108×10^8 kg/yr⁻¹ taken here for the SST injection is equivalent to about 135 Concorde.)

The model run was for 3 years, at which time stationary state again had not been achieved (Fig. B-8). However, the ratio of corridor and hemispheric depletions to global depletion did appear to have settled down as follows (Table B-9).

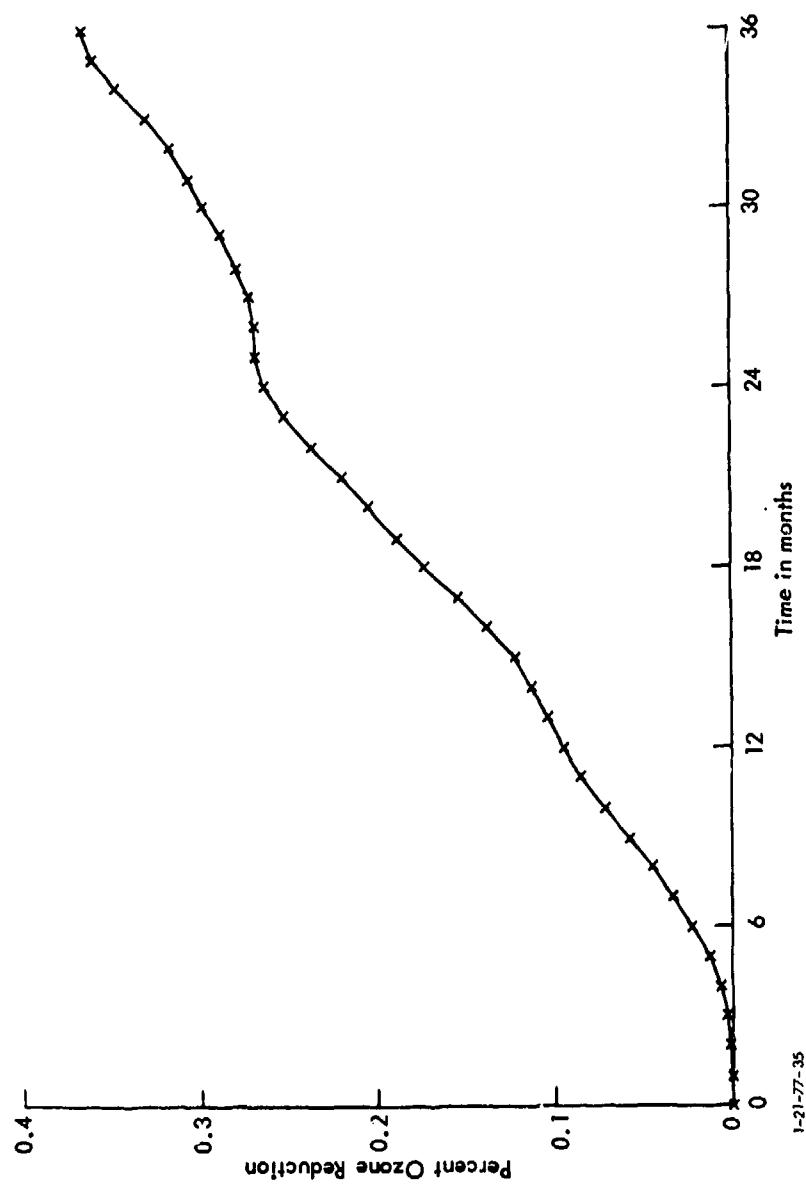


FIGURE B-8. Percentage Reduction in Total Global Ozone Amount

TABLE B-9. RATIO OF NORTHERN HEMISPHERE AND 30° N-60° N CORRIDOR OZONE REDUCTIONS TO THE GLOBAL REDUCTIONS
SOURCE: COMESA, 1975

Integration Time (months)	Northern Hemisphere/ Global	30° to 60° N/Global
6	1.83	2.30
9	1.77	2.39
12	1.85	2.39
15	1.68	2.10
18	1.52	1.73
21	1.58	1.92
24	1.68	2.10
27	1.53	1.87
30	1.46	1.62
33	1.45	1.65
36	1.52	1.88

These figures are not far from those used in CIAP, although the comparison is, in fact, improper in that no 2-D runs at subsonic injection altitudes were carried out in CIAP and much (if not most) of the depletion found in these runs is due to subsonic fleets.

The average global ozone depletion found after 3 years was 0.37 percent. However, the depletion had not shown much evidence (Fig. B-8) of leveling off, so no estimate of the final effect is possible. The depletion was found to be maximum at the North Pole, with a minimum in the equatorial region and another smaller maximum at the South Pole.

B.4.5 COMESA Comparison of Different Model Results

COMESA compared these results to CIAP and NAS results for Concorde aircraft also (COMESA report, p. 386); their results for combined Concorde/subsonic fleets are also discussed further. The results for Concorde aircraft and their comparison follows (Table B-10).

TABLE B-10. COMESA/CIAP COMPARISON

Model	K _z	NO ₂ 10 ⁸ kg/yr	Global Ozone Reduction, %	30-60° Corridor Factor	Corridor Ozone Reduction, %	Normalized** Corridor Reduction, %
COMESA A(d)	Chang	9.5	1.0	1.8*	1.8	0.11
COMESA B3	Chang	1.08	0.12	1.8*	0.22	0.12
COMESA B6	Hunten	1.08	0.14	1.8*	0.25	0.13
CIAP Average	-	0.578	-	2.0	0.39	0.39
NAS Average	-	0.628	-	2.0	0.72	0.66

*Based on COMESA 2-D results.

**To CIAP injection at 0.578×10^8 kg NO₂/yr.

The COMESA report results (p. 386), assuming 8×10^5 kg/yr NO_x /Concorde, indicate about 600 Concorde would be required to cause a 1 percent O_3 depletion in the 30° to 60° N corridor. About half the value will correspond to a global average, and about one-fourth as a Southern Hemisphere average. The effects are thus about one-sixth those of the NAS and one-third those of CIAP. The CIAP values, of course, included the NAS results in the averaging process.

The COMESA report does not note the 2-km adjustment to aircraft altitude used by NAS and by CIAP in applying the NAS model. They again note their results which imply an insensitivity to K_z (COMESA report, p. 387).

COMESA also notes that their ozone depletion results are about half those found by Chang for the same K_z . They comment that the diurnal treatment may reduce the effects, but do not note their use of a smaller rate constant (6.7×10^{-11} rather than 2×10^{-10}) for the $\text{OH} + \text{HO}_2$ reaction.*

The COMESA results for the combined fleets of subsonic and supersonic aircraft are given in Table B-11.

TABLE B-11. OZONE REDUCTIONS FOR COMBINED FLEETS, COMESA MODELS

Model	K_z	Injection as NO_2 kg/yr $^{-1} \times 10^8$ (SST + Subsonic)	Percentage Ozone Reduction, Annual, Global Average	Percentage Ozone Reduction, Annual, Hemispheric Average	Percentage Ozone Reduction 30-60° N Corridor
COMESA A(f)	Chang	(9.5 + 9.5) ^a	1.0 ^b	1.53 ^{c,b}	1.82 ^{d,b}
COMESA B2	Chang	(1.08 + 9.16) ^a	0.24	0.37 ^c	0.43 ^d
COMESA B5	Hunten	(1.08 + 9.16) ^a	0.39	0.60 ^c	0.71 ^d
COMESA 2-D	-	(1.08 + 9.16) ^a	0.37 ^b	0.56 ^b	0.70 ^b

^aFirst figure is SST injection at 16-18 km; second is subsonic at 11-13 km.

^bAt the end of three years, model has not attained a stationary state.

^cCalculated using a conversion factor of 1.53 based on 2-D model results and assumed to apply to both SST and subsonic aircraft flight altitudes.

^dCalculated similarly using a conversion factor of 1.82 based on 2-D model results.

The 2-D result appeared to be headed (Fig. 3) for a higher ozone depletion value than in run B5 but, as noted earlier, no estimate of the stationary state can be made. The superficial agreement in the final two (lower right hand) items should be discounted.

Finally, the COMESA report (p. 388) argues that "the reduction of ozone by present subsonic fleets (which is widely regarded as being negligible) will be less than doubled by addition of a hundred or more Concorde-like SSTs and a change of this magnitude will be quite undetectable."

*The greater natural NO_x burden used by COMESA is also a factor. See p. B-6.

APPENDIX C

ON THE USE OF Zr-95 DATA FROM CHINESE ATMOSPHERIC
THERMONUCLEAR EXPLOSIONS TO STUDY ATMOSPHERIC
MOTIONS IN A ONE-DIMENSIONAL PARAMETERIZATION

E. Bauer
R. C. Oliver
W. Wasylkiwskyj

ACKNOWLEDGMENT

We should like to thank J. D. Mahlman and K. Telegadas who reviewed this material, and D. M. Hunten who reviewed an earlier version.

APPENDIX C

ON THE USE OF Zr-95 DATA FROM CHINESE ATMOSPHERIC THERMONUCLEAR EXPLOSIONS TO STUDY ATMOSPHERIC MOTIONS IN A ONE-DIMENSIONAL PARAMETERIZATION

C.1 INTRODUCTION AND SUMMARY

Here we analyze the detailed data reported by the National Oceanic and Atmospheric Administration (NOAA) (Telegadas, 1974, 76) on transport of zirconium-95 from five Chinese 3-Mt thermonuclear explosions which deposited their debris clouds at approximately 18-km altitude and 40° N and 90° E, in terms of one-dimensional diffusive transport into the troposphere. The motivation for this work is that the dynamics of oxides of nitrogen and other materials injected into the lower stratosphere by (Concorde/Tu-144) SSTs in the general region of 15-km to 18-km altitude, 40° N to 60° N latitude, is not well known, and one-dimensional parameterizations of these dynamics by different authors vary substantially. (See Appendix D this report).*

The zirconium-95 data examined here show strong seasonal variation, with rapid transport into the troposphere in winter and slow transport in summer and fall, which implies advective rather than diffusive behavior.

A technique is developed here that allows data from pulsed sources at different seasons to be used to parameterize mean stratospheric dynamics and thus to estimate the annual mean residence time (burden/flux) for continuous sources. A correction is made for sedimentation of the radioactive aerosols which carry the zirconium-95. We calculate both injection coefficients and mean atmospheric residence times by our technique, and compare them to values derived by various other one-dimensional (1-D) parameterization of stratospheric transport.

The present results support Chang's parameterization of lower stratospheric dynamics better than Hunten's parameterization. The results are thus in disagreement with results based on excess carbon-14, as analyzed by Johnston et al., (1976) who found the Hunten parameterization to be preferable.

*We believe these data analyzed here to be more directly applicable to the SST problems than data from other tests, which took place near the equator or at 75° N. These data have not previously been analyzed in this context.

C.2 OBJECTIVE, OUTLINE, AND A CAVEAT

The objective of this work is to compare mean motions in the lower stratosphere as evidenced by the zirconium-95 data to those implied by existing 1-D parameterizations of such motions. A major problem in doing so is to establish a relation between pulsed and continuous injection for the altitude/latitude regime of interest. Note that we do not develop an eddy diffusivity profile; rather, we develop effective mean eddy diffusivities and the resultant injection coefficients and residence times between 18 km and the local tropopause, and compare these injection coefficients and residence times to those derived from published profiles.

In carrying out the effort, we first review the data base, and then present an analytic model for gaseous diffusion--initially neglecting the sedimentation of the fine aerosols that carry the radioactivity--using a simplified model for the eddy diffusivity profile. The correction for sedimentation is made, and calculations carried out with and without this correction. Effects of uncertainties in mean tropopause height are then considered. Conclusions relating to continuous rather than pulsed injections are then drawn. Finally, the results and approximations are discussed in the context of other data that have been used to give eddy diffusivity profiles, residence times, and injection coefficients.

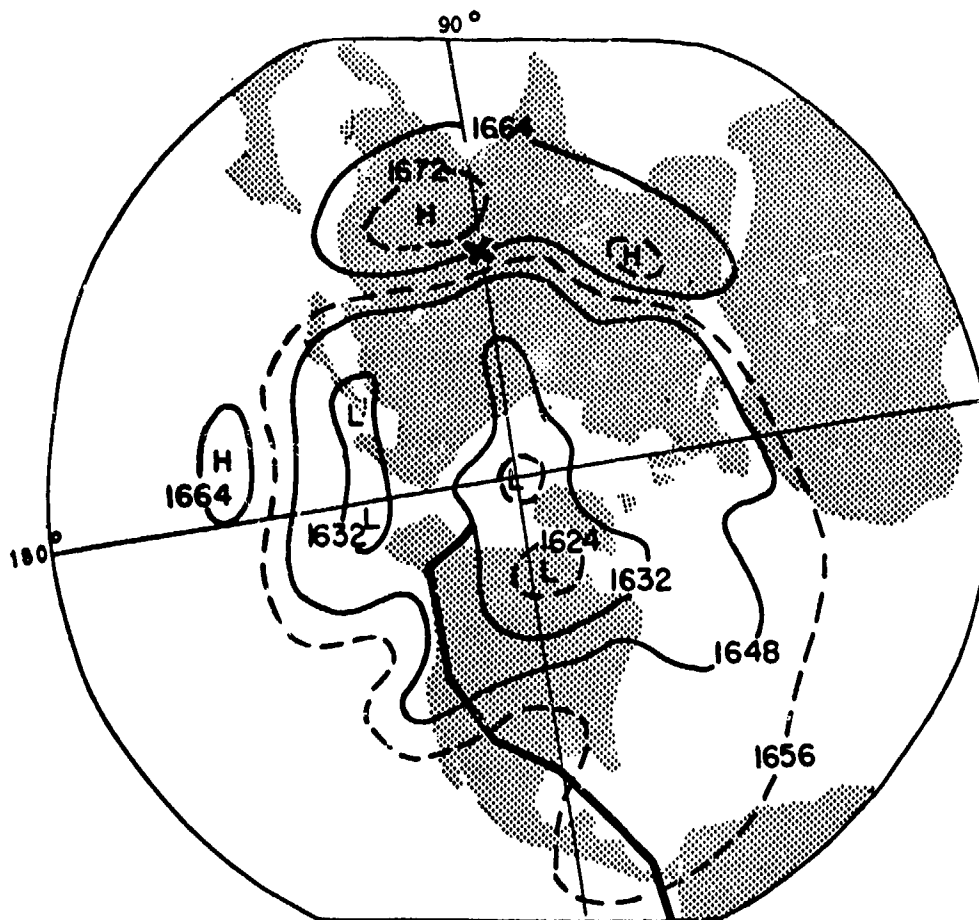
While this discussion deals with a 1-D parameterization of atmospheric dynamics, we do not regard 1-D parameterizations as adequate; a significant motivation for this study has been the fact that eddy-diffusivity profiles based on data collected at different latitudes show significant differences, and, in the present case, there is also strong evidence for variation with season. Nevertheless, because policy decisions* have used results from 1-D parameterized models, we consider it important to review any data which may provide validation tests for such models. In this context, reference should be made to the work of Johnston et al. (1975) in which excess carbon-14 was used as a tracer, also the NAS report (pp. 146-149); these data and their limitations are discussed in Section 3.

C.3 EXPERIMENTAL DATA

C.3.1 Discussion

The U.S. ERDA "Airstream" program has involved sampling radioactive debris with high-flying aircraft (RB-57F, flying at 15 km to 20 km altitudes along a flight path shown (for the Northern Hemisphere) in Fig. C-1. These flights, at regular intervals, are supplemented by occasional balloon probes,

*See, e.g., Environmental Impact Statement--Concorde.



1-31-77-2

FIGURE C-1. Height (decameters) of the 100-mb Surface on June 17, 1967 (0000 GMT). Cross denotes location of the Chinese test site, bold solid line denotes the approximate position of the Airstream sampling corridor
Source: Telegadas, 1974

which are flown mainly from San Angelo, Texas (32° N, 101° W), and which go to higher altitudes.

At the initiation of the Airstream program, indeed as part of the motivation, it was believed that East-West transport is fast relative to North-South or vertical transport, so that the Airstream corridor, which goes along the West Coast of North and South America from 72° N down to 50° S (more recently 10° S), provides an effective zonal average profile some weeks after a detonation at the Chinese test site at Lop Nor (40° N, 90° E). Partly as a result of the program, we now know that the assumption that the distribution observed along the American meridians some 2 to 16 weeks after the detonation is representative of the average concentration of the nuclear cloud is unlikely to be valid in all cases. This assumption, made by Telegadas in deriving an estimate of the vertical distribution of radioactivity with height, introduces some uncertainty in the data. However, we are concerned generally with later times (although we do comment on apparent early-time behavior), and here we concern ourselves only with a 1-D parameterization. To some extent, we are concerned with the height distribution of radioactivity in the stratosphere, but our primary concern is with the rate of removal of radioactive debris from the stratosphere on a global basis. Among other parameters (such as altitude, season, and type of injection), this removal rate will vary with the latitude of injection, so that the analysis that follows applies specifically only to the latitude under study, i.e., 40° or generally midlatitudes.

C.3.2 Data Presentation

The data are described in terms of altitude/latitude profiles presented every 3 months in terms of a stratospheric burden of the isotope zirconium-95 (half-life 65 days), decay-corrected to the time of detonation. The integrated stratospheric burdens of zirconium-95 for the various Chinese 3-Mt thermonuclear explosions computed by Telegadas (1974, 1976, are shown in Fig. C-2. (Tabulated data are given in Table C-1). These are the basic experimental data analyzed here.

Some representative altitude profiles are given in Fig. C-3. Note that according to the data, the peak in activity moves upward about 2 km in the 16 weeks following the 17 June 1967 test (the 27 June 1973 test shows similar behavior), but downward about 4 km in the same period following the 14 October 1970 test when compared to an initial distribution based on a composite of all the Chinese 3-Mt tests. This is certainly not consistent with the concept of diffusive motion, but implies that large-scale winds which show time (seasonal?) variations are significant. Indeed, we see in Fig. C-2, that for a summer injection there is no significant decrease in stratospheric

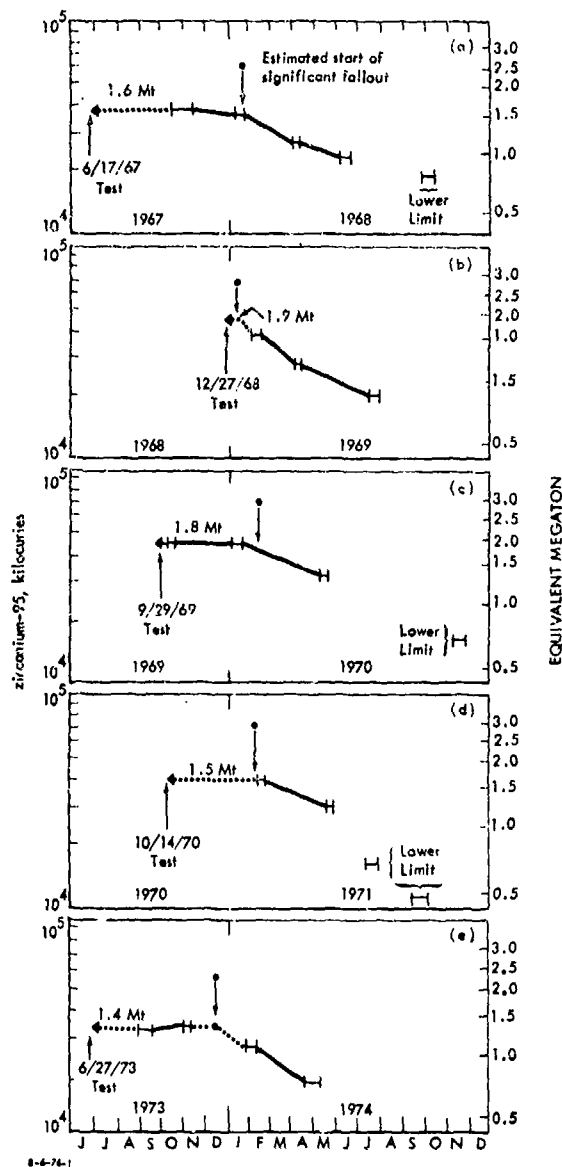


FIGURE C-2. Stratospheric Zirconium-95 Burdens (decay-corrected) Following the Chinese Nuclear Tests. Observed burdens are indicated by the short horizontal lines.
Source: Telegadas, 1974

burden until midwinter, while with a winter injection of tracer, the stratospheric burden decreases steadily.

It should be noted that, in a simple 1-D diffusive model, the tropopause height is critical to the quantitative interpretation of the data. Unfortunately, the tropopause height in the region of interest is highly variable, certainly seasonally, and at times even on a day-to-day basis; a rapid decrease with latitude (typically 2-km decrease between 40° N and 50° N) is usually evident, and considerable variation occurs with longitude, particularly over Eastern Asia. [See, for example, CIAP Monograph 1 (1975) pp. 2-5 to 2-8; also Leifer et al. (1976), Figs. 1-4.] The proper mean tropopause height is thus not easy to establish. In the following analysis, we make no effort to establish a seasonally or longitudinally weighted mean; rather, we use, for initial purposes, a value (11 km) based on reported values by Telegadas (1974) at the times and places of the tests, as shown in Fig. C-3, and then examine the sensitivity of the results to a change in this value (to 14 km). The value of 11 km is not inappropriate for the December-February quarter, but is 1/2- to 1-km low for the March-May quarter, 3- or 4-km low for the June-August

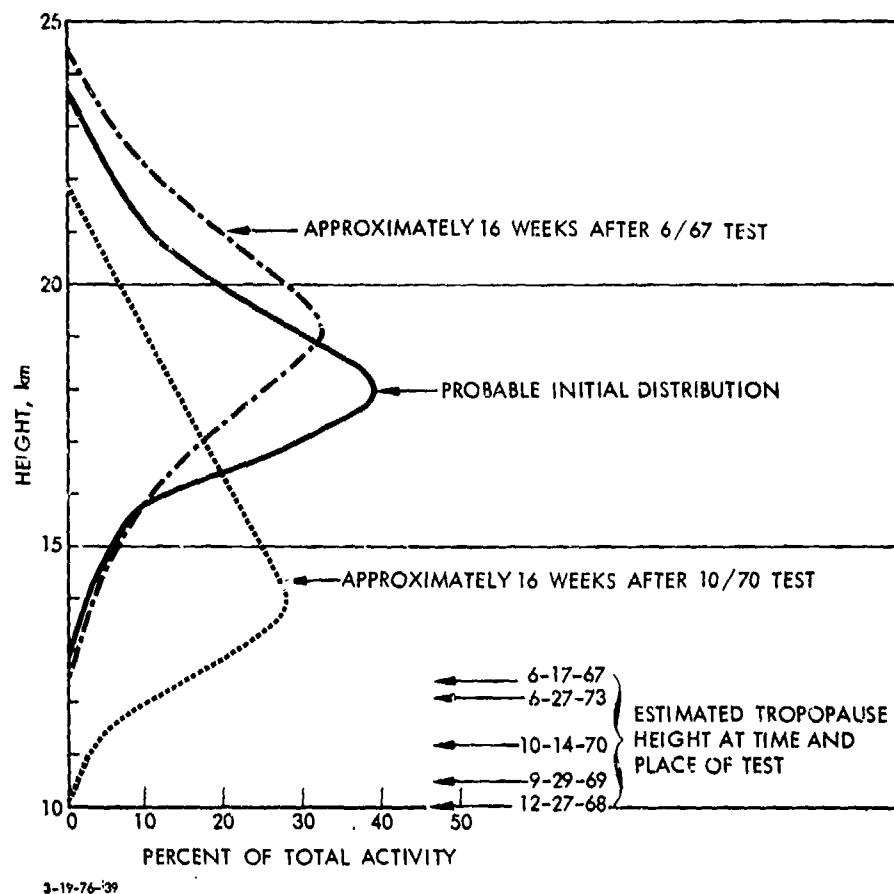


FIGURE C-3. Effective Vertical Transport of Radioactivity Estimated by Telegadas (1974, from Figs. 44 and 45). The profiles were obtained by normalizing the total radioactivity observed during the relevant Airstream flights (see Fig. C-1 for the Airstream flight corridor) and smoothing over 5000-ft vertical intervals. Note the difference in behavior following June and October injections.

quarter, and about 3-km low for the September-November quarter (see e.g., Reiter, et al. (1975) pp. 2-5 to 2-8).

Note that J.F. Louis (private communication, May 1976), who analyzed the 1967-1970 data with a 2-D model, treated the effective latitude of injection of the 1967 debris at 55° N rather than 40° N; evidently, the cloud from that detonation was caught in the Central Asian summer high-pressure cell and thus took a relatively long time before it was zonally spread. This is one clear instance where the use of zonal averaging to give

TABLE C-1. Stratospheric Inventory of Zirconium-95
Resulting from Chinese Tests
SOURCE: Telegades 1974, 1976

Date	Predominantly Chinese Debris, kilocuries
17 June 1967 Test (kilocuries decay corrected to 17 June 1967)	
July 17 - August 8, 1967	6,400 ^a
October 7 - November 9, 1967	38,500
January 8 - January 21, 1968	36,400
April 1 - April 7, 1968	27,200
May 30 - June 15, 1968	23,000
September 28 - October 6, 1968	18,600 ^b
27 December 1968 Test (kilocuries decay corrected to 27 December 1968) ^c	
February 3 - February 19, 1968	38,500
April 6 - April 9, 1969	27,800
July 14 - July 29, 1969	19,500
29 September 1969 Test (kilocuries decay corrected to 29 September 1969) ^d	
October 13 - October 17, 1969	44,700
January 5 - January 20, 1970	45,300
May 6 - May 11, 1970	32,200
August 17 - August 22, 1970	18,800 ^e
14 October 1970 Test (kilocuries decay corrected to 14 October 1970) ^f	
November 2 - November 6, 1970	^a
February 22 - February 27, 1971	38,400
May 22 - May 28, 1971	29,800
July 19 - July 23, 1971	14,600 ^g
October 4 - October 6, 1971	11,800 ^g
27 June 1973 Test (kilocuries decay corrected to 27 June 1973)	
September 5 - September 19, 1973	33,200
October 30 - November 9, 1973	34,700
January 22 - February 2, 1974	28,300
April 12 - April 29, 1974	19,800

- a. Due to the synoptic pattern, very little fresh debris was sampled.
- b. Lower limit due to the French 1968 debris overwhelming regions occupied by the Chinese 1967 debris.
- c. Northern Hemisphere zirconium-95 stratospheric background burden prior to test, based on September 28 - October 6, 1968 observations, estimated as 170 kilocuries of zirconium-95.
- d. Northern Hemisphere zirconium-95 stratospheric background burden prior to test, based on July 14 - July 29, 1969 observations, estimated as 910 kilocuries of zirconium-95.
- e. Lower limit due to the French 1970 debris overwhelming regions occupied by the Chinese 1969 debris.
- f. Northern Hemisphere zirconium-95 stratospheric background burden prior to test, based on August 17 - August 22, 1970 observations, estimated as 400 kilocuries of zirconium-95.
- g. Lower limit due to the French 1971 debris overwhelming regions occupied by the Chinese 1970 debris.

a 2-D model (not to speak of 1-D parameterization!) would seem to be inadequate, at least at relatively early times.

C.4 PROCEDURE AND DATA REDUCTION FOR TIME-DEPENDENT DATA

C.4.1 The Model

We treat the stratosphere as a region of constant and relatively small eddy diffusivity coefficient K , characterized by a tropopause at height z_0 , below which transport is very much faster; the eddy diffusivity profile is taken as

$$K(z) = \begin{cases} K, & \text{constant, in the stratosphere, i.e., for } z > z_0 \\ K_t, & \text{constant, in the troposphere, i.e., for } z < z_0 \end{cases} \quad (1)$$

where, typically, $K_t \approx 10 K$. This simple K -profile was used by Machta (1974) and by Crutzen (1974); it is used here because in this way we can obtain an analytic solution for transport in the stratosphere. In fact, we do nothing with the tropospheric portion of the solution except when we convert data from pulsed injections to steady-state loadings in Section C.5, at which point we take $K_t = 10^5 \text{ cm}^2/\text{sec}$ based on values used by several modelers.

We also assume an isothermal stratosphere, so that in the region of interest

$$N(z) = n_0 e^{-(z-z_0)/H}, \quad (2)$$

where $n(z)$ = total particle number density at height z , $n_0 = n(z_0)$, and the "scale height" $H = kT/Mg$ is taken as 6.3 km (corresponding to $T = 216 \text{ K}$). In the region from 10 km to 20 km, which is of direct interest here, the assumption of constant temperature is quite well satisfied.

In the spirit of the assumption of Eq. (1) for the K -profile, we initially ignore sedimentation (postponing discussion to Section C.4.3 below), and write a diffusion equation for the mixing ratio $f(z,t)$ of our injectant, which is defined as

$$f(z,t) = \frac{\text{[number of injectant molecules (particles) per cm}^3 \text{ at height } z \text{ and time } t]}{\text{total number of air molecules per cm}^3 \text{ at height } z, n(z)} \quad (3)$$

Since the injectant is assumed to be chemically inert, at least in the stratosphere, in a diffusive model $f(z,t)$ is assumed to satisfy the following equation,

$$(\partial/\partial z)[n(z)K(z)\partial f/\partial z] = n(z) \partial f/\partial t, \quad (4)$$

which, in the stratosphere, with hypotheses (1) and (2), becomes

$$\partial^2 f/\partial z^2 - (1/H)\partial f/\partial z = (1/K)\partial f/\partial t. \quad (5)$$

The problem is to solve Eq. (5) with the initial condition

$$f(z,0) = q\delta(z - z_1), \quad (6)$$

corresponding to instantaneous point injection at height z_1 ; in fact, the initial injection is not precisely a delta-function injection, so there is a slight time correction, as discussed in Section 2.3.

The solution of Eqs. (5 and 6) can be shown (see Addendum) to be

$$f(z,t) = q(4\pi Kt)^{-1/2} \exp \left\{ -(Kt/4) \left[(1/H) - (z - z_1)/Kt \right]^2 \right\}. \quad (7)$$

Figure C-4 shows the general character of the solution. We assume some kind of a sink either in the troposphere (rainout/washout, or conceivably, chemical destruction) or at the ground. If either diffusion or disappearance in the troposphere is "efficiently fast," the details of $f(z,t)$ in the troposphere are not important, and thus we may just ask for the total stratospheric burden,

$$B_{\text{strat}}(t) = \int_{z_0}^{\infty} n(z)f(z,t)dz. \quad (8)$$

Note that an assumption has been made here, in that we have simply extended the solution (7), which really only applies to $K(z) = K$ (i.e., for $z > z_0$), to lower altitudes, by ignoring any change in $f(z,t)$ due to the different behavior in the troposphere. Or, stated alternatively, the model treats the diffusion process as though it were taking place in an infinite atmosphere extending in both directions from the point of injection, and we compute the burden above a given point which represents the tropopause. By this assumption, the stratospheric burden of material of Eq. (8) is given by the following expression:

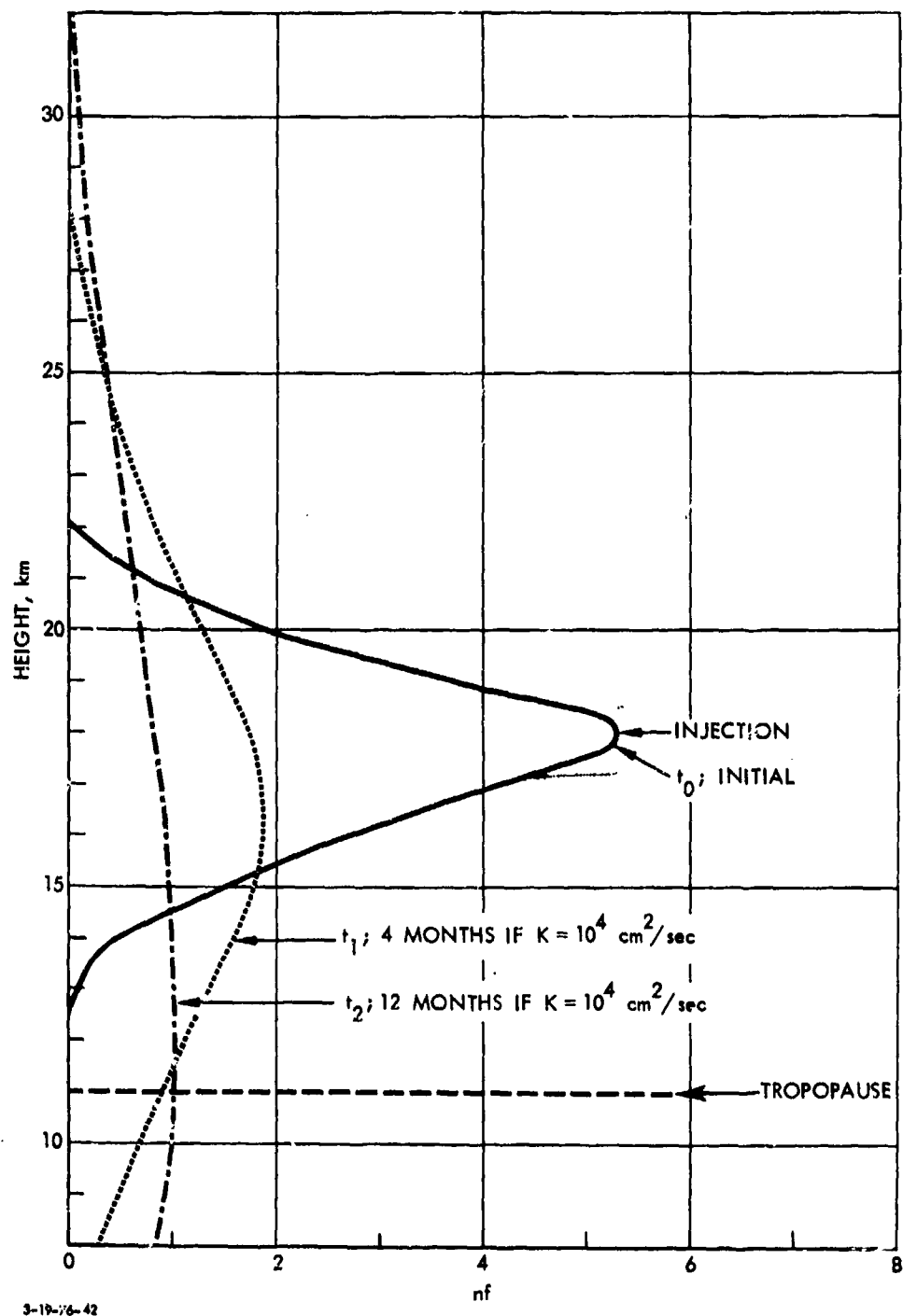


FIGURE C-4. Sketch of the Overall Character of the Solution for Injection at $z_1 = 18 \text{ km}$. We show nf , the total number of tracer particles per unit volume

$$B_{\text{strat}}(t) = n_0 q e^{-(z_{1,0}/H)} U(x_0) , \quad (9a)$$

$$x_0 = 1/2(Kt)^{1/2} \left[(1/H) - (z_{1,0}/Kt) \right] ; z_{1,0} = z_1 - z_0 , \quad (9b)$$

$$U(x_0) = \begin{cases} 1/2(1 + \text{erf } x_0) & \text{for } x_0 < 0 \\ 1/2(1 - \text{erf } x_0) & \text{for } x_0 > 0 \end{cases} . \quad (9c)$$

The overall relationship between time t , x_0 , and $U(x_0)$ is given below:

<u>time t</u>	<u>small</u>	<u>$H z_{1,0}/K$</u>	<u>large</u>
x_0	large, negative	0	$(Kt)^{1/2}/2H$
$U(x_0)$	1	0.5	$1/2(1 - \text{erf } x_0) \rightarrow 0 \text{ as } t \rightarrow \infty$

The physical meaning of Eq. (9) is relatively clear-cut. The quantity $q n_0 e^{-(z_{1,0}/H)}$ in Eq. (9a) is the total number of molecules per unit area injected at $t = 0$ at $z = z_1$; x_0 is a time-dependent variable, and $U(x_0)$ is the fraction of injected material that remains in the stratosphere after time t characterized by $x_0(t)$. The function $U(x_0)$ is shown in Fig. C-5.

A simple way to determine K is to find that time, $t_{1/2}$, at which the stratospheric burden of injectant is half its initial value. Evidently, this corresponds to the condition

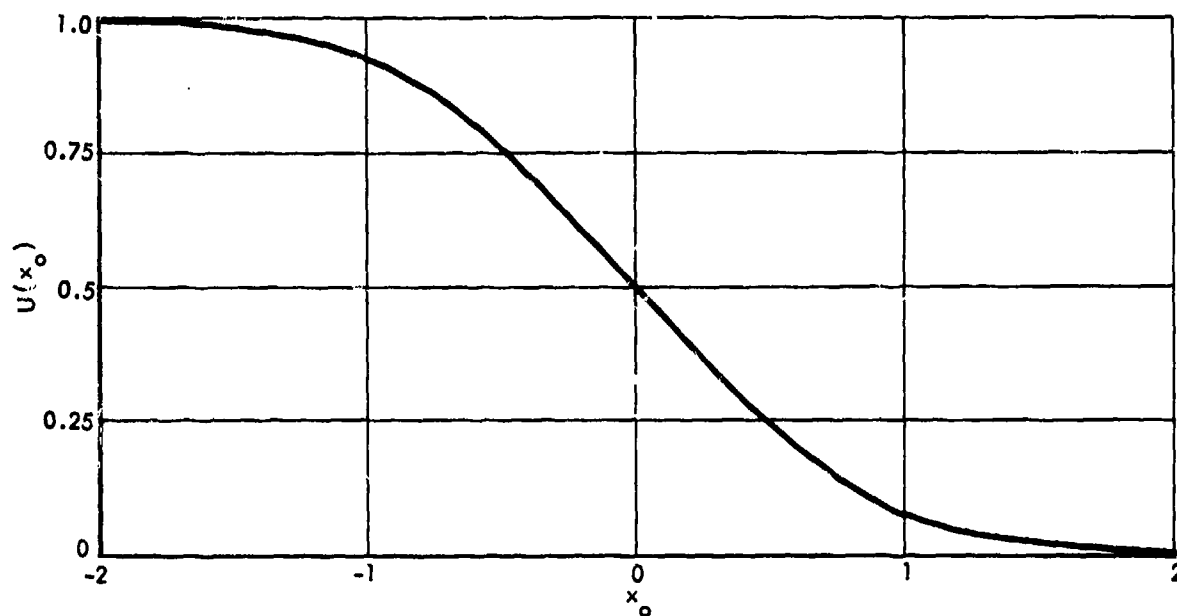
$$t_{1/2} = H z_{1,0}/K ,$$

or

$$K = H z_{1,0}/t_{1/2} .$$

(10)

Note that, the product $K t_{1/2}$ is directly proportional to $z_{1,0}$. K values are thus sensitive to the tropopause height selected. However, as will be demonstrated later, the height of the tropopause also enters in computing the steady-state loading of the stratosphere from an aircraft source, and thus there is a compensation between uncertainties in the value of K and the choice of tropopause height.



3-19-76-43

FIGURE C-5. The Function $U(x_0)$ Which Measures the Reduction in Tracer Burden with Time.

C.4.2 Initial Condition

The initial zirconium-95 profile shown in Fig. C-3 can be fitted quite well to a Gaussian profile:

$$f(z, t_0) = f_0 \exp \left\{ -(z - z_1)^2 / \sigma_0^2 \right\} , \quad (11)$$

with $\sigma_0 = 2.15$ km, which can be reconciled with the initial conditions of Eq. (6) by the equivalence

$$\sigma_0^2 = 4 K t_0 .$$

With the typical mean value $K = 10^4$ cm²/sec, $t_0 = 0.44$ months,* which is so short compared to the observation times shown in Fig. C-2 that the assumption of a delta-function profile for $f(z, t = 0)$ --see Eq. (6)--won't cause any trouble, only the time of detonation must be taken as $t = t_0$ rather than as $t = 0$ when presenting experimental data.

*We define a month as $1/12$ of a year = 2.63×10^6 sec.

C.4.3 Correction for Sedimentation

Zirconium-95, like most other radioactive isotopes, is carried on small particles whose mean radius lies in the range 0.02 μm to 0.15 μm * (see Drevinsky and Pecci, 1965; Telegadas and List, 1969). We assume that the density of the particles is $\rho = 2 \text{ g/cm}^3$, as did Telegadas and List (1969). Radioactive isotopes make up only a small fraction of the mass of aerosols associated with fallout, and a value $\rho = 2.5 \text{ g/cm}^3$ is often assumed for them (Telegadas, NOAA, private communication). However, the sedimentation velocities we use are calculated for smooth spheres, which would fall faster than the irregular particles which are, in fact, produced, thus compensating, to some extent, for a possible underestimate in density.

Particles of this size and density have a small, but not negligible Stokes velocity of sedimentation: for $\rho = 2 \text{ g/cm}^3$, particles of radius $R = 0.1 \mu\text{m}$ have a sedimentation velocity $v_s = 3.6 \times 10^{-3} \text{ cm/sec}$ at an altitude of 18 km (see, e.g., Junge, et al., 1961), which corresponds to a net settling of about 100 m per month. One way to correct for sedimentation is to assume that the mean injection height falls with the effective sedimentation speed v_s . Thus, the effective injection height above the tropopause is

$$\tilde{z}_{1,0}(t) = z_{1,0} - \int_0^t v_s[R, \tilde{z}_{1,0}(t)] dt, \quad (13)$$

since the sedimentation speed depends on radius and on ambient height (or density). A plot of $\tilde{z}_1(t)$ is given in Fig. C-6, for $\rho = 2 \text{ g/cm}^3$, $R = 0.1 \mu\text{m}$.

With this correction, we replace x_0 of Eq. (9) by

$$\tilde{x}_0 = \sqrt{2(Kt)^{1/2} \left[(1/H) - (\tilde{z}_{1,0}(t)/Kt) \right]}, \quad (14)$$

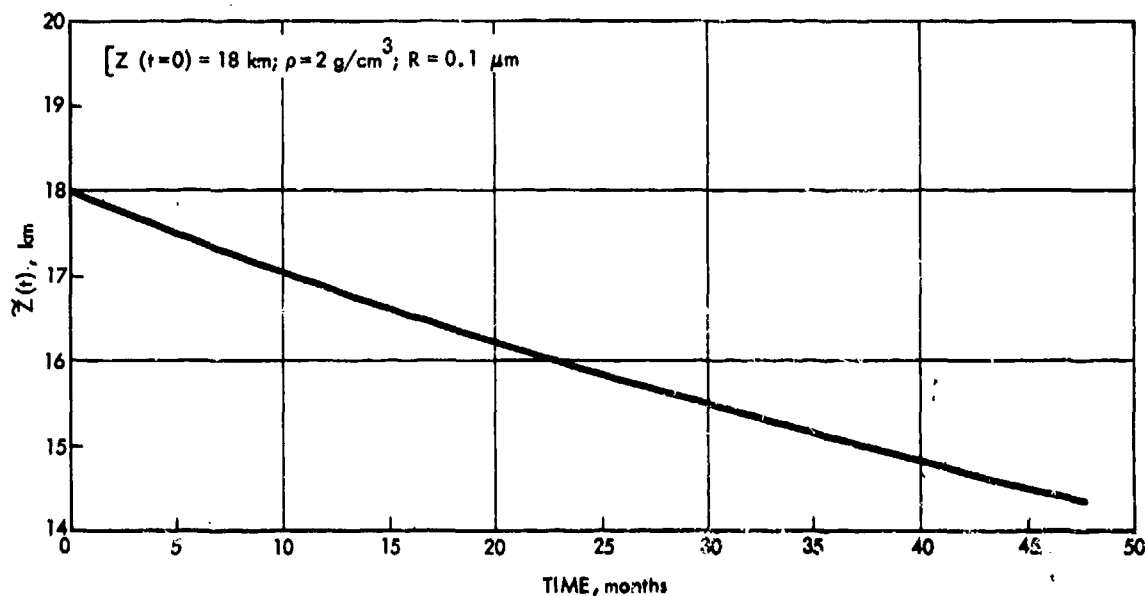
and thus $U(x_0)$ by $U(\tilde{x}_0)$.

C.4.4 Data Reduction to Find Effective K Values

C.4.4.1 Tropopause Height Taken as 11 km

To reduce the data, we normalize the tracer concentrations shown in Fig. C-2 (see Table C-1 for the actual data used) to give:

*It has been suggested (H.S. Johnston, private communication, 1975) that the actual aerosols carrying the radioactive tracers may be significantly larger than is indicated by the existing sampling techniques (cf., Drevinsky and Pecci, 1965; Telegadas and List, 1969). Clearly, this suggestion needs to be verified.



7-20-76-17

FIGURE C-6. Effective Injection Height for Aerosols as a Function of Time, $\bar{z}(t)$

$$A_{\text{exp}}(t) = \frac{\text{tracer burden (corrected for decay)}}{\text{maximum burden observed for the event}} \quad (15)$$

This quantity is shown in Fig. C-7, where we also show

$$A_{\text{calc}}(t) = U(x_0) \quad (16a)$$

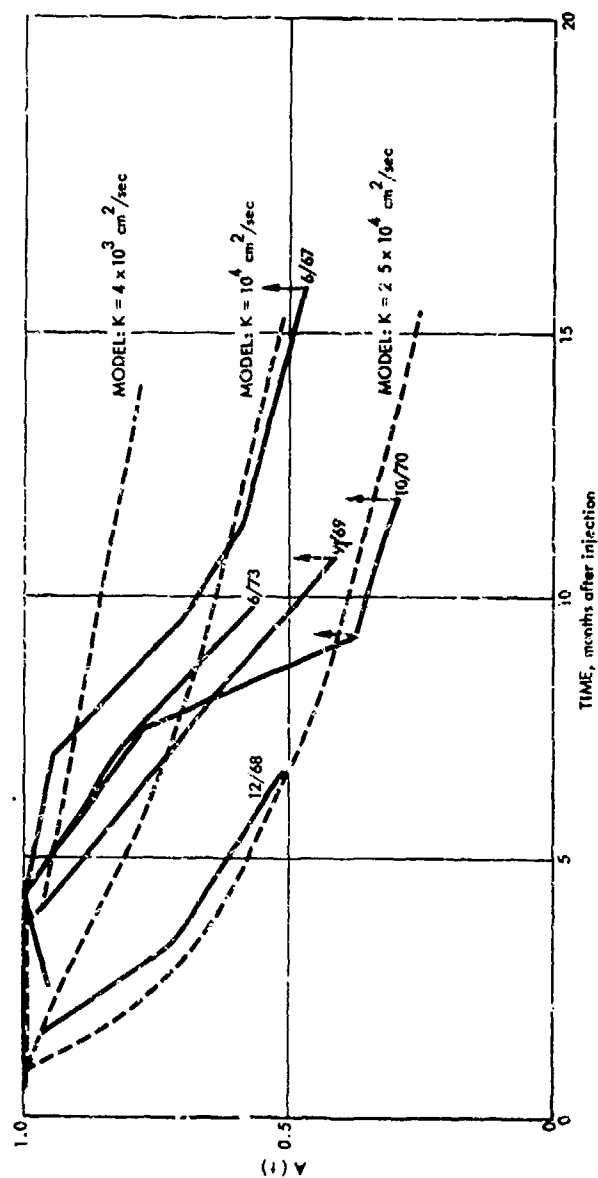
for the following set of parameters.

- $z_1 = 18$ km (height of injection),
- $z_0 = 11$ km (approximate mean tropopause height at the times of the various injections),
- $H = 6.30$ km (atmospheric scale height in the stratosphere).

In Fig. C-8, we compare $A_{\text{calc}}(t)$ and

$$\tilde{A}_{\text{calc}}(t) = U(\tilde{x}_0), \quad (16b)$$

which gives a plausible correction for sedimentation, having been computed for $\rho = 2.0 \text{ g/cm}^3$, $R = 0.1 \text{ um}$.



7-20-76-18

FIGURE C-7. Decay of Stratospheric Tracer Burden as a Function of Time. Comparison of results from the Chinese tests (from Telagadas, 1974, 1976) with the predictions of a model without sedimentation for various eddy diffusivity (K) coefficients. Note that the final data points marked with an arrow are lower-bound values, as the radioactivity data from the Chinese tests were obscured by new fallout from later (French) tests. Tropopause height taken as 11 km.

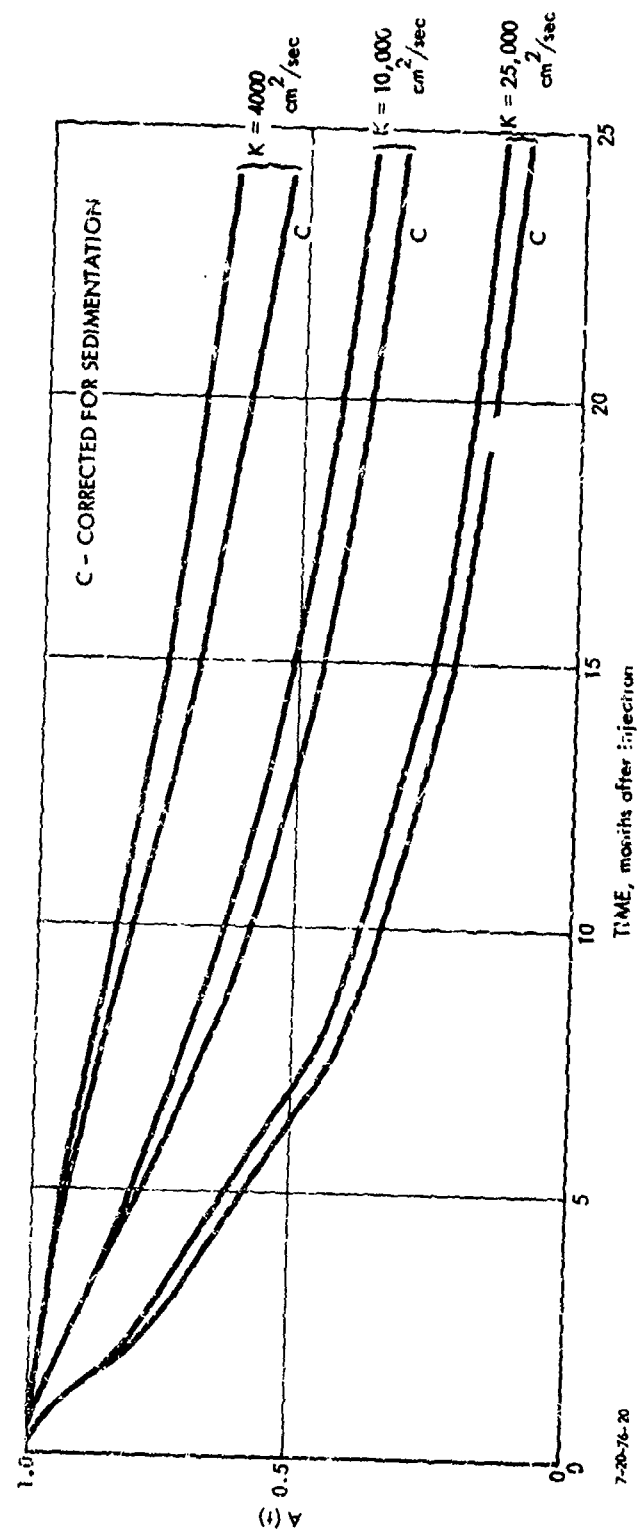


FIGURE C-8. Change of Stratospheric Tracer Burden with Time: Possible Effects of Sedimentation. We compute sedimentation effects for aerosols of $\rho = 2 \text{ g/cm}^3$, $R = 0.1 \text{ } \mu\text{m}$, according to the model of Section C.4.3. Tropopause height taken as 11 km.

In Fig. C-9 we show the time it takes for a stratospheric burden to decrease to 60 percent of its peak value following an injection, i.e., from Eqs. (15) and (16),

$$0.6 = A_{\text{calc}}(t_{0.6,\text{exp}}) \text{ or } \tilde{A}_{\text{calc}}(t_{0.6,\text{calc}}) \quad (17)$$

Figure C-8 shows $t_{0.6,\text{calc}}$ as a function of eddy diffusivity K , computed with and without sedimentation, and also indicates the experimental values of $t_{0.6}$.*

Table C-2 is an expansion of the results of Fig. C-9, which lists the effective K -values needed to reproduce the observed values of $t_{0.6}$, with and without sedimentation. The following points may be noted:

- Overall, values of K from $(0.9 \text{ to } 2.6) \times 10^4 \text{ cm}^2/\text{sec}$ encompass the $t_{0.6}$ data.
- The effect of sedimentation is of comparable significance for all values of K within the range $(1.0 \text{ to } 2.5) \times 10^4 \text{ cm}^2/\text{sec}$.
- There is seasonal variation in the data, with summer injection resulting in slow fallout or small effective K -values; note also the significant variation between the June 1967 and June 1973 values, which indicates the lack of detailed reproducibility of the data.

TABLE C-2. Effective K -values (in $10^4 \text{ cm}^2/\text{sec} = \text{m}^2/\text{sec}$) from $t_{0.6}$ values for the various Chinese tests, computed with and without sedimentation. Tropopause height taken as 11 km.

Date of test	K_{eff} (without sedimentation)	K_{eff} (with sedimentation)
6/67	1.0	0.9
12/68	2.6	2.1
9/69	1.4	1.1
10/70	1.4	1.2
6/73	1.2	1.1

Figure C-7, which shows the time-dependence of the activity function, $A(t)$, rather than the values of $t_{0.6}$, indicates that the present model represents the data quite imperfectly, and the proper year-round mean

*We show $t_{0.6}$ rather than $t_{0.5}$ since we do not have reliable experimental values for $t_{0.5}$ because of subsequent (French) nuclear explosions. See Table C-1.

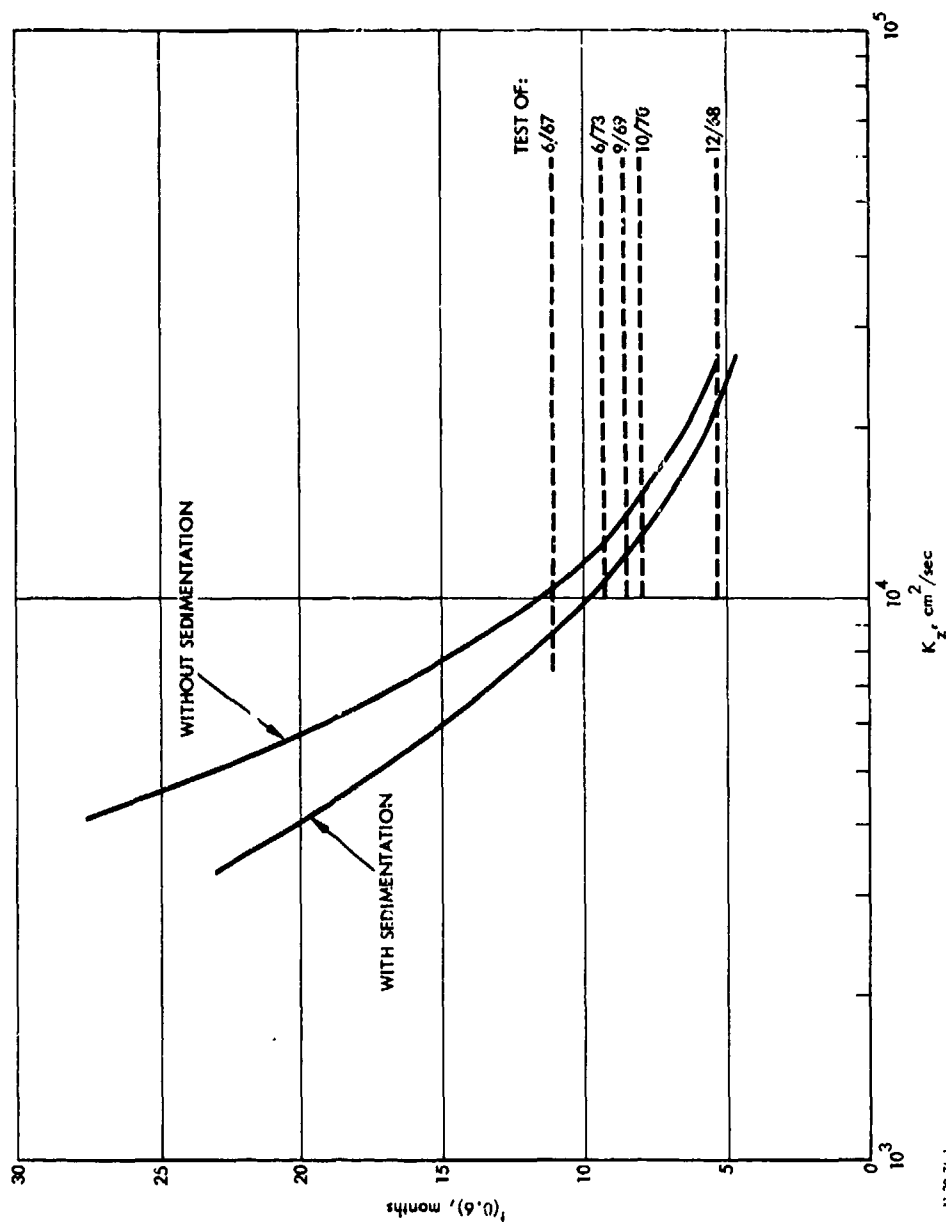


FIGURE C-9. Time for Stratospheric Tracer Burden to Decrease to 60 Percent of Its Peak Value, $t_{0.6}$, Computed With and Without Sedimentation, Shown as a Function of Eddy Diffusivity K_z . The corresponding decay times calculated from the various nuclear explosions are also shown. Tropopause height taken at 11 km.

K-values to represent the results can be debated. Nevertheless, for times greater than 6 months, the range $(1.0 \text{ to } 2.5) \times 10^4 \text{ cm}^2/\text{sec}$ encompasses all the data.

C.4.4.2 Tropopause Height Taken as 14 km

In earlier discussion, it was pointed out that the tropopause height varies substantially during the year. Insofar as the constant mixing ratio lines tend to parallel the tropopause height as a function of latitude, it might be argued that the initial cloud rise noted after the June injections was related to an increase in tropopause height, with the distance to the tropopause staying more or less constant. We choose, however, to consider the possibility that the mean "diffusion distance" to be transited by the debris was considerably less than the 7 km implied by an 18-km injection over an 11-km tropopause, related to the fact that mean annual tropopause heights are probably considerably above 11 km. For this purpose, we now give, without repeating the details, the results which would follow if the tropopause height were taken as 14 km, a value probably on the high side as an annual mean. The results are given in Fig. C-10, and summarized in Table C-3 below.

TABLE C-3. Effective K-values (in $10^4 \text{ cm}^2/\text{sec} = \text{m}^2/\text{sec}$) from to, 6 values for the various Chinese tests, computed with and without sedimentation. Tropopause height taken as 14 km.

<u>Date of test</u>	<u>K_{eff} (without sedimentation)</u>	<u>K_{eff} (with sedimentation)</u>
6/67	0.5	0.4
12/68	1.1	0.9
9/69	0.7	0.5
10/70	0.7	0.6
6/73	0.6	0.5

With this assumption, effective K-values are found to be about half those shown earlier, with values ranging from 4,000 to 10,000 cm^2/sec covering the data. As noted earlier, however, the diffusional distance is now considerably reduced, so that the total resistance to downward transport is not changed to the degree that K_z is changed. To evaluate the effects, we now consider continuous injections of pollutants, using the diffusion coefficients now developed.

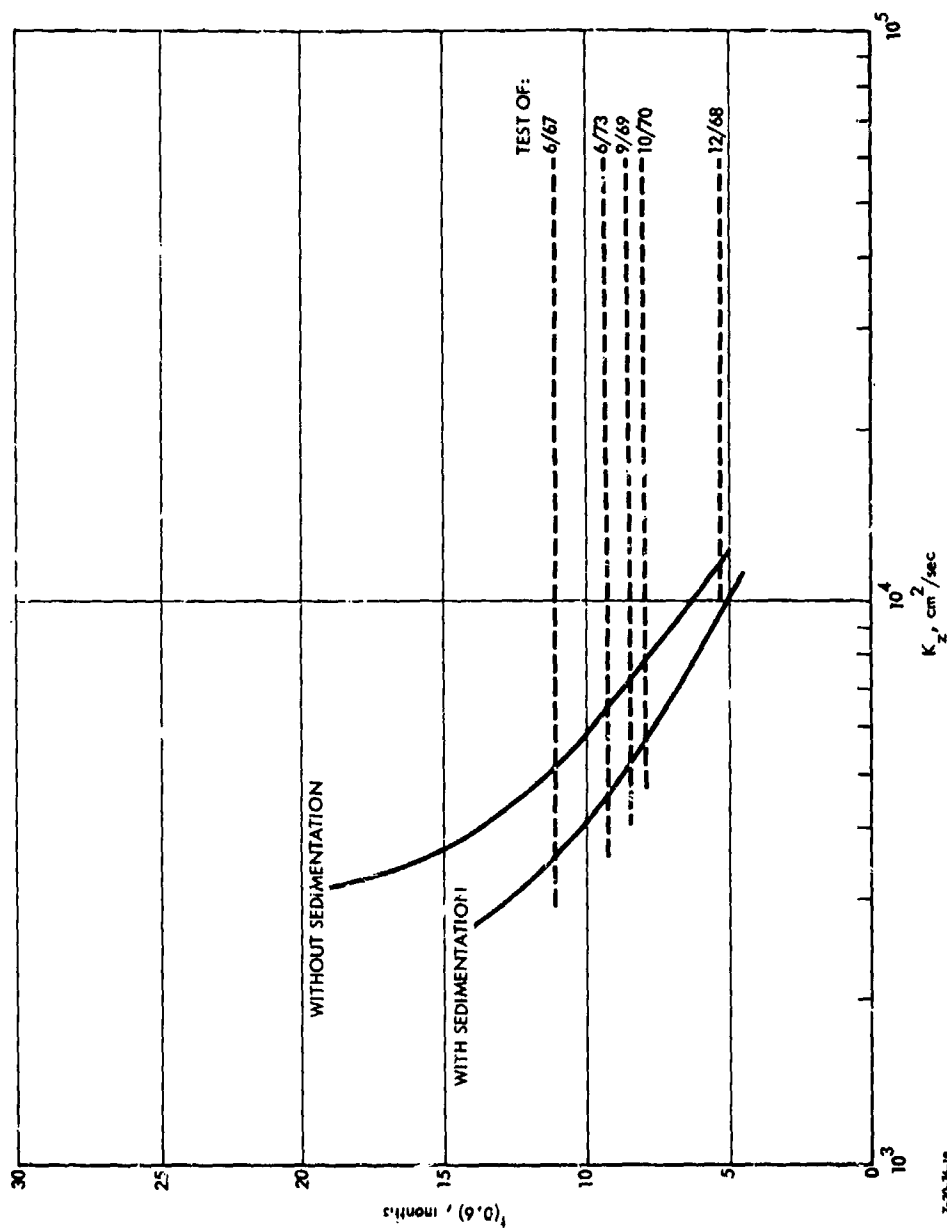


FIGURE C-10. Time for Stratospheric Tracer Burden to Decrease to 60 Percent of the Peak Value, $t(0.6)$, Computed With and Without Sedimentation, Shown as a Function of Eddy Diffusivity K_z . The corresponding decay times calculated from the various nuclear explosions are also shown. Tropopause height taken as 14 km.

C.5 EXTENSION TO CONTINUOUS INJECTIONS AND COMPARISON TO OTHER DATA

C.5.1 Procedures to Find Residence Times and Injection Coefficients for Continuous Injection

Given the effective stratospheric K-values deduced from the preceding analysis of the zirconium-95 data, it is possible to compute atmospheric residence times and injection coefficients for continuous injection of tracers (injected at 18-km altitude and 40° N latitude) by using the model for a K-profile as defined in Eq. (1).

For a model of continuous injection, we define the residence time $T_c(z)$ as follows:

$$\text{Residence time } T_c(z) = \frac{\text{burden of tracer in atmosphere, } B(z)}{\text{flux of tracer, } F(z)} \quad (18)$$

This is computed as follows. If the mixing ratio of the tracer is $f(z,t)$ and the total particle density at height z is $n(z)$, then for injection at height z_1 , the diffusion equation satisfied by $f(z,t)$ is

$$(\partial/\partial z, Kn\partial f/\partial z + v_g nf) = n\partial f/\partial t + Q\delta(z - z_1) \quad (19)$$

In a steady-state situation (such as would correspond to continuous injection), we have

$$\partial f/\partial t = 0, \text{ i.e., } f = f(z) \text{ only,} \quad (20)$$

and thus Eq. (19) can be integrated once with respect to z to give

$$\left. \begin{aligned} Kn\partial f/\partial z + v_g nf &= A \text{ for } z < z_1 & (a) \\ Kn\partial f/\partial z + v_g nf &= A + Q \text{ for } z > z_1 & (b) \end{aligned} \right\} \quad (21)$$

cf., Junge, et al. (1961), Hunten (1975). Here A and Q are constants (i.e., independent of z); for the case of precipitation-scavengable tracer, which is inert in the stratosphere, $Q = F(z)$. The function $f(z)/A$ for $z < z_1$ is the "injection coefficient" of McElroy, et al. (1974).

$$\left. \begin{aligned} B(z_1) &= B_L(z_1) + B_G(z_1) & (a) \\ B_L(z_1) &= \int_0^{z_1} n(z)f(z)dz & (b) \\ B_G(z_1) &= \int_{z_1}^{\infty} n(z)f(z)dz & (c) \end{aligned} \right\} \quad (22)$$

There are some questions about boundary conditions which are discussed elsewhere (Appendix D); typically, one may assume a perfect sink at the ground, $z = 0$, so that $f(0) = 0$, and there is also a question about the constant of integration A; the simplest thing to assume is that there is no net flux above the point of injection, so that $A = -Q$.

For the simple two-step profile used here, assuming an isothermal stratosphere with constant eddy diffusivity, and a constant but numerically different value in the troposphere, and for a gas (no sedimentation), analytical expressions for the injection coefficient and residence time can be developed, as follows:

injection coefficient α , for $z_1 > z_0 = f(z_1)/A$,

$$\alpha = \left(\frac{H}{K n_0} \right) \left[e^{(z_1 - z_0)/H} - 1 \right] + \frac{H_t}{K_t n_0} \left[1 - e^{-z_0/H_t} \right], \quad (23)$$

and residence time, t_R , for $z_1 > z_0$,

$$t_R = \frac{H}{K} (z_1 - z_0) + \frac{H_t}{K_t} \left[z_0 - H_t \left(1 - e^{-z_0/H_t} \right) \right]. \quad (24)$$

For aerosols, the treatment is more complex (see Appendix D). Here, however, we confine the discussion to gaseous injections, which are of greatest interest.

Given these formulae, we can compute injection coefficients and residence times for various values of the spatial mean eddy diffusivity coefficient (between 18 km and the tropopause) as derived from the experimental data. We can also compare the values to injection coefficients and residence times computed for published profiles, as described in Appendix D. Before doing so, however, some discussion of the appropriate mean on a time-weighted basis is necessary.

Let us reexamine how material leaves the stratosphere. From Fig. C-2, it appears that material injected in summer does not leave at all until the following winter, so that in some sense, the eddy diffusivity during the summer months can be argued to be effectively zero (although, of course, material injected in summer does leave eventually, with K-values, based on $t_{0.6}$ values, of order 10,000 cm²/sec, assuming an 11-km tropopause, or of order 4,000 cm²/sec, assuming a 14-km tropopause).

It is not obvious how to weight these various data properly, but one can put some bounds on the average behavior by simply averaging summer and winter values. Assuming an 11-km tropopause, K-values of between 0 and 10,000 cm²/sec might be used for summer injection; for winter injection, values of 20,000 to 25,000 cm²/sec seem reasonable. The corresponding values, with a 14-km tropopause assumption, are 4,000 and 10,000 cm²/sec. The simplest possible assumption seems to be that the atmosphere is characterized by winter behavior and summer behavior for equal periods; time-averaged K-values with the 11-km assumption would thus be in the range of 10,000 (i.e., $\frac{0 + 20,000}{2}$) to 17,500 (i.e., $\frac{10,000 + 25,000}{2}$) cm²/sec; for the 14-km assumption the values would be in the range of 4,000 to 7,000 cm²/sec. We now use this range of values to estimate injection coefficients and residence times, and compare the results to values generated for published profiles (Appendix D).

To compute injection coefficients and mean residence times, we use Eqs. (23/24) with the following numerical values:

$$H = 6.3 \text{ km (T = 216 K in the stratosphere)}$$

$$H_t = 7.3 \text{ km (T = 250 K in the troposphere)}$$

$$n_0 = 7.585 \times 10^{18} \text{ mol/cm}^3 \text{ (at 11 km, U.S. 1962 Standard Atmosphere)}$$

$$\text{or } 4.738 \times 10^{18} \text{ mol/cm}^2 \text{ (at 14 km; same source)}$$

$$z_0 = 11 \text{ km or } 14 \text{ km (mean tropopause height)}$$

$$z_1 = 18 \text{ km (effective injection height)}$$

$$K_t = 10^5 \text{ cm}^2/\text{sec for the troposphere}$$

With these constants, the equations become simply

$$\alpha_{11} = \frac{1.6925 \times 10^{-13}}{K_{11}} + 7.49 \times 10^{-19} \text{ (cm}^2\text{-sec)}$$

$$\alpha_{14} = \frac{1.1179 \times 10^{-13}}{K_{14}} + 1.314 \times 10^{-18} \text{ (cm}^2\text{-sec)}$$

$$t_{R11} = \frac{1.395 \times 10^4}{K_{11}} + 0.12 \text{ (years)}$$

$$t_{R14} = \frac{7.97 \times 10^3}{K_{14}} + 0.19 \text{ (years)}$$

C.5.2 Results and Comparison to Other Data

Injection coefficients developed by these procedures are compared to those computed for a variety of K_z profiles from the literature (see Appendix D) are given in Table C-4.

TABLE C-4. Comparison of results from different models for 18-km injection

<u>Source</u>	<u>$10^{-17} \frac{\alpha}{\text{cm}^2\text{-sec}}$</u>	<u>t_R yr</u>
This analysis		
$K_z = 1 \times 10^4$ (11-km tropopause)	1.8	1.5
$K_z = 1.75 \times 10^4$ (11-km tropopause)	1.0	0.95
$K_z = 5 \times 10^3$ (14-km tropopause)	2.4	1.8
$K_z = 7 \times 10^3$ (14-km tropopause)	1.7	1.3
Chang/1974 (18 km)	1.7	1.4
Chang/1976 (18 km)	1.8	1.6
Hunten/1974 (18 km)	4.6	3.6
Hunten/1974 (+ 2) (18 km, latitude adjusted to 20 km)	7.1	4.6
Crutzen/1974 (18 km)	1.8	1.7
Crutzen-Isaksen/1975 (18 km)	1.9	1.7
Wofsy/1975 (18 km)	3.2	2.6

Note that the large uncertainty in K_z introduced by changes in assumed tropopause height have relatively little impact when converted to injection coefficients or residence times.

These results may also be compared with the analysis of HTO (T=Tritium) data by Mason and Östlund (1976), who estimate a characteristic time of two years for removal (e-folding) of water vapor deposited in the lower stratosphere, and K-values of order $(2 \text{ to } 3) \times 10^4$ cm/sec.

Note also that ozone depletion estimates by the NAS correlation procedure (NAS report, p. 119) are dependent on α and not on residence time. It is evident why the NAS procedure gives much larger ozone depletions than does the Chang model, for example. Large values of α derive from small values of K_z near the tropopause.

Note also that this analysis applies to restricted conditions of injections at 18 km and 40° N. The comparison to published profiles involves only a comparison of integrated resistance to downward transport from 18 km to the ground; it says nothing about the shapes of the profiles.

These data suggest that the Chang/1974 and Crutzen profiles, at least in terms of their integrated transport characteristics from 18 km to the tropopause, may be the most appropriate for use for flight near 40° N. These results are thus in disagreement with the results of Johnston et al., presented at the 4th CIAP Conference, February 4-7, 1975, who analyzed data on excess carbon-14 and found the Hunten profile to be the most appropriate.

C.5 SOME FURTHER COMMENTS

The preceding analysis uses only the radioactive aerosol data. We did apply the same mathematical technique also to the excess carbon-14 (actually $C^{14}O_2$) data from the 1961-62 Soviet nuclear test series, but have not reported on that work for the following principal reasons:

- a. There are anomalies in the overall carbon-14 budget, possibly due to lack of adequate sampling at sufficiently high altitudes (see main text, Section 3.2.10a).
- b. We do not know the effective height of carbon-14 injected by the Soviet tests, which produced the bulk of the excess carbon-14, but the tests used were much larger than the Chinese tests (one rated at 57 Mt) and presumably put debris much higher than the 18-km region of maximum interest.
- c. Tracers injected at 75° N, as from the Soviet tests, seem less relevant to the aircraft question than are tracers deposited in mid-latitudes. Excess carbon-14 from the Chinese tests is so small in quantity that it apparently can not be adequately monitored.
- d. While $C^{14}O_2$ is not subject to sedimentation as are aerosols, it is only weakly scavenged in the troposphere and thus the majority of the excess $C^{14}O_2$ is undoubtedly recycled into the stratosphere. This effect can be taken into account (cf, e.g., Johnston et al. (1975)), but it does introduce an additional uncertainty.

It should also be noted that there may be conceptual differences between the approach used here and that of Johnston et al. (1975). Here we consider the source to be in a given latitude, and the entire global troposphere to be the sink. Johnston et al. (1975), on the other hand, by correcting for "leakage" to the southern hemisphere, appear to be considering a globally distributed source with more nearly true one-dimensional transport to the troposphere.

The present data, like all the individual sets of available data [e.g., carbon-14, tritium oxide, tungsten-185, rhodium-102, cadmium-109, and plutonium-238 (from Snap reentry), midlatitude methane profiles, meteorological data, etc.] all involve numerous uncertainties, and we do not regard any single

set of data as being conclusive. Nevertheless, we hope to reexamine the carbon-14 data with a modification of the present formalism to attempt to bound the overall transport coefficients predicted by this tracer.

ADDENDUM - APPENDIX C

SOLUTION OF A ONE-DIMENSIONAL DIFFUSION EQUATION

W. Wasylkiwskyj

ADDENDUM - APPENDIX C

$$\frac{\partial}{\partial z} \left[K n(z) \frac{\partial f(z,t)}{\partial z} \right] = n(z) \frac{\partial f(z,t)}{\partial t} , \quad (\text{E.2.1})$$

$$n(z) = n(0) e^{-z/H} , \quad -\infty < z < \infty .$$

$$K = \text{constant} .$$

The problem is to solve Eq. (E-1) for $f(z,t)$ when $f(z,0)$ is prescribed.

Since $n(z)$ is an exponential, differentiation transforms Eq. (E.2.1) into an equivalent problem.

$$\frac{\partial^2 f}{\partial z^2} - \frac{1}{H} \frac{\partial f}{\partial z} = \frac{1}{K} \frac{\partial f}{\partial t} . \quad (\text{E.2.2})$$

Equation (E.2.2) can be solved by Fourier transform. Thus, let

$$f(z,t) = \frac{1}{2\pi} \int_{-\infty}^{\infty} e^{i\xi z} F(\xi,t) d\xi , \quad (\text{E.2.3})$$

where $F(\xi,t)$ depends on time, but not on z . Inserting Eq. (E.2.3) in Eq. (E.2.2) yields

$$\frac{dF(\xi,t)}{dt} = - \left(\xi^2 + \frac{i\xi}{H} \right) K F(\xi,t) , \quad (\text{E.2.4})$$

and one finds

$$F(\xi,t) = g(\xi) e^{-Kt \left[\xi^2 + \frac{i\xi}{H} \right]} , \quad (\text{E.2.5})$$

where $g(\xi)$ is the Fourier transform with respect to z of the initial distribution $f(z,0)$:

$$g(\xi) = \int_{-\infty}^{\infty} e^{-1\xi z^1} f(z^1, 0) dz^1. \quad (E.2.6)$$

After combining Eq. (E.2.6) with Eq. (E.2.5) and substituting in (3), one obtains

$$f(z, t) = \frac{1}{2\pi} \int_{-\infty}^{\infty} dz^1 f(z^1, 0) \int_{-\infty}^{\infty} d\xi e^{i\xi(z - z^1) - \left[Kt \xi^2 + \frac{1\xi}{H} \right]}. \quad (E.2.7)$$

The integral with respect to ξ is essentially the Fourier transform of a gaussian error function. The integration can be carried out by the usual technique of completing the square in ξ of the argument of the exponent. Thus one finds

$$\begin{aligned} i\xi(z - z^1) - Kt \left[\xi^2 + \frac{1\xi}{H} \right] &= -Kt \left\{ \xi^2 + \frac{1\xi}{H} - 1 \frac{\xi(z - z^1)}{Kt} \right\} \\ &= -Kt \left\{ \xi^2 + 1 \left[\frac{1}{H} - \frac{(z - z^1)}{Kt} \right] \xi \right\} \\ &= -Kt \left\{ \xi^2 + 1 \left[\frac{1}{H} - \frac{z - z^1}{Kt} \right] \xi - \frac{1}{4} \left[\frac{1}{H} - \frac{z - z^1}{Kt} \right]^2 + \frac{1}{4} \left[\frac{1}{H} - \frac{z - z^1}{Kt} \right]^2 \right\} \\ &= -Kt \left\{ \xi + \frac{1}{2} \left[\frac{1}{H} - \frac{z - z^1}{Kt} \right] \right\}^2 - \frac{Kt}{4} \left[\frac{1}{H} - \frac{z - z^1}{Kt} \right]^2. \end{aligned}$$

After replacing the argument of the exponent in Eq. (E.2.3) by the preceding equivalent algebraic expression, one obtains

$$f(z, t) = \frac{1}{2\pi} \int_{-\infty}^{\infty} dz^1 f(z^1, 0) e^{-\frac{Kt}{4} \left[\frac{1}{H} - \frac{z - z^1}{Kt} \right]^2} \int_{-\infty}^{\infty} e^{-Kt \left\{ \xi + \frac{1}{2} \left[\frac{1}{H} - \frac{z - z^1}{Kt} \right] \right\}^2} d\xi. \quad (E.2.8)$$

Putting $\xi + \frac{1}{2} \left[\frac{1}{H} - \frac{z - z^1}{Kt} \right] = x$ in the last integral, one obtains

$$\int_{-\infty}^{\infty} e^{-Ktx^2} dz = \sqrt{\frac{\pi}{Kt}}.$$

Consequently Eq. (E.2.8) may be written as the single integral

$$f(z,t) = \frac{1}{\sqrt{4\pi Kt}} \int_{-\infty}^{\infty} f(z^1,0) e^{-\frac{Kt}{4} \left[\frac{1}{H} - \frac{z - z^1}{Kt} \right]^2} dz^1. \quad (E.2.9)$$

Equation (E.2.9) is the complete solution of Eq. (E.2.1) for any prescribed initial distribution $f(z^1,0)$. In particular, if

$$f(z,0) = q\delta(z - z_1),$$

i.e., $f(z,0)$ is a Dirac delta-function with area weighting q , Eq. (E.2.9) yields

$$f(z,t) = \frac{q}{\sqrt{4\pi Kt}} e^{-\frac{Kt}{4} \left[\frac{1}{H} - \frac{z - z_1}{Kt} \right]^2}. \quad (E.2.10)$$

For related work, see, e.g., Martin (1976).

APPENDIX D

COMPUTATIONS OF INJECTION COEFFICIENTS AND
RESIDENCE TIMES FOR 1-D MODELS

E. Bauer

K.A. Gardner

APPENDIX D

COMPUTATIONS OF INJECTION COEFFICIENTS AND RESIDENCE TIMES FOR 1-D MODELS

D.1 INTRODUCTION AND SUMMARY

In numerous upper atmospheric problems, one is concerned with the interaction of radiative, dynamic, and chemical factors. Because of the complexities involved, it is often desirable to simplify dynamics to the utmost, through use of a one-dimensional (1-D) model, in which all the mechanisms by which materials are moved upward or downward in the real atmosphere are parameterized, as a function of altitude, by an eddy diffusivity or K_z coefficient. Typical profiles are shown in Figs. D-1 and D-2.

The eddy diffusivity profile selected has certain implications with regard to stratospheric sources of pollutants. In particular, if one assumes a sink (or sinks) for the pollutant, one can calculate a corresponding "residence time," defined here as the ratio of burden/flux at steady state, for each altitude of injection. This burden may be of interest in estimating climatic effects, for example. Or as used in the National Academy of Sciences (NAS) report (pp. 116, 142), for gases, one can calculate an injection coefficient, assuming no sink above the point of injection, which gives the augmentation in mixing ratio above the aircraft source altitude. This augmented mixing ratio, by correlation with detailed chemical kinetics runs, can be used to estimate, for example, effects of NO_x on ozone for various cases, greatly simplifying the computational problem. Here we develop injection coefficients for gases, and residence times for both gases and particles, for various K_z profiles of interest.

D.2 PROBLEM DEFINITION

Specifically, we address the following problem. Given a profile of the eddy diffusion coefficient, $K(z)$, as a function of height z , and also a profile for the Stokes flow sedimentation velocity $u(a, z)$ for aerosols of radius a (and specified density--actually we take $\rho = 2 \text{ /cm}^3$), to compute the mean atmospheric residence time for a (gaseous or particulate, but chemically inert) tracer injected into the atmosphere at height z_1 and extracted essentially at ground level, $z_0 = 0$.

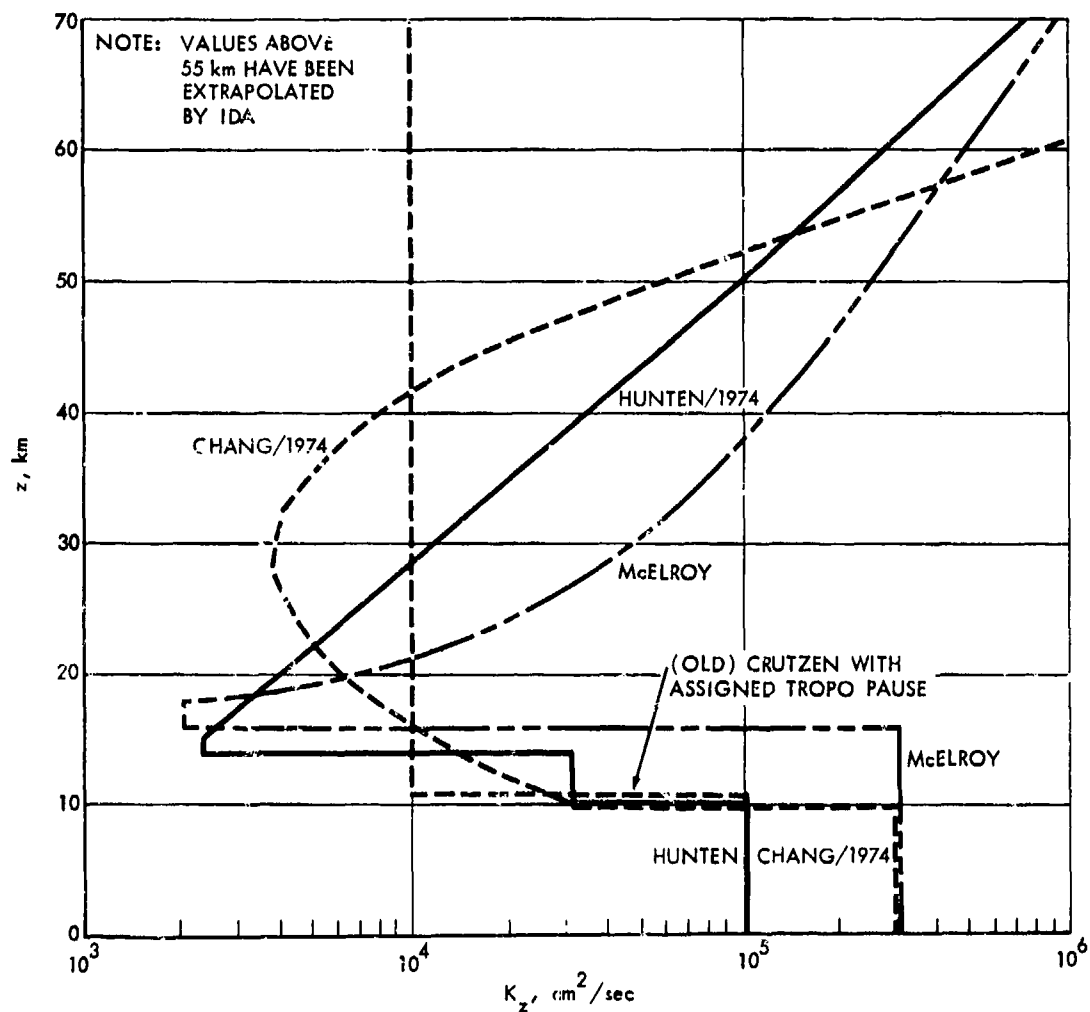


FIGURE D-1. Three Eddy Diffusivity Profiles used During CIAP in 1974

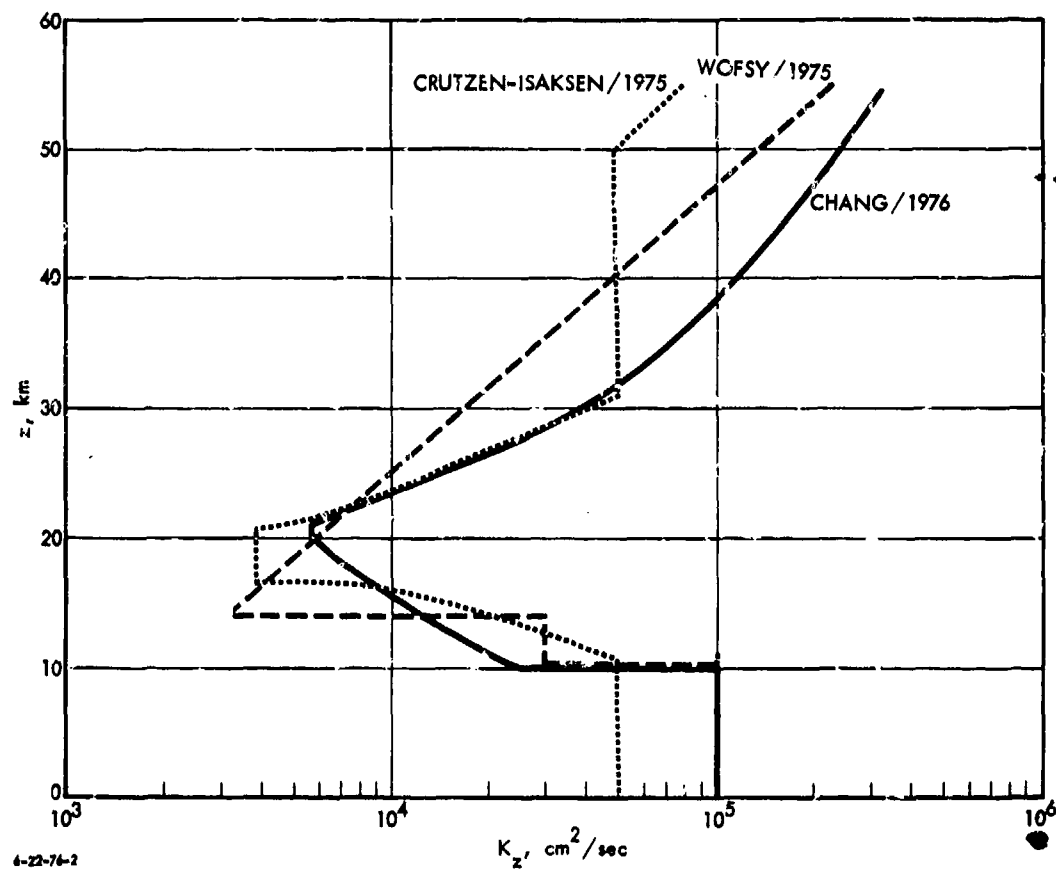


FIGURE D-2. Three Recent Eddy Diffusivity Profiles

This is a very simple problem, as long as one limits consideration to the height range $z_0 < z < z_1$, but, in fact, some of the injected material always diffuses above the point of injection, and now we ask what happens in a steady-state situation. Here we make three different assumptions:

Case (i): Following Hunten (1975), one may assume that the tracer simply fills up the region above the point of injection at constant mixing ratios. This is satisfactory for gases, but not for aerosols, for which sedimentation opposes the effect of diffusion above the point of injection, and thus we make a different assumption:

Case (ii): One assumes that the mixing ratio vanishes at some large height z_2 because there is, in fact, an additional sink there *

Case (iii): One assumes no net flux above the point of injection. This is a reasonable model for tracers for which there is no high-altitude sink; in fact, it provides a generalization to case (i) for the case of aerosols. We emphasize this case, and present tables of results.

Here we address these problems quantitatively, starting with various K_z profiles (see Figs. D-1 and D-2), and with profiles of sedimentation velocity $u(a,z)$ due to Junge et al. (1961), we compute injection coefficients and residence times (see Fig. D-3).

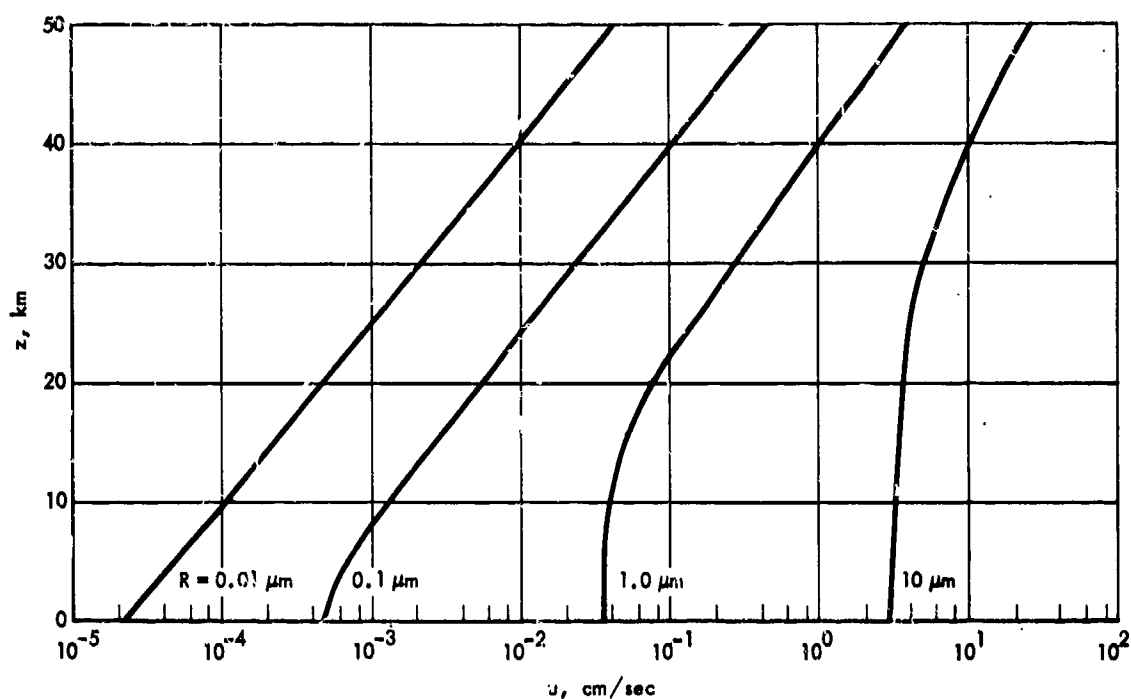
The injection coefficient for gases, α , follows that of McElroy et al. (1974), and of the NAS report (1975), p. 116:

$$\text{injection coefficient } \alpha \text{ (cm}^2\text{-sec)} = \frac{\text{mixing ratio at or above height of injection, } X}{\text{injection rate, } Q} \quad (1)$$

(mol/cm²-sec)

which relates the augmented mixing ratio X , which is taken to be constant at or above the point of injection, to the injection rate Q . However, for the case of aerosols which are subject to sedimentation, the mixing ratio is not constant above the altitude of injection, and thus we work with a modification of this concept.

*Physical interpretations of this high-altitude sink include the following: (a) There is actually a photochemical sink at high altitude, which exists for many tracers (e.g., N_2O , CH_4 , halocarbons). (b) If z_2 is sufficiently large, the effect of this upper boundary condition is, in fact, negligible for heights below z_3 , say, because a negligible quantity of tracer actually gets to high altitudes, either on account of the falloff of total density with height, or indeed because of sedimentation. Note also that sulfuric acid aerosols may evaporate at middle stratospheric altitudes (ca. 30 km), as shown by Hamill, et al. (1976); this evaporation is not a true sink, however, as the sulfuric acid vapor must eventually, in a 1-D global model, diffuse downward and be removed in the troposphere.



(Source: Junge, Chagnon & Manson, 1961.)

3-19-76-26

FIGURE D-3. Sedimentation Velocity for Spheres of Density 2 gm/cm³
Source: Junge, et al. (1961)

We define a mean residence time as

$$\text{residence time of tracer at height } z_1 \equiv \frac{\text{burden in atmosphere, } B(z_1)}{\text{flux of tracer}} \quad (2)$$

Some auxiliary definitions that are used here are the following:

$$\left. \begin{aligned} \text{Burden} &= \text{burden below point of injection, } B_L(z_1) \\ &+ \text{burden above the point of injection, } B_G(z_1) \end{aligned} \right\} \quad (3)$$

$$\left. \begin{aligned} \text{Flux of tracer below point of injection} &= A \\ (\text{units: particles (area} \times \text{time)}) & \quad (a) \\ \text{Flux of tracer going above } z_1 &= G(z_1) \quad (b) \\ \text{Flux of tracer going below } z_1 &= G(z_1) \end{aligned} \right\} \quad (4)$$

where, of course, $G = 0$ for cases (1) and (iii) by definition.*

*The quantity G gives a measure of the importance of the upper boundary condition, in particular of the upper sink. The quantity Q of Eq. (1) is given by $A(1 + G)$.

The present calculations are done numerically, using a computer program which is described briefly in Addendum 1. However, a particularly simple case can be done analytically. Thus, in Addendum 2, we treat an isothermal atmosphere for which the air molecule number density at height z , $n(z)$, is given by the formula

$$n(z) = n_0 e^{-z/H}; \quad H = kT/Mg = \text{constant} \sim 7 \text{ km}, \quad (5)$$

and we also assume

$$\left. \begin{aligned} K(z) &= \text{constant, independent of } z & (a) \\ u(a,z) &= u(a), \text{ i.e., independent of } z & (b) \end{aligned} \right\} \quad (6)$$

Figs. D-1, D-2, and D-3 show that, in particular, the assumptions (6a,b) are not correct, but this analytical model may be useful for qualitative and diagnostic discussions.

The mathematics used is outlined in Section D.3, and the results are presented in Section D.4.

D.3 THE MATHEMATICAL PROBLEM

D.3.1 Introduction

In this analysis, the mixing ratio $f = f(z)$ is used as primary variable; thus, at altitude z , where the total number density is $n(z)$, the number density of tracer species is $f(z) n(z)$. For a source of strength Q at $z = z_1$, the diffusion equation satisfied by $f(z)$ in a 1-D situation is

$$(\partial/\partial z) (Kn \partial f/\partial z + u n f) = n \partial f/\partial t + Q \delta(z - z_1). \quad (7)$$

In a steady-state situation, $\partial/\partial t \equiv 0$, and thus the diffusion Eq. (7) can be integrated once with respect to z to give

$$K n df/dz + u n f = A \text{ for } z < z_1 \quad (8a)$$

$$K n df/dz + u n f = (A + Q) \text{ for } z > z_1 \quad (8b)$$

Cf. Hunten (1975a); Junge et al. (1961); A and Q are constants, independent of z .

At the ground there is a "perfect sink," defined as

$$f(z = z_0 = 0) = 0. \quad (9)$$

We now wish to integrate Eq. (8) for $z_0 < z < z_1$, using Eq. (9) as lower boundary condition:

$$\begin{aligned}
 y(z) &= \int_0^z (u/K) dz' & (a) \\
 f_L(z) &= e^{-y(z)} \int_0^z (A/Kn) e^{y(z')} dz' & (b)
 \end{aligned}
 \tag{10}$$

For the region $z > z_1$, we have a certain ambiguity, as was pointed out in Section D.1. For a gas, we may simply consider case (i), i.e., following Hunten (1975), we say:

Case (i), Constant Augmentation in Mixing Ratio Above the Altitude of Injection

In this case:

$$f(z > z_1) = f(z_1) \tag{11}$$

which in this model would apply to a gas with no sink above the injection altitude.

This is clearly not satisfactory for an aerosol, for which sedimentation tends to reduce the mixing ratio above the point of injection. Here, then, we consider two further possible cases, (ii) and (iii).

Case (ii), The "Upper Sink" at $z = z_2$

Here we consider that there exists a

$$z_2 > z_1 \text{ such that } f(z_2) = 0; f(z_1 < z < z_2) = f_G(z) . \tag{12}$$

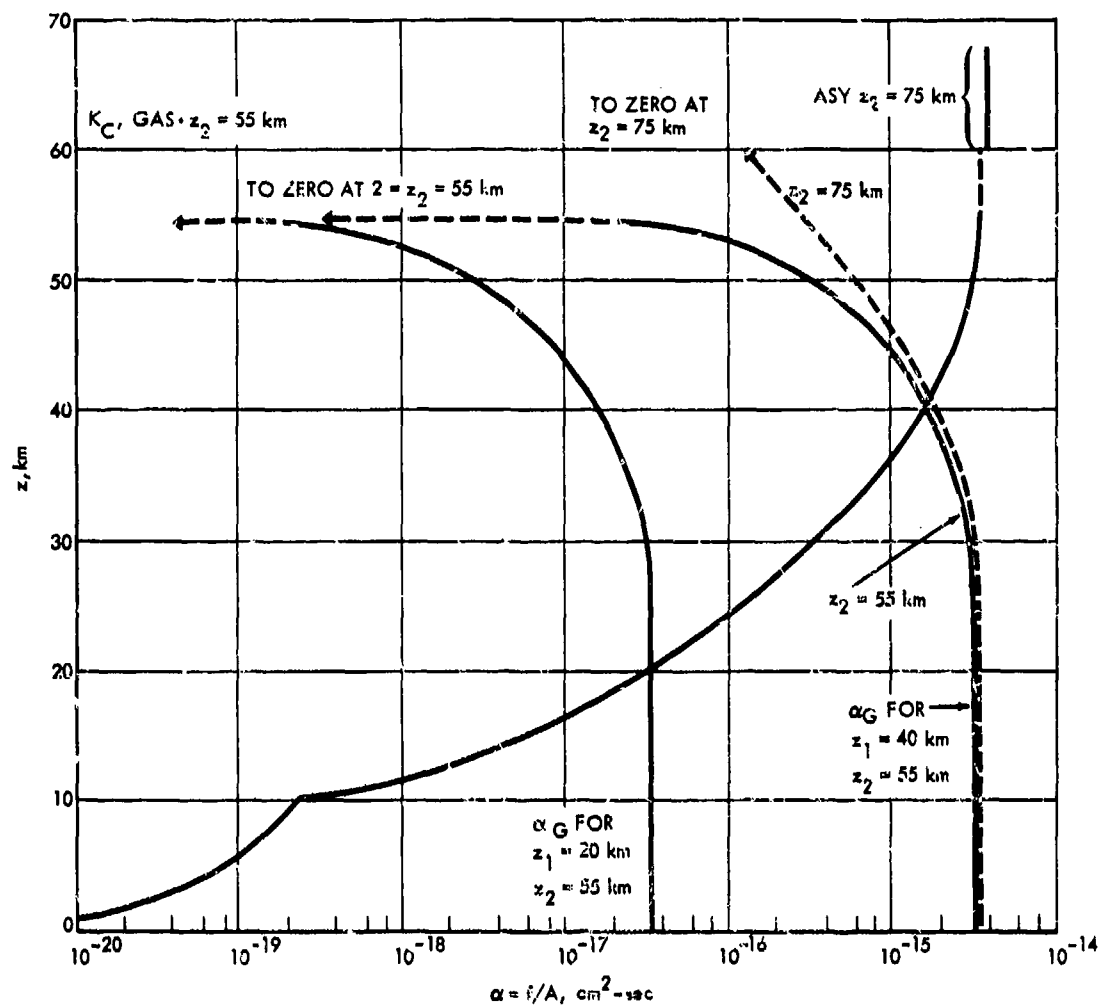
To evaluate $f_G(z)$, we must integrate Eq. (8b) with the boundary condition

$$f_G(z_2) = 0 . \tag{12}$$

The solution is still undetermined by an arbitrary scale factor, which is set by the condition that $f(z)$ must be continuous at $z = z_1$, so that

$$f_G(z_1) = f_L(z_1) . \tag{13}$$

In Fig. D-4 we show examples of $\alpha (= f_L/A, \text{ where } A = 1 \text{ particle/cm}^2\text{-sec})$, of f_L and f_G for gases (i.e., no sedimentation) for K_G ; we also show f_G for the cases $z_1 = 20 \text{ km}$ and $z_1 = 40 \text{ km}$; for different values of z_1 , one simply multiplies the f_G curve by a different scale factor $G(z)$ to satisfy condition (13) at a different value of z_1 . The function $f_G(z)$ is given by the following expression:



1-24-77-35

FIGURE D-4. General Character of the Solution for Eddy Diffusivity Profile K_C . We show $\alpha_L = f_L/A$ (McElroy's α), below the point of injection, and also $\alpha_G = f_G/A$ [case (11), for injection altitudes $z_1 = 20$ and 40 km] for an "upper sink" at $z_2 = 55$ and 75 km, all for a gas.

$$f_G(z) = G(z_1) [f_L(z_2) - f_L(z)] \quad (14a)$$

$$G(z_1) = f_L(z_L) / [f_L(z_2) - f_L(z_1)] , \quad (14b)$$

unless $A + Q = 0$, which corresponds to case (iii).*

The scaling factor $g(z)$ of Eqs. (4b) and (14) is shown in Fig. D-5 for a gas, for $K = K_M$ and K_G , and in Fig. D-6 we show $G(z)$ for K_H for both gases and particles, parameterized also with z_2 , and assuming a sink at 55 km. We see that for injection of gases above 20 km the magnitude of the upward-going flux may be as large as 10 percent of that of the downward-going flux, but, for aerosols, the effect is, of course, smaller, in that sedimentation permits less material to travel upward. Note that the figures for f_L and for $G(z)$ have discontinuities in slope at the same point as the eddy diffusivity profiles of Figs. D-1 and D-2.

For case (ii), the residence time defined in Eq. (2) is

$$T(z_1) = [B_L(z_1) + B_G(z_1)] / [1 + G(z_1)] , \quad (15)$$

where $B_L(z_1)$ and $B_G(z_1)$ are defined in Eq. (3) as, respectively, the burden of injectant below and above the point of injection, z_1 , while $G(z_1)$ is defined in Eq. (4) as the ratio of flux going upward from the point of injection to the flux going downward. Calculations have been made for an upper sink at $z_2 = 55$ km and 75 km. In Fig. D-7, we show $T(z_1)$ for a gas, comparing case (i) (constant mixing ratio above the point of injection) with case (ii) for $z_2 = 55$ km and 75 km.

Above 30 km to 35 km the residence time computed for case (ii) actually decreases with increasing altitude; this occurs because of the upper sink at $z = z_2$. In other words, at sufficiently high altitude, material flows upward to be lost rather than downward. Depending on the actual properties of the tracer which is studied, this may be physically meaningful, or it may be an indication that the model is not appropriate for the particular injectant under consideration. Note that the effect of the "upper sink" at $z_2 = 55$ km shows as low as $z_1 = 20$ km, where $G(z_1) = 0.06$. It is thus clear that the effect of the upper boundary conditions persists to relatively low altitudes. Accordingly, we also consider case (iii), which is a different way to treat the upper boundary condition, and which will be more appropriate for some tracers (e.g., aerosols).

*Recall that $f_L(z)$ is not a solution of Eq. (8b) in the range $z_1 < z$ if $A + Q = 0$.

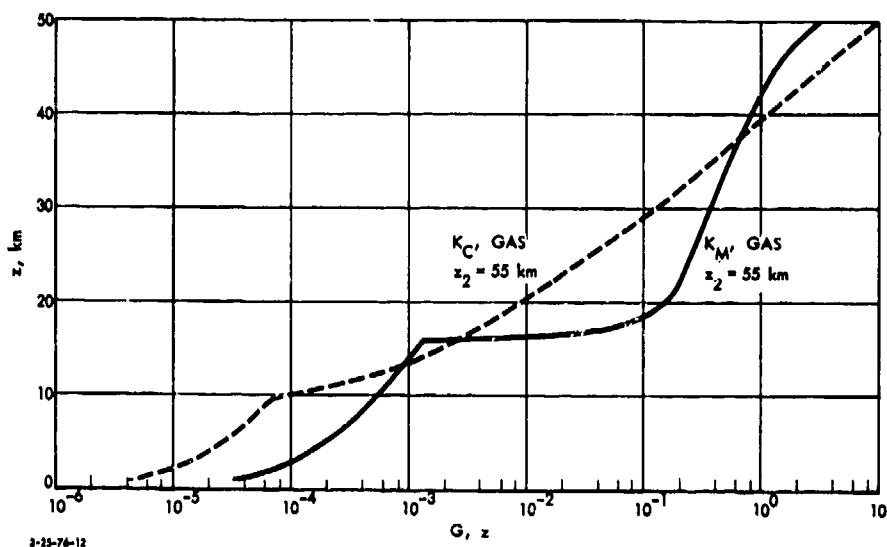


FIGURE D-5. Case (ii): Scaling factor $G(z_1)$ for $K = K_C$ and K_M for gases, $z_2 = 55$ km

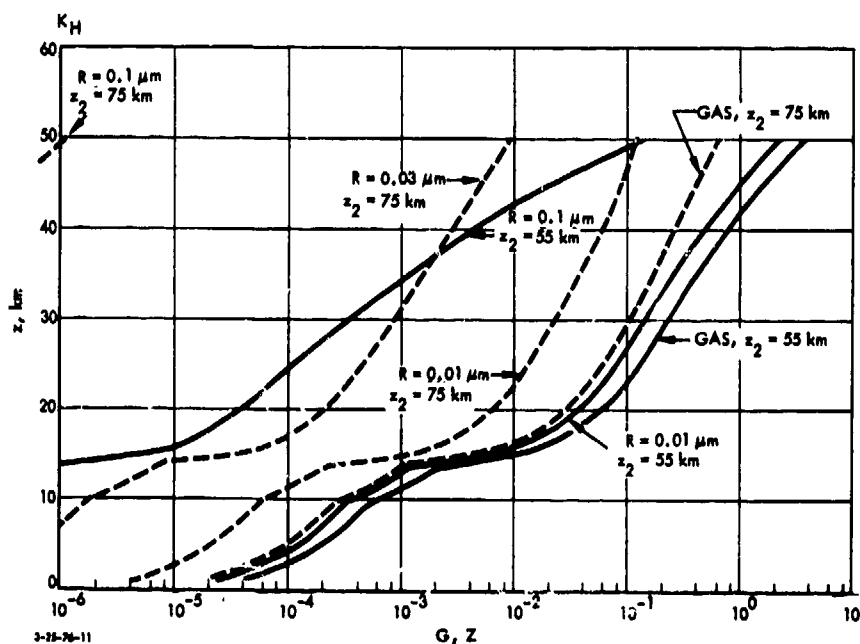
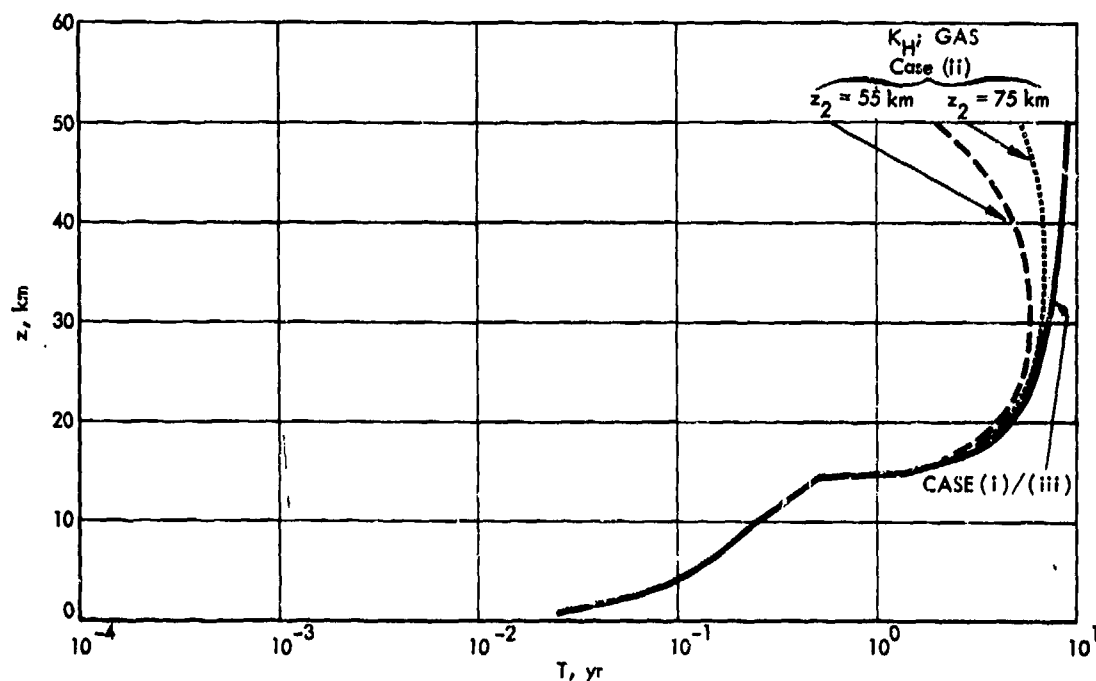


FIGURE D-6. Case (ii): The scaling factor $G(z_1)$, which gives the ratio of flux going above the point of injection, z_1 , to the flux going below the point of injection, for $K = K_H$, gases and aerosols, $z_2 = 55$ and 75 km.



3-25-76-13

FIGURE D-7. Residence Time for a Gas, $K = K_H$, for Cases (i)/(iii) and Case (ii) with $z_2 = 55$ and 75 km.

Case (iii), No Flux Above the Point of Injection

Let us return to Eq. (8); $Kn \, df/dz + unf = \text{net flux}$. Since now there is no net flux above the point of injection, we have

$$A = -Q, \quad (16)$$

so that above the point of injection, $f(z) = f_U(z)$, which satisfies the following equation:

$$Kn \, df_U/dz + un \, f_U = 0, \quad (17)$$

a special case of Eq. (8), whose solution is

$$f_U = f_{u,o} e^{-y(z)}, \quad (18)$$

where $f_{u,o}$ is a constant and where $y(z)$ is defined by Eq. (10). In fact, it is convenient to express f_U in terms of $f(z_1) = f_L(z_1)$, and thus we put

$$f_U(z) = f(z_1) e^{-n(z)} \quad (18a)$$

$$n(z) = \int_{z_1}^z (u/K) dz' = y(z) - y(a_1) . \quad (18b)$$

Note that for the case of a gas, $u = 0 = y(z)$ and $n(z)$, and thus case (iii) reduces to case (i).

In Figs. D-8 and D-9 we show residence times for gases and aerosols for $K = K_C$ and $K = K_H$.

D.3.2 Computed Results

Detailed data are given in Tables D-1 through D-8. The atmospheric properties and settling velocities $u(a,z)$ used are shown in Table D-1. Two particle sizes, 0.1 μ m and 0.3 μ m radius are shown; these are considered to be of the greatest interest to the problems at hand, as 0.1 μ m particles are typical of sulfate aerosols (Hidalgo, CIAP Report of Findings, 1974, p. E-135).

The following K_z cases are given, with sources as follows:

<u>K_z</u>	<u>Source</u>
Chang/1974*	CIAP Report of Findings, p. 19
Chang/1976*	Private communication, 1976
Crutzen	Crutzen, 1974**
Hunten	CIAP Report of Findings, p. 19
McElroy	McElroy, 1974
Wofsy	Wofsy, 1975
Crutzen-Isaksen	Lawrence Livermore Laboratory, private communication, 1976

* Sometimes referred to as "Old Chang" and "New Chang", respectively.

** We have assigned a tropopause at 11 km to the Crutzen (1974) K_z representation.

The tabulated results agree reasonably well with those tabulated (for Chang/1974 and Hunten) in the CIAP Report of Findings (p.25). However, increasing discrepancies, the source of which is unclear, appear above about 25 km in the Chang/1974 case. Also, the injection coefficients in the Hunten case do not match precisely those given by formula in the NAS report (pp. 117-118). One source of discrepancy may be that the term "Hunten K_z " profile involves some ambiguity, the data on p. 116 of the NAS report differ somewhat from the plot (p. 142, NAS report) and from that attributed to Hunten in the CIAP Report of Findings (p. 29). We have used

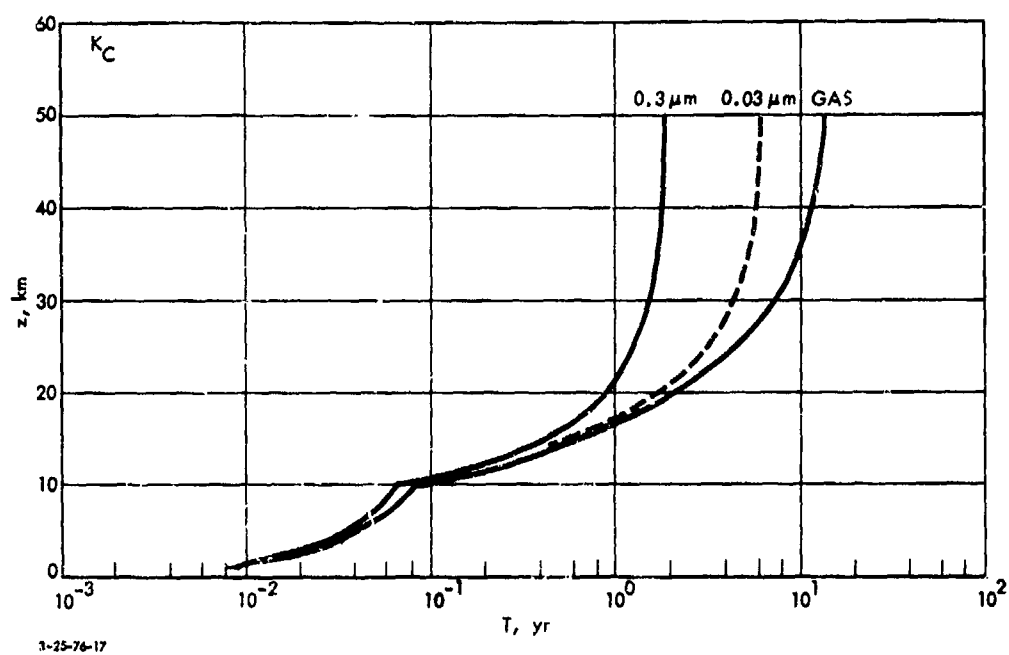


FIGURE D-8. Mean Atmospheric Residence Time for Gases and Aerosols, Case (iii), $K = K_C$.

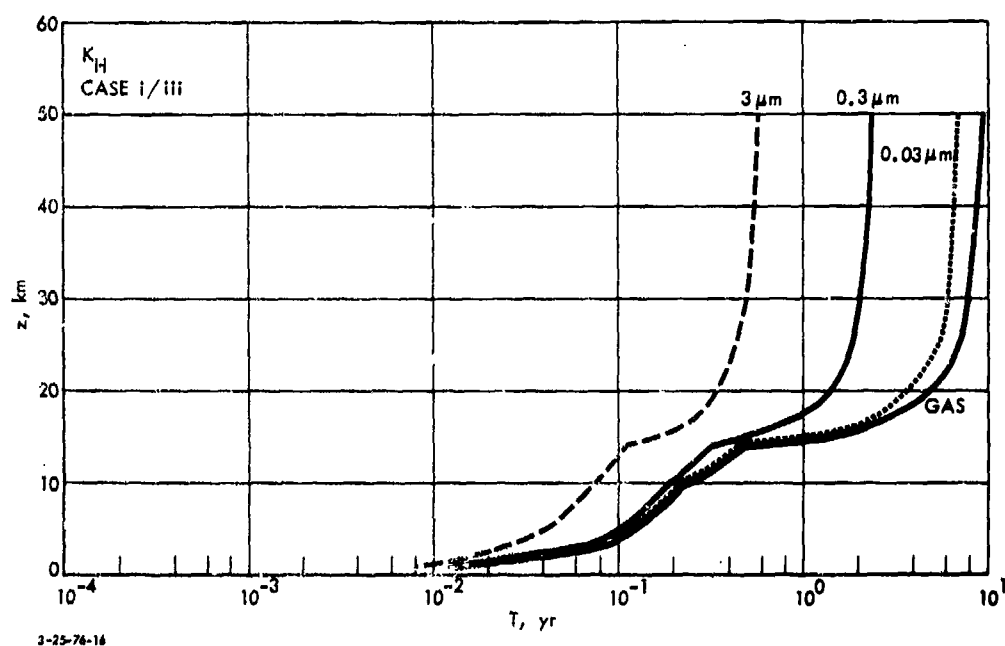


FIGURE D-9. Mean Atmospheric Residence Time for Gases and Aerosols, Case (iii), $K = K_H$.

the latter values. However, we have also used the Hunten analytical formulas in computations of effects presented in Volume 1, as these permit computations at nonintegral altitudes.

Note that the NAS report, (p. 118) recommends that the injection coefficient for aircraft operating in midlatitudes, should be taken 2 km above aircraft flight altitude to allow for the 2-km difference between the tropopause height at Palestine, Texas, for which latitude his K_z profile was developed, and the tropopause height at typical aircraft latitudes.

TABLE D-1. ATMOSPHERIC PROPERTIES AND PARTICULATE SETTLING VELOCITIES USED

Z, km	M mol/cm ³	Atmospheric Properties		Z, km	Particulate Settling Velocities (cm/sec)	
		Int (N) 0 to Z mol/cm ²	Int (N) Z to Inf mol/cm ²		R=0.10µm	R=0.30µm
0	2.550E-19	0.43000E+20	2.18374E+20	0	4.800E-06	1.900E-03
1	2.310E-15	4.42566E+19	1.99876E+20	1	5.000E-06	1.900E-03
2	2.090E-11	4.01467E+19	1.69820E+20	2	5.200E-06	2.100E-03
3	1.890E-07	3.61870E+19	1.49120E+20	3	5.400E-06	2.300E-03
4	1.700E-03	3.2333E+19	1.31187E+20	4	5.600E-06	2.500E-03
5	1.530E-01	2.8633E+19	1.15851E+20	5	5.800E-06	2.700E-03
6	1.370E-01	2.5173E+19	1.02951E+20	6	6.000E-06	2.900E-03
7	1.230E-01	2.1960E+19	9.1574E+19	7	6.200E-06	3.100E-03
8	1.100E-01	1.8970E+19	8.1574E+19	8	6.400E-06	3.300E-03
9	9.710E-02	1.6170E+19	7.2954E+19	9	6.600E-06	3.500E-03
10	8.600E-02	1.3670E+19	6.5717E+19	10	6.800E-06	3.700E-03
11	7.540E-02	1.1440E+19	5.9574E+19	11	7.000E-06	3.900E-03
12	6.490E-02	9.5300E+18	5.4374E+19	12	7.200E-06	4.100E-03
13	5.540E-02	7.9533E+18	4.9987E+19	13	7.400E-06	4.300E-03
14	4.740E-02	6.6500E+18	4.6274E+19	14	7.600E-06	4.500E-03
15	4.050E-02	5.5950E+18	4.3174E+19	15	7.800E-06	4.700E-03
16	3.460E-02	4.7433E+18	4.0574E+19	16	8.000E-06	4.900E-03
17	2.960E-02	4.0600E+18	3.8474E+19	17	8.200E-06	5.100E-03
18	2.530E-02	3.5130E+18	3.6774E+19	18	8.400E-06	5.300E-03
19	2.160E-02	3.0767E+18	3.5474E+19	19	8.600E-06	5.500E-03
20	1.850E-02	2.7367E+18	3.4474E+19	20	8.800E-06	5.700E-03
21	1.570E-02	2.4800E+18	3.3674E+19	21	9.000E-06	5.900E-03
22	1.340E-02	2.2833E+18	3.2974E+19	22	9.200E-06	6.100E-03
23	1.140E-02	2.0700E+18	3.2474E+19	23	9.400E-06	6.300E-03
24	9.740E-03	1.8433E+18	3.2074E+19	24	9.600E-06	6.500E-03
25	8.300E-03	1.6133E+18	3.1774E+19	25	9.800E-06	6.700E-03
26	7.100E-03	1.3800E+18	3.1574E+19	26	1.000E-05	6.900E-03
27	6.090E-03	1.1600E+18	3.1474E+19	27	1.020E-05	7.100E-03
28	5.210E-03	9.6133E+17	3.1474E+19	28	1.040E-05	7.300E-03
29	4.470E-03	7.8000E+17	3.1574E+19	29	1.060E-05	7.500E-03
30	3.830E-03	6.2433E+17	3.1774E+19	30	1.080E-05	7.700E-03
31	3.290E-03	4.8900E+17	3.2074E+19	31	1.100E-05	7.900E-03
32	2.820E-03	3.6933E+17	3.2474E+19	32	1.120E-05	8.100E-03
33	2.410E-03	2.6100E+17	3.2974E+19	33	1.140E-05	8.300E-03
34	2.060E-03	1.7000E+17	3.3674E+19	34	1.160E-05	8.500E-03
35	1.760E-03	1.0000E+17	3.4474E+19	35	1.180E-05	8.700E-03
36	1.510E-03	5.9000E+16	3.5474E+19	36	1.200E-05	8.900E-03
37	1.300E-03	3.4000E+16	3.6774E+19	37	1.220E-05	9.100E-03
38	1.120E-03	1.9000E+16	3.8474E+19	38	1.240E-05	9.300E-03
39	9.600E-04	1.0000E+16	4.0574E+19	39	1.260E-05	9.500E-03
40	8.200E-04	5.0000E+15	4.2974E+19	40	1.280E-05	9.700E-03
41	7.000E-04	2.4000E+15	4.5774E+19	41	1.300E-05	9.900E-03
42	6.000E-04	1.1000E+15	4.8974E+19	42	1.320E-05	1.010E-02
43	5.100E-04	5.0000E+14	5.2574E+19	43	1.340E-05	1.030E-02
44	4.400E-04	2.4000E+14	5.6574E+19	44	1.360E-05	1.050E-02
45	3.800E-04	1.1000E+14	6.0974E+19	45	1.380E-05	1.070E-02
46	3.200E-04	5.0000E+13	6.5774E+19	46	1.400E-05	1.090E-02
47	2.700E-04	2.4000E+13	7.0974E+19	47	1.420E-05	1.110E-02
48	2.300E-04	1.1000E+13	7.6574E+19	48	1.440E-05	1.130E-02
49	2.000E-04	5.0000E+12	8.2574E+19	49	1.460E-05	1.150E-02
50	1.700E-04	2.4000E+12	8.8974E+19	50	1.480E-05	1.170E-02

BEST AVAILABLE COPY

BEST AVAILABLE COPY

TABLE D-2. MCELROY K_Z PROFILE

Z, km	F ₀ , cm ² /sec	S, cm ² /sec	Gates	Residence Times, yr	
				R = 0.1μm	R = 0.3μm
0	3.066E-05	1.375E-20	0.000E+00	0.011E-02	0.040E-02
1	3.000E-05	2.001E-20	1.000E+00	1.000E-02	1.000E-02
2	3.000E-05	4.001E-20	2.000E+00	2.000E-02	2.000E-02
3	3.000E-05	6.001E-20	3.000E+00	3.000E-02	3.000E-02
4	3.000E-05	8.001E-20	4.000E+00	4.000E-02	4.000E-02
5	3.000E-05	1.000E-19	5.000E+00	5.000E-02	5.000E-02
6	3.000E-05	1.200E-19	6.000E+00	6.000E-02	6.000E-02
7	3.000E-05	1.400E-19	7.000E+00	7.000E-02	7.000E-02
8	3.000E-05	1.600E-19	8.000E+00	8.000E-02	8.000E-02
9	3.000E-05	1.800E-19	9.000E+00	9.000E-02	9.000E-02
10	3.000E-05	2.000E-19	1.000E+01	1.000E-01	1.000E-01
11	3.000E-05	2.200E-19	1.200E+01	1.200E-01	1.200E-01
12	3.000E-05	2.400E-19	1.400E+01	1.400E-01	1.400E-01
13	3.000E-05	2.600E-19	1.600E+01	1.600E-01	1.600E-01
14	3.000E-05	2.800E-19	1.800E+01	1.800E-01	1.800E-01
15	3.000E-05	3.000E-19	2.000E+01	2.000E-01	2.000E-01
16	3.000E-05	3.200E-19	2.200E+01	2.200E-01	2.200E-01
17	3.000E-05	3.400E-19	2.400E+01	2.400E-01	2.400E-01
18	3.000E-05	3.600E-19	2.600E+01	2.600E-01	2.600E-01
19	3.000E-05	3.800E-19	2.800E+01	2.800E-01	2.800E-01
20	3.000E-05	4.000E-19	3.000E+01	3.000E-01	3.000E-01
21	3.000E-05	4.200E-19	3.200E+01	3.200E-01	3.200E-01
22	3.000E-05	4.400E-19	3.400E+01	3.400E-01	3.400E-01
23	3.000E-05	4.600E-19	3.600E+01	3.600E-01	3.600E-01
24	3.000E-05	4.800E-19	3.800E+01	3.800E-01	3.800E-01
25	3.000E-05	5.000E-19	4.000E+01	4.000E-01	4.000E-01
26	3.000E-05	5.200E-19	4.200E+01	4.200E-01	4.200E-01
27	3.000E-05	5.400E-19	4.400E+01	4.400E-01	4.400E-01
28	3.000E-05	5.600E-19	4.600E+01	4.600E-01	4.600E-01
29	3.000E-05	5.800E-19	4.800E+01	4.800E-01	4.800E-01
30	3.000E-05	6.000E-19	5.000E+01	5.000E-01	5.000E-01
31	3.000E-05	6.200E-19	5.200E+01	5.200E-01	5.200E-01
32	3.000E-05	6.400E-19	5.400E+01	5.400E-01	5.400E-01
33	3.000E-05	6.600E-19	5.600E+01	5.600E-01	5.600E-01
34	3.000E-05	6.800E-19	5.800E+01	5.800E-01	5.800E-01
35	3.000E-05	7.000E-19	6.000E+01	6.000E-01	6.000E-01
36	3.000E-05	7.200E-19	6.200E+01	6.200E-01	6.200E-01
37	3.000E-05	7.400E-19	6.400E+01	6.400E-01	6.400E-01
38	3.000E-05	7.600E-19	6.600E+01	6.600E-01	6.600E-01
39	3.000E-05	7.800E-19	6.800E+01	6.800E-01	6.800E-01
40	3.000E-05	8.000E-19	7.000E+01	7.000E-01	7.000E-01
41	3.000E-05	8.200E-19	7.200E+01	7.200E-01	7.200E-01
42	3.000E-05	8.400E-19	7.400E+01	7.400E-01	7.400E-01
43	3.000E-05	8.600E-19	7.600E+01	7.600E-01	7.600E-01
44	3.000E-05	8.800E-19	7.800E+01	7.800E-01	7.800E-01
45	3.000E-05	9.000E-19	8.000E+01	8.000E-01	8.000E-01
46	3.000E-05	9.200E-19	8.200E+01	8.200E-01	8.200E-01
47	3.000E-05	9.400E-19	8.400E+01	8.400E-01	8.400E-01
48	3.000E-05	9.600E-19	8.600E+01	8.600E-01	8.600E-01
49	3.000E-05	9.800E-19	8.800E+01	8.800E-01	8.800E-01
50	3.000E-05	1.000E-18	9.000E+01	9.000E-01	9.000E-01

*Also, same value as at level 1 km below; i.e., double-valued at this level.

TABLE D-3a. CHANG/1974 K_z PROFILE

Z, km	K _z , cm ² /sec	α, cm ² -sec	Residence Times, yr		Z, km	K _z , cm ² /sec	α, cm ² -sec	Gases	Residence Times, yr	
			R = 0.1 μm	R = 0.3 μm					R = 0.1 μm	R = 0.3 μm
1	3.00E-05	9.37E-20	0.50E-03	0.93E-03	1	1.00E-05	9.37E-20	2.00E-12	2.00E-12	2.00E-12
2	3.00E-05	2.49E-20	1.74E-02	1.54E-02	2	1.00E-05	6.11E-19	7.70E-12	4.00E-12	4.00E-12
3	3.00E-05	4.57E-20	2.50E-02	2.50E-02	3	1.00E-05	1.82E-18	1.00E-11	7.00E-12	6.00E-12
4	3.00E-05	6.28E-20	3.15E-02	3.00E-02	4	1.00E-05	2.28E-18	1.00E-11	1.00E-11	1.00E-11
5	3.00E-05	9.49E-20	4.21E-02	3.75E-02	5	1.00E-05	2.28E-18	1.00E-11	1.00E-11	1.00E-11
6	3.00E-05	1.48E-19	5.04E-02	4.46E-02	6	1.00E-05	4.12E-18	1.00E-11	1.00E-11	1.00E-11
7	3.00E-05	1.33E-19	5.74E-02	5.01E-02	7	1.00E-05	4.12E-18	1.00E-11	1.00E-11	1.00E-11
8	3.00E-05	1.42E-19	6.51E-02	5.94E-02	8	1.00E-05	5.07E-18	2.00E-11	2.00E-11	2.00E-11
9	3.00E-05	1.55E-19	7.24E-02	6.44E-02	9	1.00E-05	5.07E-18	2.00E-11	2.00E-11	2.00E-11
10	2.10E-04	2.31E-19	7.94E-02	6.44E-02	10	1.00E-05	5.07E-18	2.00E-11	2.00E-11	2.00E-11
11	2.10E-04	7.40E-19	1.04E-01	1.29E-01	11	1.00E-05	1.21E-18	2.00E-11	2.00E-11	2.00E-11
12	1.80E-04	7.40E-19	1.04E-01	1.29E-01	12	1.00E-05	1.21E-18	2.00E-11	2.00E-11	2.00E-11
13	1.80E-04	1.44E-18	1.04E-01	1.29E-01	13	1.00E-05	1.21E-18	2.00E-11	2.00E-11	2.00E-11
14	1.80E-04	3.01E-18	1.04E-01	1.29E-01	14	1.00E-05	1.21E-18	2.00E-11	2.00E-11	2.00E-11
15	1.07E-04	5.49E-18	1.04E-01	1.29E-01	15	1.00E-05	1.21E-18	2.00E-11	2.00E-11	2.00E-11
16	6.55E-05	9.40E-18	1.04E-01	1.29E-01	16	1.00E-05	1.21E-18	2.00E-11	2.00E-11	2.00E-11
17	7.50E-05	1.22E-17	1.04E-01	1.29E-01	17	1.00E-05	1.21E-18	2.00E-11	2.00E-11	2.00E-11
18	7.50E-05	1.70E-17	1.04E-01	1.29E-01	18	1.00E-05	1.21E-18	2.00E-11	2.00E-11	2.00E-11
19	2.32E-03	2.32E-17	1.04E-01	1.29E-01	19	1.00E-05	1.21E-18	2.00E-11	2.00E-11	2.00E-11
20	5.48E-03	3.10E-17	1.04E-01	1.29E-01	20	1.00E-05	1.21E-18	2.00E-11	2.00E-11	2.00E-11
21	5.48E-03	4.28E-17	1.04E-01	1.29E-01	21	1.00E-05	1.21E-18	2.00E-11	2.00E-11	2.00E-11
22	4.74E-03	5.60E-17	1.04E-01	1.29E-01	22	1.00E-05	1.21E-18	2.00E-11	2.00E-11	2.00E-11
23	4.74E-03	7.44E-17	1.04E-01	1.29E-01	23	1.00E-05	1.21E-18	2.00E-11	2.00E-11	2.00E-11
24	4.74E-03	9.57E-17	1.04E-01	1.29E-01	24	1.00E-05	1.21E-18	2.00E-11	2.00E-11	2.00E-11
25	3.71E-03	1.23E-16	1.04E-01	1.29E-01	25	1.00E-05	1.21E-18	2.00E-11	2.00E-11	2.00E-11
26	3.71E-03	1.57E-16	1.04E-01	1.29E-01	26	1.00E-05	1.21E-18	2.00E-11	2.00E-11	2.00E-11
27	3.71E-03	1.97E-16	1.04E-01	1.29E-01	27	1.00E-05	1.21E-18	2.00E-11	2.00E-11	2.00E-11
28	3.71E-03	2.42E-16	1.04E-01	1.29E-01	28	1.00E-05	1.21E-18	2.00E-11	2.00E-11	2.00E-11
29	3.71E-03	2.92E-16	1.04E-01	1.29E-01	29	1.00E-05	1.21E-18	2.00E-11	2.00E-11	2.00E-11
30	3.71E-03	3.42E-16	1.04E-01	1.29E-01	30	1.00E-05	1.21E-18	2.00E-11	2.00E-11	2.00E-11
31	3.71E-03	3.92E-16	1.04E-01	1.29E-01	31	1.00E-05	1.21E-18	2.00E-11	2.00E-11	2.00E-11
32	3.71E-03	4.42E-16	1.04E-01	1.29E-01	32	1.00E-05	1.21E-18	2.00E-11	2.00E-11	2.00E-11
33	3.71E-03	4.92E-16	1.04E-01	1.29E-01	33	1.00E-05	1.21E-18	2.00E-11	2.00E-11	2.00E-11
34	3.71E-03	5.42E-16	1.04E-01	1.29E-01	34	1.00E-05	1.21E-18	2.00E-11	2.00E-11	2.00E-11
35	3.71E-03	5.92E-16	1.04E-01	1.29E-01	35	1.00E-05	1.21E-18	2.00E-11	2.00E-11	2.00E-11
36	3.71E-03	6.42E-16	1.04E-01	1.29E-01	36	1.00E-05	1.21E-18	2.00E-11	2.00E-11	2.00E-11
37	3.71E-03	6.92E-16	1.04E-01	1.29E-01	37	1.00E-05	1.21E-18	2.00E-11	2.00E-11	2.00E-11
38	3.71E-03	7.42E-16	1.04E-01	1.29E-01	38	1.00E-05	1.21E-18	2.00E-11	2.00E-11	2.00E-11
39	3.71E-03	7.92E-16	1.04E-01	1.29E-01	39	1.00E-05	1.21E-18	2.00E-11	2.00E-11	2.00E-11
40	3.71E-03	8.42E-16	1.04E-01	1.29E-01	40	1.00E-05	1.21E-18	2.00E-11	2.00E-11	2.00E-11
41	3.71E-03	8.92E-16	1.04E-01	1.29E-01	41	1.00E-05	1.21E-18	2.00E-11	2.00E-11	2.00E-11
42	3.71E-03	9.42E-16	1.04E-01	1.29E-01	42	1.00E-05	1.21E-18	2.00E-11	2.00E-11	2.00E-11
43	3.71E-03	9.92E-16	1.04E-01	1.29E-01	43	1.00E-05	1.21E-18	2.00E-11	2.00E-11	2.00E-11
44	3.71E-03	1.04E-15	1.04E-01	1.29E-01	44	1.00E-05	1.21E-18	2.00E-11	2.00E-11	2.00E-11
45	3.71E-03	1.09E-15	1.04E-01	1.29E-01	45	1.00E-05	1.21E-18	2.00E-11	2.00E-11	2.00E-11
46	3.71E-03	1.14E-15	1.04E-01	1.29E-01	46	1.00E-05	1.21E-18	2.00E-11	2.00E-11	2.00E-11
47	3.71E-03	1.19E-15	1.04E-01	1.29E-01	47	1.00E-05	1.21E-18	2.00E-11	2.00E-11	2.00E-11
48	3.71E-03	1.24E-15	1.04E-01	1.29E-01	48	1.00E-05	1.21E-18	2.00E-11	2.00E-11	2.00E-11
49	3.71E-03	1.29E-15	1.04E-01	1.29E-01	49	1.00E-05	1.21E-18	2.00E-11	2.00E-11	2.00E-11
50	3.71E-03	1.34E-15	1.04E-01	1.29E-01	50	1.00E-05	1.21E-18	2.00E-11	2.00E-11	2.00E-11

*Also, same value as at level 1 km below; i.e.,
double-valued at this level.

Low Level Radiation
 Permit All Level Radiation

BEST AVAILABLE COPY

TABLE D-4. HUNTEN/1974 K_Z PROFILE

Z, km	K _Z , cm ² /sec	g, cm ² /sec	Residence Times, yr	
			R = 0.1um	R = 0.3um
1	1.00E+05	1.12E+20	2.44E+12	2.31E+12
2	1.00E+05	1.47E+20	2.44E+12	2.31E+12
3	1.00E+05	1.37E+20	7.74E+12	6.73E+12
4	1.00E+05	1.02E+19	1.42E+12	1.17E+12
5	1.00E+05	1.02E+19	1.42E+12	1.17E+12
6	1.00E+05	1.02E+19	1.42E+12	1.17E+12
7	1.00E+05	1.02E+19	1.42E+12	1.17E+12
8	1.00E+05	1.02E+19	1.42E+12	1.17E+12
9	1.00E+05	1.02E+19	1.42E+12	1.17E+12
10	1.00E+05	1.02E+19	1.42E+12	1.17E+12
11	1.00E+05	1.02E+19	1.42E+12	1.17E+12
12	1.00E+05	1.02E+19	1.42E+12	1.17E+12
13	1.00E+05	1.02E+19	1.42E+12	1.17E+12
14	1.00E+05	1.02E+19	1.42E+12	1.17E+12
15	1.00E+05	1.02E+19	1.42E+12	1.17E+12
16	1.00E+05	1.02E+19	1.42E+12	1.17E+12
17	1.00E+05	1.02E+19	1.42E+12	1.17E+12
18	1.00E+05	1.02E+19	1.42E+12	1.17E+12
19	1.00E+05	1.02E+19	1.42E+12	1.17E+12
20	1.00E+05	1.02E+19	1.42E+12	1.17E+12
21	1.00E+05	1.02E+19	1.42E+12	1.17E+12
22	1.00E+05	1.02E+19	1.42E+12	1.17E+12
23	1.00E+05	1.02E+19	1.42E+12	1.17E+12
24	1.00E+05	1.02E+19	1.42E+12	1.17E+12
25	1.00E+05	1.02E+19	1.42E+12	1.17E+12
26	1.00E+05	1.02E+19	1.42E+12	1.17E+12
27	1.00E+05	1.02E+19	1.42E+12	1.17E+12
28	1.00E+05	1.02E+19	1.42E+12	1.17E+12
29	1.00E+05	1.02E+19	1.42E+12	1.17E+12
30	1.00E+05	1.02E+19	1.42E+12	1.17E+12
31	1.00E+05	1.02E+19	1.42E+12	1.17E+12
32	1.00E+05	1.02E+19	1.42E+12	1.17E+12
33	1.00E+05	1.02E+19	1.42E+12	1.17E+12
34	1.00E+05	1.02E+19	1.42E+12	1.17E+12
35	1.00E+05	1.02E+19	1.42E+12	1.17E+12
36	1.00E+05	1.02E+19	1.42E+12	1.17E+12
37	1.00E+05	1.02E+19	1.42E+12	1.17E+12
38	1.00E+05	1.02E+19	1.42E+12	1.17E+12
39	1.00E+05	1.02E+19	1.42E+12	1.17E+12
40	1.00E+05	1.02E+19	1.42E+12	1.17E+12
41	1.00E+05	1.02E+19	1.42E+12	1.17E+12
42	1.00E+05	1.02E+19	1.42E+12	1.17E+12
43	1.00E+05	1.02E+19	1.42E+12	1.17E+12
44	1.00E+05	1.02E+19	1.42E+12	1.17E+12
45	1.00E+05	1.02E+19	1.42E+12	1.17E+12
46	1.00E+05	1.02E+19	1.42E+12	1.17E+12
47	1.00E+05	1.02E+19	1.42E+12	1.17E+12
48	1.00E+05	1.02E+19	1.42E+12	1.17E+12
49	1.00E+05	1.02E+19	1.42E+12	1.17E+12
50	1.00E+05	1.02E+19	1.42E+12	1.17E+12

*Also, same value as at level 1 km below; i.e., double-valued at this level.

TABLE D-5. CRUTZEN/1974* K_Z PROFILE

Z, km	K _Z , cm ² /sec	g, cm ² /sec	Residence Times, yr	
			R = 0.1um	R = 0.3um
1	1.00E+05	1.12E+20	2.44E+12	2.31E+12
2	1.00E+05	1.47E+20	2.44E+12	2.31E+12
3	1.00E+05	1.37E+20	7.74E+12	6.73E+12
4	1.00E+05	1.02E+19	1.42E+12	1.17E+12
5	1.00E+05	1.02E+19	1.42E+12	1.17E+12
6	1.00E+05	1.02E+19	1.42E+12	1.17E+12
7	1.00E+05	1.02E+19	1.42E+12	1.17E+12
8	1.00E+05	1.02E+19	1.42E+12	1.17E+12
9	1.00E+05	1.02E+19	1.42E+12	1.17E+12
10	1.00E+05	1.02E+19	1.42E+12	1.17E+12
11	1.00E+05	1.02E+19	1.42E+12	1.17E+12
12	1.00E+05	1.02E+19	1.42E+12	1.17E+12
13	1.00E+05	1.02E+19	1.42E+12	1.17E+12
14	1.00E+05	1.02E+19	1.42E+12	1.17E+12
15	1.00E+05	1.02E+19	1.42E+12	1.17E+12
16	1.00E+05	1.02E+19	1.42E+12	1.17E+12
17	1.00E+05	1.02E+19	1.42E+12	1.17E+12
18	1.00E+05	1.02E+19	1.42E+12	1.17E+12
19	1.00E+05	1.02E+19	1.42E+12	1.17E+12
20	1.00E+05	1.02E+19	1.42E+12	1.17E+12
21	1.00E+05	1.02E+19	1.42E+12	1.17E+12
22	1.00E+05	1.02E+19	1.42E+12	1.17E+12
23	1.00E+05	1.02E+19	1.42E+12	1.17E+12
24	1.00E+05	1.02E+19	1.42E+12	1.17E+12
25	1.00E+05	1.02E+19	1.42E+12	1.17E+12
26	1.00E+05	1.02E+19	1.42E+12	1.17E+12
27	1.00E+05	1.02E+19	1.42E+12	1.17E+12
28	1.00E+05	1.02E+19	1.42E+12	1.17E+12
29	1.00E+05	1.02E+19	1.42E+12	1.17E+12
30	1.00E+05	1.02E+19	1.42E+12	1.17E+12
31	1.00E+05	1.02E+19	1.42E+12	1.17E+12
32	1.00E+05	1.02E+19	1.42E+12	1.17E+12
33	1.00E+05	1.02E+19	1.42E+12	1.17E+12
34	1.00E+05	1.02E+19	1.42E+12	1.17E+12
35	1.00E+05	1.02E+19	1.42E+12	1.17E+12
36	1.00E+05	1.02E+19	1.42E+12	1.17E+12
37	1.00E+05	1.02E+19	1.42E+12	1.17E+12
38	1.00E+05	1.02E+19	1.42E+12	1.17E+12
39	1.00E+05	1.02E+19	1.42E+12	1.17E+12
40	1.00E+05	1.02E+19	1.42E+12	1.17E+12
41	1.00E+05	1.02E+19	1.42E+12	1.17E+12
42	1.00E+05	1.02E+19	1.42E+12	1.17E+12
43	1.00E+05	1.02E+19	1.42E+12	1.17E+12
44	1.00E+05	1.02E+19	1.42E+12	1.17E+12
45	1.00E+05	1.02E+19	1.42E+12	1.17E+12
46	1.00E+05	1.02E+19	1.42E+12	1.17E+12
47	1.00E+05	1.02E+19	1.42E+12	1.17E+12
48	1.00E+05	1.02E+19	1.42E+12	1.17E+12
49	1.00E+05	1.02E+19	1.42E+12	1.17E+12
50	1.00E+05	1.02E+19	1.42E+12	1.17E+12

*As interpreted by IBA.
 *Also, same value as at level 1 km below, i.e., double-valued at this level.

TABLE D-6. WOFSY/1975 K₂ PROFILE

Z, km	K ₂ , cm ² /sec	Q ₂ , cm ² /sec	Residence Times, yr	
			R = 0.1μm	R = 0.3μm
1	1.00E+00	0.10E+00	0.50E+02	0.30E+02
2	1.00E+00	0.10E+00	0.50E+02	0.30E+02
3	1.00E+00	0.10E+00	0.50E+02	0.30E+02
4	1.00E+00	0.10E+00	0.50E+02	0.30E+02
5	1.00E+00	0.10E+00	0.50E+02	0.30E+02
6	1.00E+00	0.10E+00	0.50E+02	0.30E+02
7	1.00E+00	0.10E+00	0.50E+02	0.30E+02
8	1.00E+00	0.10E+00	0.50E+02	0.30E+02
9	1.00E+00	0.10E+00	0.50E+02	0.30E+02
10	1.00E+00	0.10E+00	0.50E+02	0.30E+02
11	1.00E+00	0.10E+00	0.50E+02	0.30E+02
12	1.00E+00	0.10E+00	0.50E+02	0.30E+02
13	1.00E+00	0.10E+00	0.50E+02	0.30E+02
14	1.00E+00	0.10E+00	0.50E+02	0.30E+02
15	1.00E+00	0.10E+00	0.50E+02	0.30E+02
16	1.00E+00	0.10E+00	0.50E+02	0.30E+02
17	1.00E+00	0.10E+00	0.50E+02	0.30E+02
18	1.00E+00	0.10E+00	0.50E+02	0.30E+02
19	1.00E+00	0.10E+00	0.50E+02	0.30E+02
20	1.00E+00	0.10E+00	0.50E+02	0.30E+02
21	1.00E+00	0.10E+00	0.50E+02	0.30E+02
22	1.00E+00	0.10E+00	0.50E+02	0.30E+02
23	1.00E+00	0.10E+00	0.50E+02	0.30E+02
24	1.00E+00	0.10E+00	0.50E+02	0.30E+02
25	1.00E+00	0.10E+00	0.50E+02	0.30E+02
26	1.00E+00	0.10E+00	0.50E+02	0.30E+02
27	1.00E+00	0.10E+00	0.50E+02	0.30E+02
28	1.00E+00	0.10E+00	0.50E+02	0.30E+02
29	1.00E+00	0.10E+00	0.50E+02	0.30E+02
30	1.00E+00	0.10E+00	0.50E+02	0.30E+02
31	1.00E+00	0.10E+00	0.50E+02	0.30E+02
32	1.00E+00	0.10E+00	0.50E+02	0.30E+02
33	1.00E+00	0.10E+00	0.50E+02	0.30E+02
34	1.00E+00	0.10E+00	0.50E+02	0.30E+02
35	1.00E+00	0.10E+00	0.50E+02	0.30E+02
36	1.00E+00	0.10E+00	0.50E+02	0.30E+02
37	1.00E+00	0.10E+00	0.50E+02	0.30E+02
38	1.00E+00	0.10E+00	0.50E+02	0.30E+02
39	1.00E+00	0.10E+00	0.50E+02	0.30E+02
40	1.00E+00	0.10E+00	0.50E+02	0.30E+02
41	1.00E+00	0.10E+00	0.50E+02	0.30E+02
42	1.00E+00	0.10E+00	0.50E+02	0.30E+02
43	1.00E+00	0.10E+00	0.50E+02	0.30E+02
44	1.00E+00	0.10E+00	0.50E+02	0.30E+02
45	1.00E+00	0.10E+00	0.50E+02	0.30E+02
46	1.00E+00	0.10E+00	0.50E+02	0.30E+02
47	1.00E+00	0.10E+00	0.50E+02	0.30E+02
48	1.00E+00	0.10E+00	0.50E+02	0.30E+02
49	1.00E+00	0.10E+00	0.50E+02	0.30E+02
50	1.00E+00	0.10E+00	0.50E+02	0.30E+02

TABLE D-7. CRUTZEN-ISAISEN/1975 K₂ PROFILE

Z, km	K ₂ , cm ² /sec	Q ₂ , cm ² /sec	Residence Times, yr	
			R = 0.1μm	R = 0.3μm
1	5.00E+00	0.25E+00	0.50E+02	0.30E+02
2	5.00E+00	0.25E+00	0.50E+02	0.30E+02
3	5.00E+00	0.25E+00	0.50E+02	0.30E+02
4	5.00E+00	0.25E+00	0.50E+02	0.30E+02
5	5.00E+00	0.25E+00	0.50E+02	0.30E+02
6	5.00E+00	0.25E+00	0.50E+02	0.30E+02
7	5.00E+00	0.25E+00	0.50E+02	0.30E+02
8	5.00E+00	0.25E+00	0.50E+02	0.30E+02
9	5.00E+00	0.25E+00	0.50E+02	0.30E+02
10	5.00E+00	0.25E+00	0.50E+02	0.30E+02
11	5.00E+00	0.25E+00	0.50E+02	0.30E+02
12	5.00E+00	0.25E+00	0.50E+02	0.30E+02
13	5.00E+00	0.25E+00	0.50E+02	0.30E+02
14	5.00E+00	0.25E+00	0.50E+02	0.30E+02
15	5.00E+00	0.25E+00	0.50E+02	0.30E+02
16	5.00E+00	0.25E+00	0.50E+02	0.30E+02
17	5.00E+00	0.25E+00	0.50E+02	0.30E+02
18	5.00E+00	0.25E+00	0.50E+02	0.30E+02
19	5.00E+00	0.25E+00	0.50E+02	0.30E+02
20	5.00E+00	0.25E+00	0.50E+02	0.30E+02
21	5.00E+00	0.25E+00	0.50E+02	0.30E+02
22	5.00E+00	0.25E+00	0.50E+02	0.30E+02
23	5.00E+00	0.25E+00	0.50E+02	0.30E+02
24	5.00E+00	0.25E+00	0.50E+02	0.30E+02
25	5.00E+00	0.25E+00	0.50E+02	0.30E+02
26	5.00E+00	0.25E+00	0.50E+02	0.30E+02
27	5.00E+00	0.25E+00	0.50E+02	0.30E+02
28	5.00E+00	0.25E+00	0.50E+02	0.30E+02
29	5.00E+00	0.25E+00	0.50E+02	0.30E+02
30	5.00E+00	0.25E+00	0.50E+02	0.30E+02
31	5.00E+00	0.25E+00	0.50E+02	0.30E+02
32	5.00E+00	0.25E+00	0.50E+02	0.30E+02
33	5.00E+00	0.25E+00	0.50E+02	0.30E+02
34	5.00E+00	0.25E+00	0.50E+02	0.30E+02
35	5.00E+00	0.25E+00	0.50E+02	0.30E+02
36	5.00E+00	0.25E+00	0.50E+02	0.30E+02
37	5.00E+00	0.25E+00	0.50E+02	0.30E+02
38	5.00E+00	0.25E+00	0.50E+02	0.30E+02
39	5.00E+00	0.25E+00	0.50E+02	0.30E+02
40	5.00E+00	0.25E+00	0.50E+02	0.30E+02
41	5.00E+00	0.25E+00	0.50E+02	0.30E+02
42	5.00E+00	0.25E+00	0.50E+02	0.30E+02
43	5.00E+00	0.25E+00	0.50E+02	0.30E+02
44	5.00E+00	0.25E+00	0.50E+02	0.30E+02
45	5.00E+00	0.25E+00	0.50E+02	0.30E+02
46	5.00E+00	0.25E+00	0.50E+02	0.30E+02
47	5.00E+00	0.25E+00	0.50E+02	0.30E+02
48	5.00E+00	0.25E+00	0.50E+02	0.30E+02
49	5.00E+00	0.25E+00	0.50E+02	0.30E+02
50	5.00E+00	0.25E+00	0.50E+02	0.30E+02

COPY AVAILABLE TO THE PUBLIC
PERMIT FULL REPRODUCTION

BEST AVAILABLE COPY

ADDENDUM 1 TO APPENDIX D

K.A. Gardner

A computer model for 1-D calculation of the atmospheric residence time of tracers is operational on IDA's CDC 6400. Program EB6 was completed in December 1975 from earlier versions (EB4, EB5) developed in April 1975.

Tables of data in the program include:

- Atmospheric number densities
- Various estimates for eddy diffusivity profile
- Arrays of sedimentation velocity for 2 g/cm^3 particles

Each of these sets of atmospheric data are for altitudes from 0 to 75 km, with values at each 1 km increment.

The program will give results for each combination of eddy diffusivity profile and sedimentation velocity array. Calculations are made for two sink altitudes, 55 km and 75 km.

The integration is done by Simpson's rule, with a 1-km step size. However, due to discontinuities in the diffusivity data, separate integrations are done between the altitudes of discontinuity and summed. This more careful treatment of these discontinuities is the primary difference between EB6 and earlier versions of the program.

The primary equations evaluated by program EB6 are

$$y(z_1) = A_1 \int_0^{z_1} u(z)/K(z) dz$$

$$f(z_1) = A_1 I(z_1)e^{-y(z)},$$

ADDENDUM 1 TO APPENDIX D

K.A. Gardner

A computer model for 1-D calculation of the atmospheric residence time of tracers is operational on IDA's CDC 6400. Program EB6 was completed in December 1975 from earlier versions (EB4, EB5) developed in April 1975.

Tables of data in the program include:

- Atmospheric number densities
- Various estimates for eddy diffusivity profile
- Arrays of sedimentation velocity for 2 g/cm^3 particles

Each of these sets of atmospheric data are for altitudes from 0 to 75 km, with values at each 1 km increment.

The program will give results for each combination of eddy diffusivity profile and sedimentation velocity array. Calculations are made for two sink altitudes, 55 km and 75 km.

The integration is done by Simpson's rule, with a 1-km step size. However, due to discontinuities in the diffusivity data, separate integrations are done between the altitudes of discontinuity and summed. This more careful treatment of these discontinuities is the primary difference between EB6 and earlier versions of the program.

The primary equations evaluated by program EB6 are

$$y(z_1) = A_1 \int_0^{z_1} u(z)/K(z) dz$$

$$f(z_1) = A_1 I(z_1)e^{-y(z)},$$

where

$$I(z_1) = \int_0^{z_1} \frac{1}{K(z_1)n(z_1)} e^{y(z)} dz$$

$$G(z_1) = \frac{I(z_1)}{I(z_2) - I(z_1)}$$

$$B_L(z_1) = (A_1 A_2) \int_0^{z_1} f(z)n(z) dz$$

$$B_G(z_1) = A_1(A_1 A_2)G(z_1) \int_{z_1}^{z_2} [I(z_2) - I(z)] e^{-y(z)} n(z) dz$$

$$T(z_1) = [B_L(z_1) + G_B(z_1)] / [1 + G(z_1)] .$$

A run of program EB6 for three profiles of $K(z)$, for gases and for aerosols of seven different radii takes approximately 1 min. of CP time and 22K octal words of core on the CDC 6400. A listing of the program follows.

TABLE D-8. COMPUTER MODEL

```

COMMON /UBLOCK/ U(176,7)
DIMENSION NA(76), TEM(5), TEM2(5), TEM3(5), RU(8), U(76), FIN(76)
DIMENSION G(76), VZ(76), IZ(76), K(76)
DIMENSION LISTK(54), LIST2(54)
DIMENSION XNG(76), XNL(76), BGINF(76)
REAL KC2(76), KM2(76), KCM(76), KW2(76)
DATA NA,K,KOFI
DATA IZL,SI/, RU/0.003,0.1,0.3,1.0,3.0,10.0/
DATA A1/E5/, A2/3.16E-3/
ID=1

IP=1
IP=0
IZ2=51
IZ1=51

C COMPLETE ATMOSPHERIC DATA WITH EXPONENTIAL
DO 4600 I=1,IZ2
  IZ(I)=1
  IF(I.GT.37) NA(I)=NA(57) * EXP((IZ(I)-56)/(-7.79))
  CONTINUE
4600 CONTINUE

DO 4710 I=1,5
  4710 TEMP(I)=0.
  IZ=0
  DO 4720 I=1,IZ1
    XNG=NA(I)
    XN=CLCINT(1,0Z,XNF,TEMP)
    XNL(I)=XN
    IZ=10
  4720 CONTINUE
C
  XNMF=7.92NA(51) * XNL(51)
  PRINT 4730, XNL(51), XNMF
  4730 FORMAT('01 INT(N) 0 TO 50',E15.6 / 'INT(N) 0 TO INF',E15.6 /
    1 '01 I 2 INT(N) 0 TO 2 INT(N) 2 TO INF')
  DO 4730 I=1,IZ1
    XNG(I)=XNMF-XNL(I)
    PRINT 4716, I,IZ(I), NA(I),XNL(I),XNG(I)
    4716 FORMAT('13,14,E11.3,2E15.6')
  4730 CONTINUE
C
  PRINT 919, (RU(IU),I=2,5)
  919 FORMAT('01 I 2 N KC2 KM2 KCR')
  1 40 U(RU,FS,2,0)
  PRINT 918, (IZ(I), NA(I),KC2(I),KM2(I),KCR(I),KW2(I),
    1 (UAT(I),J=1,4),I=1,IZ2)
  918 FORMAT('13,14,E11.3)
C
DO 580 I=1,IZ2
  580 U(I)=0.
C
C LOOP FOR U'S TO BE USED - VARIOUS R'S
C

```


TABLE D-8. COMPUTER MODELS (Cont.)

```

C      FUNCTION CLCINT (YOLD,DX,Y,T)
C      SUBROUTINE TO DO SIMPSON'S RULE INTEGRATION AS DONE BY GE ROUTINE
C      CLCINT - WRITTEN 1 MAY 75 FOR DO. BAUER - KG
C
C      DIMENSION T(5)
C      SUMO=T(2)
C      SUMO=T(1)
C      YOLDER=T(3)
C      YOLD=T(4)
C      IN=T(5)
C
C      IF (DX.NE.0.) GO TO 200
C      CLCINT=0.
C      GO TO 390
C
C      200  CONTINUE
C      IF (SUMO.NE.0.) GO TO 250
C      SUMO=DX/2.* (Y+YOLD)
C      CLCINT=SUMO
C      IN=1
C      GO TO 390
C
C      250  IN=3-IN
C      IF (IN.EQ.1) GO TO 300
C      SUMO=SUMO + DX/3. * (YOLDER+.5*YOLD+Y)
C      CLCINT=SUMO
C      GO TO 390
C
C      300  CONTINUE
C      SUMO=SUMO + DX/3. * (YOLDER+.5*YOLD+Y)
C      CLCINT=SUMO
C
C      390  CONTINUE
C      YOLDER=YOLD
C      YOLD=Y
C      T(1)=SUMO
C      T(2)=SUMO
C      T(3)=YOLDER
C      T(4)=YOLD
C      T(5)=IN+.001
C      RETURN
C      END

```


TABLE D-9. VARIABLES

A1	Constant for conversion of units = 10^5 cm/km	LISTM }	Matrix of discontinuities in K arrays
A2	Constant for conversion of units = $10^5 \text{ cm/km} \times 3.169 \times 10^{-12} \text{ yr/sec}$	LIST2 }	(#discont's, #K's) for determination of integration limits
BG	Burden above the point of injection (yr)	NA	Array of atmospheric number density (cm^{-3})
BGF	Integrand for calculation of BG	NK	Name of K array used
BL	Burden below the point of injection (yr)	PSUM	Result of integration for BG calculation from $z = 0$ to last altitude of data discontinuity
BLEG	BL + BG	RU	Array of particle radii for U arrays
BLF	Integrand for calculations of BL	SUM	Integral for BG calculation
BLSUM	Result of BL integration from $z = 0$ to last discontinuity in F	T	Atmospheric residence time (yr.)
CICINT	Function to calculate integral by Simpson's Rule	TEMP	Arrays for temporary storage of sums for integral calculation
DZ	Integration interval	TEMP2 }	
F	Particle mixing ratio ($\text{cm}^3/\text{sec}/\text{particle} = 1/\text{flux}$)	TEMP3 }	
FF	Integrand for calculation of F below the point of injection	U	Array of sedimentation velocities used
FINT	Integral for calculation of F below the point of injection	U1, U2, .. U7	Arrays of sedimentation velocity data for density = $2g/\text{cm}^3$ (cm/sec)
FINTSUM	Result of FINT integration from $z = 0$ to last discontinuity in K	UA	Matrix of arrays U1 through U7
G	Flux ratio = flux above Z/flux below Z	YZ	Integral for calculation of FINT = $\int u/k$
I(z)	I(z) in program description is called FINT in program	YZP	Integrand for YZ calculation
IC	Index for choice of K array	YZSUM	Integral YZ from $z = 0$ to z for last K discontinuity
ID	Interval between data points Used to set DZ		
IU	Index for choice of U array		
IE	Each value of IU refers to a particle radius		
IZL	Array of altitudes		
IZL	Maximum altitude for G, BL, BG and T calculations		
IZZ	Index for altitude of sink = altitude + ID		
K	Array of diffusivity coefficients used		
KC, KH, KM	Arrays of diffusivity data (cm^2/sec)		
KOFI	Value of K used at altitude		

ADDENDUM 2 TO APPENDIX D

THE ANALYTIC MODEL "A"

For the simple case of an isothermal atmosphere with K and u independent of height [see Eqs. (5), (6)], the whole problem can be solved analytically. In particular

$$y(z) = (u/K)z \equiv b z \quad (D.2.1)$$

$$f_L(z) = e^{-y} \int_0^z (A/Kn) e^y dz \equiv e^{-y} A I_1(z) \quad (D.2.2)$$

$$I_1(z) = [K n_0 (b + H^{-1})]^{-1} [e^{(b + H^{-1})z} - 1] \quad (D.2.3)$$

$$c \equiv b + H^{-1} \quad (D.2.4)$$

$$B_L(z_1) = \int_0^{z_1} f_L(z) n(z) dz = (A/Kc^2) [c z_1 - 1 + e^c z_1] \quad (D.2.5)$$

Case (i).

$$f(z > z_1) = f(z_1)$$

$$B_{G,1}(z_1) = f(z_1) n(z_1)/H \quad (D.2.6)$$

Case (ii)

$$z_2 > z_1 \text{ such that } f_G(z_2) = 0$$

$$f_G(z) = G(z) \begin{cases} [f_L(z_2) - f_L(z)] & z_1 < z < z_2 \\ z > z_2 \end{cases} \quad (D.2.7)$$

[See Eq. (13)] (Indept. A)

$$B_{G,11}(z_1) = G(z_1) \int_{z_1}^{z_2} n(z) [f_L(z_2) - f_L(z)] dz \quad (D.2.8)$$

Case (iii)

No net flux above the point of injection, i.e., $A + Q = 0$ in Eq. (8b) so that for $z > z_1$, $f = f_U(z)$, a solution of Eq. (17) or of

$$d(\ln f_U)/dz + b = 0 \quad (D.2.9)$$

$$f_U(z) = f_L(z_1) e^{b(z_1 - z)} \quad (D.2.10)$$

$$B_{G,111}(z_1) = f_L(z_1) n(z_1)/c \quad (D.2.11)$$

APPENDIX E

EMISSION CONSTRAINTS ON NEW SSTs: AN APPROACH

R. C. Oliver

APPENDIX E

EMISSION CONSTRAINTS ON NEW SSTs: AN APPROACH

E.1 INTRODUCTION AND SUMMARY

It is implicit in the treatment in the CIAP Report of Findings that an environmentally acceptable SST fleet can be built up by reducing NO_x emission indices and fuel sulfur content as fleet size grows or as new aircraft are introduced. In this appendix, some of the questions involved are reconsidered, estimating fleet sizes permitted by various criteria for given emission indices, or emission indices required for specific fleets. The tentative HAPP guidelines on ozone depletion (< 0.5 percent) and on climatic effects ($< 0.1\text{-K}$ surface temperature change) are used. Fleet size (or, crudely, passenger miles delivered) is characterized for purposes here by annual fuel consumption at altitude. The possible numbers of aircraft included under certain assumptions are illustrated in several cases. The procedures used are based on information available as of September, 1976.

In view of the considerable uncertainty in NO_x emission indices with current technology (Section 2), in NO_x effects on the ozone column, and in the various climatic effects, it is evident that calculations of the type to follow are, at best, illustrative. Nevertheless, it is believed that the approach provides some useful, if obviously preliminary, information, as follows:

- a. If future SSTs operate at the cruise altitudes implied by past designs, lower-mach-number SSTs (mach 2 or below) will more easily meet environmental requirements than will higher-mach-number SSTs (mach 2.7 or above).
- b. With ozone reduction calculational procedures as used in CIAP, permissible fleet sizes would very likely be unattractive economically with present NO_x emission indices. If, however, the ozone column sensitivity to NO_x emissions is as low as suggested by some of the results from Lawrence Livermore Laboratories (Section 3), large fleets would be permitted by the 0.5 percent criterion, particularly if cruise is at about 17 km (mach 2), or below.

c. If an ozone reduction constraint is met by low NO_x engines or by an accepted revision in the chemistry involved, an 0.1-K climatic constraint due to water vapor emissions may limit fleet sizes, particularly if cruise is at about 20 km (mach 2.7), or above.

d. The need to use low sulfur fuels is not clearly established.

Note that the discussion which follows applies only to those environmental matters discussed in the CIAP report and elsewhere in this report; thus sonic boom and aircraft noise, e.g., which may in fact be critical environmental problems, are not discussed.*

E.2 GUIDELINES AND BASIS FOR PROCEDURES

As guidelines, the tentative maximum aircraft-induced levels of environmental change suggested by HAPP (1975) of 0.5 percent reduction in ozone and 0.1-K change in mean Northern Hemisphere temperature will be applied. For exploratory purposes here, the reduction in ozone will be further specified to be that computed as in CIAP, using "corridor-adjusted" 1-D model results; the change in mean temperature will be that computed by the 1-D CCTT model of Ramanathan (1974), generally without adjustment for ice-albedo feedback effects (see Section 4, main text). The 0.1-K criterion will be explored both in terms of changes due to individual exhaust ingredients and net changes assuming additivity. SSTs operating over the mach 1.6 to mach 3 range will be considered, cruising at altitudes from 15 to 22 km, as implied by the empirical data plotted in Fig. E 1.

E.3 FUEL FLOW LIMITS WITH CURRENT EMISSION INDICES

In this section, in order to gain some appreciation of potential environmental constraints on SSTs, the allowable fuel flows per year with today's emission indicators (as understood in CIAP)**and HAPP guidelines are computed under various assumptions. Fuel flow per year is a rough measure of passenger-miles delivered and of the number of aircraft (of particular types) operating, and should not be extremely sensitive to whether the aircraft is designed for, say, mach 1.6 or mach 3. (At mach 1.6, however, the fuel consumption per passenger-mile may be somewhat lower than at mach 3). A fuel-flow parameter, of course, begs more complex questions as to optimum aircraft size and speed

*Boom pressure jump increases approximately as $(M^2-1)^{1/8}$, M being mach number, and as $Z^{-3/4}$, Z being altitude (Wilson, 1962). If aircraft operate along the q-Z curve shown in Fig. E-1, the sonic boom overpressure changes little between mach 2 and mach 7 for constant-length aircraft. Shape and size, and temperature and wind gradients all enter.

**That is, based on probe sampling techniques. See Section 2.2.3.

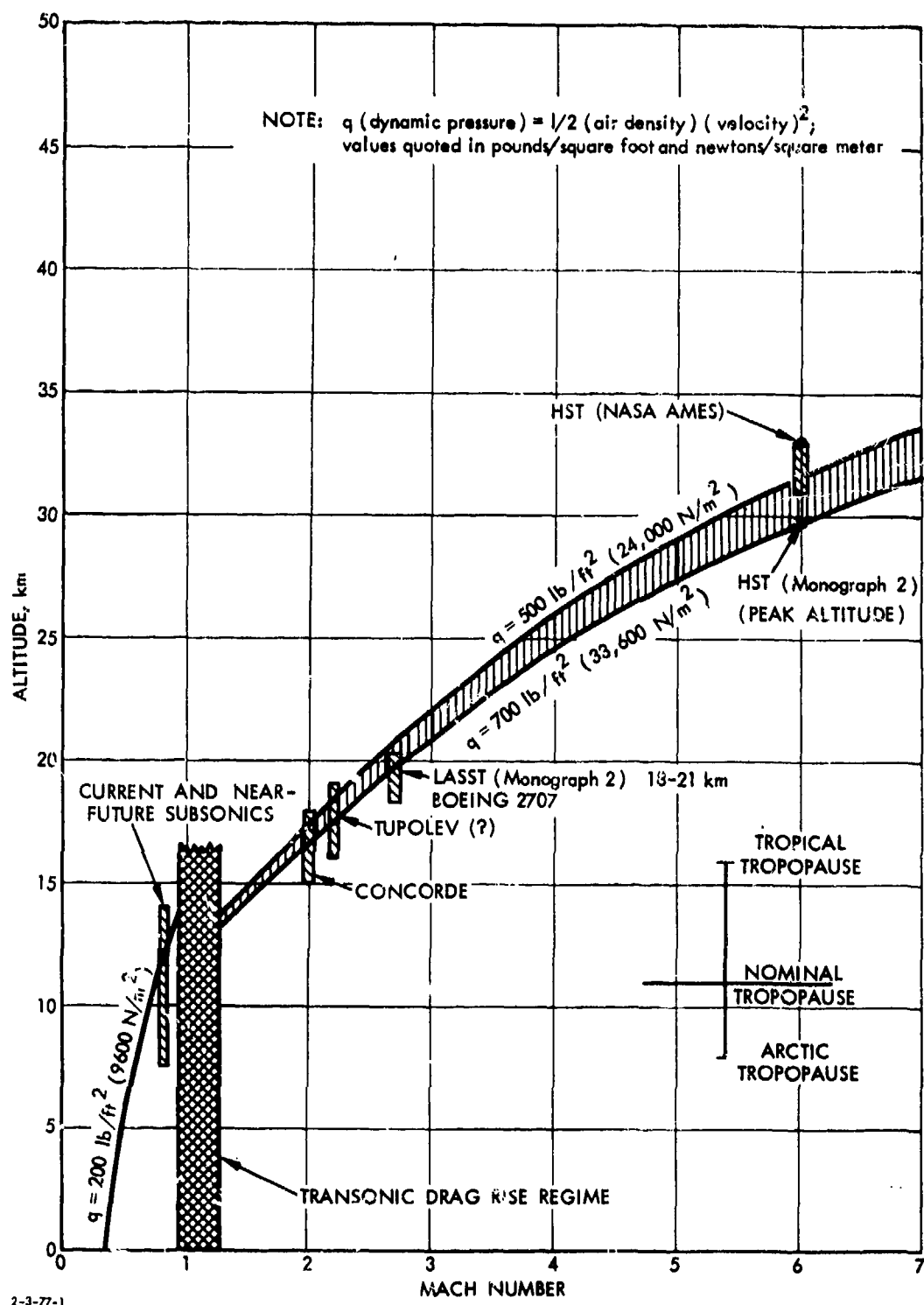


FIGURE E-1. APPARENT OPTIMAL ALTITUDE AS A FUNCTION OF MACH NUMBER (VELOCITY)

from the standpoint of profitability; such questions are beyond the scope of this discussion. Note, however, that while most U.S. SST proponents think in terms of mach 2.7 (see, e.g., Ferri, 1975), at least one large aerospace firm considers (or has considered) large mach 2 aircraft to be preferable (Fink, 1973).

The ozone-change constraint is tied to NO_x emissions (and perhaps in an ill-defined way to water emissions), while the climate-change constraint is tied largely to water vapor emissions and particulates (see Section 4). In order to demonstrate which constraint controls, the fuel flow rate which leads to 0.5 percent depletion in the region of the flight corridor with a NO_x emission index of 18 is first calculated for three available models; the fuel flow rate for which the computed water vapor warming (CCTT, $\chi = 100$, hemisphere factor of 1.4) is then estimated without inclusion of any compensating effects, using procedures described in Section 4 of this report. The sulfate question is treated later. Results are shown in Fig. E-2 and in Table E-1. Note first, for the $\text{NO}_x\text{-O}_3$ question, the following numbers from Table E-1.

TABLE E-1. Fuel Flows at Altitude (10^9 kg/yr) Leading to 0.5 Percent Ozone Depletion, at Emission Index $\text{NO}_x = 18$ gm/kg as NO_2

Altitude, km	CIAP Chemistry ($K_{19} = 2 \times 10^{-10}$ cm ³ /sec *)			Revised Chemistry ($K_{19} = 2 \times 10^{-11}$ cm ³ /sec *)	
	Huntten/1974 K_z (+2) **	CIAP	Chang/1974 K_z	Chang/1974 K_z ***	
15	3.63	5.60	12.28	30 (extrapolated)	
17	2.16	3.17	5.94	15	
20	1.28	1.67	2.40	5	
22	0.964	1.19	1.56	3 (extrapolated)	

* K_{19} refers to the $\text{OH} + \text{H}_2$ reaction to give $\text{H}_2\text{O} + \text{O}_2$.

**The +2 refers to the NAS/1975 recommendation and midlatitude traffic effects be computed by increasing the aircraft altitude by 2 km.

***Approximate, based on Duwer et al., 1976. A factor of 2.5 on ozone reduction is assumed at 15 km to 17 km and a factor of 2.0 at 20 km to 22 km. As the multiplier appears to increase with decreasing altitude, the value at 15 km may be low.

Note that the maximum yearly fuel flow permitted by the NAS/1975 or CIAP/1974 models is 12.28×10^9 kg if operating at 15-km altitude (about mach 1.6); revision of K_{19} increases this to about 3×10^{10} kg/yr. By way of comparison, according to the NAS/1975 (p. 29), 100 Concorde-type aircraft use 3.49×10^9 kg fuel per year, and 100 "large SSTs" use 9.13×10^9 kg/yr. Five hundred "large SSTs," as often discussed, using these figures, would require 4.57×10^{10} kg/yr.

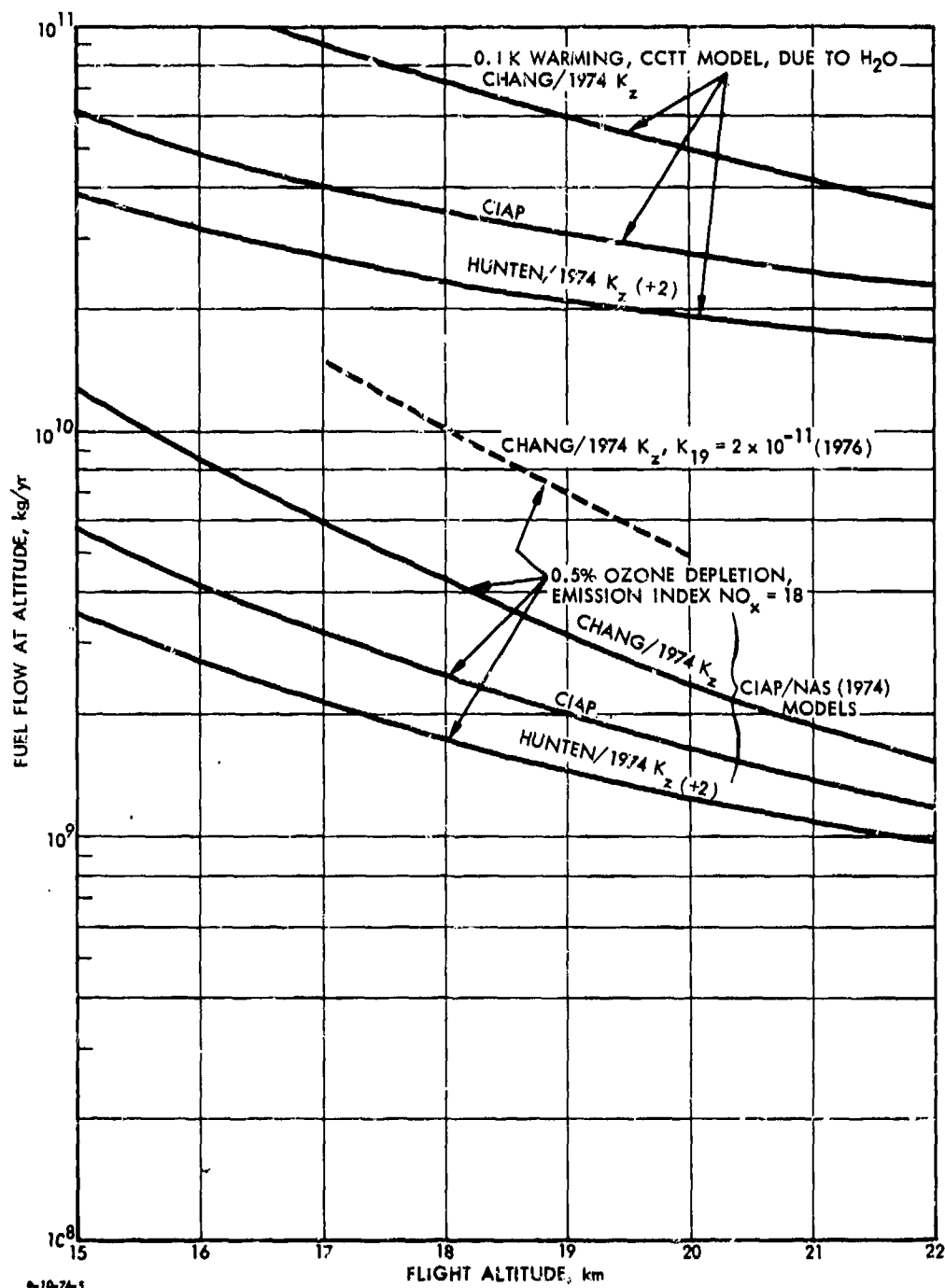


FIGURE E-2. Fuel Flow as Permitted by Various Criteria and Models. Procedures described in CIAP and in NAS/1975 are used to adjust 1-D results to give "corridor" and hemispheric means. The Hunten/1974 (+2) refers to the recommendation (NAS/1975) that aircraft altitudes be raised 2 km to give "corridor" effects.

The Chang/1974 K_z model, with revised K_{19} , would permit about 100 (15/3.5) or 430 Concorde-type aircraft at 17 km, or about 100 (5/9) or 55 "large SSTs" at 20 km. The NAS/1975 model would permit only 14 advanced SSTs at 20 km.

The different models also show different altitude sensitivities. The Chang/1974 K_u profile shows greater improvement with lower altitude flight than does the Hunten/1974 K_z profile. The results show that 4 (Hunten) to 8 (Chang) times as much fuel can be tolerated for a given ozone depletion at 15 km as at 22 km at the same emission index.*

It is, of course, self-evident that if the set of reaction rates happen to be such, that the net effect on the ozone column by SSTs at 17 km or 20 km is zero, as is possible (see Section 3), then no ozone constraint would apply. It should be cautioned, however, that these are 1-D results and averages which might net positive and negative effects in different geographical regimes could be misleading.

Fuel flow rates for the 0.1-K temperature change from the water vapor component are also shown on Fig. E-2. This constraint permits some tenfold larger fuel flows than does the NO_x constraint with an emission index of 18 gm/kg. A sulfate constraint would give even larger fuel flows by these models. The water vapor computations are based on a residence time model, according to the CCTT model ($\Delta T = 1.0 \frac{\Delta H_{2O}}{H_{2O}} H_F$, where ΔH_{2O} is the fuel flow rate $\times 1.25 \times$ residence time, H_{2O} is 1.78×10^{12} kg water, and H_F is 1.4, the hemisphere factor). The data are tabulated below.

The observation that considerably more fuel flow is allowed at all altitudes by the climate change criterion than the 0.5 percent ozone criterion, with current emission indices, would still apply if the 1.5 factor for ice-albedo feedback were applied to the ΔT calculation. Climatic constraints may nevertheless be significant, if compensation effects are ignored. Thus, the 0.1-K criterion permits only 2.77×10^{10} kg fuel per year at 20 km by the CIAP model, or about 3×10^{10} kg/yr at the 19.5 km mean altitude for mach 2.7 aircraft as used in CIAP, versus 4.57×10^{10} called for by the 500 SST fleet referred to above. The 3×10^{10} figure corresponds to about 330

*It should be pointed out that, at constant combustor inlet temperature the NO_x emission index will vary roughly as $p^{1/2}$. The square root of the pressure ratio between 22 km and 15 km is about 1.7. If this effect is applicable (and it depends on engine design), the 4 to 8 factor drops to 2.3 to 4.6; also, higher, as opposed to lower altitudes are desirable for sonic boom minimization, but this effect is small.

TABLE E-2. Fuel flow rates for which water vapor emissions lead to 1.0 K warming, ignoring other effects, 10^9 kg/yr, for several models

Altitude, km	Stratospheric Residence Time,* yr			Allowable Fuel Flows, 10^9 kg/yr		
	Chang/1974	Hunten/1974 (+2)	CIAP	Chang/1974	Hunten/1974 (+2)	CIAP
15	0.67	2.66	1.67	151.8	38.2	60.9
17	1.11	3.88	2.49	91.6	26.2	40.8
20	2.01	5.30	3.67	50.6	19.2	27.7
22	2.82	6.02	4.42	36.1	16.9	23.0

*See Fig. 4.1 main text.

aircraft; with an additional 1.5 ice-albedo feedback factor, this drops to 220 aircraft. With the Hunten model, and the 1.5 factor, this drops further to 150 aircraft. The Chang model, without the 1.5 factor, would permit over 500 mach 2.7 aircraft. At lower altitudes, more aircraft are permitted by these models, but the improvements are less dramatic than for the ozone case. (Note again that there is considerable question about how the water models should be applied.)

It thus appears that should low NO_x engines be developed, or revised chemistry show ozone effects to be minimal, so that ozone depletion is not controlling, climatic effects may restrict advanced (mach 2.7) fleets to modest sizes, if such effects are based on available models and residence time approaches and compensating effects are not considered. The questions clearly need further study.

E.4 EMISSION INDEX VALUES NEEDED FOR VARIOUS HYPOTHESIZED FLEETS

E.4.1 NO_x Emission Indices

Before proceeding, a point should be made with regard to the effects on ozone of very low emission index engines, i.e., engines with very high ratios of water to NO_x in their exhaust. It will be remembered that the first ozone depletion controversy with regard to SSTs came about because of presumed destructive water effects on ozone (Hearings, 1971). Later, a revision of water reaction rates essentially eliminated this aspect of the question and, in fact, at a later time Crutzen (1974) reported that an increase in stratospheric water vapor caused an increase in ozone, by tying up reactive NO_x as HNO_3 ; in Crutzen's work a doubling of water vapor led to a 1.5 percent increase in ozone. McElroy et al. (1974) found a 0.1 percent increase for a 24 percent increase in water (see p. 161, NAS report). The Crutzen finding led this author (Oliver, 1974) to note that if Crutzen's findings

were true, an emission index of about 0.3 for NO_x would be compensated (in a 1-D model) by the water vapor effect; further, the water vapor and sulfate effects were in opposite directions, so that, as noted then, a "zero impact" SST could be postulated, "zero impact" referring only to net changes in ozone and surface temperature according to 1-D models. (The memo, however, was intended more as a call for study of interactive effects than a conclusion.) The concept was subsequently given considerable publicity by Ferri (1975). Unfortunately, however, subsequent studies have failed to confirm Crutzen's computation, as mentioned, e.g., in Section 3 of this report. The problem is that great precision is needed in both the rates of all the water reactions and in atmospheric dynamics before such a prediction can be established. At the present time, no reliable statement, other than an expression of ignorance, can be made about the combined effects of water and NO_x emissions, where the ratio of water to NO_x is very large, as would be the case, for example, if the NO_x emission index is brought to 0.3 or thereabouts. In the following calculations, water is thus assumed to have no effect on ozone, but where emission index values less than 1.0 are called for, the values are underlined to emphasize the questions mentioned here.

With these caveats, the figures given in Table E-3 follow directly from the figures given earlier, assuming linearity:

In view of evident difficulties (EPA Hearings, 27-28 January 1976) in meeting current EPA goals which, in effect, call for about a twofold reduction in NO_x emission index at takeoff, it would appear that great difficulty will be encountered in reaching the very low levels called for above by any of the models.* It is true that through use of very lean premixed combustion (Blazowski, CIAP Monograph 2; Roffe and Ferri et al., 1976), very low emission indices have been attained in the laboratory, but reliable and operable engines using such techniques may or may not be achievable. The emission index requirement is eased by operating at lower altitudes, and perhaps with smaller rather than larger aircraft (to minimize R&D cost requirements and the number of required aircraft to achieve profitability).

E.4.2 Sulfur Contents

The effects of water vapor on climate are, according to available models, opposite in sign to those of sulfur. It appears to be a matter of viewpoint whether or not the net effects should be computed: the CIAP report implicitly recommended against doing so, while the COMESA report argued for doing so. Because of the uncertainty in knowledge of climatic effects, it can be argued that the computed effects of no single component should exceed the 0.1-K

*Again the possibility must be recognized that NO_x emission indices are higher than given by probe sampling (Section 2.2.3).

TABLE E-3. NO_x Emission Indices Leading to 0.5 Percent Ozone Depletion as a Function of Yearly Fuel Flow. *

Fuel Flow, 10^{10} kg/yr	Operating Altitude, km			
	15	17	20	22
CIAP (1974) Chemistry, $K_{19} = 2 \times 10^{-10} \text{ cm}^3/\text{sec}$				
Hunten/1974 $K_z (+2)$				
1	6.53	3.89	2.30	1.74
3	2.18	1.30	<u>0.77</u>	<u>0.58</u>
10	0.65	<u>0.39</u>	<u>0.23</u>	<u>0.17</u>
CIAP				
1	10.08	5.71	3.01	2.14
3	3.36	1.90	1.00	<u>0.71</u>
10	1.01	<u>0.57</u>	<u>0.30</u>	<u>0.21</u>
Chang/1974 K_z				
1	22.10	10.69	4.32	2.81
3	7.37	3.56	1.44	<u>0.94</u>
10	2.21	1.07	<u>0.43</u>	<u>0.28</u>
$K_{19} = 2 \times 10^{-11} \text{ cm}^3/\text{sec}$ (1976) **				
Chang/1974 K_z				
1	55.0	27.0	8.6	5.6
3	18.0	8.9	2.9	1.9
10	5.5	2.7	<u>0.9</u>	<u>0.6</u>

*Underscores denote NO_x emission index values of less than 1.0, indicating greater uncertainties in effects due to simultaneous water vapor emissions.

**Assumes factor on ozone reduction of 2.5 at 15 km and 17 km and a factor of 2.0 at 20 km and 22 km.

criterion mentioned. Conversely, it can be argued that if the best available scientific evaluation of the effects of aircraft exhaust on climate show that effects can be minimized by adjusting the ratio of certain ingredients, it would seem imprudent not to take whatever steps are needed to minimize computed climatic changes, as the penalties of any such change, positive or negative, may be significant in some areas. Other criteria, such as stratospheric optical thickness changes (see Section E-5) could then be invoked to minimize total changes in stratospheric composition.

The approach to balancing the effects is straightforward if the simple models presented earlier are used. However, in view of the uncertainties, there seems little point in going beyond the simplest of comparisons. Thus, in CIAP and COMESA, if ozone and NO_2 effects were excluded, it was found that the cooling effects on mean surface temperature of fuel containing 0.05 percent sulfur was about twice the warming effects of water vapor; on this basis, fuel should simply be desulfurized to approximately 0.025 percent to compensate the effects. With results as presented earlier (Table 4-6, main text), the net warming effect of gases is about 2 to 7 times [or more, with Pollack et al. (1976a) results] the cooling effect of aerosols. To compensate, the sulfur content should, on this basis, be increased by 2 to 7 times, i.e., to 0.1 to 0.35 percent to balance the effects. A limit exists, however, in that the maximum sulfur content in Jet A or A-1 fuel is limited by specification to 0.3 percent.

As indicated in Section 4 (this report), until internally consistent model results, with interactions and, preferably, with 2-D or more sophisticated models are available, exercises such as the above are largely devoid of meaning other than to emphasize the need for such studies before fuel requirements are established.

E.5 CHANGES IN STRATOSPHERIC OPTICAL THICKNESS: ANOTHER POSSIBLE CONSTRAINT

The CIAP Report of Findings treats a 10 percent change in stratospheric optical thickness due to added aerosols as one possible constraint. A 10 percent change (i.e., 0.002) in stratospheric optical thickness corresponds to a surface temperature change of about 0.07 K (by procedures in CIAP Report of Findings, p. 43) or slightly less (0.06 K), using Pollack-Toon procedures (p. F-116, Report of Findings), so that this constraint is more severe than a 0.1-K constraint based on the partial climatic effects of sulfate particulates. However, even by the CIAP* procedures wherein the residence times of particles are treated as equal to those of gases, the fleets permitted by this constraint are quite large: thus (p. 101, Report of Findings) at today's nominal 0.05 percent fuel sulfur, 2070 Concorde's are permitted by this criterion at 15 km to 18 km on 1100 equal-size SSTs (consuming the same annual fuel flow as Concorde's) at 18 km to 21 km. If an advanced SST is assumed, using 52,000 kg/hr rather than the Concorde's 19,100 kg/hr (p. 101, Report of Findings) at 18 km to 21 km, the corresponding number of aircraft is 404; with the correction for settling, however, the number becomes correspondingly larger, approaching 1000 aircraft.

*These procedures, however, did not include the 2-km adjustment for flight altitude recommended by Hunten. This correction would reduce the quoted numbers by about 30 percent.

The suggested optical thickness change criterion thus seems to be less significant than either ozone change or warming due to water vapor; unless high sulfur fuels are used.

E.6 FINAL CAVEAT

An important topic not treated here relates to the risks associated with uncertainties in the various estimates of effects. This question would need more detailed examination before "acceptability" of some specific fleet could be considered to be established.

APPENDIX F

CALCULATIONS OF TIME-DEPENDENT HYPOTHETICAL SST FLEET EFFECTS
ON OZONE REDUCTION AND MEAN SURFACE TEMPERATURE

R. C. Oliver

APPENDIX F

CALCULATIONS OF TIME-DEPENDENT HYPOTHETICAL SST FLEET EFFECTS ON OZONE REDUCTION AND MEAN SURFACE TEMPERATURE

F.1 INTRODUCTION AND SUMMARY

Because aircraft fleets would be expected to change with time, it would be of obvious interest to be able to predict any resulting effects as a function of time. Unfortunately, as discussed at some length in Sections 3 and 4 of this report, there are still many uncertainties regarding the magnitude and, in some cases, even the direction of changes that would occur even with steady-state operation of hypothetical fleets. The same difficulties obviously apply in estimating time-dependent effects, and these difficulties are increased by questions about rates of response and perhaps by initial phenomena which differ in direction from steady-state phenomena. Some of this, on the ozone question, was discussed in Section 3 of this report; here the time-dependent question is pursued one step further to include also, for illustration purposes, possible time-dependent aspects of changes in mean surface temperature. The procedures used are fundamentally those available at the end of CIAP, modified somewhat for present purposes; in view of the uncertainties in these procedures, it is probably best to consider the results as being indicative of the types of information--preferably however in more than one dimension--that modelers may eventually be asked to provide.

The case examined assumes a fleet of 378 Concorde-type SSTs building up over a 25-year period, thereafter, for model purposes, remaining constant in size and emissions. This fleet is one postulated in CIAP as being necessary to meet SST requirements in the "1990 upper-bound" traffic case, although this time frame has been extended. The effects of time lags in ozone reduction and climatic changes are illustrated. Effects of NO_x reduction and fuel desulfurization, the range of values which can be generated, without going outside the framework of the models, is shown.

This work was carried out in the spring of 1976, using information available at that time. Its tenuous nature cannot be overemphasized. Detailed procedures are included.

F.2 FLEET SELECTED AND RESULTS OBTAINED

The fleet is assumed to grow according to a Gompertz-type growth curve, as in CIAP Monograph 2. Specifically, the fleet is assumed to grow according to:

$$N_{\text{aircraft}} = 500[\exp(-4.125) \times (0.89384)^{(I-1)}] \text{ for } I = 1 \text{ to } 25,$$

and 378 thereafter.

This expression calls for about 8 aircraft at year 1, 12 aircraft at year 2, 36 aircraft at year 5, 111 aircraft at year 10, 212 aircraft at year 15, 306 aircraft at year 20, and 378 aircraft at year 25. The fleet is held constant at 378 aircraft after year 25 to show steady-state effects. The 378-aircraft figure comes from the CIAP 1990 upper-bound fleet for the case where the only SST class assumed to be available in the Concorde-Tupolev, but the time frame has been extended.

It is assumed for purposes here that new engines, combustors, or aircraft with lower emission indices will be brought into service in time to prevent ozone depletion, using the CIAP model, from exceeding 0.5 percent in the Northern Hemisphere. The uncontrolled emissions case is also considered. The results are given in Fig. F-1, detailed input data for which follow (Table F-1). Figure F-1 is based on the CIAP procedures; the procedures are based on Chang/1974 and Hunten/1974 profiles. Table F-1 includes only the 16.5-km emissions, which dominate the effects; the figure includes both 13.5- and 16.5-km emissions.

Several points should be noted about Fig. F-1. First, it should be reemphasized that the case is a hypothetical one, and the procedures involve many uncertainties. Also, the emission reduction schedule, implying instantaneity, is obviously unrealistic. Nevertheless, certain features should be noted, which may (or may not) be qualitatively correct, but (particularly items 3 and 4 below) are certainly poorly established.

1. The ozone depletion lags the fleet buildup by several (2-3) years.
2. The climatic changes are small and will lag some additional years behind the other changes--perhaps 5-10 years. The lag shown assumed a 6.5-year response time (which may, in fact, be too long).
3. The particulate cooling and ozone depletion, according to this model, are insufficient to compensate for H_2O and NO_2 warming. Desulfurization would increase net warming.
4. NO_x reduction, again by this model, by reducing the ozone depletion, results in a somewhat larger net warming.

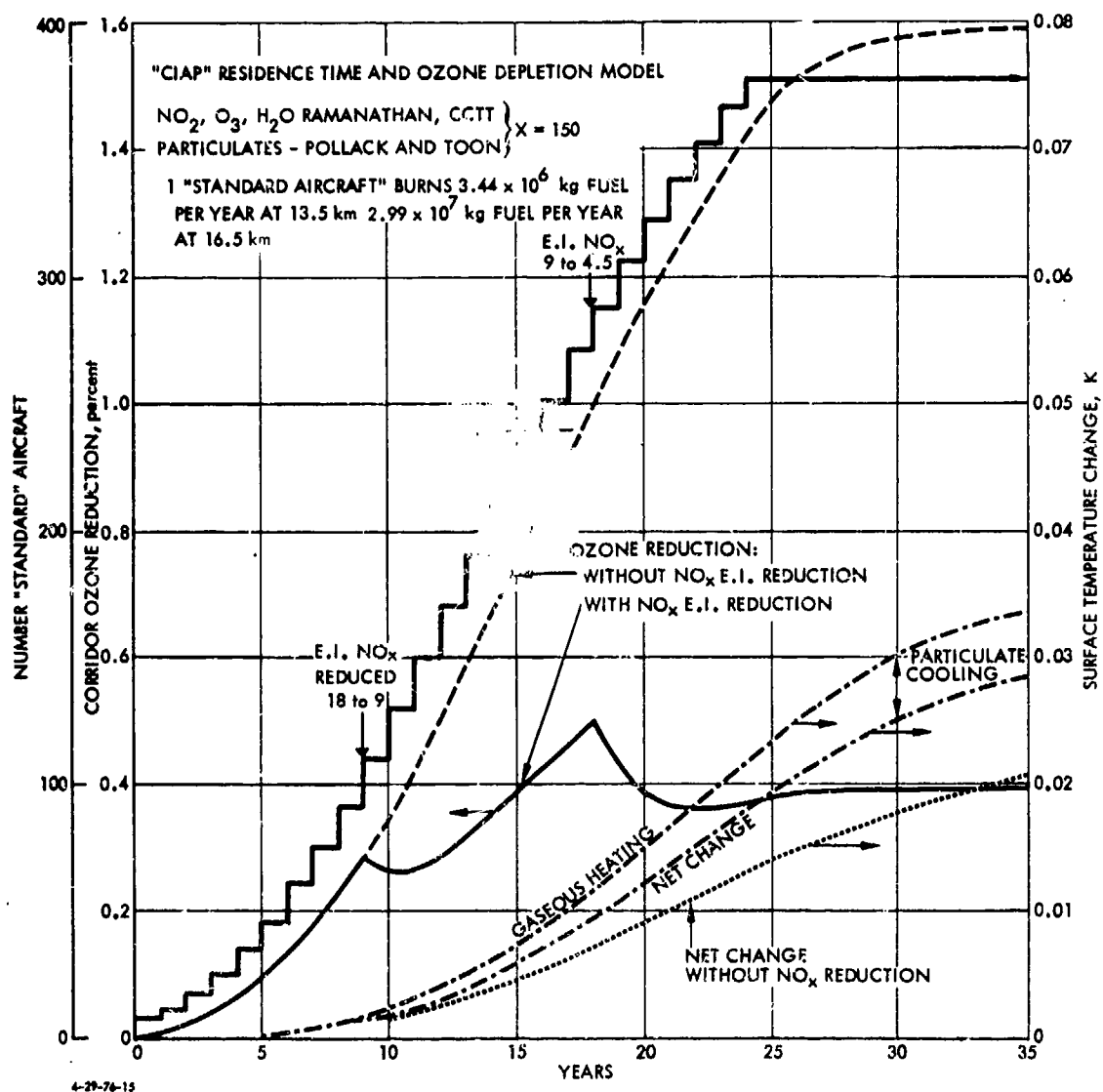


FIGURE F-1. Model-Generated Effects of Hypothetical SST Fleet Building up with Time. The procedures used and thus the results plotted are exceedingly tentative.

TABLE F-1. INPUT DATA FOR FIGURE F-1

	<u>Chang</u>	<u>Hunten*</u>	<u>CIAP</u>
Stratospheric residence time, gases, yr			
13.5 km	0.426	1.550	0.980
16.5 km	0.990	3.620	2.305
Residence times, 0.3μ, yr**			
13.5 km	0.297	0.705	0.501
16.5 km	0.560	1.240	0.900
Ozone depletion, %, global average @ 10 ⁸ kg NO _x /yr†			
13.5 km	0.0585	0.2047	0.1316
16.5 km	0.1733	0.5760	0.3747
Fuel flow kg/yr			
13.5 km (total)			1.3 x 10 ⁹
per aircraft			3.44 x 10 ⁶
16.5 km (total)			11.3 x 10 ⁹
per aircraft			2.99 x 10 ⁷
Emission indexes			
NO _x , g/kg			4.5, 18
H ₂ O			1250
Sulfates (as 75% H ₂ SO ₄)			2.04
Background data, natural atmosphere			
Global stratospheric water, kg			1.78 x 10 ¹²
Global stratospheric NO ₂			1.58 x 10 ⁹
Fraction, NO ₂ of odd nitrogen			0.27
Climate response time, yr to "e-fold"			6.5
Fleet buildup assumption: number aircraft =			
500[exp(-4.135(0.89384) ^(I-1))] for I = 1 to 25, 378 thereafter			
Model: Constant cloud-top temperature with X = 150 for gases			
Pollack and Toon's results, p. F-116, Report of Findings,			
for particulates			
Pollutant 70 percent in Northern Hemisphere			

*Includes 2-km adjustment on flight altitude, as recommended by NAS/1975.

**Based on calculations by E. Bauer (Appendix D).

†Ozone depletions assumed to be linear.

F.3 EFFECTS OF MODEL ASSUMPTIONS

In order to gain some insight into the range of numbers which can be generated within these modeling approaches, Table F-2 has been prepared. The effects tabulated therein are "steady-state" values,* resulting from continued operation of the hypothetical 378 aircraft fleet postulated in Fig. F-1; the emissions at 13.5 km have however been ignored. Assumptions include two emission indices on NO_x (4.5 and 18), three K_z profiles (in effect), and two estimates of possible climate change coefficient (α). For the uncontrolled emission case ($\text{E.I. NO}_x = 18$), the net climate change estimates (if summing of positive and negative changes is permitted, and this is indeed questionable) vary by about 17-fold, from 0.00203 to 0.0341 K. For the controlled NO_x emission case ($\text{E.I. NO}_x = 4.5$), the range is 0.00383 to 0.0484 K. These figures by no means exhaust the range of possible results for, with use of Coakley's (1976) low values for water vapor heating, or of different optical properties for aerosols or with a lesser correction for particulate setting, small negative values of net temperature change could be obtained. In general, however, a larger cooling effect from aerosols lead to a net temperature change closer to zero. The entire computational effort assumes 0.05 percent sulfur in the fuel, and this figure is neither precise nor necessarily invariant with time.

*After decades, not after thousands of years (see CIAP Monograph 4, p. 7-47, also Chapter 4, this report).

TABLE F-2. STEADY-STATE CLIMATIC EFFECTS (1-9 MODELS)

Assumed fleet and emissions (13.5-km emissions ignored; see also Table F-1)					
Fuel	11.3 x 10 ⁹ kg/yr				
Altitude	16.5 km				
Route	North Atlantic				
E.I.(s)NO _x	(a) 4.5 g/kg; (b) 16.0 g/kg				
E.I.H ₂ O	1250 g/kg				
E.I.Sulfate	2.04 g/kg as 75 percent H ₂ SO ₄ ; 0.05 percent sulfur; 0.3 μm particles, assumed				
NO _x rate(s)	5.085 x 10 ⁷ ; 2.034 x 10 ⁸ kg/yr				
H ₂ O rate	1.4125 x 10 ¹⁰ kg/yr				
Sulfate rate	2.3052 x 10 ⁷ kg/yr				
		Chang/1974	Hunten/1974	CIAP	
		(a)* (b)*	(a)* (b)*	(a)*	(b)*
Gas residence time, yr		0.99	3.62	2.305	
Particle residence time, yr		0.56	1.24	0.90	
Pollutant burdens					
H ₂ O (10 ¹⁰ kg)		1.398	5.113	3.256	
NO _x (10 ⁷ kg) as NO ₂		5.034; 20.136	18.408; 73.632	11.721; 46.884	
Sulfate (10 ⁷ kg)		1.291	2.858	2.075	

*Column (a) corresponds to the fleet in which NO_x emissions are controlled, and column (b) to the uncontrolled case.

TABLE F-2. (CONTINUED)

	<u>Chang/1974</u>		<u>Hunten/1974</u>		<u>CIAP</u>	
	(a)	(b)	(a)	(b)	(a)	(b)
Changes, global average						
$\Delta \text{H}_2\text{O}/\text{H}_2\text{O}$	0.00785		0.02872		0.01829	
$\Delta \text{NO}_2/\text{NO}_2$	0.00860; 0.0344		0.03146; 0.1258		0.02003; 0.0801	
ΔS ($\mu\text{g}/\text{m}^3$, in $5.1 \times 10^{18} \text{ m}^3$)	0.00253		0.00560		0.00407	
$-\Delta \text{O}_3/\text{O}_3$, percent	0.0881; 0.352;		0.2929; 1.172		0.1905; 0.762	

Temperature Coefficients

	<u>CCTA*, X = 100</u>		<u>CCTT**, X = 150</u>	
$\Delta \text{H}_2\text{O}/\text{H}_2\text{O}$	0.6		1.50	
$\Delta \text{NO}_2/\text{NO}_2$	0.0278		0.06675	
$-\Delta \text{O}_3/\text{O}_3$	0.76		1.875	
ΔS ; Pollack-Toon**	0.61		0.915	
Coakley-Schneider**	0.46		0.69	
Luther**	1.10		1.65	
CIAP**	0.90		1.35	

*Does not apply to the coefficients on ΔS .

**These coefficients are from the CIAP report, p. F-116. Lower values are associated with the most recent study (see Section 4).

TABLE F-2. (CONTINUED)

Mean Temperature Changes, Northern Hemisphere

Species Changed	CCTA, X = 100, HF = 1.4		CIAP	
	Chang/1974 (a)	(b)	(a)	(b)
H ₂ O	0.0066	0.0241	0.0154	
NO ₂	0.00033; 0.00134	0.00122; 0.00490	0.00078; 0.00312	
O ₃	-0.000937; -0.003750	-0.003116; -0.01247	-0.00203; -0.00811	
Sulfates (Pollack-Toon)	-0.00216	-0.00478	-0.00348	
(Net)*	0.00383; 0.00203	0.0174; 0.0118	0.0107; 0.00693	
CCTT, X = 150, HF = 1.4				
H ₂ O	0.0165	0.0603	0.0384	
NO ₂	0.00080; 0.00321	0.00294; 0.01176	0.001872; 0.00749	
O ₃	-0.00231; -0.009251	-0.00769; -0.03075	-0.00500; -0.0290	
Sulfates	-0.00324	-0.00717	-0.00521	
(Net)*	0.01175; 0.0072	0.0484; 0.0341	0.0301; 0.0207	

*It may not be valid to net these effects, as different assumptions are involved in the modeling.

ADDENDUM - APPENDIX F

TIME-DEPENDENT EFFECTS PROGRAM

General

The procedure involves consideration of aircraft fleets operating in up to four altitude bands, each with time-varying fuel flow rates and with time-varying emission indices; for the SST case presented in Fig. F-1 only two bands were used. The fleets are assumed to change in a stepwise year-by-year fashion. This procedure permits any growth curve to be approximated. Burdens of pollutants are computed as a function of time in each band independently. In this example, all effects are assumed to be linearly additive; had large ozone reductions been under consideration, a program modification would have been necessary to prevent total ozone reductions from exceeding 100 percent. Ozone reductions at a given time are taken as a function of the burden of NO_x , without consideration of any delays due to kinetic or transport factors; the procedure thus treats response times and residence times to be equal, an assumption which is erroneous in general but does not introduce serious errors for SST altitudes. For temperature change total response time is largely controlled by the climatic response time.

Climatic effects are computed for SO_2 (sulfates), H_2O , NO_x , and O_3 changes independently. As a matter of interest, the sulfate (particulate) cooling effect and the summed gas effects (O_3 , H_2O , NO_2) are reported separately as well as being summed. Climatic effects are computed from burdens and from injection rates in each band. Provision is made for inclusion of an initial temperature anomaly if desired. Particulates are permitted to have different residence time than gases.

Climatic effects modeled are only those available under CIAP, with correction for sedimentation of aerosols.

Pollutant Burdens and Climatic Temperature Changes

The assumption is that mean temperature (T) responds as follows, if displaced from a reference temperature (T_R)

$$\frac{dT}{dt} = -\lambda(T - T_R) , \quad (\text{F.1.1})$$

where $\lambda=1/C$, C being a climatic response time (in years).

In this work, it is assumed that T_R is related to a steady-state pollution-free temperature (T_0), according to

$$T_R = T_0 - \alpha q(t) , \quad (F.1.2)$$

where α is a temperature coefficient, and $q(t)$ is the quantity of pollutant material present at time (t).

It follows that, in general,

$$(T - T_0) = (T - T_0)_{t_0} e^{-\lambda(t-t_0)} + \int_{t_0}^t e^{-\lambda(t-\tau)} [-\alpha \lambda q(\tau)] d\tau . \quad (F.1.3)$$

For an idealized stratosphere, in which foreign materials are removed at a rate proportionate to their quantity present, but to which material is being continuously added at a rate $\dot{p}(t)$

$$\frac{dq}{dt} + kq = \dot{p}(t) , \quad (F.1.4)$$

for which, if $\dot{p}(t)$ can be considered constant over a certain time period, $t-t_0$, Eq. (F.1.4) becomes

$$q(t) = q_{t_0} e^{-k(t-t_0)} + \frac{\dot{p}}{k} \left[1 - e^{-k(t-t_0)} \right] , \quad (F.1.5)$$

which for each constituent, in each altitude band, can be substituted into Eq. (F.1.3), to obtain Eq. (F.1.6).

$$(T - T_0) = (T - T_0)_{t_0} e^{-\lambda(t-t_0)} + \sum_{i,j} \frac{\alpha_{i,j} q_{i,j}(t_0)}{k_{i,j} - \lambda} \left(e^{-k_{i,j}(t-t_0)} e^{-\lambda(t-t_0)} \right) - \sum_{i,j} \left[\frac{\alpha_{i,j} \dot{p}_{i,j}}{k} \left(1 - e^{-\lambda(t-t_0)} \right) + \frac{\lambda}{k_{i,j} - \lambda} \left(e^{-k_{i,j}(t-t_0)} e^{-\lambda(t-t_0)} \right) \right] , \quad (F.1.6)$$

where i refers to constituents and j refers to altitude band.

As noted earlier, $t-t_0$ here is taken in one-year increments, and \dot{p} is taken as the average yearly injection rate of each pollutant.

Equation (F.1.6) is the basis of the computational program. The burden (q) and injection rate (\dot{p}) of each temperature-changing material are computed on a year-to-year basis. The injection rate is the yearly average fuel flow rate times the emission index for that year.

As a first step in the computations, global average effects are determined. These effects are then computed for the hemisphere (or corridor) of interest by inclusion of appropriate weighting factors. Computations specific to the Northern Hemisphere are included in the material presented in the main text.

Machine Program and Output

A listing of the machine program as written follows, along with two illustrative output cases for the hypothetical 378-SST example just described. In one case, NO_x emissions are assumed to be controlled; in the other, they are uncontrolled. The CIAP model is used in the output attached. Nomenclature follows.

Ex-14

2803 CONTINUE
2804 CASE = 1
2805 IF (CASE .EQ. 1) GO TO 281
2806 CASE = 2 FOR CIAP, CASE = 2 FOR HUNTEN, CASE = 3 FOR CHANG
2807 IF (CASE .EQ. 2) GO TO 282
2808 IF (CASE .EQ. 3) GO TO 283
2809 CONTINUE

CIAP MODEL

```

468 DO3CF2 = CDELO3*DO33
469 DO3CF1 = CDELO3*DO34
470 SCV1 = SOXB1*CS*HF1/5.1E9
471 SCV2 = SOXB2*CS*HF2/5.1E9
472 SCV3 = SOXB3*CS*HF3/5.1E9
473 SCV4 = SOXB4*CS*HF4/5.1E9
474 SCV5 = SOXB5*CS*HF5/5.1E9
475 SCV6 = SOXB6*CS*HF6/5.1E9
476 SCV7 = SOXB7*CS*HF7/5.1E9
477 SCV8 = SOXB8*CS*HF8/5.1E9
478 SCV9 = SOXB9*CS*HF9/5.1E9
479 SCV10 = SOXB10*CS*HF10/5.1E9
480 SCV11 = SOXB11*CS*HF11/5.1E9
481 SCV12 = SOXB12*CS*HF12/5.1E9
482 SCV13 = SOXB13*CS*HF13/5.1E9
483 SCV14 = SOXB14*CS*HF14/5.1E9
484 SCV15 = SOXB15*CS*HF15/5.1E9
485 SCV16 = SOXB16*CS*HF16/5.1E9
486 SCV17 = SOXB17*CS*HF17/5.1E9
487 SCV18 = SOXB18*CS*HF18/5.1E9
488 SCV19 = SOXB19*CS*HF19/5.1E9
489 SCV20 = SOXB20*CS*HF20/5.1E9
490 SCV21 = SOXB21*CS*HF21/5.1E9
491 SCV22 = SOXB22*CS*HF22/5.1E9
492 SCV23 = SOXB23*CS*HF23/5.1E9
493 SCV24 = SOXB24*CS*HF24/5.1E9
494 SCV25 = SOXB25*CS*HF25/5.1E9
495 SCV26 = SOXB26*CS*HF26/5.1E9
496 SCV27 = SOXB27*CS*HF27/5.1E9
497 SCV28 = SOXB28*CS*HF28/5.1E9
498 SCV29 = SOXB29*CS*HF29/5.1E9
499 SCV30 = SOXB30*CS*HF30/5.1E9
500 SCV31 = SOXB31*CS*HF31/5.1E9
501 SCV32 = SOXB32*CS*HF32/5.1E9
502 SCV33 = SOXB33*CS*HF33/5.1E9
503 SCV34 = SOXB34*CS*HF34/5.1E9
504 SCV35 = SOXB35*CS*HF35/5.1E9
505 SCV36 = SOXB36*CS*HF36/5.1E9
506 SCV37 = SOXB37*CS*HF37/5.1E9
507 SCV38 = SOXB38*CS*HF38/5.1E9
508 SCV39 = SOXB39*CS*HF39/5.1E9
509 SCV40 = SOXB40*CS*HF40/5.1E9
510 SCV41 = SOXB41*CS*HF41/5.1E9
511 SCV42 = SOXB42*CS*HF42/5.1E9
512 SCV43 = SOXB43*CS*HF43/5.1E9
513 SCV44 = SOXB44*CS*HF44/5.1E9
514 SCV45 = SOXB45*CS*HF45/5.1E9
515 SCV46 = SOXB46*CS*HF46/5.1E9
516 SCV47 = SOXB47*CS*HF47/5.1E9
517 SCV48 = SOXB48*CS*HF48/5.1E9
518 SCV49 = SOXB49*CS*HF49/5.1E9
519 SCV50 = SOXB50*CS*HF50/5.1E9
520 SCV51 = SOXB51*CS*HF51/5.1E9
521 SCV52 = SOXB52*CS*HF52/5.1E9
522 SCV53 = SOXB53*CS*HF53/5.1E9
523 SCV54 = SOXB54*CS*HF54/5.1E9
524 SCV55 = SOXB55*CS*HF55/5.1E9
525 SCV56 = SOXB56*CS*HF56/5.1E9
526 SCV57 = SOXB57*CS*HF57/5.1E9
527 SCV58 = SOXB58*CS*HF58/5.1E9
528 SCV59 = SOXB59*CS*HF59/5.1E9
529 SCV60 = SOXB60*CS*HF60/5.1E9
530 SCV61 = SOXB61*CS*HF61/5.1E9
531 SCV62 = SOXB62*CS*HF62/5.1E9
532 SCV63 = SOXB63*CS*HF63/5.1E9
533 SCV64 = SOXB64*CS*HF64/5.1E9
534 SCV65 = SOXB65*CS*HF65/5.1E9
535 SCV66 = SOXB66*CS*HF66/5.1E9
536 SCV67 = SOXB67*CS*HF67/5.1E9
537 SCV68 = SOXB68*CS*HF68/5.1E9
538 SCV69 = SOXB69*CS*HF69/5.1E9
539 SCV70 = SOXB70*CS*HF70/5.1E9
540 SCV71 = SOXB71*CS*HF71/5.1E9
541 SCV72 = SOXB72*CS*HF72/5.1E9
542 SCV73 = SOXB73*CS*HF73/5.1E9
543 SCV74 = SOXB74*CS*HF74/5.1E9
544 SCV75 = SOXB75*CS*HF75/5.1E9
545 SCV76 = SOXB76*CS*HF76/5.1E9
546 SCV77 = SOXB77*CS*HF77/5.1E9
547 SCV78 = SOXB78*CS*HF78/5.1E9
548 SCV79 = SOXB79*CS*HF79/5.1E9
549 SCV80 = SOXB80*CS*HF80/5.1E9
550 SCV81 = SOXB81*CS*HF81/5.1E9
551 SCV82 = SOXB82*CS*HF82/5.1E9
552 SCV83 = SOXB83*CS*HF83/5.1E9
553 SCV84 = SOXB84*CS*HF84/5.1E9
554 SCV85 = SOXB85*CS*HF85/5.1E9
555 SCV86 = SOXB86*CS*HF86/5.1E9
556 SCV87 = SOXB87*CS*HF87/5.1E9
557 SCV88 = SOXB88*CS*HF88/5.1E9
558 SCV89 = SOXB89*CS*HF89/5.1E9
559 SCV90 = SOXB90*CS*HF90/5.1E9
560 SCV91 = SOXB91*CS*HF91/5.1E9
561 SCV92 = SOXB92*CS*HF92/5.1E9
562 SCV93 = SOXB93*CS*HF93/5.1E9
563 SCV94 = SOXB94*CS*HF94/5.1E9
564 SCV95 = SOXB95*CS*HF95/5.1E9
565 SCV96 = SOXB96*CS*HF96/5.1E9
566 SCV97 = SOXB97*CS*HF97/5.1E9
567 SCV98 = SOXB98*CS*HF98/5.1E9
568 SCV99 = SOXB99*CS*HF99/5.1E9
569 SCV100 = SOXB100*CS*HF100/5.1E9
570 SCV101 = SOXB101*CS*HF101/5.1E9
571 SCV102 = SOXB102*CS*HF102/5.1E9
572 SCV103 = SOXB103*CS*HF103/5.1E9
573 SCV104 = SOXB104*CS*HF104/5.1E9
574 SCV105 = SOXB105*CS*HF105/5.1E9
575 SCV106 = SOXB106*CS*HF106/5.1E9
576 SCV107 = SOXB107*CS*HF107/5.1E9
577 SCV108 = SOXB108*CS*HF108/5.1E9
578 SCV109 = SOXB109*CS*HF109/5.1E9
579 SCV110 = SOXB110*CS*HF110/5.1E9
580 SCV111 = SOXB111*CS*HF111/5.1E9
581 SCV112 = SOXB112*CS*HF112/5.1E9
582 SCV113 = SOXB113*CS*HF113/5.1E9
583 SCV114 = SOXB114*CS*HF114/5.1E9
584 SCV115 = SOXB115*CS*HF115/5.1E9
585 SCV116 = SOXB116*CS*HF116/5.1E9
586 SCV117 = SOXB117*CS*HF117/5.1E9
587 SCV118 = SOXB118*CS*HF118/5.1E9
588 SCV119 = SOXB119*CS*HF119/5.1E9
589 SCV120 = SOXB120*CS*HF120/5.1E9
590 SCV121 = SOXB121*CS*HF121/5.1E9
591 SCV122 = SOXB122*CS*HF122/5.1E9
592 SCV123 = SOXB123*CS*HF123/5.1E9
593 SCV124 = SOXB124*CS*HF124/5.1E9
594 SCV125 = SOXB125*CS*HF125/5.1E9
595 SCV126 = SOXB126*CS*HF126/5.1E9
596 SCV127 = SOXB127*CS*HF127/5.1E9
597 SCV128 = SOXB128*CS*HF128/5.1E9
598 SCV129 = SOXB129*CS*HF129/5.1E9
599 SCV130 = SOXB130*CS*HF130/5.1E9
600 SCV131 = SOXB131*CS*HF131/5.1E9
601 SCV132 = SOXB132*CS*HF132/5.1E9
602 SCV133 = SOXB133*CS*HF133/5.1E9
603 SCV134 = SOXB134*CS*HF134/5.1E9
604 SCV135 = SOXB135*CS*HF135/5.1E9
605 SCV136 = SOXB136*CS*HF136/5.1E9
606 SCV137 = SOXB137*CS*HF137/5.1E9
607 SCV138 = SOXB138*CS*HF138/5.1E9
608 SCV139 = SOXB139*CS*HF139/5.1E9
609 SCV140 = SOXB140*CS*HF140/5.1E9
610 SCV141 = SOXB141*CS*HF141/5.1E9
611 SCV142 = SOXB142*CS*HF142/5.1E9
612 SCV143 = SOXB143*CS*HF143/5.1E9
613 SCV144 = SOXB144*CS*HF144/5.1E9
614 SCV145 = SOXB145*CS*HF145/5.1E9
615 SCV146 = SOXB146*CS*HF146/5.1E9
616 SCV147 = SOXB147*CS*HF147/5.1E9
617 SCV148 = SOXB148*CS*HF148/5.1E9
618 SCV149 = SOXB149*CS*HF149/5.1E9
619 SCV150 = SOXB150*CS*HF150/5.1E9
620 SCV151 = SOXB151*CS*HF151/5.1E9
621 SCV152 = SOXB152*CS*HF152/5.1E9
622 SCV153 = SOXB153*CS*HF153/5.1E9
623 SCV154 = SOXB154*CS*HF154/5.1E9
624 SCV155 = SOXB155*CS*HF155/5.1E9
625 SCV156 = SOXB156*CS*HF156/5.1E9
626 SCV157 = SOXB157*
```

ILLUSTRATIVE EFFECTS. HYPOTHETICAL SST FLEET.
WITHOUT EMISSION CONTROLS.

YEAR	FBTE9 KG	DELTS DEG K	DELTG DEG K	DELT DEG K	DELO3 CORR. PERCENT
1	0.21	-0.0000	0.0000	0.0000	-0.0122
2	0.46	-0.0000	0.0001	0.0000	-0.0266
3	0.77	-0.0000	0.0001	0.0001	-0.0448
4	1.18	-0.0001	0.0003	0.0002	-0.0681
5	1.68	-0.0001	0.0004	0.0003	-0.0975
6	2.31	-0.0002	0.0007	0.0005	-0.1337
7	3.06	-0.0003	0.0010	0.0007	-0.1772
8	3.94	-0.0004	0.0013	0.0010	-0.2280
9	4.94	-0.0005	0.0018	0.0013	-0.2859
10	6.05	-0.0006	0.0024	0.0017	-0.3504
11	7.26	-0.0008	0.0031	0.0022	-0.4207
12	8.56	-0.0009	0.0040	0.0027	-0.4958
13	9.92	-0.0011	0.0051	0.0034	-0.5747
14	11.32	-0.0013	0.0062	0.0040	-0.6564
15	12.76	-0.0015	0.0075	0.0048	-0.7397
16	14.20	-0.0018	0.0088	0.0056	-0.8235
17	15.64	-0.0020	0.0102	0.0064	-0.9089
18	17.06	-0.0022	0.0116	0.0073	-0.9890
19	18.43	-0.0025	0.0132	0.0083	-1.0691
20	19.77	-0.0028	0.0148	0.0092	-1.1465
21	21.05	-0.0030	0.0166	0.0102	-1.2208
22	22.27	-0.0033	0.0184	0.0111	-1.2915
23	23.42	-0.0035	0.0201	0.0121	-1.3585
24	24.50	-0.0037	0.0219	0.0131	-1.4215
25	25.52	-0.0040	0.0236	0.0140	-1.4806
26	26.47	-0.0042	0.0252	0.0149	-1.5182
27	26.58	-0.0044	0.0267	0.0158	-1.5424
28	26.85	-0.0045	0.0281	0.0165	-1.5580
29	27.02	-0.0047	0.0293	0.0172	-1.5681
30	27.13	-0.0048	0.0303	0.0179	-1.5746
31	27.20	-0.0049	0.0313	0.0184	-1.5788
32	27.25	-0.0050	0.0321	0.0189	-1.5815
33	27.28	-0.0051	0.0328	0.0193	-1.5833
34	27.30	-0.0051	0.0334	0.0196	-1.5845
35	27.31	-0.0052	0.0339	0.0199	-1.5852
36	27.32	-0.0052	0.0343	0.0202	-1.5857
37	27.33	-0.0053	0.0347	0.0204	-1.5860
38	27.33	-0.0053	0.0351	0.0206	-1.5862
39	27.33	-0.0054	0.0355	0.0208	-1.5863
40	27.33	-0.0054	0.0358	0.0209	-1.5864
41	27.33	-0.0054	0.0360	0.0211	-1.5865
42	27.34	-0.0054	0.0361	0.0212	-1.5865
43	27.34	-0.0054	0.0361	0.0213	-1.5865
44	27.34	-0.0055	0.0364	0.0214	-1.5865
45	27.34	-0.0055	0.0366	0.0215	-1.5866
46	27.34	-0.0055	0.0366	0.0215	-1.5866
47	27.34	-0.0055	0.0366	0.0215	-1.5866
48	27.34	-0.0055	0.0366	0.0216	-1.5866
49	27.34	-0.0055	0.0366	0.0216	-1.5866
50	27.34	-0.0055	0.0366	0.0216	-1.5866

ILLUSTRATIVE EFFECTS. HYPOTHETICAL SST FLEET.
WITH EMISSION CONTROLS.

YEAR	FBTE9 KG	DELTS DEG K	DELTG DEG K	DELT DEG K	DELO3 CORR. PERCENT
1	0.21	-0.0000	0.0000	0.0000	-0.0122
2	0.46	-0.0000	0.0001	0.0000	-0.0266
3	0.77	-0.0000	0.0001	0.0001	-0.0448
4	1.18	-0.0001	0.0003	0.0002	-0.0681
5	1.68	-0.0001	0.0004	0.0003	-0.0975
6	2.31	-0.0002	0.0007	0.0005	-0.1337
7	3.06	-0.0003	0.0010	0.0007	-0.1772
8	3.94	-0.0004	0.0013	0.0010	-0.2280
9	4.94	-0.0005	0.0018	0.0013	-0.2859
10	6.05	-0.0006	0.0024	0.0018	-0.3504
11	7.26	-0.0008	0.0031	0.0024	-0.4207
12	8.56	-0.0009	0.0040	0.0031	-0.4958
13	9.92	-0.0011	0.0051	0.0040	-0.5747
14	11.32	-0.0013	0.0062	0.0049	-0.6564
15	12.76	-0.0015	0.0075	0.0059	-0.7397
16	14.20	-0.0018	0.0088	0.0070	-0.8235
17	15.64	-0.0020	0.0102	0.0082	-0.9089
18	17.06	-0.0022	0.0116	0.0094	-0.9890
19	18.43	-0.0025	0.0132	0.0107	-1.0691
20	19.77	-0.0028	0.0148	0.0121	-1.1465
21	21.05	-0.0030	0.0166	0.0136	-1.2208
22	22.27	-0.0033	0.0184	0.0151	-1.2915
23	23.42	-0.0035	0.0201	0.0166	-1.3585
24	24.50	-0.0037	0.0219	0.0181	-1.4215
25	25.52	-0.0040	0.0236	0.0196	-1.4806
26	26.47	-0.0042	0.0252	0.0210	-1.5182
27	26.58	-0.0044	0.0267	0.0223	-1.5424
28	26.85	-0.0045	0.0281	0.0235	-1.5580
29	27.02	-0.0047	0.0293	0.0246	-1.5681
30	27.13	-0.0048	0.0303	0.0255	-1.5746
31	27.20	-0.0049	0.0313	0.0264	-1.5815
32	27.25	-0.0050	0.0321	0.0271	-1.5833
33	27.28	-0.0051	0.0328	0.0277	-1.5845
34	27.30	-0.0051	0.0334	0.0282	-1.5852
35	27.31	-0.0052	0.0339	0.0287	-1.5857
36	27.32	-0.0052	0.0343	0.0291	-1.5860
37	27.33	-0.0053	0.0347	0.0294	-1.5862
38	27.33	-0.0053	0.0351	0.0297	-1.5863
39	27.33	-0.0054	0.0355	0.0300	-1.5864
40	27.33	-0.0054	0.0358	0.0302	-1.5865
41	27.33	-0.0054	0.0360	0.0306	-1.5865
42	27.34	-0.0054	0.0361	0.0307	-1.5865
43	27.34	-0.0055	0.0364	0.0308	-1.5865
44	27.34	-0.0055	0.0366	0.0309	-1.5866
45	27.34	-0.0055	0.0366	0.0310	-1.5866
46	27.34	-0.0055	0.0366	0.0311	-1.5866
47	27.34	-0.0055	0.0366	0.0311	-1.5866
48	27.34	-0.0055	0.0366	0.0312	-1.5866
49	27.34	-0.0055	0.0366	0.0312	-1.5866
50	27.34	-0.0055	0.0366	0.0312	-1.5866

NOMENCLATURE FOR RCO 81

C2, C3	Fuel flow rates, kg/yr/aircraft, in bands 2 and 3	XNBL, etc.	NO _x burden in band 1 as NO ₂
F2(I), F3(I)	Fuel flow rate/yr, in bands 2 and 3, for year I	SOXBL, etc.	Particulate burden in band 1 (as 75 percent H ₂ SO ₄)
EMI(I), etc.	NO _x emission index in band 1 for year I	H2OBL, etc.	Water burden in band 1
ESI(I), etc.	Particulates emission index in band 1 for year I	FBT	Total fuel burden
CONTRL	If set = 0, no NO _x or SO _x controls; if set = 1, NO _x and SO _x controls are imposed as a function of time	CBAGL, etc.	Climatic approach factor (per year) based on gaseous burden, in band 1
CASE	Defined	CBASL, etc.	Climatic approach factor (per year) based on particles, in band 1
OSFL, etc.	Ozone destruction, percent/10 ⁹ kg (burden) of NO _x in band 1, global average (here assumed in linear region)	CHL, etc.	Climatic coefficient due to combined effects of NO ₂ addition (CHL) and ozone depletion (CDEL03) per unit of NO _x addition used for yearly additions
RL, etc.	Residence time, which here is taken as equal to response time	XNCFI, etc.	Climate change, K, at steady state due to burden of NO ₂ , from band 1
PFI, etc.	Particle factor; ratio of particle residence time to gas residence time	DOJL, etc.	Ozone depletion due to NO _x burden in band 1
EHL, etc.	Emission index for H ₂ O in band 1, etc.	DOJCFI, etc.	Climate change, K, at steady state due to ozone depletion, from band 1
H2O3F	Percent ozone change for a doubling of stratospheric water vapor; i.e., for a burden of 1.78 x 10 ¹² kg of H ₂ O	SOXCFI, etc.	Climate change, K, at steady state due to particle burden, from band 1
HFI, etc.	Hemisphere factor, a multiplier on the global change, in band 1	H2OCFI, etc.	Climate change, K, at steady state due to water burden, from band 1
CH	Cooling coefficient, K/fractional change in water vapor (at steady state)	DELTS	Temperature change at year J resulting from particles
CN	Cooling coefficient, K/fractional change in NO ₂ (1.58 x 10 ⁹ kg natural)	LMI(J), etc.	NO _x emission index corrected for water effects
CS	Cooling coefficient/μg/m ³ , with m ³ taken as 2.55 x 10 ¹⁸	DELTG	Temperature change at year J resulting from gaseous additions
CDELO3	Cooling coefficient/fractional change in ozone	DELT	Total temperature change
DELTZ	Initial temperature anomaly	DELO3	Percentage change in ozone, Northern Hemisphere corridor
C	Climate response time	Other terminology follows directly.	
FBI, etc.	Fuel burden in band 1 (burned fuel as kerosene)		

APPENDIX G

DETECTABILITY OF ENVIRONMENTAL CHANGES
CAUSED BY AIRCRAFT EFFLUENTS -- SOME COMMENTS

R. C. Oliver

APPENDIX G

DETECTABILITY OF ENVIRONMENTAL CHANGES CAUSED BY AIRCRAFT EFFLUENTS -- SOME COMMENTS

G.1 INTRODUCTION AND SUMMARY

In this brief section, some comments are offered on the detectability of aircraft-induced changes in ozone or in climate which, according to theory, should result from some particular aircraft source. It is noted, with regard to ozone column changes, that the detectability problem varies with the type of perturbation: A pulsed event, such as a nuclear weapons test or a solar proton event, differs from a "step" event (a large fleet of aircraft beginning and continuing operations) and both differ from a gradually increasing source, such as a fleet building up with time or the increasing release of chlorofluoromethanes in the troposphere. Effects from the gradually increasing source would be the most difficult to assign unambiguously as to cause. Detectability will be enhanced by combining models, meteorology, and atmospheric measurements at various latitudes and altitudes. Climatic changes are more difficult to detect and credible means to ascribe and distribute the causes do not seem to be at hand.

In all cases, because of time delays, control procedures must be anticipatory and based on mathematical models; the purpose of "known cause"- "measured effect" studies is to validate such models.

G.2 DETECTABILITY OF AIRCRAFT-INDUCED CHANGES IN OZONE

The detectability of changes in mean ozone, averaged over some time period and geographical region, is a subject in apparent need of additional work. Thus, the CIAP Report of Findings (pp. 70-73, 82), based on an interpretation and extrapolation of arguments presented by Pittock (1974), concludes that a change due to aircraft of 0.5 percent per decade is "barely discernible" (with 95 percent confidence) after 10 years of observation; however, Angell and Korshover (1975) report values of annual percentage changes over specific stations as low as 0.1 percent. Also, if Pittock's arguments are examined further, it would seem questionable that the figure of 0.5 percent quoted in the CIAP Report of Findings can be justified; in fact, the 10-year, 95-percent confidence line value given by Pittock with an "ideal global network" is about 1.9 percent. According to Pittock, removal of the mean annual cycle would reduce this by a factor of 2 or so;

more, however, apparently by reducing the time required to detect a given change than the change noticeable at a given time. If so, to use Pittcock's curve, an ideal global network would permit detection of a change of 0.7 percent in 10 years rather than 20 years as plotted by Pittcock. In the CIAP Report of Findings (p. 76), it is assumed that 81, rather than Pittcock's 9 independent ozone stations, can be established, but the CIAP report does not note the possible correction for mean annual cycle.

The trend detection problem is a difficult one, and subject to severe errors in interpretation, as pointed out by Birrer (1974), who notes that the slope of a trend line, and indeed the sign, depends on the starting point and end points used in estimating the trend, that different period lengths may yield quite different trend values, and varying amplitudes can strengthen or weaken these effects; also, the longer the period analyzed, the smaller the trend values found. He concludes that "Definitely periods of 5-10 years are too short to make any statements about the future."

Another problem alluded to by Birrer results from the fact of large-scale flow patterns in ozone; that is, the variation in ozone with longitude. Should these patterns shift, a single station would find an apparent, but in a sense a spurious, change in ozone. Obviously, if perhaps to a lesser degree, a global network of land-based stations would be subject to the same problem. Note, for example, Fig. G-1, taken from ICAS (1975), which shows the longitudinal variations of ozone and the nonuniform distribution of stations.

A point which must be considered in detecting aircraft-induced effects on ozone is that numerous possible causes of ozone change have been identified, of which aircraft-induced changes, in the absence of large SST fleets, would be a small part. The potential causative agents of ozone change include changes in halocarbons, nitrous oxide, nuclear detonations, and solar phenomena.

In this connection, it should be noted that fundamental differences exist between tropospheric surface sources of possible ozone-destroying ingredients, and stratospheric sources in terms of time lags and perhaps in global uniformity of effects. Stratospheric measurements of halocarbon-derived species as a function of time could provide the information on which the effects of halogens on ozone would be separated out.

The obvious way to improve on the ozone measurement situation is to utilize satellites to continuously record global ozone levels, necessarily, however, coupled with ground stations for periodic recalibration. The type of data obtained are described by Heath (1974). A number of problems--data handling alone being a significant one--arise, which we have not

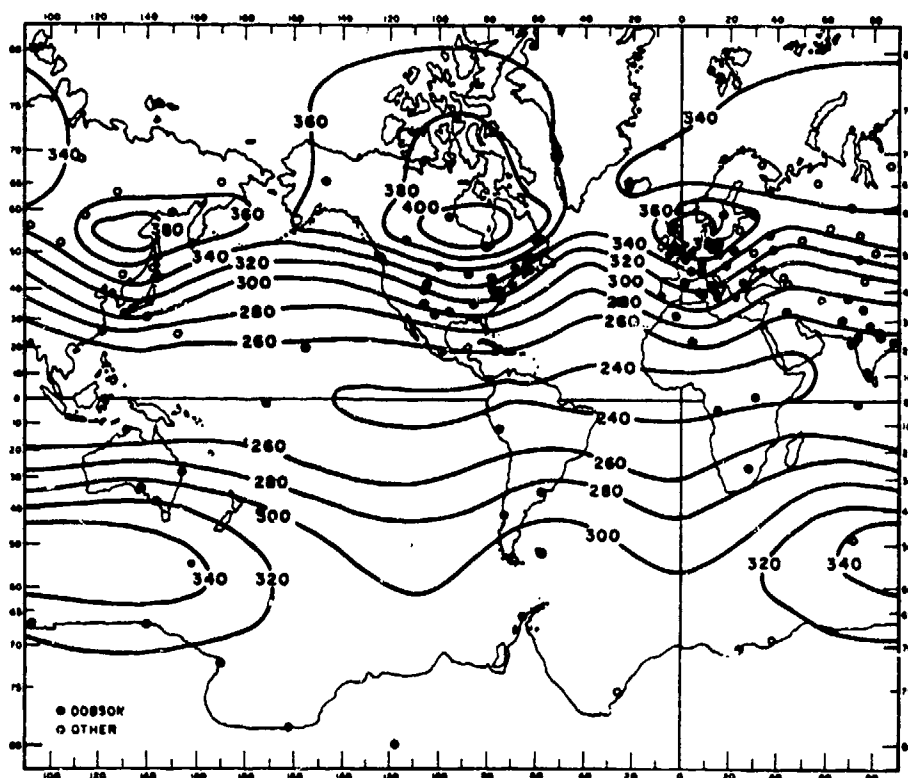


FIGURE G-1. The Mean Global Total Ozone Distribution with the Ozone Amount given in Units of m-atm-cm (after Gebhart, Bojkov, and London, 1970)
Source: ICAS, 1975

attempted to evaluate. We note, however, that the satellite data reported by Lovill (Fig. 35, p. 70, CIAP Report of Findings), which purport to show up to 10 percent changes in global ozone inventory over time periods of a few days, have been attacked as being unrealistic in a physical sense. One problem associated with Nimbus 4, interference by the South Atlantic anomaly, will be minimized in Nimbus G by inclusion of a chopper circuit. Nimbus G is scheduled for launch in the last quarter of 1978. The high-altitude (30 mbar to 0.4 mbar) data collected by Nimbus 4 are affected by the anomaly, but the error introduced has little effect on the global total ozone or zonal-averaged ozone maps (Heath, 1976).

Much of the above discussion, and the CIAP treatment, refers to detections of trends. While it is recognized that aircraft traffic generally increases as a function of time, the question of trends and their

detectability and predictability may, in fact, not be particularly relevant.* Thus, for an instantaneous event, such as ozone depletion following the large solar proton event of August 1972 (Crutzen, 1975), the question of trends does not enter; rather, a stepwise change in ozone level, which is most detectable in certain latitudes and above certain altitudes (where the change involved is a significant percentage of the column) is looked for. While aircraft effluents will cause a more diffuse effect on ozone, both geographically in terms of the total column and vertically in terms of distribution than does a solar proton absorption event, the principle that changes should be sought where and when changes are predicted is still valid. A square wave source, such as a suddenly imposed constant fleet of SSTs, is clearly a different problem from a detectability standpoint than would be a fleet growing gradually with time. Most likely, aircraft effluents, as from an SST fleet, would vary to some degree seasonally, and change year by year. Such changes would modulate ozone columns and ozone concentrations (and certain trace species) at various altitudes and latitudes and, if some measure of aircraft effluent deposition were available, one could, by coupling in model predictions, know where, at what altitudes, and when to look for changes having the highest signal-to-noise ratio. Emission rates could be obtained either directly from known fuel consumption and emission indexes, or indirectly from measures of some tracer constituent (such as vanadium naturally in the kerosene, or perhaps an ingredient purposely added in known amounts). By this approach, one would, in effect, add an extra dimension (or more) to the Pittock analysis, minimizing the questions associated with other changes caused by solar cycles, halocarbons, etc., and should improve the information content thereby. This sort of "pattern analysis" is implicit in the CIAP Report of Findings discussion on monitoring, but not clearly distinguished from trend questions, etc., as in the Pittock analysis.

Returning for a moment to an earlier discussion as to whether ozone changes and trends of a few tenths of a percent could be detected over a time period of a few years, considering the arguments raised by Pittock (1974) and Birrer (1974), and the data reported by ICAS (1975), it should be noted that Angell and Korshover (1975) appear to be simply reporting data as measured (and smoothed in some cases) for certain stations and groups of stations; they point out that some of the data, for example, are not significant at the 5 percent level. They state further that in their opinion, "it is impractical to determine a precise average on a hemispheric or global scale." In general, however, it should be noted that the Angell

*See also Section G.4.

and Korshover approach is one which couples in a great deal of meteorological and background data in the detection of effects rather than one which takes a purely statistical approach, so that the detectability of changes would seem to be enhanced.*

G.3 DETECTABILITY OF AIRCRAFT-INDUCED CHANGES IN CLIMATE

This problem is a far more difficult one than that of detecting changes in ozone. Again, aircraft effects would be expected to be small relative to other effects (e.g., CO_2 from combustion). Certain effects might be noticed and measured, e.g., the incidence of contrails, and perhaps the aircraft contribution to stratospheric particulates (soot, H_2SO_4) and optical depth, etc., might be determined by some tie of trace metal content of stratospheric particulates to the fuel composition. But in view of the theoretical problems involved in predicting (or establishing) climate change, the small expected changes mixed among larger expected changes and the poorly known time lags involved, it would appear that, at present at least, no credible means for detecting aircraft-induced changes in climate can be proposed. Any policy decisions or climate change will necessarily be based almost entirely on modeling results without the benefits of validation.**

G.4 PURPOSE

The purpose of efforts to detect aircraft-induced changes must not be forgotten. The basic purpose, in this author's opinion at least, is model validation. Effects will lag and corrective procedures must anticipate fleet growth; by the time actual fleet effects are measurable unambiguously, the changes involved could be unacceptably large. Model validation, however, may be achievable, if imperfectly, by examination of a variety of perturbations, including nuclear weapons tests, solar proton events, etc.

*See Tribus (1970) for a discussion of the misuse of statistics in connection with cloud seeding. He argues that "most existing statistical approaches do not permit us to use all that we really know."

**Reference here is to the combined effects of aircraft exhaust products. Some partial validation of the effects of aerosols can be claimed in examining the volcanic and climate records (see Oliver, 1976).

PRINCIPAL REFERENCES

- CIAP Report of Findings*, Grobecker, A.J., S.C. Coroniti, R.H. Cannon, Jr., "The Effects of Stratospheric Pollution by Aircraft," Final Report, U.S. Department of Transportation, Climatic Impact Assessment Program, DOT-TST-75-58, December 1974.
- CIAP Monograph 1*, "The Natural Stratosphere of 1974," U.S. Department of Transportation, Climatic Impact Assessment Program, DOT-TST-75-51, September 1975.
- CIAP Monograph 2*, "Propulsion Effluents in the Stratosphere," U.S. Department of Transportation, Climatic Impact Assessment Program, DOT-TST-75-52, September 1975.
- CIAP Monograph 3*, "The Stratosphere Perturbed by Propulsion Effluents," U.S. Department of Transportation, Climatic Impact Assessment Program, DOT-TST-75-53, September 1975.
- CIAP Monograph 4*, "The Natural and Radiatively Perturbed Troposphere," U.S. Department of Transportation, Climatic Impact Assessment Program, DOT-TST-75-54, September 1975.
- CIAP Monograph 5*, "Impacts of Climatic Change on the Biosphere," Part 1-- Ultraviolet Radiation Effects, U.S. Department of Transportation, Climatic Impact Assessment Program, DOT-TST-75-55, September 1975.
- CIAP Monograph 5*, "Impacts of Climatic Change on the Biosphere," Part 2-- Climatic Effects, U.S. Department of Transportation, Climatic Impact Assessment Program, DOT-TST-75-55, September 1975.
- CIAP Monograph 6*, "Economic and Social Measures of Biologic and Climatic Change," U.S. Department of Transportation, Climatic Impact Assessment Program, DOT-TST-75-56, September 1975.
- COMESA, *The Report of the Committee on Meteorological Effects of Stratospheric Aircraft*, 1972-1975.
- NAS (National Academy of Sciences), *Environmental Impact of Stratospheric Flight: Biological and Climatic Effects of Aircraft Emissions in the Stratosphere*, National Academy of Sciences, 1975.
- NAS (National Academy of Sciences), *Halocarbons: Environmental Effects of Chlorofluoromethane Release*, 1976.
- NAS (National Academy of Sciences), *Halocarbons: Effects on Stratospheric Ozone*, 1976a.

GENERAL REFERENCES

- Alyea, F.N., D.M. Cunnold, R.G. Prinn, "Stratospheric Ozone Destruction by Aircraft-Induced Nitrogen Oxides," *Science*, 188, pp. 117-125, 11 April 1975.
- Alyea, F.N., D.M. Cunnold, and R.G. Prinn, *Stratospheric Ozone Destruction by SST-Induced NO_x: First Results From a Dynamical-Chemical Circulation Model*, MIT Special Scientific Report, COO-2249-4, September 1974.
- Anderson, J.G., "The Absolute Concentration of OH(X²π) in the Earth's Stratosphere," *Geophys. Res. Letters*, 3, 3, March 1976.
- Angell, J.K. and J. Korshover, *Global Analysis of Recent Total-Ozone Fluctuations*, February 1975, as cited in ICAS 18a-FY75, "The Possible Impact of Fluorocarbons and Halocarbons on Ozone," Interdepartmental Committee for Atmospheric Sciences, Federal Council for Science and Technology, Science and Technology Policy Office, National Science Foundation, May 1975.
- Arthur D. Little, Inc., *Stratospheric Emissions Due to Current and Projected Aircraft Operations*, C77327-10, (draft report), August 1976.
- Australian Academy of Science, *Atmospheric Effects of Supersonic Aircraft*, Reports of the Australian Academy of Science, Number 15, February 1972.
- Bach, Wilfrid, "Global Air Pollution and Climatic Change," *Revs. of Geophys. & Space Physics*, 14, 3, pp. 429-474, August 1976.
- Bahr, D.W., "Attainment of Ultra-Low NO_x Emissions Levels in Aircraft Turbine Engines," *Proceedings of the 4th Conference on the Climatic Impact Assessment Program*, U.S. Department of Transportation, DOT-TSC-OST-75-38, 4-7 February 1975, published August 1976.
- Bauer, E., "Dispersion of the Tracers in the Atmosphere and Ocean, Survey and Comparison of Experimental Data," *J. Geophys. Res.*, 79, pp. 789-795, 1974.
- Bauer, E. and F.R. Gilmore presented at the 4th CIAP Conference, "The Effects of Atmospheric Nuclear Explosions on Total Ozone," also *Rev. Geophys. & Space Physics*, 13, 4 November, pp. 451-458, August 1975.
- Birrer, W.M., "Some Critical Remarks on Trend Analysis of Total Ozone Data," *Pure and Applied Geophysics (PAGEOPN)*, 112, pp. 523-532, (III), 1974.
- Blackmer, A.M., and J.M. Bremner, "Potential of Soil as a Sink for Atmospheric Nitrous Oxide," *Geophys. Res. Letters*, 3, 12, pp. 739-742, December 1976.
- Borucki, W.J., R.C. Whitten, V.R. Watson, H.J. Woodward, C.A. Riegel, L.A. Capone, and T. Becker, "Model Predictions of Latitude-Dependent Ozone Depletion Due to Supersonic Transport Operations," *AIAA Journal*, 14, 12, December 1976.
- Budyko, M.I., *Climate and Life*, International Geophysics Series, Vol. 18, D.H. Miller (ed., English edition), Academic Press, 1974.

- Callis, L.B., V. Ramanathan, R.E. Boughner, and B.R. Barkstrom, *The Stratosphere: Scattering Effects, A Coupled 1-D Model and Thermal Balance Effects*, NASA/Langley, preprint, 1975.
- Cess, R.D., "Global Climate Change: An Investigation of Atmospheric Feedback Mechanisms," *Tellus XXVII*, 3, 1975.
- Cess, R.D., "Radiative Transfer Due to Atmospheric Water Vapor: Global Considerations of the Earth's Energy Balance," *J. Quant. Spectrosc. Radiat. Transfer*, 14, pp. 861-871, Pergamon Press, 1974.
- Chameides, W.L. and D.H. Stedman, "Tropospheric Ozone: Coupling Transport and Photochemistry," presented at *The Non-Urban Tropospheric Composition Meeting*, AGU/AMS, Hollywood, Florida, 10-12 November 1976.
- Chameides, W.L. and J.C.G. Walker, "A Time-Dependent Photochemical Model for Ozone Near the Ground," *J. Geophys. Res.*, 81, 3, pp. 413-420, 20 January 1976.
- Chameides, W.L. and J.C.G. Walker, "A Photochemical Theory of Tropospheric Ozone," *J. Geophys. Res.*, 78, 36, pp. 8751-8760, 20 December 1973.
- Chapman, S., "A Theory of Upper-Atmospheric Ozone," *Mem. Roy. Meteorol. Society*, 3, pp. 103-125, 1930.
- Chang, Julius S., "Uncertainties in the Validation of Parameterized Transport in 1-D Models of the Stratosphere," *Proceedings of the 4th Conference of the Climatic Impact Assessment Program*, U.S. Department of Transportation, DOT-TSC-OST-75-38, 4-7 February 1975, published August 1976.
- Chatfield, R. and H. Harrison, "Ozone in the Remote Troposphere: Mixing Versus Photochemistry," *J. Geophys. Res.*, 81, 3, pp. 421-423, 20 January 1976.
- Coakley, J.A. and G.W. Grams, "Relative Influence of Visible and Infrared Optical Properties of a Stratospheric Aerosol Layer on the Global Climate," *J. Appl. Meteorol.*, 15, pp. 679-691, July 1976.
- COVOS, Bertin, M., R. Borshi, G. Brasseur, R. Joattor, M. Maignan, *Models Mathematiques de la Stratosphere Comite' d'Etudes Sur Les Consequences des Vols Stratospheriques*, Rapport No. 6A, 14 October 1976.
- Craig, P.M., paper presented at the AGU Meeting, Washington, D.C., 14 April 1976.
- Crutzen, P.J., "The Sensitivity of the Ozone Layer to Changes in Soil and Ocean Parameters," *AGU Meeting*, Washington, D.C., 14 April 1976.
- Crutzen, P.J., "Upper Limits on Atmospheric Ozone Reductions Following Increased Application of Fixed Nitrogen to the Soil," *Geophys. Res. Letters*, 3, 3, pp. 169-172, March 1976a.
- Crutzen, P.J., "The Possible Importance of CSO for the Sulfate Layer of the Stratosphere," *Geophys. Res. Letters*, 3, 2, pp. 73-76, February 1976b.
- Crutzen, P.J., "A Two-Dimensional Photochemical Model of the Atmosphere Below 55 km; Estimates of Natural and Man-Caused Ozone Perturbations Due to NO_x," presented at the *4th CIAP Conference*, Cambridge, Mass., 4-7 February 1975.
- Crutzen, P.J., "A Review of Upper Atmospheric Photochemistry," paper presented at the International Association of Geomagnetism and Aeronomy Symposium, Kyoto, Japan, 10-12 September 1973, *Can. J. Chem.*, 52, 8, pp. 1569-1581, 1974.

- Crutzen, P.J., "Photochemical Reactions Initiated by and Influencing Ozone in Unpolluted Tropospheric Air," *Tellus XXVI*, 1-2, 1974a.
- Crutzen, P.J., "A Discussion of the Chemistry of Some Minor Constituents in the Stratosphere and Troposphere," *Pure and Applied Geophysics (PAGEOPH)*, 106-108 (V-VII), 1973.
- Crutzen, P.J., "SSTs--A Threat to the Earth's Ozone Shield," *Ambio*, 1, pp. 41-51, 1972.
- Crutzen, P.J., "Ozone Production Rates in an Oxygen-Hydrogen-Nitrogen Oxide Atmosphere," *J. Geophys. Res.*, 76, pp. 7311-7327, 1971.
- Crutzen, P.J., I.A. Isaksen, and J.R. McAfee, "The Impact of the Chlorocarbon Industry on the Ozone Layer," submitted to *J. Geophys. Res.*, 1976.
- Crutzen, P.J., I.A. Isaksen, and G.C. Reid, "Solar Proton Events: Stratospheric Sources of Nitric Oxide," *Science*, 189, pp. 457-459, 8 August 1975.
- CTAB (Commerce Technical Advisory Board), U.S. Department of Commerce, *Environmental Aspects of the Supersonic Transport*, May 1972.
- Cunnold, D.M. and F.N. Alyea, *Transport Processes and Trace Constituents in the Stratosphere*, U.S. Department of Transportation and U.S. Energy Research and Development Administration, COO-2249-4, Final Report, May 1, 1972-June 30, 1975.
- Cunnold, D.M., F.N. Alyea, R.F. Prinn, "Relative Effects on Atmospheric Ozone of Latitude and Altitude of Supersonic Aircraft," *AIAA J.*, 15, 3, pp. 337-345, March 1977.
- Cutchis, P., "Stratospheric Ozone Depletion and Solar Ultraviolet Radiation on Earth," *Science*, 184, 5 April 1974.
- Danielsen, E.F. and V.A. Mohnen, "Project Dustorm Report: Ozone Measurements and Meteorological Analyses of Tropopause Folding," presented at *The Non-Urban Tropospheric Composition Meeting, AGU/AMS*, Hollywood, Florida, 10-12 November, 1976.
- Davidson, D.L., and A.F. Domal, *Emission Measurements of a J93 Turbojet Engine*, Report No. FAA-RD-73-66, Arnold Engineering Development Center, Arnold Air Force Station, Tennessee 37389, September 1973.
- DeMore, W.B. and F. Tschuikow-Roux, "Temperature Dependence of the Reactions of OH and HO₂ with O₃," *J. Phys. Chem.*, 78, pp. 1447-1451, 1974.
- Dickinson, R.E., "Solar Variability and the Lower Atmosphere," *Bull. Amer. Meteorol. Soc.*, 56, 12, pp. 1240-1248, December 1975.
- Dimitriadis, B., M.C. Dodge, J.J. Bufalini, K.L. Demerjian, A.P. Altshuler, correspondence to editor, *Environmental Science and Technology*, 10, 9, pp. 934-936, September 1976.
- Drevinsky, P.J., and J. Pecci, "Size and Vertical Distribution of Stratospheric Radioactive Aerosols," in A.W. Klement, ed., *Radioactive Fallout From Nuclear Weapons Tests*, USAEC Publication, Symposium Series No. 5. pp. 158-182, November 1965.
- Duewer, W.J., D.J. Wuebbles, and J.S. Chang, "Effect of NO Photolysis of NO_y Mixing Ratios," Lawrence Livermore Laboratory, *Preprint UCRL-78613*, April 1976.
- Duewer, W.H., D.J. Wuebbles, H.W. Ellsaesser, and J.S. Chang, "NO_x Catalytic Ozone Destruction: Sensitivity to Rate Coefficients," Lawrence Livermore Laboratory, *Preprint UCRL-77917 Rev. 1*, August 1976a. See also *J. Geophys. Res.*, 82, 6, pp. 935-942, February 20, 1977.

- Duewer, W.H., D.J. Wuebbles, H.W. Ellsaesser, J.S. Chang, *Author Reply to Comments by Johnston and Nelson*, UCRL-78854 Preprint, November 1976b.
- Dütsch, H.U., "Photochemistry of Atmospheric Ozone," *Advances in Geophysics*, 15, 219-322, 1971.
- English, J.M., and Guo-An-Pan, "Global Emissions in the Stratosphere," Appendix A, Chapter 8 of *CIAP Monograph 2, Propulsion Effluents in the Stratosphere*, DOT-TST-75-52, September 1975.
- EPA (Environmental Protection Agency) Public Hearings on Control of Air Pollution from Aircraft and Aircraft Engines, January 27-28, 1976.
- FAA (Federal Aviation Administration), *Concorde Supersonic Transport Aircraft; Final Environmental Impact Statement*, Vol. 1, U.S. Department of Transportation, September 1975.
- Fabian, P., "Comments on 'A Photochemical Theory of Tropospheric Ozone'," by W. Chameides and J.C.G. Walker, *J. Geophys. Res.*, 79, 27, pp. 4124-4125, 20 September 1974.
- Ferri, Antonio, "Possibilities and Goals for the Future SST," AIAA Paper 74-254, paper presented at AIAA 13th Aerospace Sciences Meeting, Pasadena, California, 20-22 January 1975.
- Few, J.D., R.J. Bryson, W.K. McGregor, *Evaluation of Probe Sampling Versus Optical In Site Measurements of Nitric Oxide Concentrations in a Jet Engine Combustion Exhaust*, ARO, Inc., AEDC-TR-76-180, prepared for Department of Transportation and Arnold Engineering Development Center, Arnold Air Force Station, Tennessee 37389, Final Report for period 2 July 1974 to 16 February 1975, January 1977.
- Fink, D.E., "Mach 2.2 SST McDonnell Douglas Aim," *Aviation Week and Space Technology*, pp. 54-55, 1 October 1973.
- Foley, H.M. and M.A. Ruderman, *Stratospheric Nitric Oxide Production from Past Nuclear Explosions, and Its Relevance to Projected SST Pollution*, IDA Paper P-984, 1972.
- Gates, W.L., *Numerical Modeling of Climatic Change: A Review of Problems and Prospects*, Rand/P-5471, July 1975.
- Greenstone, R., *The Possibility That Changes in Cloudiness Will Compensate for Changes in Ozone and Lead to Natural Protection Against Ultraviolet Radiation in Technical Information and Documentation Support of the High Altitude Pollution Program*, Operations Research Inc., Draft of Final Report, No. 1099, October 29, 1976.
- Gryvnak, D.A. and D.E. Burch, *Monitoring NO and CO in Aircraft Jet Exhausts by a Gas-Filter Correlation Technique*, AFAPL-TR-75-101, Aeronutronic Ford Corp., January 1976.
- Gulliksen, S., "Tritium Content of Rain in Trondheim," *J. Geophys. Res.*, 75, 12, pp. 2247-2249, 20 April 1970.
- Hamill, P., O.B. Toon, C.S. Kiang, *A Physical Model of the Stratospheric Aerosol Particles*, unpublished, 1976.
- Hamill, P., R.P. Turco, O.B. Toon, R.C. Whitten, C.S. Kiang, "A 1-D Model of the Stratospheric Aerosol Layer," preprint submitted to *Geophys. Res. Letters*, 1976.
- HAPP (High Altitude Pollution Program), U.S. Department of Transportation, Federal Aviation Administration, Office of Environmental Quality, Initial Planning Documentation, 16 June 1975.

- Harries, J.E., "The Distribution of Water Vapor in the Stratosphere," *Rev. Geophys. & Space Physics*, 14, 4, pp. 565-575, November 1976.
- Harries, J.E., "Measurements of Stratospheric Water Vapor Using Infrared Techniques," *J. Atmos. Sci.*, 30, 1691-1698, 1973.
- Harshvardhan and R.D. Cess, "Stratospheric Aerosols: Effect Upon Atmospheric Temperature and Global Climate," *Tellus XXVIII*, 1, 1976.
- Hearings Before a Subcommittee of the Congress on Appropriations, House of Representatives, 92nd Congress, First Session, *Civil Supersonic Aircraft Development SST*, 1971.
- McDonald, James., *ibid*, pp. 299-342, 1971.
- Machta, L., *ibid*, p. 445.
- Hearings Before the Senate Committee on Appropriations, *Civil Supersonic Aircraft Development (SST)*, H.J. Res. 468, 92nd Congress, First Session, 1971.
- Newell, R.E., *ibid*, pp. 135-175, 1971.
- Heath, D.F., "Recent Advances in Satellite Observations of Solar Variability and Global Atmospheric Ozone," *IUGG/IAMAP Proceedings of the International Conference on Structure, Composition and General Circulation of the Upper and Lower Atmospheres and Possible Anthropogenic Perturbations*, Vol. II, University of Melbourne, Australia, 14-25 January 1974.
- Heath, D.F., A.J. Krueger, P.J. Crutzen, *Influence of a Solar Proton Event on Stratospheric Ozone*, Report X-912-76-712, Goddard Space Flight Center, June 1976.
- Hidalgo, H. and P.J. Crutzen, "The Tropospheric and Stratospheric Composition Perturbed by NO_x Emissions of High Altitude Aircraft," Presented at *The Non-Urban Tropospheric Composition Symposium*, Miami, Florida, 9-12 November 1976.
- Hunt, B.G., "Some Possible Photochemical and Modeling Implications of a Very Dry Stratosphere Obtained with a General Circulation Model," *Proceedings of the International Conference on Structure, Composition and General Circulation of the Upper and Lower Atmospheres and Possible Anthropogenic Perturbations*, Vol. 1, pp. 871-880, Melbourne, Australia, 14-25 January 1974.
- Hunten, D.M., "The Philosophy of One-Dimensional Modeling," *Proceedings of the 4th Conference on the Climatic Impact Assessment Program*, U.S. Department of Transportation, DOT-TSC-OST-75-38, 4-7 February 1975, published August 1976.
- Hunten, D.M., "Estimates of Stratospheric Pollution by an Analytic Model," *Proc. Nat. Acad. Sci. USA, Geophysics*, 72, 12, pp. 4711-4715, December 1975.
- Hunten, D.M., "Residence Times of Aerosols and Gases in the Stratosphere," *Geophys. Res. Letters*, 2, 27, 1975a.
- ICAO/OACI/NKAO, *Technical Panel on Supersonic Transport Operations, 5th Meeting*, Doc 9132, SSTP/5, Montreal, Canada, 25 November - 13 December 1974.
- ICAS, *The Possible Impact of Fluorocarbons and Halocarbons on Ozone*, 18a-FY75. Interdepartmental Committee for Atmospheric Sciences, Federal Council for Science and Technology, Science and Technology Policy Office, National Science Foundation, May 1975.
- Johnston, H.S., "Analysis of the Independent Variables in the Perturbation of Stratospheric Ozone by Nitrogen Fertilizers," AGU meeting, Washington, D.C., 14 April 1976.
- Johnston, H.S., "Expected Short-Term Local Effects of Nuclear Bombs on Stratospheric Ozone, presented at the AGU Meeting, 6-10 December 1976, San Francisco, Calif. Abstract appears on p. 970, *EOS Trans.*, 57, 12, December 1976a.

- Johnston, H.S., "Global Ozone Balance in the Natural Stratosphere," *Revs. of Geophys. & Space Physics*, 13, 5, pp. 637-649, November 1975.
- Johnston, H.S., "Reduction of Stratospheric Ozone by Nitrogen Oxide Catalysts from Supersonic Transport Exhaust," *Science*, 173, pp. 517-522; "Catalytic Reduction of Stratospheric Ozone by Nitrogen Oxides, UCRL Rep. No. 20568, pp. 1-106, 1971.
- Johnston, H.S., D. Kattenhorn, and G. Whitten, "Use of Excess Carbon-14 Data to Calibrate Models of Stratospheric Ozone Depletion by Supersonic Transports, University of California, LBL-3548, 1975. See also 4th CIAP Conference Report, February 4-7, 1975, pp. 156-174, published August 1976.
- Johnston, H.S., D. Kattenhorn, G. Whitten, "Use of Excess C-14 Data to Calibrate Models of Stratospheric Ozone Depletion by SSTs," *J. Geophys. Res.*, 81, p. 368, 1976.
- Johnston, H.S., and E. Quitevis, "The Oxides of Nitrogen With Respect to Urban Smog, Supersonic Transports, and Global Methane," *International Congress of Radiation Research*, Seattle, Washington, 14-20 July 1974.
- Johnston, H.S., G. Whitten, and J. Birks, "Effect of Nuclear Explosions on Stratospheric Nitric Oxide and Ozone," *J. Geophys. Res.*, 78, 37, pp. 6107-6135, 20 September 1973.
- Johnston, H.S., and R. Graham, "Photochemistry of NO_x and HNO_x Compounds," *Can. J. Chem.*, 8, 1415-1423, 1974.
- Junge, C.E., "Residence Time and Variability of Tropospheric Trace Gases," *Tellus XXVI*, 4, pp. 477-488, 1974.
- Junge, C.E., G.W. Chagnon, J.E. Manson, "Stratospheric Aerosols," *J. Meteorol.*, 18, p. 81, 1961.
- Kuhn, P., "Airborne Observations of Contrail Effects on the Thermal Radiation Budget," *J. Atmos. Sci.*, pp. 937-942, September 1970.
- Leach, J.F., M.S. Morris, and P. Wardman, "Distribution of Emissions in the Stratosphere from Present and Future High-Altitude Aircraft," presented at the 3rd Conference on Climatic Impact Assessment Program, U.S. Department of Transportation, DOT-TSC-OST-74-15, 26 February-1 March 1974.
- Leifer, R., M. Schonberg, L. Toonkel, *Updating Stratospheric Inventories to July 1975*, USERDA Report No. HASL-306, p. I-127, July 1976.
- Liu, S.C., R.J. Cicerone, T.M. Donahue, W.L. Chameides, "Limitation of Fertilizer Induced Ozone Reduction by the Long Lifetime of the Reservoir of Fixed Nitrogen," *Geophys. Res. Letters*, 3, 3, pp. 157-160, March 1976.
- Liu, S.C., T.M. Donahue, R.J. Cicerone, W.L. Chameides, "Effect of Water Vapor on the Destruction of Ozone in the Stratosphere Perturbed by Cl_x or NO_x Pollutants," *J. Geophys. Res.*, 81, 18, pp. 3111-3118, 20 June 1976a.
- London, J., "The Distribution of Total Ozone in the Northern Hemisphere," *Beitr. Phys. Atmos.*, 36, 254-263, 1963.
- Louis, J.F., *PH.D. Thesis*, Astro-Geophysics Department, University of Colorado, Boulder, Colorado, 1974.
- Luther, F.M., *Monthly Mean Values of Eddy Diffusion Coefficients in the Lower Stratosphere*, AIAA Paper 73-498, Denver, Colorado, June 11-13, 1973.
- Luther, F.M., D.J. Wuebbles, J.S. Chang, *Temperature Feedback in a Stratospheric Model*, Lawrence Livermore Laboratory UCRL-77298, March 1976.

- Lyon, T.F., W.O. Colley, M.J. Kenworthy, and D.W. Bahr, *Development of Emissions Measurement Techniques for Afterburning Turbine Engines*, AFAPL-TR-75-52, General Electric Co., October 1975.
- Machta, L., "Global Scale Atmospheric Mixing," *Advances in Geophys.*, 18B, p. 33, 1974.
- Machta, L., "Prediction of CO₂ in the Atmosphere," *Carbon and the Biosphere*, Proceedings of the 24th Brookhaven Symposium on Biology, Upton, N.Y., 1972, CONF-720510, G.M. Woodwell and E.V. Pecan (ed.), USAEC, August 1973.
- Machta, L., R.J. List, M.E. Smith, Jr., H. Oeschger, "Use of Natural Radioactivities to Estimate Large Scale Precipitation Scavenging," *AEC Symposium Series #22, Precipitation Scavenging*, p. 465, December 1970.
- Mahlman, J.D., "Some Fundamental Limitations of Simplified-Transport Models as Implied by Results from a Three-Dimensional General Circulation/Tracer Model," *Proceedings of the 4th Conference on the Climatic Impact Assessment Program*, U.S. Department of Transportation, DOT-TSC-OST-75-38, pp. 132-146, 4-7 February 1975, published August 1976.
- Mahlman, J.D., "Preliminary Results from a Three-Dimensional General-Circulation/Tracer Model," *Proceedings of 2nd CIAP Conference*, pp. 321-337, November 1972.
- Manabe, S. and R.T. Wetherald, "Thermal Equilibrium of the Atmosphere with a Given Distribution of Relative Humidity," *J. Atmos. Sci.*, 24, 3, pp. 241-259, May 1967.
- Mason, A.S. and H.G. Östlund, "Atmospheric HT and HTO 3. Vertical Transport of Water in the Stratosphere," *J. Geophys. Res.* 81, pp. 5349-5352 30, 20 October, 1976.
- Mastenbrook, H.J., "Water Vapor Measurements in the Lower Stratosphere," *Can. J. Chem.*, 52, pp. 1527-1531, 1974.
- McElroy, M.B., S.C. Wofsy, J.E. Penner, and J.C. McConnell, "Atmospheric Ozone: Possible Impact of Stratospheric Aviation," *J. Atmos. Sci.*, 31, pp. 287-303, January 1974.
- McElroy, M.B., S.C. Wofsy, Y.L. Yung, "Agricultural Perturbations of the Nitrogen Cycle and Related Impacts on N₂O and Ozone," *AGU Meeting*, Washington, D.C., 14 April 1976.
- Martin, B., "Critical Evaluation of Residence Times Calculated Using the Exponential Approximation," *J. Geophys. Res.*, 81, 5349, 1976.
- Molina, M.J., and F.S. Rowland, "Stratospheric Sink for Chlorofluoromethanes--Chlorine Atom-Catalyzed Destruction of Ozone," *Nature*, 249, pp. 810-812, 1974.
- National Academy of Sciences, *Biological Impacts of Increased Intensities of Solar Ultraviolet Radiation*, NAE, 1973.
- Newell, R.E., "The Global Circulation of Atmospheric Pollutants," *Scientific American*, 224, pp. 32-42, January 1971.
- Oliver, R.C., "On the Response of Hemisphere Mean Temperature to Stratospheric Dust: An Empirical Approach," *J. Appl. Meteorol.*, 15, 9, pp. 933-950, September 1976.
- Oliver, R.C., memorandum to A.J. Grobecker, 15 July 1974, "The Zero Impact SST Concept," (distributed to the NAS Engine Panel at Woods Hole, Mass.).
- Ört, A.H., and E.M. Rasmusson, *Atmospheric Circulation Statistics*, NOAA Prof. Paper No. 5, Geophysical Fluid Dynamics Laboratory, Princeton, N.J., 1971.

- Pena, J.A. and C.L. Hosler, "Freezing of Supercooled Clouds Induced by Shock Waves," presented at *Second National Conference on Weather Modification*, 6-9 April 1970, Santa Barbara, Calif., sponsored by National Science Foundation, pp. 347-351.
- Penndorf, R., *Critical Analysis of Field Measurement Data*, Interim Technical Report No. 2, DOT-FATQWA-3866, 11 November 1976.
- Pittock, A.B., "Ozone Climatology, Trends and the Monitoring Problem," *Proceedings of the IAMAP/IAPSO International Conference on Structure, Composition and General Circulation of the Upper and Lower Atmospheres and Possible Anthropogenic Perturbations*, 14-25 January 1974, Melbourne, Australia, Vol. I.
- Pollack, J.B., O.B. Toon, C. Sagan, A. Summers, B. Baldwin, W. VanCamp, "Volcanic Explosions and Climatic Change: A Theoretical Assessment," *J. Geophys. Res.*, 81, 6, pp. 1071-1083, 20 February 1976.
- Pollack, J.B., O.B. Toon, A. Summers, W. VanCamp, B. Baldwin, "Estimates of the Climatic Impact of Aerosols Produced by Space Shuttles, SSTs, and Other High Flying Aircraft," *J. Appl. Meteorol.*, 15, pp. 247-258, March 1976a.
- Prabhakara, C., "Effects of Non-Photochemical Processes on the Meridional Distribution and Total Amount of Ozone in the Atmosphere," *Monthly Weather Review*, 91, 9, pp. 411-431, September 1963.
- Prinn, R.F., F.N. Alyea, D.M. Cunnold, "Stratospheric Distribution of Odd Nitrogen and Odd Hydrogen in a Two-Dimensional Model," *J. Geophys. Res.*, 80, 36, pp. 4997-5004, 20 December 1975.
- Prinn, R.F., F.N. Alyea, D.M. Cunnold, A. Katz, "The Distribution of Odd Nitrogen and Odd Hydrogen in the Natural and Perturbed Stratosphere," presented at the *2nd International Conference on the Environmental Impact of Aerospace Operations in the High Atmosphere*, American Meteorological Society, Boston, Mass., 1974.
- Ramanathan, V., Calculations provided to H. Hidalgo and summarized in *CIAP Report of Findings*, p. F-125, 1974.
- Ramanathan, V., "Radiative Transfer Within the Earth's Troposphere and Stratosphere: A Simplified Radiative Convective Model," *J. Atm. Sci.*, 33 pp. 1330-1346, July 1976.
- Ramanathan, V., L.B. Callis, R.E. Boughner, *Sensitivity of Surface Temperature and Atmospheric Temperature to Perturbations in the Stratospheric Concentration of Ozone and Nitrogen-Dioxide*, NASA-Langley Research Center, Hampton, Va., 1976a.
- Reck, R.A., "Stratospheric Ozone Effects on Temperature," *Science*, pp. 557-559, 7 May 1976.
- Reiter, Elmar E., "Stratospheric-Tropospheric Exchange Processes," *Revs. of Geophys. & Space Physics*, 13, 4, pp. 459-474, August 1975.
- Report to the Subcommittee on Science, Research and Development of the Committee on Science and Astronautics*, U.S. House of Representatives, 92nd Congress, First Session, Chapter Three, "The Supersonic Transport," pp. 685-748, April 25, 1969, Revised April 15, 1971.
- Ridley, B.A., M. McFarland, J.T. Bruin, H.I. Schiff, and J.C. McConnell, *Sunrise Measurements of Stratospheric Nitric Oxide*, York University, Departments of Chemistry and Physics, Downsview, Ontario, Canada, 1976.
- Roffe, Gerald, and Antonio Ferri, *Effect of Premixing Quality on Oxides of Nitrogen in Gas Turbine Combustors*, NASA CR-2657, February 1976.

- Rosen, J.M. and D.J. Hofmann, "Vertical Diffusion Coefficients Derived from the Spreading of a Volcanic Dust Cloud," *Report No. GM-32*, University of Wyoming, Department of Physics & Astronomy, July 1975.
- Schneider, S.H., "Cloudiness as a Global Climatic Feedback Mechanism: The Effects on the Radiation Balance and Surface Temperature of Variations in Cloudiness," *J. Atm. Sci.*, 29, pp. 1413-1422, 1972.
- Schneider, S.H. and R.E. Dickinson, "Climate Modeling," *Rev. Geophys. and Space Phys.*, 12, pp. 447-493, 1974.
- Schneider, S.H. and C. Mass, "Volcanic Dust, Sunspots, and Temperature Trends," *Science*, 190, 4216, pp. 741-746, 21 November 1975.
- Schulze, R., "Increase of Carcinogenic Ultraviolet Radiation Due to Reduction in Ozone Concentration in the Atmosphere," *Proceedings of the International Conference on Structure, Composition and General Circulation of the Upper and Lower Atmospheres and Possible Anthropogenic Perturbations*, Vol. 1, pp. 479-493, Melbourne, Australia, 14-25 January 1974.
- Schütz, K., C.E. Junge, R. Beck, and B. Albrecht, "Studies of Atmospheric N₂O," *J. Geophys. Res.*, 75, 12, p. 2230, 20 April 1970.
- Scott, C.J., "A Review of Olympus 593 Engine Emissions During High-Altitude Concorde Flights," a paper presented at the *2nd COMESA-COVOS Symposium*, Oxford, England, 24-26 September 1974.
- SCEP, *Report of the Study of Critical Environmental Programs*, "Man's Impact on the Global Environment," Massachusetts Institute of Technology, 1970.
- Seitz, H.B., B. Davidson, J.P. Friend, H.W. Teely, *Final Report on Project Streak Numerical Models of Transport, Diffusion and Fallout of Stratospheric Radioactive Material*, Report NYO-3654-4, prepared for Isotopes, Inc., Westwood, N.J., 1968.
- Smagorinsky, J., "Global Atmospheric Modeling and the Numerical Simulation of Climate," *Weather and Climate Modification*, pp. 633-686, W.N. Hess (ed.), Wiley, N.Y., 1974.
- SRI (Stanford Research Institute), Randall J. Podenza, *Forecasts of Aircraft Activity: By Altitude, World Region, and Aircraft Type*, (draft) 1976.
- Stickse, P.R., "The Annual Variation of Total Ozone in the Southern Hemisphere," *Monthly Weather Rev.*, 98, pp. 787-788, 1970.
- Telegadas, K., *Radioactivity Distribution in the Stratosphere From the Chinese High Yield Nuclear Test of June 27, 1973*, USERDA Report No. HASL-298, p. I-7, January 1976.
- Telegadas, K., *Radioactivity Distribution in the Stratosphere From Chinese and French High Yield Nuclear Tests (1967-1970)*, USERDA Report No. HASL-281, p. I-3, April 1971.
- Telegadas, K., *The Seasonal Atmospheric Distribution and Inventories of Excess Carbon-14 from March 1955 to July 1969*, Health and Safety Laboratory Report-243, 1971.
- Telegadas, K., *The Seasonal Stratospheric Distribution and Inventories of Excess Carbon-14 from March 1955 to July 1969*, Health and Safety Laboratory Report 243, U.S. AEC, 1971.
- Telegadas, K., and Robert J. List, "Are Particulate Radioactive Tracers Indicative of Stratospheric Motions?," *J. Geophys. Res.*, 74, 6, pp. 1339-1350, March 15, 1969.

Tribus, M., "Physical View of Cloud Seeding," *Science*, 168, 3928, pp. 201-211, 10 April 1970.

United Kingdom Department of the Environment, "Chlorofluorocarbons and Their Effect on Stratospheric Ozone," *Pollution Paper No. 5*, 1976.

Widhopf, G., L. Glatt, R. Kramer, "A Two-Dimensional Time-Dependent Photochemical Model of the Atmosphere," final report, Aerospace Corporation, October 1976. See also "Results of a Phenomenological Two-Dimensional Time-Dependent Photochemical Model of the Atmosphere," *AIAA preprint 77-131*, 24-26 January 1977.

Wilson, Jr., Herbert A., "Sonic Boom," *Scientific American*, 206, 1, pp. 36-43, January 1962.

Wofsy, S.C. and M.B. McElroy, "On Vertical Mixing on the Upper Stratosphere," *J. Geophys. Res.*, 78, p. 2619, 1973.

Zinn, J. and C.D. Sutherland, *Stratospheric Chemistry Computations*, LA-6111-MS, Los Alamos Scientific Laboratory, New Mexico, October 1975.